

SYNTHESES, STRUCTURES AND PHYSICAL PROPERTIES OF SOME LANTHANIDE COMPLEXES AND ORGANIC SALTS

A THESIS

*Submitted in partial fulfilment of the
requirements for the award of the degree*

of

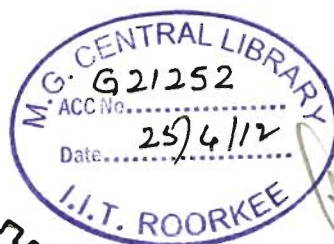
DOCTOR OF PHILOSOPHY

in

CHEMISTRY

by

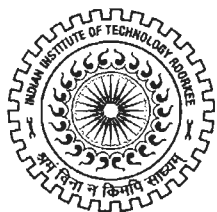
NIDHI GOEL



DEPARTMENT OF CHEMISTRY
INDIAN INSTITUTE OF TECHNOLOGY ROORKEE
ROORKEE-247 667 (INDIA)

JULY, 2011

**©INDIAN INSTITUTE OF TECHNOLOGY ROORKEE, ROORKEE-2011
ALL RIGHTS RESERVED**



INDIAN INSTITUTE OF TECHNOLOGY ROORKEE ROORKEE

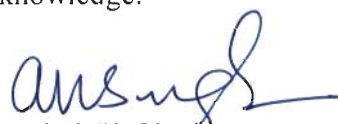
CANDIDATE'S DECLARATION


I hereby certify that the work which is being presented in the thesis entitled **SYNTHESES, STRUCTURES AND PHYSICAL PROPERTIES OF SOME LANTHANIDE COMPLEXES AND ORGANIC SALTS**, in partial fulfilment of the requirements for the award of the Degree of Doctor of Philosophy and submitted in the Department of Chemistry of the Indian Institute of Technology Roorkee, Roorkee is an authentic record of my own work carried out during a period from August 2006 to July 2011 under the supervision of Dr. Udai P. Singh, Professor, Dr. Ashok K. Singh, Professor, Department of Chemistry, Indian Institute of Technology Roorkee, Roorkee.

The matter presented in this thesis has not been submitted by me for the award of any other degree of this or any other Institute.


(NIDHI GOEL)

This is certifying that the above statement made by the candidate is correct to the best of our knowledge.

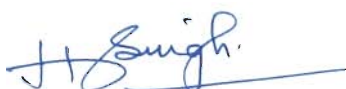

(Ashok K. Singh)
Supervisor


(Udai P. Singh)
Supervisor

Dated: 14.07.2011

The Ph.D. Viva-Voice Examination of Ms. Nidhi Goel, Research Scholar, has been held on ...17...10...2011.


Signature of Supervisors


Signature of External Examiner


SRE Chairman


HOD

ACKNOWLEDGEMENT

When you start something big, you never know where it is going to lead you, but if the intentions are good and determination intact, ways are made and destinations found. The journey may or may not be easy but one thing, which you definitely need, is the guidance and support of someone and that someone in my case is, Almighty, "The God".

I am indebted to my supervisor, Prof. Udai P. Singh, who exemplified to me the meaning of research with his distinct vision and meticulous guidance. At this day of my career, when I pause to look back to my research period I find that at every stage his perpetual encouragement, constructive criticism and above all morale boosting inspiration served a vital source to bring the present work to conclusion. Further his bold initiative and compromising gesture made a highly challenging path feasible.

I owe my sincere thanks to Prof. Ashok K. Singh, who generously gave his valuable time for detailed and constructive comments.

I am highly grateful to Prof. V. K. Gupta and Prof. Kamaluddin, the present and the former Heads of the Department of Chemistry, Indian Institute of Technology-Roorkee for providing me with the necessary facilities and support to carry out these investigations.

My sincere thanks to Prof. Gurdeep Singh and Prathibha Mam, DDU Gorakhpur University for useful discussions on explosion delay analysis.

The financial assistance provided by Council of Scientific and Industrial Research (CSIR), New Delhi that made my research work very smooth and prompt, is gratefully acknowledged.

With great pleasure I would like to thank my lab mates for their support and cooperation. I am also grateful to all the members of Chemistry Department for their cooperation and timely help which provided a good environment to develop my skills as a researcher.

I will always cherish my friendship with Dinesh, Manu, Rashmi and Sandeep who contributed directly or indirectly towards successful completion of this project in their own special way. Their help and co-operation are unforgettable.

"Family is the compass that guide us", Where would I be without my family? My parents deserve a special line of respect and sincere gratitude for their unending love,

inseparable support and prayers during my Ph.D. experience. These pages wouldn't be sufficient to mention the enormous efforts made by my parents to educate me and to take care of my entire requirements.

I am in dearth of proper words to express my abounding feelings to my sister, sweetie and niece chotu for their encouragement and the love they showed on me at every stage.

At the end, I am extremely grateful to those people, whose names have been unknowingly left, thank you very much for your prayers. It had really helped a lot. I apologize and believe that they will be always with me as they were during the times of need.

Nidhi Goel

ABSTRACT

Lanthanides are termed rare-earth elements; they are not rare in nature because their levels in the earth's crust are often equal to or higher than those of some physiologically significant elements. Although the members are very similar from a chemical point of view due to the shielding of 4f valence electrons by the completely filled $5s^2$ and $5p^6$ orbital but each of them has its own very specific physical properties including color, luminescent behavior and nuclear magnetic properties. Studies based on lanthanide ions are of special challenge due to their specific electronic, magnetic or spectroscopic properties result from a precise description of coordination sphere around the metal ions. Coordination compounds of lanthanides have found a variety of application in material science including contrast agents, superconductors, magnetic materials, catalyst and anticancer agents. Due to these attractive features, the coordination and supramolecular chemistry of lanthanide complexes have attracted much attention.

For the sake of convenience, the work embodied in the thesis is presented in the following chapter:

The **first** chapter of the thesis is the general introduction and presents an up to date survey of literature related to the various lanthanide complexes, organic compounds (salts), their photophysical properties and thermal analysis respectively. The different types of complexes and salts related to the present research have been posed in the context of the cited work.

Some pH dependent europium (III) and gadolinium (III) complexes viz., $[\text{Eu}(\text{phen})_2\text{Cl}_3\text{CH}_3\text{OH}]$, $[\text{Eu}(2,6\text{-DNP})_3\text{phenCH}_3\text{OH}]$, $[\text{Eu}(2,6\text{-DNP})_3\text{phen}(\text{OH})].\text{Hphen}$, $[\text{Eu}(2,6\text{-DNP})_3\text{bipyOH}_2]$, $[\text{Eu}(2,6\text{-DNP})_3\text{bipy}(\text{OH})].\text{Hbipy}$, $[\text{Gd}(\text{phen})_2(\text{NO}_3)_2]$, $[\text{Gd}(2,6\text{-DNP})_3\text{phenCH}_3\text{OH}]$, $[\text{Gd}(2,6\text{-DNP})_3\text{phen}(\text{OH})_2].(\text{Hphen})_2$, $[\text{Gd}(2,6\text{-DNP})_3\text{bipyOH}_2]$, $[\text{Gd}(\text{DNP})_3\text{bipy}(\text{OH})].\text{Hbipy}$ having 2,6-dinitrophenol (2,6-DNP), 1,10-phenanthroline (phen) and 2,2'-bipyridine (bipy) ligands have been synthesized and characterized by different physico-chemical methods including single crystal X-ray crystallography are presented in chapter **two**. Their thermal properties have been studied by thermogravimetric analysis (TG) and demonstrated that the final product after decomposition was stable oxide (Eu_2O_3 and Gd_2O_3) for all these complexes. The thermal stability of these complexes decreases in the order:

$[M(2,6\text{-DNP})_3\text{phen}(\text{OH})].\text{Hphen} > [M(2,6\text{-DNP})_3\text{bipy}(\text{OH})].\text{Hbipy} > [M(2,6\text{-DNP})_3\text{phen}(\text{CH}_3\text{OH})] > [M(2,6\text{-DNP})_3\text{bipyOH}_2] > [\text{Eu}(\text{phen})_2\text{Cl}_3\text{CH}_3\text{OH}] / [\text{Gd}(\text{phen})_2(\text{NO}_3)_3]$, (M = Eu, Gd). Isothermal thermogravimetric study in the range of 410-450 °C and 270-310 °C has been performed for Eu(III) and Gd(III) complexes respectively, while the kinetics of thermal decomposition was evaluated by applying model fitting as well as an isoconversional methods. To investigate the response of these complexes under the condition of rapid heating, ignition delay (D_i) has been measured.

The **third** chapter of the thesis deals with the syntheses of some lanthanide [Ln(III) = Gd(III), Eu(III), Tb(III)] complexes viz., $[\text{Gd}(\text{tptz})\text{Cl}_2(\text{OH}_2)_4].\text{Cl}.4\text{H}_2\text{O}$, $[\text{Gd}(\text{tptz})(\text{SCN})_3(\text{CH}_3\text{OH})_2\text{OH}_2].\text{CH}_3\text{OH}$, $[\text{Gd}(\text{tptz})(\text{OBz})_2(\mu\text{-OBz})\text{OH}_2]_2.\text{H}_2\text{O}$, $[\text{Gd}(\text{phen})\text{Cl}_2(\text{OH}_2)_4].\text{Cl}.\text{CH}_3\text{OH}$, $[\text{Gd}(\text{phen})_2(\text{SCN})_3\text{CH}_3\text{OH}].\text{phen}$, $[\text{OH}_2(\text{phen})(2\text{-pyca})_2\text{Gd}_1(\mu\text{-ox})\text{Gd}_2(2\text{-pyca})_2(\text{phen})\text{OH}_2].6\text{H}_2\text{O}$, $[\text{Eu}(\text{tptz})\text{Cl}_3(\text{CH}_3\text{OH})_2].\text{CH}_3\text{OH}$, $[\text{Eu}(\text{tptz})(\text{SCN})_3(\text{CH}_3\text{OH})_2\text{OH}_2].\text{CH}_3\text{OH}$, $[\text{OH}_2(\text{OBz})_2(\text{tptz})\text{Eu}_1(\mu\text{-OBz})_2\text{Eu}_2(\text{tptz})(\text{OBz})_2\text{OH}_2].\text{CH}_3\text{OH}.7\text{H}_2\text{O}$, $[\text{Eu}(\text{phen})_2(\text{SCN})_3\text{CH}_3\text{-OH}].\text{phen}$, $[\text{OH}_2(\text{phen})(2\text{-pyca})_2\text{Eu}_1(\mu\text{-ox})\text{Eu}_2(2\text{-pyca})_2(\text{phen})\text{OH}_2].6\text{H}_2\text{O}$, $[\text{Tb}(\text{tptz})\text{Cl}_3(\text{CH}_3\text{-OH})_2].\text{CH}_3\text{OH}$, $[\text{Tb}(\text{tptz})(\text{SCN})_3(\text{CH}_3\text{OH})_2\text{OH}_2].\text{CH}_3\text{OH}$, $\{[\text{Tb}_1(\text{tptz})(\text{OBz})_2(\mu\text{-OBz})]_2.[\text{Tb}_2(\text{tptz})(\text{OBz})_3\text{CH}_3\text{OH}]\}.\text{CH}_3\text{OH}.2\text{H}_2\text{O}$, $[\text{Tb}(\text{phen})_2\text{Cl}_3\text{OH}_2].\text{CH}_3\text{OH}$, $[\text{Tb}(\text{phen})_2(\text{SCN})_3\text{CH}_3\text{-OH}].\text{phen}$, $[\text{OH}_2(\text{phen})(2\text{-pyca})_2\text{Tb}_1(\mu\text{-ox})\text{Tb}_2(2\text{-pyca})_2(\text{phen})\text{OH}_2].6\text{H}_2\text{O}$ where 2,4,6-tris(2-pyridyl)-1,3,5-triazine, 1,10-phenanthroline, KSCN, sodium benzoate (NaOBz), 2-pyrazine carboxylic acid (2-pyca) act as supporting ligands. These complexes have been characterized by different methods including IR and single crystal X-ray crystallography. These complexes were tested for photophysical and thermal behavior. The complexes $[\text{Gd}(\text{tptz})(\text{SCN})_3(\text{CH}_3\text{OH})_2\text{OH}_2].\text{CH}_3\text{OH}$, $[\text{Eu}(\text{tptz})(\text{SCN})_3(\text{CH}_3\text{OH})_2\text{OH}_2].\text{CH}_3\text{OH}$, $[\text{Tb}(\text{tptz})(\text{SCN})_3(\text{CH}_3\text{OH})_2\text{OH}_2].\text{CH}_3\text{OH}$ are mononuclear and show the three dimensional pseudo host-guest like supramolecular structure along 'c' axis. The same reaction in presence of sodium benzoate gave binuclear bridged complexes $[\text{Gd}(\text{tptz})(\text{OBz})_2(\mu\text{-OBz})\text{OH}_2]_2.\text{H}_2\text{O}$, $[\text{OH}_2(\text{OBz})_2(\text{tptz})\text{Eu}_1(\mu\text{-OBz})_2\text{Eu}_2(\text{tptz})(\text{OBz})_2\text{OH}_2].\text{CH}_3\text{OH}.7\text{H}_2\text{O}$, $\{[\text{Tb}_1(\text{tptz})(\text{OBz})_2(\mu\text{-OBz})]_2.[\text{Tb}_2(\text{tptz})(\text{OBz})_3\text{CH}_3\text{OH}]\}.\text{CH}_3\text{OH}.2\text{H}_2\text{O}$. The photophysical properties of these complexes have been studied with ultraviolet absorption, excitation and emission spectral studies. Thermogravimetric analysis showed that after complete decomposition, all complexes resulted in the formation of thermally stable lanthanide oxide (Ln_2O_3).

The chapter **four** of the thesis deals with the preparation of salts having picric acid $[(\text{OH})(\text{NO}_2)_3\text{C}_6\text{H}_2]$ (PA) and nitrogen-rich heterocycles like different ditopic pyrazoles [PzH,

$\text{Pz}^{\text{Me}_2\text{H}}$, $\text{Pz}^{\text{Ph,MeH}}$, H_2dmpz], 1,10-phenanthroline (phen), 2,2';6',2''-terpyridine (terpy), hexamethylenetetramine (hmta), 2,4,6-tris(2-pyridyl)-1,3,5-triazine (tptz), urea, 1H-1,2,4-triazole-3,5-diamine (guanazole), cyclohexane-1,2-diamine (1,2-DACH), 6-phenyl-1,3,5-triazine-2,4-diamine (benzoguanamine). The reaction of picric acid with other components resulted in the formation of various types of salts as $[\text{2PA}^-\text{.2PzH}_2^+\text{.OH}_2]$, $[\text{PA}^-\text{.Pz}^{\text{Me}_2\text{H}_2^+}]$, $[\text{PA}^-\text{.Pz}^{\text{Ph,MeH}_2^+}\text{.CH}_3\text{OH}]$, $[\text{2PA}^-\text{.2H}_2\text{dmpzH}^+\text{.CH}_3\text{CN}]$ $[\text{PA}^-\text{.phenH}^+\text{.CH}_3\text{OH}]$, $[\text{2PA}^-\text{.terpyH}_2^{+2}]$, $[\text{PA}^-\text{.hmta}]$, $[\text{3PA}^-\text{.tptzH}_3^{+3}]$, $[\text{PA}^-\text{.Uronium}]$, $[\text{PA}^-\text{.3,5-diamino-1,2,4-triazolium}]$, $[\text{PA}^-\text{.1/2cyclohexane-1,2-diaminium}]$, $[\text{PA}^-\text{.6-phenyl-2,4-diamino-1,3,5-triazinium}]$. Due to presence of nitrogen-rich heterocycles, each salt contains infinite two or three dimensional structures held together by primary $\text{N-H}\cdots\text{O}$, $\text{O-H}\cdots\text{N}$, $\text{O-H}\cdots\text{O}$ hydrogen bonds and secondary $\text{C-H}\cdots\text{O}$ interactions. The structures and harmonic vibration frequencies of the complexes were calculated in terms of the density functional theory. The orientation of molecule remains same in both the solid and the gaseous phase. Theoretical studies suggested that the structures remain the same in both solid and gaseous phase, and the hydrogen bond interaction energy largely depends on the nitrogen-rich heterocycles in different salts. The thermal decomposition of these salts has been studied by thermogravimetry (TGA), derivative thermogravimetric (DTG) and differential thermal analysis (DTA). Kinetic parameters have been evaluated using models fitting and isoconversional methods.

The material reagents, synthetic procedures, experimental details, theoretical calculation, ignition delay measurement, thermal kinetic analysis and different type of spectroscopic measurements are described in chapter **five** of the thesis. Methods for the preparation of different type complexes with Ln(III) and also synthesis of organic salt have been reported.

LIST OF PUBLICATIONS

1. Udai P. Singh, **Nidhi Goel**, Gurdip Singh, Pratibha Srivastava “pH-Dependent host-guest complexes of europium (III) and gadolinium (III): Syntheses, structural and thermal studies” *Inorganica Chimica Acta*, (*Under review*)
2. **Nidhi Goel**, Udai P. Singh, A. K. Singh, Gurdip Singh, Pratibha Srivastava “Thermolysis of supramolecular synthons of picric acid-substituted pyrazoles: Syntheses, structural and computational study” *Combustion and Flame*, (*Communicated*)
3. Gurdip Singh, Inder Pal Singh Kapoor, Dinesh Kumar, Udai P. Singh, **Nidhi Goel** “Preparation, X-ray crystallography and thermal decomposition of transition metal perchlorate complexes with perchlorate and 2,2'-bipyridyl ligands” *Inorganica Chimica Acta*, **362**, 4091 (2009).
4. Sudesh T. Manjare, Ray j. Butcher, **Nidhi Goel**, Udai P. Singh, Harkesh B. Singh “1-(2-Bromobenzyl)-3-isopropylbenzimidazol-2-one” *Acta Crystallographica, Section E*, **E65**, o2836 (2009).
5. Inder Pal Singh Kapoor, Manisha Kapoor, Gurdip Singh, Udai P. Singh, **Nidhi Goel** “Preparation, characterization and thermolysis of nitrate and perchlorate salts of 2,4,6-trimethylaniline” *Journal of Hazardous Materials*, **173**, 173 (2010).
6. Kaushik Ghosh, Nidhi Tyagi, Pramod Kumar, Udai P. Singh, **Nidhi Goel** “Stabilization of Mn(II) and Mn(III) in mononuclear complexes derived from tridentate ligands with N₂O donors: Synthesis, crystal structure, superoxide dismutase activity and DNA interaction studies” *Journal of Inorganic Biochemistry*, **104**, 9 (2010).
7. Kaushik Ghosh, Sushil Kumar, Rajan Kumar, Udai P. Singh, **Nidhi Goel** “Oxidative cyclization of phenolic schiff base and synthesis of cyclometallated ruthenium nitrosyl complex: Photoinduced NO release by visible light” *Inorganic Chemistry*, **49**, 7235 (2010).
8. Kaushik Ghosh, Sushil Kumar, Rajan Kumar, Udai P. Singh, **Nidhi Goel** “Photocleavage of coordinated NO under visible light from two different classes of organometallic ruthenium nitrosyl complexes: Reversible binding of phenolato function” *Organometallics*, **30**, 2498 (2011).
9. Kaushik Ghosh, Pramod Kumar, Nidhi Tyagi, Udai P. Singh, **Nidhi Goel** “Synthesis, structural characterization and DNA interaction studies on a novel copper complex: Nuclease activity via self-activation” *Inorganic Chemistry Communications*, **14**, 489 (2011).

10. K. Selvakumar, Harkesh B. Singh, **Nidhi Goel**, Udai P. Singh “Methyl ester eunction: An intramolecular electrophilic trap for the isolation of aryltellurenyl hydroxide and diorganotellurium dihydroxide” *Organometallics*, xxx, 000 (2011).
11. Dinesh Kumar, Inder Pal Singh Kapoor and Gurdip Singh, Udai P. Singh, **Nidhi Goel** “Preparation, X-ray crystallography and thermolysis of transition metal nitrates of 2, 2'-bipyridine” *Journal of Thermal Analysis and Calorimetry*, (2011) (*Accepted*).
12. Inder Pal Singh Kapoor, Manisha Kapoor, Gurdip Singh, Udai P. Singh, **Nidhi Goel** “Preparation, characterization and thermolysis of nitrate salts of aminopyridine” *Combustion and Flame*, (2011) (*Accepted*)

CONFERENCES / SYMPOSIUM / WORKSHOPS

1. Participated in “9th CRSI, National Symposium in Chemistry (NSC-9), University of Delhi, India, 1st-4th Feb., (2007).
2. Participated in 2nd CRSI-RSC Symposium on the Chemical Sciences, Indian Institute of Science, Bangalore, India, (2008).
3. **Nidhi Goel**, Udai P. Singh, A. K. Singh “Syntheses, structural, photophysical and thermal properties of some gadolinium (III) & europium (III) complexes”, 10th CRSI National Symposium in Chemistry (NSC-10), Indian Institute of Science, Bangalore, India, P-165 (2008) (Poster Presentation).
4. **Nidhi Goel**, Udai P. Singh “Synthesis, Structural and Explosive Studies of some Europium (III) Complexes” First National Symposium & Exhibition on Trends in Explosive Technology, Terminal Ballistics Research Laboratory Sector-30 Chandigarh, India, (2008) (Poster Presentation).
5. **Nidhi Goel**, Udai P. Singh “Supramolecular synthesis of binary co-crystals”, Symposium on Modern Trends in Inorganic Chemistry MTIC – XIII, Indian Institute of Science, Bangalore, India, P-103 (2009) (Poster Presentation).
6. **Nidhi Goel**, Udai P. Singh, A. K. Singh “Thermolysis of supramolecular synthons of picric acid-substituted pyrazoles: Syntheses, structural and computational study”, 13th CRSI National Symposium in Chemistry (NSC-13), KIIT, University, Bhubaneswar, India, P-129 (2011) (Poster Presentation).
7. Participated in “4th Conference on recent trends in instrumental methods of analysis, Department of Chemistry, Indian Institute of Technology Roorkee, India, 18-20th Feb., (2011).
8. Participated in two days National Workshop on “Techniques and challenges for structure solution in chemical crystallography”, sponsored by Bruker-AXS, Germany. Indian Institute of Technology Roorkee, India, August 31st-01st Sep., (2007).
9. Participated in two days International Workshop on “Chemical evolution and origin of life”, Indian Institute of Technology Roorkee, India, 05-07th March (2010).

CONTENTS

	Page No.
CANDIDATE'S DECLARATION	
ACKNOWLEDGEMENT	i
ABSTRACT	iii
LIST OF PUBLICATIONS	vii
CHAPTER-1: GENERAL INTRODUCTION	1
CHAPTER-2: pH-DEPENDENT HOST-GUEST COMPLEXES OF EUROPIUM (III) AND GADOLINIUM (III): SYNTHESSES, STRUCTURAL AND THERMAL STUDIES	27
CHAPTER-3: SYNTHESSES, STRUCTURAL, PHOTOPHYSICAL AND THERMAL STUDIES OF SOME LANTHANIDE (III) COMPLEXES	99
CHAPTER-4: SYNTHESSES, STRUCTURAL, COMPUTATIONAL AND THERMAL STUDIES OF SALTS WITH PICRIC ACID AS ONE COMPONENT	187
CHAPTER-5: EXPERIMENTAL	301

CHAPTER-1

General Introduction

Lanthanides are f-block elements with atomic number from 57 to 71. In nature, they never exist as pure elements, but only as sparsely distributed minerals. Although lanthanides are termed rare-earth elements; they are not rare in nature because their levels in the earth's crust are often equal to or higher than those of some physiologically significant elements. The lanthanide series is characterized by a gradual filling of the 4f shell. Since, in most cases, the 4f electrons are chemically inert and atomic like, all lanthanides behave in a very similar manner and basic properties such as the atomic volume, bulk modulus and melting temperature vary in a more or less regular manner across the series [1]. Their unique chemical similarity is due to the shielding of 4f valence electrons by the completely filled $5s^2$ and $5p^6$ orbitals. Although the members are very similar from a chemical point of view, each of them has its own very specific physical properties including color, luminescent behavior and nuclear magnetic properties. The ionic radii of lanthanides range from 0.1034 nm (Ce) to 0.0848 nm (Lu), the values being relatively higher than those in other elements with the same oxidation number. Despite the high charge, the large size of the Ln(III) ions results in low charge density and their compounds are predominately ionic in character. The lanthanide (III) ions are typical 'A' type cations in the Ahrlansd-Chat-Davies sense or hard acid in the Pearson sense, so they tend to bound to ligands containing pure oxygen donors (e.g. oxalate ion, β -diketonate ions), mixed oxygen-nitrogen donors (e.g. polyamine-polycarboxylate ions) and nitrogen donors (e.g. 1,10-phenanthroline, bipyridine, terpyridine). The past several years have witnessed the rapid growth of interest in the lanthanides and their coordination chemistry. Studies based on lanthanide ions are of special challenge due to their specific electronic, magnetic or spectroscopic properties result from a precise description of coordination sphere around the metal ions. Coordination compounds of lanthanides have found a variety of application in material science including contrast agents, superconductors, magnetic materials, catalyst and anticancer agents [2-5]. Restricting our discussion on the luminescent and thermal properties of lanthanide complexes, the following recent literatures have been cited.

LUMINESCENT PROPERTIES

The emission from lanthanide ions has been utilized extensively in biological systems. The applications range from luminescent labels of biologically relevant molecules and detection of cellular functions *in vivo* to the elucidation of structures and function of enzymes and proteins. The emission from lanthanides has proven useful as a sensitive detection method in biological systems. The valance 4f electrons of trivalent lanthanide ions are well shielded

from the environment by the outer core 5s and 5p electrons and are minimally involved in bonding. The ligand field splitting for Ln(III) complexes is very small, so radiation less decay processes are relatively inefficient, and emission from these complexes is common. The absorption and emission spectra of Ln(III) complexes consist of sharp and narrow bands corresponding to *f-f* transitions of the metal ion. Direct excitation with UV radiation into the Ln(III) *f-f* transitions leads to weak emission, because of the poor ability of ions to absorb light. The photoluminescent intensities of lanthanide complexes are strongly dependent on their organic composition [6-8]. Organic ligands do a better job at absorbing light where ligand excitation is followed by the intramolecular energy transfer from the ligand triplet state to lower lying emissive lanthanide excited state. The organic chromophore acts like some sort of antenna. The most commonly used antenna moieties are based upon pyridine, bipyridine, terpyridine, phenanthroline, 2,4,6-tris(2-pyridyl)-1,3,5-triazine and various derivatives of pyrazole.

Zhang et al. [9] synthesized six new homodinuclear lanthanide (III) complexes with a flexible tripodal carboxylate ligand [$H_3L = 3,3'-(2-((3\text{-carboxynaphthalen-2-yl}oxy)methyl)-2-(4\text{-methylphenylsulfonamido})propane-1,3\text{-diyl})bis(oxy)di-2\text{-naphthoic acid}$], of formulae $[Ln_2L_2(DMF)_4] \cdot 4DMF$ ($Ln = La, Nd, Eu, Gd, Tb, Dy$, $DMF = N, N\text{-Dimethylformamide}$). The crystal structures revealed that these complexes are isostructural, and molecules are connected from 0D to 3D supramolecular structures by hydrogen bonds. They also investigated the photophysical property of the Eu(III) complex and the magnetic property of Gd(III) complex. Ramya et al. [10] synthesized three new binuclear lanthanide complexes of general formula $[Ln_2(L)_6(H_2O)_4]$ [$Ln = Tb$ (**1**), Eu (**2**) and Gd (**3**)] supported by the novel aromatic carboxylate ligand 4-(dibenzylamino)benzoic acid (HL). Complex **1** exhibited high green luminescence efficiency in the solid state with a quantum yield of 82%. On the other hand, poor luminescence efficiency has been noted for the Eu^{3+} -4-(dibenzylamino)benzoate complex. Choi et al. [11] reported the lanthanide-based metal-organic frameworks (Ln-MOFs) and investigated the photoinduced electron transfer between the excited Eu-MOF nanoparticles and various organic compounds, such as aromatic sulfides and amines. From the time resolved emission measurements, the bimolecular quenching rate constants of luminescence from the Eu^{3+} ions in the MOF framework by electron donors were determined and explained in terms of the Marcus theory of electron-transfer reactions. Furthermore, spatially resolved emission quenching images obtained by confocal fluorescence microscopy revealed that small (large)

emission, excitation of emission spectra and lifetimes of both europium (III) complexes in solid state as well as in methanol solution at 77 and 300 K. On the basis of optical studies, they proved efficient sensitized luminescence and proposed the probable energy transfer mechanism. Liu et al. [16] synthesized a series of complexes of poly(N,N-diethylacrylamide-co-methacrylicacid) (PDEA-co-MAA) with Ln(III) (Ln = La, Eu, Tb). They also studied the luminescence spectra of Eu(III) and Tb(III) complexes in solid state. The complexes exhibited strong characteristic luminescence of Eu(III) and Tb(III) ions, while the luminescence intensity depends on the content of DEA and Ln(III) ions. Shyni et al. [17] synthesized three new homodinuclear lanthanide (III) complexes of xanthene-9-carboxylic acid, $[\text{Ln}_2(\text{XA})_6(\text{DMSO})_2(\text{H}_2\text{O})_2]$ (Ln = Eu (**1**), Tb (**2**) and Gd (**3**); HXA = xanthene-9-carboxylic acid; DMSO = dimethylsulfoxide) (Fig. 1.2). They also investigated the photophysical properties of these complexes in the solid state at room temperature.

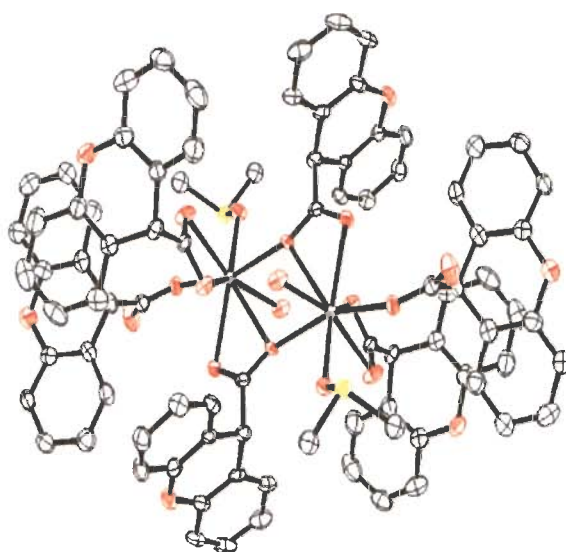


Fig. 1.2: Crystal structure of $\text{Eu}_2(\text{XA})_6(\text{DMSO})_2(\text{H}_2\text{O})_2$

Tanase et al. [18] synthesized the mononuclear complexes of formula $[\text{Ln}(\text{pcam})_3](\text{CF}_3\text{SO}_3)_3$ (Ln = Eu, Tb; pcam = pyridine-2,6-dicarboxamide) by the reactions of pyridine-2,6-dicarboxamide with Eu(III) and Tb(III) triflates. Both the Eu(III) and Tb(III) complexes exhibited efficient ligand sensitized luminescence in the visible region with lifetimes of 1.9 ms and 2.2 ms, respectively, in the solid state. Tang et al. [19] reported the synthesis of solid complexes of lanthanide isothiocyanates with an amide-type tripodal ligand, 2,2',2''-nitrilotris-(N-phenylmethyl)-acetamide. They also investigated the luminescent properties of the Sm(III),

Eu(III), Tb(III), Dy(III) isothiocyanate complexes in solid state and the Tb(III) complex in solvents. Jang et al. [20] synthesized two dinuclear Eu(III) complexes by employing β -diketones and 2,2'-bipyrimidine (bpm) as sensitizing ligands for the Eu^{+3} ion and a bridging ligand, respectively. The use of dibenzoylmethane (dbm) and trifluorothenoylacetone (tta) as β -diketones gave $[\text{Eu}_2(\text{dbm})_6(\text{bpm})]$ (**1**) and $[\text{Eu}_2(\text{tta})_6(\text{bpm})]$ (**2**). The analysis of the absorption, excitation and emission spectra of the dinuclear complexes along with a comparison with analogous mononuclear complexes containing the same β -diketone ligands and 1,10-phenanthroline (phen) suggested that the dinuclear complexes followed the luminescence mechanism of general Ln(III) complexes. Soares-Santos et al. [21] prepared samarium (III) complexes of Hpic, HpicOH and H_2nicO and determined the crystal structures of $\text{K}_2[\text{Sm}_2(\text{pic})_6(\mu\text{-pic})_2] \cdot 7.5\text{H}_2\text{O}$, $[\text{Sm}(\text{picOH})_2(\mu\text{-HpicO})(\text{H}_2\text{O})] \cdot 3\text{H}_2\text{O}$ and $[\text{Sm}(\text{HnicO})_2(\mu\text{-HnicO})(\text{H}_2\text{O})] \cdot 5\text{H}_2\text{O}$ complexes by single crystal X-ray diffraction studies. The X-ray crystal structures showed one-dimensional polymeric chains for all complexes presenting N, O- or O, O- chelation for the ligands (Fig. 1.3).

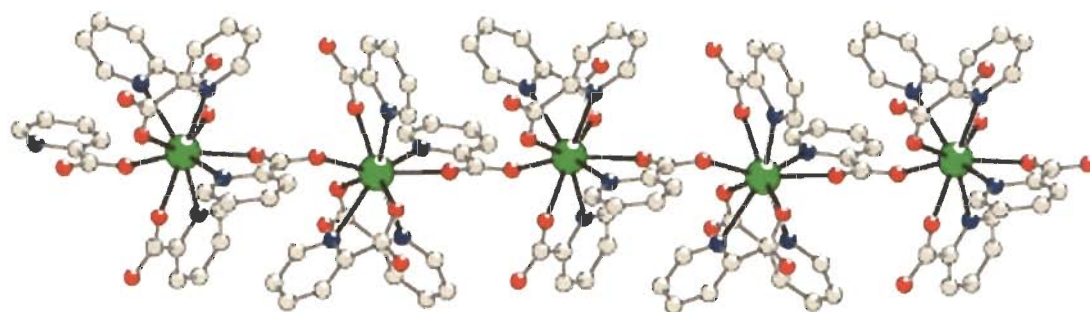


Fig. 1.3: Perspective views of one dimensional $[\text{Sm}_2(\text{pic})_6(\mu\text{-pic})_2]_n^{2n-}$ coordination polymer. They also reported that all these complexes exhibited room temperature emission spectra on excitation at 325 nm. The emission spectra of the complexes were composed of a series of straight lines, assigned to the Sm(III) intra- $4f^5$ transitions, $^4G_{5/2} \rightarrow ^6H_{5/2, 7/2, 9/2, 11/2}$ and of a large broad band in the range of 380-680 nm for all the complexes, which may arise from the ligands excited states. Wang et al. [22] synthesized a novel 6-hydroxy chromone-3-carbaldehyde benzoyl hydrazone (L) ligand and its samarium (III) complex with the composition $[\text{SmL}_2(\text{NO}_3)_2]\text{NO}_3$. The molecular structure of this complex demonstrated that the samarium ion is ten coordinated (Fig.1.4) and showed characteristic line emission of $f-f$ transitions of metal ion when they are excited with UV light.

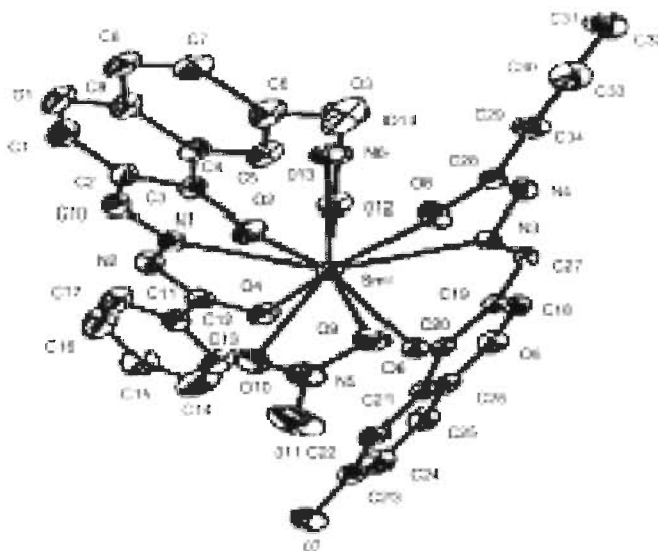


Fig. 1.4: Crystal structure of Sm(III) complex with hydrazone

Lenaerts et al. [23] reported that the luminescent Tb(III) complex covalently coupled to an organic–inorganic hybrid material by immobilization of $[\text{Tb}(\text{C}_5\text{H}_4\text{NCO}_2)_3(\text{phen})(\text{H}_2\text{O})_2]$ complex on the sol–gel glass matrix and showed a green photoluminescence upon irradiation with UV light. Oyang et al. [24] prepared different Tb(III) complexes like $[\text{TbL}_3(\text{DMSO})(\text{H}_2\text{O})_2]$, $[\text{TbL}_3(\text{DMF})(\text{H}_2\text{O})_2]$ and $[\text{TbL}_3(\text{bipy})(\text{H}_2\text{O})_2] \cdot 2\text{H}_2\text{O}$ (HL = amino benzoic acid) and reported their crystal structures. All these complexes were binuclear with two carboxyl groups, act bidentate bridges between two Tb(III) ions. They also calculated the fluorescence life time of the $^5\text{D}_4$ state energy and the emission quantum yield for all the complexes, and found that the complex $[\text{TbL}_3(\text{DMSO})(\text{H}_2\text{O})_2]$ showed the highest emission quantum yield (0.91) and the fluorescence life time (610 μs). Qu et al. [25] reported the hydrothermal synthesis of a coordination polymer with $[\text{Eu}_2(\text{BDC})_3(\text{H}_2\text{O})_2]_n$ composition (BDC = 1,3-benzenedicarboxylate). In the X-ray structure of this complex, all H_2BDC molecules were completely deprotonated and all the oxygen atoms from the carboxylic groups of BDC anions take part in coordination with the metal ions. The BDC anions adopted only one type of coordination mode: two bridging bidentates to coordinate with Eu(III) ions. They also investigated the luminescence properties of the above coordination polymer. Song et al. [26] used hydrothermal reaction for the synthesis of one novel samarium coordination polymer $[\text{Sm}(\text{Hdipic})(\text{dipic})(\text{H}_2\text{O})_2 \cdot 4\text{H}_2\text{O}]_n$ (Fig. 1.5). Single crystal X-ray studies revealed that one

bridged dipic anion connects two adjacent samarium ions and formed one dimensional chain. They have also reported their emission properties.

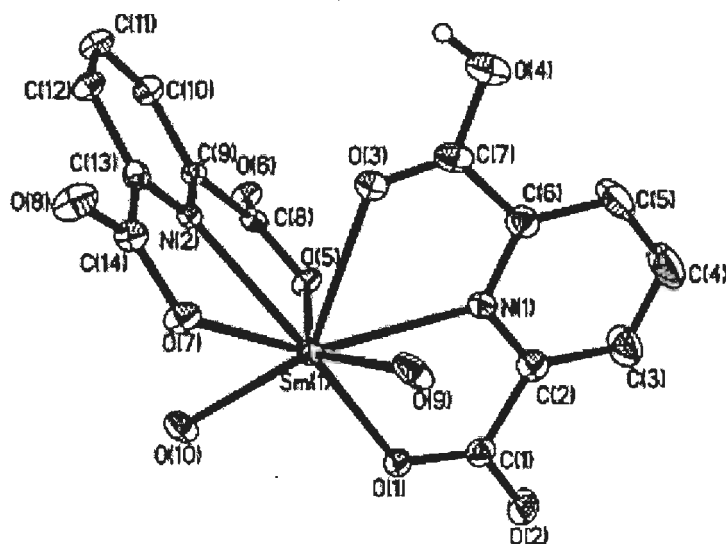


Fig. 1.5: Crystal structure of $[\text{Sm}(\text{Hdipic})(\text{dipic})(\text{H}_2\text{O})_{2.4}\text{H}_2\text{O}]_n$

Liu et al. [27] reported the preparation of a supramolecular europium coordination polymer with the composition $\{[\text{Eu}(\text{IA})_{1.5}(\text{phen})]\cdot\text{H}_2\text{O}\}_n$ (IA = itaconic acid) and structurally characterized by single crystal X-ray diffraction. In the crystal structure (Fig. 1.6), the IA ligands exhibited tetra and pentadentate coordination modes.

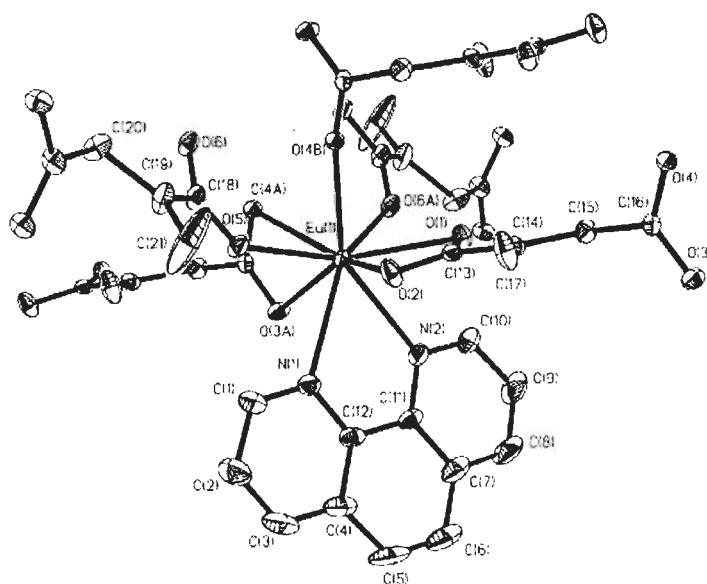


Fig. 1.6: Coordination environment of the Eu(III) ion in $\{[\text{Eu}(\text{IA})_{1.5}(\text{phen})]\cdot\text{H}_2\text{O}\}_n$

Zheng et al. [28] synthesized three isostructural 2-D square grid coordination polymers $[\text{Ln}_2(\text{NDC})_3(\text{phen})_2(\text{H}_2\text{O})_2]$ ($\text{Ln} = \text{La}$ (1), Eu (2), Ho (3), $\text{NDC} = 1,4\text{-naphthalenedicarboxylate}$, $\text{phen} = 1,10\text{-phenanthroline}$) by hydrothermal reactions of lanthanide chloride with 1,4-naphthalenedicarboxylic acid and phen. The asymmetric unit of 2 consists of $[\text{Eu}_2(\text{NDC})_3(\text{phen})_2(\text{H}_2\text{O})_2]$ as a building unit (Fig. 1.7). There are two independent $\text{Eu}(\text{III})$ ions where Eu1 and Eu2 are both eight coordinated with N_2O_6 donor set in a dodecahedral environment. They also investigated the photophysical and magnetic properties of these complexes.

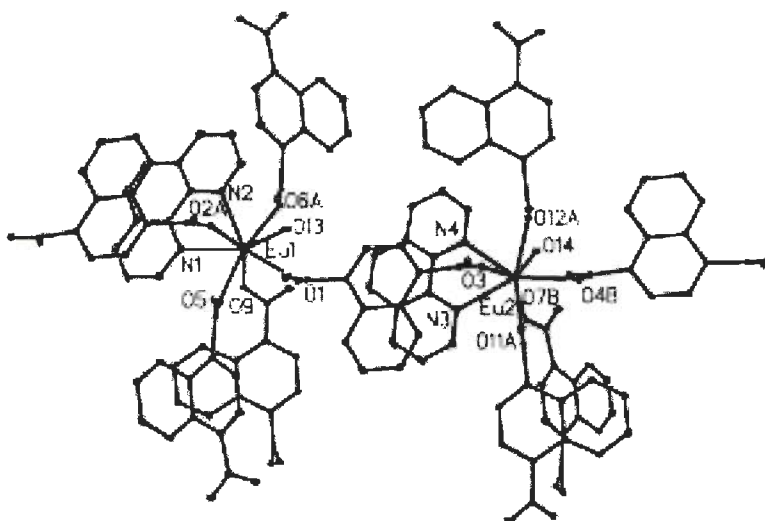


Fig. 1.7: Coordination environment of $[\text{Eu}_2(\text{NDC})_3(\text{phen})_2(\text{H}_2\text{O})_2]$

The two dimensional coordination polymers were assembled into three dimensional network via $\text{O-H}\cdots\text{O}$ hydrogen bonding between coordinated water molecules and uncoordinated carboxylate oxygen atoms of the 1,4 naphthalenedicarboxylate anions in the adjacent layer. The excitation spectra at 77 K of above compound were obtained by setting 16235 and 16204 cm^{-1} as the analyzing wave numbers. Scanning in the range of 578.0-581.0 nm revealed two sharp excitation peaks, which showed that there are two $\text{Eu}(\text{III})$ ion sites. Zhang et al. [29] reported the synthesis, structure and luminescent properties of a new terbium (III) β -diketimate complex of composition $[\{(2,6\text{-Me}_2\text{C}_6\text{H}_3)\text{NC}(\text{Me})_2\text{CH}\}\text{Tb-Cl}(\text{THF})(\mu\text{-Cl})_2\text{Li}(\text{THF})_2]$. Single crystal X-ray analysis revealed that this complex was binuclear (Fig.1.8). They suggested that due to an efficient energy transfer from the ligand to the central $\text{Tb}(\text{III})$, this complex showed a strong emission corresponding to $\text{Tb}(\text{III})$ $^5\text{D}_4 \rightarrow ^7\text{F}_j$ ($j = 6, 5, 4, 3$) transitions with $^5\text{D}_4 \rightarrow ^7\text{F}_5$ (550 nm) green emission as the most prominent group.

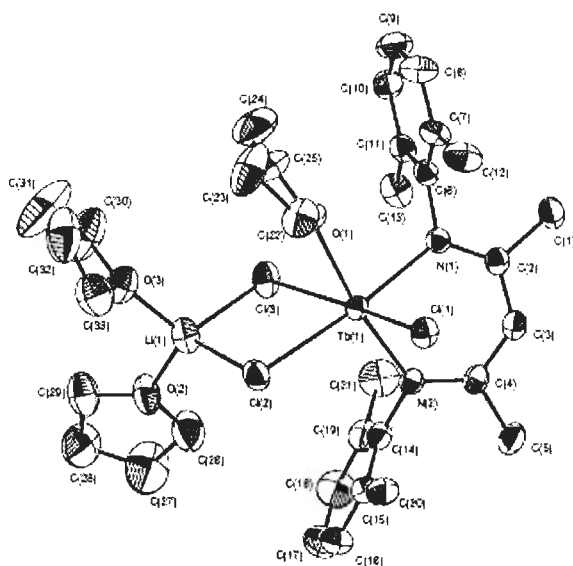


Fig. 1.8: Crystal structure of $[\{(2,6\text{-Me}_2\text{C}_6\text{H}_3)\text{NC}(\text{Me})\}_2\text{CH}]\text{TbCl}(\text{THF})(\mu\text{-Cl})_2\text{Li}(\text{THF})_2$

A binuclear terbium complex $[\text{Tb}_2(\text{Hsal})_8(\text{H}_2\text{O})_2][(\text{Hphen})_2] \cdot 2\text{H}_2\text{O}$ [$\text{Hsal} = o\text{-HOC}_6\text{H}_4\text{COO}^-$] was synthesized and characterized by elemental analysis, molar conductance, IR, UV-VIS, X-ray powder diffraction, thermogravimetric analysis and fluorescence [30]. The single crystal X-ray study showed the presence of hydrogen bonding, $\pi\text{-}\pi$ stacking interactions and electrostatic attractions in two-dimensional supramolecular structure of this compound. The solid state luminescence behavior of this complex was also studied. Barja et al. [31] reported the structures and properties of dimeric $[\text{Tb}_2(\text{CH}_3\text{COO})_6(\text{H}_2\text{O})_4] \cdot 4\text{H}_2\text{O}$, $[\text{Tb}_2(\text{CF}_3\text{COO})_6(\text{H}_2\text{O})_6]$ and of mononuclear $[\text{Tb}(\text{Hoda})_3] \cdot \text{H}_2\text{O} \cdot \text{H}_2\text{O}$ complexes. They also recorded the luminescence emission spectra of powder samples and of aqua solutions of all these complexes. Barja et al. also prepared a homometallic terbium (III) trans-2-butenoate polymer of composition $[\{\text{Tb}(\text{MeCH}=\text{CHCO}_2)_3(\text{H}_2\text{O})\} \cdot \text{MeCH}=\text{CHCO}_2\text{H}]_n$ and their dimeric 1,10-phenanthroline derivative $[\{\text{Tb}_2(\text{MeCH}=\text{CHCO}_2)_6 \cdot (\text{phen})_2 \cdot 2\text{H}_2\text{O}\}]_n$ and characterized by single crystal X-ray analysis [32]. As shown in X-ray structure, the Tb(III) coordination polymer crystallized in the centrosymmetric space group P-1 ($Z = 2$), as the polymeric chains were built up by TbO_9 units along 'c' axis. In crystal structure of dimeric 1,10-phenanthroline derivative of above complex, each Tb(III) ion was coordinated to three trans-2-butenoates and one phenanthroline with nine coordinated Tb(III) center in a monocapped square antiprism geometry. They also found that the luminescence excitation and emission spectra of microcrystalline powder samples of Tb(III) complexes were very similar and the metal centered transitions bands $^5\text{D}_4 \rightarrow ^7\text{F}_j$ ($j = 6, 5, 4$ and 3) were observed at 489, 544, 585 and 621

nm. Soares-Santos et al. [33] reported the synthesis and structural characterization of a new Tb(III) complex with 2,6-dihydroxybenzoic acid and its single crystal X-ray diffraction studies revealed that the complex crystallizes in the chiral and non-centrosymmetric $P2_1$ space group (Fig. 1.9).

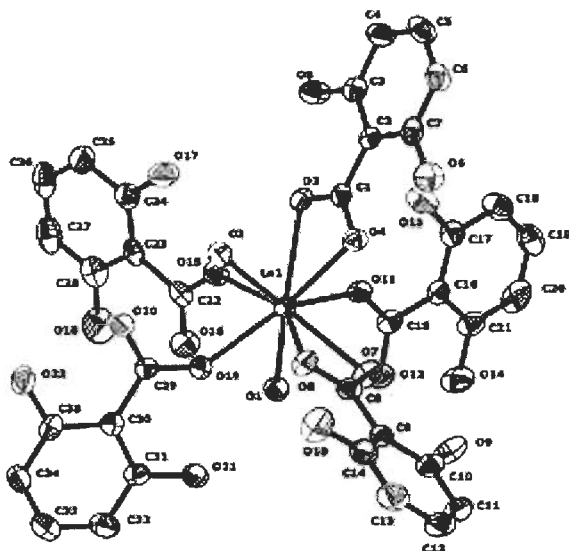


Fig. 1.9: Chiral complex anion, $[Tb(2,6-dhb)_5(H_2O)_2]^{2-}$

An interesting feature of the crystal was the medium-intensity hydrogen bond between the water molecule and the hydroxy group of the neighboring $[Ln(2,6-dhb)_5(H_2O)_2]^{2-}$ complex resulted in the formation of a hydrogen-bonded metal chain which runs along the ‘a’ direction of the unit cell (Fig. 1.10).

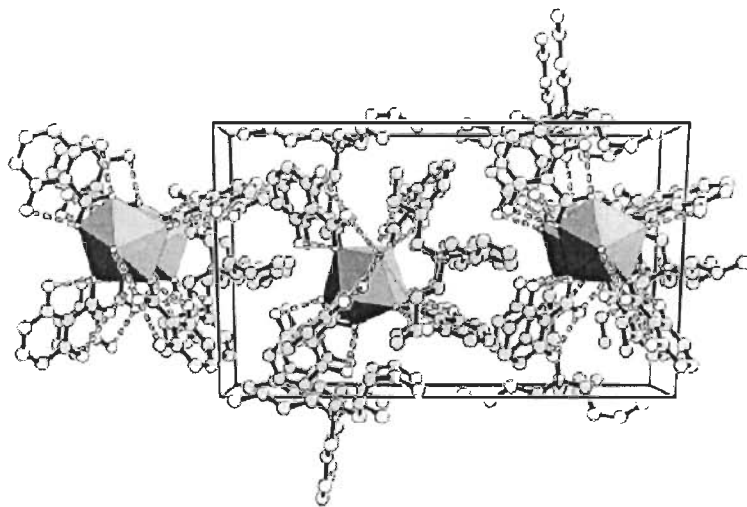


Fig. 1.10: Perspective along the ‘a’ axis of $[nBu_4N]_2[Tb(2,6-dhb)_5(H_2O)_2]$

They also described for the first time the luminescent properties of the Tb(III) complex with the 2,6-dihydroxybenzoate ligand. Wan et al. [34] synthesized some coordination polymers

like $[\text{Eu}(1,2\text{-BDC})(1,2\text{-HBDC})(\text{phen})(\text{H}_2\text{O})]_n$, $[\text{Eu}(1,3\text{-BDC})_3(\text{phen})_2(\text{H}_2\text{O})_2]_n \cdot 4n\text{H}_2\text{O}$ and $[\text{Eu}(1,4\text{-BDC})_{3/2}(\text{phen})(\text{H}_2\text{O})]_n$ by hydrothermal reactions of europium (III) chloride with three isomers of H_2BDC , phen and characterized by single crystal X-ray diffraction. Their crystal structure and packing views are given in Fig. 1.11-1.12.

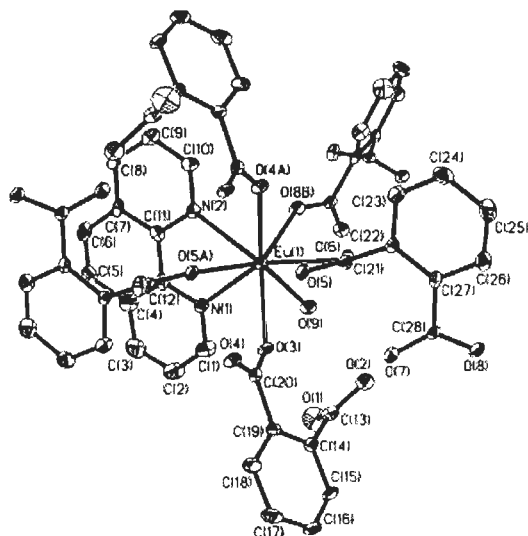


Fig. 1.11: Asymmetric unit of $[\text{Eu}(1,2\text{-BDC})(1,2\text{-HBDC})(\text{phen})(\text{H}_2\text{O})]_n$

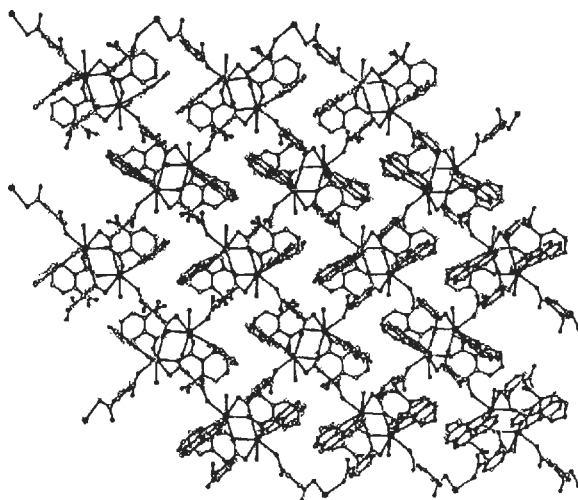


Fig. 1.12: Packing diagram of $[\text{Eu}(1,2\text{-BDC})(1,2\text{-HBDC})(\text{phen})(\text{H}_2\text{O})]_n$ along 'a' axis

Out of above three coordination polymers, $[\text{Eu}(1,2\text{-BDC})(1,2\text{-HBDC})(\text{phen})(\text{H}_2\text{O})]_n$ exhibited intense red fluorescence under UV light. Wang et al. [35] reported a binuclear europium complex $[\text{Eu}(\text{m-BrBA})_3(\text{H}_2\text{O})(\text{phen})]_2$ in the ethanol solution and characterized structurally by X-ray diffraction. In above complex, each $\text{Eu}(\text{III})$ ion is coordinated to one 1,10-phenanthroline molecule, one monodentate carboxylate group, one water molecule and four

bridging carboxylate. The excitation and luminescence spectra of the title complex measured at room temperature showed that the title complex emitted red fluorescence under UV light. The intensity of the luminescence band arising from $^5D_0 \rightarrow ^7F_2$ transition was most intense.

THERMAL PROPERTIES OF LANTHANIDE COMPLEXES

The lanthanide metal complexes with nitrophenols as high energetic materials have been the subject of fairly extensive investigation in thermal and combustion properties. On thermolysis, these complexes release the chemical energy available in them and produce gaseous decomposition product and solid residues. Harrowfield et al. [36] reported the single crystal room-temperature X-ray studies on hydrated specimens (deposited from aqueous solutions) of the sequence of trivalent lanthanoid picrates La \rightarrow Tb. They found that the latter form is frequently found partially desolvated toward the undecahydrate without loss of crystal integrity, as water is lost from tunnels in the lattice, with the actual hydrate stoichiometry dependent on the history of the specimen. In both sets of compounds, similar complex species $[Ln(pic)_2(OH_2)_6]^+$ are observed, with one picrate uncoordinated as counter ion and six lattice water molecules. The lanthanoid ion is > 8 -coordinated, one of the coordinated picrate moieties being quasibidentate, with an ortho-nitro group oxygen atom having a long contact to the metal atom in both series. Yun et al. [37] synthesized the Ln(III) complexes, $[Sm(pic)_2(H_2O)_6]Pic \cdot 6H_2O$ (**1**) and $[Ho(pic)(H_2O)_7](pic)_2 \cdot 3H_2O$ (**2**) using picrate ligand and their crystal structures were analyzed by X-ray diffraction methods (Fig. 1.13). Based on the results of the TG-DTG and DSC thermal analysis, it was analyzed that the lanthanide picrate complexes **1** and **2** are thermally decomposed in three distinctive stages, the dehydration, the picrate decomposition and the formation of the metal oxide.

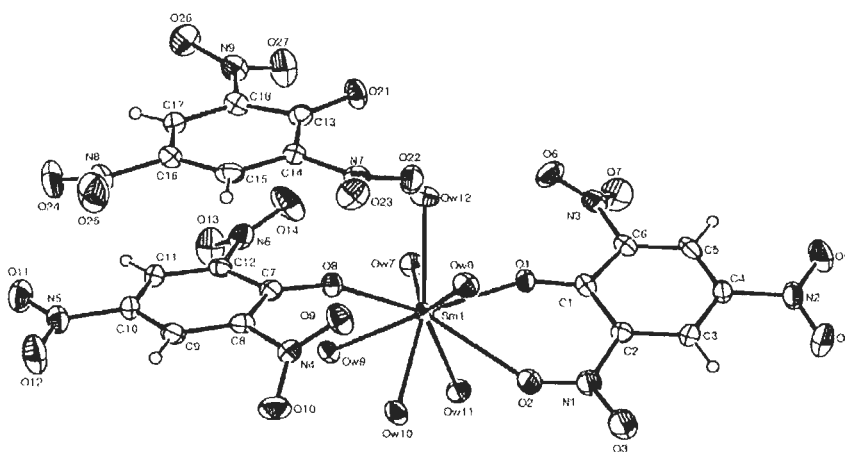


Fig. 1.13: Crystal structure of $[Sm(pic)_2(H_2O)_6]Pic \cdot 6H_2O$

Yun et al. [38] reported the title complexes $[M(\text{NTO})_2(\text{H}_2\text{O})_6]\cdot\text{NO}_3\cdot 2\text{H}_2\text{O}$ with NTO ligand ($M = \text{Gd}, \text{Ho}$) (Fig. 1.14). Based on the results of TG-DTG thermal analysis, the thermal decomposition reaction of complexes was analyzed to have three distinctive stages such as the dehydration of water, the cleavage of NTO ring, decomposition of NO_3 ion and the formation of metal oxide. The DSC curve appears to indicate that dehydration process is composed of three steps. The three dehydration stages occurred in the temperature range of 30–186 °C. The total mass loss for these three dehydration steps is 22.5% due to the mass loss of two crystalline and six coordinated water molecules.

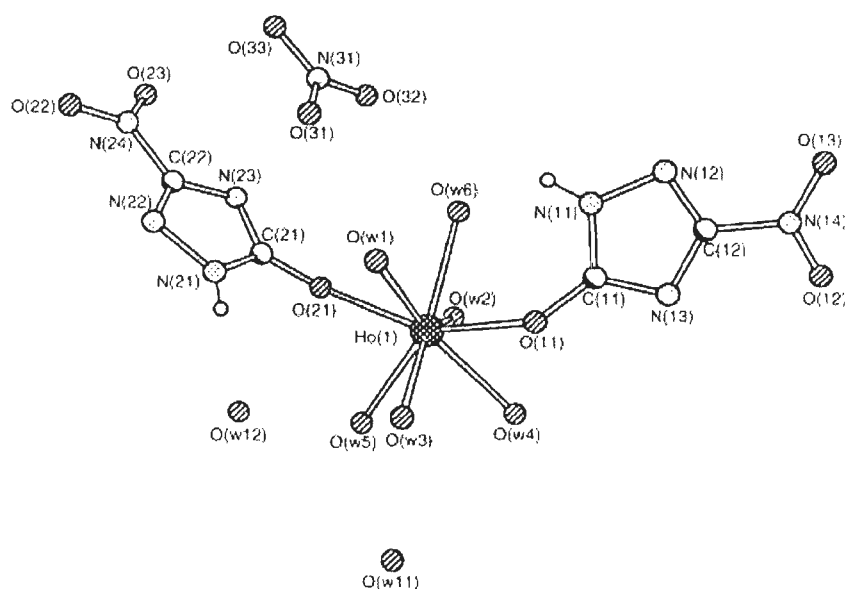


Fig. 1.14: Crystal structure of $[\text{Ho}(\text{NTO})_2(\text{H}_2\text{O})_6]\cdot\text{NO}_3\cdot 2\text{H}_2\text{O}$

Yan et al. [39] reported the thermal decomposition process and mechanism of lanthanide complexes with N-phenylanthranilic acid. On heating in air atmosphere, the TG-DTA curves of La^{3+} , Pr^{3+} , Nd^{3+} complexes showed three processes (two dehydrations and one decomposition), while the TG-DTA curves of Gd^{3+} , Eu^{3+} , Tb^{3+} , Sm^{3+} , Dy^{3+} complexes showed two processes (one dehydration and one decomposition), the final products are rare earth oxides. On heating in nitrogen atmosphere, the TG-DTA curves of all the complexes showed two processes, the final products are the mixtures of lanthanide oxides and carbon. Jr et al. [40] synthesized and characterized the hydrated lanthanide picrates with a composition of $\text{Ln}(\text{pic})_3\cdot x\text{H}_2\text{O}$ ($\text{Ln} = \text{La}, \text{Lu}, \text{Y}$). The results showed that the thermal decomposition of hydrated lanthanide picrates occurs in three similar groups, allowing the study of the thermal stability and the determination of the different number of hydration water molecules. These

compounds were explosives and their thermal decomposition occurs in highly exothermic events. Jr et al. [41] also reported the lanthanide picrates complexes with DTSO₂ (1,3-dithiane-1,3-dioxide) ligand (Fig. 1.15). Thermal decomposition of these compounds by TG-DTG and DSC were performed. It was found that the compounds are comprised in a single isomorphous series and their thermal decomposition occurs as exothermic events. The final products were found to be lanthanide dioxysulfates.

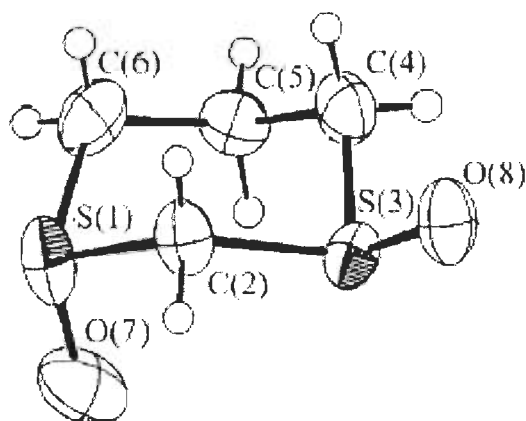


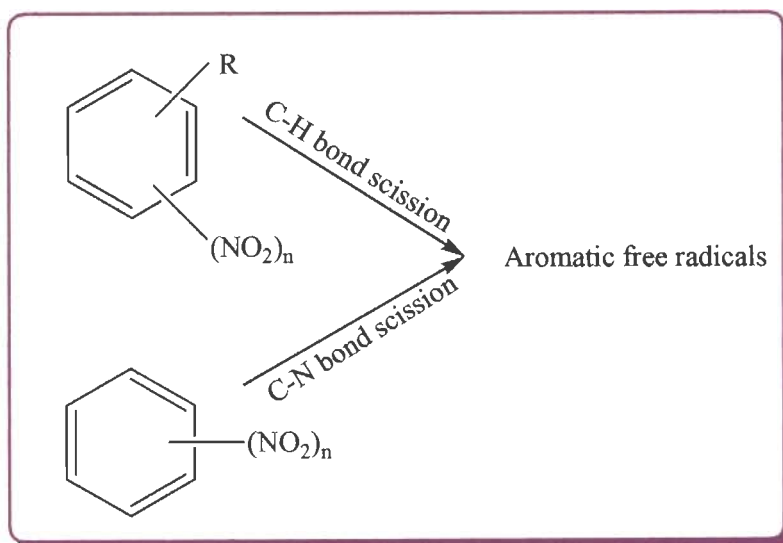
Fig. 1.15: Crystal structure of trans-DTSO₂

Nakagawa et al. [42] reported the lanthanoid (III) picrates (Ln = La, Ce, Pr, Nd, Sm, Eu, Gd, Dy and Yb) from picric acid. Combustion analysis, ICP emission analysis and UV spectrophotometry showed that the light lanthanoid picrate, i.e. Ln = La-Gd, are all undecahydrates, while the heavy ones, Dy and Yb, are octahydrates. An examination, by TG-DTA has revealed that these hydrates, being fairly stable in air at ambient temperature, are quite labile to give partially or completely dehydrated samples upon drying under vacuum, in a desiccator, and / or at elevated temperatures just above 30 °C. Boncher et al. [43] reported polycrystalline lanthanide sulfide materials, formed at low temperatures using a single-source precursor based on the lanthanide dithiocarbamate complex. Thermal decomposition of a single-source lanthanide dithiocarbamate precursor was successfully employed to obtain lanthanide chalcogenide materials. Brzyska and Ozga [44] studied the thermal decomposition in air of mephenamates of yttrium and lanthanides from La(III) to Lu(III). During heating, the hydrated complexes Ln(C₁₅H₁₄O₂N)₃.nH₂O (n = 3-14) lose water of crystallization in one (Y, La-Sm, Gd-Lu) or two steps (Eu), then anhydrous (Sm, Gd, Dy, Tm, Lu) or lower hydrated (Y, La-Nd, Eu, Tb, Ho, Er, Yb) complexes decompose directly to oxides or with intermediate formation of very unstable oxycarbonates (La, Nd). Sallama and Mahmoudb [45] investigated

the complex-formation of the lanthanide (III) cations with D-penicillamine methyl ester in acidic and neutral media. The macroscopic protonation constants of the ligand and the formation constants of $[\text{Ln.Pme}]_2^+$, $[\text{L}(\text{Pme})_2]^+$, $[\text{Ln.Pme.OH}]^+$ and $[\text{Ln.Pme}(\text{OH})_2]$ complexes have been determined from pH-metric data using BEST computer program. They also studied that the complexes decompose in four steps as shown by their TG and DTA analysis with the formation of $\text{Ln}_2(\text{SO}_4)_3$ as a final product. Christos et al. [46] reported the neutral complexes of the general formula $[\text{Ln}(3\text{-OCH}_3\text{-salO})_3]$, by the reaction of a lanthanide (III) nitrate ($\text{Ln} = \text{Pr, Nd, Gd, Dy, Er}$) with 3-methoxy-salicylaldehyde (3-OCH₃-salOH). They also analyzed the released products, due to the thermal decomposition by on-line coupling MS spectrometer to the thermobalance in argon, allowed to prove the proposed decomposition stages. In order to confirm the stability scale provided on the basis of the onset decomposition temperature, a kinetic analysis of the three decomposition stages was made using the Kissinger equation, while the complex nature of the decomposition kinetics was revealed by the isoconversional Ozawa—Flynn—Wall method. Tian et al. [47] synthesized two complexes of $[\text{Ln}(\text{CA})_3\text{bipy}]_2$ ($\text{Ln} = \text{Tb and Dy}$; $\text{CA} = \text{cinnamate}$; $\text{bipy} = 2,2'\text{-bipyridine}$) and characterized by elemental analysis, infrared spectra, ultraviolet spectra, thermogravimetry and differential thermogravimetry techniques. The thermal decomposition behavior of the two complexes under a static air atmosphere was discussed by thermogravimetry and differential thermogravimetry. The non-isothermal kinetics was investigated by using a double equal-double steps method, the non-linear integral isoconversional method and the Starink method. The mechanism functions of the first decomposition step of the two complexes were also determined. Ye et al. [48] synthesized a series of lanthanide complexes with the 4-ethylbenzoic acid ligand (4-eba), $[\text{Ln}(4\text{-eba})_3(\text{phen})]_2$ ($\text{Ln} = \text{Nd (1), Sm (2), Eu (3), Tb (4), Dy (5) and Ho (6)}$; $\text{phen} = 1,10\text{-phenanthroline}$). They also discussed the thermal analysis of the six complexes by TG-DTG techniques. The activation energy E values of the first decomposition stage for complexes 1–6 were calculated by integral isoconversional non-linear (NL-INT) and Ozawa iteration methods, respectively. Wang et al. [49] reported the Sm(III) complex with 1,10-phenanthroline (phen) and 5-chloro-2-methoxybenzoate (5-Cl-2-MOBA). The crystal and molecular structure of the complex, as well as its molecular formula and composition $[\text{Sm}(5\text{-Cl-2-MOBA})_3\text{phen}]_2$, were determined by single crystal X-ray diffraction, elementary analyses, infrared (IR) and thermogravimetric-differential thermogravimetric (TG-DTG) measurements. Yun et al. [50] reported the Tb(III) complex containing 2,4-

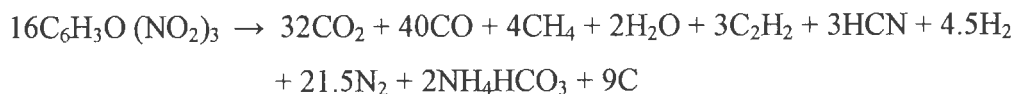
dinitrobenzoate (2,4-DNB), $\text{Tb}(\text{2,4-DNB})_3(\text{H}_2\text{O})_2 \cdot \text{C}_2\text{H}_5\text{OH}$. This complex crystallized in the triclinic space group P-1, where the eight-coordinated Tb ion with six carboxylate groups and two water molecules forms a slightly distorted square antiprism. They also studied the thermal properties of the terbium complex. Czyłkowska and Markiewicz [51] synthesized novel mixed-ligand complexes $\text{Dy}(\text{4-bipy})(\text{CCl}_2\text{HCOO})_3 \cdot \text{H}_2\text{O}$ and $\text{Ln}(\text{4-bipy})_{1.5}(\text{CCl}_3\text{COO})_3 \cdot 2\text{H}_2\text{O}$ (where $\text{Ln}(\text{III}) = \text{Ce}, \text{Nd}$). They also studied the thermal properties of complexes in the solid state under non-isothermal conditions in air atmosphere.

The research conducted on energetic materials during last years has also led to the discovery of various types of organic compounds and salts which can be used as a component in the propellants and explosives. Propellants are chemicals which are used to produce the thrust required to propel the rockets. These are the main source of chemical energy [52] for modern space launch vehicles such as rockets and missiles. Polynitro compounds, which have high energy parameters, are used as constituents of explosive compositions and solid-rocket propellants [53]. Kamlet and Adolph [54] reported that the impact sensitivities of organic high explosives are primarily functions of the rates of the thermal decomposition processes taking place in the temperature regimes generated under the impact hammer. For classes of explosives with similar decomposition mechanisms, there appear to be statistically significant linear relationships (sensitivity/composition trends) between logarithmic 50% impact heights and OB_{100} values. They also showed that polynitroaromatic explosives containing a C-H linkage alpha to the aromatic ring are more sensitive as a class than explosives lacking such a linkage. Gilbert and Leccacorvi [55] reported that the dinitrobenzene (DNB) can be prepared either by the nitration of benzene or by the oxidation of nitroaniline. The explosive decomposition products of DNB are CO_2 , CO , H_2 , N_2 , CH_4 , HCN , C_2H_2 , NH_4HCO_3 , C and its VOD is 6100 m/s. Kamlet et al. [56] demonstrated the relationship between impact sensitivity with the structures of high explosives and found that the initiation step in polynitroaromatics, is presumably a scission of the C- NO_2 bond where C- NO_2 homolysis to form NO and an aromatic radical, is a dominant decomposition channel. But those having C-H bond alpha to the polynitroaromatic ring, decompose by C-H bond scission as shown in scheme 1.1.



Scheme 1.1: C-H and C-N bond scission in polynitroaromatics

Urbanski [57] reported that 2,4,6-trinitrophenol (picric acid) is of the greatest importance and thermal decomposition of picric acid can be represented as follows:



Thermal decomposition of 5-nitro-2,4-dihydro-3H-1,2,4-triazole-3-one (NTO) have been carried out by Rothgery et al. [58]. They observed that the stability of NTO is to aging of the sample. Kinetic analysis suggested an auto-catalytic mechanism and the decomposition mechanism changed abruptly at 212 °C where an ignition occurred. Formation of $\cdot\text{NO}_2$ radical by C-NO₂ cleavage, with the rupture of the adjacent C-N bond appears to be the probable mechanism in the thermal decomposition of NTO.

Heterocycles like pyrazolo-pyrazole generally have a higher density and oxygen balance, important parameters for increasing the performance of an energetic material, than their carbocyclic analogues. Mikhailov et al. [59] developed a method of synthesis of 2,6-diazido-3,5-dicyanopyridine, 2,4,6-triazido-3,5-dicyanopyridine, 2,3,4,5-tetraazido-6-cyanopyridine and determined the heats of formation and explosive properties of compounds. The replacement of endocyclic nitrogen atoms by C-CN fragments in the aromatic ring of polyazides strongly reduces the explosive risk of these compounds with retention of the energetic properties of the molecules. Kapoor et al. [60] synthesized four phenylene-diammonium dinitrate salts. They also studied their thermal properties by using thermogravimetry (TG) and simultaneous thermogravimetry-differential scanning calorimetry

(TG–DSC). Singh et al. [61] prepared six dimethylanilinium chlorides (DMACl) and studied their thermal decomposition properties by TG and DSC techniques. They also evaluated the kinetic parameters from the isothermal and non-isothermal TG data. Singh et al. [62] reported the thermolysis of dimethylanilinium nitrates (DMAN) by TG, DTA, ignition delay, impact and friction sensitivity measurements. Although kinetics of the thermal decomposition of these salts were evaluated by fitting TG data in nine-mechanism-based kinetic models, only Avrami Erofeev ($n = 2, 3$) and contracting area ($n = 2$) gave the best fits. Felix et al. [63] studied the thermal analysis of RDX and its three plastic bonded explosives (PBXs) by using various thermo analytical techniques, under different conditions. The thermal analyses did not show any significant reduction in thermal stability of RDX. Kinetic analysis of isothermal TG data was made by model fitting methods as well as a model free isoconversional method. Kapoor et al. [64] synthesized hydrogen sulphate, nitrate and perchlorate salts of diphenylamine and evaluated their thermal decomposition by TG (static air) and DSC (inert atmosphere). The diphenylammonium hydrogen sulphate under thermal and microwave irradiation formed 4-(phenylamino) benzenesulphonic acid by sulphonation process, whereas nitrate and perchlorate salts did not form corresponding nitro and perchloro derivatives, rather they ignite and explode, respectively, to form gaseous products along with a residual carbon. Kapoor et al. [65] synthesized three salts of phenylenediammonium and studied their thermal decomposition by thermogravimetry (TG), differential thermal analysis (DTA) and explosion delay (D_E) measurements. They also found that the oxidation-reduction reactions near the surface of thermolysing perchlorates may be responsible for the decomposition, followed by explosion.

The above literature revealed that the luminescent and thermal properties of lanthanide complexes with 1,10-phenanthroline (phen), 2,2'-bipyridine (bipy), 2,4,6-tris(2-pyridyl)-1,3,5-triazine (tptz) as primary ligands and 2,6-dinitrophenol (2,6-DNP), Sodium benzoate (NaOBz), 2-pyrazinecarboxylic acid (2-pyca) as secondary ligands have not been reported in details. Accordingly in present thesis, we have attempted the structural, photophysical and thermal properties of lanthanide (III) [$Ln = \text{Eu, Gd, Tb}$] complexes as well as the thermal kinetic analysis of various organic salts.

REFERENCES

1. Johansson, B., Brooks, M. S. S., in "Handbook on the physics and chemistry of the rare earths", edited by Gschneidner, K. A., Eyring, L., Lander, G. H., Choppin, G. R., North-Holland, Amsterdam, Vol. 17 (1993), p. 149 (Chapter 112).
2. (a) Ballato, J., Lewis, J. S. and Holloway P., "Display applications of rare-earth-doped materials", Mater. Res. Soc. Bull., **24**, 51 (1999). (b) Ma, L., Evans, O. R., Foxman, B. M. and Lin W., "Luminescent lanthanide coordination polymers", Inorg. Chem., **38**, 5837 (1999).
3. (a) Caravan, P., Ellison, J. J. and McMurry, T. J., "Gadolinium (III) chelates as MRI contrast agents: Structure, dynamics and applications", Chem. Rev., **99**, 2293 (1999). (b) Bianchi, A., Calabi, L., Corana, F., Fontana, S., Losi, P., Maiocchi, A., Paleari, L. and Valtancoli, B., "Thermodynamic and structural properties of Gd(III) complexes with polyamino-polycarboxylic ligands: Basic compounds for the development of MRI contrast agents", Coord. Chem. Rev., **204**, 309 (2000). (c) Reichert, D. E., Lewis, J. S. and Anderson, C. J., "Metal complexes as diagnostic tools", Coord. Chem. Rev., **184**, 3 (1999).
4. (a) Volkert, W. A., Goeckeler, W. F., Ehrhardt, G. J. and Ketrting, A. R., "Therapeutic radionuclides: Production and decay property considerations", J. Nucl. Med., **32**, 174 (1991). (b) Li, W. P., Ma, D. S., Higginbotham, C., Hoffman, T., Ketrting, A. R., Cutler, C. S. and Jurisson, S. S., "Development of an *in vitro* model for assessing the *in vivo* stability of lanthanide chelates", Nucl. Med. Biol., **28**, 145 (2001).
5. Wang, K., Li, R., Cheng, Y. and Zhu, B., "Lanthanides-the future drugs?", Coord. Chem. Rev., **190**, 297 (1999).
6. Desilva, A. P., Gunaratne, H. Q. N., Gunnlaugsson, T., Huxley, A. J. M., McCoy, C. P., Rademacher, J. T. and Rice, T. E., "Signaling recognition events with fluorescent sensors and switches", Chem. Rev., **97**, 1515 (1997).
7. Yang, C., Chen, X. -M., Zhang, W. -H., Chen, J., Yang, Y. -S. and Gong, M. -L., "Synthesis, crystal structure and luminescence properties of a europium (III) complex with a new planar aromatic tridentate N₃ ligand", J. Chem. Soc., Dalton Trans., **8**, 1767 (1996).
8. Mehrotra, C. and Bohra, R., "Metal carboxylates", New York, Academic Press (1983).
9. Zhang, A. -J., Wang, Y. -W., Dou, W., Dong, M., Zhang, Y. -L., Tang, Y., Liu, W. -S. and Peng, Y., "Synthesis, crystal structures, luminescent and magnetic properties of homodinuclear

- lanthanide complexes with a flexible tripodal carboxylate ligand”, *Dalton Trans.*, **40**, 2844 (2011).
10. Ramya, A. R., Reddy, M. L. P., Cowley, A. H. and Vasudevan, K. V., “Synthesis, crystal structure and photoluminescence of homodinuclear lanthanide 4-(dibenzylamino)benzoate complexes”, *Inorg. Chem.*, **49**, 2407 (2010).
 11. Choi, J. R., Tachikawa, T., Fujitsuka, M. and Majima, T., “Europium-based metal-organic framework as a photocatalyst for the one-electron oxidation of organic compounds”, *Langmuir*, **26**, 10437 (2010).
 12. An, B. -L., Song, J., Cheah, K. -W., Ren, Y. -Y. and Cheng, Z. -X., “Structure and NIR luminescence of lanthanide (III) complexes with an organic tridentate ligand”, *Inorg. Chim. Acta*, **362**, 3196 (2009).
 13. Lv, Y., Zhanga, J., Caoa, W. and Fua, Y., “Enhanced luminescence of novel rare earth complexes $\text{Eu}(\text{3,5-DNBA})_3\text{phen}$ in nano- TiO_2 ”, *Spectrochim. Acta, Part A*, **72**, 22 (2009).
 14. Remya, P. N., Biju, S., Reddy, M. L. P., Cowley, A. H. and Findlater, M., “1D molecular ladder of the ionic complex of terbium-4-sebacoylbis(1-phenyl-3-methyl-5-pyrazolonate) and sodium dibenzo-18-crown-6: Synthesis, crystal structure and photophysical properties”, *Inorg. Chem.*, **47**, 7396 (2008).
 15. Puchalska, M., Tyrk., I. T., Trush, V. and Legendziewicz, J., “Structural characteristic and luminescence properties of first known example of a pair of europium (III) complexes of phosphoroazo-derivative of β -diketone with inner and both inner and outer sphere 2,2'-bipyridine”, *J. Alloys Comp.*, **451**, 264 (2008).
 16. Liu, T., Fang, J., Zhang, Y. and Zeng, Z., “Synthesis, characterization and luminescent properties of lanthanide complexes with poly(N,N-diethylacrylamide-co-methacrylic acid)”, *Synth. React. Inorg. Met.-Org. Chem.*, **38**, 695 (2008).
 17. Shyni, R., Biju, S., Reddy, M. L. P., Cowley, A. H. and Findlater, M., “Synthesis, crystal structures, and photophysical properties of homodinuclear lanthanide xanthene-9-carboxylates”, *Inorg. Chem.*, **46**, 11025 (2007).
 18. Tanase, S., Gallego, P. M., Gelder, R. D. and Fu, W. T., “Synthesis, crystal structure and photophysical properties of europium (III) and terbium (III) complexes with pyridine-2,6-dicarboxamide”, *Inorg. Chim. Acta*, **360**, 102 (2007).

19. Tang, K. -Z., Li, Y. -F, Tang, Y., Liu, W. -S., Tang, M. and Tan, M. -Y., "Synthesis and luminescent properties of the lanthanide isothiocyanate complexes with an amide-type tripodal ligand", *Spectrochim. Acta, Part A*, **67**, 858 (2007).
20. Jang, H., Shin, C. -H., Jung, B. -J., Kim, D. -H., Shim, H. -K. and Do, Y., "Synthesis and characterization of dinuclear europium complexes showing pure red electroluminescence", *Eur. J. Inorg. Chem.*, **2006**, 718 (2006).
21. Soares-Santos, P. C. R., Almeida Paz, F. A., Sà Ferreira, R. A., Klinowski, J., Carlos, L. D., Trindade, T. and Nogueira, H. I. S., "Coordination modes of pyridine-carboxylic acid derivatives in samarium (III) complexes", *Polyhedron*, **25**, 2471 (2006).
22. Wang, B. -D., Yang, Z. -Y., Zhang, D. -W. and Wang, Y., "Synthesis, structure, infrared and fluorescence spectra of new rare earth complexes with 6-hydroxy chromone-3-carbaldehyde benzoyl hydrazone", *Spectrochim. Acta*, **A63**, 213 (2006).
23. Lenaerts, P., Warland, C. G. and Binnemans, K., "Luminescent europium (III) and terbium (III) nicotinate complexes covalently linked to a 1,10-phenanthroline functionalized sol-gel glass", *J. Lumin.*, **117**, 163 (2006).
24. Oyang, L., Sun, H. -L., Wang, X. -Y., Li, J. -R, Nie, D. -B., Fu, W. -F., Gao, S. and Yu, K. -B., "Crystal structure and luminescence property of ternary terbium p-aminobenzoic acid complexes with different second ligands", *J. Mol. Struct.*, **740**, 175 (2005).
25. Qu, Y., Ke, Y., Lu, S., Fan, R., Pan, G. and Li, J., "Hydrothermal synthesis, structures and spectroscopy of 2D lanthanide coordination polymers built from helical chains: $[\text{Ln}_2(\text{BDC})_3(\text{H}_2\text{O})_2]_n$ (Ln = Sm, Eu, BDC = 1,3-benzenedicarboxylate)", *J. Mol. Struct.*, **734**, 7 (2005).
26. Song, Y. -S., Yan, B. and Chen, Z. -X., "Two novel lanthanide 1-D chain coordination polymers of pyridinedicarboxylic acids: Hydrothermal synthesis, structure and luminescent properties", *J. Mol. Struct.*, **750**, 101 (2005).
27. Liu, C. -B., Yu, M. -X., Zheng, X. -J., Jin, L. -P., Gao, S. and Lu, S. -Z., "Structural change of supramolecular coordination polymers of itaconic acid and 1,10-phenanthroline along lanthanide series", *Inorg. Chim. Acta*, **358**, 2687 (2005).
28. Zheng, X. -J., Jin, L. -P., Gao, S. and Lu, S. -Z., "New ternary lanthanide coordination polymers of 1,4-naphthalenedicarboxylate with phenanthroline", *Inorg. Chem. Commun.*, **8**, 72 (2005).

29. Zhang, Z. -Q., Shen, Q., Zhang, Y., Yao, Y. -M. and Lin, J., “Synthesis and characterization of β -diketiminato terbium complex”, *Inorg. Chem. Commun.*, **7**, 305 (2004).
30. Yin, M. -C., Ai, C. -C., Yuan, L. -J., Wang, C. -W. and Sun, J. -T., “Synthesis, structure and luminescent property of a binuclear terbium complex $[\text{Tb}_2(\text{Hsal})_8(\text{H}_2\text{O})_2] [(\text{Hphen})_2] \cdot 2\text{H}_2\text{O}$ ”, *J. Mol. Struct.*, **691**, 33 (2004).
31. Barja, B., Baggio, R., Garland, M. T., Aramendia, P. F., Peña, O. and Perec, M., “Crystal structure and luminescent properties of terbium (III) carboxylates”, *Inorg. Chim. Acta*, **346**, 187 (2003).
32. Barja, B., Aramendia, P., Baggio, R., Garland, M. T., Pena, O. and Perec, M., “Europium (III) and terbium (III) trans-2-butenoates: Synthesis, crystal structures and properties”, *Inorg. Chim. Acta*, **355**, 183 (2003).
33. Soares-Santos, P. C. R., Nogueira, H. I. S., Almeida Paz, F. A., Sá Ferreira, R. A., Carlos, L. D., Klinowski, J. and Trindade, T., “Lanthanide complexes of 2,6-dihydroxybenzoic acid: Synthesis, crystal structures and luminescent properties of $[\text{nBu}_4\text{N}]_2[\text{Ln}(2,6\text{-dihb})_5(\text{H}_2\text{O})_2]$ (Ln = Sm, and Tb)”, *Eur. J. Inorg. Chem.*, **2003**, 3609 (2003).
34. Wan, Y., Zhang, L., Jin, L., Gao, S. and Lu, S., “High-dimensional architectures from the self-assembly of lanthanide ions with benzenedicarboxylates and 1,10-phenanthroline”, *Inorg. Chem.*, **42**, 4985 (2003).
35. Wang, R. -F., Wang, S. -P. and Zhang, J. -J., “Crystal structure and properties of $[\text{Eu}(\text{m-BrBA})_3(\text{H}_2\text{O})(\text{phen})]_2$ ”, *J. Mol. Struct.*, **648**, 151 (2003).
36. Harrowfield, J. M., Lu, W., Skelton, B. W. and White, A. H., “Structural systematics of rare earth complexes. I. structural characterization of lanthanoid (III) picrate hydrates: Monoclinic ($\text{P}2_1/\text{C}$) (Quasi-)dodecahydrates of the related $\text{La} \rightarrow \text{Pr}$ and $\text{Nd} \rightarrow \text{Tb}$ families”, *Aus. J. Chem.*, **47**, 321 (1994).
37. Yun, S. -S., Kang, S. K., Suh, H. -R., Suh, H. -S., Lee, E. K., Kim, J. -K. and Kim, C. -H., “Lanthanide complexes of some high energetic compounds (II), crystal structures and thermal properties of picrate complexes”, *Bull. Korean Chem. Soc.*, **26**, 1197 (2005).
38. Yun, S. -S., Kim, J. -K. and Kim, C. -H., “Lanthanide complexes of some high energetic compounds (I), crystal structures and thermal properties of 3-nitro-1,2,4-triazole-5-one (NTO) complexes”, *J. Alloys Comp.*, **408**, 945 (2006).

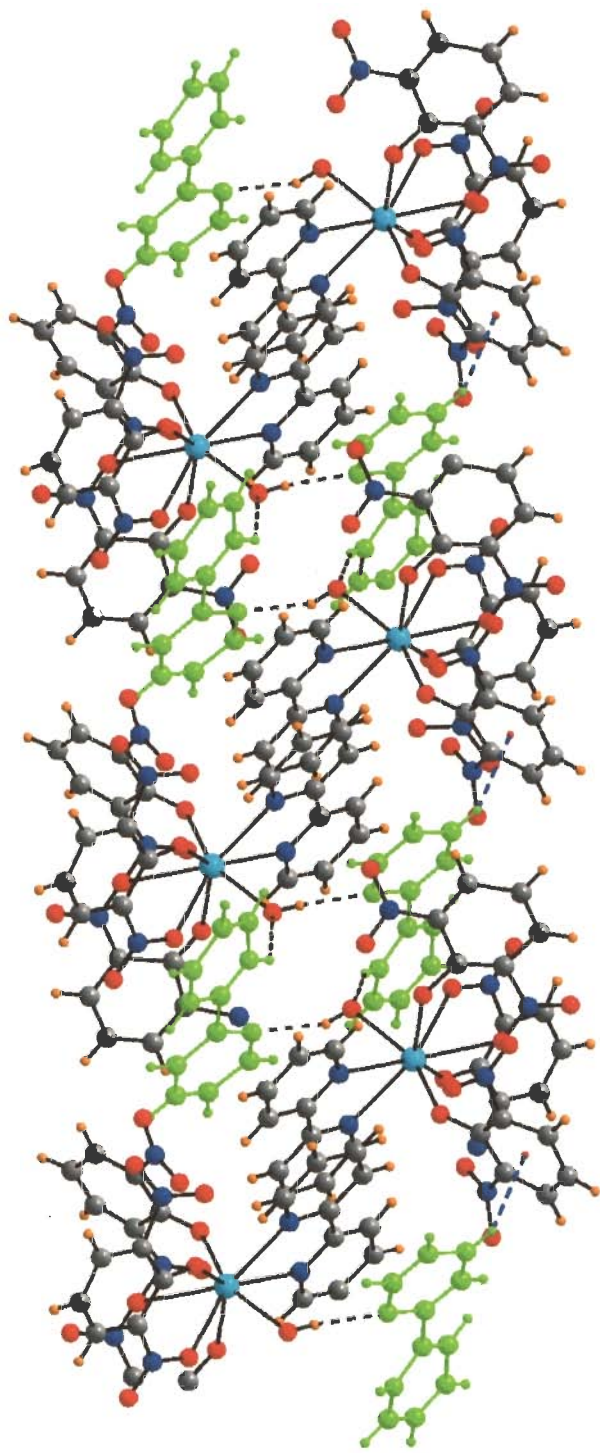
39. Yan, B., Zhang, H. J., Zhou, G. L. and Ni, J. Z., "Different thermal decomposition process of lanthanide complexes with N-phenylanthranilic acid in air and nitrogen atmosphere", *Chem. Pap.*, **57**, 83 (2003).
40. Jr, P. M., Matos, J. R., Mercuri, L. P., Araújo, M. P. B. M., Vicentini, G. and Zinner, L. B., "Thermal decomposition of hydrated lanthanide picrates by TG/DTG and DSC analyses", *J. Therm. Anal. Calorim.*, **67**, 465 (2002).
41. Jr, P. M., Máduar, M. F., Schpectorand, J. Z. and Matos, J. R. "Thermal decomposition and structural study of lanthanide complexes with trans-1,3-dithiane-1,3-dioxide", *J. Therm. Anal. Calorim.*, **87**, 793 (2007).
42. Nakagawa, K., Amita, K., Mizuno, H., Inoue, Y. and Hakushi, T., "Preparation of some lanthanoid picrates and the behavior of their water of hydration", *Bull. Chem. Soc.*, **60**, 2037 (1987).
43. Boncher, W. L., Regulacio, M. D. and Stoll, S. L., "Thermolysis of lanthanide dithiocarbamate complexes", *J. Solid State Chem.*, **183**, 52 (2010).
44. Brzyska, W. and Ozga, W., "Thermal decomposition of yttrium and lanthanide complexes with mephenamic acid", *Thermochim. Acta*, **195**, 149 (1992).
45. Sallama, S. A. and Mahmoudb, M. A., "Lanthanide complexes with D-penicillamine methyl ester: Formation constants, spectral and thermal properties", *Z. Naturforsch., B: Chem. Sci.*, **61b**, 139 (2006).
46. Christos, P., Stefano, V. and Maria, L. -K., "Lanthanide complexes of 3-methoxy-salicylaldehyde: Thermal and kinetic investigation by simultaneous TG/DTG-DTA coupled with MS", *J. Therm. Anal. Calorim.*, **99**, 319 (2010).
47. Tian, L., Ren, N., Zhang, J. J., Liu, H. M., Sun, S. J., Ye, H. M. and Wu, K. Z., "Synthesis and thermal decomposition kinetics of two lanthanide complexes with cinnamic acid and 2,2'-bipyridine", *J. Therm. Anal. Calorim.*, **99**, 349 (2010).
48. Ye, H. -M., Ren, N., Zhang, J. -J., Sun, S. -J. and Wang, J. -F., "Crystal structures, luminescent and thermal properties of a new series of lanthanide complexes with 4-ethylbenzoic acid", *New J. Chem.*, **34**, 533 (2010).
49. Wang, J. -F., Zhang, D. -H., Liu, X., Wu, K. -Z. and Zhang, J. -J., "Synthesis, crystal structure, and thermal decomposition kinetics of the ternary complex $[\text{Sm}(\text{5-Cl-2-MOBA})_3\text{phen}]_2$ ", *J. Chem. Eng. Data*, **55**, 5608 (2010).

50. Yun, S. -S., Park, Y. -B., Yeon, J. -H., Kim, E. -J. and Kim, D., "Crystal structure, thermal and magnetic properties of 2,4-dinitrobenzoatoterbium (III) complex", *J. Coord. Chem.*, **60**, 2703 (2007).
51. Czylkowska, A. and Markiewicz, M., "Coordination behaviour and thermolysis of some rare-earth complexes with 4,4'-bipyridine and di- or trichloroacetates", *J. Therm. Anal. Calorim.*, **100**, 717 (2010).
52. Holzmann, R. T., "Chemical Rockets, Flame and Explosives Technology", Marcell Dekker Inc, New York (1969) p. 1.
53. Energetic Condensed Systems. A Brief Encyclopedic Dictionary [in Russian], Yanus, -K., Moscow (1999).
54. Kamlet, M. J. and Adolph, H. G., "The relationship of impact sensitivity with structure of organic high explosives: II. Polynitroaromatic explosives", *Propellants Explos.*, **4**, 30 (1979).
55. Gilbert, E. E. and Leccacorvi, J. R., "A simplified oxidative preparation of aromatic nitro compounds", *Propellants Explos.*, **1**, 89 (1976).
56. Kamlet, M. J., "The relationship between impact sensitivity with structure of organic high explosives: I. Polynitro aliphatic explosives", *Proceedings VI International Symposium, Detonation, San Diego, CA* (1976).
57. Urbanski, T., "Chemistry and Technology of Explosives", Vol. 1, Pergamon, PWN -Polish Scientific Publishers, Warszawa (1965).
58. Rothgery, E. F., Audette, D. E., Wedlich, R. C. and Csejka, D. A., "The study of the thermal decomposition of 3-nitro-1,2,4-triazol-5-one (NTO) by DSC, TGA-MS and ARC", *Thermochim. Acta*, **185**, 235 (1991).
59. Mikhailov, Y., Chapyshev, S. and Nedel'ko, V., "Synthesis, thermal stability, heats of formation and explosive properties of cyano-substituted di-, tri- and tetraazidopyridines", *Russ. Chem. Bull. Int. Ed.*, **58**, 2097 (2009).
60. Kapoor, I. P. S., Srivastava, P. and Singh, G., "Preparation, characterization and thermolysis of phenylenediammonium dinitrate salts", *J. Hazard. Mater.*, **150**, 687 (2008).
61. Singh, G., Kapoor, I. P. S. and Kaur, J., "Studies on (non) energetic compounds. Part-14: Thermal decomposition of dimethylanilinium chlorides", *Thermochim. Acta*, **338**, 45 (1999).
62. Singh, G., Kapoor, I. P. S. and Mannan, S. M., "Studies on energetic compounds Part 3: Kinetics of thermolysis of dimethylanilinium nitrates", *Thermochim. Acta*, **262**, 117 (1995).

63. Felix, S. P., Singh, G. and Soni, P., "Studies on energetic compounds Part 31: Thermolysis and kinetics of RDX and some of its plastic bonded explosives", *Thermochim. Acta*, **426**, 131 (2005).
64. Kapoor, I. P. S., Kapoor, M. and Singh, G., "Thermolysis of hydrogen sulphate, nitrate and perchlorate salts of diphenylamine. Part LXVIII", *J. Therm. Anal. Calorim.*, **102**, 723 (2010).
65. Kapoor, I. P. S., Shrivastava, P., Singh, G., Singh, U. P. and Frohlich, R., "Preparation, crystal structure and thermolysis of phenylenediammonium diperchlorate salts", *J. Phys. Chem. A*, **112**, 652 (2008).

CHAPTER-2

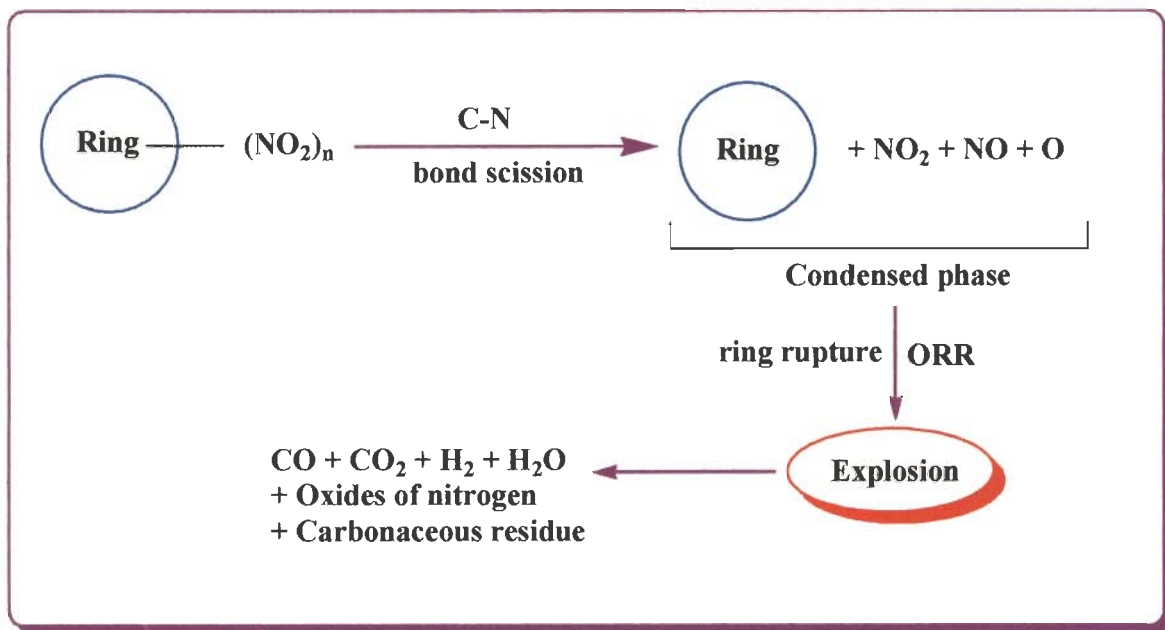
***pH-Dependent Host-Guest
Complexes of Europium (III)
and Gadolinium (III):
Syntheses, Structural and
Thermal Studies***



Both polynitro aromatic and aliphatic compounds have been extensively studied as high energetic compounds [1, 2]. Presence of even one nitro group is sufficient to increase the thermal decomposition of aromatic compounds as nitrates are powerful oxidizing agent and decompose at elevated temperature to give oxygen as one of the major product. Nevertheless, aromatic compounds which have two or more nitro groups, exhibit distinctly marked explosive properties. Keshavarza et al. [3] reported a new method for activation energy or the Arrhenius parameter E_a of the thermolysis in the condensed state for different polynitro arenes as an important class of energetic molecules. The methodology assumes that E_a of a polynitro arene with general formula $C_aH_bN_cO_d$ can be expressed as a function of optimized elemental composition as well as the contribution of specific molecular structural parameters. They also reported the new method which can predict E_a of the thermolysis under conditions of Soviet Manometric Method (SMM) and suggested that the proposed new method can also be used to predict E_a of three polynitro arenes, i.e. DIPAM and NTFA. Stepanov et al. [4] studied the effect of chemical structure on the thermal stability of multifunctional gem-trinitro compounds and found that depending on the structure of the compounds, the decomposition rate changes by more than two orders of magnitude, which is due not only to the effect of substituents but also to the different mechanisms of the rate-determining stage of the process. Singh et al. [5] reported the thermolysis of 3-amino-5-nitro-1,2,4-triazole (ANTA) using thermogravimetry-differential thermal analysis (TG-DTG-DTA) and differential scanning calorimetry (DSC) techniques in N_2 atmosphere. They found that the decomposition of ANTA occurred in two steps i.e. first step corresponds to the removal of NO_2 followed by ring rupture and various condensed phase processes leading to the formation of CO_2 , N_2O , HCN and HCNO. Rao and Yoganasimhan [6] reported the mode of decomposition of 2,4,N-trinitro anilino acetic acid [glycine, N-(2,4 dinitrophenyl), N-nitro] and its methyl and ethyl esters from a study of the kinetic parameters of their thermal decomposition using DTA, isolation and identification of some of the nonvolatile products of decomposition. From which, they concluded that these compounds decompose through the scission of N- NO_2 bond. Singh and Pandey [7] synthesized the nitrate complexes of copper, nickel and zinc with diethylenetriamine (dien) i.e. $[Cu(dien)_2](NO_3)_2$, $[Ni(dien)_2](NO_3)_2 \cdot 2H_2O$ and $[Zn(dien)_2](NO_3)_2$. The kinetic parameters for both non-isothermal and isothermal decomposition of the complexes were evaluated by employing Coats-Redfern (C-R) method and Avrami-Erofeev (A-E) equations ($n = 2$ and 3), respectively. They also reported that all these complexes were found to be insensitive towards

impact of 2 Kg mass hammer up to the height limit (110 cm) of the instrument used. Singh and Felix [8] reported the crystal structure, thermolysis and applications of 5-nitro-2,4-dihydro-3H-1,2,4-triazole-3-one (NTO). They also summarized the various studies dealing with applications of NTO as a high-energetic material. Ferenc et al. [9] reported the physico-chemical properties of 4-chloro-2-nitrobenzoates of Co(II), Ni(II) and Cu(II). All analysed 4-chloro-2-nitrobenzoates are polycrystalline compounds with colors depending on the central ions: pink for Co(II), green for Ni(II) and blue for Cu(II) complexes. Their thermal decomposition was studied only in the range of 293–523 K, because it was found that on heating in air above 523 K, 4-chloro-2-nitrobenzoates decomposed explosively. Hydrated complexes lose crystallization water molecules in one step and anhydrous compounds are formed. The final products of their decomposition are the oxides of the respective transition metals. From the results, they concluded that during dehydration process no transformation of nitro group to nitrite takes place.

The explosive characteristics depend on properties such as shear strength and molecular orientations of the crystalline material [10-12]. Zeman et al. [13] and Zeman [14] have correlated the thermal decomposition kinetics of polynitro aromatic explosives at lower temperatures with heat of explosion, detonation characteristics. They also specified the thermal stabilities of polynitroaromatic compounds by means of non-isothermal DTA and determined the initial temperatures of the exotherms T_D , as well as the Piloyan decomposition activation energies, E , of the compounds. The thermal decomposition of polynitro organic compounds involves simple bond scission prior to explosion. A notable feature of these reactions is the fact that the aromatic ring remains intact. The next stage of thermolysis involves propagation reaction which involves exothermic oxidation/reduction reactions leading to the formation of low molecular weight and thermodynamically stable gaseous products. It has been also proved that the dissociation of ring does not occur until most of the attached substituents are removed. The thermolysis of polynitro aromatic compounds begins with one or more endothermic initiation steps. These steps involve C-NO₂ homolysis, and NO₂ or NO are formed which attack the aromatic ring producing CO and CO₂. The overall unified thermolysis mechanism can be suggested in scheme 2.1.



where $n = 2, 3, 4, \dots$

ORR = Oxidation reduction reaction

Scheme 2.1: Schematic illustration of the thermolysis mechanism

2,6-dinitrophenol (2,6-DNP) is one of the six possible dinitrophenol forms used in the synthesis of dyes, other organic chemicals, wood preservatives, explosives and insecticides. The absence of nitro groups at the para position on 2,6-DNP makes the nitro group at ortho position be involved strongly in chelate formation i.e. it can coordinate in different ways when it is present in solution, and the coordination mode again changes when one more ligand is present in same solution. Yun et al. [15] reported the crystal structure of a (2,6-dinitrophenolato)lithium complex $[\text{Li}(2,6\text{-DNP})(\text{H}_2\text{O})]_2 \cdot 2\text{H}_2\text{O}$ which is centrosymmetric in nature (Fig. 2.1). They also reported the thermal decomposition of this dimeric complex which occurs in two steps i.e. first between 57 and 80 °C, corresponds to dehydration and the second, between 330 and 370 °C, corresponds to decomposition of the complex with explosion.

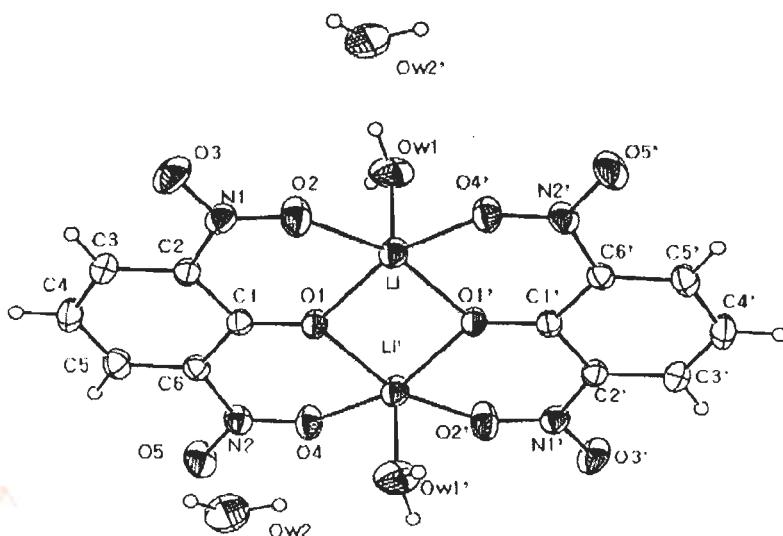


Fig. 2.1: Crystal structure of $[\text{Li}(2,6\text{-DNP})(\text{H}_2\text{O})]_2 \cdot 2\text{H}_2\text{O}$

Yun et al. [16] further reported the Ln(III) complexes with 2,6-dinitrophenol ligand, $[\text{La}_2(2,6\text{-DNP})_6(\text{H}_2\text{O})_4] \cdot 4\text{H}_2\text{O}$ and $[\text{Tb}(2,6\text{-DNP})_3(\text{H}_2\text{O})_3]$ (Fig. 2.2). Based on the results of TG-DTG and DSC thermal analysis, they suggested that the lanthanide 2,6-DNP complexes were thermally decomposed in three distinctive stages, the dehydration, the 2,6-DNP decomposition and the formation of the metal oxide.

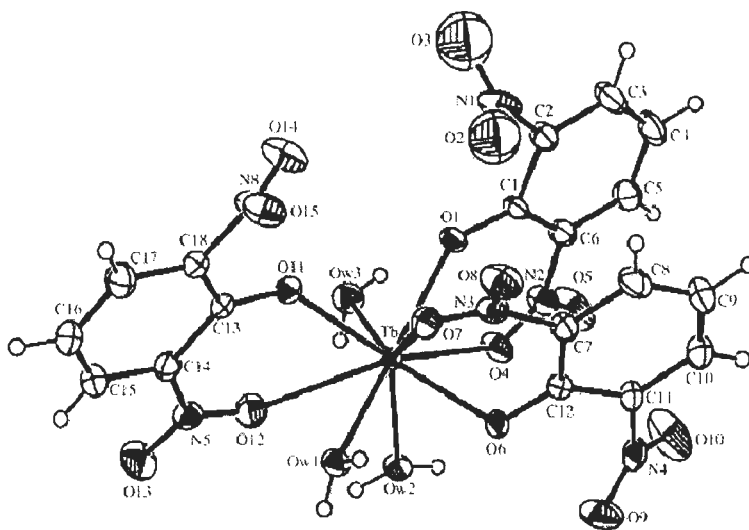


Fig. 2.2: Crystal structure of $[\text{Tb}(2,6\text{-DNP})_3(\text{H}_2\text{O})_3]$

Yun et al. [17] synthesized the lanthanide complexes of 2,6-DNP with Y(III) beside Ce(III), Pm(III), Lu(III) and analyzed their crystal structures by X-ray diffractions methods. La(III) ion formed the dimeric complex $[\text{La}_2(2,6\text{-DNP})_6(\text{H}_2\text{O})_4] \cdot 4\text{H}_2\text{O}$, while the rest of Ln(III) ions

formed the monomeric complexes $[\text{Ln}(2,6\text{-DNP})_3(\text{H}_2\text{O})_3]$. He found that in the La(III) complex, the significance of the structure is the presence of the bridged ligands and the terminal ligands in the bimetallic compound. The thermal properties of these complexes were also studied by TG-DTG and DSC thermal analysis method. Based on the results of TG-DTG and DSC analysis, he also proposed the thermal decomposition mechanism of the complexes i.e. the complexes were thermally decomposed in three distinctive stages, the dehydration, the 2,6-DNP decomposition, and the formation of the metal oxide. Kim et al. [18] reported the formation of $[\text{Ho}(2,6\text{-DNP})_3(\text{H}_2\text{O})_3]$, where Ho^{+3} is nine coordinated via three bidentate 2,6-DNP and three water molecules (Fig. 2.3) and discussed the dependences of metal to ligand bond lengths according to the atomic number of lanthanide elements. They also studied the thermal properties of lanthanide complexes by TG-DTG and DSC thermal analysis methods.

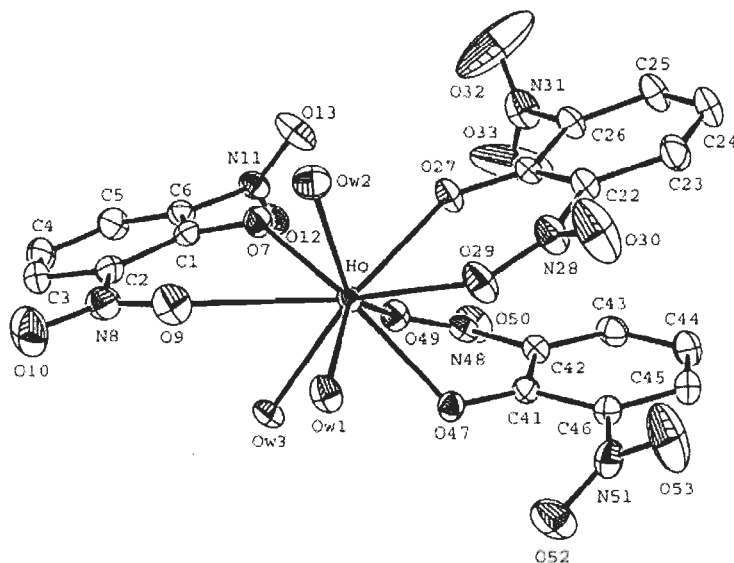


Fig. 2.3: Crystal structure of $[\text{Ho}(2,6\text{-DNP})_3(\text{H}_2\text{O})_3]$

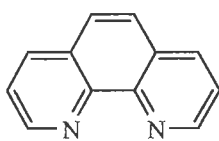
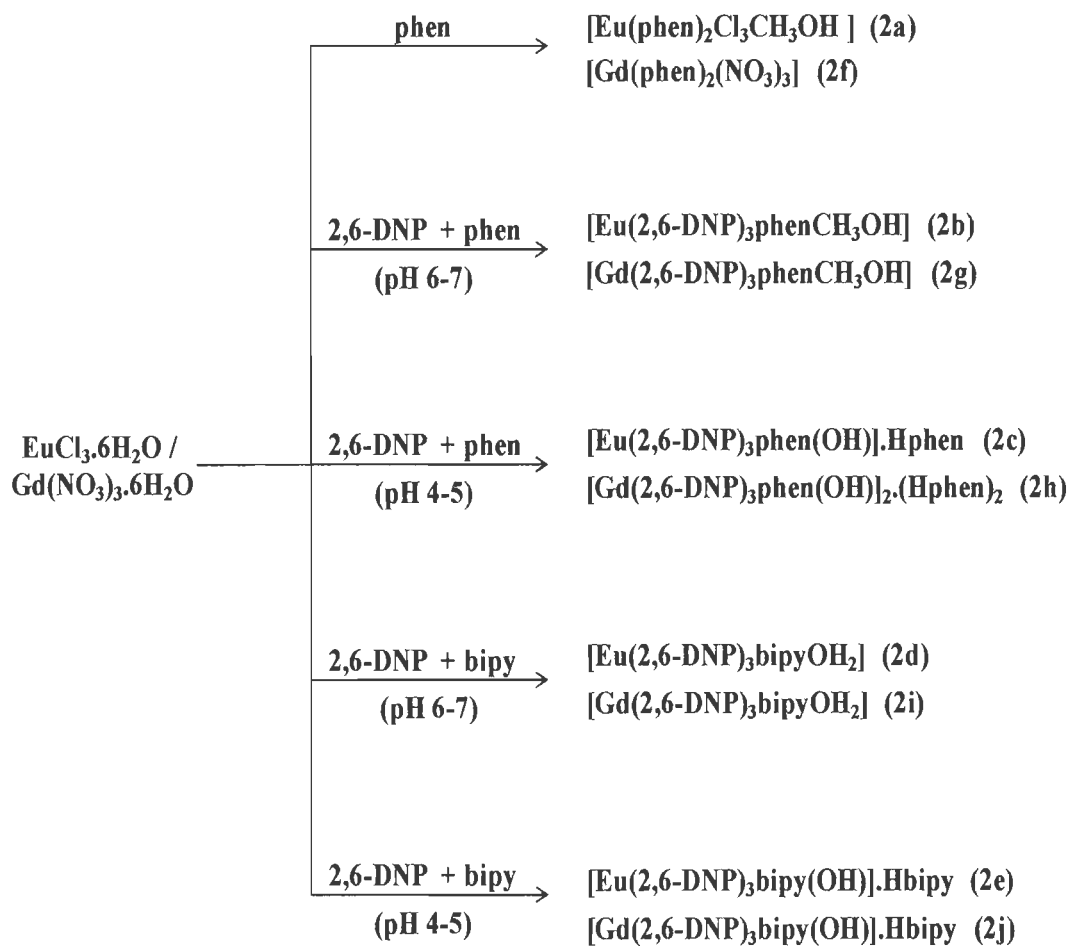
Suh et al. [19] reported the synthesis of nine-coordinated $[\text{Nd}(\text{C}_6\text{H}_3\text{N}_2\text{O}_5)_3(\text{H}_2\text{O})_3]$ system with a slightly distorted tricapped trigonal prismatic coordination geometry. The Nd(III) ion is coordinated to three H_2O and by three bidentate 2,6-dinitrophenolate ligands. The coordinated NO_2 groups are almost coplanar with the benzene rings. Suh et al. [20] also reported the formation of compound $[\text{Y}(\text{C}_6\text{H}_3\text{N}_2\text{O}_5)_3(\text{H}_2\text{O})_3]$, where Y atom is nine-coordinated with a slightly distorted tricapped trigonal prismatic coordination geometry. The Y(III) ion is coordinated to three bidentate 2,6-dinitrophenolate ligands and three water molecules. Aly et al. [21] compared the reactivity of the coordinated monodentate oxine and of the bidentate anion in the complexes $\text{ThOx}_4 \cdot \text{HOx}$ and $\text{UO}_2\text{Ox}_2 \cdot \text{HOx}$ ($\text{HOx} = \text{oxine}$) by the reaction of these

complexes with nitrophenols. The mixed ligand complexes isolated were formulated as $\text{ThOx}_4 \cdot 2\text{Hph}$ and as $\text{UO}_2\text{Ox}_2 \cdot \text{Hph}$ [Hph = picric acid and 2,4-dinitrophenol for Th(IV) and also 2,6-dinitrophenol for U(VI)]. They tentatively suggested the structures with the formation of hydrogen bonds between the oxygen atom of the chelated oxinate and that of the nitrophenol. Layton et al. [22] synthesized the adducts between the alkali-metal salts of 1-nitroso-2-naphthol, o-nitrophenol, 2,4- and 2,6-dinitrophenol and ligands viz., 1,10-phenanthroline, or 2,9-dimethyl-1,10-phenanthroline.

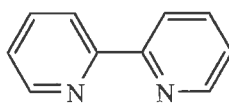
The above literature revealed that the syntheses of lanthanide complexes, described in this chapter are not available in literature. The present chapter reports the syntheses of the lanthanide metal complexes with phen and bipy in the presence of secondary ligand 2,6-dinitrophenol at different pH. Thermal stability of these complexes has been studied by means of thermogravimetric analysis, while kinetic parameters have been evaluated using models fitting and isoconversional methods. The possible pathways of thermolysis of these salts have also been proposed.

RESULTS AND DISCUSSION

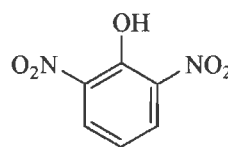
The syntheses of the complexes **2a-2j** were carried out by the stoichiometric combination of lanthanide chloride ($\text{MCl}_3 \cdot 6\text{H}_2\text{O}$, $\text{M} = \text{Eu}, \text{Gd}$), 1,10-phenanthroline (phen) / 2,2'-bipyridine (bipy) and 2,6-dinitrophenol (2,6-DNP) in methanol. Reaction of 1,10-phenanthroline with europium (III) chloride and gadolinium (III) nitrate resulted in the formation of complex $[\text{Eu}(\text{phen})_2\text{Cl}_3\text{CH}_3\text{OH}]$ (**2a**) and $[\text{Gd}(\text{phen})_2(\text{NO}_3)_3]$ (**2f**), whereas in the presence of 2,6-DNP at pH 6-7, the same reaction yielded the complex $[\text{Eu}(2,6\text{-DNP})_3\text{phenCH}_3\text{OH}]$ (**2b**) and $[\text{Gd}(2,6\text{-DNP})_3\text{phenCH}_3\text{OH}]$ (**2g**). This reaction at pH 4-5 gave the complexes $[\text{Eu}(2,6\text{-DNP})_3\text{phen}(\text{OH})] \cdot \text{Hphen}$ (**2c**) and $[\text{Gd}(2,6\text{-DNP})_3\text{phen}(\text{OH})]_2 \cdot (\text{Hphen})_2$ (**2h**). The complexes $[\text{Eu}(2,6\text{-DNP})_3\text{bipyOH}_2]$ (**2d**) / $[\text{Gd}(2,6\text{-DNP})_3\text{bipyOH}_2]$ (**2i**) and $[\text{Eu}(2,6\text{-DNP})_3\text{bipy}(\text{OH})] \cdot \text{Hbipy}$ (**2e**) / $[\text{Gd}(2,6\text{-DNP})_3\text{bipy}(\text{OH})] \cdot \text{Hbipy}$ (**2j**) were prepared by the reaction of lanthanide (III) chloride with 2,2'-bipyridine and 2,6-DNP at pH 6-7 and pH 4-5, respectively as given in scheme 2.2. The different formulations were confirmed by elemental analysis and crystallographic structure analysis of these complexes. The crystallographic data, structure refinement parameters, selected bond lengths and bond angles are listed in Table 2.1-2.18. The selected hydrogen bonding data are summarized in Table 2.19.



1,10-phenanthroline
(phen)



2,2'-bipyridine
(bipy)



2,6-dinitrophenol
(2,6-DNP)

Scheme 2.2: Scheme for the synthesis of complexes **2a-2j**

Infrared spectra

The presence of coordinated 2,6-dinitrophenolate anions are suggested by strong bands at 1566, 1538 cm^{-1} and 1365, 1336 cm^{-1} [23]. The frequencies were split into two bands for $\nu_s(\text{NO}_2)$, exhibiting the 2,6-dinitrophenolate coordination through phenolic oxygen and oxygen of one ortho-nitro group, behaving as a bidentate [23, 24]. The band attributed to $\nu(\text{NO})$ at 988-940 cm^{-1} was shifted to 938 cm^{-1} , indicating the coordination of 2,6-dinitrophenolate anion through the oxygen atom [25] for **2b-2j**. In complex **2a-2c**, **2f-2h**, the C=C and C=N ring stretching vibrations bands in the region 1650-1400 cm^{-1} indicates the coordination of phen to the metal center while in complexes **2d**, **2e**, **2i**, **2j**, the stretching bands C=C (1577 cm^{-1}) and C=N (1558 cm^{-1}) in free bipy shifted to 1596 cm^{-1} and 1568 cm^{-1} on complex formation suggested that bipy ligands coordinated to the lanthanide metal centre through the nitrogen atoms [26]. The out of plane the hydrogen deformation vibration of free phen and bipy are obtained at 735 and 845 cm^{-1} . The broad absorption appears at around 3350 cm^{-1} [27], the typical stretching of alcohol hydroxyl, indicating the presence of methanol in complex **2a**, **2b**, **2g**, and the IR spectra of the complexes show strong bands in the range of 3545-3320 cm^{-1} assignable to $\nu(\text{OH})$ stretching vibrations of coordinated water and OH molecules [28] in complex **2c-2e**, **2h-2j**.

Crystal structure of [Eu(phen)₂Cl₃CH₃OH] (**2a**)

The single crystal X-ray diffraction studies confirmed the formulation of **2a** as [Eu(phen)₂Cl₃CH₃OH] and the molecular structure is given in Fig. 2.4. The complex crystallizes in the orthorhombic system with space group P 2₁ 2₁ 2₁ (Z = 4). The structure analysis demonstrated that complex **2a** contains mononuclear europium centre, where the europium is coordinated by four N atoms (N1, N2, N3, N4) from two phen ligands and three chloride ions (Cl1, Cl2, Cl3). The coordination polyhedron is completed by coordination of one O-atom (O1) of methanol molecule with total coordination number eight. A coordinated polyhedron around Eu⁺³ ion is square-antiprism; atoms N1, Cl1, O1, Cl2 and N2, N3, N4, Cl3 form upper and lower square planes, respectively (Fig. 2.5). Eu-N bond distances of coordinated phen ligands are in the range of 2.581(6) - 2.642(6) Å, while the Eu-O1 bond distance of coordinated methanol is 2.497(5) Å which is in good agreement with the reported values for lanthanide complexes with methanol coordination [29, 30]. The crystal packing shows the presence of C-H...Cl intermolecular and intramolecular interactions between hydrogen atoms of phen ligand, methyl group of methanol and chloride atoms which are in the

range of 2.639 – 2.869 Å. C-H $\cdots\pi$ interactions [C11-H11 $\cdots\pi$, 3.135 and 3.305 Å; C17-H17 $\cdots\pi$, 3.389 Å; C18-H18 $\cdots\pi$, 3.406 Å] are also observed between two phen ligands of neighboring complexes (Fig. 2.6). A pseudo host-guest architecture along the ‘a’ axis is observed due to the presence of C-H $\cdots\pi$ interactions between two complexes (Fig. 2.7).

Crystal structure of [Eu(2,6-DNP)₃phenCH₃OH] (2b)

This complex crystallizes in monoclinic space group P 21/n. The molecular structure of **2b** is shown in Fig. 2.8 where the europium centre is nine coordinated with two N-atoms (N1, N2) from one phen, six O-atoms (O1, O2, O3, O4, O5, O6) from three 2,6-DNP and one O-atom (O7) from coordinated methanol molecule. Eu⁺³ ion forms three six-membered chelate rings with each 2,6-DNP through an O-atom of the nitro group and an O-atom of the phenolate group, whereas the phen ligand coordinates to Eu⁺³ ion, forming a five membered ring. A coordinated polyhedron around Eu⁺³ ion is slightly distorted tricapped trigonal prism (Fig. 2.9). The Eu-O bond distances to the nitro groups are in the range of 2.518(3) - 2.782(5) Å, while the Eu-O bond distances to the phenolate groups are in the range of 2.268(7) - 2.302(4) Å. The average Eu-O bond distance to the nitro group is 2.616 Å which is slightly smaller than the reported value i.e. 2.664 Å, whereas the average Eu-O bond distance to the phenolate group is 2.292 Å which is slightly greater than the reported value in Tb-2,6-DNP complexes [16]. The Eu-N bond distances of coordinated phen ligands are in the range of 2.577(7) - 2.606(3) Å which is shorter as compare to complex **2a**. The intermolecular C-H \cdots O [C31-H31B \cdots O10, 2.899(4) Å] interactions between hydrogen atoms of methyl group of methanol and O-atom of nitro group of 2,6-DNP and $\pi\cdots\pi$ [3.544(3) Å] interactions with neighboring molecules, resulted in the formation of two dimensional structure (Fig. 2.10).

Crystal structure of [Eu(2,6-DNP)₃phen(OH)].Hphen (2c)

The complex **2c** crystallizes in triclinic space group P-1 and the europium centre is eight coordinated with two N-atoms (N1, N2) from one phen, five O-atoms (O2, O3, O4, O5, O6) from three 2,6-DNP and one O-atom (O1) from coordinated deprotonated water molecule (Fig. 2.11). The structure also contains uncoordinated protonated phen molecule in the lattice. Eu⁺³ ion forms two six-membered chelate rings with two 2,6-DNP through an O-atom of the nitro group and an O-atom of the phenolate group but one 2,6-DNP is coordinated to the europium centre in monodentate manner through the single O-atom of phenolate group, whereas the phen ligand coordinates to Eu⁺³ ion, forming a five membered ring. A coordinated polyhedron around Eu⁺³ ion is slightly distorted square-antiprism; atoms N1, O1, O5, O6 and

N2, O2, O3, O4 form upper and lower square planes, respectively (Fig. 2.12). The Eu-O bond distances to the nitro groups are in the range of 2.543(5) - 2.555(3) Å, while the Eu-O distances to the phenolate groups are in the range of 2.236(6) - 2.313(4) Å. Eu-O4 bond distance [2.236(6) Å] is shorter than the Eu-O2 [2.289(4) Å] and Eu-O6 [2.313(4) Å]. The average Eu-O bond distances to the phenolate group and nitro group is 2.279 Å and 2.549 Å, respectively which are smaller as compare to complex **2b**. The Eu-N bond distances of coordinated phen ligands are in the range of 2.569(4) - 2.588(4) Å which is shorter as compare to the complex **2a**, **2b**. The crystal packing shows that one mononuclear complex intermolecularly hydrogen bonded to the neighboring complex via C-H...O [C22-H22...O16, 2.947(10) Å; C29-H29...O12, 2.918(7) Å; C38-H38...O13, 2.606(11) Å; C39-H39...O13, 3.153(9) Å] and C-H... π [C21-H21... π , 3.456(5) Å] interactions. These different non-covalent interactions among host molecules cause the formation of cavity to accommodate the guest (Hphen) as shown in Fig. 2.13a and 2.13b. It is also observed that the hydrogen atoms of the coordinated deprotonated water molecule (O1) is involved in extensive hydrogen bonding with the nitrogen atom (N3) of Hphen molecule present in lattice and protonated nitrogen (N4) with the coordinated oxygen (O1) of deprotonated water molecule via O1-H1A...N3, 2.197(36) Å and N4-H4A...O1, 2.058(3) Å intermolecular interactions (Fig. 2.14a and 2.14b).

Crystal structure of [Eu(2,6-DNP)₃bipyOH₂] (**2d**)

The coordination geometry in **2d** (Fig. 2.15) is same as in complex **2b** in which metal centre is coordinated with two N-atoms (N1, N2) from one bipy, six O-atoms (O2, O3, O4, O5, O6, O7) from three 2,6-DNP and one O-atom (O1) from coordinated water molecule instead of methanol molecule as compared to **2b**. A coordinated polyhedron around Eu⁺³ ion is slightly distorted tricapped trigonal prism (Fig. 2.16). The Eu-O bond distances to the nitro groups [2.348(10) - 2.663(15) Å] are greater than the phenolate groups [2.281(10) - 2.741(9) Å], while the Eu-N bond distances of coordinated bipy ligand are in the range of 2.542(9) - 2.569(10) Å. Like complex **2c**, in complex **2d** also one molecule is non-covalently hydrogen bonded to the neighboring molecule through the C-H...O [C3-H3...O8, 2.535(15) Å; C7-H7...O3, 2.668(12) Å; C9-H9...O4, 2.651(14) Å; C9-H9...O11, 2.671(16) Å and O...O [O1...O5, 2.994(18) Å; O1...O6, 2.609(18) Å; O1...O13, 3.023(17) Å] intermolecular interactions and resulted in the formation of two dimensional sheet like structure (Fig. 2.17).

Crystal structure of [Eu(2,6-DNP)₃bipy(OH)].Hbipy (2e)

This complex is isomorphous with the complex **2c** containing bipy ligand instead of phen (Fig. 2.18). The europium centre is eight coordinated with two N-atoms (N1, N2) from one phen, five O-atoms (O2, O3, O4, O5, O7) from three 2,6-DNP and one O-atom (O1) from coordinated water molecule. The structure also contains uncoordinated Hbipy molecule in the lattice which involve in extensive hydrogen bonding. A coordinated polyhedron around Eu⁺³ ion is distorted square-antiprism; atoms N1, O2, O3, O7 and N2, O1, O4, O5 form upper and lower square planes, respectively (Fig. 2.19). The Eu-O bond distances to the nitro groups are in the range of 2.565(25) Å and 2.562(50) Å, while the Eu-O distances to the phenolate groups are in the range of 2.279(16) - 2.314(24) Å. The Eu-N bond distances of coordinated bipy ligands are 2.568(35) - 2.595(40) Å which is slightly shorter than in complex **2c**. The crystal packing shows that the C-H...O [C9-H9...O14, 2.475(35) Å; C13-H13...O13, 3.047(29) Å; C14-H14...O13, 3.095(49) Å; C27-H27...O16, 2.387(32) Å] and C-H...π [C27-H27...π, 3.440(64) Å] non-covalent interactions between one host to other give spiral packing with cavity (Fig. 2.20a and 2.20b). The cavity is occupied by Hbipy through different non-covalent interactions viz., O1-H1A...N4, 2.037(16) Å and N3-H3A...O1, 2.142(27) Å (Fig. 2.21a and 2.21b).

Crystal structure of [Gd(phen)₂(NO₃)₃] (2f)

Single crystal X-ray studies reveal that the complex **2f** crystallizes in a monoclinic space group C 2/c (Z = 4). The molecular structure is shown in Fig. 2.22. The analysis demonstrated that the complex is monomeric where gadolinium atom is coordinated by four nitrogen atoms of two bidentate phenanthroline ligands and six oxygen atoms from three nitrate ions having coordination number ten. A coordinated polyhedron around Gd⁺³ ion is bicapped square-antiprism; atoms N1, N2, O1, O4 form upper and lower square planes, respectively which are capped by oxygen atoms (O2) (Fig. 2.23). The Gd-O bond distances are in the range of 2.481(6) - 2.542(31) Å, while the Gd-N bond distances of coordinated phen ligands are 2.526(12) - 2.582(6) Å. The structural analysis shows that one mononuclear complex non-covalently hydrogen bonded to the neighboring complexes via C-H...O [C3-H3...O1, 2.746(15) Å; C4-H4...O5, 2.469(9) Å; C8-H8...O1, 2.578(6) Å; C12-H12...O1, 2.789(19) Å] interactions and resulted in the formation of sheet like network (Fig. 2.24).

Crystal structure of [Gd(2,6-DNP)₃phenCH₃OH] (2g)

Fig. 2.25 shows the coordination geometry and atom labeling in the crystal structure of complex **2g**, whose unit cell consists of one gadolinium ion, three 2,6-dinitrophenol, one phenanthroline and one methanol molecule. The structural feature of complex is that the presence of three 2,6-DNP ligands coordinated in bidentate fashion directly to the metal ion. The skeletal structure around the Gd(III) ion forms a slightly distorted tri-capped trigonal prism. The oxygen atoms of nitro groups, O_n (3,4,6) lie close enough to the metal atom to be considered to have a significant bidentate interaction. Therefore, Gd(III) ion forms three six-membered chelate rings with each 2,6-DNP through an O_n (3,4,6) atom of the nitro group and an O_p (2,5,7) atom of the phenolate group; in the chelate rings, O_p (2,5,7)-Gd-O_n(3,4,6) lie around 54°. Fig. 2.26 shows the coordination polyhedron of the Gd(III) ion of the complex. The Gd-O bond distances to the nitro groups are in the range of 2.490(2) - 2.697(3) Å, while the Gd-O bond distances to the phenolate groups are in the range of 2.272(4) - 2.307(2) Å. The average Gd-O bond distance to the nitro group is 2.571 Å, whereas the average Gd-O bond distance to the phenolate group is 2.291 Å. The Gd-N bond distances of coordinated phen ligands are in the range of 2.554(4) - 2.589(2) Å. One unit cell consist of four mononuclear unit of gadolinium which are hydrogen bonded to each other via C-H...π and π...π intermolecular interactions. C-H...π interactions are very weak which are in the range of 3.755 Å, while π...π interactions are 3.480 Å as shown in Fig. 2.27. Other non-covalent interactions are O...O which are in the range of 2.976(4) – 2.986(5) Å. All these intermolecular interactions are involved in the formation of two dimensional structures (Fig. 2.28).

Crystal structure of [Gd(2,6-DNP)₃phen(OH)]₂·(Hphen)₂ (2h)

The crystal structure for complex **2h** is presented in Fig. 2.29. The structural feature of complex **2h** is that three 2,6-DNP and one deprotonated water molecules are coordinated directly to the gadolinium atom in the inner coordination sphere, while one protonated phenanthroline is freely occupied in lattice. A coordinated polyhedron around Gd⁺³ ion is distorted square-antiprism; atoms N1, O1, O3, O5 and N2, O2, O4, O6 form upper and lower square planes, respectively (Fig. 2.30). The Gd-O bond distances to the nitro groups are in the range of 2.523(13) - 2.539(11) Å, while the Gd-O distances to the phenolate groups are in the range of 2.227(14) - 2.318(14) Å. Gd-O6 bond distances [2.227(14) Å] is shorter than the Gd-O2 [2.318(14) Å] and Gd-O5 [2.277(11) Å]. The average Gd-O bond distance to the phenolate group and nitro group is 2.274 Å and 2.531 Å, respectively. The Gd-N bond distances of

coordinated phen ligands are in the range of 2.542(11) - 2.568(12) Å which is very similar to Gd-N bond distance of **2g**. The crystal packing shows that one mononuclear complex intermolecularly hydrogen bonded to the neighboring complex via C-H...O [C2-H2...O29, 2.397(16) Å; C3-H3...O29, 3.272(14) Å; C28-H28...O26, 2.540(1) Å; C29-H29...O19, 2.818(15) Å; C44-H44...O11, 3.102(17) Å; C45-H45...O11, 2.897(17) Å; C57-H57...O10, 2.882(19) Å; C57-H57...O16, 2.782(18) Å] interactions. The different non-covalent interactions among host molecules create a cavity for the guest Hphen as shown in Fig. 2.31a and 2.31b. The hydrogen atoms of the coordinated deprotonated water molecule shows the extensive hydrogen bonding with the nitrogen atom of Hphen molecule present in lattice and protonated nitrogen with the coordinated oxygen of deprotonated water molecule [(i) O1-H1A...N10, 1.960(14) Å; O17-H17A...N11, 2.113(13) Å; (ii) N12-H12...O1, 2.078(9) Å; N9-H9A...O17, 2.053(8) Å]. The protonated phen molecule also hydrogen bonded to the host molecule via C32-H32...O7, 2.611(13) Å; C33-H33...O7, 3.188(11) Å and C33-H33...O8, 2.983(19) Å non-covalent interactions (Fig. 2.32a and 2.32b). All these intermolecular interactions are involved in making the host-guest supramolecular motif.

Crystal structure of [Gd(2,6-DNP)₃bipy(OH)].Hbipy (2j**)**

This compound crystallizes in the triclinic space group P-1 ($Z = 2$). The molecular structure, shown in Fig. 2.33, reveals a central gadolinium atom situated in a coordination sphere composed of five oxygen and two nitrogen atoms from 2,6-DNP and bipy ligands, respectively. The coordination geometry is completed with one oxygen atom from deprotonated water molecule. The structure also contains uncoordinated Hbipy molecule in the lattice which involve in extensive hydrogen bonding. The coordination polyhedron, shown in Fig. 2.34, can be described as a distorted square antiprism. The Gd-O bond distances to the nitro groups are in the range of 2.531(6) Å and 2.561(3) Å, while the Gd-O distances to the phenolate groups are in the range of 2.279(6) - 2.305(3) Å. The Gd-N bond distances of coordinated bipy ligands are 2.533(4) - 2.589(4) Å. The crystal packing shows that the C-H...O [C3-H3...O13, 2.702(3) Å; C4-H4...O12, 2.648(5) Å; C15-H15...O5, 2.453(4) Å; C7-H7A...O12, 2.731(6) Å; C25-H25...O16, 2.396(4) Å] and C-H... π [C3-H3... π , 3.421(9) Å; C7-H7A... π , 3.444(9) Å] interactions between host molecules help to create a cavity as shown in Fig. 2.35a and 2.35b. This cavity is occupied by Hbipy through different non-covalent interactions viz., O15-H35...N9, 2.179(55) Å; N10-H10...O15, 2.028(1) Å; C38-H38...O6, 2.559(3) Å and C38-H38... π , 3.288(9) Å as shown in Fig. 2.36a and 2.36b.

Thermal analysis

To check the thermal stability of the complexes in solid state, TGA of representative complexes **2a-2j** are recorded (Fig. 2.37 - 2.38) and thermal decomposition data are given in Table 2.20. Thermogravimetric analysis indicated that complexes **2a-2j** are stable up to about 100 °C but at higher temperatures, curves showed irregular pattern until plateau reached in between 700 and 800 °C due to the formation of thermally stable lanthanide oxide (Ln_2O_3). According to TG curve, thermal decomposition process of complex **2a** can be divided into three stages. The first weight loss of 4.31% between 114.0 and 134.0 °C corresponds to the release of methanol molecule. The second weight loss 28.40% was observed in between 189.0 and 238.0 °C may be due to the release of one phenanthroline molecule. The third weight loss of 44.45% corresponds to the release of another phenanthroline and three chloride molecules. The above pattern of degradation was also supported by the differences in different bond lengths (Table 2.19). The complexes **2b**, **2g** show the same pattern of thermal decomposition in TG curve, exhibited three well-separated weight loss stages. In first step, one methanol molecule with ~ 3.2% mass loss (106-133 °C) in complex **2b**, ~ 3.02% mass loss (142-186 °C) in complex **2g** leaves out, while one phen molecule (178-234 °C) with 20.17% mass loss for **2b**, (336-400 °C) with 19.53% mass loss for **2g** release in next second step. In third stage, three 2,6-DNP molecules are released with 58.77% and 59.31% weight loss in complex **2b** and **2g**, respectively. The complexes **2c**, **2h** with host-guest structures follow the similar constellation in TG curve and decomposition occurs in five well separated stages. The first weight loss of 1.64% (151-154 °C), 1.43% (136-142 °C) occurred due to the loss of deprotonated water molecule in complex **2c** and **2h**, respectively. The second weight loss of 16.72% (154-275 °C) and 17.48% (142-300 °C) corresponds to the loss of non-coordinated Hphen molecule, whereas the third weight loss of 17.04%, 17.67% was due the release of another coordinated phen molecule in **2c** and **2h**, respectively. One 2,6-DNP molecule releases between 309-441 °C (~15.85% mass loss) and 342-536 °C (~15.99% mass loss), while another two 2,6-DNP release between 441-496 °C (~33.44%), 539-609 °C (~32.01%) in **2c** and **2h**, respectively. The complexes **2d**, **2i** decompose in three different steps including removal of coordinated water molecule in first step with 1.98% mass loss (107-132 °C) and 1.79% mass loss (151-179 °C), whereas phen molecule releases in the temperature range of 178-232 °C with 16.38% mass loss, 295-401 °C with 16.21% mass loss, respectively. In third stage, three 2,6-DNP molecules are released with 59.21% and 60.69% weight loss in complex **2d** and **2i**, respectively. The

complexes **2e**, **2j** follow the same thermal decomposition pattern and occur in five well separated stages. The first weight loss of 1.72% (151-154 °C), 1.57% (138-146 °C) occurred due to the loss of deprotonated water molecule in complex **2e** and **2j**, respectively. The second weight loss of 14.13% (154-279 °C) and 14.39% (146-301 °C) corresponds to the loss of non-coordinated Hbipy molecule, whereas the third weight loss of 14.68%, 14.23% was due the release of another coordinated bipy molecule in complex **2e** and **2j**, respectively. One 2,6-DNP molecule releases between 300-447 °C (~16.96% mass loss) and 350-549 °C (~16.16% mass loss), while another two 2,6-DNP release between 447-486 °C (~34.53%), 549-613 °C (~33.87%) in **2e** and **2j**, respectively. The release of 2,6-DNP molecules in two stages may be correlated with different europium–oxygen bond lengths of coordinated 2,6-DNP and their coordination mode. The TG curve indicates that complex **2f** decomposes immediately after melting and the decomposition continues up to 435 °C with about 81.9% weight loss, corresponds to release of two molecules of phen and three molecules of coordinated nitrates.

The kinetics of thermal decomposition of these complexes was evaluated using fourteen mechanism based kinetic models, shown in Table 2.21. Different parameters such as slope, correlation coefficients etc. were calculated by different models, and with the help of these parameters activation energy for thermal decomposition were also calculated (Fig. 2.39 and 2.42). In the model fitting method, the kinetics is analyzed by choosing a “best fit” model based on the value of correlation coefficient r close to 1. Since the kinetics was done in very lower range of α , values of activation energies (E_a) obtained from different models for a particular sample are nearly equal. As reported in Table 2.22-2.23, the order of activation energies obtained from isoconversional method for europium (Eu) and gadolinium (Gd) complexes follow the same order. It is difficult to assign a single value of E_a to a particular process taking place in such a complex solid state decomposition. The isoconversional method shows that the thermolysis of these complexes is not as simple as indicated by model fitting method. As can be seen from Fig. 2.40 and 2.43, for a particular complex, each activation energy has separate value at different α . It is true [31] that energetic materials appear to have reaction characteristics that are generally consistent with the isoconversional principle as long as the confinement conditions are constant and appropriate to the intended application. Moreover, these complexes have been found to be stable at room temperature, but experience has shown that when subjected sudden to high temperature, they ignite.

Following equation

$$dQ_H/dt = d_H/dt - dq/dt \dots\dots\dots(1)$$

Where dQ_H/dt is the net rate of heat gain in the system, d_H/dt is the rate of heat produced by pre-ignition reactions, dq/dt is the rate of heat dissipation.

Ignition will occur when

$$Q_H = H' \dots\dots\dots (2)$$

Where H' = minimum amount of heat required to raise the temperature of the system to the point of ignition. From eq.ⁿ (2), it follows that

$$Q_H = H - q \dots\dots\dots (3)$$

Where H = total heat produced by pre-ignition reactions. The ignition would occur only if

$$H - q \geq H'$$

The total heat produced by the pre-ignition reactions must be greater than H' by the amount of heat dissipated. Thus

$$H = H' + q \dots\dots\dots (4)$$

The following equation was derived by Freeman and Gordon [32].

$$t_{id} = Ae^{\Delta H^*/RT} \dots\dots\dots (5)$$

Where ΔH^* is the heat of activation and is approximately equal to activation energy (E^*). If the activities of the reactants do not change significantly during pre-ignition reactions, the log of the time of ignition should be a linear function of the reciprocal of the absolute temperature, and the relation comes out to be as given in Eq.ⁿ. (5).

Ignition delay and activation energy in the temperature range 400-460 °C for complexes **2a-2e** and 410-450 °C for complexes **2f-2j** are reported in Table 2.24-2.25. E_a values obtained from the kinetic analysis data, suggest that this could be thermal stability order which is also following the same trend. The difference in activation energy (E_a) for complexes

obtained from kinetic analysis is much greater than from ignition delay (E_a^*). This is due to sudden heating in ignition delay. The activation energy for ignition (E_a^*) of both europium and gadolinium complexes **2a-2j** are in decreasing order, $[M(2,6-DNP)_3phen(OH)].Hphen > [M(2,6-DNP)_3bipy(OH)].Hbipy > [M(2,6-DNP)_3phenCH_3OH] > [M(2,6-DNP)_3bipyOH_2] > [Eu(phen)_2Cl_3CH_3OH] / [Gd(phen)_2(NO_3)_3]$, ($M = Eu, Gd$). E_a^* was determined from the slope of a plot of $\ln(D_i)$ vs. $1/T$ as shown in Fig. 2.41 and 2.44. The highest value of D_i and E_a^* for complex **2c/2h** and **2e/2j** suggests that these are the most stable due to the more non-covalent interactions between the mononuclear complex and protonated 1,10-phenanthroline and 2,2'-bipyridine molecules present in the lattice of these complexes. From the above calculation, it is clear that the value of activation energy for Gd complexes is higher than that of Eu. This may be attributed to the half-filled valence shell electronic configuration of Gd^{+3} ion (f^7 system) and the greater electronic charge density on Gd atom than Eu [33]. The OB values reported in Table 2.24-2.25, suggest that these complexes belong to low explosives.

CONCLUSION

We have reported first time the pH dependent host-guest complexes of Ln(III) [Eu, Gd]. At pH 6-7, the coordination number of complex is nine but at pH 4-5 the coordination number reduce to eight and contain a guest molecule in lattice which are protonated as we know that the phen/bipy ligands are more stronger base than the water molecule i.e. these ligands have more tendency to get the proton than water [34]. The greater coordination number in complex **2b**, **2d**, **2g**, **2i** may also be responsible for non host-guest structure of the complexes. The presence of a maximum number of non-covalent interactions in **2c**, **2e**, **2h**, **2j** may be responsible for the creation of a pseudocavity for trapping the guest molecule and assembled a three dimensional supramolecular architecture. The thermal studies carried out using non-isothermal and isothermal TG in air, provide an understanding of the nature of energetic complexes during thermal analysis i.e. thermal decomposition occurs in multistage and the corresponding metal oxides were found to be formed. The isoconversional method shows that the mechanism of thermal decomposition changes as the reaction proceeds. The thermal stability is found in the order $Gd > Eu$.

Table 2.1: Crystal data and structure refinement for [Eu(phen)₂Cl₃CH₃OH] (2a)

Empirical formula	C ₂₅ H ₁₉ Cl ₃ N ₄ OEu*
Color	Colorless
Formula weight (g mol ⁻¹)	649.76
Crystal System	orthorhombic
Space Group	P 21 21 21
a (Å)	11.079(5)
b (Å)	11.677(6)
c (Å)	18.431(9)
α (°)	90.00
β (°)	90.00
γ (°)	90.00
V (Å ³)	2384.8(2)
Crystal size (mm)	0.27 x 0.21 x 0.17
Z	4
ρ _{calcd} (g m ⁻³)	1.810
μ	2.993
F (000)	1276
θ range for data collection	2.06-29.54
limiting indices	-15 ≤ h ≤ 10 -16 ≤ k ≤ 16 -25 ≤ l ≤ 22
No. of measured reflections	6654
No. of observed reflections	6104
Data/ restraints/parameters	6654/0/298
*R1 (I > 2σ(I))	0.043
R1 (all data)	0.050
*wR2 (I > 2σ(I))	0.129
wR2 (all data)	0.138

$$^*R1 = \frac{\sum ||F_o| - |F_c||}{\sum |F_o|}, wR2 = \left\{ \frac{\sum [w(F_o^2 - F_c^2)^2]}{\sum w(F_o^2)^2} \right\}^{1/2}$$

* Hydrogen is not added on methanol molecule

Table 2.2: Selected Bond Distances (Å) and Bond Angles (°) for [Eu(phen)₂Cl₃CH₃OH] (2a)

Bond Distances

Eu1—N1	2.627(6)	Eu1—O1	2.497(5)
Eu1—N2	2.642(6)	Eu1—Cl1	2.700(2)
Eu1—N3	2.588(6)	Eu1—Cl2	2.673(2)
Eu1—N4	2.581(6)	Eu1—Cl3	2.742(2)

Bond Angles

N1—Eu1—N2	63.03(17)	N4—Eu1—Cl1	138.07(13)
N1—Eu1—Cl1	75.25(13)	N4—Eu1—Cl2	84.47(13)
N1—Eu1—Cl2	82.07(13)	N4—Eu1—Cl3	71.48(13)
N2—Eu1—Cl2	142.41(13)	O1—Eu1—N1	133.00(17)
N2—Eu1—Cl3	70.37(13)	O1—Eu1—N2	141.24(17)
N3—Eu1—N1	138.72(17)	O1—Eu1—N3	71.57(16)
N3—Eu1—N2	78.25(17)	O1—Eu1—N4	70.32(18)
N3—Eu1—Cl1	83.72(13)	O1—Eu1—Cl1	74.91(12)
N3—Eu1—Cl2	138.68(13)	O1—Eu1—Cl2	73.28(12)
N3—Eu1—Cl3	102.85(13)	O1—Eu1—Cl3	139.45(11)
N4—Eu1—N1	146.64(17)	Cl1—Eu1—Cl3	145.54(5)
N4—Eu1—N2	116.79(17)	Cl2—Eu1—Cl1	107.33(5)
N4—Eu1—N3	63.72(17)	Cl2—Eu1—Cl3	90.07(5)

Table 2.3: Crystal data and structure refinement for [Eu(2,6-DNP)₃phenCH₃OH] (2b)

Empirical formula	C ₃₁ H ₂₁ N ₈ O ₁₆ Eu
Color	Yellow
Formula weight (g mol ⁻¹)	913.53
Crystal System	Monoclinic
Space Group	P 21/n
a (Å)	9.998(12)
b (Å)	17.253(19)
c (Å)	19.296(2)
α (°)	90.00
β (°)	91.39(6)
γ (°)	90.00
V (Å ³)	3327.6(6)
Crystal size (mm)	0.31 x 0.23 x 0.18
Z	4
ρ _{calcd} (g m ⁻³)	1.824
μ	1.977
F (000)	1816
θ range for data collection	1.58-33.28
limiting indices	-14 ≤ h ≤ 15 -26 ≤ k ≤ 26 -29 ≤ l ≤ 29
No. of measured reflections	12499
No. of observed reflections	8672
Data/ restraints/parameters	12499/0/506
R1 (I > 2σ(I))	0.034
R1 (all data)	0.063
wR2 (I > 2σ(I))	0.121
wR2 (all data)	0.138

Table 2.4: Selected Bond Distances (Å) and Bond Angles (°) for [Eu(2,6-DNP)₃phen CH₃OH] (2b)

Bond Distances

Eu1—N1	2.606(3)	Eu1—O4	2.518(3)
Eu1—N2	2.577(7)	Eu1—O	2.549(4)
Eu1—O1	2.268(7)	Eu1—O6	2.302(4)
Eu1—O2	2.782(5)	Eu1—O7	2.442(6)
Eu1—O3	2.308(2)		

Bond Angles

N1—Eu1—O2	129.10(8)	O4—Eu1—O2	65.34(9)
N2—Eu1—N1	63.15(9)	O4—Eu1—O5	72.18(9)
N2—Eu1—O2	127.51(9)	O5—Eu1—N1	99.51(9)
O1—Eu1—O2	62.72(9)	O5—Eu1—N2	71.42(9)
O1—Eu1—O3	88.46(9)	O5—Eu1—O2	131.38(9)
O1—Eu1—O4	127.84(9)	O6—Eu1—N1	74.24(8)
O1—Eu1—O5	147.12(10)	O6—Eu1—N2	111.49(8)
O1—Eu1—O6	138.87(9)	O6—Eu1—O3	132.23(8)
O1—Eu1—O7	79.9(1)	O6—Eu1—O4	74.75(8)
O3—Eu1—N1	140.95(8)	O6—Eu1—O5	65.70(8)
O3—Eu1—N2	78.88(8)	O6—Eu1—O7	68.13(9)
O3—Eu1—O2	67.75(8)	O7—Eu1—N1	80.03(9)
O3—Eu1—O4	67.73(8)	O7—Eu1—N2	140.54(9)
O3—Eu1—O5	75.24(10)	O7—Eu1—O2	65.93(9)
O3—Eu1—O7	132.44(9)	O7—Eu1—O4	83.67(9)
O4—Eu1—N1	148.53(8)	O7—Eu1—O5	131.93(10)
O4—Eu1—N2	135.48(9)		

Table 2.5: Crystal data and structure refinement for [Eu(2,6-DNP)₃phen(OH)].Hphen (2c)

Empirical formula	C ₄₂ H ₂₇ N ₁₀ O ₁₆ Eu
Color	Yellow
Formula weight (g mol ⁻¹)	1079.71
Crystal System	Triclinic
Space Group	P -1
a (Å)	12.089(11)
b (Å)	13.004(12)
c (Å)	14.650(14)
α (°)	91.03(2)
β (°)	103.16(2)
γ (°)	109.79(3)
V (Å ³)	2098.8(3)
Crystal size (mm)	0.26 x 0.24 x 0.17
Z	2
ρ _{calcd} (g m ⁻³)	1.709
μ	1.583
F (000)	1104
θ range for data collection	1.85-27.99
limiting indices	-15 ≤ h ≤ 13 -9 ≤ k ≤ 17 -19 ≤ l ≤ 19
No. of measured reflections	9574
No. of observed reflections	7715
Data/ restraints/parameters	9574/0/630
R1 (I > 2σ(I))	0.037
R1 (all data)	0.052
wR2 (I > 2σ(I))	0.088
wR2 (all data)	0.096

**Table 2.6: Selected Bond Distances (Å) and Bond Angles (°) for [Eu(2,6-DNP)₃phen(OH)].
Hphen (2c)**

Bond Distances

Eu1—N1	2.588(4)	Eu1—O3	2.555(3)
Eu1—N2	2.569(4)	Eu1—O4	2.236(6)
Eu1—O1	2.364(6)	Eu1—O5	2.543(5)
Eu1—O2	2.289(4)	Eu1—O6	2.313(4)

Bond Angles

N2—Eu1—N1	63.45(10)	O4—Eu1—O1	151.39(11)
O1—Eu1—N1	79.24(9)	O4—Eu1—O2	96.30(12)
O1—Eu1—N2	77.42(10)	O4—Eu1—O3	71.44(10)
O2—Eu1—N1	142.57(10)	O4—Eu1—O5	137.60(12)
O2—Eu1—N2	79.26(11)	O4—Eu1—O6	104.76(12)
O2—Eu1—O1	90.14(10)	O5—Eu1—N1	134.65(9)
O2—Eu1—O3	67.02(9)	O5—Eu1—N2	136.36(10)
O2—Eu1—O5	71.83(9)	O5—Eu1—O3	66.43(8)
O2—Eu1—O6	135.28(11)	O6—Eu1—N1	80.91(11)
O3—Eu1—N1	140.96(9)	O6—Eu1—N2	143.63(11)
O3—Eu1—N2	129.54(9)	O6—Eu1—O1	89.57(11)
O4—Eu1—N1	78.79(12)	O6—Eu1—O3	82.84(10)
O4—Eu1—N2	76.47(12)	O6—Eu1—O5	65.96(11)

Table 2.7: Crystal data and structure refinement for [Eu(2,6-DNP)₃bipyOH₂] (2d)

Empirical formula	C ₂₈ H ₁₇ N ₈ O ₁₆ Eu
Color	Yellow
Formula weight (g mol ⁻¹)	873.47
Crystal System	Monoclinic
Space Group	P 21/c
a (Å)	6.988(12)
b (Å)	23.961(4)
c (Å)	18.979(3)
α (°)	90.00
β (°)	100.61
γ (°)	90.00
V (Å ³)	3123.5(9)
Crystal size (mm)	0.32 x 0.26 x 0.23
Z	4
ρ _{calcd} (g m ⁻³)	1.857
μ	2.102
F (000)	1782
θ range for data collection	1.38-29.91
limiting indices	-9 ≤ h ≤ 4 -25 ≤ k ≤ 33 -26 ≤ l ≤ 25
No. of measured reflections	6813
No. of observed reflections	3889
Data/ restraints/parameters	6813/0/517
R1 (I > 2σ(I))	0.096
R1 (all data)	0.127
wR2 (I > 2σ(I))	0.297
wR2 (all data)	0.309

* Hydrogen is not added on water molecule.



Table 2.8: Selected Bond Distances (Å) and Bond Angles (°) for [Eu(2,6-DNP)₃bipyOH₂] (2d)

Bond Distances

Eu1—O1	2.449(9)	Eu1—O6	2.348(10)
Eu1—O2	2.301(12)	Eu1—O7	2.741(9)
Eu1—O3	2.663(15)	Eu1—N1	2.542(9)
Eu1—O4	2.566(9)	Eu1—N2	2.569(10)
Eu1—O5	2.281(10)		

Bond Angles

N1—Eu1—N2	63.43(30)	O4—Eu1—N2	142.89(30)
N1—Eu1—O3	81.82(38)	O4—Eu1—O3	71.51(36)
N1—Eu1—O4	153.26(30)	O4—Eu1—O7	121.17(29)
N2—Eu1—O3	143.18(36)	O4—Eu1—C23	69.70(32)
N2—Eu1—O7	65.57(29)	O5—Eu1—N1	135.17(33)
N2—Eu1—C23	119.63(32)	O5—Eu1—N2	83.39(32)
O1—Eu1—N1	123.16(34)	O5—Eu1—O1	72.03(33)
O1—Eu1—N2	76.91(34)	O5—Eu1—O2	138.85(38)
O1—Eu1—O4	72.70(36)	O5—Eu1—O3	132.69(39)
O1—Eu1—O3	116.56(39)	O5—Eu1—O4	67.41(32)
O1—Eu1—O7	129.63(32)	O5—Eu1—O6	85.60(33)
O1—Eu1—C23	131.66(32)	O5—Eu1—O7	71.40(31)
O2—Eu1—N1	77.47(37)	O5—Eu1—C23	66.16(32)
O2—Eu1—N2	96.39(36)	O6—Eu1—N1	91.39(34)
O2—Eu1—O1	67.95(39)	O6—Eu1—N2	127.42(33)
O2—Eu1—O3	62.66(42)	O6—Eu1—O1	145.35(34)
O2—Eu1—O4	91.56(36)	O6—Eu1—O3	61.21(39)
O2—Eu1—O6	123.75(39)	O6—Eu1—O4	74.39(34)
O2—Eu1—O7	145.14(35)	O6—Eu1—O7	62.18(32)
O2—Eu1—C23	140.73(37)	O6—Eu1—C23	19.53(33)
O3—Eu1—O7	113.62(35)	O7—Eu1—C23	55.90(31)
O3—Eu1—C23	78.50(38)		

Table 2.9: Crystal data and structure refinement for [Eu(2,6-DNP)₃bipy(OH)].Hbipy (2e)

Empirical formula	C ₃₈ H ₂₇ N ₁₀ O ₁₆ Eu
Color	Yellow
Formula weight (g mol ⁻¹)	1031.67
Crystal System	Triclinic
Space Group	P -1
a (Å)	12.192(5)
b (Å)	12.927(5)
c (Å)	14.378(5)
α (°)	88.62(3)
β (°)	82.67(3)
γ (°)	63.80(2)
V (Å ³)	2015.2(14)
Crystal size (mm)	0.36 x 0.24 x 0.18
Z	2
ρ _{calcd} (g m ⁻³)	1.700
μ	1.644
F (000)	1032
θ range for data collection	1.89-23.87
limiting indices	-14 ≤ h ≤ 14 -15 ≤ k ≤ 15 -17 ≤ l ≤ 17
No. of measured reflections	7110
No. of observed reflections	3330
Data/ restraints/parameters	7110/0/588
R1 (I>2σ(I))	0.060
R1 (all data)	0.128
wR2 (I>2σ(I))	0.136
wR2 (all data)	0.186

Table 2.10: Selected Bond Distances (Å) and Bond Angles (°) for [Eu(2,6-DNP)₃bipy(OH)]·Hbipy (2e)

Bond Distances

Eu1—N1	2.568(35)	Eu1—O3	2.565(25)
Eu1—N2	2.595(40)	Eu1—O4	2.562(50)
Eu1—O1	2.401(58)	Eu1—O5	2.314(24)
Eu1—O2	2.279(16)	Eu1—O7	2.295(44)

Bond Angles

N2—Eu1—N1	63.10(32)	O4—Eu1—O3	65.05(32)
N2—Eu1—O3	145.46(34)	O5—Eu1—N1	143.40(38)
N2—Eu1—O4	132.18(32)	O5—Eu1—N2	80.60(37)
O1—Eu1—O3	131.70(34)	O5—Eu1—O1	89.09(37)
O1—Eu1—O4	68.48(33)	O5—Eu1—O3	83.59(38)
O2—Eu1—N1	79.57(36)	O5—Eu1—O4	65.58(36)
O2—Eu1—N2	141.72(36)	O7—Eu1—N1	75.60(39)
O2—Eu1—O1	87.09(34)	O7—Eu1—N2	84.08(36)
O2—Eu1—O3	66.50(34)	O7—Eu1—O1	154.43(37)
O2—Eu1—O4	71.37(35)	O7—Eu1—O2	95.12(39)
O2—Eu1—O5	134.98(41)	O7—Eu1—O3	71.33(37)
O3—Eu1—N1	129.25(34)	O7—Eu1—O4	136.21(38)
O4—Eu1—N1	137.39(33)	O7—Eu1—O5	106.64(42)

Table 2.11: Crystal data and structure refinement for [Gd(phen)₂(NO₃)₃] (2f)

Empirical formula	C ₂₄ H ₁₆ N ₇ O ₉ Gd
Color	Colorless
Formula weight (g mol ⁻¹)	703.69
Crystal System	Monoclinic
Space Group	C 2/c
a (Å)	11.177(7)
b (Å)	17.883(12)
c (Å)	12.999(9)
α (°)	90.00
β (°)	100.34(2)
γ (°)	90.00
V (Å ³)	2556(3)
Crystal size (mm)	0.25 x 0.19 x 0.14
Z	4
ρ _{calcd} (g m ⁻³)	1.829
μ	2.663
F (000)	1380
θ range for data collection	2.17-35.27
limiting indices	-16 ≤ h ≤ 17 -26 ≤ k ≤ 25 -18 ≤ l ≤ 20
No. of measured reflections	4245
No. of observed reflections	2993
Data/ restraints/parameters	4245/0/187
R1 (I>2σ(I))	0.054
R1 (all data)	0.098
wR2 (I>2σ(I))	0.144
wR2 (all data)	0.207

Table 2.12: Selected Bond Distances (Å) and Bond Angles (°) for [Gd(phen)₂(NO₃)₃] (2f)

Bond Distances

Gd1—N1 ¹	2.526(12)	Gd1—O1	2.481(6)
Gd1—N1	2.526(12)	Gd1—O2 ¹	2.542(31)
Gd1—N2 ¹	2.582(6)	Gd1—O2	2.542(31)
Gd1—N2	2.582(6)	Gd1—O4 ¹	2.491(6)
Gd1—O1 ¹	2.481(6)	Gd1—O4	2.491(6)

Bond Angles

O1 ¹ —Gd1—O1	142.75(19)	O4—Gd1—O2	103.99(23)
O1 ¹ —Gd1—O4 ¹	71.51(20)	N1 ¹ —Gd1—O2	69.61(19)
O1—Gd1—O4 ¹	74.97(20)	N1—Gd1—O2	69.61(19)
O1 ¹ —Gd1—O4	74.97(20)	O2 ¹ —Gd1—O2	171.60(22)
O1 ¹ —Gd1—O4	74.97(20)	O1 ¹ —Gd1—N2 ¹	142.12(19)
O4 ¹ —Gd1—O4	50.98(18)	O1—Gd1—N2 ¹	74.91(20)
O1 ¹ —Gd1—N1 ¹	72.35(18)	O4 ¹ —Gd1—N2 ¹	136.67(18)
O1—Gd1—N1 ¹	120.40(18)	O4—Gd1—N2 ¹	140.15(18)
O4 ¹ —Gd1—N1 ¹	84.86(23)	N1 ¹ —Gd1—N2 ¹	84.27(17)
O4—Gd1—N1 ¹	131.55(20)	N1—Gd1—N2 ¹	64.75(17)
O1 ¹ —Gd1—N1	120.40(18)	O2 ¹ —Gd1—N2 ¹	118.83(19)
O1—Gd1—N1	72.35(18)	O2—Gd1—N2 ¹	68.84(19)
O4 ¹ —Gd1—N1	131.55(20)	O1 ¹ —Gd1—N2	74.91(20)
O4—Gd1—N1	84.86(23)	O1—Gd1—N2	142.12(19)
N1 ¹ —Gd1—N1	142.94(17)	O4 ¹ —Gd1—N2	140.15(18)
O1 ¹ —Gd1—O2 ¹	50.80(21)	O4—Gd1—N2	136.67(18)
O1—Gd1—O2 ¹	125.82(21)	N1 ¹ —Gd1—N2	64.75(17)
O4 ¹ —Gd1—O2 ¹	103.99(23)	N1—Gd1—N2	84.27(17)
O4—Gd1—O2 ¹	68.03(22)	O2 ¹ —Gd1—N2	68.84(19)
N1 ¹ —Gd1—O2 ¹	113.26(19)	O2—Gd1—N2	118.83(19)
N1—Gd1—O2 ¹	69.61(19)	N2 ¹ —Gd1—N2	68.18(17)
O1 ¹ —Gd1—O2	125.82(21)	O1 ¹ —Gd1—N3 ¹	25.87(18)
O1—Gd1—O2	50.80(21)	N2i—Gd1—N3i	134.57(18)
O1—Gd1—N3 ¹	139.61(19)	N2—Gd1—N3i	69.92(19)
O4 ¹ —Gd1—N3 ¹	87.85(21)	N3—O1—Gd1	97.11(41)
O4—Gd1—N3 ¹	69.32(20)	N3—O2—Gd1	95.52(50)
N1 ¹ —Gd1—N3 ¹	93.34(18)	N4—O4—Gd1	95.64(29)
N1—Gd1—N3 ¹	94.54(18)	C5—N1—Gd1	121.75(46)
O2 ¹ —Gd1—N3 ¹	24.93(21)	C1—N1—Gd1	119.45(38)
O2—Gd1—N3 ¹	151.06(21)	C6—N2—Gd1	123.67(45)
O4 ¹ —Gd1—O2	68.03(22)	C10—N2—Gd1	116.53(39)

Table 2.13: Crystal data and structure refinement for [Gd(2,6-DNP)₃phenCH₃OH] (2g)

Empirical formula	C ₃₁ H ₂₁ N ₈ O ₁₆ Gd
Color	Yellow
Formula weight (g mol ⁻¹)	918.81
Crystal System	Monoclinic
Space Group	P 21/n
a (Å)	9.765(9)
b (Å)	17.139(14)
c (Å)	19.271(16)
α (°)	90.00
β (°)	91.51(3)
γ (°)	90.00
V (Å ³)	3224.6(5)
Crystal size (mm)	0.33 x 0.27 x 0.19
Z	4
ρ _{calcd} (g m ⁻³)	1.893
μ	2.152
F (000)	1820.0
θ range for data collection	1.59-31.86
limiting indices	-14 ≤ h ≤ 14 -25 ≤ k ≤ 25 -28 ≤ l ≤ 28
No. of measured reflections	11064
No. of observed reflections	9003
Data/ restraints/parameters	11064/0/495
R1 (I > 2σ(I))	0.030
R1 (all data)	0.044
wR2 (I > 2σ(I))	0.093
wR2 (all data)	0.11

Table 2.14: Selected Bond Distances (Å) and Bond Angles (°) for [Gd(2,6-DNP)₃phen CH₃OH] (2g)

Bond Distances

Gd1—N1	2.589(2)	Gd1—O4	2.490(2)
Gd1—N2	2.554(4)	Gd1—O5	2.307(2)
Gd1—O1	2.415(3)	Gd1—O6	2.697(3)
Gd1—O2	2.296(3)	Gd1—O7	2.272(4)
Gd1—O3	2.527(2)		

Bond Angles

O7—Gd1—O2	137.57(7)	O1—Gd1—N1	80.09(7)
O7—Gd1—O5	89.35(7)	O4—Gd1—N1	148.30(7)
O2—Gd1—O5	132.91(7)	O3—Gd1—N1	100.00(6)
O7—Gd1—O1	80.27(7)	N2—Gd1—N1	63.53(7)
O2—Gd1—O1	68.09(7)	O7—Gd1—O6	64.23(6)
O5—Gd1—O1	133.00(7)	O2—Gd1—O6	121.33(6)
O7—Gd1—O4	129.86(7)	O5—Gd1—O6	68.51(6)
O2—Gd1—O4	75.06(7)	O1—Gd1—O6	65.69(6)
O5—Gd1—O4	68.53(7)	O4—Gd1—O6	65.83(6)
O1—Gd1—O4	83.55(6)	O3—Gd1—O6	131.24(6)
O7—Gd1—O3	146.61(7)	N2—Gd1—O6	127.74(6)
O2—Gd1—O3	65.94(6)	N1—Gd1—O6	128.74(6)
O5—Gd1—O3	74.77(7)	N5—O3—Gd1	136.80(16)
O1—Gd1—O3	131.82(6)	N4—O4—Gd1	136.46(17)
O4—Gd1—O3	71.59(6)	C18—O5—Gd1	137.24(17)
O7—Gd1—N2	76.93(7)	C22—O7—Gd1	139.17(18)
O2—Gd1—N2	110.90(7)	N8—O6—Gd1	128.40(15)
O5—Gd1—N2	77.92(7)	C27—O1—Gd1	132.72(16)
O1—Gd1—N2	141.15(7)	C9—N1—Gd1	124.01(18)
O4—Gd1—N2	134.93(7)	C11—N1—Gd1	117.38(16)
O3—Gd1—N2	71.16(6)	C1—N2—Gd1	122.38(18)
O7—Gd1—N1	73.61(7)	C4—N2—Gd1	118.57(16)
O2—Gd1—N1	73.69(7)	C17—O2—Gd1	137.60(17)
O5—Gd1—N1	140.28(7)		

Table 2.15: Crystal data and structure refinement for [Gd(2,6-DNP)₃phen(OH)]₂·(Hphen)₂ (2h)

Empirical formula	C ₈₄ H ₅₄ N ₂₀ O ₃₂ Gd ₂
Color	Yellow
Formula weight (g mol ⁻¹)	2169.95
Crystal System	Triclinic
Space Group	P 1
a (Å)	12.044(15)
b (Å)	13.021(15)
c (Å)	14.660(16)
α (°)	90.76(7)
β (°)	103.23(7)
γ (°)	109.60(6)
V (Å ³)	2098.1(4)
Crystal size (mm)	0.33x 0.24 x 0.17
Z	2
ρ _{calcd} (g m ⁻³)	1.717
μ	1.670
F (000)	1082
θ range for data collection	2.04 - 39.48
limiting indices	-21 ≤ h ≤ 21 -16 ≤ k ≤ 23 -24 ≤ l ≤ 26
No. of measured reflections	31281
No. of observed reflections	21486
Data/ restraints/parameters	31281 /3/1235
R1 (I>2σ(I))	0.035
R1 (all data)	0.063
wR2 (I>2σ(I))	0.095
wR2 (all data)	0.120

Table 2.16: Selected Bond Distances (Å) and Bond Angles (°) for [Gd(2,6-DNP)₃phen(OH)]₂·(Hphen)₂ (2h)

Bond Distances

Gd1—N1	2.544(12)	Gd2—N13	2.568(13)
Gd1—N2	2.579(13)	Gd2—N14	2.555(12)
Gd1—O1	2.375(16)	Gd2—O17	2.351(16)
Gd1—O2	2.318(14)	Gd2—O18	2.285(13)
Gd1—O3	2.523(13)	Gd2—O19	2.547(11)
Gd1—O4	2.539(11)	Gd2—O20	2.525(13)
Gd1—O5	2.277(11)	Gd2—O21	2.285(13)
Gd1—O6	2.227(14)	Gd2—O22	2.253(14)

Bond Angles

O6—Gd1—O5	99.75(32)	O22—Gd2—O21	104.81(39)
O6—Gd1—O2	99.87(37)	O22—Gd2—O18	95.39(36)
O5—Gd1—O2	135.29(36)	O21—Gd2—O18	135.96(39)
O6—Gd1—O1	152.01(32)	O22—Gd2—O17	151.19(31)
O5—Gd1—O1	90.01(31)	O21—Gd2—O17	90.46(30)
O2—Gd1—O1	91.03(32)	O18—Gd2—O17	89.88(31)
O6—Gd1—O3	136.80(32)	O22—Gd2—O20	138.09(34)
O5—Gd1—O3	71.53(26)	O21—Gd2—O20	66.37(33)
O2—Gd1—O3	66.66(34)	O18—Gd2—O20	72.41(31)
O1—Gd1—O3	71.18(29)	O17—Gd2—O20	70.37(28)
O6—Gd1—O4	71.18(29)	O22—Gd2—O19	71.27(31)
O5—Gd1—O4	67.45(28)	O21—Gd2—O19	82.23(32)
O2—Gd1—O4	81.7(3)	O18—Gd2—O19	67.69(31)
O1—Gd1—O4	136.34(26)	O17—Gd2—O19	136.03(26)
O3—Gd1—O4	66.41(26)	O20—Gd2—O19	66.99(26)
O6—Gd1—N1	78.57(32)	O22—Gd2—N14	75.90(33)
O5—Gd1—N1	79.47(31)	O21—Gd2—N14	143.76(34)
O2—Gd1—N1	143.94(34)	O18—Gd2—N14	78.75(33)
O1—Gd1—N1	77.54(27)	O17—Gd2—N14	77.42(26)
O3—Gd1—N1	136.71(29)	O20—Gd2—N14	136.18(28)
O4—Gd1—N1	129.55(27)	O19—Gd2—N14	129.61(28)
O6—Gd1—N2	77.09(30)	O22—Gd2—N13	78.98(33)
O5—Gd1—N2	143.12(27)	O21—Gd2—N13	80.80(33)
O2—Gd1—N2	80.60(33)	O18—Gd2—N13	142.19(33)
O1—Gd1—N2	79.41(29)	O17—Gd2—N13	79.59(27)
O3—Gd1—N2	134.73(25)	O20—Gd2—N13	134.42(28)
O4—Gd1—N2	140.14(28)	O19—Gd2—N13	140.44(28)
N1—Gd1—N2	63.80(29)	N14—Gd2—N13	63.56(28)

Table 2.17: Crystal data and structure refinement for [Gd(2,6-DNP)₃bipy(OH)].Hbipy (2j)

Empirical formula	C ₃₈ H ₂₇ N ₁₀ O ₁₆ Gd
Color	Yellow
Formula weight (g mol ⁻¹)	1036.95
Crystal System	Triclinic
Space Group	P -1
a (Å)	11.849(7)
b (Å)	12.964(7)
c (Å)	14.227(7)
α (°)	88.51(3)
β (°)	82.08(3)
γ (°)	63.60(3)
V (Å ³)	1937.83(18)
Crystal size (mm)	0.32X0.26X0.21
Z	2
ρ _{calcd} (g m ⁻³)	1.777
μ	1.803
F (000)	1034
θ range for data collection	1.75 - 37.65
limiting indices	-20 ≤ h ≤ 20
	-22 ≤ k ≤ 22
	-24 ≤ l ≤ 21
No. of measured reflections	20419
No. of observed reflections	17485
Data/ restraints/parameters	20419 /0/590
R1 (I>2σ(I))	0.031
R1 (all data)	0.042
wR2 (I>2σ(I))	0.087
wR2 (all data)	0.10

Table 2.18: Selected Bond Distances (Å) and Bond Angles (°) for [Gd(2,6-DNP)₃bipy(OH)].Hbipy (2j)

Bond Distances

Gd1—N1	2.553(4)	Gd1—O3	2.561(3)
Gd1—N2	2.589(4)	Gd1—O4	2.531(6)
Gd1—O1	2.350(6)	Gd1—O5	2.305(3)
Gd1—O2	2.288(2)	Gd1—O6	2.279(6)

Bond Angles

O6—Gd1—O2	100.84(5)	N1—Gd1—O3	127.85(5)
O6—Gd1—O5	98.44(6)	O6—Gd1—N2	82.18(5)
O2—Gd1—O5	136.41(6)	O2—Gd1—N2	141.30(5)
O6—Gd1—O1	155.32(5)	O5—Gd1—N2	79.82(5)
O2—Gd1—O1	85.87(5)	O1—Gd1—N2	78.06(5)
O5—Gd1—O1	92.49(6)	O4—Gd1—N2	132.53(5)
O6—Gd1—O4	133.68(5)	N1—Gd1—N2	62.58(5)
O2—Gd1—O4	71.58(5)	O3—Gd1—N2	145.46(5)
O5—Gd1—O4	66.83(5)	C11—O5—Gd1	139.68(14)
O1—Gd1—O4	70.99(5)	N4—O4—Gd1	133.71(13)
O6—Gd1—N1	78.58(5)	C17—O2—Gd1	142.79(13)
O2—Gd1—N1	80.05(6)	N5—O3—Gd1	136.96(12)
O5—Gd1—N1	142.38(6)	C23—O6—Gd1	141.66(12)
O1—Gd1—N1	79.26(5)	Gd1—O1—H2	115.76(271)
O4—Gd1—N1	139.80(5)	Gd1—O1—H1	119.39(403)
O6—Gd1—O3	70.19(5)	C1—N1—Gd1	118.44(13)
O2—Gd1—O3	66.68(5)	C5—N1—Gd1	122.91(11)
O5—Gd1—O3	84.07(5)	C10—N2—Gd1	119.53(13)
O1—Gd1—O3	133.30(5)	C6—N2—Gd1	122.04(11)
O4—Gd1—O3	64.90(5)		

Table 2.19: Non-covalent interactions for 2a, 2c-2f, 2h, 2j (Å and °)

S.N	D-H...A	d(D-H)	d(H-A)	d(D-A)	<(DHA)>
1.	[Eu(phen)₂Cl₃CH₃OH] (2a)				
	C12-H12...Cl1	0.930(7)	2.782(2)	3.457	130.2
	C13-H13...Cl1	0.930(7)	2.643(2)	3.533	160.6
	C20-H20...Cl1	0.930(7)	2.639(2)	3.527	159.8
	C23-H23...Cl1	0.930(7)	2.728(2)	3.555	148.7
	C1-H1...Cl2	0.931(8)	2.736(2)	3.382	127.2
	C14-H14...Cl2	0.930(7)	2.658(1)	3.580	171.5
	C21-H21...Cl2	0.930(7)	2.809(2)	3.489	130.8
	C28-H28B...Cl2	0.960(7)	2.869(2)	3.803	164.6
	C11-H11...Cl3	0.929(8)	2.775(2)	3.487	134.1
2.	[Eu(2,6-DNP)₃phen(OH)].Hphen (2c)				
	O1-H1A...N3	0.645(33)	2.197(36)	2.829	166.8
	N4-H4A...O1	0.860(3)	2.058(3)	2.788	142.3
	C9-H9...O7	0.931(7)	2.422(7)	3.249	147.9
	C22-H22...O16	0.930(6)	2.947(10)	3.366	108.9
	C31-H31...O8	0.930(7)	2.581(6)	3.284	132.7
	C29-H29...O12	0.930(7)	2.918(7)	3.661	137.8
	C38-H38...O13	0.93(1)	2.606(11)	3.353	137.7
	C39-H39...O13	0.931(9)	3.153(9)	3.628	113.7
3.	[Eu(2,6-DNP)₃bipyOH₂] (2d)				
	C3-H3...O8	0.932(24)	2.535(15)	3.398	154.1
	C7-H7...O3	0.932(20)	2.668(12)	3.447	141.4
	C9-H9...O4	0.931(11)	2.651(14)	3.345	131.8
	C9-H9...O11	0.931(11)	2.671(16)	3.469	144.2
	C12-H12A...O12	0.931(22)	2.609(18)	3.265	127.9
4.	[Eu(2,6-DNP)₃bipy(OH)].Hbipy (2e)				
	O1-H1A...N4	0.819(4)	2.037(16)	2.820	159.9
	N3-H3A...O1	0.860(2)	2.142(27)	2.861	140.8
	C13-H13...O13	0.932(29)	3.047(29)	3.682	126.7
	C14-H14...O13	0.927(29)	3.095(49)	3.686	123.2
	C9-H9...O14	0.930(23)	2.475(35)	3.367	160.7
	C27-H27...O16	0.931(25)	2.387(32)	3.278	160.1
5.	[Gd(phen)₂(NO₃)₃] (2f)				
	C3-H3...O1	0.929(8)	2.746(15)	3.478	136.3
	C4-H4...O5	0.931(8)	2.469(9)	3.315	151.2
	C8-H8...O1	0.931(9)	2.578(6)	3.503	172.5
	C12-H12...O1	0.930(1)	2.789(19)	3.495	133.6

6.	[Gd(2,6-DNP)₃phen(OH)]₂·(Hphen)₂ (2h)				
	O1-H1A...N10	0.820(1)	1.960(14)	2.749	160.9
	O17-H17A...N11	0.820(8)	2.113(13)	2.873	153.8
	N12-H12...O1	0.860(11)	2.078(9)	2.779	138.2
	N9-H9A...O17	0.860(8)	2.053(8)	2.812	146.7
	C2-H2...O29	0.930(2)	2.397(16)	3.211	146.1
	C3-H3...O29	0.930(19)	3.272(14)	3.660	107.4
	C28-H28...O26	0.930(15)	2.540(1)	3.225	130.7
	C29-H29...O19	0.930(2)	2.818(15)	3.582	140.1
	C32-H32...O7	0.929(33)	2.611(13)	3.341	135.7
	C33-H33...O7	0.932(20)	3.188(11)	3.663	113.6
	C33-H33...O8	0.932(20)	2.983(19)	3.682	132.9
	C44-H44...O11	0.929(19)	3.102(17)	3.641	118.7
	C45-H45...O11	0.931(16)	2.897(17)	3.538	127.1
	C57-H57...O10	0.930(16)	2.882(19)	3.071	92.81
	C57-H57...O16	0.930(16)	2.782(18)	3.564	142.3
7.	[Gd(2,6-DNP)₃bipy(OH)]·Hbipy (2j)				
	O15-H35...N9	0.610(53)	2.179(55)	2.782	169.7
	N10-H10...O15	0.859(2)	2.028(1)	2.768	143.8
	C3-H3...O13	0.930(3)	2.702(3)	3.334	125.9
	C4-H4...O12	0.929(3)	2.648(5)	3.610	162.7
	C7-H7A...O12	0.930(2)	2.731(6)	3.456	157.9
	C15-H15...O5	0.930(3)	2.453(4)	3.249	143.6
	C25-H25...O16	0.930(3)	2.396(4)	3.301	164.2
	C38-H38...O6	0.929(3)	2.559(3)	3.189	125.4

Table 2.20: TG-DTG phenomenological data of 2a-2j under air atmosphere

S. N	Stage	DTG peak (Temp. °C)	Mass loss (%)		Constituents lost
			obs.	calc.	
1.	[Eu(phen)₂Cl₃CH₃OH] (2a)				
	I.	154.0 °C	4.31	4.80	one methanol molecule
	II.	376.0 °C	28.40	29.90	one phenanthroline
	III.	501.0 °C	44.45	44.90	one phenanthroline, three chlorides
2.	[Eu(2,6-DNP)₃phenCH₃OH] (2b)				
	I.	114.0 °C	3.2	3.5	one methanol molecule
	II.	237.0 °C	20.17	21.6	one phenanthroline
	III.	455.0 °C	58.77	59.89	Three 2,6-DNP molecules
3.	[Eu(2,6-DNP)₃phen(OH)].Hphen (2c)				
	I.	153.0 °C	1.64	1.66	one deprotonated water molecule
	II.	204.0 °C	16.72	18.31	protonated phen (noncoordinated)
	III.	299.0 °C	17.04	18.31	one phenanthroline
	IV.	398.0 °C	15.85	16.89	one 2,6-DNP molecule
	V.	464.0 °C	33.44	33.98	Two 2,6-DNP molecules
4.	[Eu(2,6-DNP)₃bipyOH₂] (2d)				
	I.	116.0 °C	1.98	2.1	one water molecule
	II.	227.0 °C	16.38	17.56	one bipyridine
	III.	443.0 °C	59.21	61.8	Three 2,6-DNP molecules
5.	[Eu(2,6-DNP)₃bipy(OH)].Hbipy (2e)				
	I.	155.0 °C	1.72	1.74	one deprotonated water molecule
	II.	214.0 °C	14.13	15.13	protonated bipy (noncoordinated)
	III.	297.0 °C	14.68	15.13	one bipyridine
	IV.	381.0 °C	16.96	17.79	one 2,6-DNP molecule
	V.	458.0 °C	34.53	35.5	Two 2,6-DNP molecules
6.	[Gd(phen)₂(NO₃)₃] (2f)				
	I.	432.0 °C	81.9	82.7	Two phen, Three nitrates
7.	[Gd(2,6-DNP)₃phenCH₃OH] (2g)				
	I.	151.0 °C	3.02	3.48	one methanol molecule
	II.	382.0 °C	19.53	21.5	one phenanthroline
	III.	591.0 °C	59.31	60.07	Three 2,6-DNP molecules
8.	[Gd(2,6-DNP)₃phen(OH)]₂.(Hphen)₂ (2h)				
	I.	139.0 °C	1.43	1.56	one deprotonated water molecule
	II.	271.0 °C	17.48	18.36	protonated phen (noncoordinated)
	III.	367.0 °C	17.67	18.27	one phenanthroline
	IV.	529.0 °C	15.99	16.96	one 2,6-DNP molecule
	V.	587.0 °C	32.01	33.92	Two 2,6-DNP molecules

9.	[Gd(2,6-DNP)₃bipyOH₂] (2i)				
	I.	167.0 °C	1.79	2.04	one water molecule
	II.	343.0 °C	16.21	17.78	one bipyridine
	III.	575.0 °C	60.69	62.82	Three 2,6-DNP molecules
10.	[Gd(2,6-DNP)₃bipy(OH)].Hbipy (2j)				
	I.	142.0 °C	1.57	1.64	one deprotonated water molecule
	II.	257.0 °C	14.39	15.15	protonated bipy (noncoordinated)
	III.	327.0 °C	14.23	15.06	one bipyridine
	IV.	467.0 °C	16.16	17.74	one 2,6-DNP molecule
	V.	591.0 °C	33.87	35.48	Two 2,6-DNP molecules

Table 2.21: Set of reaction models applied to describe thermal decomposition of solids

S. N	Reaction model	f(α)	g(α)
1.	Power law	$4 \alpha^{3/4}$	$\alpha^{1/4}$
2.	Power law	$3 \alpha^{2/3}$	$\alpha^{1/3}$
3.	Power law	$2 \alpha^{1/2}$	$\alpha^{1/2}$
4.	Power law	$2/3 \alpha^{-1/2}$	$\alpha^{3/2}$
5.	One-dimensional diffusion	$1/2 \alpha^{-1}$	α^2
6.	Mampel (first order)	$1 - \alpha$	$-\ln(1 - \alpha)$
7.	Avrami-Erofeev	$4(1 - \alpha)[-\ln(1 - \alpha)]^{3/4}$	$[-\ln(1 - \alpha)]^{1/4}$
8.	Avrami-Erofeev	$3(1 - \alpha)[-\ln(1 - \alpha)]^{2/3}$	$[-\ln(1 - \alpha)]^{1/3}$
9.	Avrami-Erofeev	$2(1 - \alpha)[-\ln(1 - \alpha)]^{1/2}$	$[-\ln(1 - \alpha)]^{1/2}$
10.	Contracting sphere	$3(1 - \alpha)^{2/3}$	$1 - (1 - \alpha)^{1/3}$
11.	Three-dimensional diffusion	$2(1 - \alpha)^{2/3}[1 - (1 - \alpha)^{1/3}]^{-1}$	$[1 - (1 - \alpha)^{1/3}]^2$
12.	Contracting cylinder	$2(1 - \alpha)^{1/2}$	$1 - (1 - \alpha)^{1/2}$
13.	Prout-Tomkins	$\alpha(1 - \alpha)$	$\ln(\alpha / 1 - \alpha)$
14.	Ginstling-Brounshtein	$3/2[(1 - \alpha)^{-1/3} - 1]^{-1}$	$[1 - (2\alpha / 3)] - (1 - \alpha)^{2/3}$

Table 2.22: Arrhenius parameters for isothermal decomposition of complexes 2a-2e

Complexes	(2a)		(2b)		(2c)		(2d)		(2e)	
	E _a	r	E _a	r	E _a	r	E _a	r	E _a	r
1	36.06	0.908	65.89	0.985	74.99	0.972	64.62	0.959	70.50	0.988
2	36.15	0.909	65.79	0.985	74.77	0.972	64.65	0.960	70.34	0.988
3	36.35	0.912	65.59	0.987	74.33	0.972	64.68	0.962	70.03	0.988
4	37.45	0.926	64.16	0.987	71.93	0.975	64.36	0.967	68.10	0.990
5	37.95	0.931	63.28	0.987	70.95	0.976	64.07	0.968	67.14	0.991
6	37.61	0.927	63.89	0.986	72.19	0.975	64.18	0.966	67.89	0.990
7	36.92	0.920	65.08	0.987	73.62	0.973	64.02	0.966	69.05	0.990
8	36.63	0.916	65.21	0.985	74.16	0.973	64.50	0.962	69.61	0.989
9	36.88	0.919	64.90	0.986	73.64	0.973	64.46	0.963	69.19	0.989
10	37.38	0.925	64.25	0.986	72.48	0.974	64.33	0.966	68.30	0.990
11	38.70	0.956	62.45	0.943	70.43	0.969	64.71	0.942	66.10	0.964
12	37.26	0.923	64.42	0.986	72.63	0.974	64.40	0.966	68.49	0.990
13	36.44	0.913	65.39	0.985	74.79	0.972	64.39	0.960	69.95	0.988
14	38.35	0.935	62.68	0.987	70.47	0.977	63.77	0.968	66.37	0.991

Table 2.23: Arrhenius parameters for isothermal decomposition of complexes 2f-2j

Complexes	(2f)		(2g)		(2h)		(2i)		(2j)	
	E _a	r	E _a	r	E _a	r	E _a	r	E _a	r
1	96.21	0.974	111.51	0.983	218.12	0.979	110.26	0.986	116.73	0.972
2	96.17	0.974	111.46	0.983	217.87	0.979	110.23	0.986	116.54	0.973
3	96.08	0.974	111.35	0.983	217.38	0.979	110.18	0.986	116.17	0.973
4	95.57	0.973	110.67	0.984	214.46	0.977	109.85	0.986	113.95	0.976
5	95.32	0.972	110.33	0.984	214.73	0.977	109.69	0.986	112.87	0.978
6	95.73	0.973	110.90	0.983	214.73	0.977	109.94	0.986	114.25	0.976
7	96.15	0.974	110.18	0.989	217.73	0.979	100.10	0.983	112.09	0.978
8	96.10	0.974	111.38	0.983	217.07	0.979	110.18	0.986	116.00	0.973
9	96.01	0.974	111.26	0.983	216.48	0.978	110.12	0.986	115.56	0.974
10	95.76	0.973	110.94	0.983	215.12	0.977	109.96	0.986	114.52	0.976
11	95.23	0.972	110.52	0.942	212.87	0.975	110.04	0.949	112.35	0.967
12	95.78	0.973	110.96	0.983	215.32	0.977	109.97	0.986	114.65	0.975
13	96.24	0.974	113.33	0.982	216.93	0.978	108.94	0.986	119.10	0.981
14	95.26	0.972	127.26	0.950	233.23	0.963	102.11	0.970	112.37	0.979

^aEnumeration of the model is as given in Table 2.21

$$E_a = \text{kJmol}^{-1}$$

Table 2.24: Ignition delay activation energy for thermal ignition (E^*) and correlation coefficient (r) for the complexes 2a-2e

S. N	D_i /s at temperature/ °C					E^* / kJmol ⁻¹ (KJ/mol)	r	OB
	400 ±1	415 ±1	430 ±1	445 ±1	460 ±1			
1.	[Eu(phen)₂Cl₃CH₃OH] (2a)							
	75	71	68	62	56	19.6	0.979	-146.51
2.	[Eu(2,6-DNP)₃phenCH₃OH] (2b)							
	92	78	71	67	63	25.0	0.977	-100.70
3.	[Eu(2,6-DNP)₃phen(OH)].Hphen (2c)							
	105	90	78	69	58	47.7	0.976	-122.26
4.	[Eu(2,6-DNP)₃bipyOH₂] (2d)							
	80	71	63	60	58	22.3	0.973	-90.46
5.	[Eu (2,6-DNP)₃bipy(OH)].Hbipy (2e)							
	100	86	78	65	57	38.4	0.995	-115.54

Table 2.25: Ignition delay activation energy for thermal ignition (E^*) and correlation coefficient (r) for the complexes 2f-2j

S. N	D_i /s at temperature/ °C					E^* / kJmol ⁻¹ (KJ/mol)	r	OB
	410 ±1	420 ±1	430 ±1	440 ±1	450 ±1			
6.	[Gd(phen)₂(NO₃)₃] (2f)							
	95	80	65	60	48	100.0	0.994	-115.96
7.	[Gd(2,6-DNP)₃phenCH₃OH] (2g)							
	82	68	59	52	40	103.0	0.991	-100.13
8.	[Gd(2,6-DNP)₃phen(OH)]₂.(Hphen)₂ (2h)							
	79	71	54	43	38	118.9	0.990	-121.66
9.	[Gd(2,6-DNP)₃bipyOH₂] (2i)							
	87	73	65	53	44	101.8	0.995	-91.74
10.	[Gd(2,6-DNP)₃bipy(OH)].Hbipy (2j)							
	76	65	512	44	36	114.1	0.997	-114.95

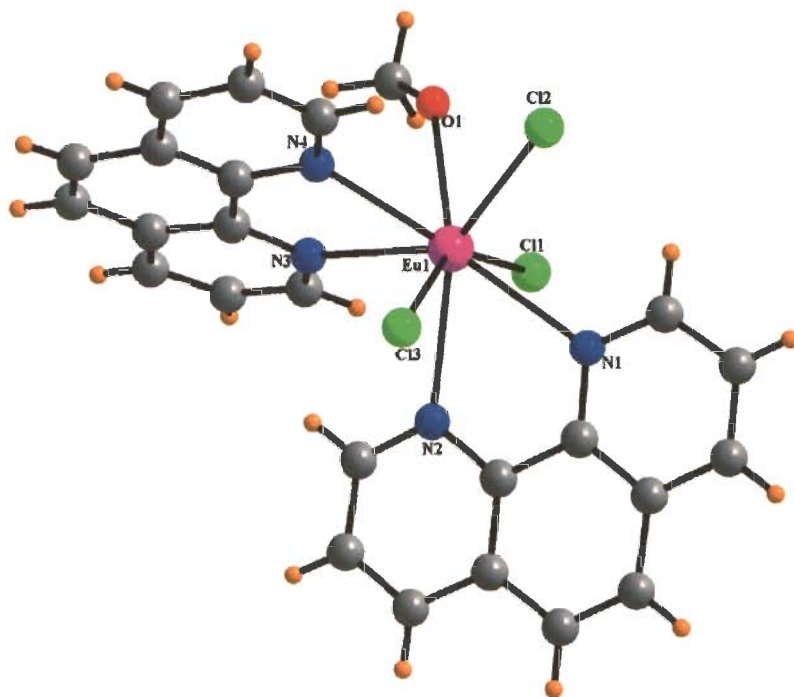


Fig. 2.4: Crystal structure of $[\text{Eu}(\text{phen})_2\text{Cl}_3\text{CH}_3\text{OH}]$ (**2a**). Color code: Eu, pink; C, grey; H, orange; O, red; N, blue; Cl, green

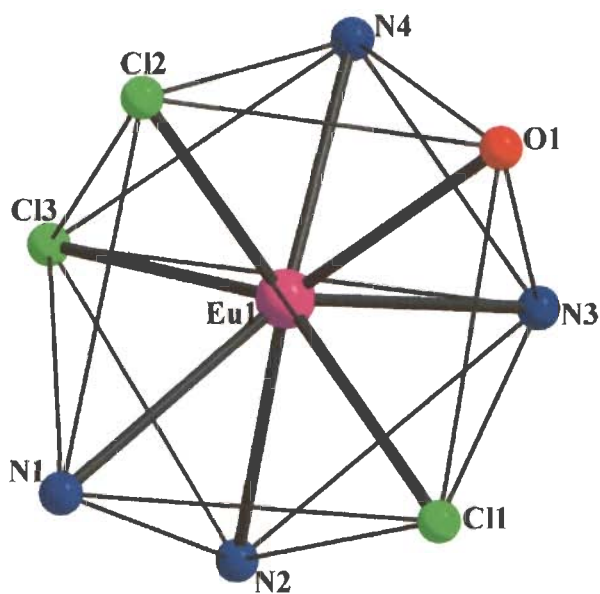


Fig. 2.5: The coordination polyhedron of the Eu^{+3} ion in **2a**. Color code: Eu, pink; O, red; N, blue; Cl, green

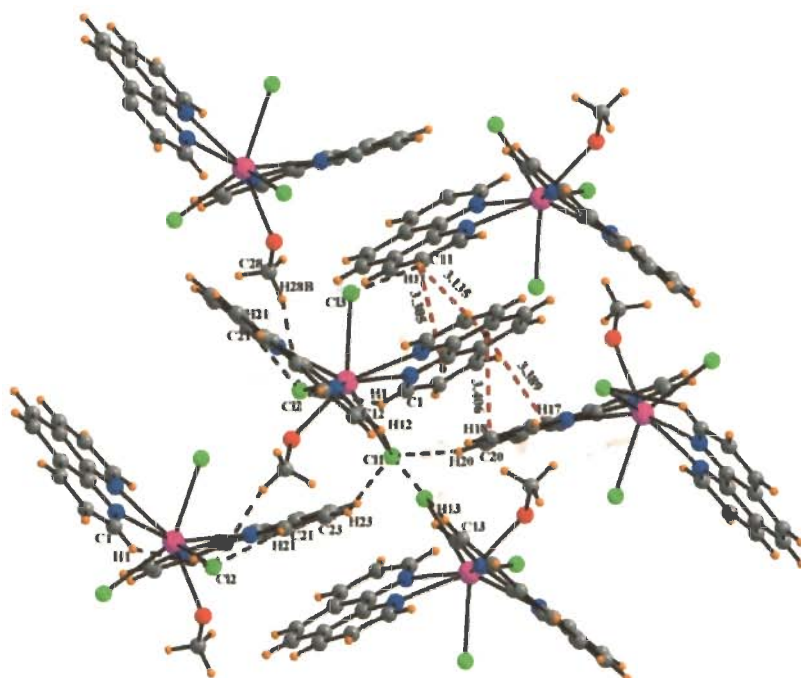


Fig. 2.6: Various C-H...Cl and C-H... π intermolecular and intermolecular interactions in **2a**. Color code: Eu, pink; C, grey; H, orange; O, red; N, blue; Cl, green

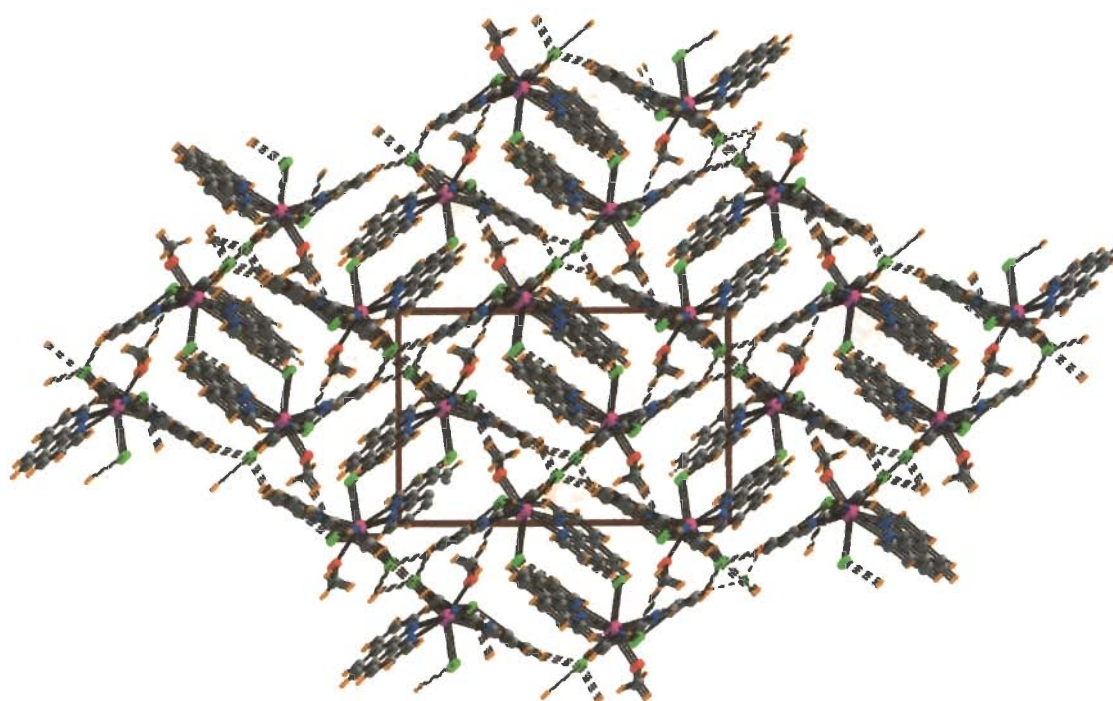


Fig. 2.7: Three dimensional pseudo host-guest structure along 'a' axis in **2a**. Color code: Eu, pink; C, grey; H, orange; O, red; N, blue; Cl, green

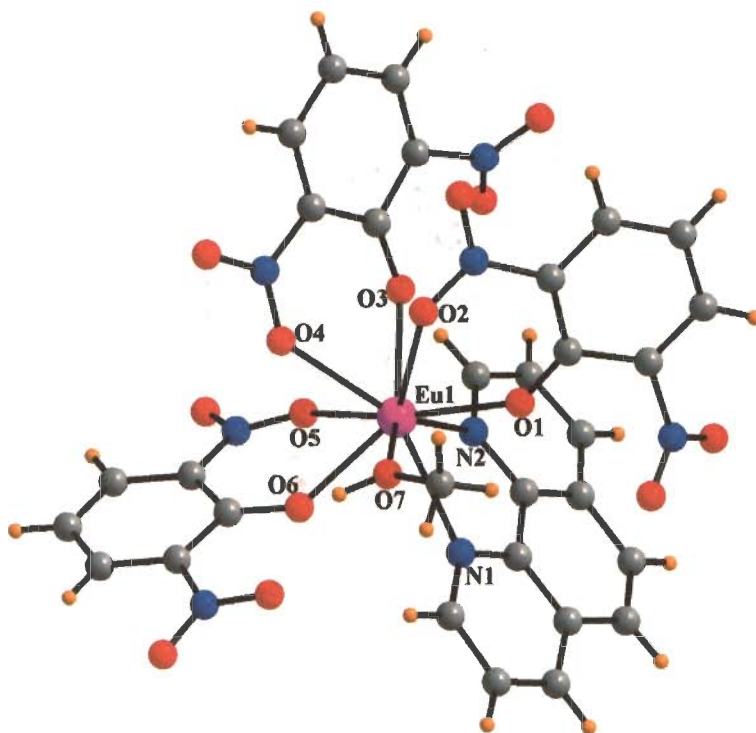


Fig. 2.8: Crystal structure of $[\text{Eu}(\text{2,6-DNP})_3\text{phenCH}_3\text{OH}]$ (**2b**). Color code: Eu, pink; C, grey; H, orange; O, red; N, blue

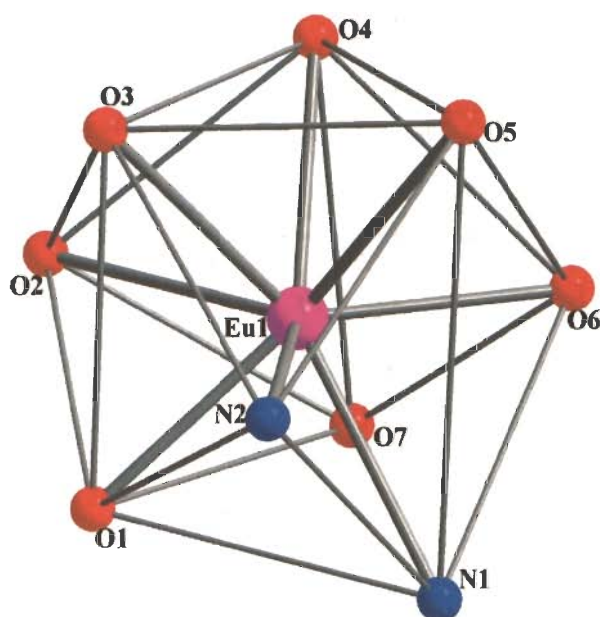


Fig. 2.9: The coordination polyhedron of the Eu^{+3} ion in **2b**. Color code: Eu, pink; O, red; N, blue

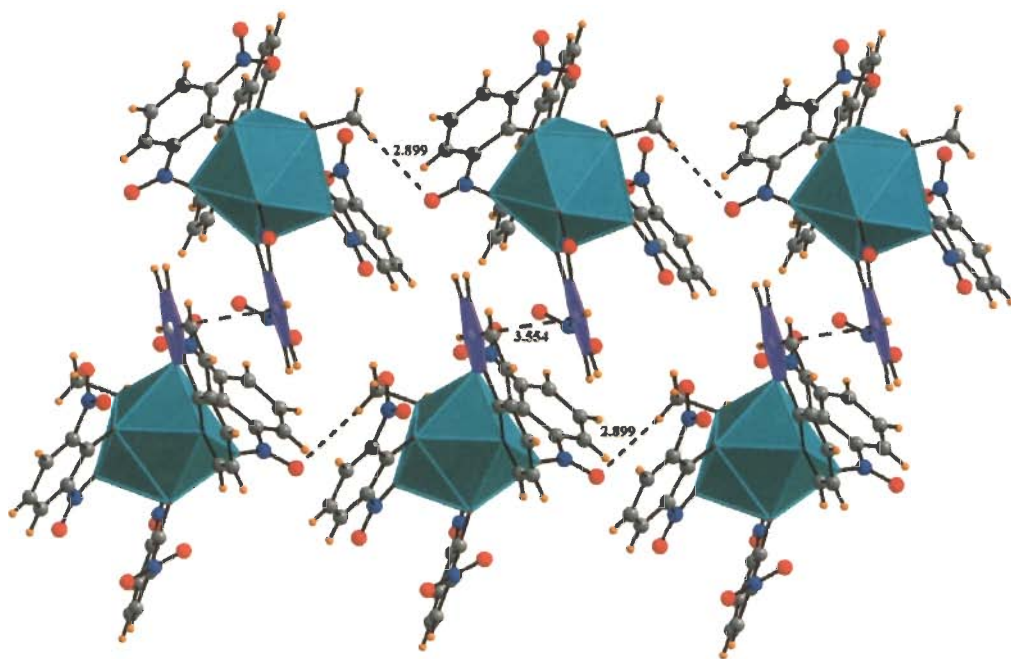


Fig. 2.10: Various C-H...O and C-H... π intermolecular interactions in **2b**. Color code: Eu, pink; C, grey; H, orange; O, red; N, blue

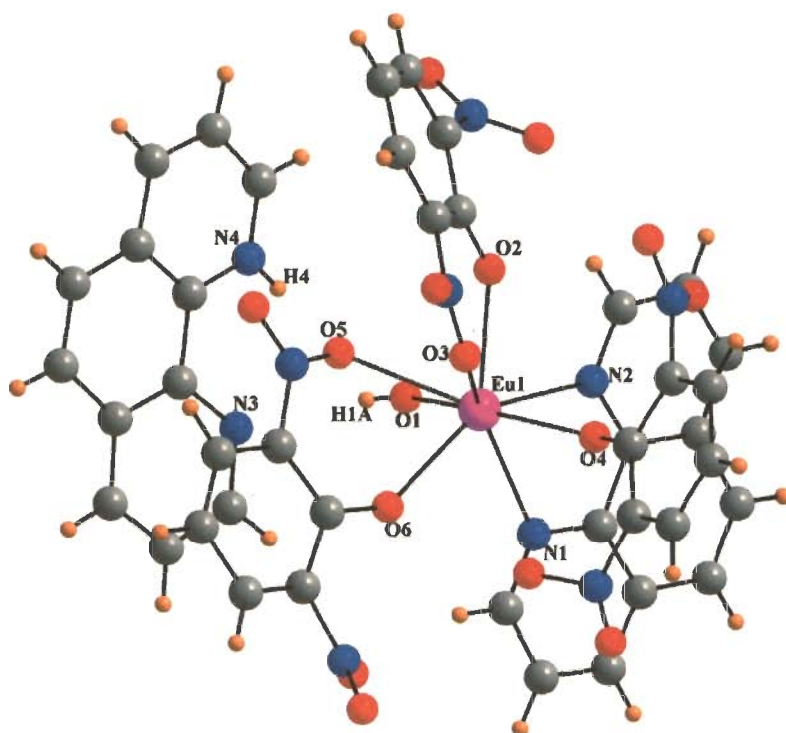


Fig. 2.11: Crystal structure of [Eu(2,6-DNP)₃phen(OH)].Hphen (**2c**). Color code: Eu, pink; C, grey; H, orange; O, red; N, blue

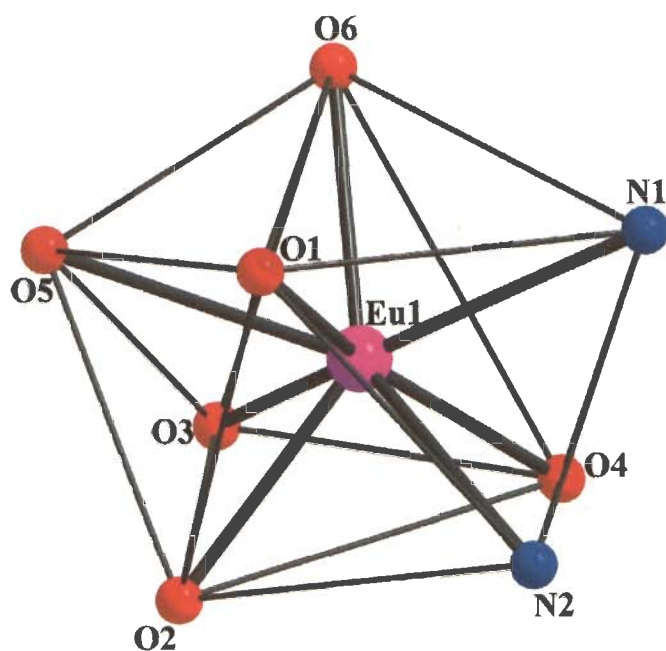


Fig. 2.12: The coordination polyhedron of the Eu^{+3} ion in **2c**. Color code: Eu, pink; O, red; N, blue

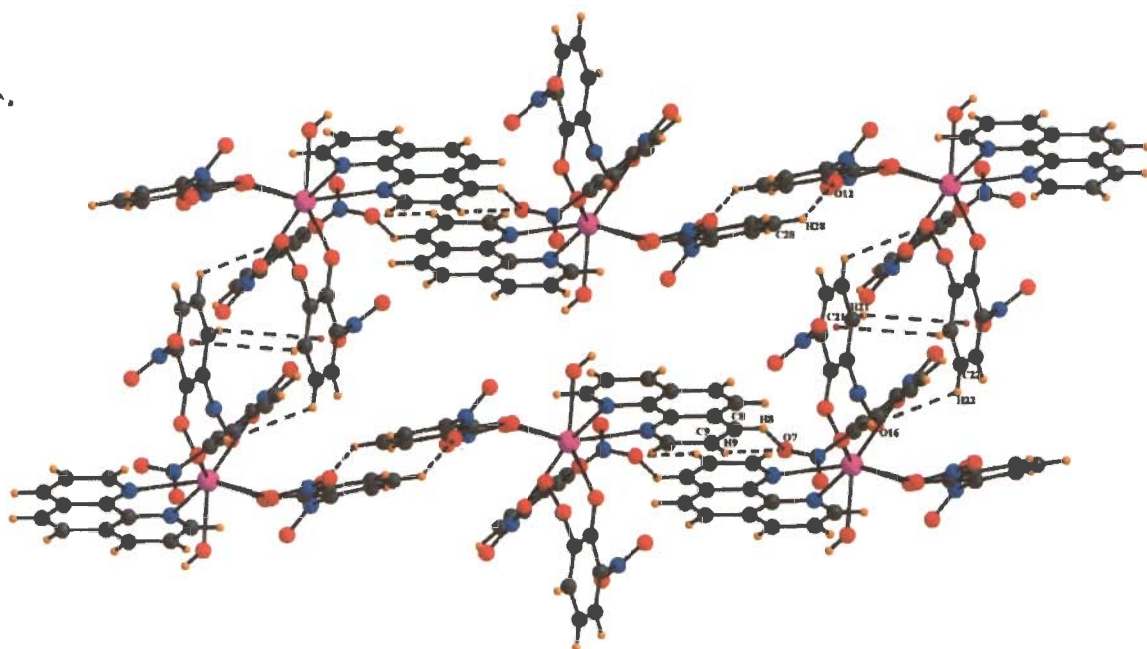
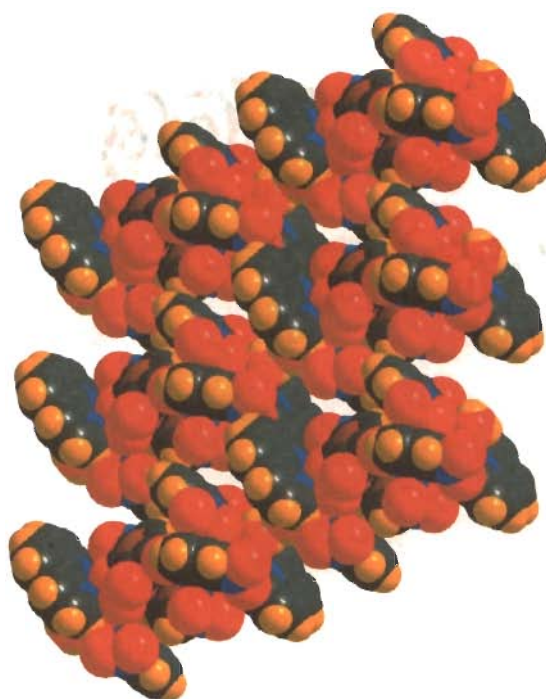


Fig. 2.13 (a): Formation of cavity among host molecules via $\text{C-H}\cdots\text{O}$ and $\text{C-H}\cdots\pi$ non-covalent interactions in **2c**. Color code: Eu, pink; C, grey; H, orange; O, red; N, blue



(b)

Fig. 2.13 (b): Space-fill model in **2c** along 'b' axis between host molecules. Color code: Eu, pink; C, grey; H, orange; O, red; N, blue

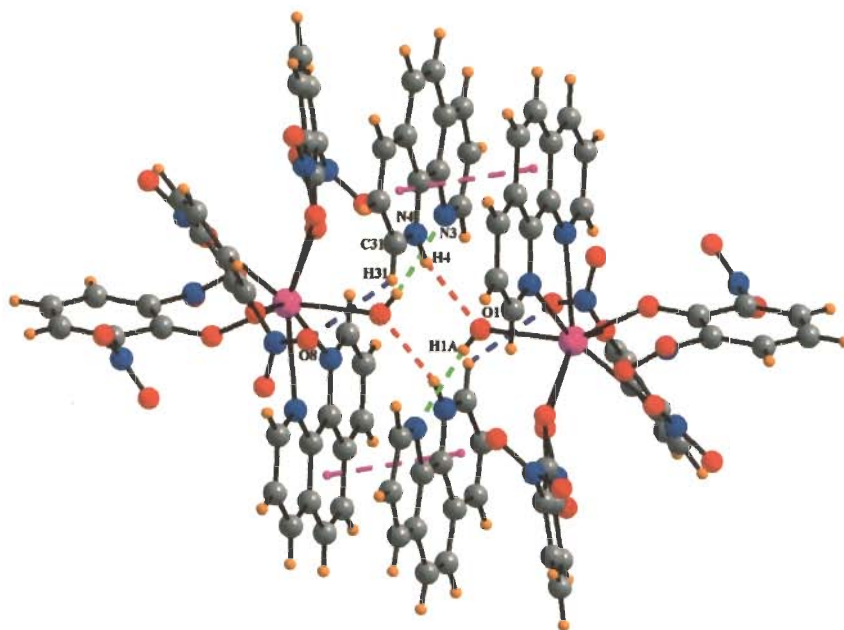
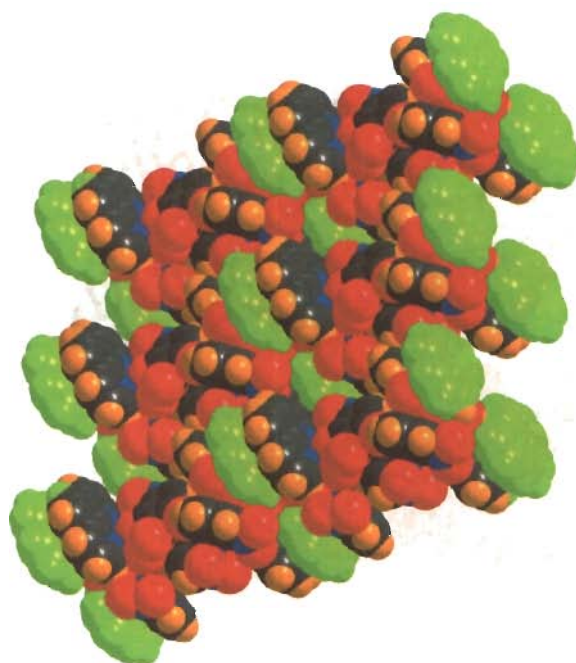


Fig. 2.14 (a): C-H...O, N-H...O, O-H...N and $\pi \cdots \pi$ non-covalent interactions between host-guest molecules in **2c**. Color code: Eu, pink; C, grey; H, orange; O, red; N, blue



(b)

Fig. 2.14 (b): Space-fill model in **2c** between host and guest molecules. Color code: Eu, pink; C, grey; H, orange; O, red; N, blue; Hphen, green

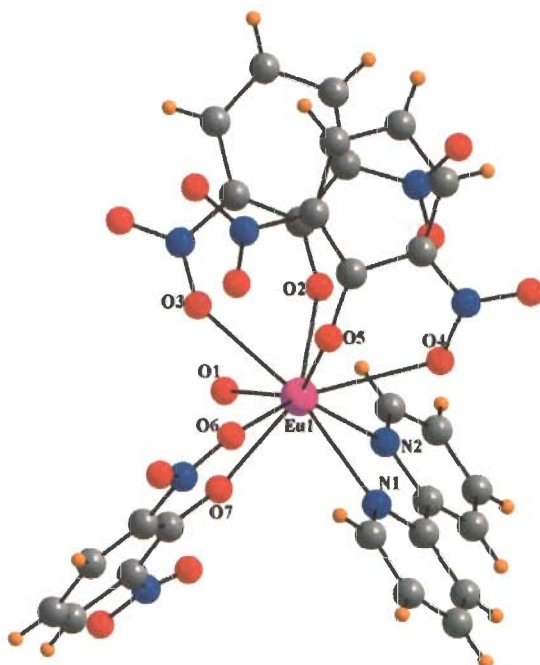


Fig. 2.15: Crystal structure of $[\text{Eu}(\text{2,6-DNP})_3\text{bipyOH}_2]$ (**2d**). Color code: Eu, pink; C, grey; H, orange; O, red; N, blue

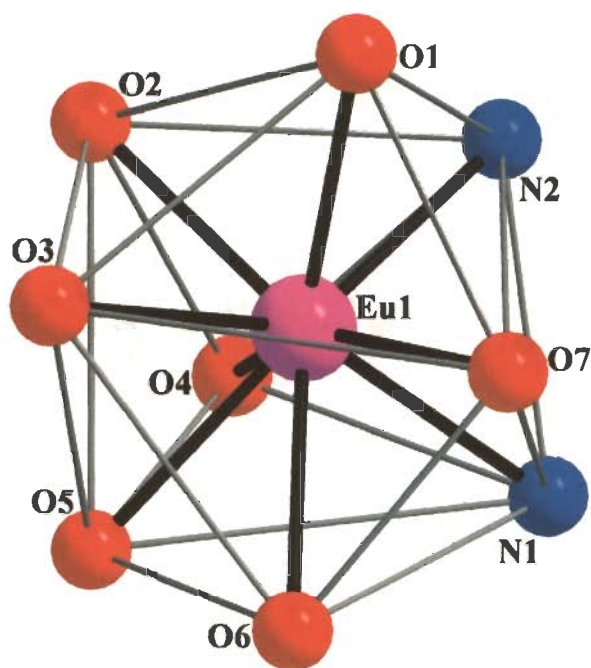


Fig. 2.16: The coordination polyhedron of the Eu^{+3} ion in **2d**. Color code: Eu, pink; O, red; N, blue

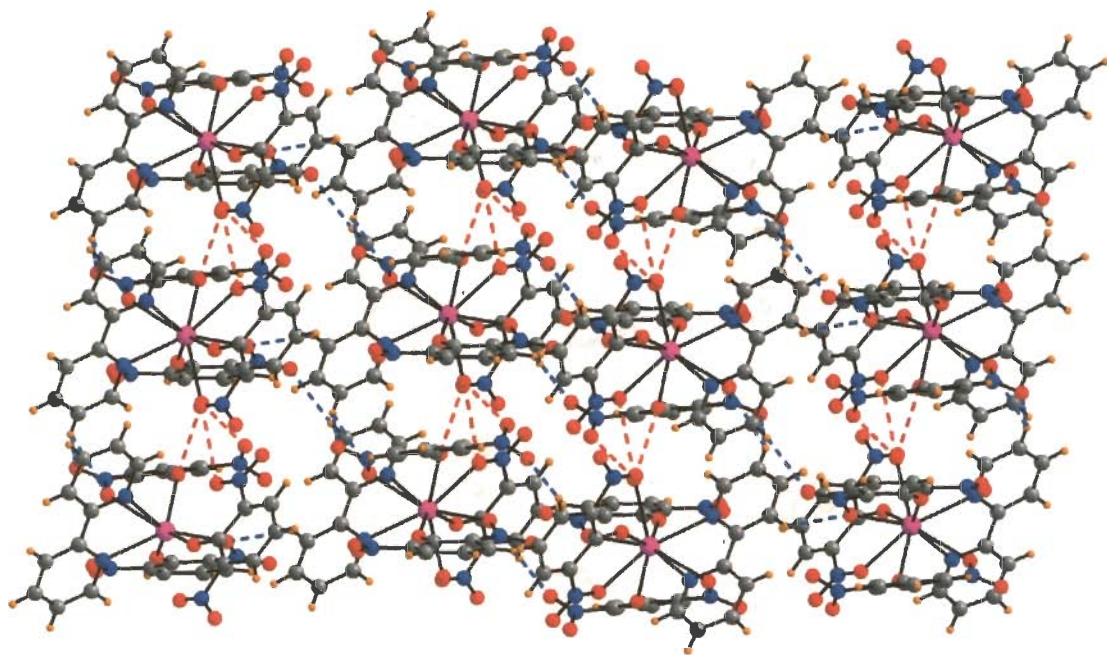


Fig. 2.17: Two dimensional sheet via C-H...O and O...O non-covalent interactions in **2d**. Color code: Eu, pink; C, grey; H, orange; O, red; N, blue

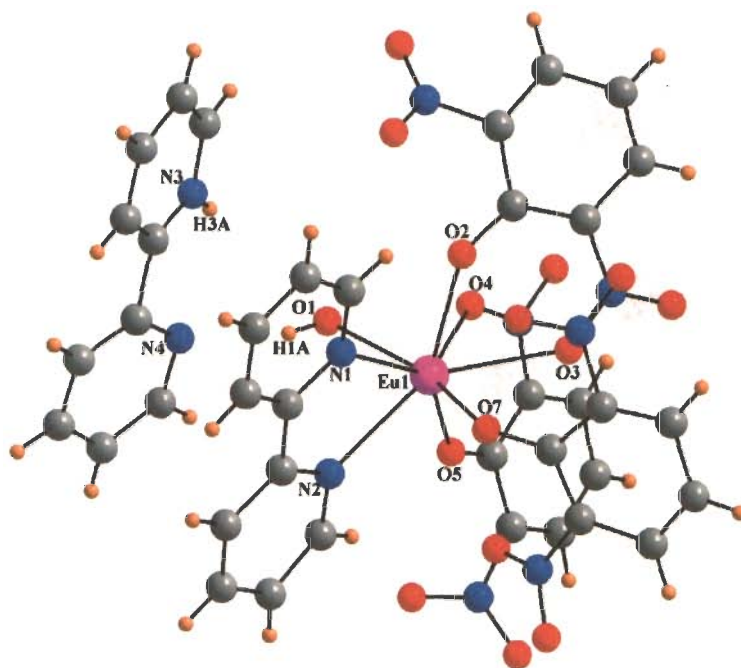


Fig. 2.18: Crystal structure of $[\text{Eu}(2,6\text{-DNP})_3\text{bipy}(\text{OH})]\cdot\text{Hbipy}$ (**2e**). Color code: Eu, pink; C, grey; H, orange; O, red; N, blue

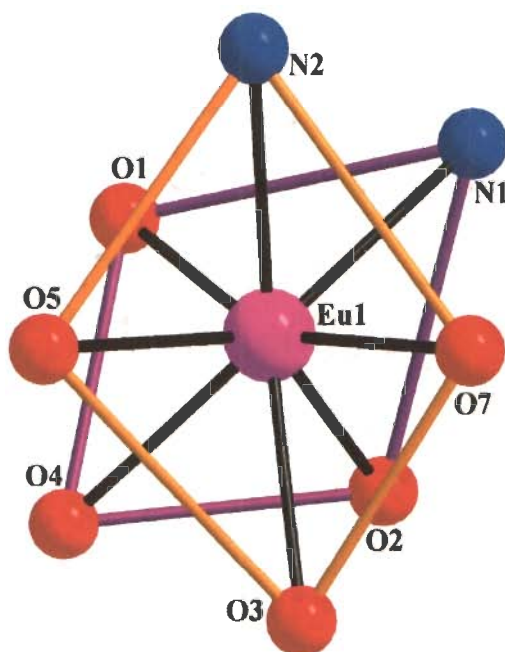


Fig. 2.19: The coordination polyhedron of the Eu^{+3} ion in **2e**. Color code: Eu, pink; O, red; N, blue

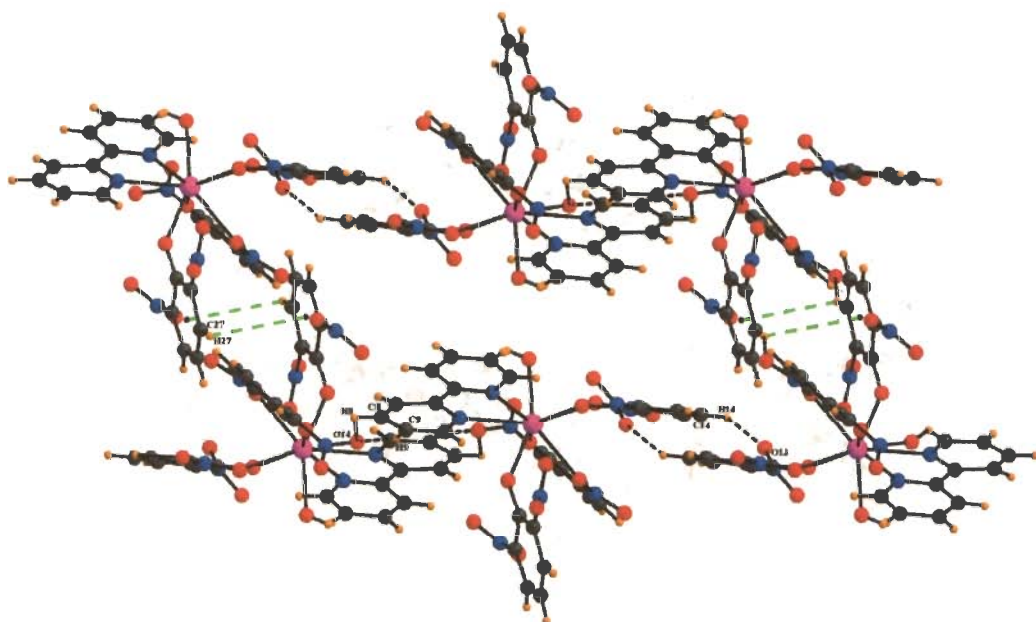


Fig. 2.20 (a): Formation of cavity among host molecules via C-H...O and C-H... π non-covalent interactions in **2e**. Color code: Eu, pink; C, grey; H, orange; O, red; N, blue

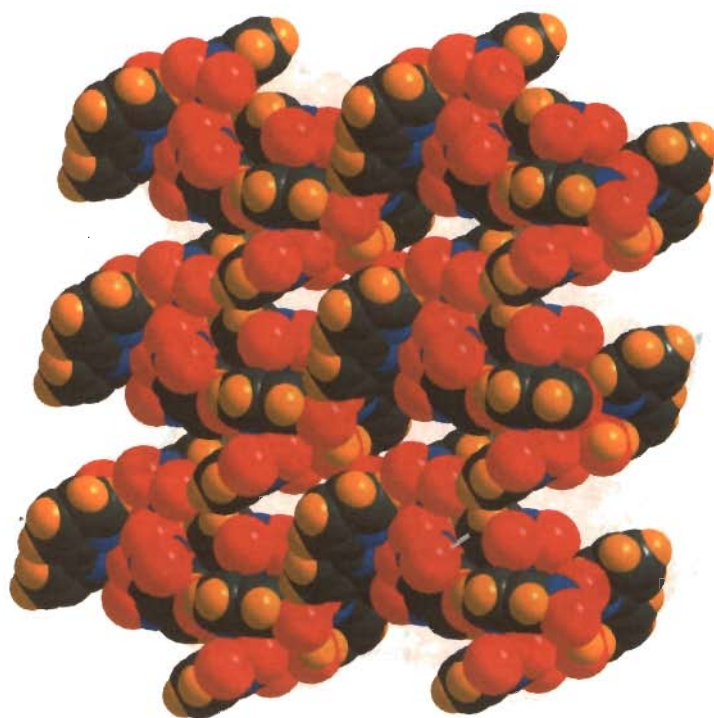


Fig. 2.20 (b): Space-fill model in **2e** along 'b' axis between host molecules. Color code: Eu, pink; C, grey; H, orange; O, red; N, blue

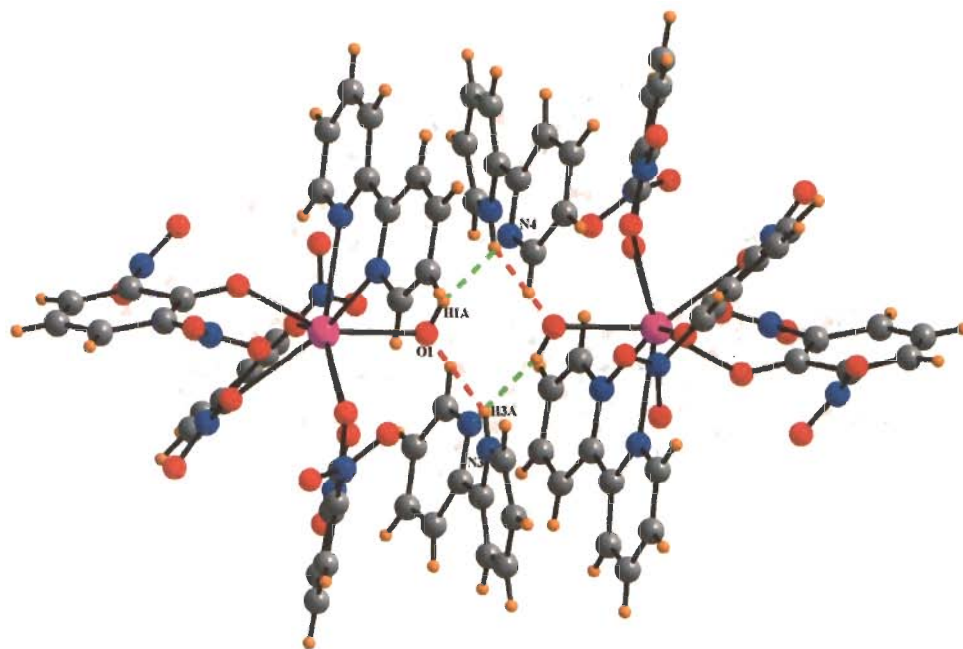


Fig. 2.21 (a): N-H...O and O-H...N non-covalent interactions between host-guest molecules in **2e**. Color code: Eu, pink; C, grey; H, orange; O, red; N, blue

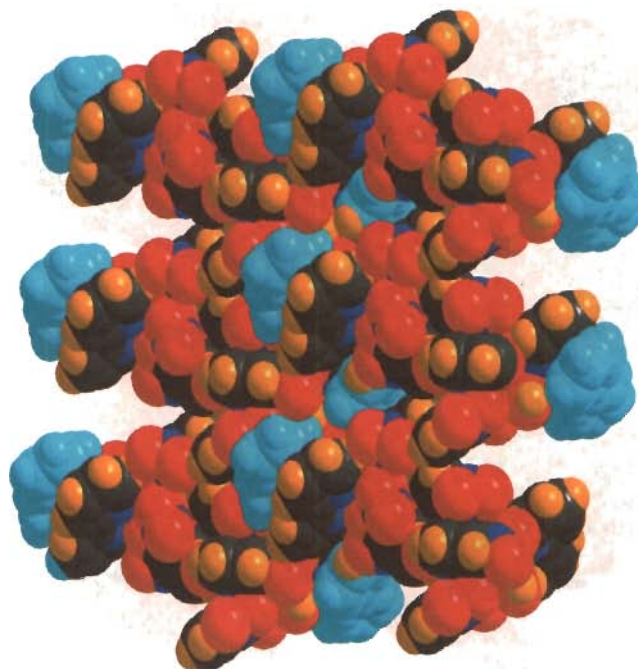


Fig. 2.21 (b): Space- fill model in **2e** between host and guest molecules. Color code: Eu, pink; C, grey; H, orange; O, red; N, blue; Hbipy, cyan

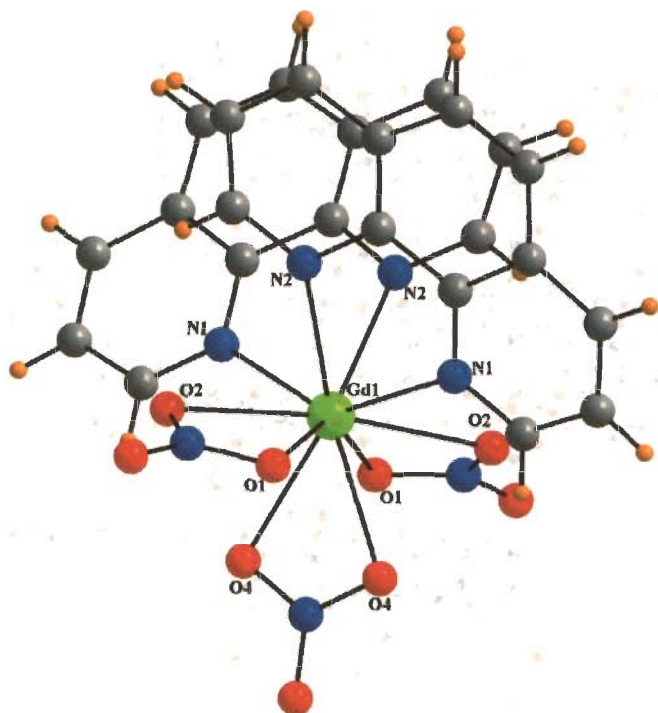


Fig. 2.22: Crystal structure of $[\text{Gd}(\text{phen})_2(\text{NO}_3)_3]$ (**2f**). Color code: Gd, green; C, grey; H, orange; O, red; N, blue

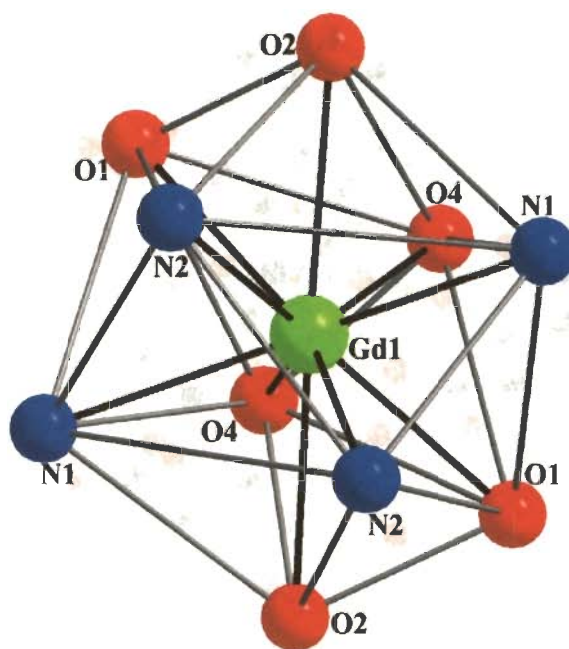


Fig. 2.23: The coordination polyhedron of the Gd^{+3} ion in **2f**. Color code: Gd, green; O, red; N, blue

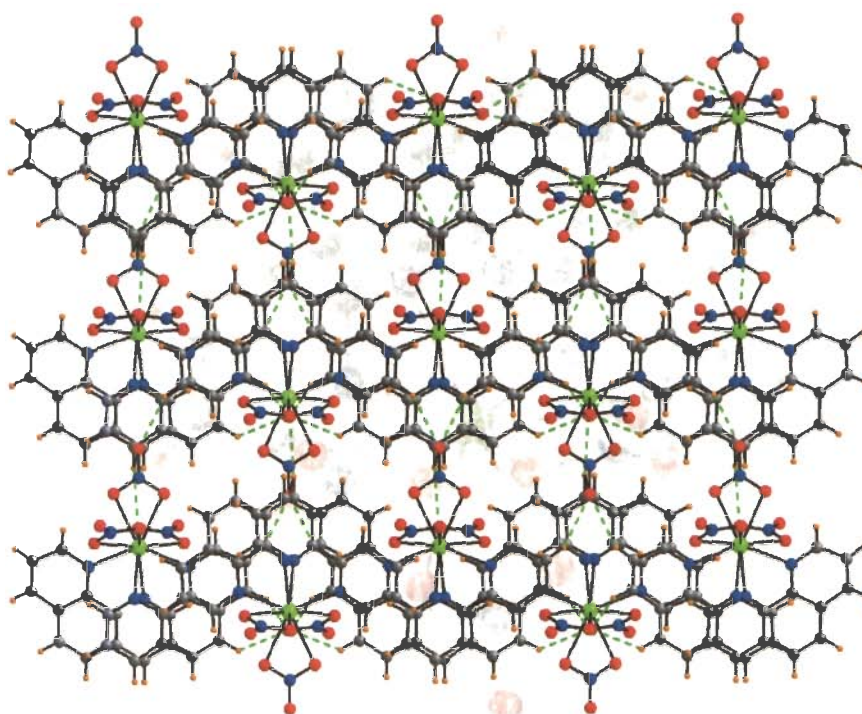


Fig. 2.24: Two dimensional sheet like structure via C-H...O non-covalent interactions in **2f**. Color code: Gd, green; C, grey; H, orange; O, red; N, blue

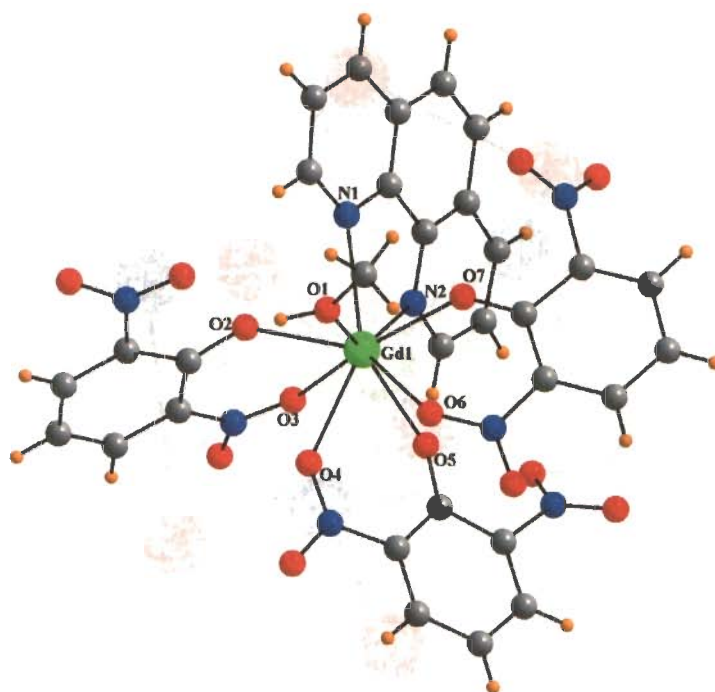


Fig. 2.25: Crystal structure of [Gd(2,6-DNP)₃phenCH₃OH] (**2g**). Color code: Gd, green; C, grey; H, orange; O, red; N, blue

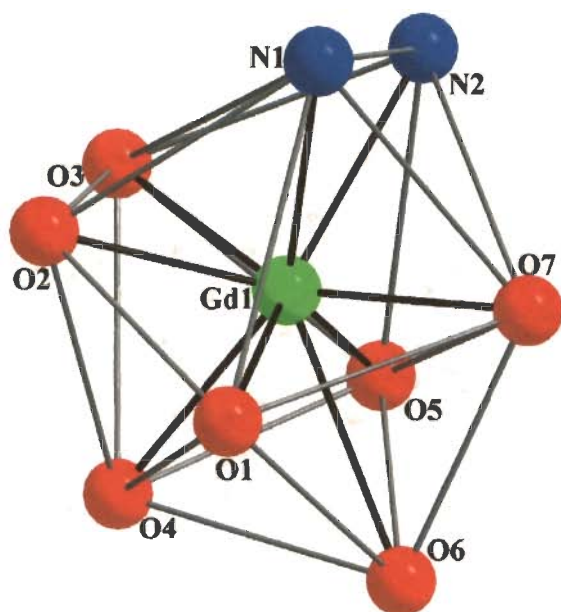


Fig. 2.26: The coordination polyhedron of the Gd^{+3} ion in **2g**. Color code: Gd, green; O, red; N, blue

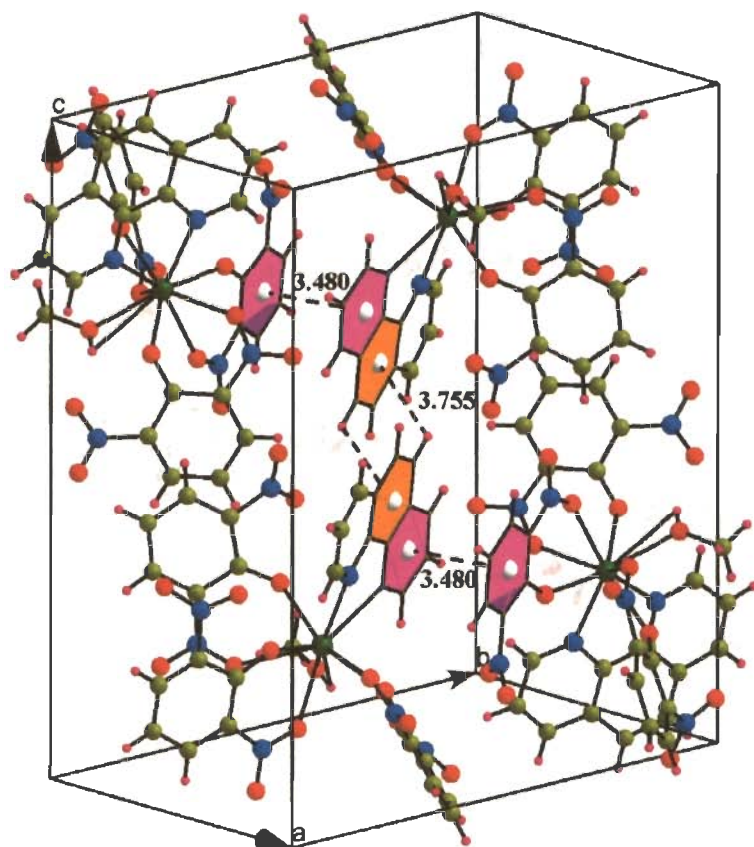


Fig. 2.27: Packing diagram of unit cell via C-H \cdots π and $\pi\cdots\pi$ non-covalent interactions in **2g**. Color code: Gd, dark green; C, green; H, pink; O, red; N, blue

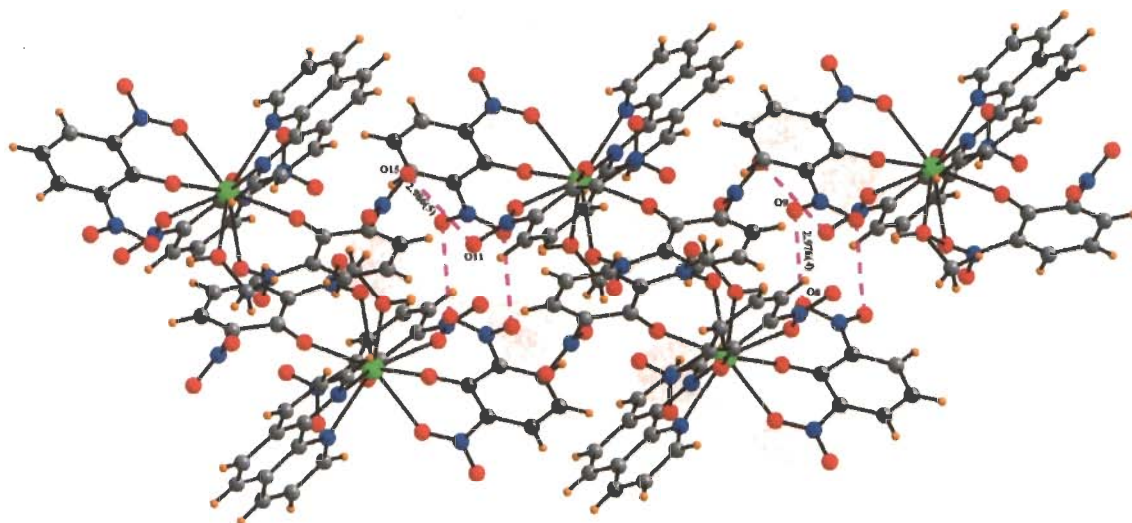


Fig. 2.28: Various O...O intermolecular interactions in **2g**. Color code: Gd, green; C, grey; H, orange; O, red; N, blue

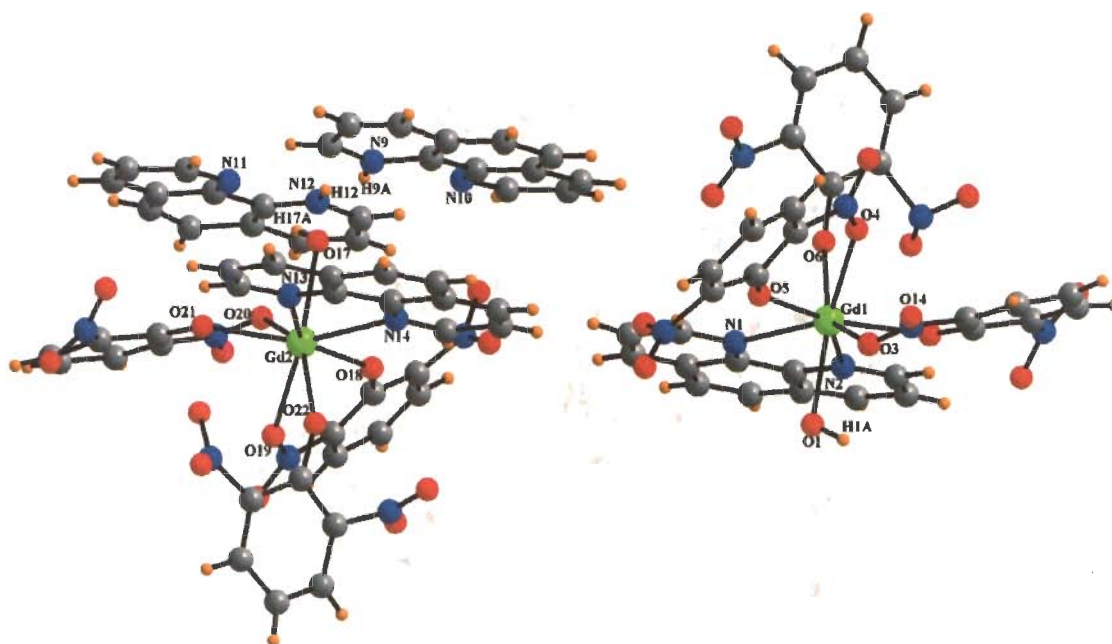


Fig. 2.29: Crystal structure of $[\text{Gd}(\text{2,6-DNP})_3\text{phen}(\text{OH})]_2 \cdot (\text{Hphen})_2$ (**2h**). Color code: Gd, green; C, grey; H, orange; O, red; N, blue

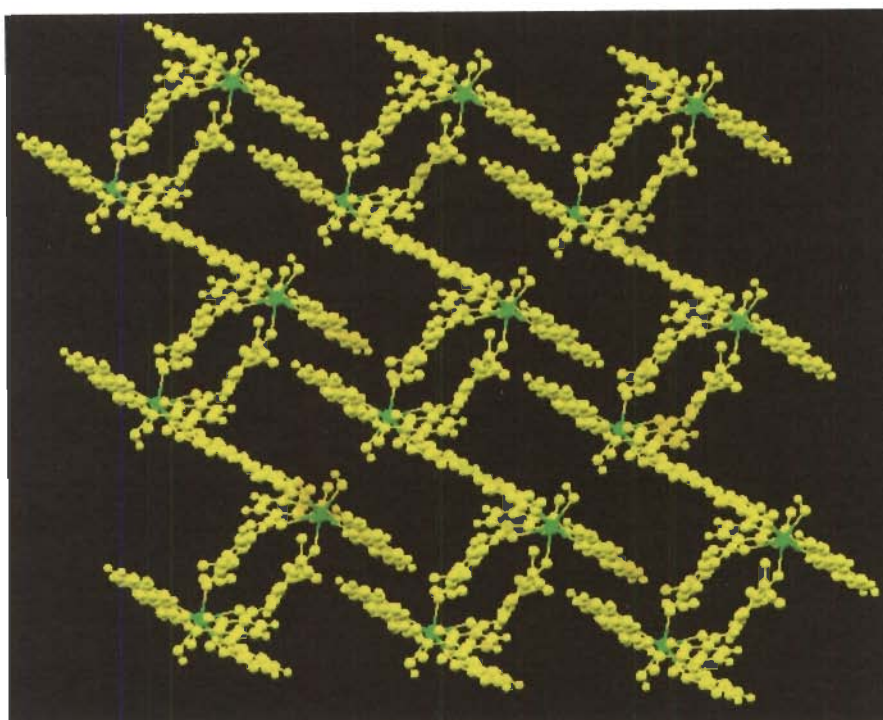


Fig. 2.31 (b): Formation of cavity among host molecules via C-H \cdots O non-covalent interactions in **2h**. Color code: Gd, green; C, H, O, N, yellow

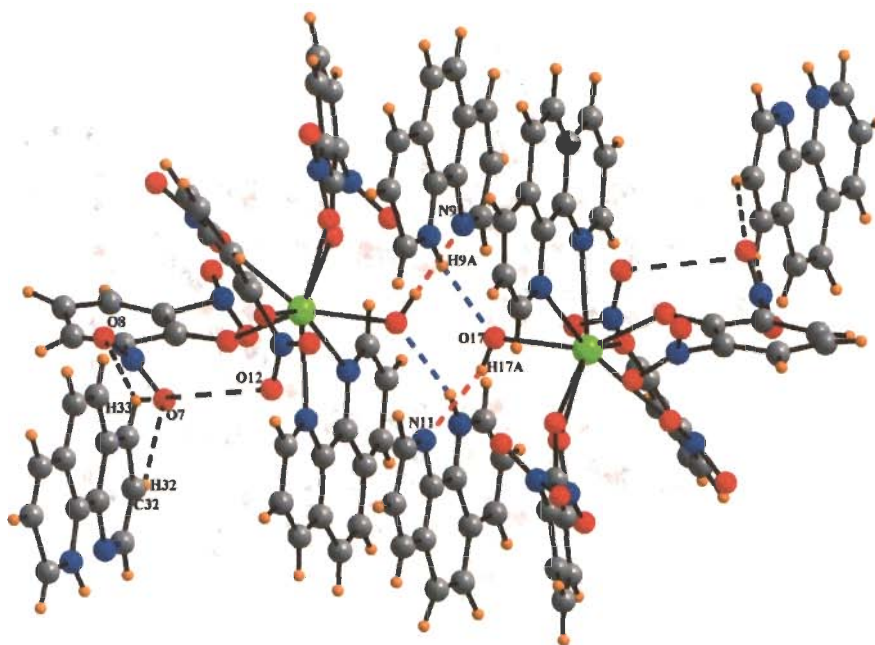


Fig. 2.32 (a): C-H \cdots O, N-H \cdots O and O-H \cdots N non-covalent interactions between host-guest molecules in **2h**. Color code: Gd, green; C, grey; H, orange; O, red; N, blue

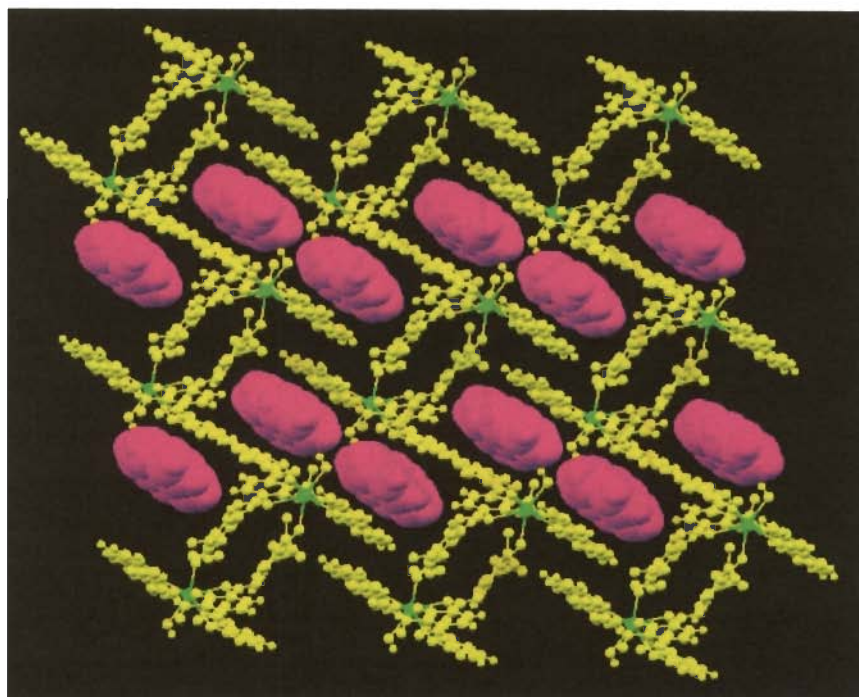


Fig. 2.32 (b): Host-guest supramolecular motif via C-H...O, N-H...O and O-H...N non-covalent interactions in **2h**. Color code: Gd, green; C, H, O, N, yellow; Hphen, purple

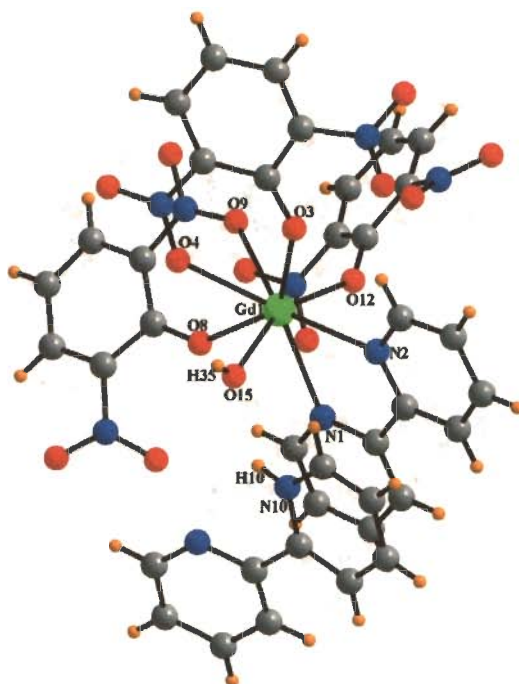


Fig. 2.33: Crystal structure of [Gd(2,6-DNP)₃bipy(OH)].Hbipy (**2j**). Color code: Gd, green; C, grey; H, orange; O, red; N, blue

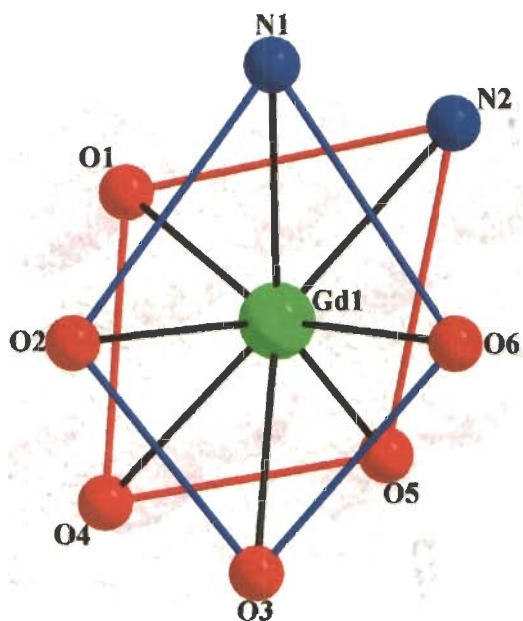


Fig. 2.34: The coordination polyhedron of the Gd^{+3} ion in **2j**. Color code: Gd, green; O, red; N, blue

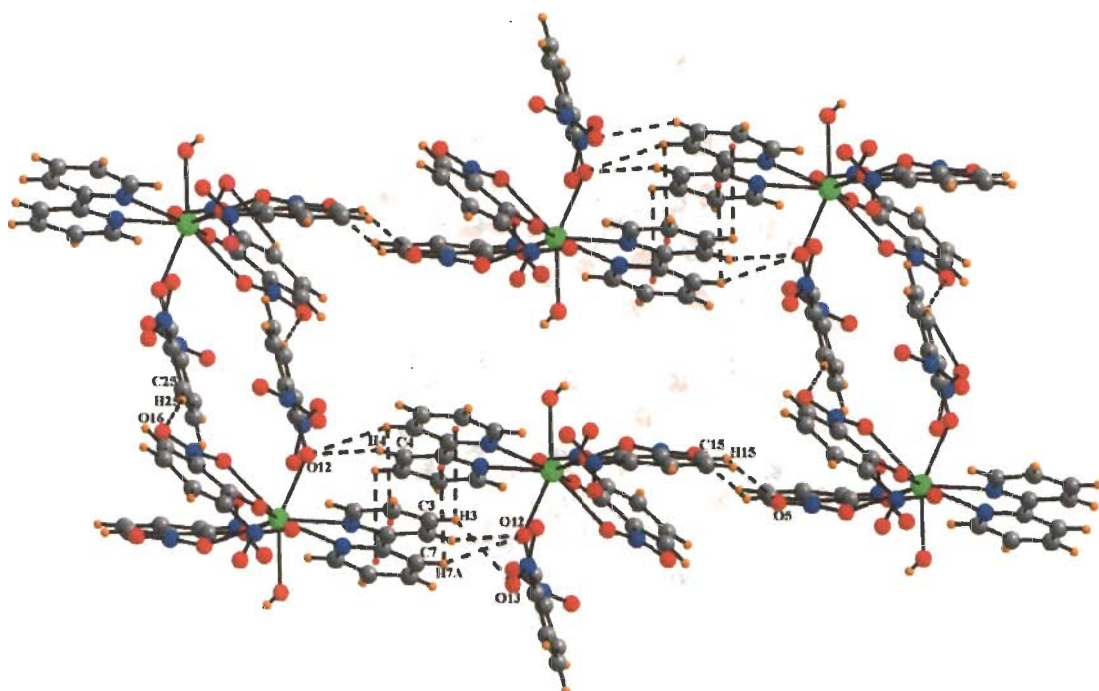


Fig. 2.35 (a): Formation of cavity among host molecules via $\text{C-H}\cdots\text{O}$ and $\text{C-H}\cdots\pi$ non-covalent interactions in **2j**. Color code: Gd, green; C, grey; H, orange; O, red; N, blue

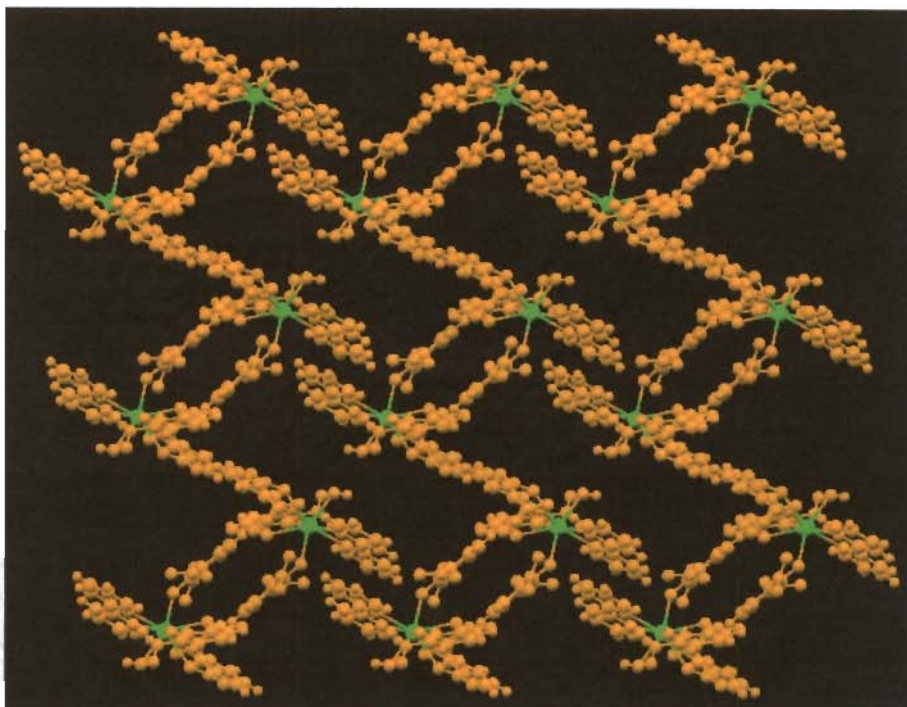


Fig. 2.35 (b): Formation of cavity among host molecules via C-H...O and C-H... π non-covalent interactions in **2j**. Color code: Gd, green; C, H, O, N, orange

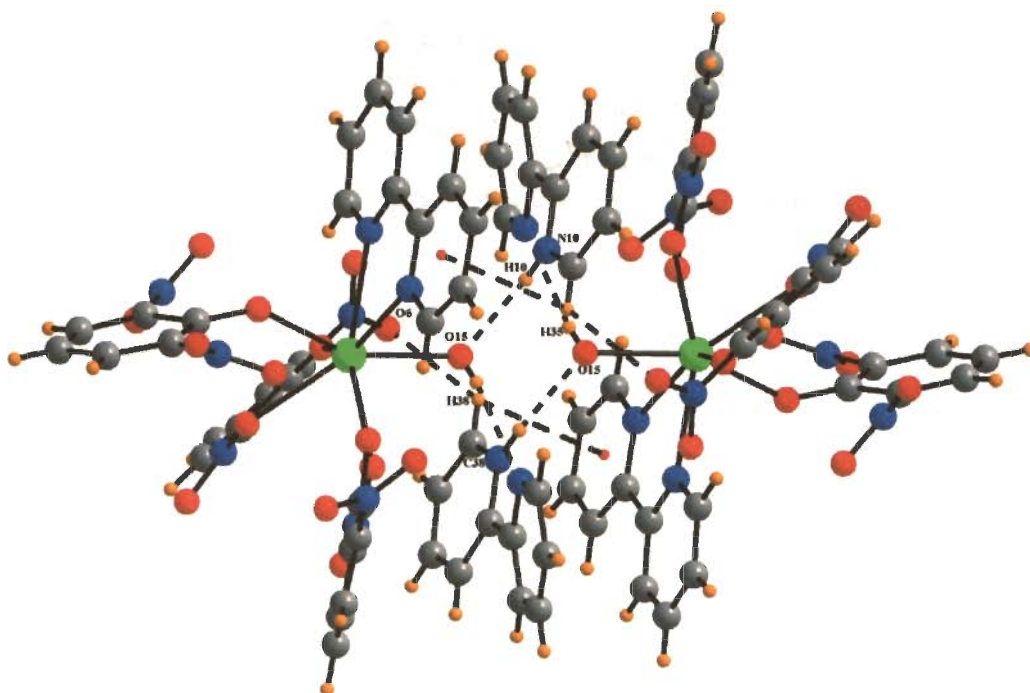


Fig. 2.36 (a): C-H... π , N-H...O and O-H...N non-covalent interactions between host-guest molecules in **2j**. Color code: Gd, green; C, grey; H, orange; O, red; N, blue

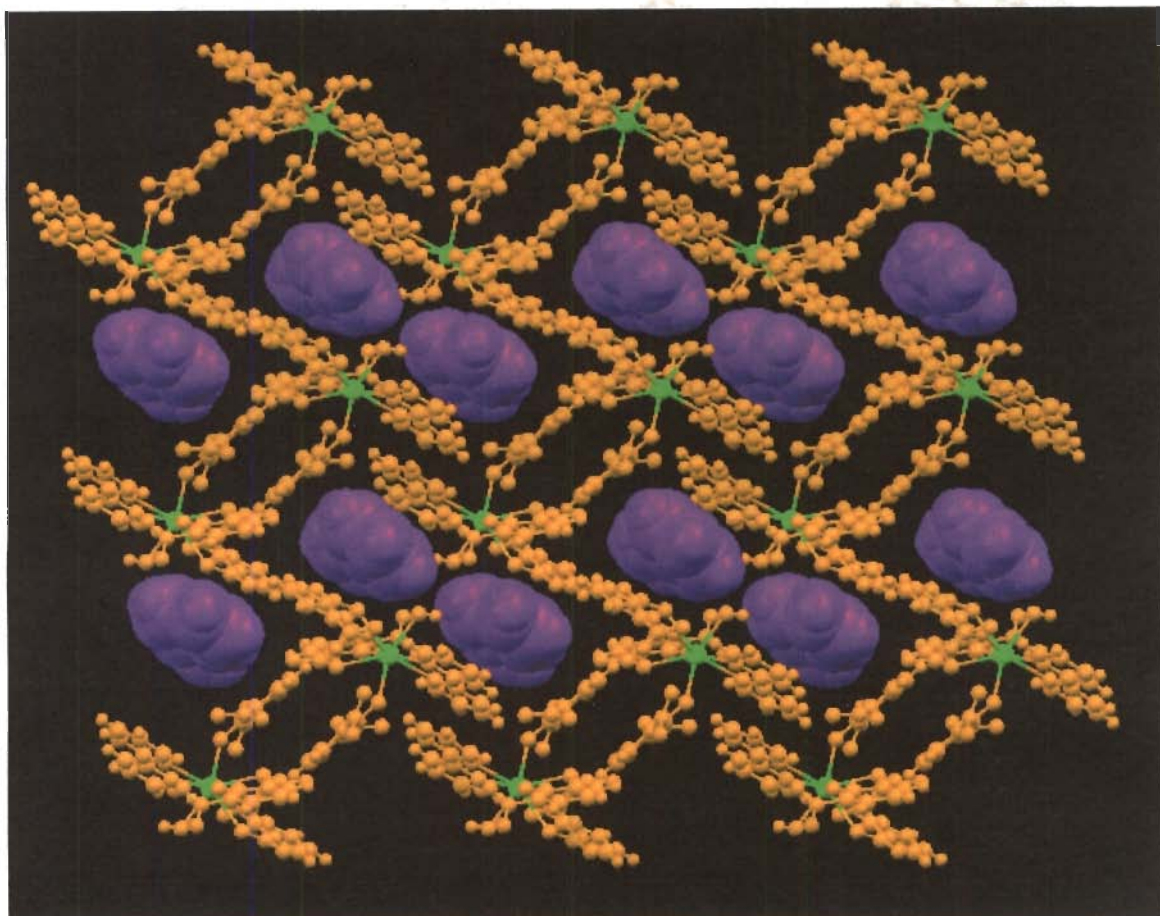


Fig. 2.36 (b): Host-guest supramolecular motif via C-H \cdots O, N-H \cdots O, O-H \cdots N and C-H \cdots π non-covalent interactions in **2j**. Color code: Gd, green; C, H, O, N, orange; Hbipy, purple

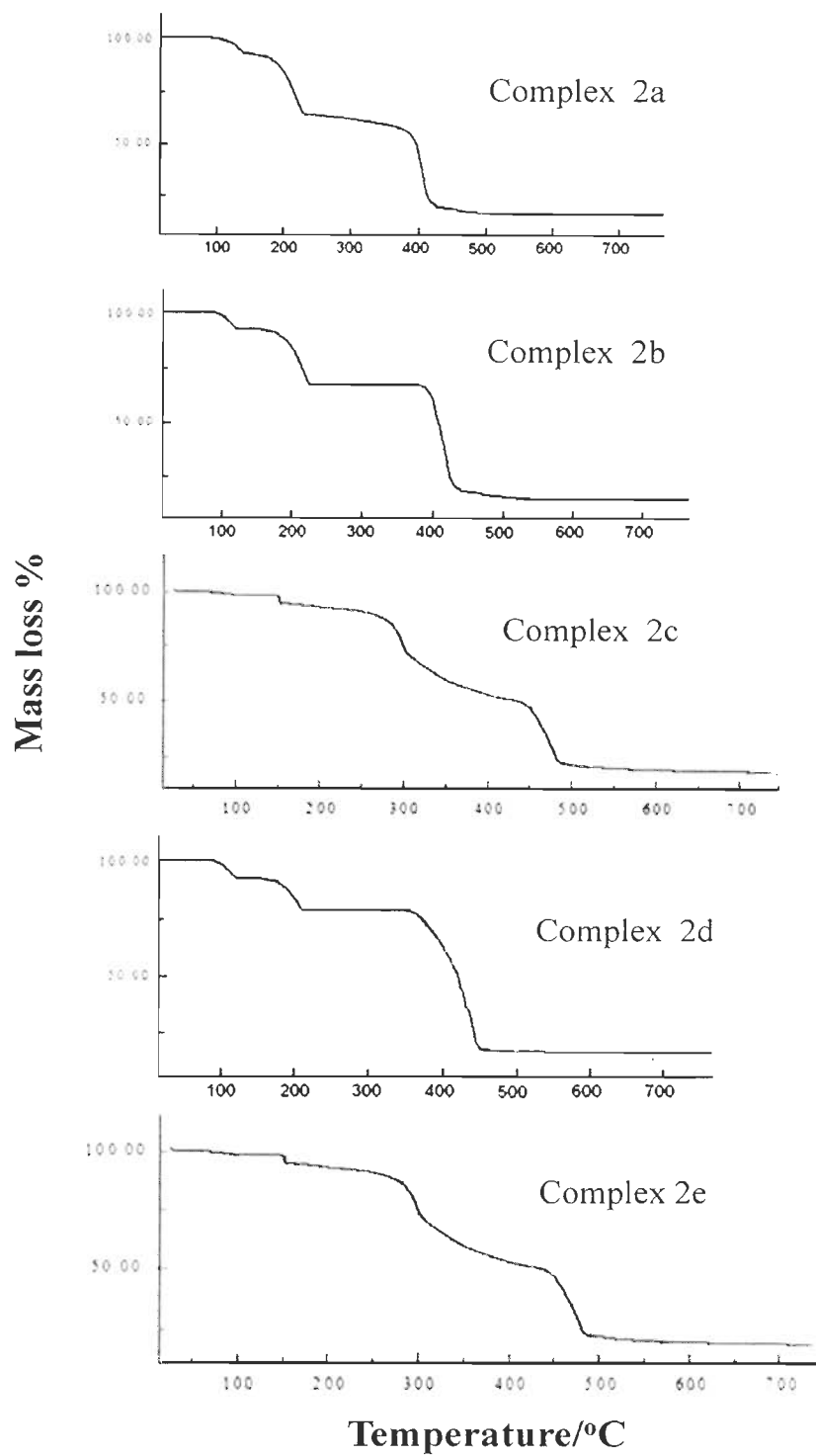


Fig. 2.37: Non-isothermal TG in air at standard atmospheric condition of 2a-2e

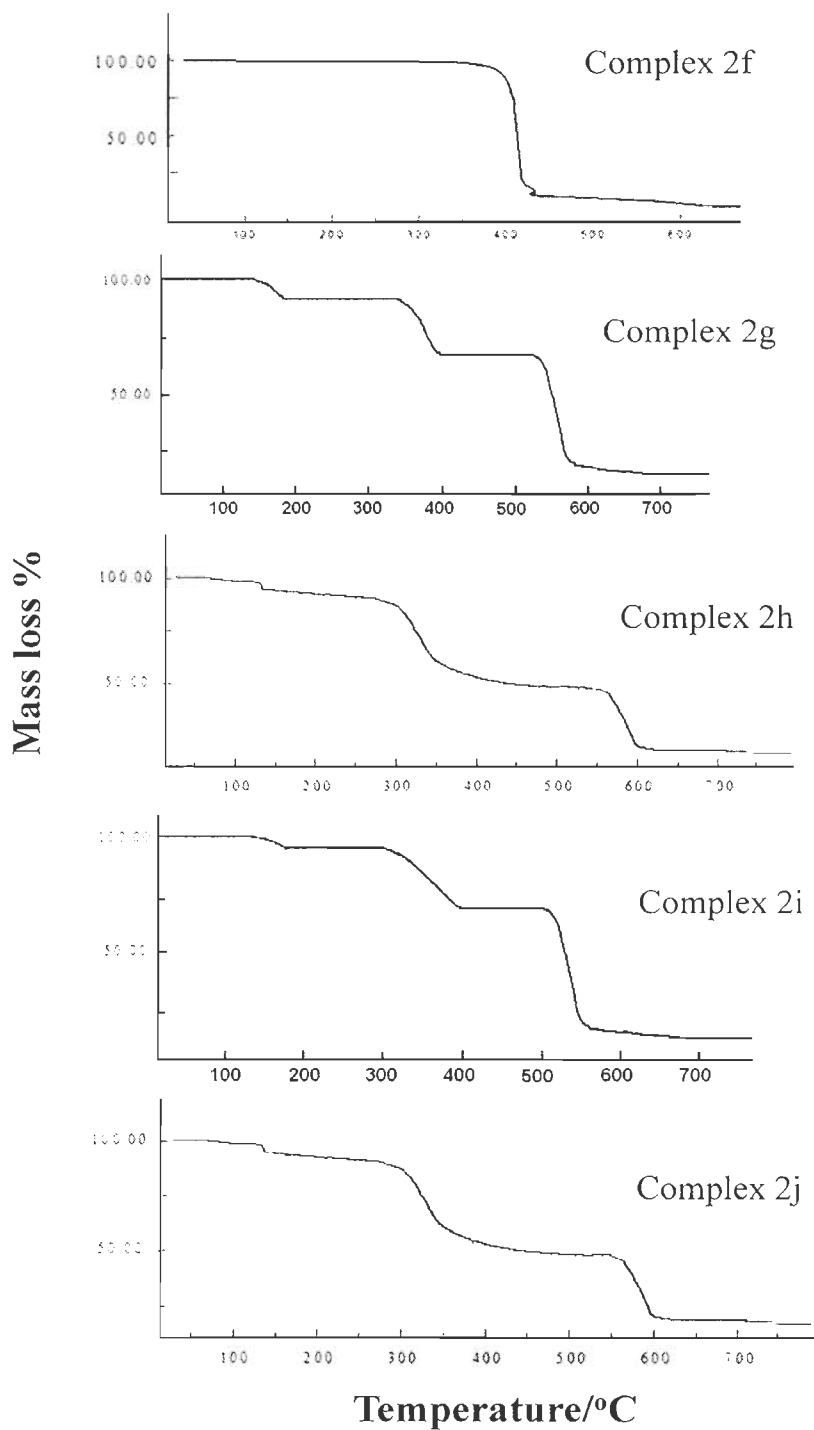
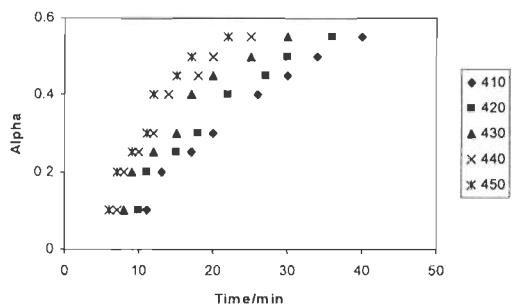
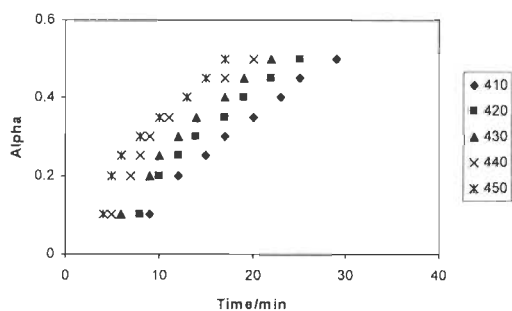


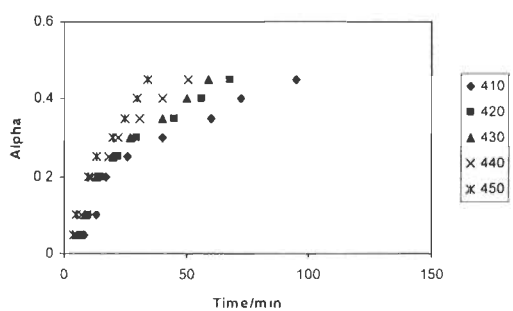
Fig. 2.38: Non-isothermal TG in air at standard atmospheric condition of 2f-2j



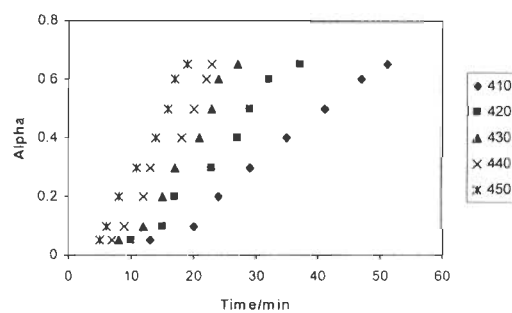
(a)



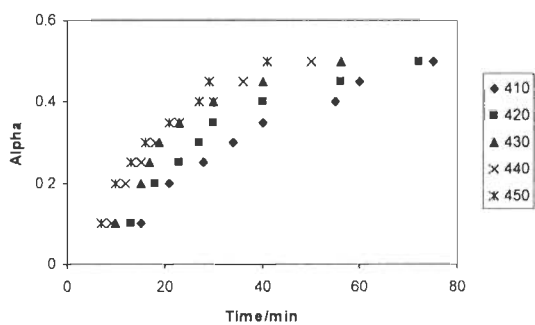
(b)



(c)



(d)



(e)

Fig. 2.39: Isothermal TG in static air atmosphere for complexes 2a-2e (a) 2a (b) 2b (c) 2c (d) 2d (e) 2e

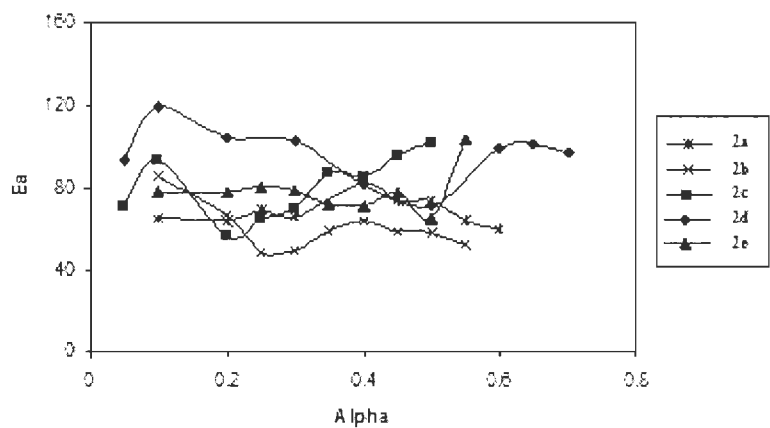


Fig. 2.40: Dependence of activation energy (E_a) on the extent of conversion (α) for 2a-2e

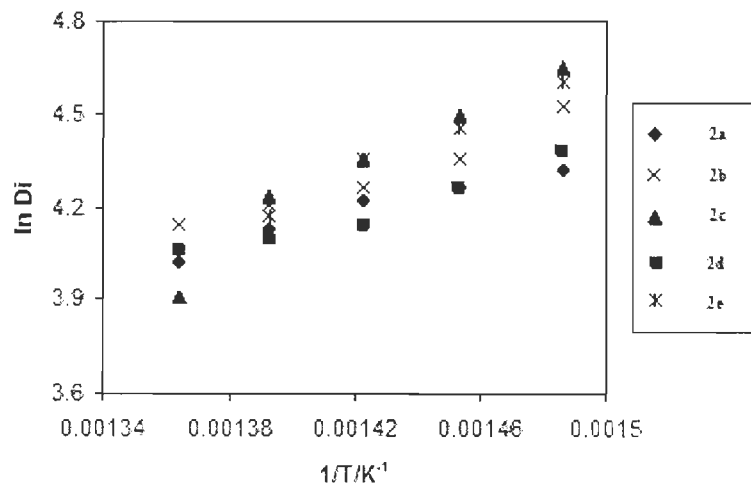
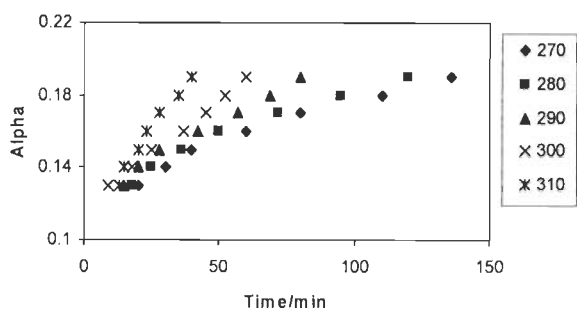
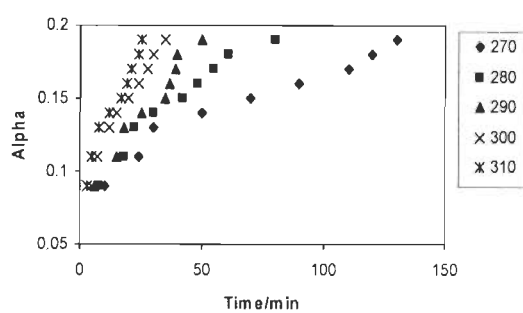


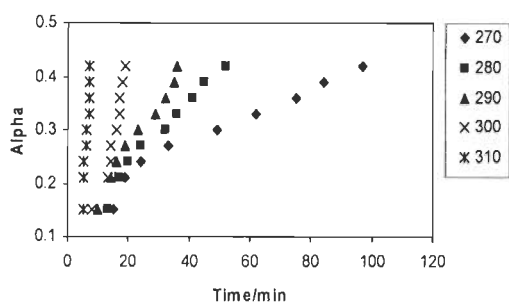
Fig. 2.41: Graph of $\ln D_i$ vs $1/T$ for 2a-2e



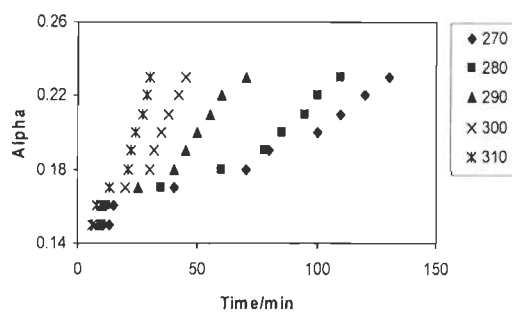
(a)



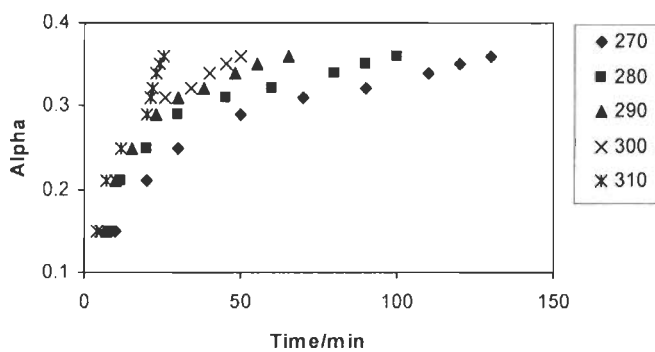
(b)



(c)



(d)



(e)

Fig. 2.42: Isothermal TG in static air atmosphere for complexes 2f-2j (a) 2f (b) 2g (c) 2h (d) 2i (e) 2j

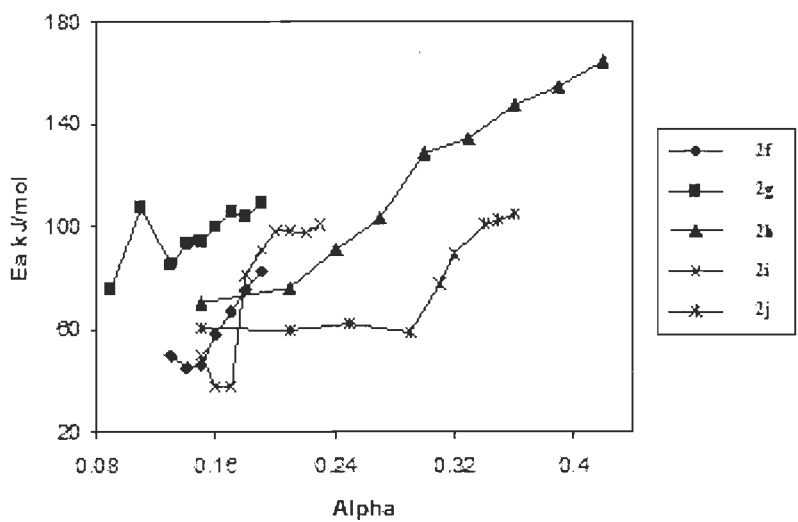


Fig. 2.43: Dependence of activation energy (E_a) on the extent of conversion (α) for 2f-2j

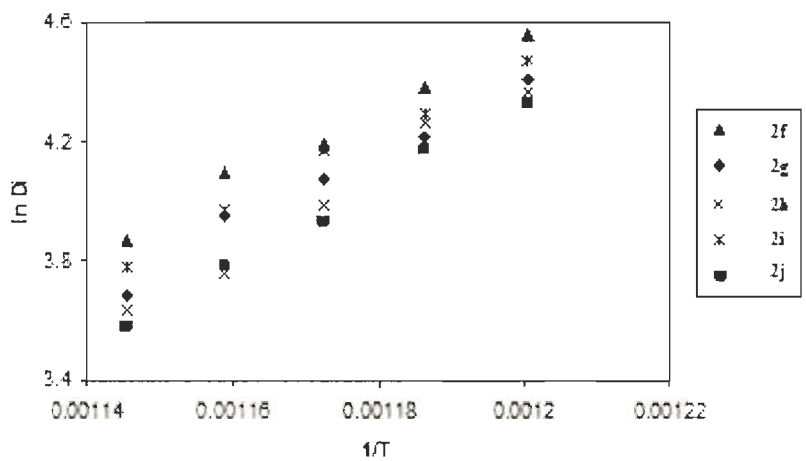


Fig. 2.44: Graph of $\ln D_i$ vs $1/T$ for 2f-2j

REFERENCES

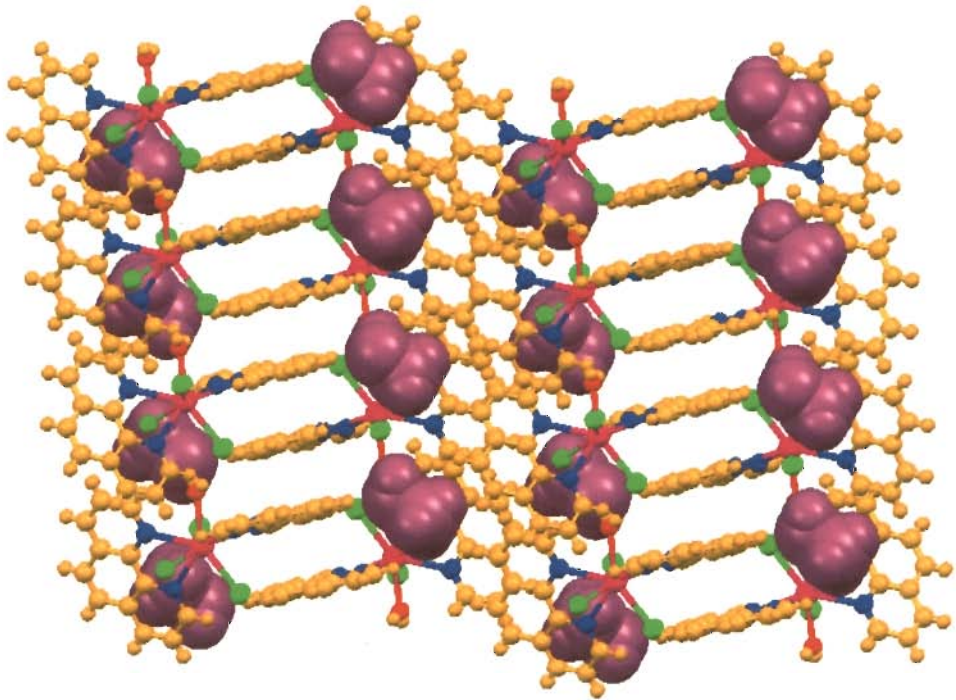
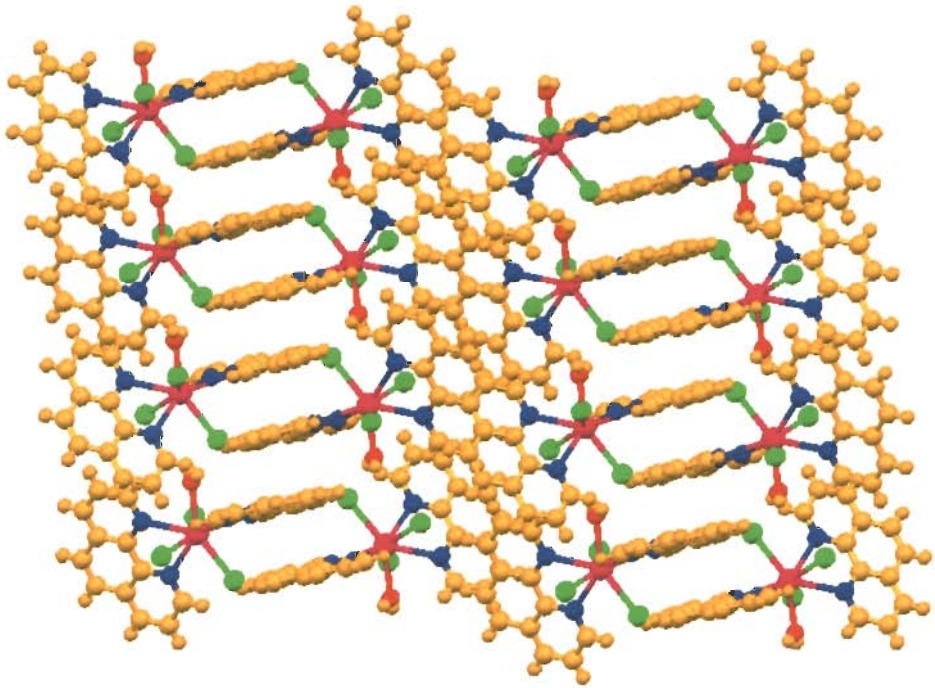
1. Singh, G., Kapoor, I. P. S., Mannan, S. M. and Tiwari, S. K., Studies on energetic compounds Part XI: Preparation and thermolysis of polynitro organic compounds”, *J. Hazard. Mater.*, **A 68**, 155 (1999).
2. Ilyushin, M. A., Bachurina, I. V., Smirnov, A. V., Tselinsky, I. V. and Shugalei, I. V., “Study of the interaction of polynitro compounds with transition metals coordination complexes with 1,5-pentamethylenetetrazole as a ligand”, *Cent. Eur. J. Energetic Mater.*, **7**, 33 (2010).
3. Keshavarza, M. H., Pouretedala, H. R., Shokrolahia, A., Zali, A. and Semnanib, A., “Predicting activation energy of thermolysis of polynitro arenes through molecular structure”, *J. Hazard. Mater.*, **160**, 142 (2008).
4. Stepanov, R. S., Kruglyakova, L. A. and Astakhov, A. M., “Thermal decomposition of polynitro compounds under non-isothermal conditions”, *Combust. Explo. Shock⁺*, **42**, 63 (2006).
5. Singh, G., Singh, C. P., Agrawal, J. P. and Sikder, A. K., “Studies on energetic compounds Part 42: Thermolysis of 5-amino-3-nitro-1,2,4-triazole (ANTA)”, *Indian J. Eng. Mater. Sci.*, **13**, 462 (2006).
6. Rao, K. U. B. and Yoganarasimhan, S. R., “Thermal decomposition of 2,4,N-trinitro anilino acetic acid and its esters”, *Journal of Chemical Sci.*, **95**, 303 (1985).
7. Singh, G. and Pandey, D. K., “Thermal studies on energetic compounds Part 30: Kinetics and mechanism of bis(diethylenetriamine) metal nitrate complexes”, *J. Therm. Anal. Calorim.*, **76**, 507 (2004).
8. Singh, G. and Felix, S. P., “Studies on energetic compounds Part 32: Crystal structure, thermolysis and applications of NTO and its salts”, *J. Mol. Struct.*, **649**, 71 (2003).
9. Ferenc, W. A., Dziewulska, A. W., Wojciechowska, M. and Ski, J. S., “Thermal, spectral and magnetic characterization of Co(II), Ni(II) and Cu(II) 4-chloro-2-nitrobenzoates”, *J. Therm. Anal. Calorim.*, **86**, 359 (2006).
10. Zamiri, A. R. and De, S., “Deformation distribution maps of β -HMX molecular crystals”, *J. Phys. D: Appl. Phys.*, **43**, 1 (2010).
11. Dick, J. J. and Ritchie, J. P., “Molecular mechanics modeling of shear and the crystal orientation dependence of the elastic precursor shock strength in pentaerythritol tetranitrate”, *J. Appl. Phys.*, **76**, 2726 (1994).

12. Bombieri, G., Pra, A. D., Benetollo, F., Zinner, K. D., Melo, M. A., Belarmino, L. D. and Vicentini, G., "The role of the picric acid in the hydrated lanthanide derivatives with neutral ligands. Synthesis and X-ray structures of hydrated neodymium, praseodymium and thulium picrate complexes with nicotinamide-N-oxide", *Inorg. Chim. Acta*, **348**, 254 (2003).
13. Zeman, S., Dimun, M. and Truchilik, S., "The relationship between kinetic data of the low-temperature thermolysis and the heats of explosion of organic polynitro compounds", *Thermochim. Acta*, **78**, 181 (1984).
14. Zeman, S., "The relationship between differential thermal analysis data and the detonation characteristics of polynitroaromatic compounds", *Thermochim. Acta*, **41**, 199 (1980).
15. Yun, S. S., Yeon, J. H., Suh, H. R., Kim, J. K., Kim, W. C. and Kang, S. K., "Crystal structure and thermal properties of a dimeric (2,6-dinitrophenolato)lithium (I) complex", *J. Coord. Chem.*, **57**, 989 (2004).
16. Yun, S. S., Suh, H. R., Suh, H. S., Kang, S. K., Kim, J. K. and Kim, C. H., "Lanthanide complexes of some high energetic compounds (III), crystal structures and thermal properties of 2,6-dinitrophenol (2,6-DNP) complexes", *J. Alloys Comp.*, **408**, 1030 (2006).
17. Yun, S. S., "Crystal structures and thermal properties of lanthanide (III) complexes of 2,6-dinitrophenol, the high energetic compounds", A poster, in Richmond, (2006).
18. Kim, E. J., Kim, C. H., Kim, J. K. and Yun, S. S., "Crystal structures and thermal properties of 2,6-dinitrophenol complexes with lanthanide series", *Bull. Korean Chem. Soc.*, **29**, 1157 (2008).
19. Suh, H. R., Suh, H. S., Yun, S. S., Lee, E. K. and Kang, S. K., "Triaquabis(2,6-dinitrophenolato)neodymium (III)", *Acta Cryst.*, **E58**, m284 (2002).
20. Suh, H. R., Suh, H. S., Yun, S. S., Lee, E. K. and Kang, S. K., "Triaquabis(2,6-dinitrophenolato- κ^2 O¹,O²)yttrium (III)", *Acta Cryst.*, **C58**, m202 (2002).
21. Aly, M. M., "The coordinative unsaturation and the reactivity of Th(IV) and U(VI) oxinates towards some haloacetic acids and nitrophenols", *J. Inorg. Nucl. Chem.*, **41**, 1737 (1979).
22. Layton, A. J., Nyholm, R. S., Banerjee, A. K., Fenton, D. E., Lestas, C. N. and Truter, M. R., "Alkali-metal complexes Part III: Adducts of 1,10-phenanthroline with alkali-metal salts of 1-nitroso-2-naphthol, o-nitrophenol, and 2,4- and 2,6-dinitrophenol", *J. Chem. Soc., A*, **18**, 94 (1970).

23. Delboni, L. F., Livia, G. O., Castellano, E. E., Zinner, L. B. and Braun, S., "Structural and luminescence studies of trivalent europium complexes with pentaethylene glycol and 18-crown-6 ligands in the presence of picrate anion", *Inorg. Chim. Acta*, **221**, 169 (1994).
24. Saleh, M. I., Kusriani, E., Adnan, R., Rahman, I. A., Saad, B., Usman, A., Fun, H. -K. and Yamin, B. M., "The crystal structure and thermal stability of [bis-picrate(pentaethylene glycol)] praseodymium (III) picrate complex", *J. Chem. Crystallogr.*, **35**, 472 (2005).
25. Mai, P. T., Herzog-Cance, M. -H., Potier, A. and Potier, J., "Etude, par spectroscopie de vibration, de deux solvants de la cellulose: La N-methyl morpholine N-oxyde and its monohydrate", *Can. J. Chem.*, **60**, 2777 (1982).
26. Shriner, R. L., "The systematic identification of organic compounds", Wiley, New York, 1980.
27. Coates, J., "Interpretation of infrared spectra: A practical approach", R. A. Meyers (Ed.) John Wiley & Sons Ltd; (2000).
28. Nakamoto, K., "Infrared and raman spectra of inorganic and coordination compounds. 3rd ed. New York: Wiley Interscience; (1978).
29. Singh, U. P., Kumar, R. and Upreti, S., "Synthesis, structural, photophysical and thermal studies of benzoate bridged Sm(III) complexes", *J. Mol. Struct.*, **831**, 97 (2007).
30. Lam, A. W. -H., Wong, W. -T., Gao, S., Wen, G. and Zhang, X. -X., "Synthesis, crystal structure, photophysical and magnetic properties of dimeric and polymeric lanthanide complexes with benzoic acid and its derivatives", *Eur. J. Inorg. Chem.*, **1**, 149 (2003).
31. Burnham, A. K. and Dinh, L. N., "A comparison of isoconversional and model-fitting approaches to kinetic parameter estimation and application predictions", *J. Therm. Anal. Calorim.*, **89**, 479 (2007).
32. Freeman, E. S. and Gorden, S., "The application of the absolute rate theory of the nitrate-magnesium, sodium nitrate- magnesium", *J. Phys. Chem.*, **60**, 867 (1956).
33. Singh, G., Kapoor, I. P. S., Kumar, D., Singh, U. P. and Goel, N., "Preparation, X-ray crystallography and thermal decomposition of transition metal perchlorate complexes with perchlorate and 2,2'-bipyridyl ligands", *Inorg. Chim. Acta*, **362**, 4091 (2009).
34. Zheng, P. -Q., Ren, Y. -P., Long, L. -S., Huang, R. -B. and Zheng, L. -S., "pH dependent assembly of Keggin-based supramolecular architecture", *Inorg. Chem.*, **44**, 1190 (2005).

CHAPTER-3

***Syntheses, Structural,
Photophysical and Thermal
Studies of Some Lanthanide
(III) Complexes***



Over the past decades, much research has been performed on the lanthanide complexes with organic ligands because these complexes can exhibit strong luminescence and have a lot of potential applications for the fluorescence probes or labels in biological immunoassay and active central species in photoluminescent materials [1-5]. Luminescence in lanthanide compounds with organic ligands proceeds throughout intramolecular energy transfer from excited ligand triplet states to the coordinated ion. The efficiency of this process depends on the efficiency of the organic ligand absorption, the ligand-to-lanthanide ion energy transfer and the lanthanide luminescence. A good correlation between the excited levels of the lanthanide and the charge transfer (CT) energy of the ligand leads to enhancement of the luminescence in such systems [6-8]. According to the molecular fragments principle, commonly used organic compounds viz., 1,10-phenanthroline, 2,2'-bipyridine and 2,4,6-tris(2-pyridyl)-1,3,5-triazine act as the energy donor and luminescence sensitizer for lanthanide ions. The compound 1,10-phenanthroline, 2,2'-bipyridine behave as bidentate ligands while 2,4,6-tris(2-pyridyl)-1,3,5-triazine (tptz), a bulky aromatic compound featuring three 2-pyridyl rings fixed on a central 1,3,5-triazine platform [9], has been widely used as a multi-dentate ligand in metal coordination chemistry. There are a few structurally characterized lanthanide complexes in which tptz acts as a tridentate ligand [10]. The tptz, by offering three coordinating atoms, protects the lanthanide ion from interacting with solvent molecules, and therefore, restrains solvent-based vibrational coupling and luminescence quenching [11]. Furthermore, the remaining nitrogen atoms allow further coordination to other metals, transition metals in particular. Thus, complicated heterometallic complexes structurally may be envisioned, for which novel magnetic as well as luminescence properties can be expected [12-14]. The complexation ability of tptz depends in part upon the size of the metal cations, which normally coordinate as a tridentate ligand to give a 1:1 metal/ligand ratio, and a considerable number of transition metals and lanthanide complexes of this ligand has been studied [15-17]. Besides this, these compounds also act as the second assistant ligands for some lanthanide complexes of carboxylates or diketonates. Lanthanide carboxylate and diketone complexes show interesting crystal structures due to the variable coordination number of metal centers as well as coordination versatility of these ligands. The donor ability of oxygen atoms toward different lanthanides [especially Eu(III), Tb(III), Sm(III), Dy(III)] increases the fluorescence intensity in lanthanides. The synthesis and structural studies of lanthanide complexes with efficient photoluminescent properties continue to be an active area of research. Several classes of ligands

have been utilized for the preparation of Ln(III) complexes. Wu et al. [18] reported two series of novel lanthanide complexes of composition $[\text{Ln}(\text{dca})_2(\text{phen})_2(\text{H}_2\text{O})_3](\text{dca})\cdot\text{phen}$ (Fig. 3.1) and $[\text{Ln}(\text{dca})_3(\text{bipy})_2(\text{H}_2\text{O})]_n$ ($\text{Ln} = \text{La}, \text{Pr}, \text{Sm}, \text{Gd}$). The crystal structure of $[\text{Sm}(\text{dca})_2(\text{phen})_2(\text{H}_2\text{O})_3](\text{dca})\cdot\text{phen}$ consisted of discrete $[\text{Sm}(\text{dca})_2(\text{phen})_2(\text{H}_2\text{O})_3]^+$ cations, dca anions and lattice phen molecules, whereas the structure of the $[\text{Sm}(\text{dca})_3(\text{bipy})_2(\text{H}_2\text{O})]_n$ was characterized by infinite chains.

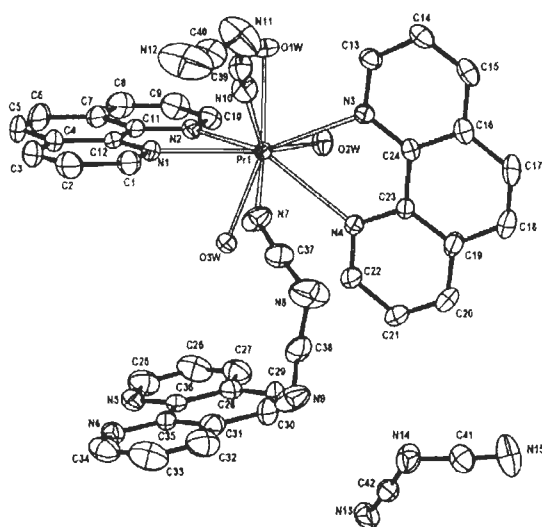


Fig. 3.1: Crystal structure of $[\text{Pr}(\text{dca})_2(\text{phen})_2(\text{H}_2\text{O})_3](\text{dca})\cdot\text{phen}$

Wang et al. [19] reported new lanthanide coordination polymers with 1,2,4,5-benzenetetracarboxylic acid, $\text{Ln}_2(-\text{betc})_2(4,4'\text{-bipyH}_2)$ ($\text{Ln} = \text{Eu}, \text{Gd}$). The crystallographic data shows that they are isostructural and possess three dimensional framework with one dimensional rhomboid channels, where the 4,4'-bipyridine molecules exist steadily via hydrogen bonds. The results of complexes indicate that 4,4'-bipyridine molecule acting as a template, plays an important role in the formation of complexes and thus has a synergistic action in the construction of three dimensional framework with large channels. Desilva et al. [20] synthesized a novel Eu(III) complex featuring three dibenzoyl methane (DBM) ligands and a Lewis base ligand 2,4,6-tris(2-pyridyl)-1,3,5-triazine (tptz). The nonacoordinate europium ion features six oxygen atoms of the three DBM ligands and three nitrogen atoms from the tptz ligand, forming a distorted monocapped square antiprism. They also studied that the electronic absorption of the complex is essentially ligand-based, while the emission is characteristic of a Eu(III) ion. It is concluded that the metal-centered red emission is promoted by the ligand-assisted energy transfer, namely the antenna effects. Wietzke et al. [21] reported

the crystal structure of the europium chloride with tptz, $[\text{Eu}(\text{tptz})\text{Cl}_3(\text{CH}_3\text{OH})_2]\cdot\text{CH}_3\text{OH}$ and shows that tptz is a better ligand than terpy in acidic media owing to its additional protonation/complexation site (Fig. 3.2).

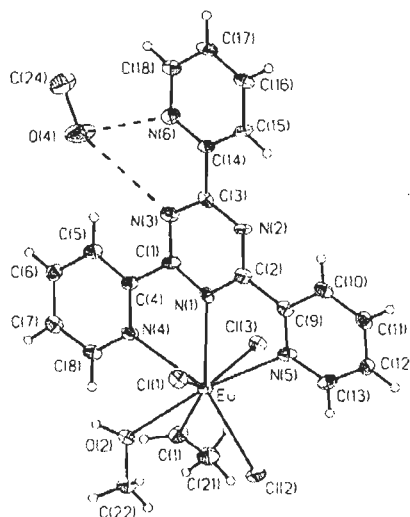


Fig. 3.2: Crystal structure of $[\text{Eu}(\text{tptz})\text{Cl}_3(\text{CH}_3\text{OH})_2]\cdot\text{CH}_3\text{OH}$

Tedmann et al. [22] reported the synthesis and characterization of seven coordinated europium complex, $[\text{EuCl}_3(\text{C}_{10}\text{H}_8\text{N}_2\text{O}_2)_2]\cdot 2\text{CH}_3\text{OH}$ as shown in Fig. 3.3. They also reported the luminescence properties of the title compound, where Eu^{3+} cation has a non-degenerate emitting level.

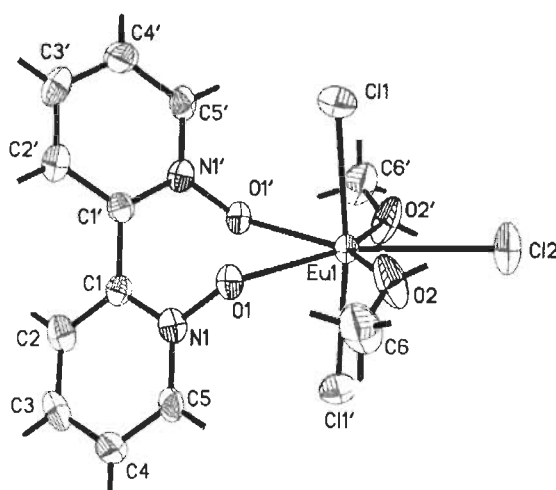


Fig. 3.3: Crystal structure of $[\text{EuCl}_3(\text{C}_{10}\text{H}_8\text{N}_2\text{O}_2)_2]\cdot 2\text{CH}_3\text{OH}$

Liu et al. [23] synthesized and characterized novel europium complex, using 2-(4-methoxy)phenyl-5-(2-pyridyl)-1,3,4-oxadiazole as a secondary ligand. They also reported its thermal stability, UV absorption and photoluminescence of this europium complex, as well as

its electroluminescence in polymer light emitting devices (PLEDs). The results show that this europium complex displayed intense UV absorption band around 350 nm and sharp red emission peaked at 612 nm with a full width at half maximum of 9 nm in chloroform. The PLEDs with this europium complex doped into a blend of poly (N-vinylcarbazole) and 5-biphenyl-2-(4-tert-butylphenyl)-1,3,4-oxadiazole exhibited a light intensity of 12 cd/m² at 24 V with a characteristic red emission of europium ion at 613 nm.

Zheng et al. [24] synthesized the binuclear europium complex [Eu₂(SA)₆(phen)₂].6H₂O (where SA = succinamate, phen = 1,10-phenanthroline) containing two crystallographically independent Eu(SA)₃(phen) species in which the Eu(III) ions have two different coordination environments (Fig. 3.4). The ⁷F₀→⁵D₀ excitation peaks at 580.16 and 580.46 nm at 77 K and the stark components of ⁵D₀→⁷F_J transitions, especially ⁵D₀→⁷F₁ and ⁵D₀→⁷F₂ emission lines, show that this complex has two Eu(III) ion sites.

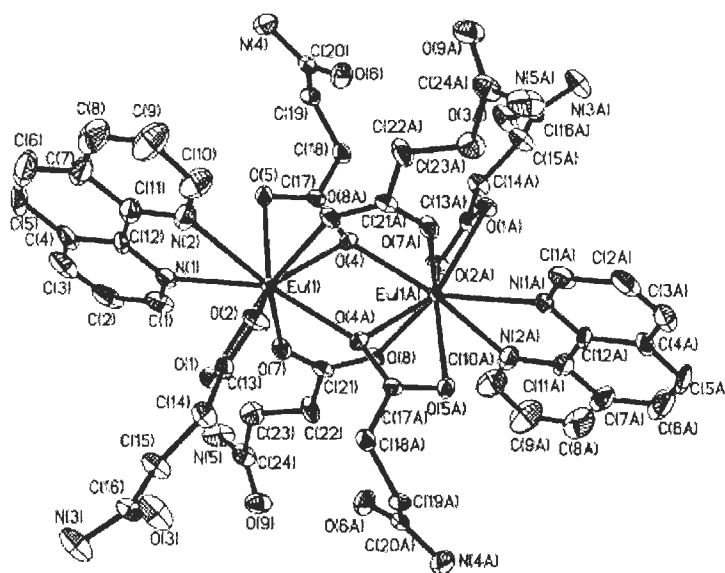


Fig. 3.4: Crystal structure of [Eu₂(SA)₆(phen)₂].6H₂O

Fukuda et al. [25] reported novel higher-order mixed chelate complex of composition [Tb(terpy)(acac)(NO₃)₂] and defined the splitting parameter, $\Delta\nu$, of the NO₃⁻ ligand, increases with decreasing ionic size across the lanthanide series. Song et al. [26] synthesized and characterized a series of lanthanide complexes with two structurally related ligands, 1,1,1,1-tetrakis{[(2'-(2-benzylaminoformyl))phenoxy] methyl} methane (L^I) and 1,1,1,1-tetrakis{[(2'-(2-picolyaminoformyl))phenoxy]methyl}methane (L^{II}) (Fig. 3.5). They also studied the luminescence properties of the resulting complexes, formed with ions and used in

fluoroimmunoassays (Ln = Eu, Tb). It is noteworthy that subtle variation of the terminal group from benzene to pyridine not only sensibly affects the overall molecular structures but also the luminescence properties as well.

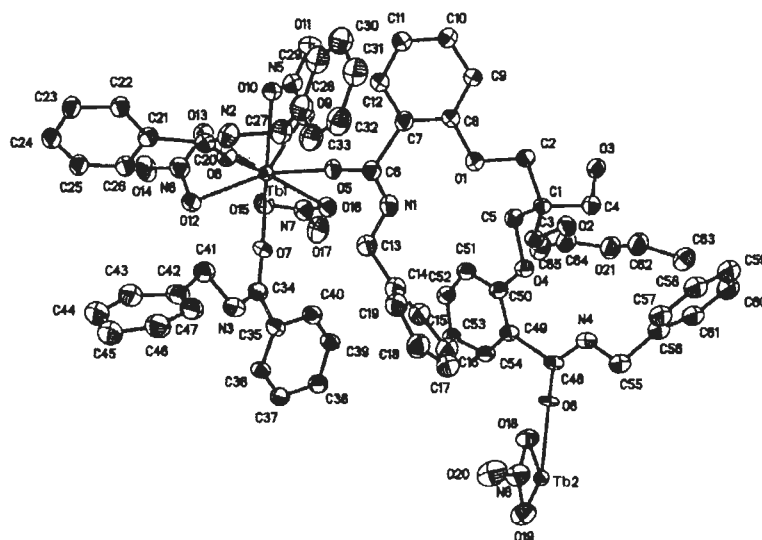


Fig. 3.5: Crystal structure of $\{[Tb_4L^1_3(NO_3)_{12} \cdot 6C_4H_{10}O]_{\infty}\}$

Song et al. [27] reported five novel lanthanide [Eu(III) (1), Tb(III) (2), Sm(III) (3), Dy(III) (4) and Gd(III) (5)] complexes with 5-Bromonicotinic acid (5-Brnic). The results reveal that $\{[Tb(5-Brnic)_3(H_2O)_3] \cdot H_2O\}_n$ (2) and $[Sm(5-Brnic)_3(H_2O)_2 \cdot H_2O]_2$ (3) exhibit different coordination geometries and crystal structures. The lowest triplet state energy of 5-Brnic was determined to be 24330 cm^{-1} corresponded to the 0–0 transition in the phosphorescence spectrum of its gadolinium complex at 411 nm. The strong luminescent emission intensities of these complexes indicated that the triplet state energy of 5-Brnic is suitable for the sensitization of luminescence of Eu(III), Tb(III), Sm(III) and Dy(III), especially for that of Tb(III) and Dy(III). Singh et al. [28] reported that the reaction of $GdCl_3$ and $TbCl_3$ with one equivalent of the potassium salt of the tridentate ligand hydrotris(pyrazol-1-yl)borate [K(tp)] and two equivalents of sodium p-X-benzoate (X = H, Cl, Br and NO_2) yielded the complexes of composition $\{[(tp)Ln(\mu\text{-p-X-OBz})_2]_2\}$ (Ln = Gd, Tb) (Fig. 3.6). The compounds consist of a seven-coordinate tetrakis carboxylato bridged dimetal unit with two capping hydrotris (pyrazolyl)borate ligands. Unit cell determinations suggested that $\{[(tp)Tb(\mu\text{-p-Cl-OBz})_2]_2\}$, and $\{[(tp)Tb(\mu\text{-p-NO}_2\text{-OBz})_2]_2\}$ are isostructural with $[(tp)Gd(\mu\text{-p-Cl-OBz})_4Gd(tp)] \cdot 4CH_2Cl_2$ and $[(tp)Tb(\mu\text{-p-Cl-OBz})_4Tb(tp)] \cdot 4CH_2Cl_2$. The luminescence properties of the unsubstituted

and para-substituted Gd and Tb benzoate complexes have been studied in solution at room temperature.

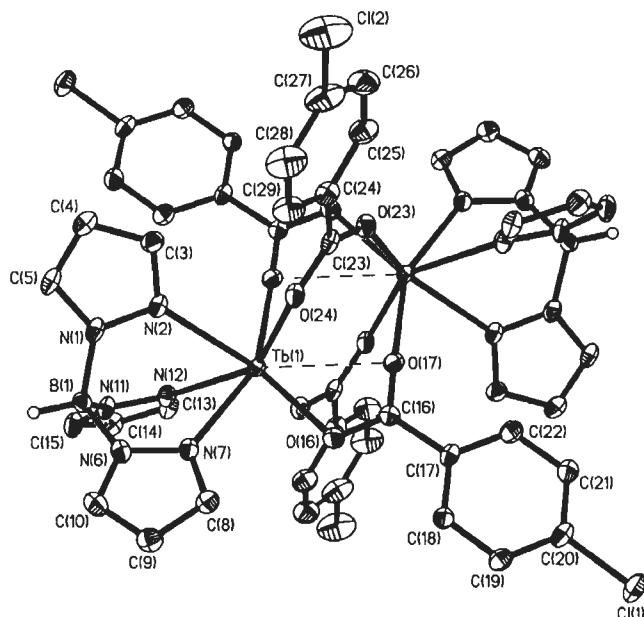


Fig. 3.6: Crystal structure of $[(tp)Tb(\mu\text{-}p\text{-Cl-OBz})_4Tb(tp)]$

Yan et al. [29] synthesized a novel quaternary dinuclear terbium complex $[Tb_2(phth)_2(Hphth)_2(phen)_2(H_2O)_4]$ where H_2phth and $phen$ are phthalic acid, 1,10-phenanthroline, respectively (Fig. 3.7). They also reported the photophysical properties which have been studied with UV absorption spectrum, excitation and emission spectrum, which exhibit strong green emission.

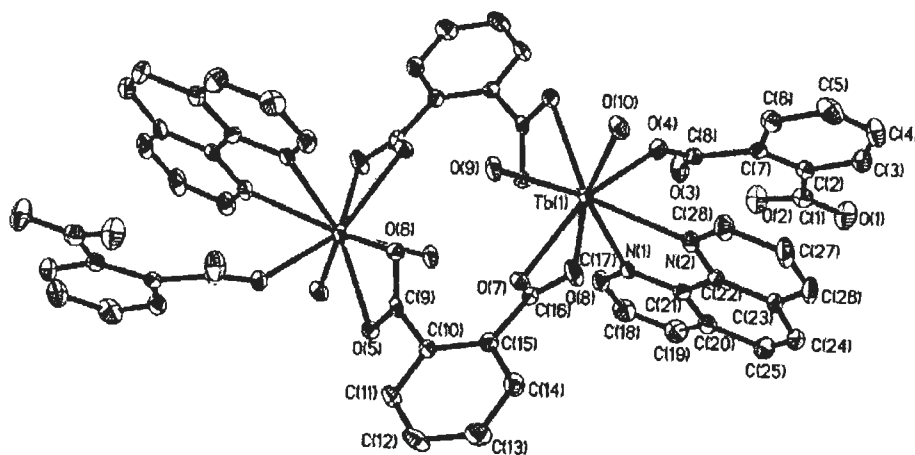


Fig. 3.7: Crystal structure of $[Tb_2(phth)_2(Hphth)_2(phen)_2(H_2O)_4]$

Li et al. [30] synthesized a series of homodinuclear Ln(III) complexes with the 4-cba ligand, $[\text{La}_2(4\text{-cba})_6(\text{phen})_2(\text{H}_2\text{O})_6]$ (**1**) (Fig. 3.8) and $[\text{Ln}_2(4\text{-cba})_6(\text{phen})_2(\text{H}_2\text{O})_2]$ ($\text{Ln} = \text{Pr}$ (**2**), Nd (**3**), Sm (**4**), Eu (**5**), Gd (**6**) and Dy (**7**); 4-Hcba = 4-cyanobenzoic acid; phen = 1,10-phenanthroline). They investigated the magnetic properties of **2-7** at variable-temperature. Complex **7** shows a significant ferromagnetic interaction between Dy(III), while no magnetic interaction exists between Gd(III) ions in **6**. In **2-5**, the value of χ_{MT} decreases with decreasing temperature but the magnetic interactions between the Ln(III) ions cannot definitely be concluded. The strong fluorescent emissions of **4**, **5**, and **7** demonstrate that ligand-to-Ln(III) energy transfer is efficient and that the coordinated water molecules do not quench their luminescence by the nonradiative dissipation of energy

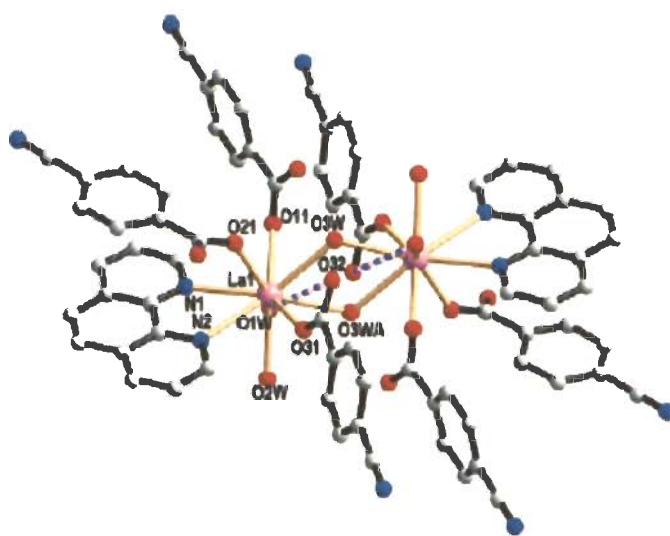


Fig. 3.8: Crystal structure of $[\text{La}_2(4\text{-cba})_6(\text{phen})_2(\text{H}_2\text{O})_6]$

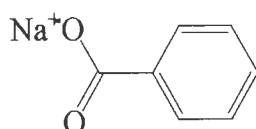
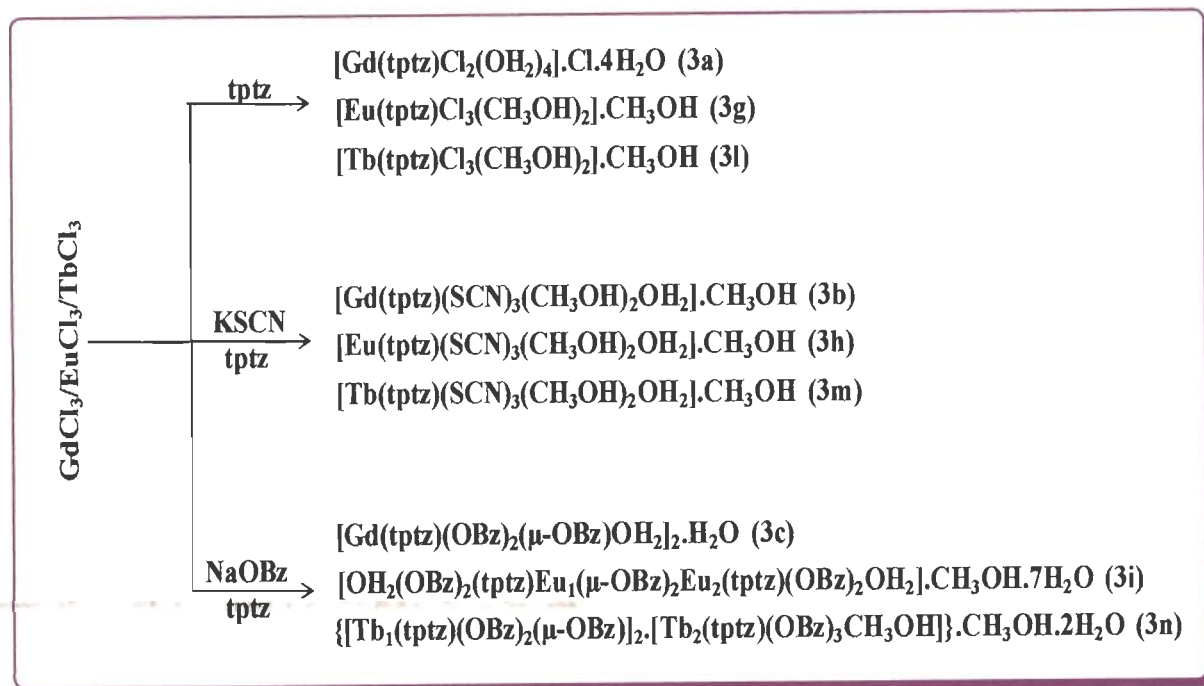
Gawryszewska and Ciunik [31] synthesized a series of lanthanide complexes with *o*-phenylenedioxydiacetic acid (PDDA) as $[\text{Ln}(\text{C}_{10}\text{H}_8\text{O}_6)_{1.5}(\text{H}_2\text{O})_3] \cdot \text{H}_2\text{O}$ where $\text{Ln} = \text{Tb(III)}$, Gd(III) , Eu(III) . Absorption, emission and excitation spectra as well as luminescence decay time measurements were used to characterize the dynamics of the excited states and to determine the ligand-to metal energy transfer mechanism for the complexes in solid state and solution. Lam et al. [32] synthesized and characterized lanthanide carboxylate complexes with benzoic acid and its derivatives. They also studied the photophysical properties of the Eu and Tb complexes i.e. the complexes exhibited sensitized luminescence in the visible spectral region but the luminescence intensities and lifetimes were very sensitive to quenching by the OH groups of methanol molecules. The solid-state magnetic properties of the Gd and Tb

complexes demonstrated the presence of weak antiferromagnetic exchange interactions at very low temperatures, caused by interaction between the neighboring ions along the chain. The above literature revealed that the syntheses of lanthanide complexes, described in this chapter are not available in details. The objective of present work is to see whether the secondary ligands would affect the structure and photophysical properties of some Ln(III) complexes, compared to its mononuclear complexes as it has been reported that the appropriate organic ligands can act as light collectors (antenna) and transfer absorbed energy to the coordinated lanthanide ion (emitter). In view of the potential applications of lanthanide complexes, this chapter reports the synthesis, structural, photophysical and thermal properties of some Ln(III) complexes with benzoate and other ligands.

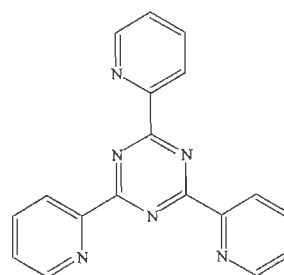
RESULTS AND DISCUSSION

The reaction of hydrated lanthanide chloride (GdCl₃, EuCl₃, TbCl₃,) with corresponding organic ligands as 2,4,6-tris(2-pyridyl)-1,3,5-triazine, 1,10-phenanthroline, KSCN, sodium benzoate (NaOBz), 2-pyrazine carboxylic acid (2-pyca) resulted in the formation of various types of metal-organic frameworks which is represented by the general scheme 3.1-3.2. The reaction of LnCl₃ with tptz and phen resulted in the formation of mononuclear complexes [Gd(tptz)Cl₂(OH₂)₄].Cl.4H₂O (**3a**), [Gd(phen)Cl₂(OH₂)₄].Cl.CH₃OH (**3d**), [Eu(tptz)Cl₃(CH₃OH)₂].CH₃OH (**3g**), [Tb(tptz)Cl₃(CH₃OH)₂].CH₃OH (**3i**), [Tb(phen)₂Cl₃OH₂].CH₃OH (**3o**), while the same reaction in the presence of KSCN give the thiocyanate complexes viz., [Gd(tptz)(SCN)₃(CH₃OH)₂OH₂].CH₃OH (**3b**), [Gd(phen)₂(SCN)₃CH₃OH].phen (**3e**), [Eu(tptz)(SCN)₃(CH₃OH)₂OH₂].CH₃OH (**3h**), [Eu(phen)₂(SCN)₃CH₃OH].phen (**3j**), [Tb(tptz)(SCN)₃(CH₃OH)₂OH₂].CH₃OH (**3m**), [Tb(phen)₂(SCN)₃CH₃OH].phen (**3p**). But when we use the secondary organic ligands as 2-pyca and OBz in the reaction mixture, the binuclear and bridged metal-organic frameworks, namely [Gd(tptz)(OBz)₂(μ-OBz)OH₂]₂.H₂O (**3c**), [OH₂(OBz)₂(tptz)Eu₁(μ-OBz)₂Eu₂(tptz)(OBz)₂OH₂].CH₃OH.7H₂O (**3i**), {[Tb₁(tptz)(OBz)₂(μ-OBz)]₂. [Tb₂(tptz)(OBz)₃CH₃OH]} .CH₃OH.2H₂O (**3n**), [OH₂(phen)(2-pyca)₂Gd₁(μ-ox)Gd₂(2-pyca)₂(phen)OH₂].6H₂O (**3f**), [OH₂(phen)(2-pyca)₂Eu₁(μ-ox)Eu₂(2-pyca)₂(phen)OH₂].6H₂O (**3k**), [OH₂(phen)(2-pyca)₂Tb₁(μ-ox)Tb₂(2-pyca)₂(phen)OH₂].6H₂O (**3q**) were obtained. The complexes **3g** and **3i** were synthesized by literature method [10, 21], and the synthesis of [Eu(phen)₂Cl₃CH₃OH] has been described in chapter 2. All these complexes were characterized by elemental analysis, infrared, thermogravimetry and X-ray crystallography. In the absence of suitable crystal, we could not collect the data for **3e**, **3p**, **3k**, **3q** complexes. The

crystallographic data, selected bond lengths, bond angles and non-covalent interactions are listed in Table 3.1 - 3.23.

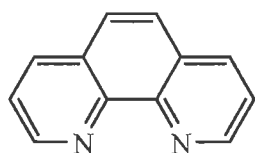
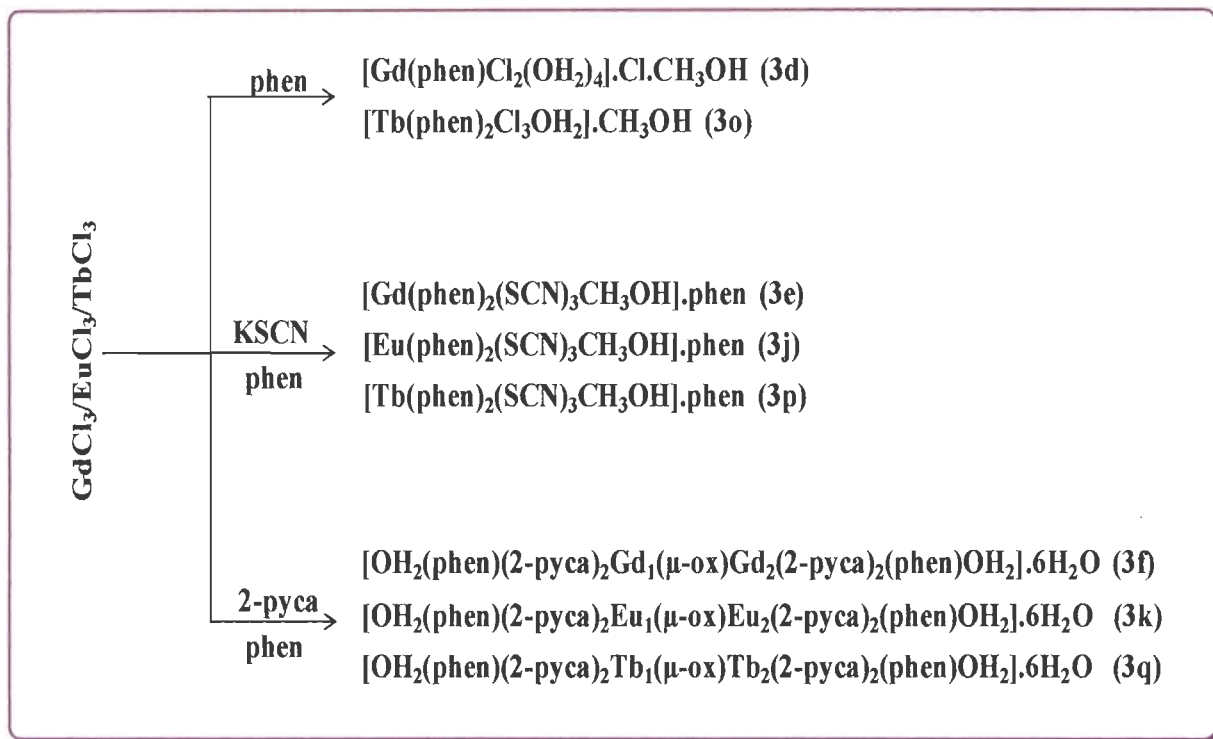


Sodium benzoate
(NaOBz)

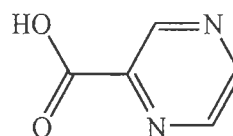


2,4,6-tris(2-pyridyl)-1,3,5-triazine
(tptz)

Scheme 3.1: Scheme for the synthesis of complexes **3a-3c**, **3g-3i**, **3l-3n**



1,10-phenanthroline
(phen)



2-pyrazine carboxylic acid
(2-pyca)

Scheme 3.2: Scheme for the synthesis of complexes **3d-3f**, **3j-3k**, **3o-3q**

Infrared spectra

The IR spectra of all the complexes show strong bands in the range of $3545\text{-}3320\text{ cm}^{-1}$ due to $\nu(\text{OH})$ stretching vibrations of lattice and / or coordinated water molecules [33]. The infrared spectra of the complex **3a-3c**, **3g-3i**, **3l-3n** gave a strong absorption as an asymmetric doublet at $1551\text{-}1522\text{ cm}^{-1}$ due to the stretching vibrations of $\nu(\text{C}=\text{C})$, $\nu(\text{C}=\text{N})$ of tptz (ca.

1530 cm⁻¹ as a strong singlet in free tptz) [17]. In complexes **3b**, **3e**, **3h**, **3j**, **3m**, **3p**, the presence of $\nu(\text{C-N})$ bands at 2067 cm⁻¹ shows the coordination of thiocyanate to the metal center through the nitrogen. The C-N stretching frequencies of thiocyanate are generally lower in the N-bonded complexes than the S-bonded complexes (near 2010 cm⁻¹) [33]. The IR bands of complexes **3c**, **3i**, **3n** in the range of 1614-1612 cm⁻¹ and 1541-1532 cm⁻¹ have been assigned to asymmetric (ν_{as}) and symmetric (ν_{s}) stretching vibrations of carboxyl group, respectively; indicating that the coordination behaviors of the benzoate groups are same in all these complexes i.e. bidentate. The position of IR bands at 1599 cm⁻¹ (ν_{as}) and 1421 cm⁻¹ (ν_{s}) are slightly different than those benzoates, which are coordinated as a bidentate. This coordination mode of the carboxylate groups was further confirmed by X-ray crystallographic studies. The C=C and C=N ring stretching vibrations bands (in the region 1650-1400 cm⁻¹) and out of plane hydrogen deformation vibrations of free phenanthroline at 845 and 735 cm⁻¹ were shifted to lower side on coordination [34] indicates the coordination of phen to the metal center. In contrast to the free acid (2-pyca) (ν_{CO} : 1721 cm⁻¹), the complexes **3f**, **3k**, **3q** show C-O absorption bands between 1635 and 1610 cm⁻¹ indicating the presence of coordinated -COO⁻ group. The bands due to the ring vibrations [33] of the pyrazine molecule are found to move to higher frequency and the band due to the carboxyl group which moves to a lower frequency, in the compounds, suggests that the nitrogen atoms in the aromatic ring and the oxygen of the carboxyl groups are coordinated to the metal atom [35, 36].

Crystal structure of [Gd(tptz)Cl₂(OH₂)₄].Cl.4H₂O (3a**)**

The single crystal X-ray studies reveal that the complex **3a** crystallizes in a monoclinic space group C1c1 ($Z = 4$). As shown in Fig. 3.9, the crystal structure of complex contains a mononuclear metal center in which gadolinium atom is coordinated by three nitrogen atoms from tptz and two terminal chlorine atoms. The coordination polyhedron is completed by four water molecules to obtain the coordination number nine. One chlorine atom is in lattice to balance the charge on the gadolinium metal center. The lattice has also four water molecules. The three coordinated six-membered rings of the tptz ligand are close to being co-planar. The gadolinium-nitrogen bond distances are in the range of 2.584(7) – 2.648(8) Å (Table 3.2). The Gd1-N2 bond distance [2.648(8) Å] is the longest bond distance among all gadolinium-nitrogen bond distances. The molecules are linked through weak non-covalent interactions viz., O3...Cl3, 3.123(9) Å; O6...Cl1, 3.166(10) Å; O6...Cl2, 3.235(11) Å; O7...Cl1, 3.299(17) Å; O7...Cl2, 2.636(17) Å; O7...Cl3, 3.091(16) Å; O1...N6, 3.202(8) Å; O2...N4, 3.033(11) Å;

O2...N6, 2.782(10) Å; O4...O5, 2.678(17) Å; O5...O8, 3.003(16) Å, resulting an entirely different three dimensional zig-zag molecular arrangement (Fig. 3.10 and 3.11).

Crystal structure of [Gd(tptz)(SCN)₃(CH₃OH)₂OH₂].CH₃OH (3b)

This complex is nine coordinated with tridentate tptz ligand, three thiocyanate, two methanol and one water molecules. One methanol molecule is present in lattice as shown in Fig. 3.12. Single crystal X-ray studies reveal that this complex crystallizes in a orthorhombic space group Pbcn ($Z = 8$). The gadolinium-nitrogen bond distances with tptz are in the range of 2.557(8) – 2.605(8) Å while with thiocyanate, these are in the range of 2.394(7) – 2.464(8) Å. The gadolinium-nitrogen bond distance with thiocyanate is shorter than with tptz. The gadolinium-oxygen bond distance is 2.426(6) Å with the water molecule, while in the range of 2.462(6) – 2.481(7) Å with the coordinated methanol molecules. The uncoordinated methanol molecule in lattice is hydrogen bonded to the coordinated thiocyanate where the methanolic oxygen act as a hydrogen donor [O4-H4...S1, 2.518(4) Å]. In addition, the methanolic oxygen (O4) also acts as hydrogen acceptor with the tptz ligand [C10-H10...O4, 2.601(11) Å]. C-H... π interactions are also present between two molecules of tptz ligands of neighboring gadolinium complexes [(i) C4-H4... π , 3.675(1) Å; (ii) C10-H10... π , 3.514(1) Å]. Other weak non-covalent interactions [O3...S2, 3.258(6) Å; S1...S1, 3.155(5) Å] are due to coordinated methanol and thiocyanate in adjacent complexes (Fig. 3.13). All these intermolecular interactions are involved to construct a three dimensional host-guest supramolecular motif along the 'a' axis where the methanol molecule acts as a guest (Fig. 3.14).

Crystal structure of [Gd(tptz)(OBz)₂(μ -OBz)OH₂]₂.H₂O (3c)

The single crystal X-ray diffraction studies confirmed the formulation of complex **3c** as being [Gd(tptz)(OBz)₂(μ -OBz)OH₂]₂.H₂O. It crystallizes in monoclinic space group P 21/c ($Z = 2$). It contains a binuclear metal center in which each gadolinium is coordinated by three nitrogen atoms from a tptz ligand and five oxygen atoms from four benzoates and one oxygen from coordinated water molecule, having coordination number nine, while one water molecule is freely present in lattice as shown in Fig. 3.15. The gadolinium atoms are separated by 4.763(11) Å. Structural studies of lanthanide carboxylate complexes have shown that the carboxylate groups may be coordinated simultaneously in three modes, namely chelating, bridging and chelating bridging [37, 38]. In present structure X-ray studies show that all the four benzoates coordinate in chelating-bridging mode within the dimeric unit i.e. one benzoate behaves as monodentate ligand, while the other as a bidentate. The other two benzoates

coordinate to the metal in a bridging mode as can be seen from the differences in bond distances of Gd-O for coordinated benzoate (Table 3.6). The gadolinium-oxygen bond distances with benzoates are 2.307(4) – 2.513(4) Å. The bridged benzoates show the shorter distance as compare to other coordinated benzoates. The gadolinium-nitrogen bond distances with tptz are in the range of 2.617(11) – 2.627(6) Å. According to Fig. 3.16, the uncoordinated water molecule non-covalently hydrogen bonded to the coordinated benzoate and tptz where it acts as an acceptor via C10-H10...O8, 2.991(27) Å; C23-H23...O8, 2.961(27) Å interactions, while the others C-H...O interactions between the adjacent complexes are C3-H3...O2, 2.573(6) Å; C4-H4...O2, 2.691(3) Å; C4-H4...O4, 2.838(7) Å; C35-H35...O7, 2.537(7) Å. A ladder like molecular rearrangement is possible along the 'b' axis due to these intermolecular hydrogen bonded interactions (Fig. 3.17).

Crystal structure of [Gd(phen)Cl₂(OH₂)₄].Cl.CH₃OH (3d)

The molecular structure of **3d** is shown in Fig. 3.18. The structure analysis demonstrated that complex **3d** contains mononuclear gadolinium center where the metal ion is coordinated by two nitrogen atoms (N1, N2) of phen ligand and two terminal chloride ions. The coordination polyhedron is completed by coordination of four water molecule with total coordination number eight. A chloride ion and also a methanol molecules crystallize in lattice where the Cl⁻ ion complete the +3 charge on the metal center. The gadolinium-nitrogen bond distances of coordinated phen ligand are in the range of 2.574(6) – 2.589(6) Å, while the gadolinium-oxygen is 2.433(6) – 2.442(7) Å. The chloride ion in lattice show non-covalent interactions [O2-H2A...Cl3, 2.416(6) Å; O4-H4A...Cl3, 2.453(4) Å; O4-H4B...Cl3, 2.374(91) Å] with the coordinated water molecules of adjacent mononuclear complex. The methanol molecule in lattice also non-covalently hydrogen bonded to coordinated water molecule via O3-H3A...O5, 1.889(9) Å; O5-H3A...O3, 1.845(6) Å interactions as shown in Fig. 3.19. These interactions cause the formation of two dimensional ladder like molecular rearrangement for this complex (Fig. 3.20).

Crystal structure of [OH₂(phen)(2-pyca)₂Gd₁(μ-ox)Gd₂(2-pyca)₂(phen)OH₂].6H₂O (3f)

The molecular structure of **3f** is depicted in Fig. 3.21. From the crystal structural study, it is clear that this is a binuclear complex and crystallizes in triclinic space group P 1 (Z = 1). Each gadolinium metal center is coordinated by two nitrogen atoms (N1, N2) from phen, two (N3, N4) from 2-pyca, one oxygen (O1) from water molecule, two (O2, O3) from 2-pyca and two (O4, O5) from oxalic acid. This reaction includes oxidative-coupling of methanol to oxalic

acid. Six water molecules are also present in lattice. One binuclear complex hydrogen bonded to the adjacent complex through C29-H29...O5, 2.693(23) Å; C15-H15... π , 3.387(15) Å intermolecular interactions (Fig. 3.22a). The freely present water molecules in lattice also show non-covalent interactions [O11...O15, 2.792(53) Å; O14...O15, 2.530(15) Å; O16...O19, 2.725(33) Å; O19...O20, 2.687(50) Å] with each other. These water molecules further interacted with coordinated water molecule and the oxygen atom of 2-pyca via C15-H15...O14, 3.387(13) Å; C19-H19...O14, 3.010(13) Å interactions as shown in Fig. 3.22b. Host-guest supramolecular network is constructed due to the presence of these intermolecular interactions.

Crystal structure of [Eu(tptz)(SCN)₃(CH₃OH)₂OH₂].CH₃OH (3h)

The europium complex **3h** crystallizes in orthorhombic space group Pbcn ($Z = 8$). It is a nine coordinated mononuclear complex with three nitrogen atoms (N1, N2, N3) of tridentate tptz ligands, three nitrogen atoms (N4, N5, N6) of thiocyanates, two methanol and one water molecules as shown in Fig. 3.23. It also contains one uncoordinated methanol solvent in lattice. The europium-nitrogen bond distances with tptz fall in the range of 2.588(3) - 2.636(5) Å while with thiocyanates, 2.434(4) – 2.470(4) Å. The Eu-N and Eu-O bond distances are larger than the Gd-N in complex **3b**. The europium-oxygen bond distances with methanol and water molecules are 2.458(3) – 2.517(4) Å which are also greater than Gd-O bond distance in the complex **3b**. The uncoordinated methanol molecule shows the intermolecular hydrogen bond interaction with the mononuclear europium complex where the oxygen atom (O4) of methanol acts as donor with the thiocyanate, O4-H4...S3, 2.535(1) Å, the methyl group of methanol also act as donor with thiocyanate, C26-H26B...S3, 2.967(2) Å. The others hydrogen bonded non-covalent interactions [O1-H1A...S2, 2.475(56) Å; C19-H19...S1, 3.176(1) Å; C20-H20...S3, 3.083(2) Å] and very weak non-covalent interactions [O2...S1, 3.189(4) Å, S3...S3, 3.176(2) Å] are shown in Fig. 3.24. There are no C-H... π interaction in this complex as in **3b**. These different non-covalent interactions cause the construction of a three dimensional pseudo host-guest supramolecular framework along the 'c' axis where methanol in lattice behaves as a guest molecule (Fig. 3.25).

Crystal structure of [OH₂(OBz)₂(tptz)Eu₁(μ -OBz)₂Eu₂(tptz)(OBz)₂OH₂].CH₃OH.7H₂O (3i)

This complex crystallizes in triclinic space group P 1 ($Z = 1$). Each metal center completes its coordination number (nine) through three nitrogen atoms from trident tptz ligands, five oxygen atoms from benzoates and one oxygen from water molecule, whereas

seven water molecules are freely present in lattice as shown in Fig. 3.26. The europium-nitrogen bond distances with tptz are in the range of 2.583(23) – 2.660(29) Å, while the europium-oxygen bond distances with benzoates are in the range of 2.236(19) – 2.524(19) Å. The bridged benzoates show the shorter distance of europium-oxygen bond as compare to terminally coordinated benzoates. The binuclear europium complex is hydrogen bonded to the neighboring complex via C-H \cdots π [C19-H19 \cdots π , 3.477(6) Å; C20-H20 \cdots π , 3.627(6) Å; C37-H37 \cdots π , 3.548(12) Å; C52-H52 \cdots π , 3.553(11) Å] intermolecular interactions. Due to these C-H \cdots π non-covalent interactions, four binuclear complex hydrogen bond to each other and construct a cavity for guest i.e. behave as a host. The seven water and one methanol molecules act as guest molecules and occupy these cavities. These free seven water molecules non-covalently bonded to each other via O \cdots O [O17 \cdots O19, 2.997(35) Å; O19 \cdots O20, 2.787(31) Å; O17 \cdots O22, 3.008(31) Å; O15 \cdots O16, 2.737(39) Å; O15 \cdots O22, 2.690(47) Å; O16 \cdots O21, 2.886(40) Å] intermolecular interactions. Three uncoordinated water molecules show the intermolecular interactions with the coordinated benzoates through O \cdots O [O4 \cdots O20, 2.703(29) Å; O13 \cdots O17, 2.892(31) Å; O10 \cdots O15, 2.851(32) Å; O14 \cdots O21, 2.878(36) Å] weak interactions. The methanol molecule also involved in non-covalent interactions [C82-H82A \cdots O20, 2.845(36) Å; C82-H82B \cdots O21, 2.121(22) Å; C82-H82C \cdots O21, 2.637(24) Å] with uncoordinated water molecules, where the methyl group acts as donor and water as an acceptor (Fig. 3.27). All these interactions help to construct an entirely different three dimensional supramolecular metal-organic framework for this complex (Fig. 3.28).

Crystal structure of [Eu(phen)₂(SCN)₃CH₃OH].phen (3j)

The complex **3j** crystallizes in the triclinic space group P-1 (Z=2) with an uncoordinated phenanthroline molecule in the asymmetric unit. Fig. 3.29 shows the molecular structure of the complex with numbering of the atom. From crystal structure, it is clear that europium is eight coordinated, bonding to four nitrogen atoms of two bidentate 1,10 phenanthroline ligands, three monodentate thiocyanate groups. The coordination polyhedron in this complex is also completed by one methanol (CH₃OH) group. The europium-nitrogen bond distances of coordinated phenanthroline ligands are in the range of 2.585(4) – 2.620(4) Å. Among all the Eu-N(phen) bond distances, Eu(1)-N(1) bond distance [2.620(4) Å] is the longest. The average Eu-N(phen) bond distance [2.601 Å] is longer as compare to average Eu-N(phen) bond distances [2.584 Å]. The europium-nitrogen (thiocyanate) bond distances are in the range of 2.435(5) – 2.452(5) Å. The Eu(1)-N(7) bond distance [2.452(5) Å] is the longest

bond distance among all three Eu-N(thiocyanate) bond distances. The average Eu-N(thiocyanate) bond distance is [2.444 Å]. For all thiocyanate ligands, the average N-C and C-S bond distances are 1.154 Å and 1.625 Å, respectively; consistent with the reported values. In **3j**, all the N-C-S bond angles [N8-C38-S2; 178.9(5)°, N7-C37-S1; 178.4(5)° and N9-C90-S3; 178.7(5)°] are approximately very close to linearity, but there is no significant difference in the Eu-N-C bond angles. The average Eu-N-C bond angle is 162.4° that concludes that all thiocyanate groups show a significant bending at the nitrogen atoms of thiocyanate ligands. The average angles involving the thiocyanate ligands at the metal center are cis-N-Eu-N of 81.41° and trans-N-Eu-N of 147.98°. The non-coordinated phenanthroline molecule in the asymmetric unit is bonded to the mononuclear complex through C-H...O [C36-H36A...O1, 3.160(5) Å] hydrogen bond between non-coordinated phenanthroline molecule and oxygen atom of coordinated methanol. The same non-coordinated phenanthroline molecule is again bonded to another mononuclear complex through C-H...S [C26-H26A...S1, 3.076(7) Å; C34-H34A...S1, 2.887(2) Å; C91-H91A...S2, 3.703(6) Å; C92-H92A...S1, 3.037(4) Å] hydrogen bond between non-coordinated phenanthroline molecule and sulfur atom of coordinated thiocyanate ligand (Fig. 3.30). In addition to this, other non-covalent interactions are weak $\pi\cdots\pi$ [3.378(5) – 3.415(2) Å] stacking interactions between the coordinated phenanthroline molecules, C-H...S [C39-H39A...S3, 3.189(4) Å] and C-H...N [C19-H19A...N8, 2.738(5) Å] from the adjacent mononuclear complex. All these interactions are involved in the formation of host-guest supramolecular architecture as shown in Fig. 3.31.

Crystal structure of [Tb(tptz)(SCN)₃(CH₃OH)₂OH₂].CH₃OH (**3m**)

The complex **3m** crystallizes in orthorhombic space group Pbcn (*Z* = 8). It is nine coordinated mononuclear complex with three nitrogen atoms (N1, N2, N3) of tridentate tptz ligands, three nitrogen atoms (N4, N5, N6) of thiocyanates, two methanol and one water molecules. It also contains the one uncoordinated methanol solvent in lattice as shown in Fig. 3.32. The terbium-nitrogen bond distances with tptz are in the range of 2.588(3) - 2.638(5) Å while with thiocyanates, they are in the range of 2.434(4) – 2.468(4) Å. The terbium-oxygen bond distances with methanol and water molecules are in the range of 2.458(3) – 2.520(4) Å. The Tb-N and Tb-O bond distances are almost same as in complex **3h**. The coordinated methanol molecule shows the intermolecular hydrogen bond interaction [O2-H2A...S2, 2.513(56) Å; C24-H24B...S1, 2.929(1) Å] with adjacent terbium complex where the oxygen atom (O2) and methyl group of methanol acts as donor with the thiocyanate. The

uncoordinated methanol molecule hydrogen bonded to coordinated thiocyanate via O4-H4...S3, 2.540(1) Å; C26-H26B...S3, 2.975(2) Å interactions. The other intermolecular interactions are C14-H14...S3, 2.931(2) Å; O3...S1, 3.188(4) Å; S3...S3, 3.178(2) Å as given in Fig. 3.33. A three dimensional pseudo host-guest supramolecular framework along the 'c' axis where methanol in lattice behaves as a guest molecule, is formed due to these non-covalent interactions (Fig. 3.34).

Crystal structure of $\{[\text{Tb}_1(\text{tptz})(\text{OBz})_2(\mu\text{-OBz})]_2\cdot[\text{Tb}_2(\text{tptz})(\text{OBz})_3\text{CH}_3\text{OH}]\}\cdot\text{CH}_3\text{OH}$.

2H₂O (3n)

The single crystal X-ray studies reveal that the unit cell consists of two crystallographically independent complex, one mononuclear and one binuclear complex with two water and one methanol molecules in lattice (Fig. 3.35). This complex crystallizes in a triclinic space group P-1 (Z = 1). In mononuclear unit, the terbium ion is in nine coordination environment, coordinated by three nitrogen atoms from tptz ligand, five oxygen atoms from three benzoates (two OBz behave as bidentate and one as monodentate). The coordination polyhedron is completed by one solvent methanol molecule. The terbium-nitrogen bond distances in this unit are in the range of 2.524(6) – 2.569(6) Å and the terbium-oxygen distances are in the range of 2.377(7) - 2.487(5) Å. In binuclear complex, each metal center is coordinated by three nitrogen atoms from tptz and six oxygen atoms from benzoates (two OBz coordinated to the metal center in bidentate manner and two in bridging mode). The different type of C-H...π interactions are present in this complex (i) binuclear moiety non-covalently hydrogen bonded to the adjacent binuclear complex through C12-H12...π, 3.148(5) Å; C13-H13...π, 3.279(7) Å; C23-H23...π, 3.389(5) Å, (ii) the two mononuclear complex is hydrogen bonded via C3-H3...π, 3.409(3) Å, (iii) mononuclear and binuclear complexes are hydrogen bonded to each other via C3-H3...π, 3.409(3) Å; C11-H11...π, 3.371(6) Å which are involved in making a cavity to occupy the methanol and water molecules. The methanol occupied the cavity through C80-H80B...O10, 1.928(5) Å, while the water molecules with oxygen atoms of benzoates and nitrogen atom of tptz via O1...O15, 2.738(8) Å; O2...O14, 2.847(8) Å; O3...O15, 2.761(7) Å; N6...O14, 2.985(8) Å intermolecular interactions, respectively (Fig. 3.36). These intermolecular interactions are responsible for the formation of an entirely different ladder like host-guest supramolecular metal-organic framework along 'c' axis as shown in Fig. 3.37.

Crystal structure of [Tb(phen)₂Cl₃OH₂].CH₃OH (**3o**)

The molecular structure and numbering of **3o** is shown in Fig. 3.38. The structure analysis demonstrated that the complex contains mononuclear terbium center, where the terbium is coordinated by four nitrogen atoms (N1, N2, N3, N4) of two phen ligands and three chloride ions. The coordination polyhedron is completed by coordination of one water molecule with total coordination number eight. A methanol molecule also crystallizes in lattice. The terbium-nitrogen bond distances of coordinated phen ligands are in the range of 2.577(2) Å – 2.586(2) Å. There are various non-covalent interactions as O-H...O, O-H...Cl, C-H... π , [O1-H30...O2, 1.877(2) Å; O1-H31...Cl2, 2.555(33) Å; O2-H2...Cl3, 2.370(1) Å; C6-H6...Cl2, 2.731(0) Å; C11-H11B... π , 3.360(2) Å] with neighboring terbium complexes as shown in Fig. 3.39. The methanol molecule in lattice also non-covalently hydrogen bonded to coordinated chloride molecule via C25-H25...Cl1, 2.922(0) Å and resulted in the formation of three dimensional ladders like packing along 'b' axis (Fig. 3.40).

Photophysical properties

Due to the smaller ligand-field splitting for Ln(III) complexes, the radiationless decay processes are relatively inefficient and emission from these complexes is common [39]. The characteristics sharp and narrow bands in the absorption and emission spectra of Ln(III) ions correspond to the *f-f* transitions. The numbers of bands depend upon the particular lanthanide ion and its electronic states arrangement. Direct excitation with UV radiation leads to weak emission because of the poor ability to absorb the light, whereas the sensitized emission in chelate complexes causes an increase (by several orders of magnitude) in the lanthanide based emission. No emission could be detected for the Gd complexes. The ultraviolet absorption spectra (spectra not shown) of the complex **3g**, shows maximum absorption bands at 298.0 nm. The fluorescence arises from intramolecular energy transfer from the ligand to the Eu(III) center. The absorption of UV radiation by the ligands produces an excited triplet state, which in turn causes an intramolecular energy transfer to the Eu(III) ion. Upon decay from the excited state, fluorescence is observed. The emission spectrum for **3g** displays bands at 585.0 nm (⁵D₀ → ⁷F₁); 612.0 nm (⁵D₀ → ⁷F₂); 644.0 nm (⁵D₀ → ⁷F₃); 698.0 nm (⁵D₀ → ⁷F₄). The intensity sequence of the peaks is – I_{5D0→7F2} > I_{5D0→7F3} > I_{5D0→7F1} > I_{5D0→7F4}. The electronic dipole transition ⁵D₀ → ⁷F₂ exhibits the highest relative emission intensity (Fig. 3.41). From the spectrum, it is clear that no emission from the ligands present in the complex are observed, indicates that a very efficient energy transfer occurs from the ligands to Eu(III) ion. Fig. 3.42

and 3.43 show the luminescence spectra of the complex **3h**, **3i** in methanol. UV-VIS absorption spectra of both complexes reveal absorption bands at $\lambda_{\max} = 292$ and 230 nm, respectively. The complex **3h** shows the emission at 585.6 nm (${}^5D_0 \rightarrow {}^7F_1$); 618.0 nm (${}^5D_0 \rightarrow {}^7F_2$); 648.4 nm (${}^5D_0 \rightarrow {}^7F_3$); 691.6 nm (${}^5D_0 \rightarrow {}^7F_4$) and the electronic dipole transition ${}^5D_0 \rightarrow {}^7F_1$ exhibits the highest relative emission intensity, while the complex **3i** shows the more emission bands with more number of transitions (${}^5D_0 \rightarrow {}^7F_{0,1,2,3,4}$) and ${}^5D_0 \rightarrow {}^7F_2$ shows the highest relative emission intensity. The ${}^5D_0 \rightarrow {}^7F_0$ transition is relatively weak and the emission band is not symmetrical. The inhomogeneous broadening of the ${}^5D_0 \rightarrow {}^7F_0$ emission band arises from the site to site variation in the local field acting on the ions. The emission spectrum of complex **3i** vary significantly from **3h** as the crystal system is triclinic, whereas the complex **3h** crystallizes in orthorhombic crystal system in Pbcn space group and in complex **3i**, benzoate groups are coordinated to the europium ions in different chelating mode. On the other hand, the emission bands for [Eu(phen)₂Cl₃CH₃OH] (described in chapter-2) (Fig. 3.44) are same as in complex **3g** but the intensity sequence is different from others due to different local coordination sites. The intensity sequence of the peaks is $I_{5D_0 \rightarrow 7F_3} > I_{5D_0 \rightarrow 7F_2} > I_{5D_0 \rightarrow 7F_1} > I_{5D_0 \rightarrow 7F_4}$. The main emission features for the complex **3j**, centered at 598.79 nm arising from electronic dipole transition ${}^5D_0 \rightarrow {}^7F_1$. The other sharp bands at 644.37 nm (${}^5D_0 \rightarrow {}^7F_3$) and 698.97 nm (${}^5D_0 \rightarrow {}^7F_4$) are also identifiable (Fig. 3.45). As shown in Fig. 3.46 and 3.51, the emission spectra contain narrow and well resolved bands which corresponds to ${}^5D_0 \rightarrow {}^7F_j$ ($j = 0-4$) and ${}^5D_4 \rightarrow {}^7F_j$ ($j = 2-6$) transition for Eu(III) **3k** and Tb(III) **3q** complexes, respectively. They show high intensive emission due to the increase in the energy of 2-pyca⁻ ligand triplet level and coordination of the nitrogen hetero atom by the lanthanide (Eu, Tb) ions. The luminescence spectrum (Fig. 3.48) of the complex **3m** indicates that the complex exhibits strong luminescence, which may arise from ${}^5D_4 \rightarrow {}^7F_j$ ($J = 6-3$) transition, a typical characteristic of Tb³⁺. The main emission occurs, as expected, in the ${}^5D_4 \rightarrow {}^7F_6$. Although the ${}^5D_4 \rightarrow {}^7F_5$, ${}^5D_4 \rightarrow {}^7F_4$ and ${}^5D_4 \rightarrow {}^7F_3$ transitions are also present. The existence of a single peak at about 486.0 nm indicates the presence of only one single emitting species corresponding to the metal center. The emission spectrum of the Tb in complex **3l**, **3o** (Fig. 3.47 and 3.50) and **3p** (Fig. is not shown), excited into lowest energy ligand centered absorption ($\lambda_{\max} = 226$ nm, 264 nm, respectively) exhibits typical narrow band features, originating from the transition from 5D_4 ground state to the 7F_j ($J = 6-0$) multiplets. The bands at 489.0 , 544.39 , 581.61 and 622.0 nm are attributed to the transition from 5D_4 state to the 7F_6 , 7F_5 , 7F_4 , 7F_3 , respectively.

These transitions have medium intensity and show moderate sensitivity to the ligand environment. The most intense band is observed at 544.39 nm and it is due to $^5D_4 \rightarrow ^7F_5$ transition. The emission spectrum (Fig. 3.49) of the complex **3n** exhibits specific maxima at ca. 488.99, 544.77, 564.98, 587.07 and 621.7 nm. The number of components of the $^5D_4 \rightarrow ^7F_5$ transition indicates the presence of more than one chemically different Tb(III) ion sites. This is the most intense peak. The complex **3i** and **3o** show similarity with each other as both are mononuclear, whereas complex **3n** is different as this contains both binuclear and mononuclear units, and have different local coordination sites. So the emission spectra are very sensitive to the structural changes in the closest environment of the Ln(III) i.e. changes in symmetry of the lanthanide complexes causes changes in fluorescence spectra as also suggested by Legendziewicz et. al. [40, 41].

Thermal study

The thermograms were recorded for all the complexes by thermogravimetry (TG) and derivative thermogravimetric (DTG) technique in the temperature range 20-800 °C at a heating rate of 10 °C min⁻¹ under air atmosphere. Thermo gravimetric analysis indicated that complexes are stable at room temperature but at higher temperatures, curves showed irregular pattern until plateau reached up to 800 °C due to the formation of thermally stable lanthanide oxides (Ln₂O₃). The thermo analytical data for complexes **3a-3q** are listed in Table 3.24. According to TG curve as shown in Fig. 3.52, thermal decomposition process of complex **3a** can be divided into two stages. The first weight loss of 14.2% between 91-125 °C corresponds to the release of one chloride and four molecules of water. These are uncoordinated and occur in lattice freely, release easily. The second weight loss 62.1% was observed in the temperature range of 350-550 °C. At 798 °C, the complex was completely degraded into Gd₂O₃. The complexes **3b**, **3h**, **3m** showed the same pattern of thermal decomposition exhibited three well-separated weight loss stages, concluded that the coordination atmosphere is same around the metal center (Fig. 3.59). In first step, one uncoordinated methanol molecule with 4.2% mass loss leaves out in the temperature range of 103-161 °C, while coordinated water, methanol and thiocyanates with ~ 32.2% mass loss release simultaneously in the temperature range of 300-450 °C. In third stage, one 2,4,6-tris(2-pyridyl)-1,3,5-triazine molecule is released with ~ 41.5% weight loss in the temperature range of 576-661 °C. Thermal decomposition of complex **3c** (Fig. 3.53) can be divided into two stages. The first weight loss of 1.0% between 76-102 °C, corresponds to the release of uncoordinated water molecule, and the second weight loss 75.1%

was observed in the temperature range of 400-524 °C. The water molecule occurs in lattice is less stable and can easily leaves out in comparison to coordinated molecules. The complex **3d** decomposes in three steps i.e. first step involves the removal of uncoordinated chloride and methanol with 11.93% mass loss at 103 °C, while coordinated chloride and water molecules leave out completely at 324 °C. The coordinated phen completely decompose at 487 °C with 35.13% weight loss in next third step (Fig. 3.54). TG curve of complex **3f** exhibited two well separated weight loss as shown in Fig. 3.55. The first weight loss of 7.3% occurred from 100-175 °C temperature due to the loss of six uncoordinated water molecules, whereas the second weight loss of 69.3% between 300 °C and 565 °C corresponds to the loss of coordinated molecules. The remaining weight, 23.4% corresponds to the percentage of Gd and O components indicated the formation of gadolinium oxide (Gd₂O₃) as final product. The complexes **3k** and **3q** show the same trend of thermal decomposition as **3f**, given in Table 3.24. TG curve of complexes **3g** and **3l** have same pattern and show that decomposition occurred in three stages. According to Fig. 3.56, in complex **3g**, the methanol molecule present in lattice releases first with 4.34% mass loss at 105-158 °C, while coordinated water, two methanol and three chloride molecules simultaneously leave out with ~ 26.83% mass loss in the temperature range of 305-467 °C and one 2,4,6-tris(2-pyridyl)-1,3,5-triazine molecule is completely removed with ~ 43.92% weight loss at 667 °C in third stage. The complex **3i** shows the same thermal decomposition pattern as complex **3c** but in **3i**, one methanol and seven water molecules are released with 7.67% weight loss in temperature range 99-131 °C in first step, while 73.19% weight loss occurs between 401-554 °C in next second step due to the rest coordinated groups (Fig. 3.57). The TG curve and thermal behavior of complex [Eu(phen)₂Cl₃CH₃OH] has been shown in chapter 2. The complex **3j** decomposes in different ways in three stages (Fig. 3.58). Non-coordinated phen releases at 291 °C with 21.8% mass loss, while the coordinated phen groups decompose at 487 °C with 43.24%. The rest coordinated thiocyanates and methanol molecules leave out at 636 °C with 19.79% weight loss in last step. The complexes **3e** and **3p** thermally decompose in the same manner as **3j** (Table 3.24). The TG thermogram clearly indicates that thermal decomposition of complex **3n** occurs in three steps (Fig. 3.60). This complex on heating first loses 2.5% of its mass at around 99 °C i.e. low temperature decomposition, resulting the loss of methanol and water molecules, occurring in lattice. Beyond this temperature, a plateau is observed where 25.51% mass loss occurs which is responsible for the removal of C₄₀H₃₁N₆O₇ at 223-326 °C. Almost complete

decomposition 49.67% occurs at around 543 °C i.e. high temperature decomposition which corresponds to the release of $C_{78}H_{54}N_{12}O_{12}$. Thermogravimetric analysis shows that the complex **3o** exhibited three weight loss stages (Fig. 3.61). The first weight loss of 4.5% in between 77-99 °C corresponds to the loss of uncoordinated methanol. The second weight loss of 17.83% occurred in between 221-319 °C corresponds to the loss of coordinated three chlorides and one water molecules, while third weight loss 57.93% occurred in between 450-550 °C corresponds to the loss of coordinated phen molecules.

CONCLUSION

In conclusion, we have reported the synthesis, structures, photophysical and thermal properties of some mononuclear and binuclear lanthanide complexes using tptz, phen, benzoate, 2-pyca ligands. All lanthanide complexes show eight or nine coordination depending on the presence of different types of ligands in the reaction mixture. The complexes **3b**, **3h**, **3m** with tptz ligand give the pseudo host-guest like supramolecular motif along 'c' axis, while in presence of benzoate in the reaction mixture, the complexes **3c**, **3i**, **3n** give the three dimensional bridging architecture. The complex **3f** is solvothermally synthesized in which two gadolinium metal centers are bridged by the oxalic acid which is formed by the oxidative coupling of methanol solvent at high pressure and temperature. The structural integrity and the highly ordered arrangement of lanthanide centers in these complexes promise their applications as structural and functional building blocks for a variety of lanthanide-containing materials. The photophysical properties of these have been studied with excitation and emission spectra and reveal the presence of single luminescent site i.e. efficient ligand-to-metal energy transfer. Thermal analysis shows that all synthesized complexes are stable at room temperature and decompose at high temperature to give stable lanthanide oxides.

Table 3.1: Crystal data and structure refinement for [Gd(tptz)Cl₂(OH₂)₄].Cl.4H₂O (3a)

Empirical formula	C ₁₈ H ₁₂ N ₆ O ₈ Cl ₃ Gd*
Color	Colorless
Formula weight (g mol ⁻¹)	703.94
Crystal System	Monoclinic
Space Group	C1c1
a (Å)	14.859(6)
b (Å)	10.632(6)
c (Å)	17.478(8)
α (°)	90.00
β (°)	93.97(3)
γ (°)	90.00
V (Å ³)	2755.0(2)
Crystal size (mm)	0.31 x 0.26 x 0.19
Z	4
ρ _{calcd} (g m ⁻³)	1.697
μ	2.748
F (000)	1364
θ range for data collection	2.34-31.49
limiting indices	-19 ≤ h ≤ 21 -15 ≤ k ≤ 14 -18 ≤ l ≤ 25
No. of measured reflections	7280
No. of observed reflections	6774
Data/ restraints/parameters	7280/2/325
R1 (I>2σ(I))	0.058
R1 (all data)	0.066
wR2 (I>2σ(I))	0.169
wR2 (all data)	0.183

*Hydrogen are not added on water molecules.

Table 3.2: Selected Bond Distances (Å) and Bond Angles (°) for [Gd(tptz)Cl₂(OH₂)₄]. Cl.4H₂O (3a)

Bond Distances

Gd1—N1	2.584(7)	Gd1—O3	2.471(9)
Gd1—N2	2.648(8)	Gd1—O4	2.409(9)
Gd1—N3	2.641(9)	Gd1—Cl1	2.494(10)
Gd1—O1	2.451(7)	Gd1—Cl2	2.418(10)
Gd1—O2	2.449(8)		

Bond Angles

O4—Gd1—Cl2	97.57(31)	O1—Gd1—N1	68.65(23)
O4—Gd1—O2	73.26(27)	O3—Gd1—N1	121.69(26)
Cl2—Gd1—O2	69.65(28)	Cl1—Gd1—N1	68.39(27)
O4—Gd1—O1	73.98(26)	O4—Gd1—N3	78.45(27)
Cl2—Gd1—O1	136.73(29)	Cl2—Gd1—N3	144.42(29)
O2—Gd1—O1	67.28(23)	O2—Gd1—N3	138.91(26)
O4—Gd1—O3	68.76(30)	O1—Gd1—N3	76.72(27)
Cl2—Gd1—O3	72.44(33)	O3—Gd1—N3	73.24(32)
O2—Gd1—O3	120.90(28)	Cl1—Gd1—N3	83.31(30)
O1—Gd1—O3	135.75(26)	N1—Gd1—N3	62.96(25)
O4—Gd1—Cl1	138.26(30)	O4—Gd1—N2	144.86(26)
Cl2—Gd1—Cl1	76.50(33)	Cl2—Gd1—N2	78.11(28)
O2—Gd1—Cl1	137.06(29)	O2—Gd1—N2	72.59(24)
O1—Gd1—Cl1	137.03(28)	O1—Gd1—N2	85.42(24)
O3—Gd1—Cl1	70.12(32)	N1—Gd1—N2	61.69(23)
O4—Gd1—N1	130.84(25)	N3—Gd1—N2	124.62(25)
O3—Gd1—N2	138.64(28)	C13—N3—Gd1	122.12(67)
Cl1—Gd1—N2	75.28(28)	C9—N3—Gd1	121.42(62)
Cl2—Gd1—N	131.56(28)	C6—N1—Gd1	124.13(52)
O2—Gd1—N1	117.40(23)	C8—N1—Gd1	121.40(52)

**Table 3.3: Crystal data and structure refinement for [Gd(tpz)(SCN)₃(CH₃OH)₂OH₂].
CH₃OH (3b)**

Empirical formula	C ₂₄ H ₂₂ N ₉ O ₄ S ₃ Gd*
Color	Yellow
Formula weight (g mol ⁻¹)	753.97
Crystal System	Orthorhombic
Space Group	P b c n
a (Å)	27.024(12)
b (Å)	14.987(7)
c (Å)	14.156(6)
α (°)	90.00
β (°)	90.00
γ (°)	90.00
V (Å ³)	5733(4)
Crystal size (mm)	0.29 x 0.23 x 0.15
Z	8
ρ _{calcd} (g m ⁻³)	1.747
μ	2.580
F (000)	2984
θ range for data collection	1.51-28.47
limiting indices	-32 ≤ h ≤ 36 -18 ≤ k ≤ 17 -11 ≤ l ≤ 18
No. of measured reflections	6755
No. of observed reflections	4118
Data/ restraints/parameters	6755/131/374
R1 (I > 2σ(I))	0.064
R1 (all data)	0.126
wR2 (I > 2σ(I))	0.158
wR2 (all data)	0.204

*Hydrogens are not added on coordinated water and methanol molecules.

Table 3.4: Selected Bond Distances (Å) and Bond Angles (°) for [Gd(tpz)(SCN)₃(CH₃OH)₂OH₂].CH₃OH (3b)

Bond Distances

Gd1—N1	2.577(8)	Gd1—N6	2.442(8)
Gd1—N2	2.557(8)	Gd1—O1	2.426(6)
Gd1—N3	2.605(8)	Gd1—O2	2.481(7)
Gd1—N4	2.394(7)	Gd1—O3	2.462(6)
Gd1—N5	2.464(8)		

Bond Angles

N4—Gd1—O1	135.79(22)	N6—Gd1—N1	78.65(25)
N4—Gd1—N6	76.97(26)	O3—Gd1—N1	140.07(22)
O1—Gd1—N6	136.32(24)	N5—Gd1—N1	144.07(26)
N4—Gd1—O3	69.66(22)	O2—Gd1—N1	78.25(23)
O1—Gd1—O3	137.93(20)	N2—Gd1—N1	62.17(26)
N6—Gd1—O3	71.90(24)	N4—Gd1—N3	79.28(24)
N4—Gd1—N5	137.70(25)	O1—Gd1—N3	80.72(21)
O1—Gd1—N5	72.94(23)	N6—Gd1—N3	141.68(24)
N6—Gd1—N5	102.23(26)	O3—Gd1—N3	71.83(22)
O3—Gd1—N5	70.08(22)	N5—Gd1—N3	76.44(25)
N4—Gd1—O2	141.58(24)	O2—Gd1—N3	139.10(22)
O1—Gd1—O2	68.88(21)	N2—Gd1—N3	62.65(24)
N6—Gd1—O2	69.05(23)	N1—Gd1—N3	124.79(24)
O3—Gd1—O2	114.01(21)	C22—O2—Gd1	148.33(57)
N5—Gd1—O2	69.05(25)	C23—O3—Gd1	131.41(54)
N4—Gd1—N2	66.82(24)	C1—N1—Gd1	121.98(61)
O1—Gd1—N2	68.97(21)	C5—N1—Gd1	122.89(59)
N6—Gd1—N2	130.57(25)	C8—N2—Gd1	122.32(61)
O3—Gd1—N2	120.99(21)	C6—N2—Gd1	122.52(58)
N5—Gd1—N2	127.20(26)	C13—N3—Gd1	122.06(59)
O2—Gd1—N2	124.91(23)	C9—N3—Gd1	120.77(57)
N4—Gd1—N1	77.97(25)	C19—N4—Gd1	169.58(75)
O1—Gd1—N1	81.90(24)	C20—N5—Gd1	179.27(76)

Table 3.5: Crystal data and structure refinement for [Gd(tpz)(OBz)₂(μ-OBz)OH₂]₂·H₂O (3c)

Empirical formula	C ₇₈ H ₅₄ N ₁₂ O ₁₆ Gd ₂ *
Color	Colorless
Formula weight (g mol ⁻¹)	1729.83
Crystal System	Monoclinic
Space Group	P 21/c
a (Å)	13.275(17)
b (Å)	15.035(17)
c (Å)	18.810(2)
α (°)	90.00
β (°)	95.91(6)
γ (°)	90.00
V (Å ³)	3734.6(8)
Crystal size (mm)	0.27 x 0.23 x 0.17
Z	2
ρ _{calcd} (g m ⁻³)	1.538
μ	1.836
F (000)	1724
θ range for data collection	1.54-28.56
limiting indices	-17 ≤ h ≤ 17 -20 ≤ k ≤ 17 -25 ≤ l ≤ 25
No. of measured reflections	9285
No. of observed reflections	6356
Data/ restraints/parameters	9285/0/487
R1 (I > 2σ(I))	0.036
R1 (all data)	0.074
wR2 (I > 2σ(I))	0.102
wR2 (all data)	0.145

*Hydrogen are not added on water molecules.

Table 3.6: Selected Bond Distances (Å) and Bond Angles (°) for [Gd(tptz)(OBz)₂(μ-OBz)OH₂]₂·H₂O (3c)

Bond Distances

Gd1—N1	2.622(3)	Gd1—O3	2.367(5)
Gd1—N2	2.617(6)	Gd1—O4	2.396(3)
Gd1—N3	2.627(6)	Gd1—O5	2.500(6)
Gd1—O1	2.513(4)	Gd1—O6 ¹	2.307(4)
Gd1—O2	2.477(8)	Gd1 ¹ —O6	2.307(4)

Bond Angles

O6 ¹ —Gd1—O3	81.10(12)	O4—Gd1—N1	139.54(10)
O6 ¹ —Gd1—O4	107.34(10)	O2—Gd1—N1	73.07(11)
O3—Gd1—O4	140.68(11)	O5—Gd1—N1	144.65(10)
O6 ¹ —Gd1—O2	128.38(11)	O1—Gd1—N1	69.01(11)
O3—Gd1—O2	131.40(12)	N2—Gd1—N1	62.32(10)
O4—Gd1—O2	73.68(11)	O6 ¹ —Gd1—N3	148.75(11)
O6 ¹ —Gd1—O5	76.99(11)	O3—Gd1—N3	80.04(12)
O3—Gd1—O5	73.14(12)	O4—Gd1—N3	73.71(10)
O4—Gd1—O5	71.74(10)	O2—Gd1—N3	82.49(11)
O2—Gd1—O5	142.28(11)	O5—Gd1—N3	73.81(11)
O6 ¹ —Gd1—O1	77.94(13)	O1—Gd1—N3	129.48(12)
O3—Gd1—O1	145.35(13)	N2—Gd1—N3	61.16(12)
O4—Gd1—O1	72.65(12)	N1—Gd1—N3	123.3(1)
O2—Gd1—O1	52.45(12)	C32—O1—Gd1	91.76(31)
O5—Gd1—O1	127.19(12)	C32—O2—Gd1	93.39(32)
O6 ¹ —Gd1—N2	129.32(11)	C33—O3—Gd1	136.69(35)
O3—Gd1—N2	63.77(12)	C25—O4—Gd1	121.42(28)
O4—Gd1—N2	123.10(11)	C25—O6—Gd1 ¹	171.93(28)
O2—Gd1—N2	68.03(11)	C1—N1—Gd1	121.55(27)
O5—Gd1—N2	121.05(11)	C5—N1—Gd1	121.16(26)
O1—Gd1—N2	110.85(12)	C8—N2—Gd1	122.03(28)
O6 ¹ —Gd1—N1	76.94(10)	C6—N2—Gd1	120.32(26)
O3—Gd1—N1	79.59(11)	C9—N3—Gd1	122.58(32)

Table 3.7: Crystal data and structure refinement for [Gd(phen)Cl₂(OH₂)₄].Cl.CH₃OH (3d)

Empirical formula	C ₁₃ H ₁₉ N ₂ O ₅ Cl ₃ Gd*
Color	Colorless
Formula weight (g mol ⁻¹)	546.86
Crystal System	Triclinic
Space Group	P -1
a (Å)	6.713(5)
b (Å)	11.045(5)
c (Å)	13.131(5)
α (°)	87.83(5)
β (°)	79.50(5)
γ (°)	80.18(5)
V (Å ³)	943.3(9)
Crystal size (mm)	0.31 x 0.23 x 0.15
Z	2
ρ _{calcd} (g m ⁻³)	1.901
μ	3.561
F (000)	528
θ range for data collection	3.13-39.98
limiting indices	-11 ≤ h ≤ 12 -15 ≤ k ≤ 19 -22 ≤ l ≤ 23
No. of measured reflections	11350
No. of observed reflections	8355
Data/ restraints/parameters	11350/0/233
R1 (I > 2σ(I))	0.037
R1 (all data)	0.062
wR2 (I > 2σ(I))	0.109
wR2 (all data)	0.150

*Hydrogen is not added on one coordinated water molecules.

Table 3.8: Selected Bond Distances (Å) and Bond Angles (°) for [Gd(phen)Cl₂(OH₂)₄].Cl .CH₃OH (3d)

Bond Distances

Gd1—N1	2.574(6)	Gd1—O3	2.433(6)
Gd1—N2	2.589(7)	Gd1—O4	2.442(7)
Gd1—O1	2.436(7)	Gd1—Cl1	2.734(7)
Gd1—O2	2.429(3)	Gd1—Cl2	2.783(9)

Bond Angles

O2—Gd1—O3	75.11(12)	O3—Gd1—Cl1	73.24(10)
O2—Gd1—O1	77.80(12)	O1—Gd1—Cl1	139.48(9)
O3—Gd1—O1	144.91(12)	O4—Gd1—Cl1	74.64(8)
O2—Gd1—O4	72.29(9)	N1—Gd1—Cl1	78.20(7)
O3—Gd1—O4	118.24(11)	N2—Gd1—Cl1	76.88(7)
O1—Gd1—O4	72.92(11)	O2—Gd1—Cl2	80.20(9)
O2—Gd1—N1	149.30(9)	O3—Gd1—Cl2	80.34(9)
O3—Gd1—N1	82.71(11)	O1—Gd1—Cl2	73.38(8)
O1—Gd1—N1	111.79(11)	O4—Gd1—Cl2	140.06(8)
O4—Gd1—N1	138.00(9)	N1—Gd1—Cl2	75.32(8)
O2—Gd1—N2	144.13(9)	N2—Gd1—Cl2	111.10(8)
O3—Gd1—N2	139.02(11)	Cl1—Gd1—Cl2	144.54(3)
O1—Gd1—N2	73.61(11)	C1—N1—Gd1	122.46(24)
O4—Gd1—N2	78.88(10)	C12—N1—Gd1	119.34(22)
N1—Gd1—N2	64.04(8)	C10—N2—Gd1	122.67(27)
O2—Gd1—Cl1	114.23(8)	C11—N2—Gd1	118.77(22)

Table 3.9: Crystal data and structure refinement for [OH₂(phen)(2-pyca)₂Gd₁(μ-ox)Gd₂(2-pyca)₂(phen)OH₂].6H₂O (3f)

Empirical formula	C ₄₆ H ₂₈ N ₁₂ O ₂₀ Gd ₂ *
Color	Colorless
Formula weight (g mol ⁻¹)	1383.31
Crystal System	Triclinic
Space Group	P 1
a (Å)	10.550(3)
b (Å)	11.814(4)
c (Å)	12.753(4)
α (°)	101.54(15)
β (°)	105.89(14)
γ (°)	111.45(14)
V (Å ³)	1340.4(7)
Crystal size (mm)	0.27 x 0.22 x 0.18
Z	1
ρ _{calcd} (g m ⁻³)	1.714
μ	2.539
F (000)	676
θ range for data collection	1.76-28.28
limiting indices	-13 ≤ h ≤ 13 -15 ≤ k ≤ 15 -16 ≤ l ≤ 16
No. of measured reflections	11055
No. of observed reflections	9228
Data/ restraints/parameters	11055 /3/721
R1 (I>2σ(I))	0.040
R1 (all data)	0.056
wR2 (I>2σ(I))	0.111
wR2 (all data)	0.140

*Hydrogen are not added on water molecules.

Table 3.10: Selected Bond Distances (Å) and Bond Angles (°) for [OH₂(phen)(2-pyca)₂Gd₁(μ-ox)Gd₂(2-pyca)₂(phen)OH₂].6H₂O (3f)

Bond Distances

Gd1—N1	2.654(27)	Gd2—N5	2.610(27)
Gd1—N2	2.609(26)	Gd2—N6	2.651(25)
Gd1—N3	2.654(30)	Gd2—N7	2.722(28)
Gd1—N4	2.692(27)	Gd2—N8	2.636(26)
Gd1—O1	2.411(30)	Gd2—O6	2.452(30)
Gd1—O2	2.409(37)	Gd2—O7	2.426(22)
Gd1—O3	2.344(27)	Gd2—O8	2.432(25)
Gd1—O4	2.409(22)	Gd2—O9	2.352(26)
Gd1—O5	2.424(24)	Gd2—O10	2.367(36)

Bond Angles

O3—Gd1—O1	82.80(59)	O1—Gd1—N1	71.13(62)
O3—Gd1—O2	127.87(62)	O2—Gd1—N1	119.78(64)
O1—Gd1—O2	148.07(58)	O5—Gd1—N1	120.33(66)
O3—Gd1—O5	144.74(63)	O4—Gd1—N1	139.71(57)
O1—Gd1—O5	75.56(56)	N2—Gd1—N1	61.89(60)
O2—Gd1—O5	73.34(61)	N3—Gd1—N1	73.75(66)
O3—Gd1—O4	80.33(54)	O3—Gd1—N4	60.77(61)
O1—Gd1—O4	73.51(54)	O1—Gd1—N4	126.93(52)
O2—Gd1—O4	100.46(59)	O2—Gd1—N4	72.85(59)
O5—Gd1—O4	67.07(56)	O5—Gd1—N4	112.27(56)
O3—Gd1—N2	137.85(60)	O4—Gd1—N4	63.95(55)
O1—Gd1—N2	90.63(58)	N2—Gd1—N4	142.33(58)
O2—Gd1—N2	72.45(62)	N3—Gd1—N4	68.79(57)
O5—Gd1—N2	70.67(57)	N1—Gd1—N4	127.37(62)
O4—Gd1—N2	137.31(50)	C10—N1—Gd1	118.62(162)
O3—Gd1—N3	78.36(63)	C11—N1—Gd1	122.5(16)
O1—Gd1—N3	143.07(56)	C24—O4—Gd1	117.14(120)
O2—Gd1—N3	63.05(62)	C1—N2—Gd1	118.36(151)
O5—Gd1—N3	134.06(61)	C12—N2—Gd1	118.39(134)
O4—Gd1—N3	132.71(58)	C22—O3—Gd1	132.46(166)
N2—Gd1—N3	82.71(61)	C21—N4—Gd1	119.51(164)
O3—Gd1—N1	76.70(67)	C18—N4—Gd1	126.83(153)
C16—N3—Gd1	116.24(144)	O9—Gd2—N7	65.62(59)

C13—N3—Gd1	126.78(159)	O10—Gd2—N7	69.01(59)
C17—O2—Gd1	124.92(152)	O8—Gd2—N7	65.62(57)
O9—Gd2—O10	128.89(63)	O7—Gd2—N7	108.89(56)
O9—Gd2—O8	82.94(58)	O6—Gd2—N7	131.08(54)
O10—Gd2—O8	98.94(57)	N5—Gd2—N7	139.62(60)
O9—Gd2—O7	145.84(58)	N8—Gd2—N7	70.10(52)
O10—Gd2—O6	148.07(55)	N6—Gd2—N7	127.65(57)
O7—Gd2—O6	77.76(55)	C23—O8—Gd2	123.82(156)
O9—Gd2—N5	135.92(61)	C24—O7—Gd2	119.09(129)
O10—Gd2—N5	73.42(60)	O10—Gd2—O7	71.45(62)
O8—Gd2—N5	136.12(58)	O8—Gd2—O7	65.39(57)
O7—Gd2—N5	71.38(58)	O9—Gd2—O6	82.15(58)
O6—Gd2—N5	89.11(56)	O10—Gd2—O6	148.07(55)
O9—Gd2—N8	77.88(54)	C23—O5—Gd1	121.73(159)
O10—Gd2—N8	65.45(52)	C25—N5—Gd2	122.01(156)
O8—Gd2—N8	135.70(51)	C36—N5—Gd2	122.0(14)
O7—Gd2—N8	133.97(52)	C34—N6—C35	114.88(172)
O6—Gd2—N8	139.28(48)	C34—N6—Gd2	128.98(155)
N5—Gd2—N8	81.40(53)	C35—N6—Gd2	116.01(121)
O9—Gd2—N6	73.05(62)	C46—O9—Gd2	128.24(145)
O10—Gd2—N6	121.88(64)	C42—N7—Gd2	133.26(157)
O8—Gd2—N6	139.15(57)	C45—N7—Gd2	107.49(123)
O7—Gd2—N6	123.29(60)	C41—N8—Gd2	127.24(155)
O6—Gd2—N6	69.33(58)	C38—N8—Gd2	113.76(124)
N5—Gd2—N6	63.49(57)	C37—O10—Gd2	125.69(182)
N8—Gd2—N6	71.02(55)		

Table 3.11: Crystal data and structure refinement for [Eu(tptz)(SCN)₃(CH₃OH)₂OH₂]. CH₃OH (3h)

Empirical formula	C ₂₄ H ₂₃ N ₉ O ₄ S ₃ Eu*
Color	Yellow
Formula weight (g mol ⁻¹)	749.69
Crystal System	Orthorhombic
Space Group	P b c n
a (Å)	27.124(3)
b (Å)	15.117(2)
c (Å)	14.291(2)
α (°)	90.00
β (°)	90.00
γ (°)	90.00
V (Å ³)	5859.8(13)
Crystal size (mm)	0.27 x 0.21 x 0.17
Z	8
ρ _{calcd} (g m ⁻³)	1.700
μ	2.402
F (000)	2984
θ range for data collection	1.50-31.64
limiting indices	-24 ≤ h ≤ 40 -19 ≤ k ≤ 20 -19 ≤ l ≤ 17
No. of measured reflections	8332
No. of observed reflections	6807
Data/ restraints/parameters	8332/0/378
R1 (I > 2σ(I))	0.041
R1 (all data)	0.057
wR2 (I > 2σ(I))	0.154
wR2 (all data)	0.172

*Hydrogen are not added on water and one methanol molecules.

Table 3.12: Selected Bond Distances (Å) and Bond Angles (°) for [Eu(tptz)(SCN)₃(CH₃OH)₂OH₂].CH₃OH (3h)

Bond Distances

Eu1—N1	2.636(5)	Eu1—N6	2.434(4)
Eu1—N2	2.588(3)	Eu1—O1	2.485(3)
Eu1—N3	2.611(4)	Eu1—O2	2.517(4)
Eu1—N4	2.470(4)	Eu1—O3	2.458(3)
Eu1—N5	2.468(4)		

Bond Angles

N6—Eu1—O3	135.43(12)	N5—Eu1—N3	144.07(12)
N6—Eu1—N5	138.18(13)	N4—Eu1—N3	77.74(13)
O3—Eu1—N5	72.97(12)	O1—Eu1—N3	139.34(10)
N6—Eu1—N4	76.73(14)	O2—Eu1—N3	77.22(12)
O3—Eu1—N4	136.19(12)	N2—Eu1—N3	62.38(11)
N5—Eu1—N4	102.91(14)	N6—Eu1—N1	79.09(13)
N6—Eu1—O1	69.25(12)	O3—Eu1—N1	80.64(10)
O3—Eu1—O1	138.48(10)	N5—Eu1—N1	77.09(13)
N5—Eu1—O1	70.91(11)	N4—Eu1—N1	142.25(14)
N4—Eu1—O1	72.52(12)	O1—Eu1—N1	71.99(10)
N6—Eu1—O2	141.11(13)	O2—Eu1—N1	139.80(11)
O3—Eu1—O2	68.45(12)	N2—Eu1—N1	61.96(11)
O3—Eu1—O2	68.45(12)	N3—Eu1—N1	124.27(13)
N4—Eu1—O2	69.37(13)	C25—O1—Eu1	130.72(25)
O1—Eu1—O2	115.78(11)	C24—O2—Eu1	147.14(27)
N6—Eu1—N2	67.07(11)	C10—N2—Eu1	122.06(25)
O3—Eu1—N2	68.36(10)	C6—N2—Eu1	122.80(26)
N5—Eu1—N2	126.80(11)	C11—N3—Eu1	121.78(27)
N4—Eu1—N2	130.29(12)	C15—N3—Eu1	121.15(31)
O1—Eu1—N2	120.61(10)	C21—N4—Eu1	164.00(38)
O2—Eu1—N2	123.55(10)	C22—N5—Eu1	178.86(33)
N6—Eu1—N3	77.48(11)	C23—N6—Eu1	170.46(37)
O3—Eu1—N3	82.01(9)		

Table 3.13: Crystal data and structure refinement for [OH₂(OBz)₂(tptz)Eu₁(μ-OBz)₂Eu₂(tptz)(OBz)₂OH₂].CH₃OH.7H₂O (3i)

Empirical formula	C ₇₉ H ₅₈ N ₁₂ O ₂₂ Eu ₂ *
Color	Colorless
Formula weight (g mol ⁻¹)	1831.32
Crystal System	Triclinic
Space Group	P 1
a (Å)	12.927(11)
b (Å)	12.930(10)
c (Å)	13.791(11)
α (°)	82.623(5)
β (°)	83.15(4)
γ (°)	64.85(4)
V (Å ³)	2064.2(3)
Crystal size (mm)	0.29 x 0.21 x 0.14
Z	1
ρ _{calcd} (g m ⁻³)	1.473
μ	1.584
F (000)	918
θ range for data collection	1.49-28.47
limiting indices	-17 ≤ h ≤ 17 -17 ≤ k ≤ 17 -18 ≤ l ≤ 18
No. of measured reflections	16186
No. of observed reflections	10729
Data/ restraints/parameters	16186/362/1038
R1 (I > 2σ(I))	0.066
R1 (all data)	0.111
wR2 (I > 2σ(I))	0.153
wR2 (all data)	0.198

*Hydrogen are not added on water molecules.

Table 3.14: Selected Bond Distances (Å) and Bond Angles (°) for [OH₂(OBz)₂(tptz)Eu₁(μ-OBz)₂Eu₂(tptz)(OBz)₂OH₂].CH₃OH.7H₂O (3i)

Bond Distances

Eu1—N4	2.583(23)	Eu2—N1	2.700(25)
Eu1—N5	2.660(29)	Eu2—N2	2.565(21)
Eu1—N6	2.650(19)	Eu2—N3	2.593(27)
Eu1—O1	2.483(19)	Eu2—O7	2.479(19)
Eu1—O2	2.436(20)	Eu2—O8	2.375(18)
Eu1—O3	2.524(19)	Eu2—O9	2.514(19)
Eu1—O4	2.507(18)	Eu2—O10	2.504(16)
Eu1—O5	2.429(17)	Eu2—O11	2.309(18)
Eu1—O6	2.236(19)	Eu2—O12	2.386(19)

Bond Angles

O6—Eu1—O5	82.41(60)	O5—Eu1—N6	67.62(59)
O6—Eu1—O2	103.55(61)	O2—Eu1—N6	121.84(61)
O5—Eu1—O2	140.85(56)	O1—Eu1—N6	122.41(61)
O6—Eu1—O1	77.95(66)	O4—Eu1—N6	69.59(62)
O5—Eu1—O1	74.11(62)	O3—Eu1—N6	112.33(56)
O2—Eu1—O1	69.61(67)	N4—Eu1—N6	62.08(57)
O6—Eu1—O4	124.36(64)	O6—Eu1—N5	79.29(70)
O5—Eu1—O4	136.5(6)	O5—Eu1—N5	76.91(64)
O2—Eu1—O4	71.55(59)	O2—Eu1—N5	142.17(68)
O1—Eu1—O4	138.96(66)	O1—Eu1—N5	145.07(73)
O6—Eu1—O3	72.87(59)	O4—Eu1—N5	75.97(74)
O5—Eu1—O3	143.80(59)	O3—Eu1—N5	72.87(71)
O2—Eu1—O3	72.16(59)	N4—Eu1—N5	123.01(70)
O1—Eu1—O3	123.88(65)	N6—Eu1—N5	60.96(67)
O4—Eu1—O3	52.47(65)	C1—O4—Eu1	92.41(149)
O6—Eu1—N4	149.95(59)	C1—O3—Eu1	93.74(164)
O5—Eu1—N4	83.73(58)	C29—O5—Eu1	140.18(157)
O2—Eu1—N4	71.98(59)	C22—O6—Eu1	168.71(158)
O1—Eu1—N4	72.65(67)	C66—O2—Eu1	136.63(161)
O4—Eu1—N4	83.30(61)	C59—N5—Eu1	120.09(178)
O6—Eu1—N6	134.02(60)	C50—N4—Eu1	122.52(149)
C54—N4—Eu1	124.26(143)	O12—Eu2—N3	78.66(67)
O11—Eu2—O8	101.74(55)	O7—Eu2—N3	144.75(72)

O11—Eu2—O12	142.02(60)	O10—Eu2—N3	71.81(69)
O8—Eu2—O12	79.66(59)	O9—Eu2—N3	72.78(69)
O11—Eu2—O7	71.19(63)	N2—Eu2—N3	63.07(72)
O8—Eu2—O7	74.67(64)	O11—Eu2—N1	73.93(61)
O12—Eu2—O7	72.75(67)	O8—Eu2—N1	147.85(59)
O11—Eu2—O10	74.28(57)	O12—Eu2—N1	85.02(64)
O8—Eu2—O10	124.92(57)	O7—Eu2—N1	73.84(69)
O12—Eu2—O10	135.96(63)	O10—Eu2—N1	85.30(63)
O7—Eu2—O10	143.36(64)	O9—Eu2—N1	128.22(61)
O11—Eu2—O9	68.62(58)	N2—Eu2—N1	61.20(61)
O8—Eu2—O9	75.66(61)	N3—Eu2—N1	124.09(71)
O12—Eu2—O9	144.77(63)	C35—N1—Eu2	115.89(175)
O7—Eu2—O9	122.84(64)	C39—N1—Eu2	119.4(14)
O10—Eu2—O9	51.23(62)	C40—N3—Eu2	124.67(176)
O11—Eu2—N2	123.31(62)	C44—N3—Eu2	120.03(179)
O8—Eu2—N2	134.69(62)	C8—O12—Eu2	140.00(167)
O12—Eu2—N2	68.19(65)	C22—O11—Eu2	143.12(159)
O7—Eu2—N2	121.50(67)	C66—O8—Eu2	171.69(162)
O10—Eu2—N2	69.52(64)	C15—O10—Eu2	93.03(152)
O9—Eu2—N2	114.21(62)	C15—O9—Eu2	92.60(159)
O11—Eu2—N3	139.30(64)	C74—N2—Eu2	126.69(167)
O8—Eu2—N3	80.37(64)	C65—N2—Eu2	123.85(161)

Table 3.15: Crystal data and structure refinement for [Eu(phen)₂(SCN)₃CH₃OH].phen (3j)

Empirical formula	C ₄₀ H ₂₇ N ₉ OS ₃ Eu*
Color	Colorless
Formula weight (g mol ⁻¹)	897.89
Crystal System	Triclinic
Space Group	P-1
a (Å)	10.386(5)
b (Å)	12.450(6) Å
c (Å)	15.497(7) Å
α (°)	96.22(2)
β (°)	105.62(2)
γ (°)	102.41(3)
V (Å ³)	1855.14(15)
Crystal size (mm)	0.29 x 0.21 x 0.17
Z	2
ρ _{calcd} (g m ⁻³)	1.607
μ	1.906
F (000)	898.0
θ range for data collection	1.39-26.06
limiting indices	-12 ≤ h ≤ 12 -15 ≤ k ≤ 15 -19 ≤ l ≤ 19
No. of measured reflections	7221
No. of observed reflections	6519
Data/ restraints/parameters	7221/0/487
R1 (I > 2σ(I))	0.044
R1 (all data)	0.052
wR2 (I > 2σ(I))	0.119
wR2 (all data)	0.134

*Hydrogen are not added on methanol molecule.

Table 3.16: Selected Bond Distances (Å) and Bond Angles (°) for [Eu(phen)₂(SCN)₃CH₃OH].phen (3j)

Bond Distances

Eu1—N1	2.620(4)	Eu1—N7	2.452(5)
Eu1—N2	2.607(4)	Eu1—N8	2.435(5)
Eu1—N3	2.594(4)	Eu1—N9	2.446(5)
Eu1—N4	2.585(4)	Eu1—O1	2.439(4)
Eu1—N5	2.468(4)		

Bond Angles

N8—Eu1—O1	141.32(15)	N4—Eu1—N3	63.85(14)
N8—Eu1—N9	79.28(17)	N8—Eu1—N2	78.96(15)
O1—Eu1—N9	77.26(15)	O1—Eu1—N2	124.05(12)
N8—Eu1—N7	83.52(16)	N9—Eu1—N2	76.86(15)
O1—Eu1—N7	130.15(15)	N7—Eu1—N2	73.42(14)
N9—Eu1—N7	147.95(17)	N4—Eu1—N2	144.59(14)
N8—Eu1—N4	109.74(17)	N3—Eu1—N2	146.95(12)
O1—Eu1—N4	70.83(15)	N8—Eu1—N1	141.79(15)
N9—Eu1—N4	137.80(16)	O1—Eu1—N1	72.17(15)
N7—Eu1—N4	73.65(16)	N9—Eu1—N1	97.87(16)
N8—Eu1—N3	72.79(15)	N7—Eu1—N1	79.42(16)
O1—Eu1—N3	73.58(12)	N4—Eu1—N1	97.87(15)
N9—Eu1—N3	81.30(15)	N3—Eu1—N1	145.01(14)
N7—Eu1—N3	118.96(14)	N2—Eu1—N1	63.50(14)

Table 3.17: Crystal data and structure refinement for [Tb(tptz)(SCN)₃(CH₃OH)₂OH₂]. CH₃OH (3m)

Empirical formula	C ₂₄ H ₂₃ N ₉ O ₄ S ₃ Tb*
Color	Yellow
Formula weight (g mol ⁻¹)	756.65
Crystal System	Orthorhombic
Space Group	P b c n
a (Å)	27.124(3)
b (Å)	15.117(2)
c (Å)	14.291(2)
α (°)	90.00
β (°)	90.00
γ (°)	90.00
V (Å ³)	5859.8(13)
Crystal size (mm)	0.26 x 0.19 x 0.13
Z	8
ρ _{calcd} (g m ⁻³)	1.715
μ	2.675
F (000)	3000.0
θ range for data collection	1.50-31.64
limiting indices	-24 ≤ h ≤ 39 -19 ≤ k ≤ 20 -19 ≤ l ≤ 21
No. of measured reflections	8564
No. of observed reflections	6789
Data/ restraints/parameters	8332/0/378
R1 (I > 2σ(I))	0.042
R1 (all data)	0.058
wR2 (I > 2σ(I))	0.158
wR2 (all data)	0.174

*Hydrogen are not added on water and one methanol molecules.

Table 3.18: Selected Bond Distances (Å) and Bond Angles (°) for [Tb(tpz)(SCN)₃(CH₃OH)₂OH₂].CH₃OH (3m)

Bond Distances

Tb1—N1	2.638(5)	Tb1—N6	2.435(4)
Tb1—N2	2.588(3)	Tb1—O1	2.458(3)
Tb1—N3	2.610(4)	Tb1—O2	2.483(3)
Tb1—N4	2.471(4)	Tb1—O3	2.520(4)
Tb1—N5	2.468(4)		

Bond Angles

N6—Tb1—O1	135.43(12)	N4—Tb1—N3	77.74(13)
N6—Tb1—N5	138.20(13)	O2—Tb1—N3	139.36(10)
O1—Tb1—N5	72.89(12)	O3—Tb1—N3	77.22(12)
N6—Tb1—N4	76.74(14)	N2—Tb1—N3	62.32(11)
O1—Tb1—N4	136.22(12)	N6—Tb1—N1	79.06(13)
N5—Tb1—N4	102.97(14)	O1—Tb1—N1	80.63(10)
N6—Tb1—O2	69.28(12)	N5—Tb1—N1	77.05(13)
O1—Tb1—O2	138.42(10)	N4—Tb1—N1	142.22(14)
N5—Tb1—O2	70.92(11)	O2—Tb1—N1	71.97(10)
N4—Tb1—O2	72.52(12)	O3—Tb1—N1	139.79(11)
N6—Tb1—O3	141.15(13)	N2—Tb1—N1	62.04(12)
O1—Tb1—O3	68.43(12)	N3—Tb1—N1	124.29(13)
N5—Tb1—O3	69.87(13)	C24—O2—Tb1	130.78(26)
N4—Tb1—O3	69.41(13)	C25—O3—Tb1	147.13(27)
O2—Tb1—O3	115.78(11)	C1—N1—Tb1	121.51(32)
N6—Tb1—N2	67.03(11)	C5—N1—Tb1	121.28(32)
O1—Tb1—N2	68.4(1)	C6—N2—C10	114.74(34)
N5—Tb1—N2	126.80(11)	C6—N2—Tb1	122.74(26)
N4—Tb1—N2	130.23(12)	C10—N2—Tb1	122.15(26)
O2—Tb1—N2	120.66(10)	C11—N3—Tb1	121.87(27)
O3—Tb1—N2	123.5(1)	C15—N3—Tb1	121.20(31)
N6—Tb1—N3	77.48(11)	C21—N4—Tb1	164.02(39)
O1—Tb1—N3	82.06(9)	C22—N5—Tb1	178.97(34)
N5—Tb1—N3	144.06(12)	C23—N6—Tb1	170.43(3)

Table 3.19: Crystal data and structure refinement for $\{[\text{Tb}_1(\text{tptz})(\text{OBz})_2(\mu\text{-OBz})]_2\cdot[\text{Tb}_2(\text{tptz})(\text{OBz})_3\text{CH}_3\text{OH}]\}\cdot\text{CH}_3\text{OH}\cdot 2\text{H}_2\text{O}$ (3n)

Empirical formula	$\text{C}_{119}\text{H}_{89}\text{N}_{18}\text{O}_{22}\text{Tb}_3^*$
Color	Colorless
Formula weight (g mol^{-1})	2599.95
Crystal System	Triclinic
Space Group	P -1
a (Å)	14.253(11)
b (Å)	15.754(13)
c (Å)	17.686(17)
α ($^\circ$)	67.53(3)
β ($^\circ$)	88.23(3)
γ ($^\circ$)	82.09(3)
V (Å ³)	3634.4(5)
Crystal size (mm)	0.33 x 0.23 x 0.19
Z	1
ρ_{calcd} (g m^{-3})	1.612
μ	2.009
F (000)	3654
θ range for data collection	1.25-27.51
limiting indices	$-13 \leq h \leq 18$ $-17 \leq k \leq 20$ $-22 \leq l \leq 22$
No. of measured reflections	15839
No. of observed reflections	11718
Data/ restraints/parameters	15839/0/994
R1 ($I > 2\sigma(I)$)	0.043
R1 (all data)	0.070
wR2 ($I > 2\sigma(I)$)	0.121
wR2 (all data)	0.155

*Hydrogens are not added on water molecules.

Table 3.20: Selected Bond Distances (Å) and Bond Angles (°) for [Tb₁(tptz)(OBz)₂(μ-OBz)]₂·[Tb₂(tptz)(OBz)₃CH₃OH]}·CH₃OH·2H₂O (3n)

Bond Distances

Tb1—N1	2.566(7)	Tb2—N7	2.569(6)
Tb1—N2	2.566(6)	Tb2—N8	2.524(6)
Tb1—N3	2.601(6)	Tb2—N9	2.554(6)
Tb1—O1	2.428(5)	Tb2—O7	2.377(7)
Tb1—O2	2.471(6)	Tb2—O8	2.444(6)
Tb1—O3	2.400(5)	Tb2—O9	2.487(5)
Tb1—O4	2.485(6)	Tb2—O10	2.438(6)
Tb1—O5	2.307(6)	Tb2—O11	2.479(6)
Tb1—O6 ¹	2.265(6)	Tb2—O12	2.286(6)
Tb1 ¹ —O6	2.265(6)		

Bond Angles

O5—Tb1—O3	78.02(17)	N2—Tb1—N1	62.79(16)
O5—Tb1—O1	73.63(16)	O5—Tb1—N3	75.98(16)
O3—Tb1—O1	143.10(15)	O3—Tb1—N3	71.42(15)
O5—Tb1—O2	79.44(16)	O1—Tb1—N3	122.28(15)
O3—Tb1—O2	142.07(15)	O2—Tb1—N3	73.76(15)
O1—Tb1—O2	53.27(14)	O4—Tb1—N3	87.43(15)
O5—Tb1—O4	131.40(16)	N2—Tb1—N3	62.63(16)
O3—Tb1—O4	53.38(14)	N1—Tb1—N3	125.34(15)
O1—Tb1—O4	147.57(15)	O6 ¹ —Tb1—O5	90.41(18)
O2—Tb1—O4	139.07(15)	O6 ¹ —Tb1—O3	79.22(16)
O5—Tb1—N2	133.74(17)	O6 ¹ —Tb1—O1	77.86(16)
O3—Tb1—N2	105.49(16)	O6 ¹ —Tb1—O2	131.06(17)
O1—Tb1—N2	111.13(15)	O6 ¹ —Tb1—O4	81.38(16)
O2—Tb1—N2	70.30(16)	O6 ¹ —Tb1—N2	135.84(17)
O4—Tb1—N2	68.78(15)	O6 ¹ —Tb1—N1	79.24(17)
O5—Tb1—N1	149.21(17)	O6 ¹ —Tb1—N3	149.54(17)
O3—Tb1—N1	127.15(15)	C1—O1—Tb1	92.33(35)
O1—Tb1—N1	75.85(15)	C1—O2—Tb1	90.57(35)
O2—Tb1—N1	85.70(15)	C8—O3—Tb1	94.76(35)
O4—Tb1—N1	76.00(15)	C8—O4—Tb1	90.72(35)
C15—O5—Tb1	147.02(44)	O9—Tb2—N8	70.22(15)
C22—N1—Tb1	120.28(35)	O12—Tb2—N9	146.51(17)

C26—N1—Tb1	121.79(39)	O7—Tb2—N9	87.66(17)
C27—N2—Tb1	121.84(41)	O10—Tb2—N9	81.10(17)
C29—N2—Tb1	122.32(38)	O8—Tb2—N9	125.13(17)
C34—N3—Tb1	121.26(39)	O11—Tb2—N9	72.00(17)
C30—N3—Tb1	121.86(36)	O9—Tb2—N9	72.29(17)
C15—O6—Tb1 ¹	168.71(43)	N8—Tb2—N9	63.68(16)
O12—Tb2—O7	77.87(17)	O12—Tb2—N7	79.62(17)
O12—Tb2—O10	84.32(16)	O7—Tb2—N7	141.17(16)
O7—Tb2—O10	127.92(16)	O10—Tb2—N7	80.24(15)
O12—Tb2—O8	81.50(16)	O8—Tb2—N7	67.53(16)
O7—Tb2—O8	78.12(16)	O11—Tb2—N7	128.37(16)
O10—Tb2—O8	146.58(15)	O9—Tb2—N7	94.88(15)
O12—Tb2—O11	75.10(16)	N8—Tb2—N7	63.30(16)
O7—Tb2—O11	74.81(16)	N9—Tb2—N7	126.68(16)
O10—Tb2—O11	53.30(15)	C40—O7—Tb2	135.24(44)
O8—Tb2—O11	147.24(15)	C41—O8—Tb2	93.86(41)
O12—Tb2—O9	131.60(15)	C41—O9—Tb2	91.69(40)
O7—Tb2—O9	77.48(15)	C48—O10—Tb2	93.79(35)
O10—Tb2—O9	142.62(14)	C48—O11—Tb2	92.52(36)
O8—Tb2—O9	52.97(14)	C55—O12—Tb2	132.03(43)
O11—Tb2—O9	135.14(14)	C62—N7—Tb2	119.96(46)
O12—Tb2—N8	139.65(16)	C66—N7—Tb2	120.45(40)
O7—Tb2—N8	141.77(16)	C69—N8—Tb2	121.55(36)
O10—Tb2—N8	74.66(15)	C67—N8—Tb2	122.15(40)
O8—Tb2—N8	97.43(16)	C74—N9—Tb2	121.49(42)
O11—Tb2—N8	115.26(15)	C70—N9—Tb2	121.02(40)

Table 3.21: Crystal data and structure refinement for [Tb(phen)₂Cl₃OH₂].CH₃OH (3o)

Empirical formula	C ₂₅ H ₂₂ N ₄ O ₂ Cl ₃ Tb
Color	Colorless
Formula weight (g mol ⁻¹)	675.75
Crystal System	Monoclinic
Space Group	P2(1)/c
a (Å)	18.024(6)
b (Å)	10.821(4)
c (Å)	12.665(5)
α (°)	90.00
β (°)	101.44(2)
γ (°)	90.00
V (Å ³)	2421.24(15)
Crystal size (mm)	0.23 x 0.17 x 0.11
Z	4
ρ _{calcd} (g m ⁻³)	1.854
μ	3.284
F (000)	2184
θ range for data collection	1.15-41.43
limiting indices	-33 ≤ h ≤ 23 -20 ≤ k ≤ 20 -23 ≤ l ≤ 21
No. of measured reflections	16246
No. of observed reflections	12863
Data/ restraints/parameters	16246/0/323
R1 (I>2σ(I))	0.027
R1 (all data)	0.044
wR2 (I>2σ(I))	0.082
wR2 (all data)	0.103

**Table 3.22: Selected Bond Distances (Å) and Bond Angles (°) for [Tb(phen)₂Cl₃OH₂].
CH₃OH (3o)**

Bond Distances

Tb1—N1	2.577(2)	Tb1—O1	2.368(1)
Tb1—N2	2.590(2)	Tb1—Cl1	2.691(2)
Tb1—N3	2.586(2)	Tb1—Cl2	2.727(2)
Tb1—N4	2.578(3)	Tb1—Cl3	2.756(0)

Bond Angles

O1—Tb1—N1	69.96(5)	N3—Tb1—Cl2	140.94(3)
O1—Tb1—N4	138.34(5)	N2—Tb1—Cl2	73.93(3)
N1—Tb1—N4	148.01(5)	Cl1—Tb1—Cl2	85.76(1)
O1—Tb1—N3	75.75(5)	O1—Tb1—Cl3	83.86(4)
N1—Tb1—N3	130.96(5)	N1—Tb1—Cl3	136.31(3)
N4—Tb1—N3	64.42(5)	N4—Tb1—Cl3	72.08(4)
O1—Tb1—N2	78.94(5)	N3—Tb1—Cl3	70.32(3)
N1—Tb1—N2	64.45(5)	N2—Tb1—Cl3	76.89(3)
N4—Tb1—N2	125.37(5)	Cl1—Tb1—Cl3	139.78(1)
N3—Tb1—N2	140.19(5)	Cl2—Tb1—Cl3	115.20(1)
O1—Tb1—Cl1	100.86(4)	C1—N1—Tb1	123.08(11)
N1—Tb1—Cl1	80.86(3)	C5—N1—Tb1	119.05(11)
N4—Tb1—Cl1	78.92(4)	C12—N2—Tb1	124.15(11)
N3—Tb1—Cl1	72.27(3)	C9—N2—Tb1	118.41(11)
N2—Tb1—Cl1	143.33(3)	C21—N3—Tb1	123.44(12)
O1—Tb1—Cl2	141.46(4)	C20—N3—Tb1	118.79(11)
N1—Tb1—Cl2	73.82(3)	C13—N4—Tb1	123.23(12)
N4—Tb1—Cl2	80.17(4)	C17—N4—Tb1	119.12(12)

Table 3.23: Non-covalent interactions (Å and °) for complexes 3b-3d, 3f, 3h-3j, 3m-3o

S. N	D-H...A	d(D-H)	d(H-A)	d(D-A)	<(DHA)>
1.	[Gd(tptz)(SCN)₃(CH₃OH)₂OH₂].CH₃OH (3b)				
	O4-H4...S1	0.820	2.518(4)	3.335	174.9
	C4-H4A...O1	0.930	2.503(7)	3.379	157.1
	C10-H10...O4	0.932	2.601(11)	3.406	144.9
	C4-H4A...π	0.930	3.675(1)	3.470	170.1
2.	[Gd(tptz)(OBz)₂(μ-OBz)OH₂]₂.H₂O (3c)				
	C3-H3...O2	0.930	2.573(6)	3.208	125.8
	C4-H4...O2	0.930	2.691(3)	3.262	120.3
	C4-H4...O4	0.930	2.838(7)	3.484	127.5
	C10-H10...O8	0.930	2.991(24)	3.875	159.4
	C23-H23...O8	0.930	2.961(22)	3.560	123.5
	C35-H35...O7	0.931	2.537(7)	3.338	144.4
3.	[Gd(phen)Cl₂(OH₂)₄].Cl.CH₃OH (3d)				
	O2-H2A...Cl3	0.820	2.416(6)	3.106	142.3
	O4-H4A...Cl3	0.821	2.453(4)	3.085	134.4
	O4-H4B...Cl3	0.886	2.374(91)	3.085	149.9
	O3-H3A...O5	0.821	1.889(9)	2.608	145.5
	O5-H5A...O3	0.820	1.845(6)	2.608	153.9
4.	[OH₂(phen)(2-pyca)₂Gd₁(μ-ox)Gd₂(2-pyca)₂(phen)OH₂].6H₂O (3f)				
	C15-H15...O14	0.927	3.387(13)	6.455	132.2
	C19-H19...O14	0.936	3.010(13)	9.523	159.2
	C29-H29...O5	0.935	2.693(23)	3.409	133.9
	C15-H15...π	0.927	3.387(15)	3.717	133.5
5.	[Eu(tptz)(SCN)₃(CH₃OH)₂OH₂].CH₃OH (3h)				
	C19-H19...S1	0.931	3.176(1)	4.091	167.8
	C20-H20...S3	0.931	3.083(2)	3.721	127.3
	C26-H26B...S3	0.961	2.967(2)	3.662	130.2
	O1-H1A...S2	0.829	2.475(56)	3.289	167.4
	O4-H4...S3	0.820	2.535(1)	3.355	177.4
6.	[OH₂(OBz)₂(tptz)Eu₁(μ-OBz)₂Eu₂(tptz)(OBz)₂OH₂].CH₃OH.7H₂O (3i)				
	C19-H19...π	0.925	3.477(6)	3.821	113.6
	C20-H20...π	0.932	3.627(6)	3.687	121.5
	C37-H37...π	0.936	3.548(12)	3.699	91.86
	C52-H52...π	0.931	3.553(11)	3.651	88.6
	C82-H82A...O20	0.959	1.887(3)	2.845	177.6

	C82-H82B...O21	0.957	2.121(22)	2.755	122.3
	C82-H82C...O21	0.960	2.637(24)	2.755	86.7
7.	[Eu(phen)₂(SCN)₃CH₃OH].phen (3j)				
	C36-H36A...O1	0.930	3.160(5)	3.359	94.20
	C26-H26A...S1	0.930	3.076(7)	3.702	126.1
	C34-H34A...S1	0.931	2.887(2)	3.716	149.0
	C92-H92A...S1	0.929	3.037(4)	3.684	128.1
	C91-H91A...S2	0.930	3.703(6)	3.907	150.1
	C39-H39A...S3	0.960	3.189(4)	3.886	130.8
	C19-H19A...N8	0.930	2.738(5)	3.499	139.7
8.	[Tb(tptz)(SCN)₃(CH₃OH)₂OH₂].CH₃OH (3m)				
	O2-H2A...S2	0.820	2.513(6)	3.290	170.8
	O4-H4...S3	0.820	2.540(1)	3.359	177.0
	C14-H14...S3	0.930	2.931(2)	3.609	132.8
	C24-H24B...S1	0.960	2.929(1)	3.729	141.5
	C26-H26B...S3	0.960	2.975(2)	3.664	129.7
9.	{[Tb₁(tptz)(OBz)₂(μ-OBz)]₂. [Tb₂(tptz)(OBz)₃CH₃OH]}.CH₃OH.2H₂O (3n)				
	C3-H3...π	0.930	3.409(3)	4.018	125.1
	C11-H11...π	0.930	3.371(6)	4.165	144.6
	C12-H12...π	0.930	3.279(7)	3.742	112.9
	C13-H13...π	0.930	3.148(5)	3.674	117.7
	C23-H23...π	0.931	3.389(5)	3.464	74.34
	C36-H36...π	0.929	3.194(5)	3.753	120.5
	C46-H46...π	0.930	3.401(6)	4.262	154.9
	C60-H60...π	0.930	3.587(7)	4.468	159.0
	C80-H80B...O10	0.960	1.928(5)	2.866	164.9
10.	[Tb(phen)₂Cl₃OH₂].CH₃OH (3o)				
	O1-H30...O2	0.820	1.877(2)	2.684	167.3
	O1-H31...Cl2	0.820	2.555(33)	3.142	172.0
	O2-H2...Cl3	0.820	2.370(1)	3.110	150.4
	C6-H6...Cl2	0.930	2.731(0)	3.626	161.8
	C25-H25B...Cl1	0.960	2.922(0)	3.652	133.7
	C11-H11B...π	0.930	3.360(2)	3.408	85.06

Table 3.24: TG-DTG phenomenological data of 3a-3q under air atmosphere

S. N	Stages	DTG peak (Temp. °C)	Mass loss (%)		Constituents lost
			Obs.	Calc.	
1.	[Gd(tptz)Cl₂(OH₂)₄].Cl.4H₂O (3a)				
	I	118 °C	14.2	14.8	One chloride, four water molecules
	II	536 °C	62.1	63.05	C ₁₈ H ₂₀ N ₆ O ₄ Cl ₂
2.	[Gd(tptz)(SCN)₃(CH₃OH)₂OH₂].CH₃OH (3b)				
	I	150 °C	3.9	4.2	One uncoordinated methanol molecule
	II	413 °C	32.2	33.6	C ₅ H ₉ N ₃ O ₃ S ₃
3.	[Gd(tptz)(OBz)₂(μ-OBz)OH₂]₂.H₂O (3c)				
	I	66 °C	1.0	1.02	One uncoordinated water molecule
	II	511 °C	75.1	76.2	C ₅₈ H ₅₈ N ₁₂ O ₁₅
4.	[Gd(phen)Cl₂(OH₂)₄].Cl.CH₃OH (3d)				
	I	91 °C	11.93	12.31	One chloride, one methanol molecules
	II	267 °C	25.67	26.08	Two chloride, four water molecules
5.	[Gd(phen)₂(SCN)₃CH₃OH].phen (3e)				
	I	281 °C	19.8	21.9	One uncoordinated phen molecule
	II	476 °C	41.7	43.8	Two coordinated phen molecules
6.	[OH₂(phen)(2-pyca)₂Gd₁(μ-ox)Gd₂(2-pyca)₂(phen)OH₂].6H₂O (3f)				
	I	129 °C	7.3	7.5	Six uncoordinated water molecules
	II	552 °C	69.33	71.48	C ₄₆ H ₃₆ N ₁₂ O ₁₄
7.	[Eu(tptz)Cl₃(CH₃OH)₂OH₂].CH₃OH (3g)				
	I	153 °C	4.19	4.67	One uncoordinated methanol molecule
	II	414 °C	26.83	27.51	C ₂ H ₁₀ Cl ₃ O ₃
8.	[Eu(tptz)(SCN)₃(CH₃OH)₂OH₂].CH₃OH (3h)				
	I	151 °C	4.1	4.2	One uncoordinated methanol molecule
	II	409 °C	32.3	33.8	C ₅ H ₉ N ₃ O ₃ S ₃
9.	[OH₂(OBz)₂(tptz)Eu₁(μ-OBz)₂Eu₂(tptz)(OBz)₂OH₂].CH₃OH.7H₂O (3i)				
	I	121 °C	7.67	8.52	One methanol, seven water molecules
	II	527 °C	73.19	74.54	C ₇₈ H ₅₈ N ₁₂ O ₁₄
10.	[Eu(phen)₂(SCN)₃CH₃OH].phen (3j)				
	I	284 °C	20.56	22.05	One uncoordinated phen molecule

	II	469 °C	42.79	44.10	Two coordinated phen molecules
	III	571 °C	19.13	20.05	C ₄ H ₃ N ₃ OS ₃
11.	[OH₂(phen)(2-pyca)₂Eu₁(μ-ox)Eu₂(2-pyca)₂(phen)OH₂].6H₂O (3k)				
	I	137 °C	6.9	7.8	Six uncoordinated water molecules
	II	559 °C	68.1	70.3	C ₄₆ H ₃₂ N ₁₂ O ₁₄
12.	[Tb(tptz)Cl₃(CH₃OH)₂OH₂].CH₃OH (3l)				
	I	153 °C	4.32	4.62	One uncoordinated methanol molecule
	II	414 °C	25.89	27.24	C ₂ H ₁₀ Cl ₃ O ₃
	III	644 °C	44.10	45.15	C ₁₈ H ₁₂ N ₆
13.	[Tb(tptz)(SCN)₃(CH₃OH)₂OH₂].CH₃OH (3m)				
	I	153 °C	4.1	4.2	One uncoordinated methanol molecule
	II	414 °C	32.43	33.58	C ₅ H ₉ N ₃ O ₃ S ₃
	III	644 °C	39.80	41.00	C ₁₈ H ₁₂ N ₆
14.	{[Tb₁(tptz)(OBz)₂(μ-OBz)]₂[Tb₂(tptz)(OBz)₃CH₃OH]}.CH₃OH.2H₂O (3n)				
	I	89 °C	2.53	2.57	One methanol, two water molecules
	II	293 °C	25.51	26.51	C ₄₀ H ₃₁ N ₆ O ₇
	III	477 °C	49.67	50.61	C ₇₈ H ₅₄ N ₁₂ O ₁₂
15.	[Tb(phen)₂Cl₃OH₂].CH₃OH (3o)				
	I	82 °C	4.5	4.7	One methanol molecule
	II	315 °C	17.83	18.35	Three chloride, one water molecules
	III	524 °C	57.93	58.66	Two phen. molecules
16.	[Tb(phen)₂(SCN)₃CH₃OH].phen (3p)				
	I	282 °C	19.79	21.88	One uncoordinated phen molecule
	II	472 °C	41.56	43.76	Two coordinated phen molecules
	III	576 °C	20.13	22.77	C ₄ H ₄ N ₃ OS ₃
17.	[OH₂(phen)(2-pyca)₂Tb₁(μ-ox)Tb₂(2-pyca)₂(phen)OH₂].6H₂O (3q)				
	I	133 °C	6.17	7.69	Six uncoordinated water molecules
	II	556 °C	67.54	69.63	C ₄₆ H ₃₂ N ₁₂ O ₁₄

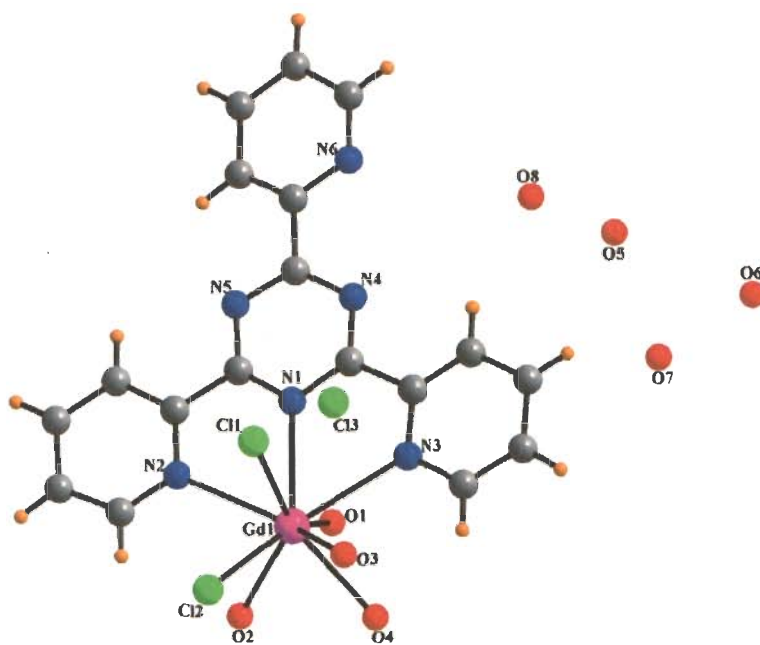


Fig. 3.9: Crystal structure of $[\text{Gd}(\text{tptz})\text{Cl}_2(\text{OH}_2)_4]\cdot\text{Cl}\cdot 4\text{H}_2\text{O}$ (**3a**). Color code: C, grey; H, orange; O, red; N, blue; Gd, purple

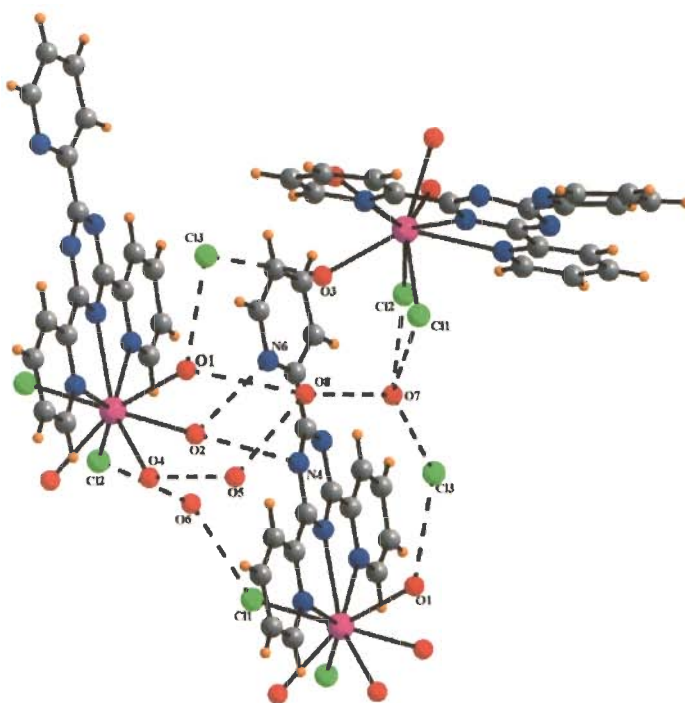


Fig. 3.10: Various non-covalent interactions in **3a**. Color code: C, grey; H, orange; O, red; N, blue; Cl, green; Gd, purple

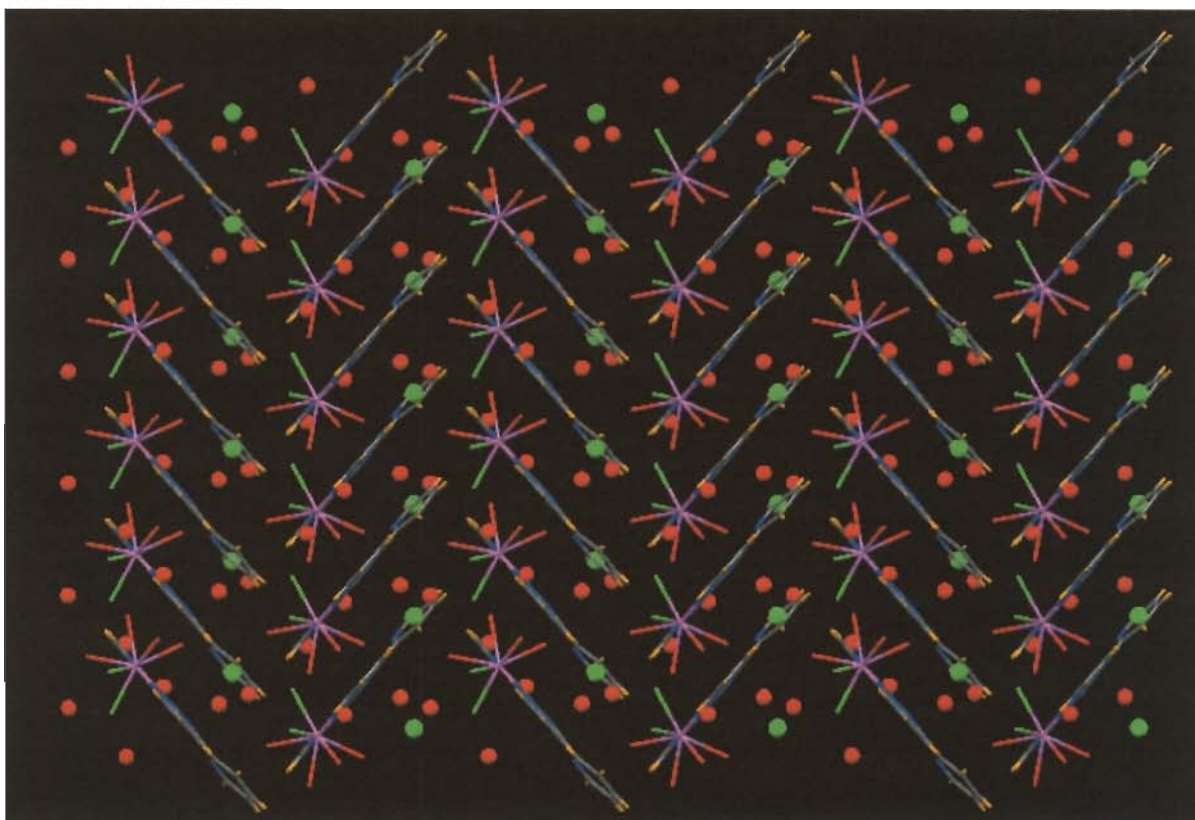


Fig. 3.11: Zig-zag molecular arrangement via O...O, N...O, Cl...O non-covalent interactions in **3a**. Color code: C, grey; H, orange; O, red; N, blue; Cl, green; Gd, purple

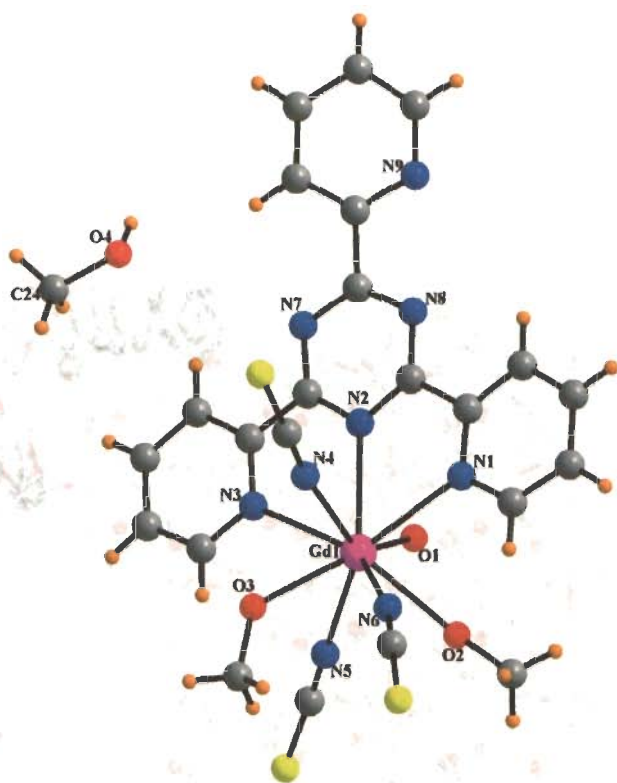
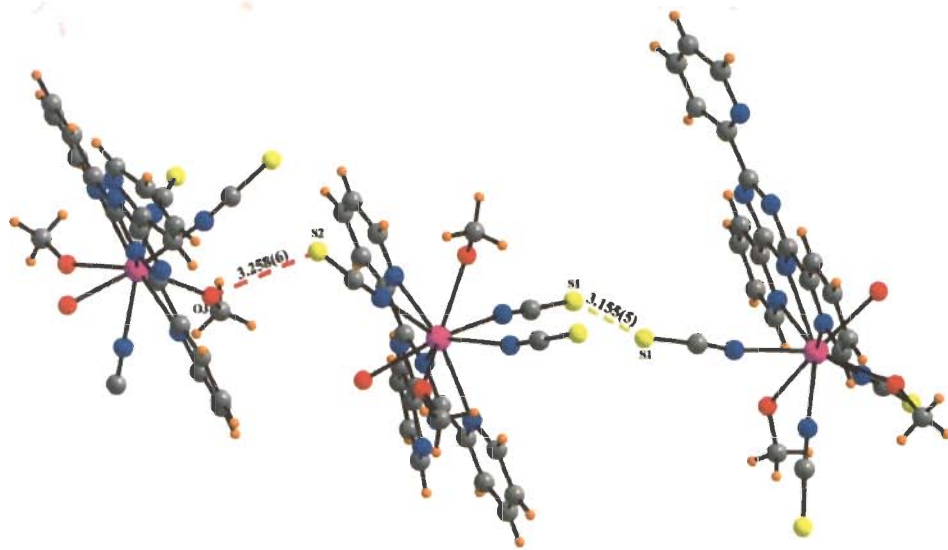
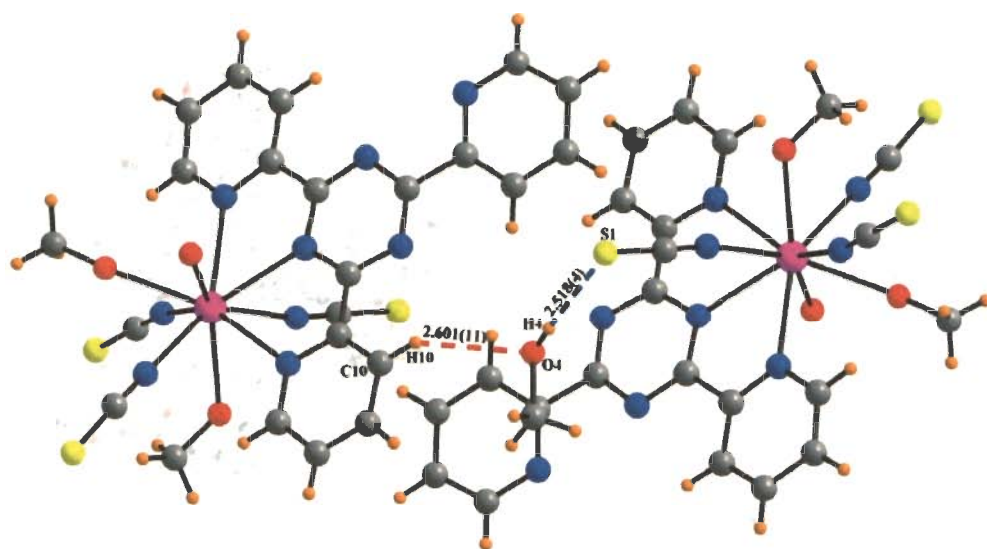


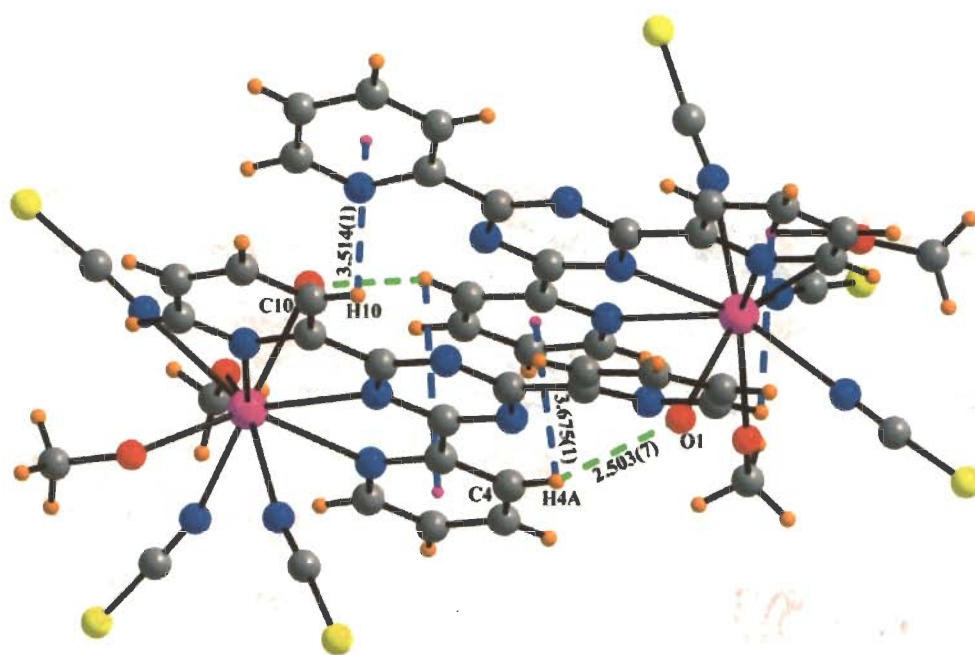
Fig. 3.12: Crystal structure of $[\text{Gd}(\text{tptz})(\text{SCN})_3(\text{CH}_3\text{OH})_2\text{OH}_2] \cdot \text{CH}_3\text{OH}$ (**3b**). Color code: C, grey; H, orange; O, red; N, blue; S, yellow; Gd, purple



(a)

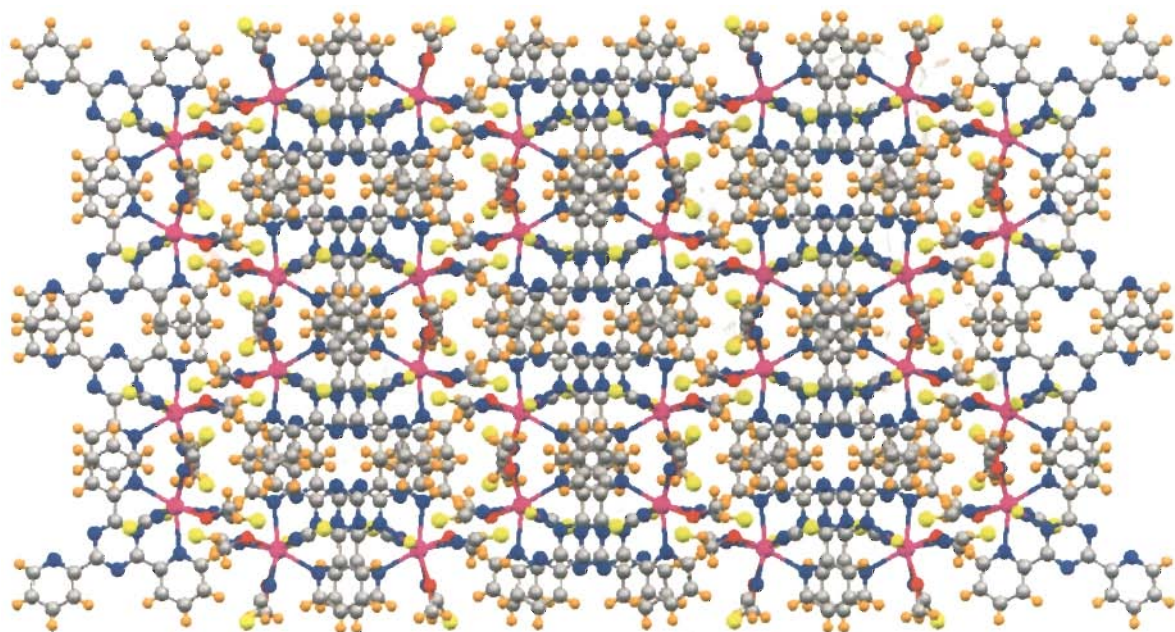


(b)

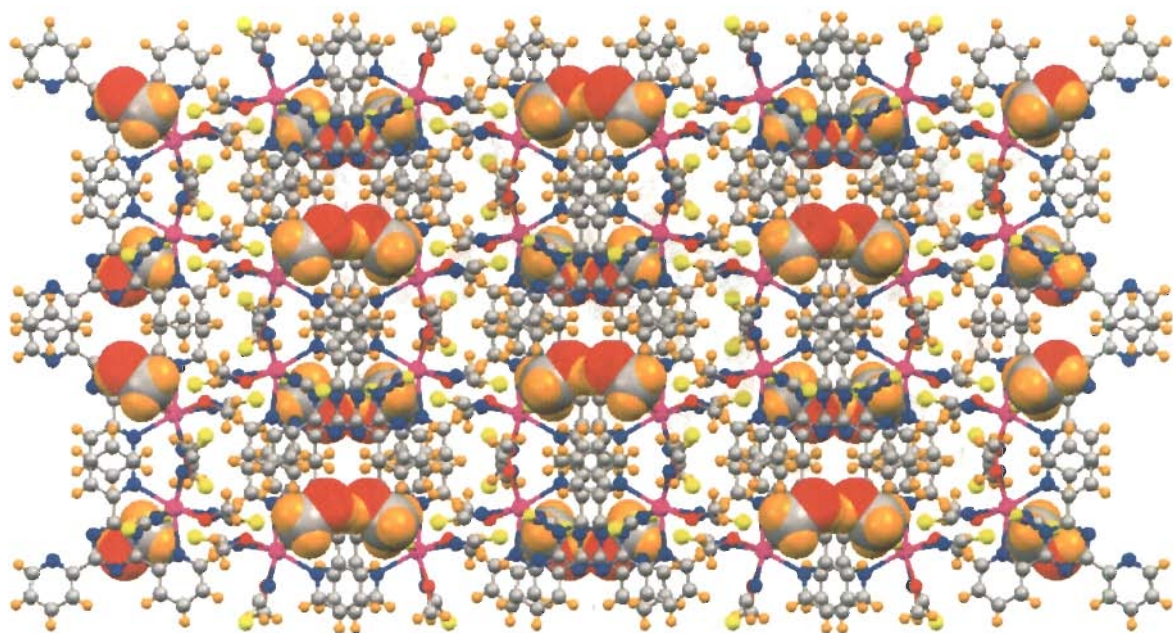


(c)

Fig. 3.13: Various non-covalent interactions in **3b** (a) S...S, O...S (b) C-H...O, O-H...S via methanol (c) C-H...O, C-H... π . Color code: C, grey; H, orange; O, red; N, blue; S, yellow; Gd, purple



(a)



(b)

Fig. 3.14: Host-guest like supramolecular motif along 'c' axis in **3b** (a) without guest (b) with guest. Color code: C, grey; H, orange; O, red; N, blue; S, yellow; Gd, purple

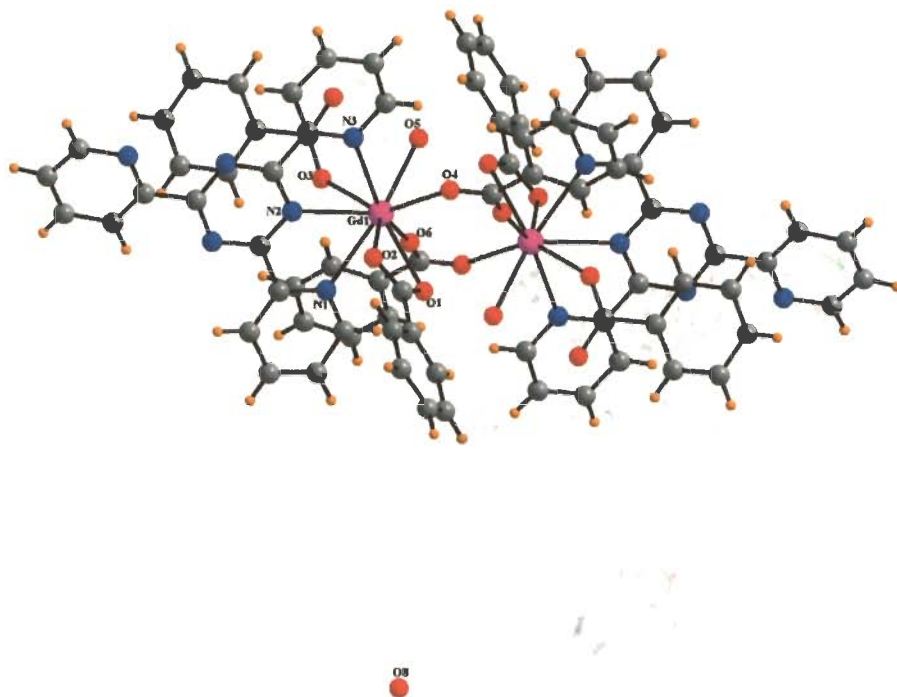


Fig. 3.15: Crystal structure of $[\text{Gd}(\text{tptz})(\text{OBz})_2(\mu\text{-OBz})\text{OH}_2]_2 \cdot \text{H}_2\text{O}$ (**3c**). Color code: C, grey; H, orange; O, red; N, blue; Gd, purple

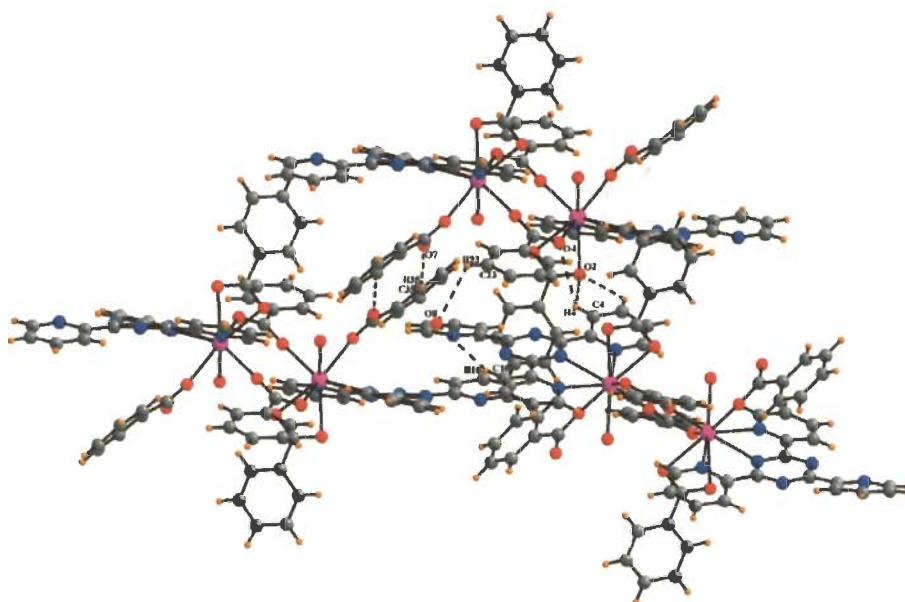


Fig. 3.16: Various C-H...O non-covalent interactions in **3c**. Color code: C, grey; H, orange; O, red; N, blue; Gd, purple

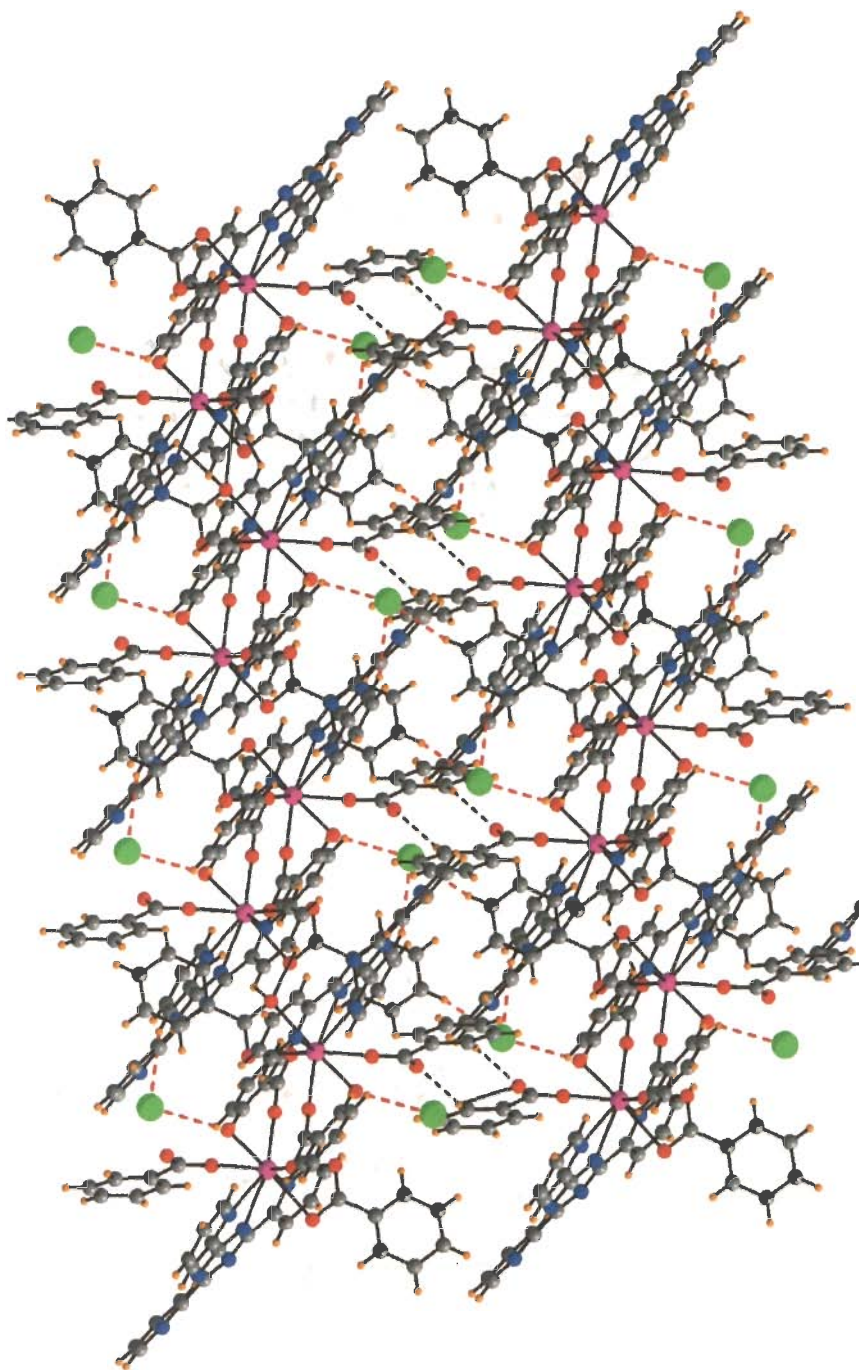


Fig. 3.17: Ladder like molecular arrangement along 'b' axis via non-covalent interactions in **3c**. Color code: C, grey; H, orange; O, red; N, blue; Gd, purple; lattice water molecule, green

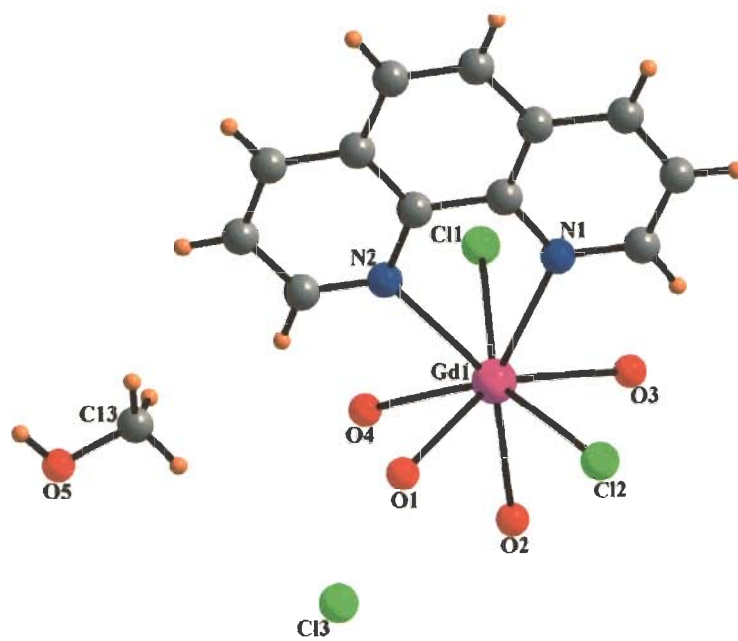


Fig. 3.18: Crystal structure of $[\text{Gd}(\text{phen})\text{Cl}_2(\text{OH}_2)_4]\cdot\text{Cl}\cdot\text{CH}_3\text{OH}$ (**3d**). Color code: C, grey; H, orange; O, red; N, blue; Cl, green; Gd, purple

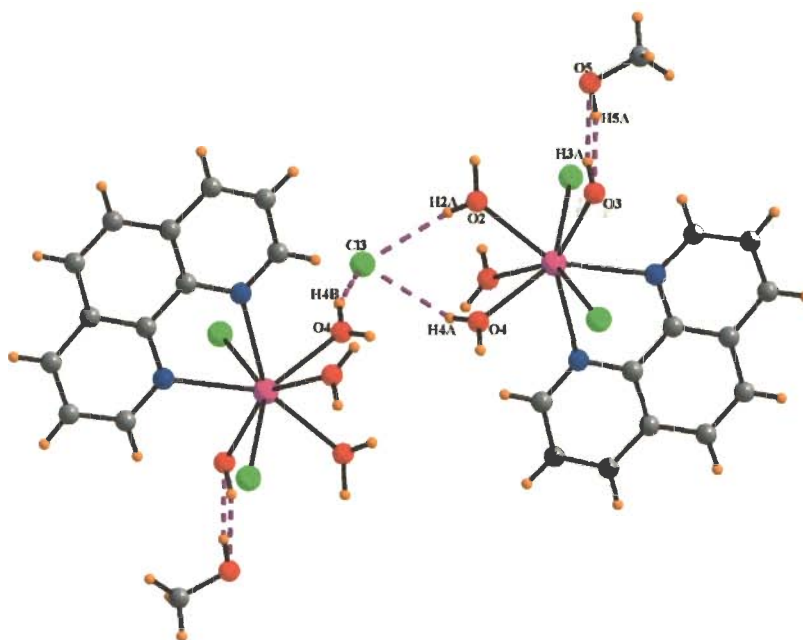


Fig. 3.19: Various O-H...Cl, O-H...O non-covalent interactions in **3d**. Color code: C, grey; H, orange; O, red; N, blue; Cl, green; Gd, purple

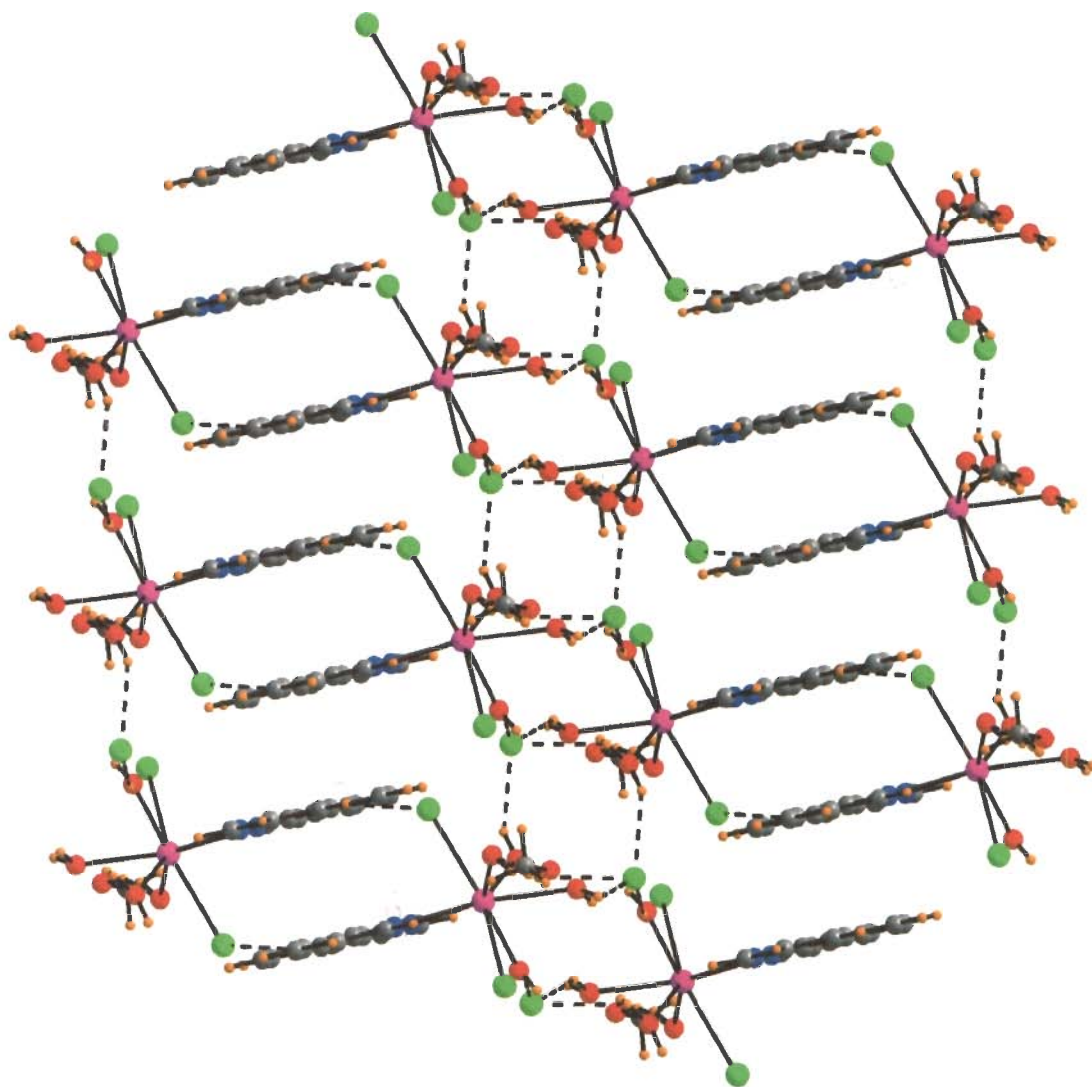


Fig. 3.20: Two dimensional view of **3d**. Color code: C, grey; H, orange; O, red; N, blue; Cl, green; Gd, purple

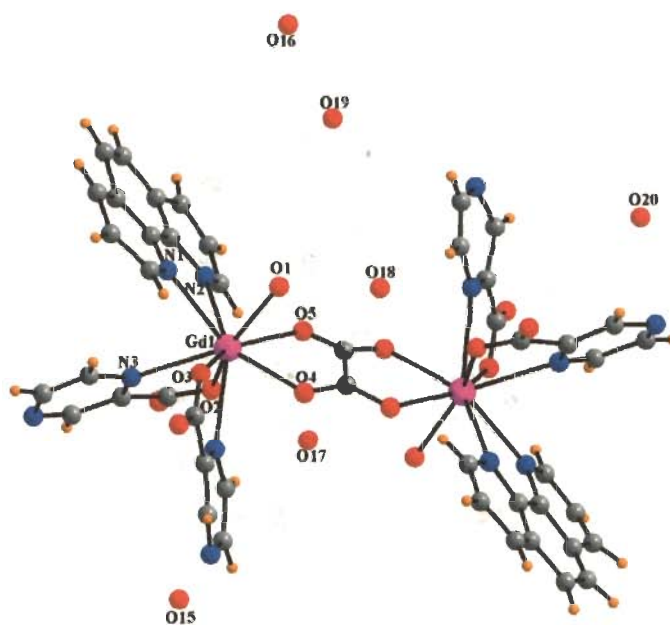


Fig. 3.21: Crystal structure of $[\text{OH}_2(\text{phen})(2\text{-pyca})_2\text{Gd}_1(\mu\text{-ox})\text{Gd}_2(2\text{-pyca})_2(\text{phen})\text{OH}_2] \cdot 6\text{H}_2\text{O}$ (**3f**). Color code: C, grey; H, orange; O, red; N, blue; Gd, purple

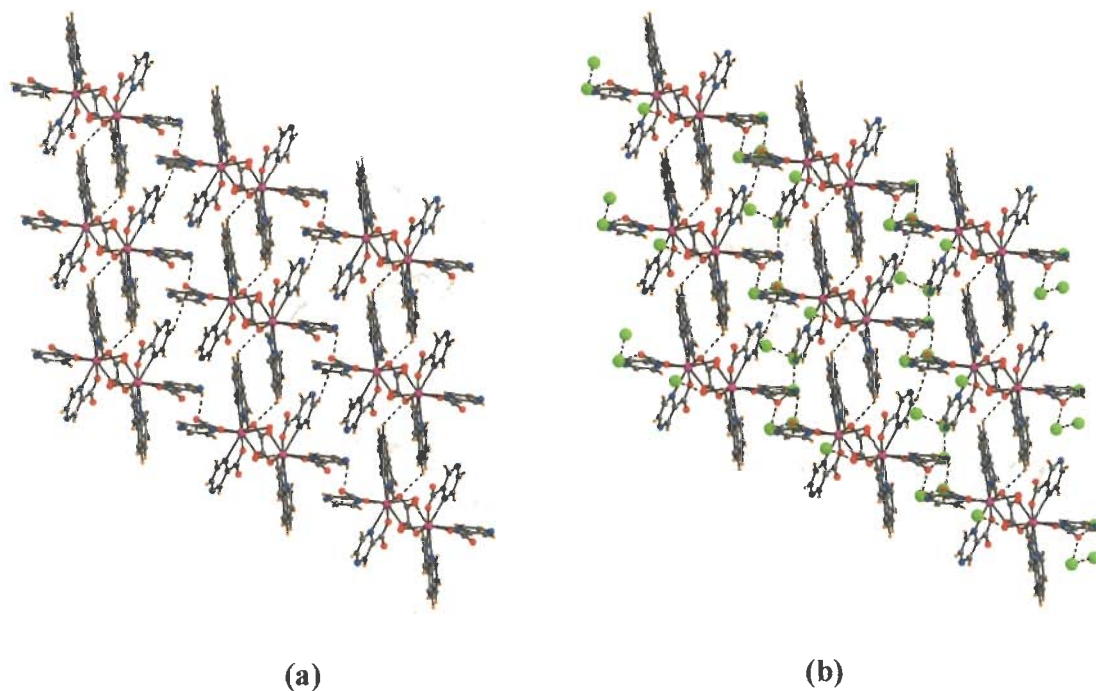


Fig. 3.22: Host-guest like supramolecular motif along 'a' axis via non-covalent interactions in **3f** (a) without guest (OH_2) (b) with guest. Color code: C, grey; H, orange; O, red; N, blue; Gd, purple; water, green

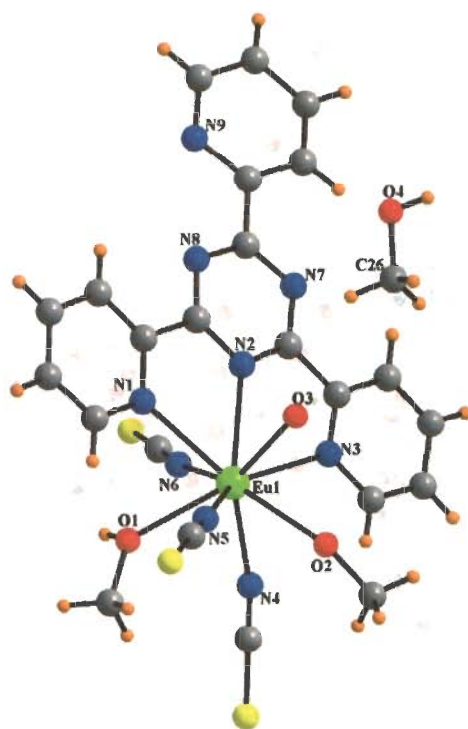


Fig. 3.23: Crystal structure of $[\text{Eu}(\text{tptz})(\text{SCN})_3(\text{CH}_3\text{OH})_2\text{OH}_2]\cdot\text{CH}_3\text{OH}$ (**3h**). Color code: C, grey; H, orange; O, red; N, blue; S, yellow; Eu, green

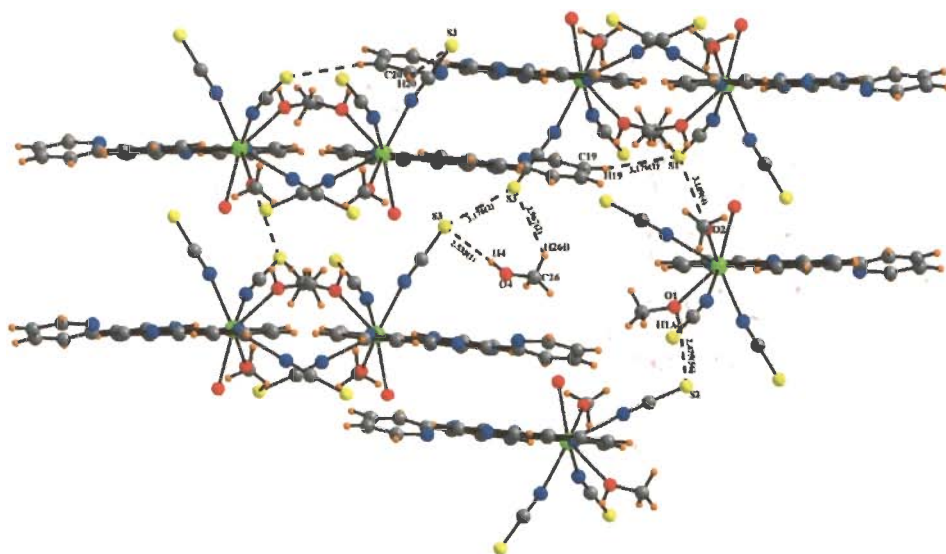
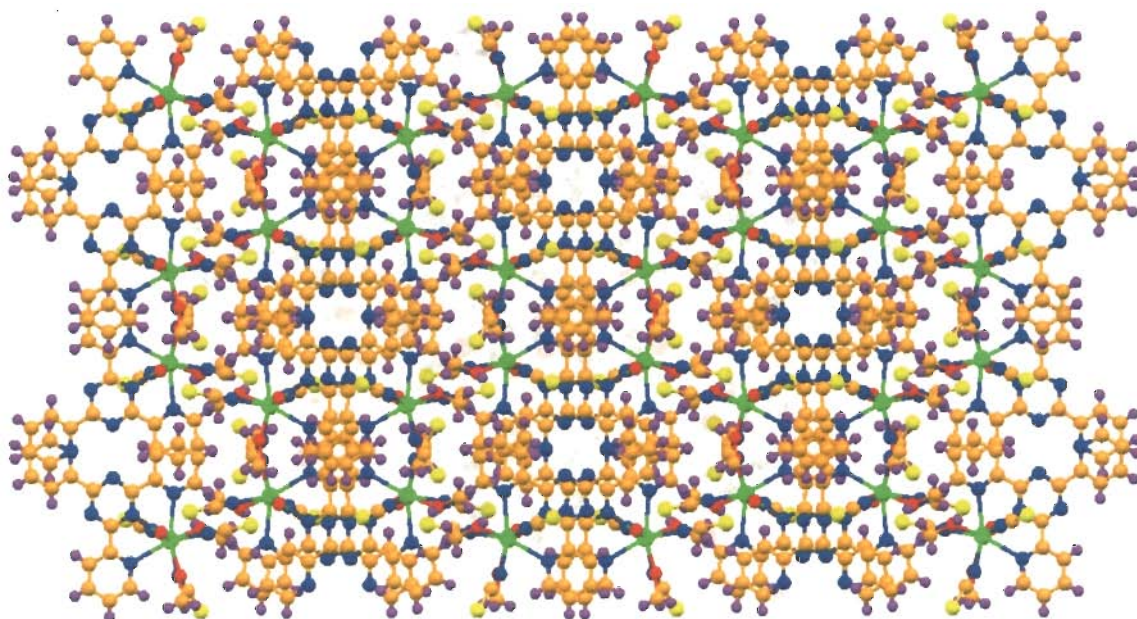
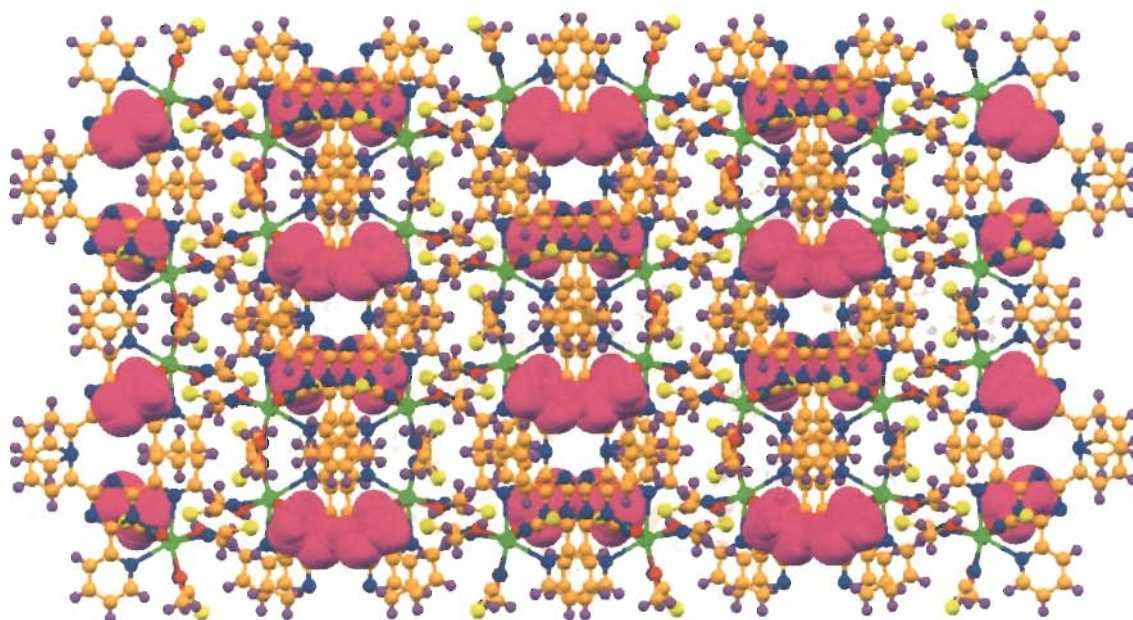


Fig. 3.24: Various C-H...O, O-H...S, S...S, O...S non-covalent interactions in **3h**. Color code: C, grey; H, orange; O, red; N, blue; S, yellow; Eu, green



(a)



(b)

Fig. 3.25: Host-guest like supramolecular motif along 'c' axis in **3h** (a) without guest (b) with guest. Color code: C, orange; H, purple; O, red; N, blue; S, yellow; Eu, green; guest (CH₃OH), pink

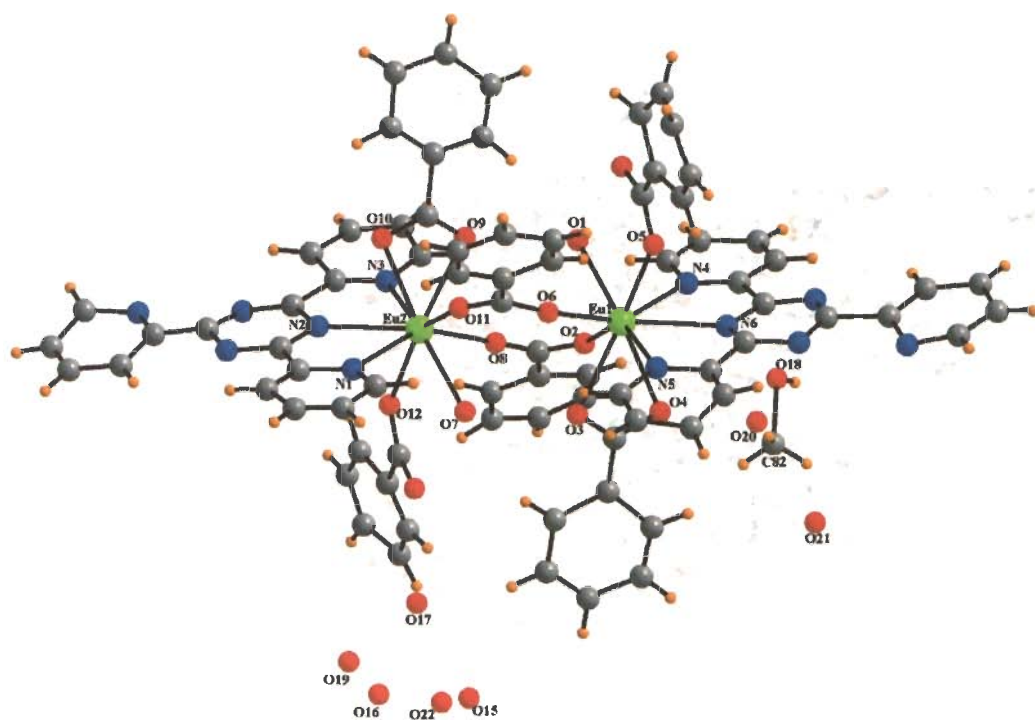


Fig. 3.26: Crystal structure of $[\text{OH}_2(\text{OBz})_2(\text{tptz})\text{Eu}_1(\mu\text{-OBz})_2\text{Eu}_2(\text{tptz})(\text{OBz})_2\text{OH}_2)] \cdot \text{CH}_3\text{OH} \cdot 7\text{H}_2\text{O}$ (**3i**). Color code: C, grey; H, orange; O, red; N, blue; Eu, green

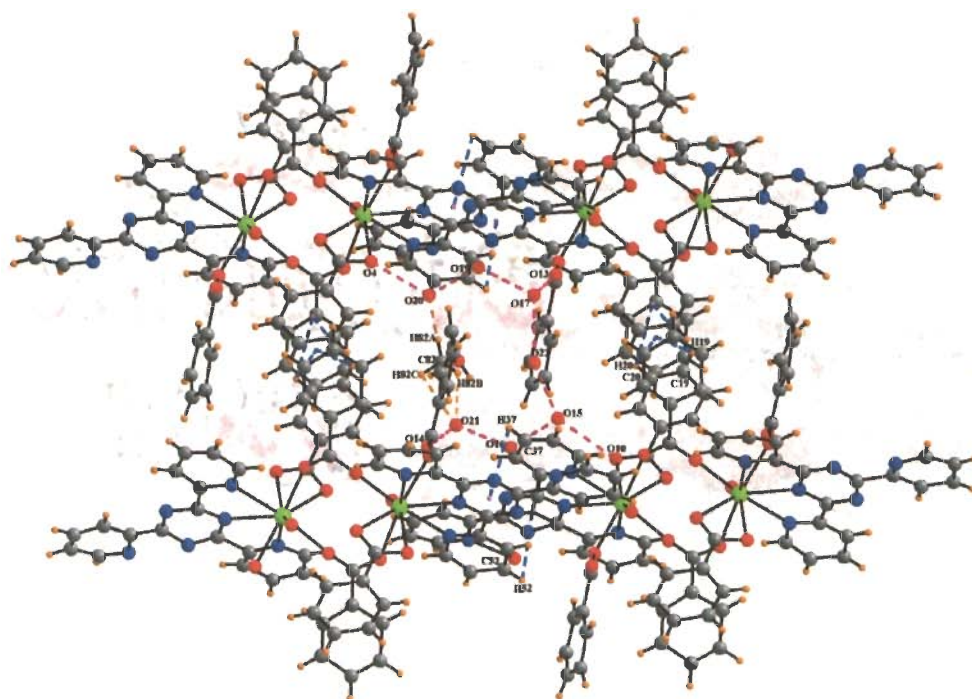
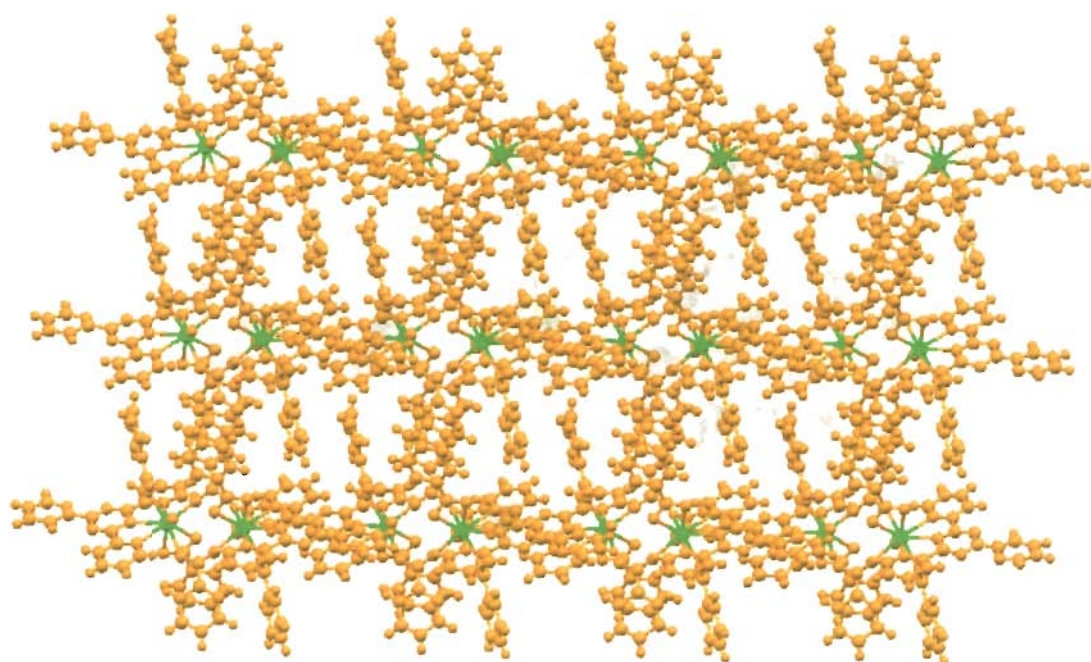
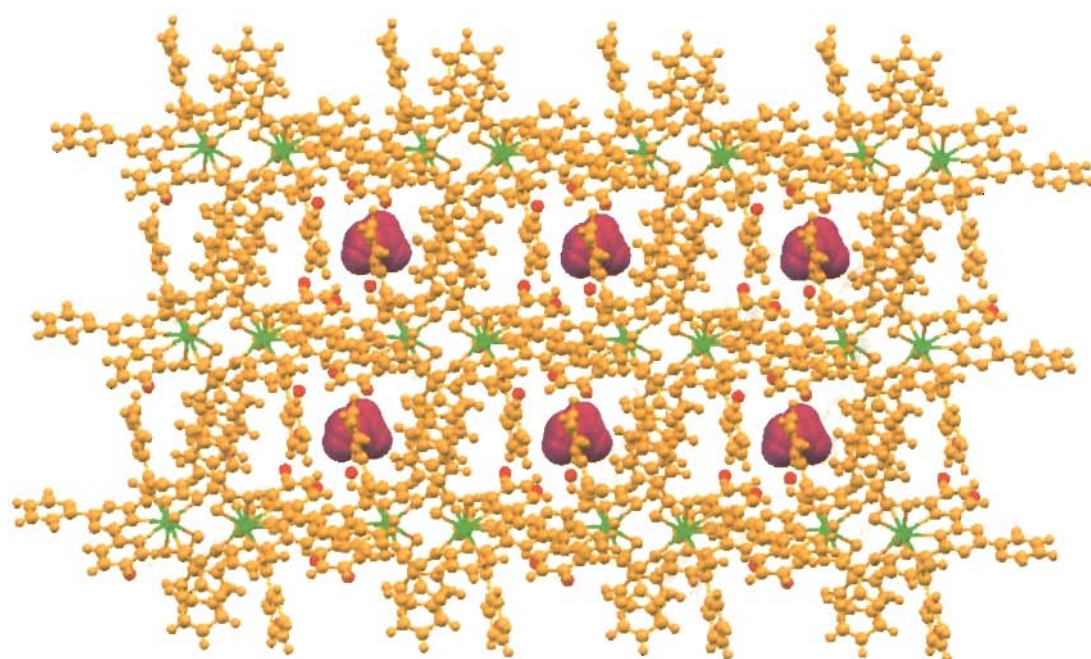


Fig. 3.27: Various non-covalent interactions in **3i**. Color code: C, grey; H, orange; O, red; N, blue; Eu, green

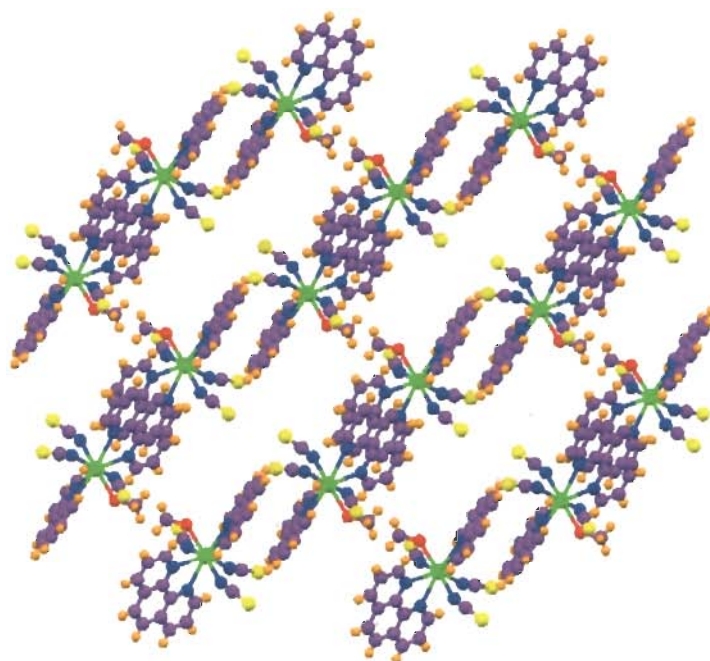


(a)

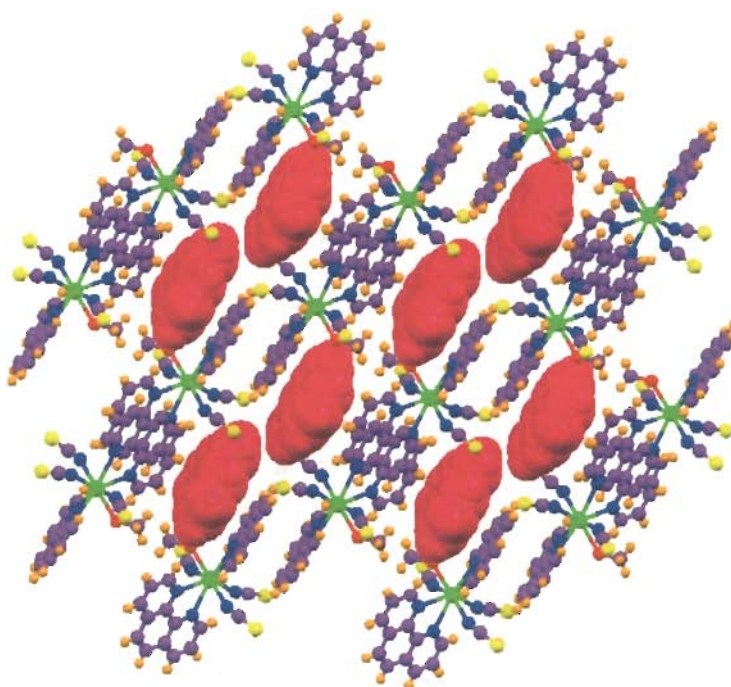


(b)

Fig. 3.28: Host-guest like supramolecular motif along 'a' axis in **3i** (a) without guest (CH_3OH , $7\text{H}_2\text{O}$) (b) with guest. Color code: C, H, O, N, S, orange; Eu, green; CH_3OH , purple water, red



(a)



(b)

Fig. 3.31: Host-guest like supramolecular motif along 'a' axis in **3j** (a) without guest (b) with guest. Color code: C, purple; H, orange; O, red; N, blue; S, yellow; Eu, green; guest (phen), pink

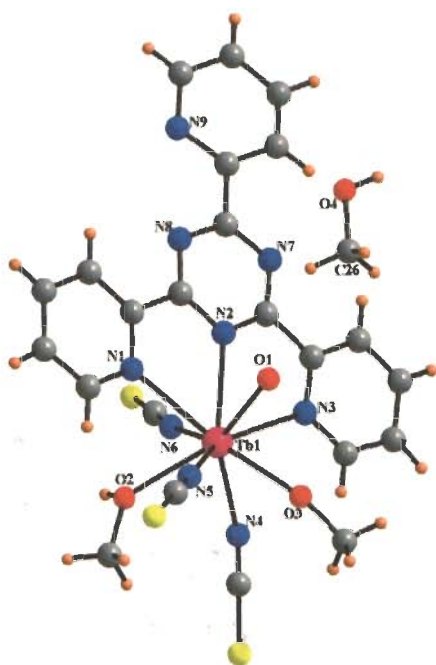


Fig. 3.32: Crystal structure of $[\text{Tb}(\text{tptz})(\text{SCN})_3(\text{CH}_3\text{OH})_2\text{OH}_2]\cdot\text{CH}_3\text{OH}$ (**3m**). Color code: C, grey; H, orange; O, red; N, blue; S, yellow; Tb, pink

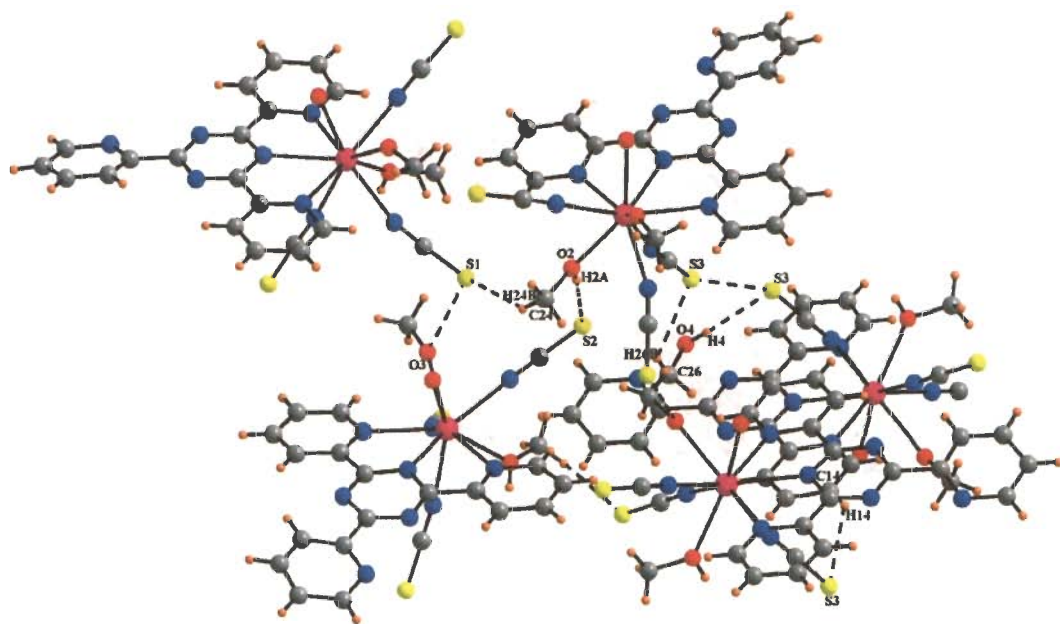
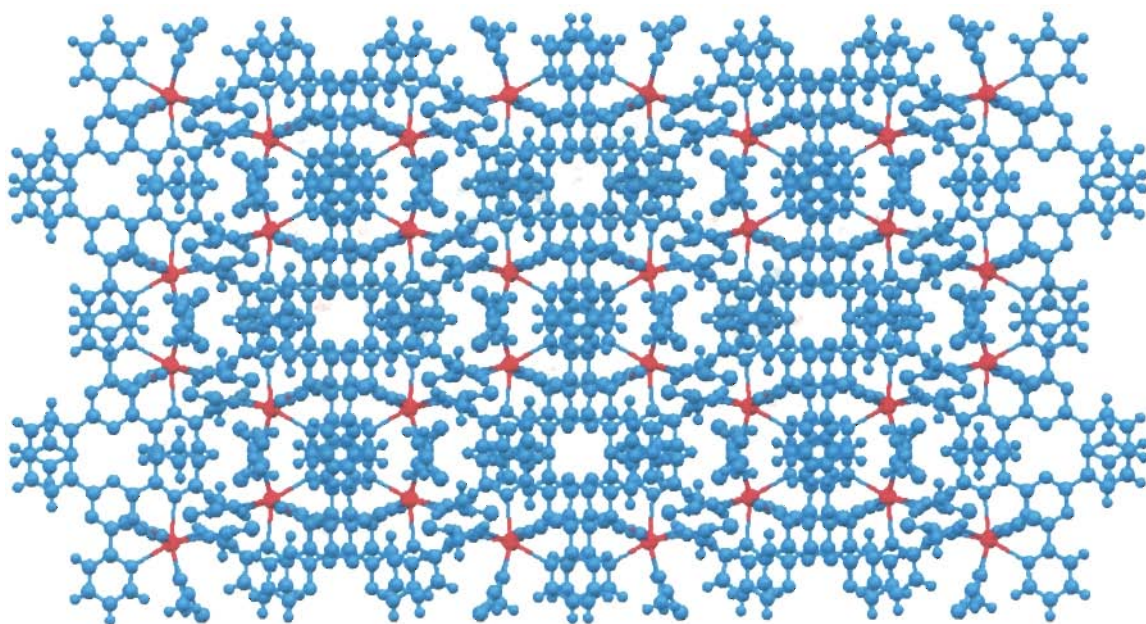
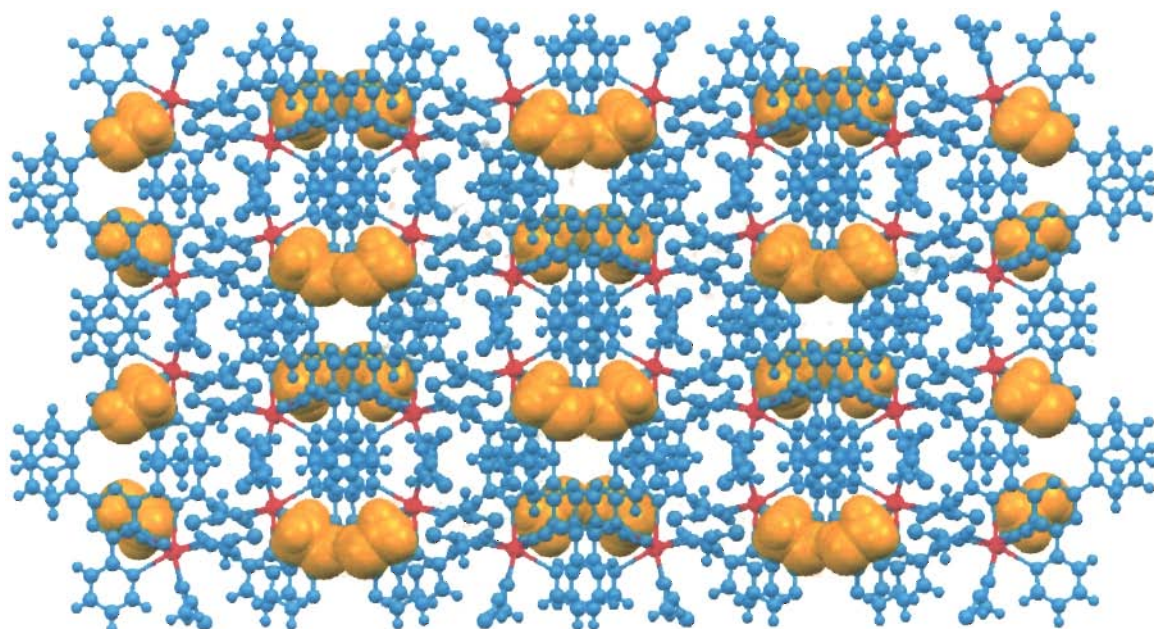


Fig. 3.33: Various C-H...O, C-H...S, O-H...S, S...S, O...S non-covalent interactions in **3m**. Color code: C, grey; H, orange; O, red; N, blue; S, yellow; Tb, pink



(a)



(b)

Fig. 3.34: Host-guest like supramolecular motif along 'c' axis in **3m** (a) without guest (b) with guest. Color code: C, H, O, N, S, blue; Tb, pink; guest (CH₃OH), orange

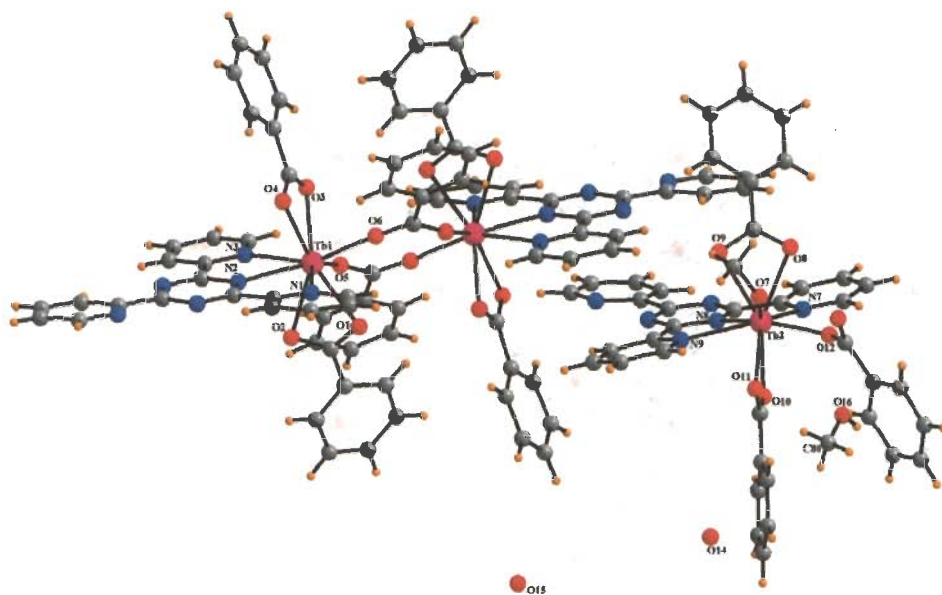


Fig. 3.35: Crystal structure of $\{[\text{Tb}_1(\text{tptz})(\text{OBz})_2(\mu\text{-OBz})]_2[\text{Tb}_2(\text{tptz})(\text{OBz})_3\text{CH}_3\text{OH}]\} \cdot \text{CH}_3\text{OH} \cdot 2\text{H}_2\text{O}$ (**3n**). Color code: C, grey; H, orange; O, red; N, blue; Tb, pink

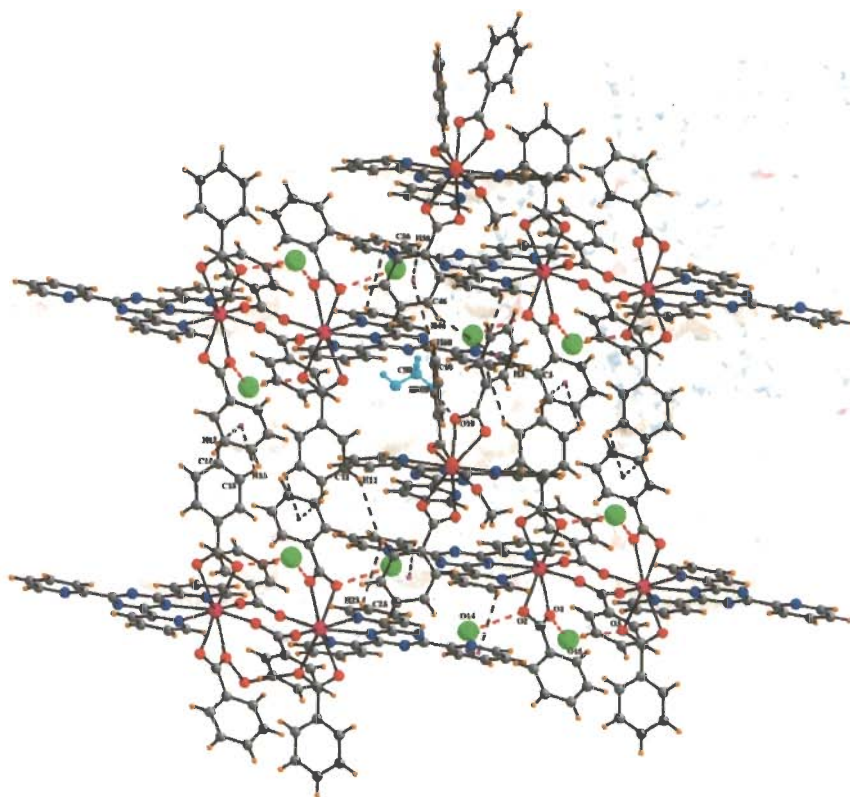
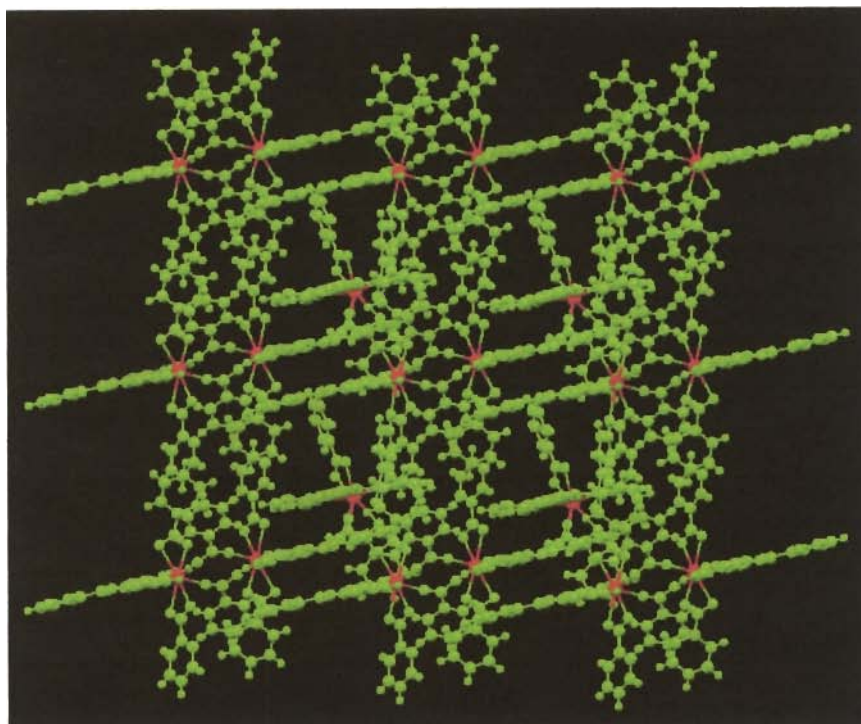
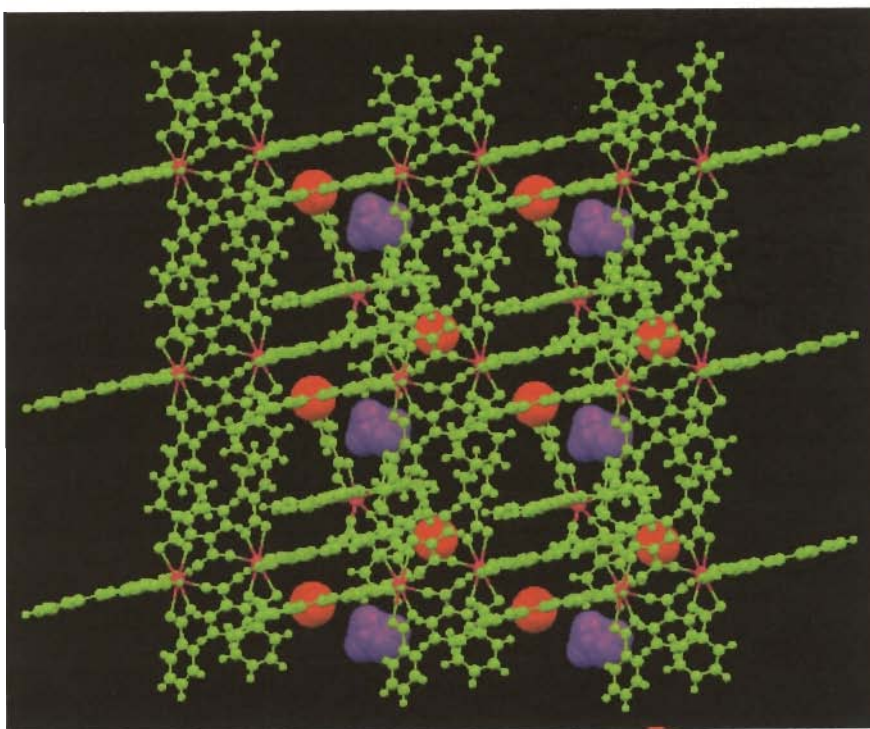


Fig. 3.36: Various non-covalent interactions in **3n**. Color code: C, grey; H, orange; O, red; N, blue; Tb, pink; methanol, cyan; water molecule, green



(a)



(b)

Fig. 3.37: Ladder like host-guest supramolecular motif along 'c' axis in **3n** (a) without guest (b) with guest. Color code: C, H, O, N, green; Tb, pink; CH₃OH, purple; water, red

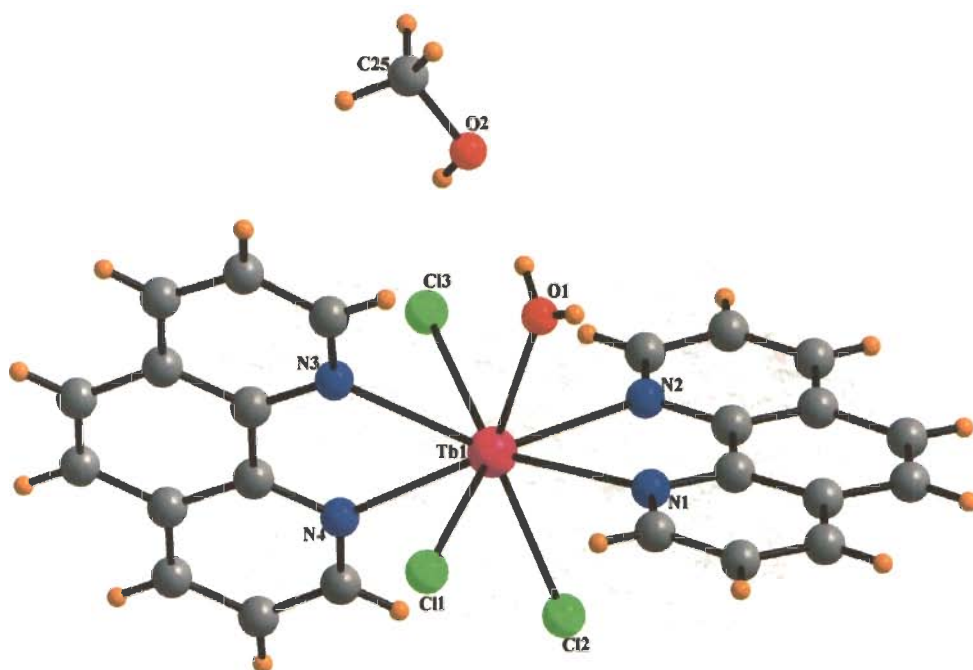


Fig. 3.38: Crystal structure of $[\text{Tb}(\text{phen})_2\text{Cl}_3\text{OH}_2]\cdot\text{CH}_3\text{OH}$ (**30**). Color code: C, grey; H, orange; O, red; N, blue; Cl, green; Tb, pink

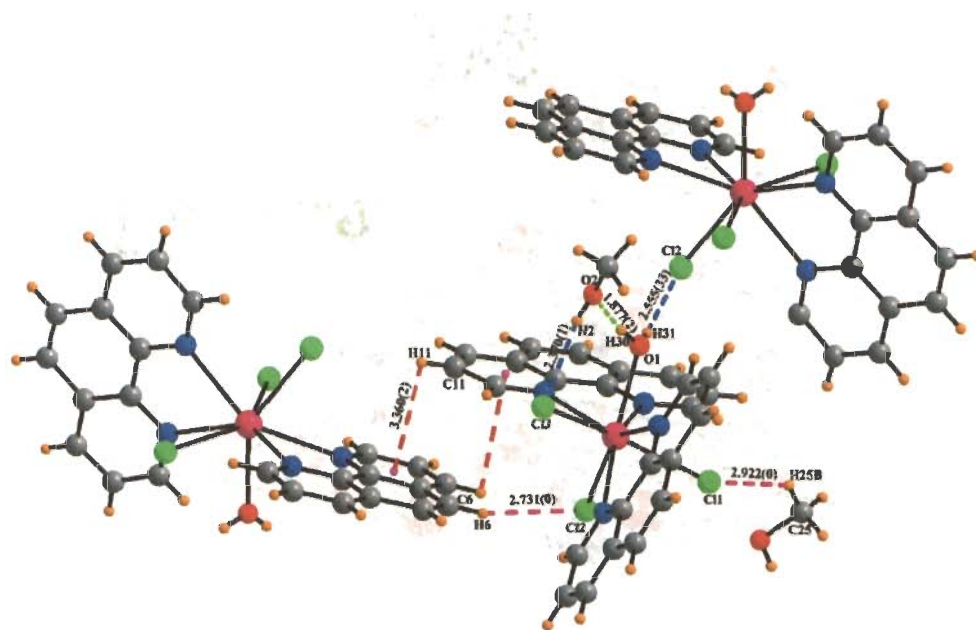
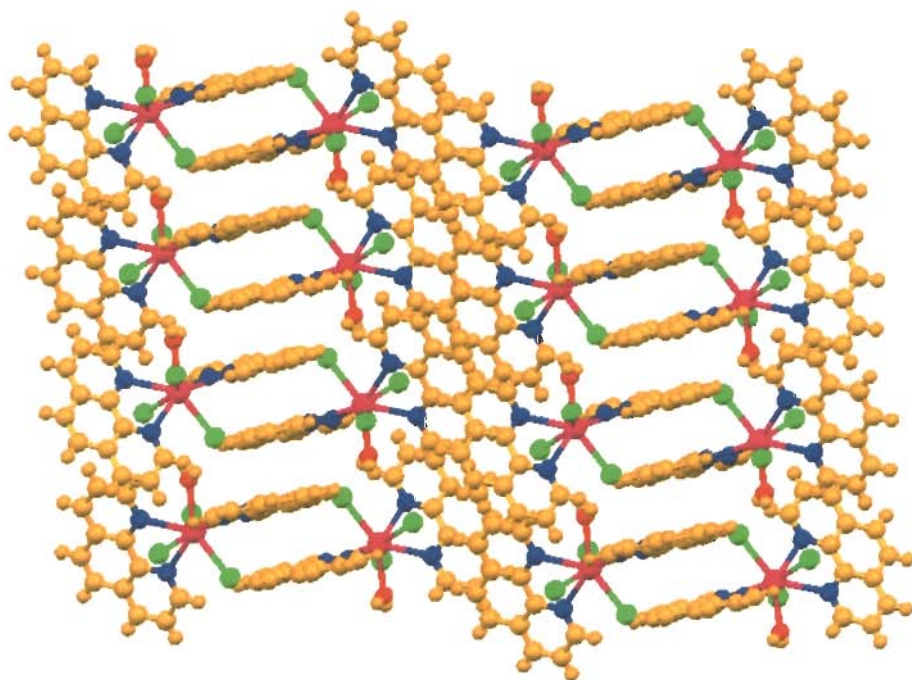
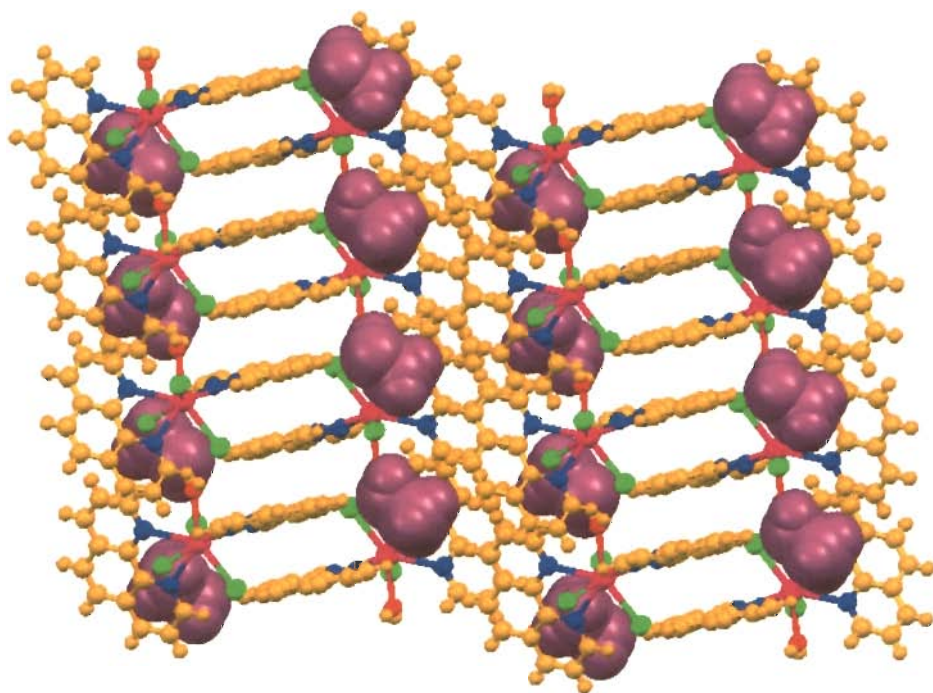


Fig. 3.39: Various C-H \cdots Cl, O-H \cdots O, O-H \cdots Cl, C-H \cdots π non-covalent interactions in **30**. Color code: C, grey; H, orange; O, red; N, blue; Cl, green; Tb, pink



(a)



(b)

Fig. 3.40: Ladder like molecular arrangement along 'b' axis for **3o** (a) without CH₃OH (b) with CH₃OH (purple). Color code: C, H, orange; O, red; N, blue; Cl, green; Tb, pink

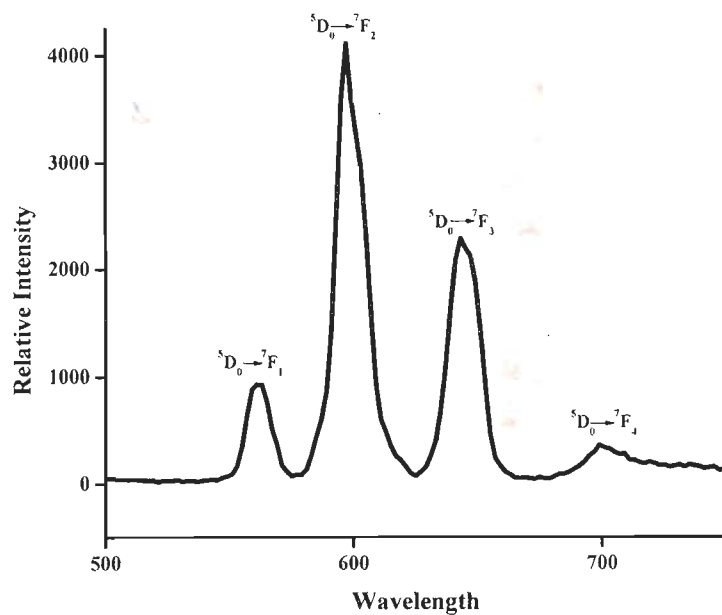


Fig. 3.41: Emission spectrum for $[\text{Eu}(\text{tptz})\text{Cl}_3(\text{CH}_3\text{OH})_2\text{OH}_2] \cdot \text{CH}_3\text{OH}$ (**3g**)

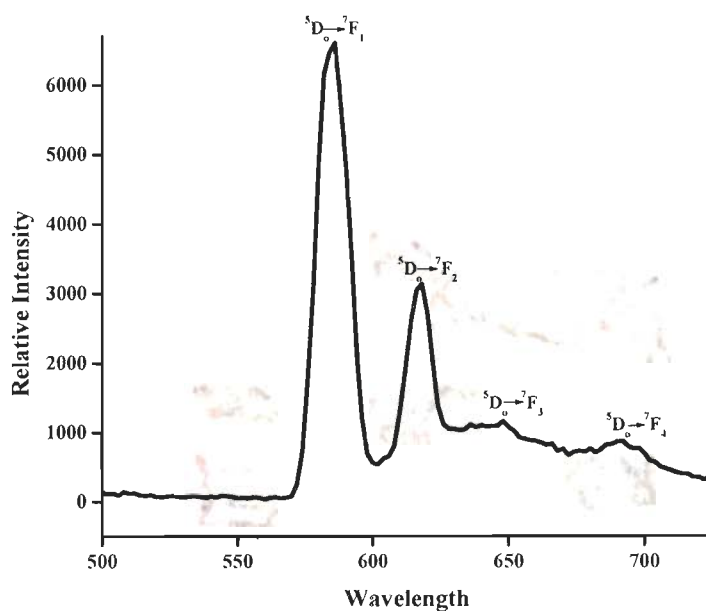


Fig. 3.42: Emission spectrum for $[\text{Eu}(\text{tptz})(\text{SCN})_3(\text{CH}_3\text{OH})_2\text{OH}_2] \cdot \text{CH}_3\text{OH}$ (**3h**)

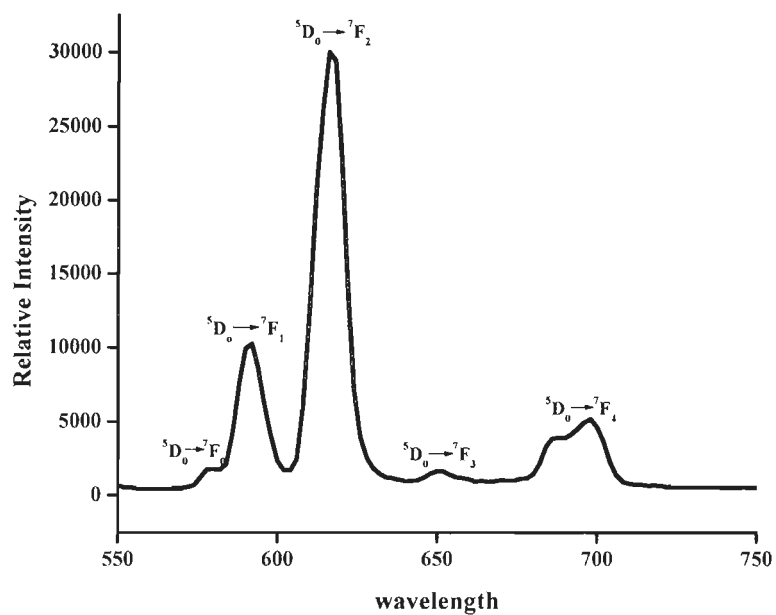


Fig. 3.43: Emission spectrum for [OH₂(OBz)₂(tptz)Eu₁(μ-OBz)₂Eu₂(tptz)(OBz)₂OH₂].CH₃OH.7H₂O (3i)

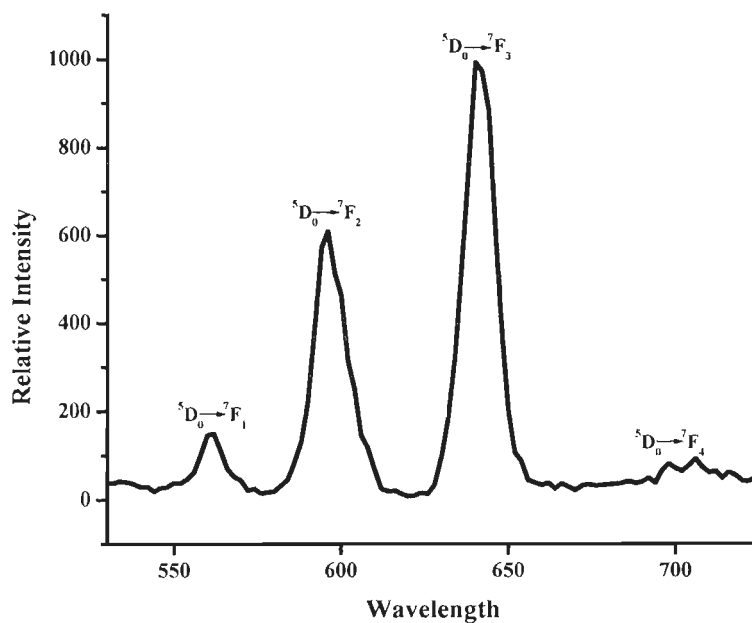


Fig. 3.44: Emission spectrum for [Eu(phen)₂Cl₃].CH₃OH

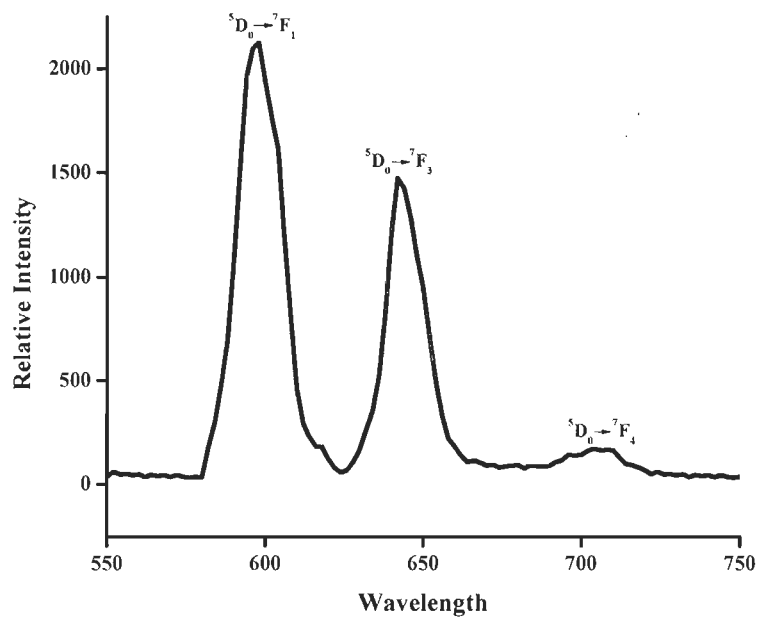


Fig. 3.45: Emission spectrum for [Eu(phen)₂(SCN)₃CH₃OH].phen (3j)

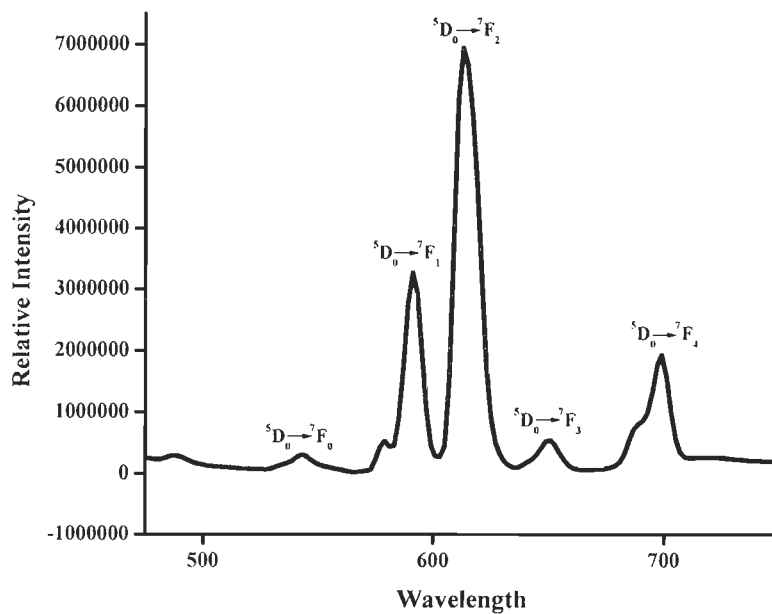


Fig. 3.46: Emission spectrum for [OH₂(phen)(2-pyca)₂Eu₁(μ-ox)Eu₂(2-pyca)₂(phen)OH₂].6H₂O (3k)

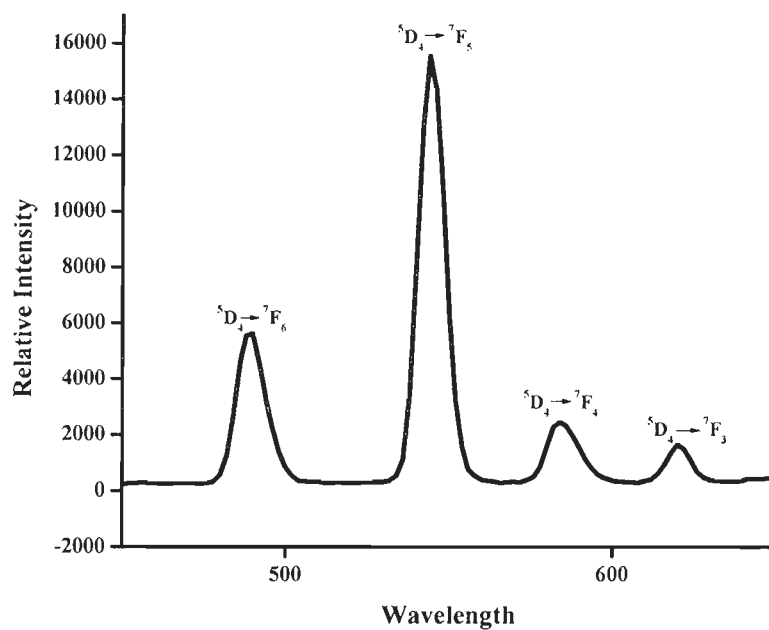


Fig. 3.47: Emission spectrum for [Tb(tptz)Cl₃(CH₃OH)₂OH₂].CH₃OH (**3l**)

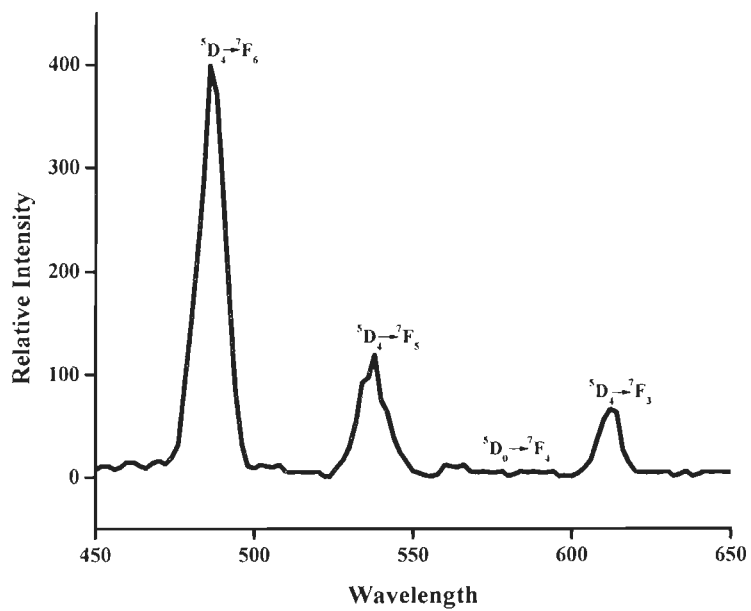


Fig. 3.48: Emission spectrum for [Tb(tptz)(SCN)₃(CH₃OH)₂OH₂].CH₃OH (**3m**)

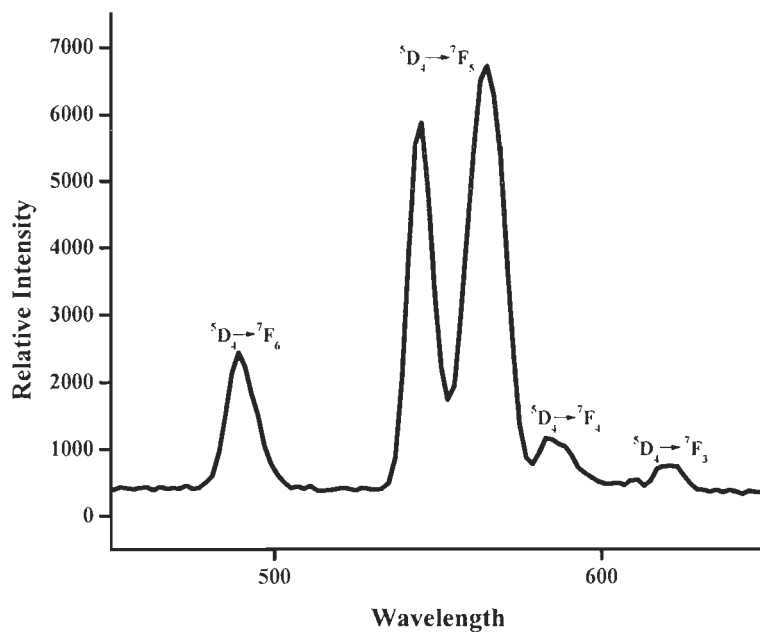


Fig. 3.49: Emission spectrum for $\{[\text{Tb}_1(\text{tptz})(\text{OBz})_2(\mu\text{-OBz})]_2 \cdot [\text{Tb}_2(\text{tptz})(\text{OBz})_3\text{CH}_3\text{OH}]\} \cdot \text{CH}_3\text{OH} \cdot 2\text{H}_2\text{O}$ (**3n**)

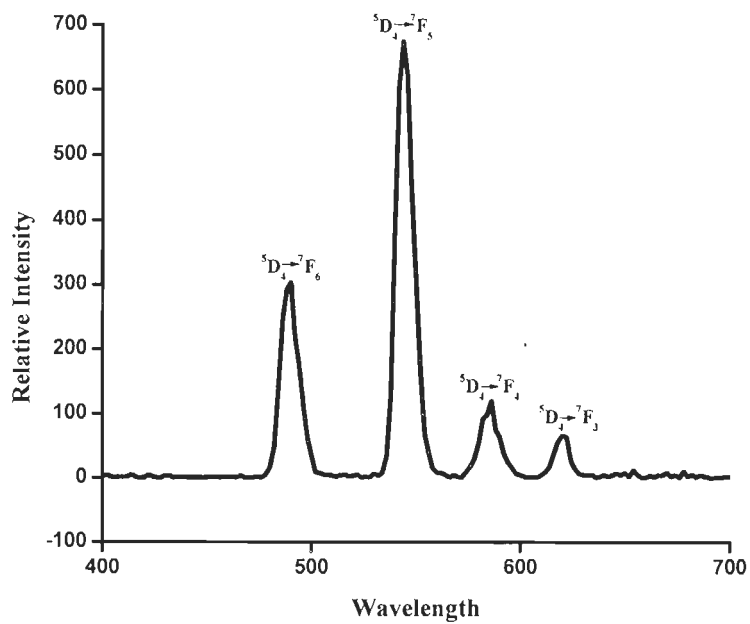


Fig. 3.50: Emission spectrum for $[\text{Tb}(\text{phen})_2\text{Cl}_3\text{OH}_2] \cdot \text{CH}_3\text{OH}$ (**3o**)

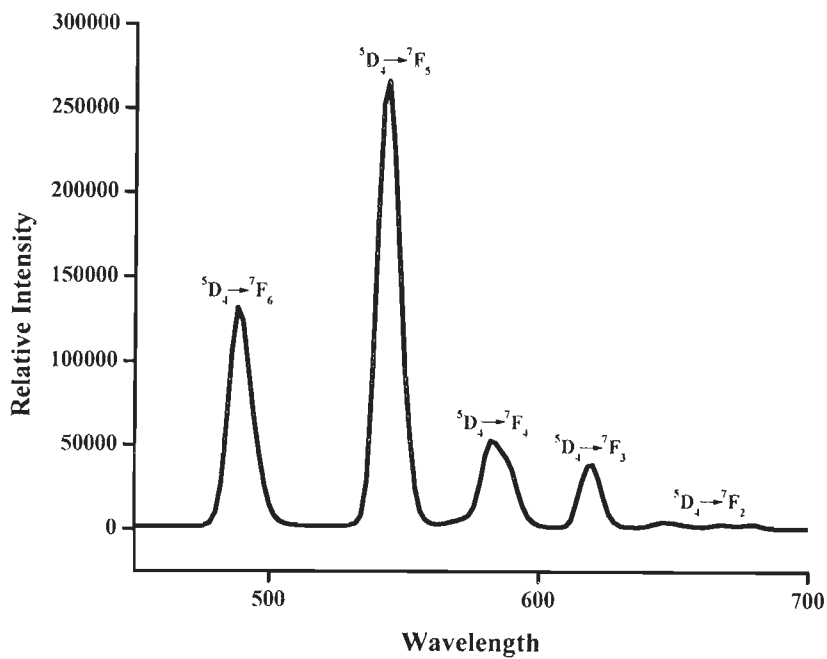


Fig. 3.51: Emission spectrum for $[\text{OH}_2(\text{phen})(2\text{-pyca})_2\text{Tb}_1(\mu\text{-ox})\text{Tb}_2(2\text{-pyca})_2(\text{phen})\text{OH}_2] \cdot 6\text{H}_2\text{O}$ (**3q**)

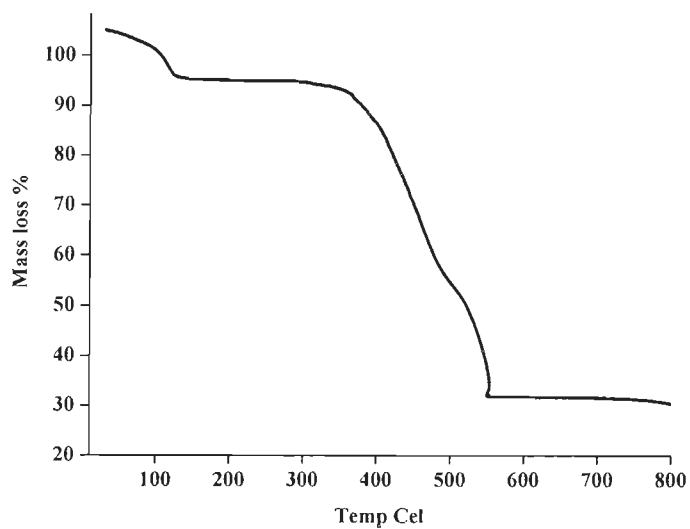


Fig. 3.52: TGA curve for $[\text{Gd}(\text{tptz})\text{Cl}_2(\text{OH}_2)_4] \cdot \text{Cl} \cdot 4\text{H}_2\text{O}$ (**3a**)

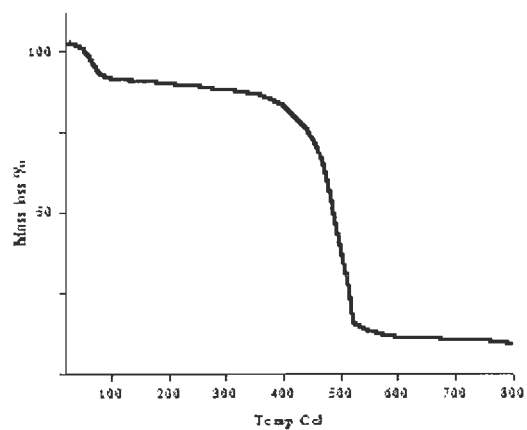


Fig. 3.53: TGA curve for $[\text{Gd}(\text{tptz})(\text{OBz})_2(\mu\text{-OBz})\text{OH}_2]_2 \cdot \text{H}_2\text{O}$ (**3c**)

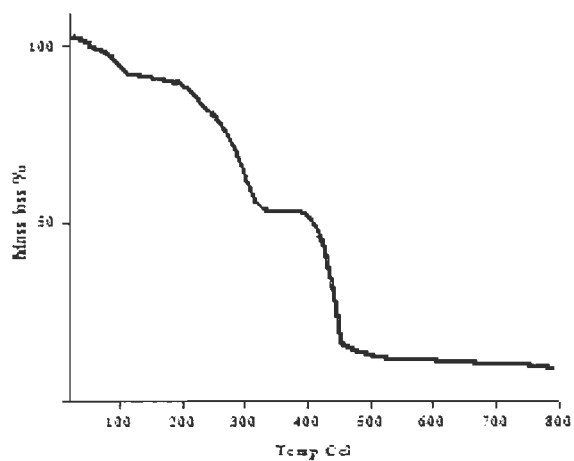


Fig. 3.54: TGA curve for $[\text{Gd}(\text{phen})\text{Cl}_2(\text{OH}_2)_4] \cdot \text{Cl} \cdot \text{CH}_3\text{OH}$ (**3d**)

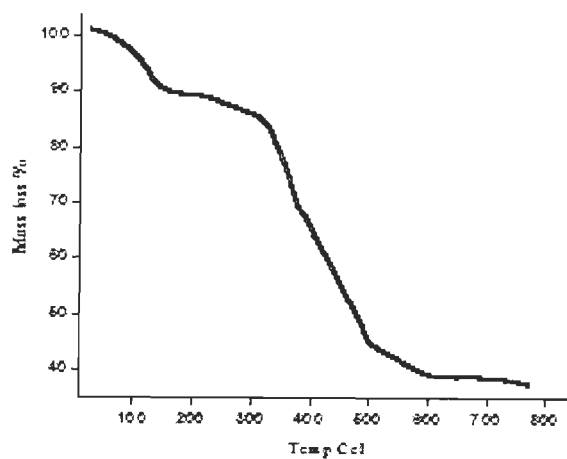


Fig. 3.55: TGA curve for $[\text{OH}_2(\text{phen})(2\text{-pyca})_2\text{Gd}_1(\mu\text{-ox})\text{Gd}_2(2\text{-pyca})_2(\text{phen})\text{OH}_2]\cdot 6\text{H}_2\text{O}$ (**3f**)

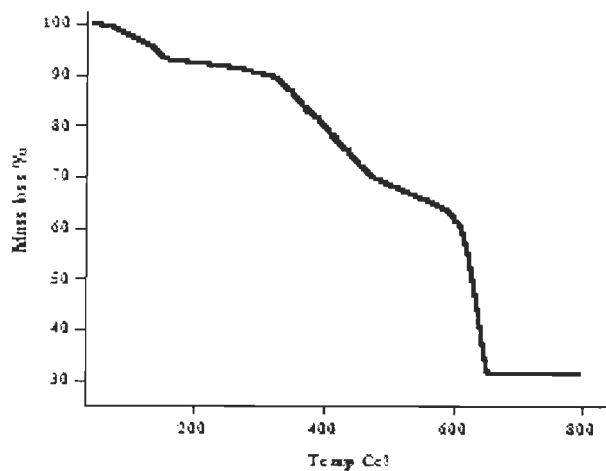


Fig. 3.56: TGA curve for $[\text{Eu}(\text{tptz})\text{Cl}_3(\text{CH}_3\text{OH})_2\text{OH}_2]\cdot \text{CH}_3\text{OH}$ (**3g**)

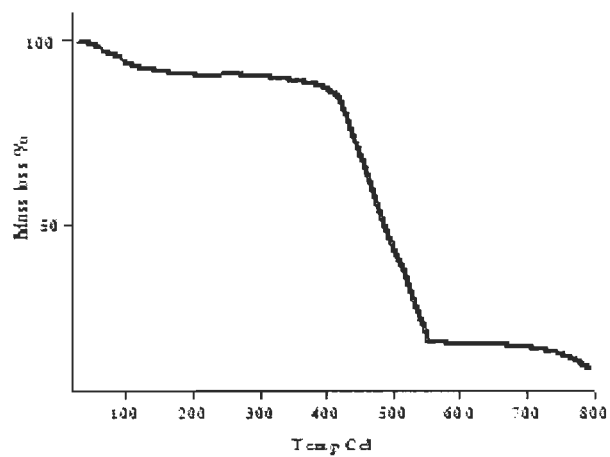


Fig. 3.57: TGA curve for $[\text{OH}_2(\text{OBz})_2(\text{tpz})\text{Eu}_1(\mu\text{-OBz})_2\text{Eu}_2(\text{tpz})(\text{OBz})_2\text{OH}_2)\cdot\text{CH}_3\text{OH}\cdot 7\text{H}_2\text{O}$ (**3i**)

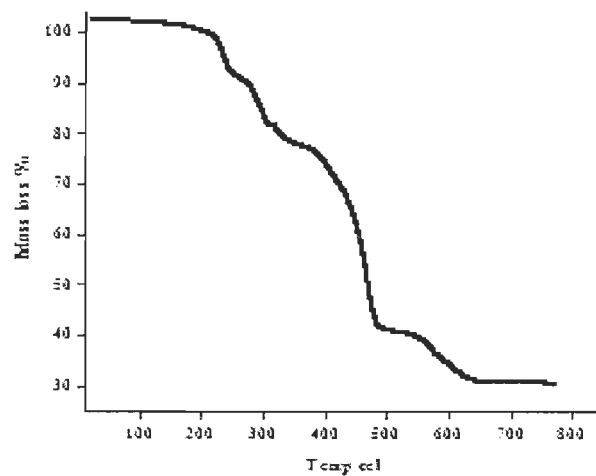


Fig. 3.58: TGA curve for $[\text{Eu}(\text{phen})_2(\text{SCN})_3\text{CH}_3\text{OH}]\cdot\text{phen}$ (**3j**)

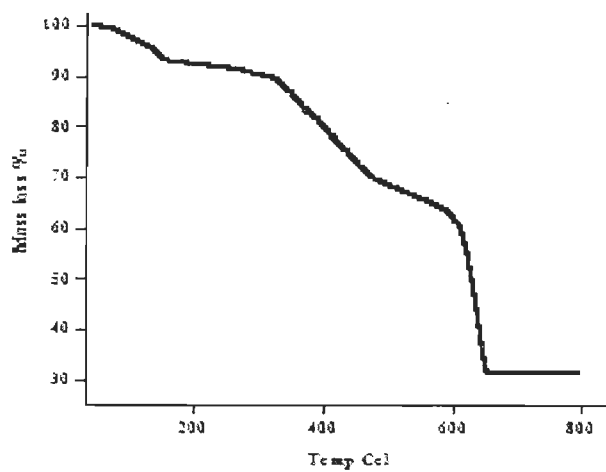


Fig. 3.59: TGA curve for $[\text{Tb}(\text{tptz})(\text{SCN})_3(\text{CH}_3\text{OH})_2\text{OH}_2] \cdot \text{CH}_3\text{OH}$ (3m)

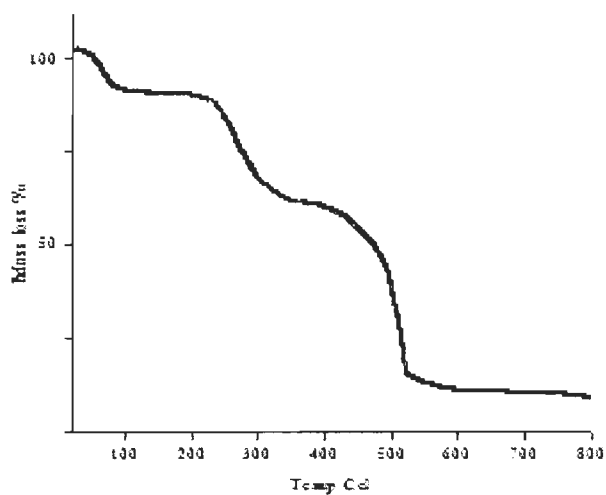


Fig. 3.60: TGA curve for $\{[\text{Tb}_1(\text{tptz})(\text{OBz})_2(\mu\text{-OBz})]_2 \cdot [\text{Tb}_2(\text{tptz})(\text{OBz})_3\text{CH}_3\text{OH}]\} \cdot \text{CH}_3\text{OH} \cdot 2\text{H}_2\text{O}$ (3n)

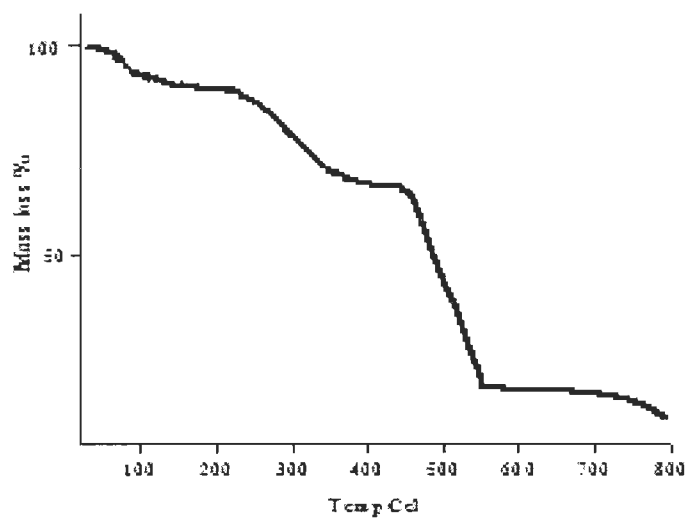


Fig. 3.61: TGA curve for [Tb(phen)₂Cl₃OH₂].CH₃OH (**3o**)

REFERENCES

1. Jin, T., Tsutsumi, A., Deguchi, Y., Machida, K. I. and Adachi, G. Y., "Luminescence property of the terbium bipyridyl complex incorporated in silica matrix by a sol-gel method", *J. Electrochem. Soc.*, **142**, L195 (1995).
2. Jin, T., Tsutsumi, A., Deguchi, Y., Machida, K. I. and Adachi, G. Y., "Preparation and luminescence characteristics of the europium and terbium complexes incorporated into a silica matrix using a sol-gel method", *J. Alloys Comp.*, **252**, 59 (1997).
3. Yan, B., Zhang, H. J. and Ni, J. Z., "Luminescence properties of rare earth (Eu^{3+} and Tb^{3+}) complexes with 1,10-phenanthroline incorporated in silica matrix by a sol-gel method", *Mater. Sci. Eng.*, **52**, 123 (1998).
4. Chuai, X. H., Zhang, H. J. and Li, F. S., "Luminescence properties of $\text{Eu}(\text{phen})_2\text{Cl}_3$ doped in sol-gel-derived SiO_2 -PEG matrix", *Mater. Lett.*, **46**, 244 (2000).
5. Yan, B. and Song, Y. S., "Spectroscopic study on the photophysical properties of lanthanide complexes with 2, 2'-bipyridine-N, N'-dioxide", *J. Fluoresc.*, **14**, 289 (2004).
6. Sabbatini, N., Guardigli, M., Manet, I., Ungaro, R., Casnati, A., Ziessel, R., Ulrich, G., Asfari, Z. and Lehn, J. -M., "Lanthanide complexes of encapsulating ligands: Luminescent devices at the molecular level", *Pure Appl. Chem.*, **67**, 135 (1995).
7. De Sá, G. F., Silva, F. R. G. and Malta, O. L., "Synthesis, spectroscopy and photophysical properties of mixed ligand complexes of europium (III) and terbium (III)", *J. Alloys Comp.*, **207**, 457 (1994).
8. Serra, O. A., Rosa, I. L. V., Nassar, E. J., Calefi, P. S. and Cardoso, P. C., "A new Tb^{3+} -diketonate complex and its inclusion in a K_2SO_4 crystal matrix: Luminescent hourglass", *J. Alloys Comp.*, **249**, 178 (1997).
9. Ionova, G., Raber, C., Guillaumont, R., Ionov, S., Madic, C. and Krupa, J. K., "A donor-acceptor model of Ln(III) complexation with terdentate nitrogen planar ligands", *N. J. Chem.*, **26**, 234 (2002).
10. Drew, M. G. B., Hudson, M. J., Iverson, P. B. and Madic, C., "[$\text{Sm}(\text{NO}_3)_3(\text{tptz})(\text{H}_2\text{O})$]. $2\text{H}_2\text{O}$ [tptz is 2,4,6-tris(2-pyridyl)-1,3,5-triazine]", *Acta. Crystallogr.*, **C 56**, 434 (2000).
11. Niyama, E., Brito, H. F., Cremona, M., Teotonio, E. E. S., Reyes, R. and Brito, G. E. S., "Synthesis and spectroscopic behavior of highly luminescent Eu^{3+} -dibenzoylmethanate (DBM) complexes with sulfoxide ligands", *Spectrochim. Acta*, **61**, 2643 (2005).

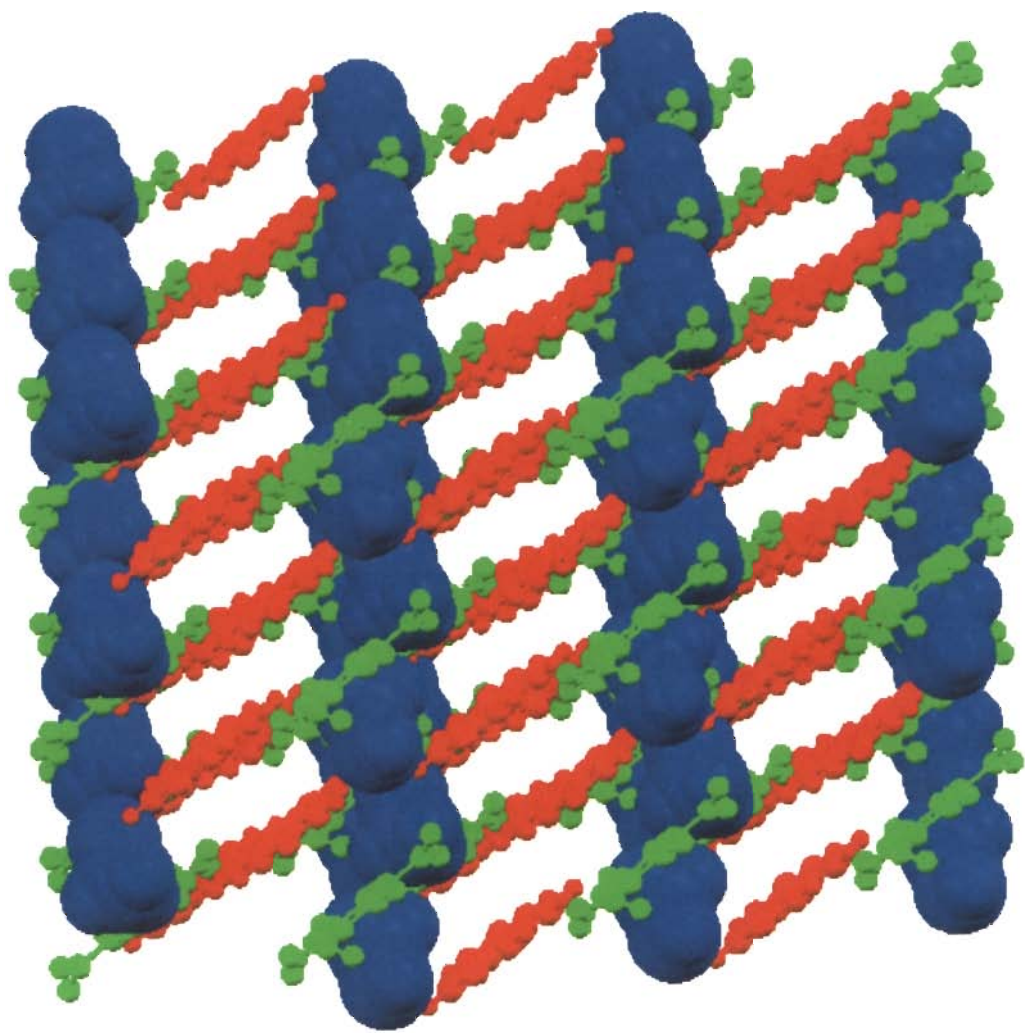
12. Xu, H. B., Shi, L. X., Zhang, L. Y., Wei, Q. H. and Chen, Z. N., "Diplatinum alkynyl chromophores as sensitizers for lanthanide luminescence in Pt₂Ln₂ and Pt₂Ln₄ (Ln = Eu, Nd, Yb) arrays with acetylidelfunctionalized bipyridine/phenanthroline", *Chem. Comm.*, **38**, 1601 (2006).
13. Coppo, P., Duat, I. M., Kozhevnikov, V. N., Hofstraat, J. W. and De Cola, L., "White-light emission from an assembly comprising luminescent iridium and europium complexes", *Angew. Chem. Int. Ed.*, **44**, 1806 (2005).
14. Davies, G. M., Pope, S. J. A., Adams, H., Faulkner, S. and Ward, M. D., "Structural and photophysical properties of coordination networks combining [Ru(bipy)(CN)₄]²⁻ anions and lanthanide (III) cations: Rates of photoinduced Ru-to-lanthanide energy transfer and sensitized near-infrared luminescence", *Inorg. Chem.*, **44**, 4656 (2005).
15. Paul, P., Tyagi, B. and Bilakhiya, A. K., "Synthesis and characterization of rhodium complexes containing 2,4,6-tris(2-pyridyl)-1,3,5-triazine and its metal-promoted hydrolytic products: Potential uses of the new complexes in electrocatalytic reduction of carbon dioxide", *Inorg. Chem.*, **37**, 5733 (1998).
16. Zibaseresht, R. and Hartshorn, R. M., "The nickel(II)/2,4,6-tris(2-pyridyl)-1,3,5-triazine system: Synthesis and crystallographic characterization of a series of complexes", *Austral. J. Chem.*, **58**, 345 (2005).
17. Zhang, L., Lu, X. Q. and Zhang, Q., "Coordination modes of diphosphines in silver (I)-diphosphine complexes mediated by 2,4,6-tris(2-pyridyl)-1,3,5-triazine (tptz)", *Trans. Met. Chem.*, **30**, 76 (2005).
18. Wu, A. -Q., Zheng, F. -K., Chen, W. -T., Cai, L. -Z., Guo, G. -C., Huang, J. -S., Dong, Z. -C. and Takano, Y., "Two series of novel rare earth complexes with dicyanamide [Ln(dca)₂(phen)₂(H₂O)₃][dca]·(phen), (Ln = Pr, Gd, and Sm) and [Ln(dca)₃(2,2'-bipy)₂(H₂O)]_n (Ln = Gd, Sm, and La): Syntheses, crystal structures and magnetic properties", *Inorg. Chem.*, **43**, 4839 (2004).
19. Wang, Y. B., Zhuang, W. J., Jin, L. P. and Lu, S. Z., "New lanthanide coordination polymers of 1,2,4,5-benzenetetracarboxylic acid and 4,4'-bipyridine with 1D channels", *J. Mol. Struct.*, **737**, 165 (2005).
20. Desilva, C. R., Wang, J. F. and Carducci, M. D., "Synthesis, structural characterization and luminescence studies of a novel europium (III) complex [Eu(DBM)₃(tptz)] (DBM:

- dibenzoylmethanate; tptz: 2,4,6-tri(2-pyridyl)-1,3,5-triazine”, *Inorg. Chim. Acta.*, **357**, 630 (2004).
21. Wietzke, R., Mazzanti, M., Latour, J. –M. and Pecaut, J., “Crystal structure and solution fluxionality of lanthanide complexes of 2,4,6-tris-2-pyridyl-1,3,5-triazine”, *Inorg. Chem.*, **38**, 3581 (1999).
 22. Tedmann, O. M., Madan, S. K., Zavalij, P. Y. and Oliver, S. R. J., “Crystal structure and fluorescence of a europium (III) complex: $\text{EuCl}_3(2,2'\text{-bipyridine N,N dioxide})\cdot 2\text{CH}_3\text{OH}$ ”, *Inorg. Chim. Acta*, **360**, 3408 (2007).
 23. Liu, Y., Liang, B., Xiao, D., Zhua, M. and Zhu, W., “Synthesis and characteristics of a europium complex using pyridyl oxadiazole derivative as a secondary ligand”, *J. Alloys Comp.*, **469**, 370 (2009).
 24. Zheng, X. J., Jin, L. P., Wang, Z. M., Yan, C. H., Lu, S. Z. and Li, Q., “Structure and photophysical properties of europium complexes of succinamic acid and 1,10-phenanthroline”, *Polyhedron*, **22**, 323 (2003).
 25. Fukuda, Y., Nakao, A. and Hayashi, K., “Syntheses and specific structures of higher-order mixed chelate lanthanide complexes containing terpyridine, acetylacetonate and nitrate ligands”, *Dalton Trans.*, **4**, 527 (2002).
 26. Song, X., Zhou, X., Liu, W., Dou, W., Ma, J., Tang, X. and Zheng, J., “Synthesis, structures and luminescence properties of lanthanide complexes with structurally related new tetrapodal ligands featuring salicylamide pendant arms”, *Inorg., Chem.* **47**, 11501 (2008).
 27. Song, Y. -S., Yan, B. and Chen, Z. -X., “Different crystal structure and photophysical properties of lanthanide complexes with 5-bromonicotinic acid”, *J. Solid State Chem.*, **177**, 3805 (2004).
 28. Singh, U. P., Tyagi, S., Sharma, C. L., Görner, H. and Weyhermüller, T., “Synthesis, molecular structure and emission properties of benzoatobridged lanthanide complexes with hydrotris(pyrazolyl)borate”, *Dalton Trans.*, **2002**, 4464 (2002).
 29. Yan, B., Song, Y. -S. and Chen, Z. -X., “A novel quaternary dinuclear luminescent terbium complex $\text{Tb}_2(\text{phth})_2(\text{Hphth})_2(\text{phen})_2(\text{H}_2\text{O})_4$: Hydrothermal synthesis, crystal structure and photophysics”, *J. Mol. Struct.*, **694**, 115 (2004).
 30. Li, Y., Zheng, F. K., Liu, Xi., Zou, W. Q., Guo, G. C., Lu, C. Z. and Huang, J. S., “Crystal structures and magnetic and luminescent properties of a series of homodinuclear lanthanide complexes with 4-cyanobenzoic ligand”, *Inorg. Chem.*, **45**, 6308 (2006).

31. Gawryszewska, P. and Ciunik, Z., "Structure and photophysical properties of new lanthanide (III) complexes $[\text{Ln}(\text{C}_{10}\text{H}_8\text{O}_6)_{1.5}(\text{H}_2\text{O})_3]\cdot\text{H}_2\text{O}$ ", *J. Photochem. Photobiol., A* **202**, 1 (2009).
32. Lam, A. W. -H., Wong, W. -T., Gao, S., Wen, G. and Zhang, X. -X., "Synthesis, crystal structure and photophysical and magnetic properties of dimeric and polymeric lanthanide complexes with benzoic acid and its derivatives", *Eur. J. Inorg. Chem.*, **2003**, 149 (2003).
33. Nakamoto, K., "Infrared spectra of inorganic and coordination compounds", John Willey & Sons, New York, 3rd edn., (1986).
34. Ferrao, J. R. and Walker, W. R., "Infrared spectra of hydroxy-bridged copper (II) compounds", *Inorg. Chem.*, **4**, 1382 (1965).
35. Lord, R. C., Martson, A. L. and Miller, F. A., "Infra-red and Raman spectra of the diazines", *Spectrochim. Acta*, **9**, 113 (1957).
36. Allan, J. R., Baird, N. D. and Kassyk, A. L., "Some first row transition metal complexes of nicotinamide and nicotinic acid", *J. Thermal Anal.*, **16**, 79 (1979).
37. Ren, N., Zhang, J. -J., Wang, R. -F. and Wang, S. -P., "Synthesis, crystal structure and thermal decomposition process of complex $[\text{Sm}(\text{BA})_3\text{phen}]_2$ ", *J. Chinese Chem. Soc.*, **53**, 293 (2006).
38. Ren, N., Zhang, J. -J., Xu, S. -L., Wang, R. -F. and Wang, S. -P., "Synthesis, crystal structure and thermal decomposition mechanism of complex $[\text{Sm}(\text{o-MBA})_3\text{phen}]_2$ ", *Thermochim. Acta*, **438**, 172 (2006).
39. Horrocks, W., Dew, Jr. and Albin, M., "Lanthanide ion luminescence in coordination chemistry and biochemistry", *Prog. Inorg. Chem.*, **31**, 1 (1984).
40. Glowiak, T., Legendziewicz, J., Huskowska, E. and Gawryszewska, P., "Ligand chirality effect on the structure and its spectroscopic consequences in $[\text{Ln}_2(\text{Ala})_4(\text{H}_2\text{O})_8](\text{ClO}_4)_6$ crystals", *Polyhedron*, **15**, 2939 (1996).
41. Legendziewicz, J., Glowiak, T., Huskowska, E. and Ngoan, D. C., "Crystal structure and spectroscopic studies of catena-diaqua-tris- μ -(L-Proline) neodymium (III) triperchlorate, $[\text{Nd}(\text{L-pro-H})_3(\text{H}_2\text{O})_2](\text{ClO}_4)_3$ ", *Polyhedron*, **7**, 2495 (1988).

CHAPTER-4

***Syntheses, Structural,
Computational and Thermal
Studies of Salts with Picric Acid
as one Component***



The nitro phenols as high energetic materials have been the subject of fairly extensive investigation of various aspects, such as the thermal and combustion properties [1], molecular structure [2], solvent extraction [3] and coordination behavior [4]. Picric acid (2,4,6-trinitrophenol) is a highly nitrated compound, basically used to produce very sensitive explosive as the NO_2 groups are the major source of oxygen in the energetic molecules, which contribute significantly to the detonation or combustion process [5]. It is also used to manufacture dyes, antiseptic agent, medicines, etching copper as well as a colorimetric reagent. Co-crystallization of picric acid with nitrogen-rich heterocycles, develop new energetic materials with higher performance or enhanced insensitivity to thermal or shock insults as the heterocycles generally have higher heat of formation, density and oxygen balance than their carbocyclic analogues [6-8]. Energetic salts based on nitrogen-rich heterocycles have been the subject of great interest in several research groups, particularly in the last couple of years as these are used extensively for both civilian and military applications. These high-nitrogen compounds [9-13] form a unique class of energetic materials whose energy is derived from their very high positive heat of formation rather than from the combustion of the carbon back bone or the ring/cage strain. Energetic materials that are salt-based often possess advantages over non-ionic molecules since these salts tend to exhibit lower vapour pressures and higher densities than their atomically similar non-ionic analogues. Five membered nitrogen-containing heterocycles are traditional centers for energetic materials. The pyrazole nucleus both thermally and hydrolytically is very stable and occupies a position similar to that of pyridine or ammonia in spectrochemical series. As a ligand, it coordinates to metals and metalloids through the 2-N but after deprotonation, the formed pyrazolate anions can coordinate through both nitrogen atoms as an exobidentate ligand of C_{2v} symmetry. The nucleophilicity of the nitrogen and their steric accessibility may be varied through appropriate ring substitution. However the literature on co-crystallization using pyrazole as one component and picric acid as other component are very limited. Llamas-Saiz et al. [14] reported the picrate of tris(pyrazol-1-yl)-1,3,5-triazine (TPT) containing water and chloroform, exists as an oxonium picrate solvated by TPT and chloroform in the solid state (Fig. 4.1). All H atoms of the oxonium cations are involved in strong hydrogen bonds joining the TPT molecule and picrate anion. They also reported that the TPT molecule mimics the crown ethers in stabilizing the H_3O^+ cation.

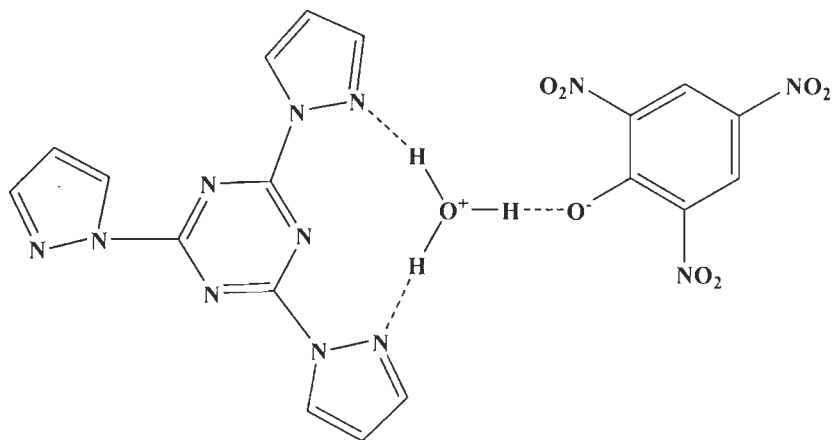


Fig. 4.1: Structure of the picrate of tris(pyrazol-1-yl)-1,3,5-triazine (TPT) containing water. Infantes et al. [15] reported the crystal structure of 3(5)-aminopyrazolium picrate salt where the anions and the cations are linked by a two dimensional network of hydrogen bonds in the 'ab' plane. They also compared the relative stability of the tautomeric forms of the 3(5)-aminopyrazolium cation using Ab initio molecular orbital methods at the HF and B3LYP levels using a 6-31G** basis set. Zaderenko et al. [16] reported the crystal structure of the diethyl 2-benzimidazol-1-ylsuccinate-picric acid (1/1) by X-ray diffraction analysis. Diethyl 2-benzimidazol-1-ylsuccinate molecules form channels along the 'a' axis, in which the picric acid molecules are located which are held together by hydrogen bonding. They also studied the ^1H NMR spectra in DMSO- d_6 solution and CP/MAS solid ^{13}C NMR of this 2-benzimidazol-1-ylsuccinate-picric acid (1/1) molecular complex, suggest that the picric acid linkage depends on the nature of the azole.

Heterocycles that contain large amounts of nitrogen are typically relatively dense, and the smaller amounts of hydrogen and carbon enhance good oxygen balance. Normally, they also have higher heats of reaction. Because a higher percentage of the decomposition products will be dinitrogen, these nitrogen-rich compounds are promising high energetic materials with high energy densities [17]. From an analysis of the structures of thermally stable explosives, it appears that introduction of amino groups into heterocycles is one of the simplest approaches to enhance their thermal stability [8]. However, until now, most research is based on compounds with both nitro and carbon-amino or nitrogen-amino substituents [8]. Dobrowolska et al. [18] reported the crystal structure of 2:1 picric acid (PAH) with tetramethylpyrazine (TMP) (Fig. 4.2). They found that the two equivalent $^+\text{NH}\cdots\text{O}^-$ hydrogen bonds are formed with the length of 2.601 Å (calculated 2.640 Å).

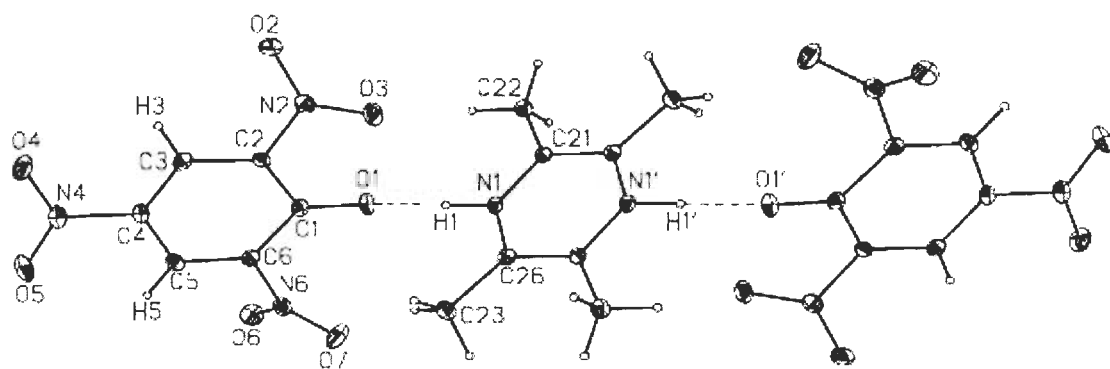


Fig. 4.2: Crystal Structure of 2PAH:tetramethylpyrazine

Jin et al. [19] reported the imidazolyl derived complex $[N,N'$ -butylenebis(imidazole):(2,4,6-trinitrophenol) $]$ $_2$. They found that in this complex, two parallel imidazolium cations and two antiparallel 2,4,6-trinitrophenolate anions formed 32-membered rings through hydrogen bonding interaction and these rings extended along the 'c' axis direction to form one dimensional railway structure. Due to presence of many weak interactions, the complex showed three dimensional layer structure. Chandramohan et al. [20] reported the synthesis of acenaphthene picrate (ACP) as shown in Fig. 4.3. They also characterized through the elemental analysis, powder XRD, NMR and FTIR techniques.

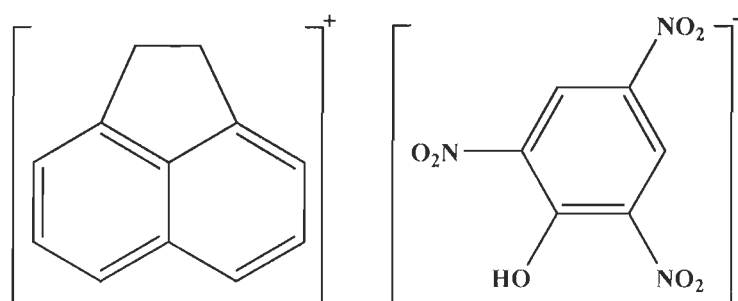


Fig. 4.3: Structure of ACP

Narayana et al. [21] reported the formation of 2-aminopyrimidinium:picrate ($C_4H_6N_3^+.C_6H_2N_3O_7^-$) compound and found that the geometric parameters of the title compound were in the usual ranges. Two nitro groups are almost coplanar with the aromatic picrate ring [dihedral angles 3.0 (2) and 4.4 (3) $^\circ$], while the third is significantly twisted out of this plane [dihedral angle 46.47 (8) $^\circ$]. Anions and cations are connected via N-H \cdots O hydrogen bonds. Smith et al. [22] reported the crystal structure of a second monoclinic polymorph of

anilinium picrate ($C_6H_8N^+ : C_6H_2N_3O_7^-$) that showed a three dimensional hydrogen-bonded polymer with strong primary interspecies interactions involving the proximal phenolate and adjacent nitro group O-atom acceptors and separate anilinium H-atom donors in two cyclic $R^2_1(6)$ associations. MacDonald et al. [23] reported the supramolecular chemistry and crystal structures of two concomitant polymorphs (**1** and **2**) of a 1:2:2 complex between betaine, imidazole and picric acid. Co-crystallization of these complexes gave discrete aggregates composed of five different molecules joined by four N-H \cdots O and four C-H \cdots O hydrogen bonds. The network of hydrogen bonds between betaine, imidazole and picric acid mimics the connectivity present in the Asp \cdots His \cdots Ser catalytic triad and serves as a structural model for hydrogen bonding in the active site of serine proteases (Fig. 4.4).

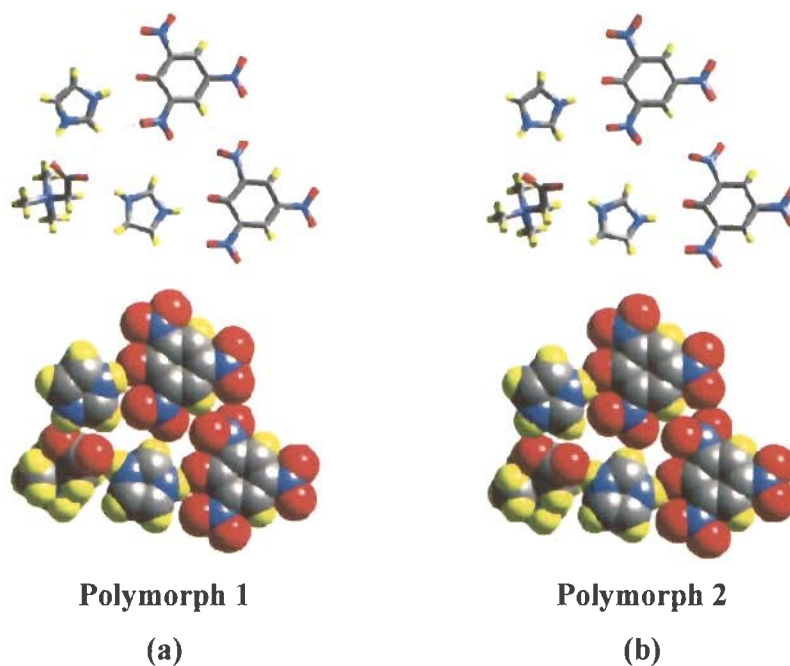


Fig. 4.4: (a & b) The supramolecular units in polymorphs **1** and **2** contain betaine, imidazolium cations, and picric acid anions in a ratio of 1:2:2, respectively. Stick and space-filling view that show the similarity in structure of the supramolecular units in **1** and **2**.

Garcia et al and Toscano [24] reported the title compound, IBA-PIC (IBA = 4-(3-indolyl) butyric acid, PIC = picric acid). The IBA-PIC complex occurred as two independent molecules with different conformations. Molecules of both IBA and picric acid lie approximately parallel to (100) in layers and π -bonding interactions across the 3.55 Å spacing.

Yamaguchi et al. [25] reported the π -molecular complex of phenanthrene:picric acid. Phenanthrene and picric acid molecules are stacked alternately along the 'c' axis, making their molecular planes parallel to each other (Fig. 4.5).

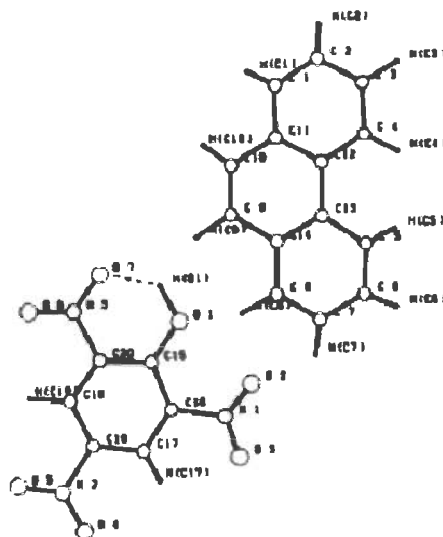


Fig. 4.5: Crystal Structure of phenanthrene:picric acid

Darwich et al. [26] reported the picrate salts using high nitrogen-content heterocycles 3,4,5-triamino-1,2,4-triazole. They also determined the sensitivity of the compounds to shock and friction by standard BAM tests revealing a low sensitivity. Yathirajan et al. [27] reported the crystal structure of phthalazin-1 (2H)-one-picric acid, and found that the three nitro groups are almost coplanar with the aromatic picrate ring [dihedral angles $10.2 (2)^\circ$, $7.62 (16)^\circ$ and $8.08 (17)^\circ$] (Fig. 4.6). They also suggested that the phthalazin-1(2H)-one molecules are connected via N-H \cdots O hydrogen bonds, forming centrosymmetric dimmers, and the molecular conformation of the picric acid is stabilized by an intramolecular O-H \cdots O hydrogen bond.

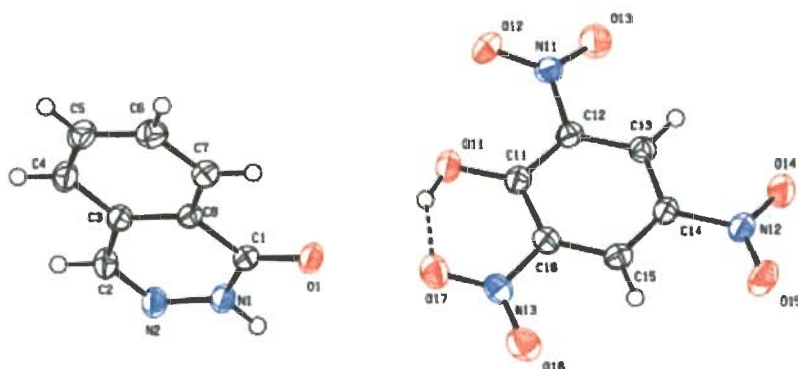


Fig. 4.6: Crystal Structure of phthalazin-1(2H)-picric acid

Muthamizhchelvan et al. [28] reported crystal structure of 2-chloroanilinium picrate (2CAP) (Fig. 4.7) where the proton from the phenolic OH group of the picric acid has been transferred to the amino group of the 2-chloroaniline. The bond lengths and angles of the picrate anion show the characteristic values, with C1-C2, 1.429(3) Å, which are longer and deviate from the regular aromatic values; the C1-O1 value is 1.270(3) Å, which is intermediate between the single and double bonds.

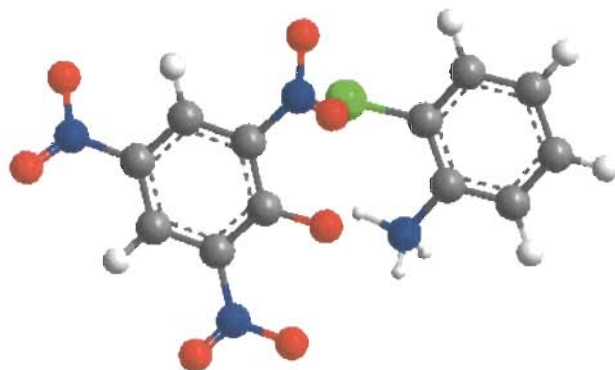


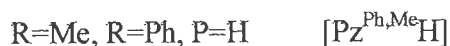
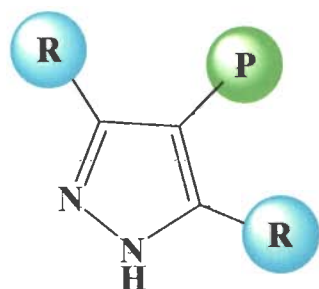
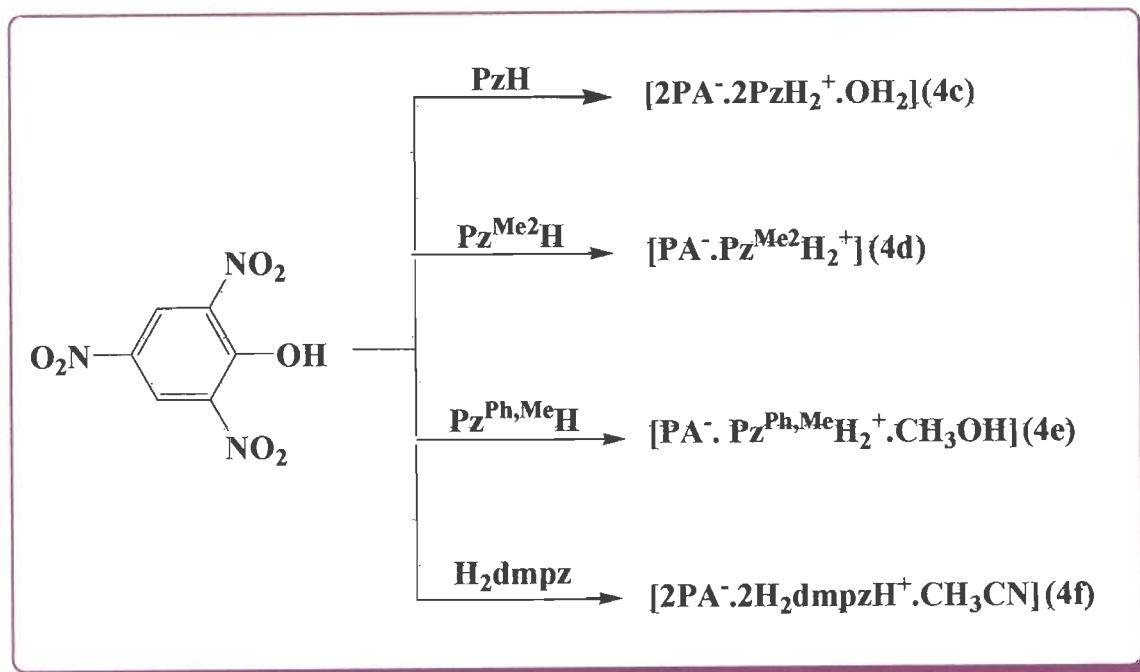
Fig. 4.7: Crystal Structure of 2-chloroanilinium picrate

Singh et al. [29] reported that the energetic salts offer many advantages over conventional energetic molecular compounds and the use of nitrogen containing anions and cations contributes to high heats of formations and high densities. Klapotke et al. [30] synthesized 1,4-dimethyl-5-aminotetrazolium-5-nitrotetrazolate in high yield from 1,4-dimethyl-5-aminotetrazolium iodide and silver 5-nitrotetrazolate. They also found that 1,4-dimethyl-5-aminotetrazolium-5-nitrotetrazolate is the first example of an energetic material which contains both tetrazole based cation and anion, and is hydrolytically stable with a high melting point of 190 °C (decomposition). Xue et al. [31] synthesized new energetic salts via the quaternization of azido or nitro derivatives of imidazole, 1,2,4-triazole and substituted derivatives of tetrazole with nitric or perchloric acid or with iodomethane followed by metathesis reaction with silver nitrate or silver perchlorate. They also confirmed the structures of 1,4-dimethyl-3-azido-1,2,4-triazolium nitrate, 3-azido-1,2,4-triazolium nitrate, 1-methyl-4-amino-1,2,4-triazolium perchlorate and 1,4-dimethyl-2-H-1,2,4-triazolium triiodide using single crystal X-ray analysis. Xue et al. [32] also synthesized new energetic salts via the quaternization of derivatives of N-aminoazoles with nitric or perchloric acid or with iodomethane followed by metathesis reaction with silver nitrate or silver perchlorate, and

found that the most of the salts exhibited good thermal stabilities and low melting points. Huynh et al. [33] reported the synthesis and properties of novel 4,4',6,6'-tetra(azido)hydrazo-1,3,5-triazine and 4,4',6,6'-tetra(azido)azo-1,3,5-triazine where the hydrazo and azo linkages not only desensitize but also dramatically increase the melting point of the polyazido products. Chavez et al. [34] synthesized and discussed the properties of various 1,2,4,5-tetrazine explosives and energetic materials. These are the nitrate and perchlorate salts of 3,6-diguanidino-1,2,4,5-tetrazine, the nitrate and perchlorate salts of 3,6-diguanidino-1,2,4,5-tetrazine-1,4-di-N-oxide, 3,6-bis(1H-1,2,3,4-tetrazol-5-ylamino)-1,2,4,5-tetrazine and its 1,4-di-N-oxide derivative, 3,3'-azobis(6-amino-1,2,4,5-tetrazine) and its oxidation products. On the basis of above literatures, it may be concluded that co-crystallization of picric acid with different types of nitrogen-rich heterocycles, described in this chapter are not available in literature. The objective of this work is to co-crystallize the picric acid with nitrogen-rich heterocycles and to see the effect of them on explosive properties of picric acid. The present chapter describes the synthesis, structural, thermal studies and theoretical calculation of some salts. Thermal stability of these salts has been studied by means of thermogravimetric and differential thermogravimetric analysis methods, while kinetic parameters have been evaluated using models fitting and isoconversional methods.

RESULTS AND DISCUSSION

3-phenyl-5-methylpyrazole [$\text{Pz}^{\text{Ph,Me}}\text{H}$] [35] (**4a**), 4-(3,5-dimethyl-4H-pyrazole-4-yl)-3,5-dimethyl-1H-pyrazole [H_2mdpz] [36] (**4b**) were synthesized by the literature method. The reaction of picric acid (2,4,6-trinitrophenol) (PA) with corresponding nitrogen-rich heterocycles as pyrazole (PzH), 3,5-dimethylpyrazole ($\text{Pz}^{\text{Me}_2}\text{H}$), 3-phenyl-5-methylpyrazole ($\text{Pz}^{\text{Ph,Me}}\text{H}$), 4-(3,5-dimethyl-4H-pyrazole-4-yl)-3,5-dimethyl-1H-pyrazole (H_2dmpz) yielded salts viz., [$2\text{PA}^- \cdot 2\text{PzH}_2^+ \cdot \text{OH}_2$] (**4c**), [$\text{PA}^- \cdot \text{Pz}^{\text{Me}_2}\text{H}_2^+$] (**4d**), [$\text{PA}^- \cdot \text{Pz}^{\text{Ph,Me}}\text{H}_2^+ \cdot \text{CH}_3\text{OH}$] (**4e**), [$2\text{PA}^- \cdot 2\text{H}_2\text{dmpzH}^+ \cdot \text{CH}_3\text{CN}$] (**4f**) as given in scheme 4.1. The different formulations were confirmed by elemental analysis, infrared and X-ray crystallography. The crystallographic, structure refinement parameters and selected hydrogen bonding data are summarized in Table 4.1 to 4.4 and 4.13.



Scheme 4.1: General method of preparation of salts **4c-4f**

Infrared spectra

The asymmetric and the symmetric stretching vibrations of $-\text{NO}_2$ group show bands at 1536 cm^{-1} and 1334 cm^{-1} , respectively [20, 37]. Usually, the asymmetric stretching vibration of the $-\text{NO}_2$ group is sensitive to the polar influences and electronic states of the nucleus. The shift of the $\nu_{\text{as}}(\text{NO}_2)$ vibration to lower frequency ($1581\text{-}1530 \text{ cm}^{-1}$) in the spectrum of the salts (**4c-4n**) compared with the free picric acid (1607 cm^{-1}) suggested the large electron density on the picric acid. The NH stretching vibration is normally observed at $3500\text{-}3400 \text{ cm}^{-1}$ which is

shifted to lower wavenumber (3102 - 3056 cm^{-1}) due to the attraction of the $-\text{NH}$ protons by the picrate anion leading to an increase in $-\text{NH}$ bond length in salts (**4c-4n**) [38]. The shifting towards lower frequency in both cases, is due to the hydrogen bonded non-covalent interactions between donor ($-\text{NH}$ protons) and acceptor (picrate anion) [39].

Crystal structure of $[\text{2PA}^-\cdot\text{2PzH}_2^+\cdot\text{OH}_2]$ (**4c**)

The salt **4c** crystallizes in the triclinic crystal system with P-1 space group. As shown in Fig. 4.8, the unit cell consists of two molecules of protonated pyrazole with four NH group, two molecules of deprotonated picric acid i.e. the acidic hydrogen of the hydroxyl group on picric acid has been transferred to the nitrogen atom of the pyrazole and a water molecule. Both deprotonated picric acid groups and protonated nitrogen atoms of both pyrazole form a cationic anionic acid-base pair via $\text{N}-\text{H}\cdots\text{O}$ [$\text{N7}-\text{H7A}\cdots\text{O1}$, 1.852(23) Å; $\text{N10}-\text{H10A}\cdots\text{O8}$, 1.930(21) Å] and $\text{C}-\text{H}\cdots\text{O}$ [$\text{C13}-\text{H13A}\cdots\text{O2}$, 2.581(1) Å; $\text{C18}-\text{H18}\cdots\text{O9}$, 2.532(1) Å] intermolecular interactions (Fig. 4.9). Due to the presence of various interactions, picrate and pyrazolate ions are self assembled in a three dimensional square shaped channels and these channels act as a host molecules for water as the guest molecule. The guest molecules are situated between the two channels through $\text{N}-\text{H}\cdots\text{O}$ [$\text{N8}-\text{H8A}\cdots\text{O15}$, 1.783(24) Å; $\text{N9}-\text{H9B}\cdots\text{O15}$, 1.921(19) Å] as well as $\text{O}-\text{H}\cdots\text{O}$ [$\text{O15}-\text{H15A}\cdots\text{O8}$, 1.969(24); $\text{O15}-\text{H15A}\cdots\text{O14}$, 2.259(22) Å; $\text{O15}-\text{H16A}\cdots\text{O1}$, 2.037(23) Å] non-covalent interactions (Fig. 4.10).

Crystal structure of $[\text{PA}^-\cdot\text{Pz}^{\text{Me}_2}\text{H}_2^+]$ (**4d**)

The unit cell of **4d** contains one molecule of anionic deprotonated picric acid and one molecule of cationic protonated 3,5-dimethyl pyrazole (Fig. 4.11). It also crystallizes in the triclinic crystal system with P-1 space group. It contains $\text{N}-\text{H}\cdots\text{O}$ [$\text{N4}-\text{H4A}\cdots\text{O1}$, 1.678(21) Å; $\text{N4}-\text{H4A}\cdots\text{O7}$, 2.298(24) Å; $\text{N5}-\text{H5}\cdots\text{O7}$, 2.362(4) Å] as well as $\text{C}-\text{H}\cdots\text{O}$ [$\text{C2}-\text{H2}\cdots\text{O6}$, 2.603(2) Å; $\text{C7}-\text{H7A}\cdots\text{O1}$, 2.606(3) Å; $\text{C9}-\text{H9}\cdots\text{O4}$, 2.639(4) Å; $\text{C11}-\text{H11B}\cdots\text{O5}$, 2.478(4) Å] non-covalent interactions which are responsible for the formation of sheet with rectangular cavities in three dimensional views (Fig. 4.12). This cavity can be used for trapping the appropriate size of guest molecule (1.2 Å).

Crystal structure of $[\text{PA}^-\cdot\text{Pz}^{\text{Ph,Me}}\text{H}_2^+\cdot\text{CH}_3\text{OH}]$ (**4e**)

The co-crystallization of picric acid and 3-phenyl-5-methylpyrazole resulted in the formation of salt **4e** which crystallizes in monoclinic system with P 1 21/c 1 space group. The methanol solvent present in lattice, binds one molecule of picrate anion and one molecule of 3-phenyl-5-methylpyrazole (Fig. 4.13). The presence of different non-covalent interactions viz.,

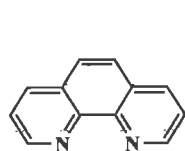
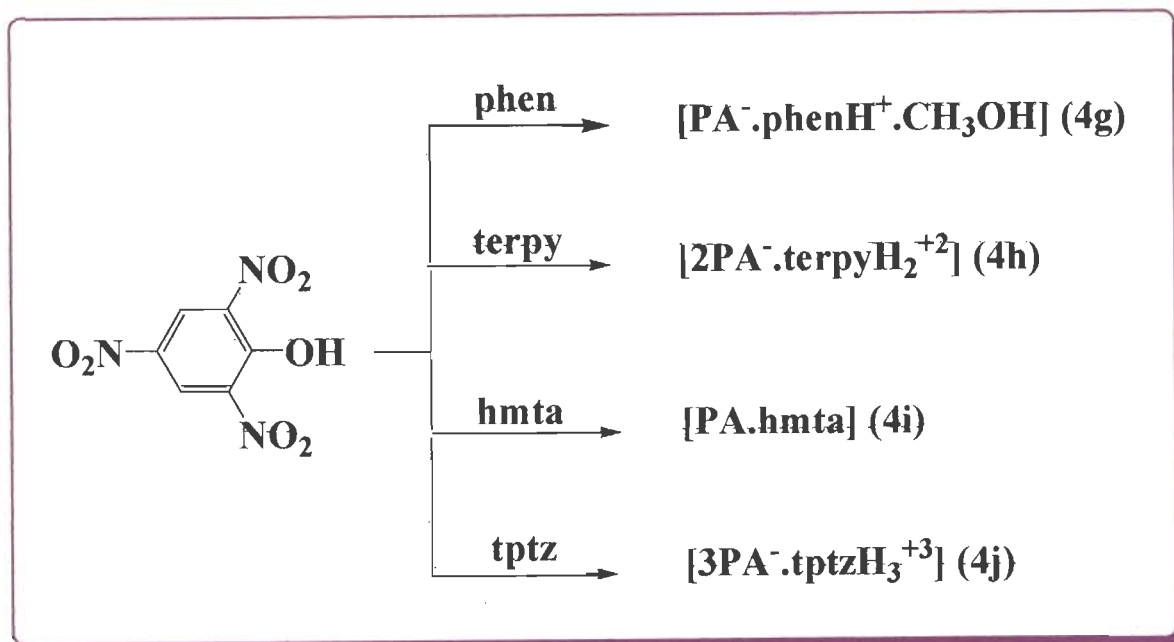
N-H...O [N1-H1...O1, 1.782(23) Å; N1-H1...O2, 2.315(21) Å; N2-H2A...O8, 1.664(22) Å], C-H...O [C1-H1C...O2, 2.355(2) Å; C6-H6...O7, 3.149(2) Å; C6-H6...O8, 2.859(2) Å; C7-H7...O7, 2.592(3) Å; C17-H17B...O5, 2.687(3) Å; C17-H17C...O6, 3.020(2) Å; C17-H17C...O7, 2.636(2) Å], O-H...O [O8-H8A...O1, 2.151(3) Å; O8-H8A...O6, 2.225(3) Å] cause the formation of host-guest structure (Fig. 4.14). Due to these interactions, cation and anion forms the cross-wires which are stacked one above the others and forms an oval shaped cavity between the two sets of cross-wires for guest methanol molecule as shown in Fig. 4.15.

Crystal structure of [2PA⁻.2H₂dmpzH⁺.CH₃CN] (4f)

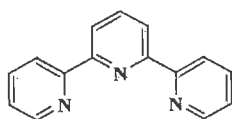
The salt **4f** with two molecules of picric acid, two molecules of 4-(3,5-dimethyl-4H-pyrazole-4-yl)-3,5-dimethyl-1H-pyrazole and one molecule of acetonitrile in unit cell, crystallizes in the monoclinic system with P 1 21/c space group (Fig. 4.16). The N-H and C-H group of pyrazole in **4f** is non-covalently interacted with O2, O8, O11, O13 and O14 atoms of picrate acceptor, forming a charge-assisted ⁺N-H...O⁻ [N13-H13A...O14, 2.792(25) Å; N14-H14A...O8, 1.800(25) Å; N14-H14A...O14, 2.284(25) Å] and ⁺C-H...O⁻ [C19-H19B...O11, 2.575(2) Å; C22-H22A...O11, 2.605(5) Å; C30-H30A...O2, 2.685(7) Å; C30-H30C...O5, 2.761(9) Å; C32-H32A...O8, 2.914(2) Å; C33-H33B...O14, 2.600(3) Å] hydrogen bonds. The presence of different non-covalent interactions resulted in the formation of host-guest structure where the host assembly was present with rectangular shaped cavity. This cavity is formed by the picrate and 4-(3,5-dimethyl-4H-pyrazole-4-yl)-3,5-dimethyl-1H-pyrazolate ions. The guest acetonitriles are located inside the cavity through C-H...N [C2-H2...N15, 2.433(9) Å; C21-H21C...N15, 2.413(3) Å] intermolecular interactions where the solvent molecule behaves as both donor and acceptor. (Fig. 4.17). All these interactions form the three dimensional zig-zag railway track like perspective view (Fig. 4.18).

The above structural studies reveals that on increasing the substituents of pyrazole ring, the number of non-covalent interactions vary from salt **4c** to **4f** which in turn causes different type of three dimensional packing view for each salt.

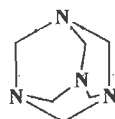
When we performed the reaction of picric acid with 1,10-phenanthroline (phen), 2,2';6',2"-terpyridine (terpy), hexamethylenetetramine (hmta), 2,4,6-tris(2-pyridyl)-1,3,5-triazine (tptz), the salts viz., [PA⁻.phenH⁺.CH₃OH] (**4g**), [2PA⁻.terpyH₂⁺²] (**4h**), [PA.hmta] (**4i**), [3PA⁻.tptzH₃⁺³] (**4j**) were obtained (scheme 4.2).



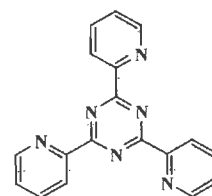
Phen



terpy



hmta



tptz

Scheme 4.2: General method of preparation of salts **4g-4j**

Crystal structure of $[PA^{\ominus}.phenH^{\oplus}.CH_3OH]$ (4g)

Salt **4g** crystallizes in the triclinic space group P-1 and the β angle is $71.296(13)^{\circ}$ (Table 4.5). In this case, there are one molecule of deprotonated picric acid, one molecule of protonated 1,10-phenanthroline and one methanol molecule in the asymmetric unit i.e. acidic hydrogen of the hydroxyl group on picric acid has been transferred to the one nitrogen atom of 1,10-phenanthroline as shown in Fig. 4.19. The protonated nitrogen (N1) shows the strong hydrogen bonding with the oxygen atom (O8) of methanol molecule via $N1-H1B \cdots O8$, 1.831(29) Å interaction. The crystal packing also shows other $C-H \cdots O$ [$C7-H7A \cdots O1$,

2.338(18) Å; C7-H7A...O2, 2.404(9) Å; C9-H9...O3, 3.016(19) Å; C11-H11...O3, 2.628(9) Å; C12-H12...O6, 2.840(21) Å; C14-H14...O7, 2.410(2) Å; C15-H15...O8, 2.839(5) Å; C16-H16...O8, 2.807(4) Å; C19-H19C...O3, 2.746(3) Å] and O-H...O [O8-H8...O1, 2.002(3) Å; O8-H8...O4, 2.419(19) Å] non-covalent interactions (Fig. 4.20). Stacking of both organic moieties with methanol molecules make three dimensional ladder like assemble where the methanol molecules act as the pillars (Fig. 4.21).

Crystal structure of [2PA⁻.terpyH₂⁺²] (4h)

Salt **4h** is in monoclinic space group P21/c (Table 4.6) with two molecules of anionic deprotonated picric acid and one molecule of cationic protonated 2,2';6',2"-terpyridine in asymmetric unit (Fig. 4.22). In this crystal structure, the two nitrogen atoms (N1, N3) of terpy molecule are protonated which show the strong hydrogen bonding with the oxygen atom (O8) of picrate anion via N-H...O [N1-H1A...O8, 2.031(110) Å; N3-H3A...O8, 1.727(49) Å] interactions. Other weak intermolecular interactions C-H...O [C4-H4...O12, 2.697(3) Å; C7-H7...O11, 2.714(3) Å; C7-H7...O12, 2.619(3) Å; C8-H8...O5, 2.949(8) Å; C9-H9...O1, 2.287(5) Å; C12-H12...O1, 2.380(4) Å; C13-H13...O2, 2.489(8) Å; C13-H13...O11, 2.600(3) Å; C14-H14...O5, 2.121(7) Å; C15-H15...O4, 2.328(7) Å] and O...O [O13...O6, 2.968(6) Å; O14...O6, 3.010(5) Å] are also present (Fig. 4.23). Due to the presence of various non-covalent interactions, the three dimensional view of **4h** shows mat-like supramolecular structure as shown in Fig. 4.24.

Crystal structure of [PA.hmta] (4i)

The co-crystallization of picric acid and hexamethylenetetramine resulted in the formation of co-crystal **4i** which crystallizes in monoclinic system with P 21/c space group (Table 4.7). The asymmetric unit contains one molecule of picric acid and one molecule of hexamethylenetetramine as shown in Fig. 4.25. It is true co-crystal i.e. no proton transfer occurs. Like previous salt, **4i** also shows different intermolecular interactions viz., C-H...O [C7-H7A...O4, 2.607(2) Å; C7-H7A...O6, 3.255(4) Å; C7-H7B...O6, 3.042(4) Å; C8-H8A...O3, 2.972(2) Å; C8-H8A...O4, 3.159(2) Å; C9-H9B...O7, 2.627(1) Å; C10-H10A...O4, 2.707(1) Å; C10-H10A...O5, 3.017(2) Å; C10-H10A...O6, 2.599(1) Å; C11-H11...O7, 2.676(2) Å], C-H...N [C7-H7A...N7, 2.800(2) Å; C8-H8A...N5, 2.858(1) Å; C9-H9B...N2, 2.924(2) Å; C10-H10A...N3, 2.977(2) Å], O-H...O [O1-H1...O3, 3.228(2) Å] and O-H...N [O1-H1...N6, 2.119(1) Å]. In this co-crystal, the intermolecular C-H...N hydrogen bond plays a key role in the self-assembly of the hmta to generate one dimensional zig-zag chain i.e. CH₂

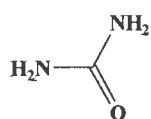
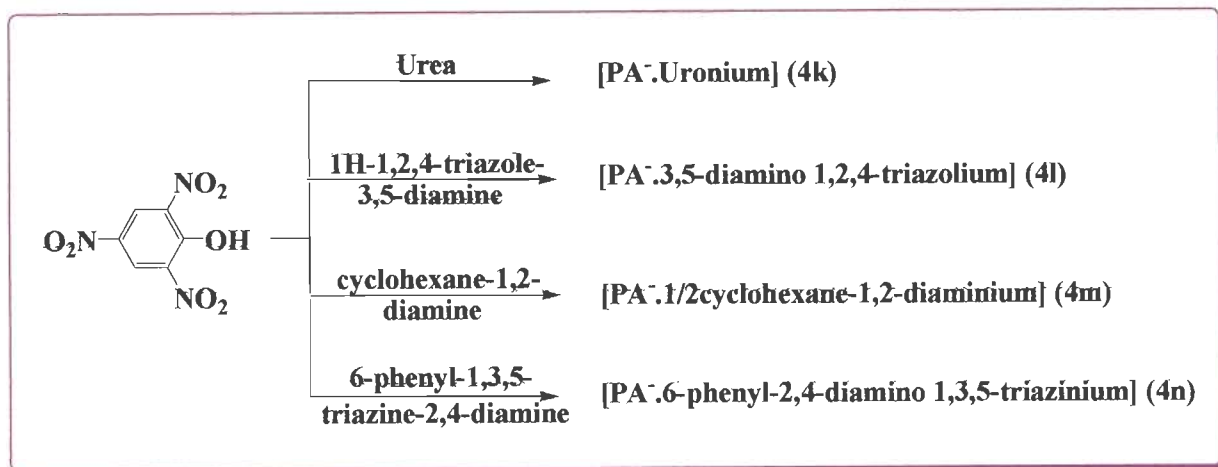
group of one hexamine forms C-H...N interaction with the nitrogen atom of the neighboring hmta, while on the other side the picric acid stack one above the other molecule through the O-H...O interactions (Fig. 4.26), resulting in an entirely different three dimensional packing as alternate channels of picric acid and hexamethylenetetramine which are hydrogen bonded to each other (Fig. 4.27).

Crystal structure of [3PA⁻.tptzH₃⁺³] (4j)

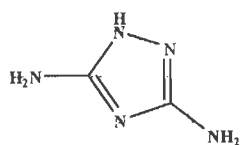
Salt **4j** in triclinic space group P-1 (Table 4.8) has one protonated 2,4,6-tris(2-pyridyl)-1,3,5-triazine cation and three picrate anions where only pyridyl nitrogen atoms (N10, N12, N15) are protonated through the proton transfer from the hydroxyl group of picric acid, resulting in the formation of ionic salt (cationic - anionic polar salt) (Fig. 4.28). As shown in Fig. 4.29, seven molecules of picrate anion are interlinked with each other through the weak non-covalent interactions O...O [O3...O10, 3.308 Å; O3...O15, 3.558 Å; O5...O9, 3.570 Å; O10...O20, 3.475 Å; O13...O17, 3.536 Å; O14...O16, 3.105 Å] and formed a pseudocavity which act as a host for tptz molecule. The guest molecule is resided in cavity with the support of N-H...O and C-H...O non-covalent intermolecular interactions. C-H and three protonated pyridyl N-H of tptz are involved in the C-H...O [C19-H19...O14, 2.484(5) Å; C19-H19...O17, 2.795(8) Å; C20-H20...O27, 2.633(5) Å; C21-H21...O18, 2.661(2) Å; C22-H22...O20, 2.839(8) Å; C28-H28...O15, 2.649(6) Å; C28-H28...O16, 2.534(6) Å; C29-H29...O15, 2.601(6) Å; C33-H33...O8, 1.955(4) Å] and N-H...O [N10-H10...O17, 2.637(24) Å; N12-H12...O8, 1.931(26) Å; N15-H15...O20, 2.243(29) Å; N15-H15...O21, 2.777(29) Å] interactions with the oxygen atom of picrate anions (Fig. 4.30). The presence of different types of non-covalent interactions between picrates and protonated 2,4,6-tris(2-pyridyl)-1,3,5-triazine in asymmetric unit gave cationic-anionic host-guest structure with entirely different packing view in comparison to others (Fig. 4.31).

The above structural studies show that on increasing the nitrogen atom, the non-covalent interactions increase step by step which are responsible to give the entirely different perspective view for **4g-4j**.

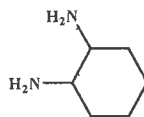
Co-crystallization of picric acid with amines viz., urea, 1H-1,2,4-triazole-3,5-diamine (guanazole), cyclohexane-1,2-diamine (1,2-DACH), 6-phenyl-1,3,5-triazine-2,4-diamine (benzoguanamine), resulted in the formation of various types of salts as [PA⁻.Uronium] (**4k**), [PA⁻.3,5-diamino-1,2,4-triazolium] (**4l**), [PA⁻.1/2cyclohexane-1,2-diaminium] (**4m**), [PA⁻.6-phenyl-2,4-diamino-1,3,5-triazinium] (**4n**), represented by the general scheme 4.3.



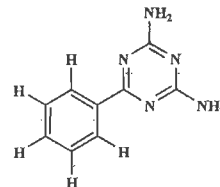
urea



1H-1,2,4-triazole-3,5-diamine



cyclohexane-1,2-diamine



6-phenyl-1,3,5-triazine-2,4-diamine

Scheme 4.3: General method of preparation of salts **4k-4n**

Crystal structure of [PA·Uronium] (4k)

The salt **4k** crystallizes in a monoclinic system having P21/c space group with $Z = 4$ (Table 4.9) as it contains one molecule of picrate and uronium in an asymmetric unit. The molecular structure is depicted in Fig. 4.32, where it shows the acidic hydrogen of the hydroxyl group on picric acid protonates the oxygen atom (O11) of urea and making the cation. The molecular packing analysis shows that the N-O (acceptor) and C-H (donor) of picrates are self dimerized with $R^2_2(10)$ motif involving C-H...O [C3-H3...O3, 2.587(7) Å; C5-H5...O5, 2.999(15) Å] interactions and also weak O...O [O5...O6, 2.889(8) Å; O3...O4, 3.198(16) Å] intermolecular interactions are present, which are responsible for one dimensional spiral molecular arrangement as shown in Fig. 4.33. The protonated oxygen (O11) of urea shows the strong hydrogen bonding with the phenolic oxygen atom (O1) of picrate via

O-H \cdots O [O11-H11 \cdots O1, 1.740(2) Å] interaction. Both organic moieties make three dimensional zig-zag arrangement along the 'c' axis through N-H \cdots O [N6-H6A \cdots O1, 2.135(6) Å; N6-H6A \cdots O2, 2.651(4) Å; N6-H6B \cdots O6, 2.701(2) Å; N6-H6B \cdots O7, 2.373(10) Å; N7-H7A \cdots O2, 2.246(8) Å; N7-H7A \cdots O3, 2.968(2) Å; N7-H7B \cdots O4, 2.625(5) Å; N7-H7B \cdots O6, 2.224(3) Å] and other C-H \cdots O, O-H \cdots O, O \cdots O non-covalent interactions (Fig. 4.34).

Crystal structure of [PA $^-$.3,5-diamino-1,2,4-triazolium] (4l)

Salt **4l** is in monoclinic space group C 2/c (Table 4.10) with one molecule of anionic deprotonated picric acid and one molecule of cationic protonated 1H-1,2,4-triazole-3,5-diamine in an asymmetric unit (Fig. 4.35). In this structure, two molecules of picrate anion are self dimerized with R 2_2 (10) motif involving C-H \cdots O [C7-H7 \cdots O6, 2.699(6) Å] interaction, and also a picrate anion is interconnected to the adjacent picrate via weak non-covalent interactions O \cdots O [O2 \cdots O4, 3.117(43) Å; O3 \cdots O4, 2.948(17) Å], create a cavity of size 1.3 Å, resulting the ribbon shaped one dimensional packing along 'ac' plane. Meanwhile, two molecules of protonated 1H-1,2,4-triazole-3,5-diamine are self dimerized with R 2_2 (8) motif involving N-H \cdots N [N4-H4 \cdots N3, 2.115(31) Å] interaction and also two triazole molecules are stacked one above other via N-H \cdots π [N4-H4A \cdots π , 3.347(47) Å; N4-H4B \cdots π , 3.302(34) Å; N5-H5B \cdots π , 3.304(6) Å] interactions, forming two dimensional layer along 'c' axis (Fig. 4.36). One molecule of cationic 1H-1,2,4-triazole-3,5-diamine attracts three molecules of picrate anions, and one N-H group of it shows the strong hydrogen bonding with the phenolic oxygen (O1) of picrate anion [N1-H1 \cdots O1, 1.932(27) Å]. Other non-covalent interactions N-H \cdots O, are in the range of 2.202(26) - 2.689(39) Å (Fig. 4.37). The resulting heteromeric synthon due to these hydrogen bonds connects the acid and base into an infinite three dimensional packing as alternate channels of picrate anions and 1H-1,2,4-triazole-3,5-diamine cations along the 'c' axis (Fig. 4.38). The mat-like supramolecular architecture along the 'a' axis for **4l** is shown in Fig. 4.39.

Crystal structure of [PA $^-$.1/2cyclohexane-1,2-diaminium] (4m)

According to Fig. 4.40, the asymmetric unit of salt **4m** contains one molecule of picrate and half molecule of 1/2cyclohexane-1,2-diaminium which crystallizes in monoclinic system with C 2/c space group (Table 4.11). In 1,2-diaminocyclohexane, both amino nitrogens (N4) are protonated by the hydroxyl group of both picric acid molecules. Picrate anions are self assembled to form a hydrogen bonded homomeric synthons through O \cdots O [O2 \cdots O6, 3.109(10) Å; O2 \cdots O7, 3.109(10) Å; O5 \cdots O7, 3.160(12) Å; O4 \cdots O6, 3.139(5) Å] and C8-H8 \cdots π [3.250(3)

Å] intermolecular interactions. The four picrates non-covalently interact via O...O, generate a cavity of size 1.54 Å (Fig. 4.41a), resulting the three dimensional spiral packing as shown in Fig. 4.41b. On the other side, 1/2cyclohexane-1,2-diaminium acts as a base and does not assembled with the same molecule but shows non-covalent interactions with four molecules of picrate anions through N-H...O [N4-H4A...O1, 2.092(18) Å; N4-H4A...O7, 2.385(6) Å; N4-H4B...O7, 2.293(16) Å, N4-H4C...O1, 1.928(8) Å; N4-H4C...O2, 2.428(30) Å]. The extended hydrogen bonding network is also formed which involves R²₂(8) graph-set association through C-H...O [C2-H2B...O6, 2.431(22) Å] intermolecular interactions (Fig. 4.42). The various non-covalent interactions present in the salt, help in the formation of pseudocavity through the self assembled interactions of acids and base where 1/2cyclohexane-1,2-diaminium act as a pseudoguest, present in the cavity (Fig. 4.43).

Crystal structure of [PA⁻.6-phenyl-2,4-diamino-1,3,5-triazinium] (4n)

The crystal structure of salt **4n** demonstrated that the asymmetric unit contain one molecule of picrate anion and one molecule of 6-phenyl-2,4-diamino-1,3,5 triazine cation, crystallizes in triclinic with space group P-1 (Table 4.12). The ionic species is formed by the transformation of the proton from the hydroxyl group of picric acid to the one nitrogen atom (N6) of 6-phenyl-2,4-diamino-1,3,5 triazine (Fig. 4.44). Crystal packing reveals that the four molecules of picrate anions are intermolecularly hydrogen bonded and make cavity of size 1.9 Å. Also two molecules of picrates are self dimerized with R²₂(10) motif through C-H...O [C5-H5A...O5, 2.722(15) Å] interactions, forms other cavity of size 1.1 Å (Fig. 4.45a). The non-covalent interactions among different picrate anions cause the formation of three dimensional zig-zag molecular arrangement along 'bc' plane as shown in Fig. 4.45b. The base 6-phenyl-2,4-diamino-1,3,5-triazinium also interconnected with other same molecule through C-H...N [C11-H11...N8, 2.572(15) Å] and N-H...N [N8-H8...N5, 2.248(13) Å] intermolecular interactions, resulted in the formation of spiral molecular structure along the 'a' axis (Fig. 4.45c). These molecules are also partially stacked one above the other via weak π...π [3.504(15) Å] interactions as shown in Fig. 4.45d. The protonated nitrogen (N6) of 6-phenyl-2,4-diamino-1,3,5-triazinium shows the strong hydrogen bonding with the phenolic oxygen (O1) of picrate i.e. N6-H6...O1 [1.920(57) Å]. Both organic moieties are held together by various non-covalent interactions viz., C-H...O [C12-H12...O4, 2.593(8) Å; C13-H13...O4, 2.728(11) Å; C14-H14...O5, 2.537(11) Å] and N-H...O [N7-H7A...O2, 2.389(15) Å and 3.003(14) Å; N7-H7A...O3, 2.377(9) Å; N7-H7B...O2, 2.227(12) Å] (Fig. 4.46). These non-

covalent interactions present between cation and anion resulted in the formation of entirely different three dimensional packing as alternate channels of picric acid and 6-phenyl-2,4-diamino-1,3,5 triazine (Fig. 4.47).

In case of these salts, the multidimensional hydrogen bonds between picrates and protonated amines control the crystal structures, and lead to the alternate stacking of cations and anions. This causes the formations of zig-zag structures.

Computational study

The optimized structural parameters of all individual nitrogen-rich heterocyclic compounds, acids and their salts were calculated at B3LYP/6-31G(d, p) basis sets and are summarized in Table 4.16. Each optimized geometries showed positive vibrational frequencies, showing that optimized structure was the global minimum on the potential energy surface. Single point energy calculations were performed, and zero point corrected total energies for various species were recorded. In addition to the characterization of these salts and co-crystals, the gas phase geometries, harmonic vibrational frequencies and binding energies of whole series are computed.

The hydrogen bond interaction energies were determined according to the following equation:

Energy calculations for salts

$$\Delta E = E_{\text{Salt}} - (E_x + E_{\text{Acid}})$$

Energy calculations for co-crystal

$$\Delta E = E_{\text{co-crystal}} - (E_x + E_{\text{Acid}})$$

Where E_{Salt} , $E_{\text{co-crystal}}$, E_x and E_{Acid} are the zero point corrected total energies of salt, co-crystal, nitrogen-rich heterocycles and acid, calculated at DFT(B3LYP)/6-31G(d,p) level of theory. We have removed the solvent and water molecules to check the relative stability.

The trend observed for the hydrogen bond interaction energy is given in Table 4.14. In case of salt **4c** and **4d**, the number of non-covalent interactions are same as both have almost same amount of hydrogen bond interaction energy. On the other hand in salt **4e** and **4f** the interaction energy are still greater than **4c** and **4d** as the numbers of non-covalent interactions are high but the factor of steric hindrance is also play an important role. The more steric hindered groups on the pyrazole ring reduce the hydrogen bond interaction energy. This is important to point out that the salt **4e** shows the more hydrogen bond interaction energy than salt **4f** due to the fact that the two pyrazole rings create the much more steric hindrance in salt **4f** as compared to salt **4e** which reduce the hydrogen bond interaction energy. In case of salts

4g-4j, the acid is same and heterocyclic organic moieties are different. DFT calculation shows that as the nitrogen atom increases stepwise, the hydrogen bond interaction energy increases in the same manner. There is a slight difference in hydrogen bond interaction energy in salt **4g** and **4h** as both salts have almost same non-covalent interactions but in case of co-crystal **4i**, the energy is almost twice as compared to salt **4g** as the nitrogen atom increases i.e. twice which shows the more intermolecular interactions and stabilize the co-crystal. The hydrogen bond interaction energy is highest in salt **4j** where the bulkiness increases due to the crystallization of more acid molecule as compared to others which show the more contribution in the strong and weak hydrogen bond interactions with the protonated 2,4,6-tris(2-pyridyl)-1,3,5-triazine. In case of salts **4k-4n**, the steric hindrance plays an important role to describe the order of hydrogen bond interaction energy. This is important to point out that the salt **4n** shows the least hydrogen bond interaction energy than others as the substituted phenyl group on the triazine ring produce the greater steric hindrance which reduces the hydrogen bond interaction energy. Along with this, the negligible difference in the energy of the optimized structure and the crystal structure of these salts and co-crystal (Table 4.15), as well as the bond lengths and angles of the salts and co-crystals (obtained from theoretical calculation and crystallographic data) as given in Table 4.16, suggests that the orientation and interaction remain almost the same both in gaseous and the solid phase (Fig. 4.48 – 4.50).

Thermal analysis

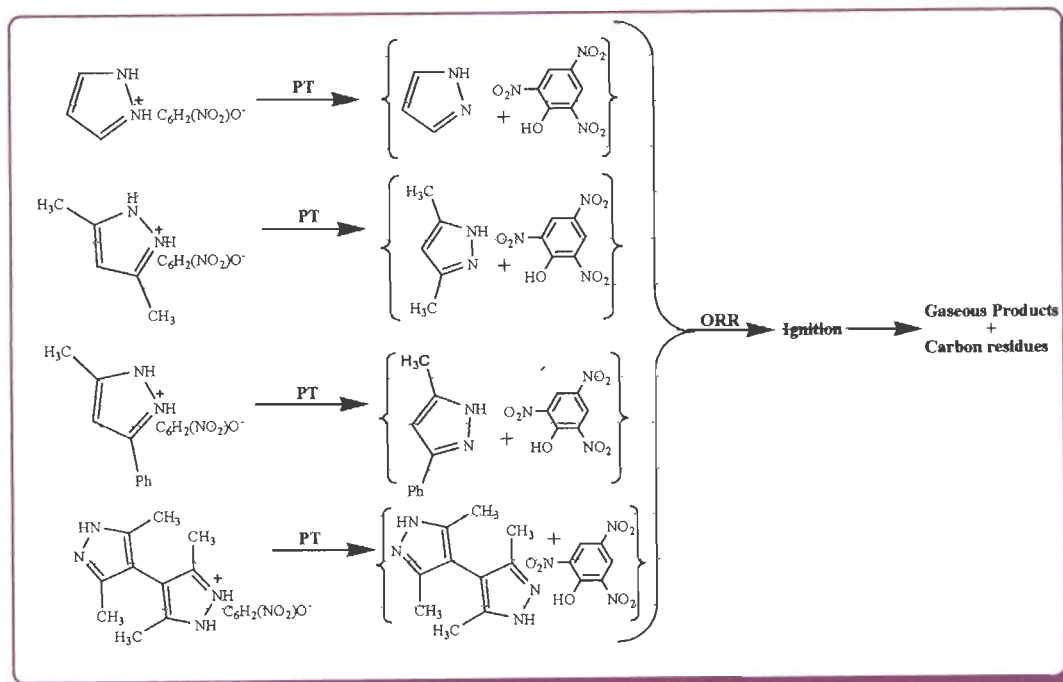
These salts are stable at room temperature and their thermal stability is demonstrated by a thermogravimetry (TG), derivative thermogravimetric (DTG) and differential thermal analysis (DTA). The thermoanalytical data for salts **4c-4n** are listed in Table 4.17 and the non-isothermal TGA-DTA curves of salts **4c-4n** are shown in Fig. 4.51-4.62. Salt **4c** shows two steps decomposition. In the first step (71-205 °C), one water molecule and protonated pyrazole leave out (~23.4% mass loss) which corresponds to endotherm at 159 °C in DTA thermogram, while in the second step (205-279 °C) one picrate ion (~ 72.8% mass loss) leaves out exothermically at 350 °C. Beyond this temperature, the explosion of resulting mass occurs with the formation of gaseous products. The TG-DTA thermogram for salt **4d** indicates that it also undergoes two stages decomposition. The first stage (~ 28.2% mass loss) corresponds to endotherm at 102 °C. In this step one molecule of 3,5-dimethyl pyrazolate (92-200 °C) leaves out. In the second stage (200-234 °C), picrate ion leaves (~ 68.5% mass loss), corresponds to exotherm at 278 °C. Three steps decomposition takes place in salt **4e**. In the first step methanol

molecule releases in the 101-225 °C temperature range (~ 7.1% mass loss) which corresponds to endotherm at 162 °C, while in next second and third steps, both 3-phenyl-5-methyl pyrazolate and picrate ions release in 225-295 °C (~ 52.8% mass loss) and 505-666 °C (~ 35.9% mass loss) temperature range, respectively. The DTA peak at 281 °C and 589 °C is exothermic for both steps, respectively. TG curve of salt **4f** exhibited three well-separated weight loss stages. In first step, acetonitrile molecule releases in 99-171 °C temperature ranges (~ 4.6% mass loss). In second step (240-289 °C), protonated H₂dmpz leaves out (~ 49.7% mass loss) exothermically at 293 °C, while picrate ion (~ 45.1% mass loss) also releases (289-689 °C) exothermically at 686 °C in third step. The non-isothermal TG thermogram clearly indicates that thermal decomposition of salt **4g** occurs in three steps. This salt on heating first loses 7.0% of its mass at around 200 °C due to the loss of methanol molecule, shows an endothermic peak at 206 °C. Beyond this temperature, a plateau corresponds to 49.1% mass loss is observed due to the removal of picrate (250-337 °C) exothermally at 319 °C. Almost complete decomposition 41.8% occurs at around 600 °C, which corresponds to the release of protonated 1,10-phenanthroline. The exothermic peak for the same appeared at 537 °C. The TG curve of salt **4h** indicates that it decomposes immediately after melting and the decomposition continues up to 314 °C with about 62.1% weight loss corresponds to release of two molecules of picrate anion. The second weight loss (34.2%) occurs in the region 420 °C to 620 °C, due to the removal of protonated 2,2';6',2''-terpyridine. The sharp exothermic peaks for both steps are occurred at 301 °C and 531 °C, respectively. The thermal decomposition process of co-crystal **4i** can be divided into two stages. The first weight loss of 60.3% between the temperature range 178-342 °C responsible for the release of picric acid, leading to appearance of first exothermic peak at 270 °C in DTA curve, while the second weight loss 36.4% was observed in between 512-711 °C, may be due to the release of hexamethylenetetramine organic moiety. This process can also be observed as exothermic in DTA at 585 °C. On the other hand in salt **4j**, weight loss occurs in a single step. The DTA reveals exactly the same changes as shown by the TGA. In the DTA curve, there is a sharp exothermic peak at 301 °C which supports the crystalline nature of **4j** [40]. The TG curve indicates that **4j** decomposes continuously between the temperature range 175-306 °C with ~ 94.5% weight loss. The salt **4k** indicates two major steps of weight loss. The first weight loss of 76.2% between 136 and 264 °C, corresponding to the release of picrate anion with a sharp exothermic peak at 188 °C in DTA, while the second weight loss of 20.4% occurs between 264 and 412 °C, responsible for

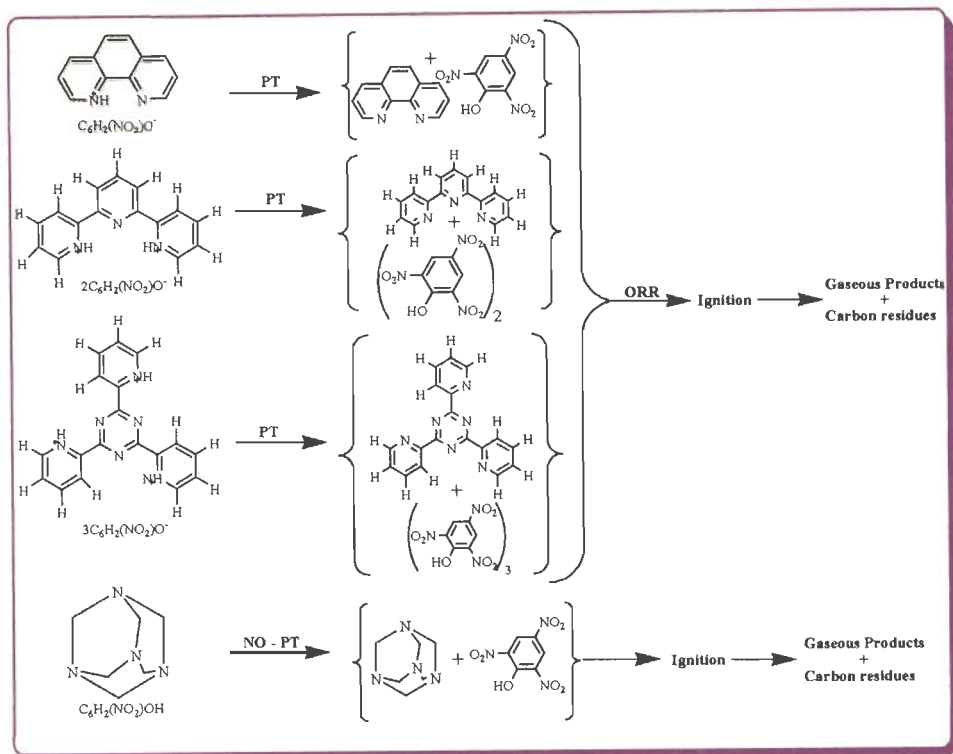
the removal of uronium cation. For this mass loss, an exothermic peak at 312 °C in DTA is obtained. According to TG curve, salt **4l** is stable up to 200 °C. The decomposition starts at 225 °C and continues up to 330 °C with 68.1% mass loss due to the release of picrate anion, whereas 1H-1,2,4-triazole-3,5-diamine cation releases completely at 689 °C. The exothermic peaks are perceived at 264 and 677 °C in DTA for both steps, respectively. The salt **4m** and **4n** also follow the same way of decomposition as others (Table 4.17). The exotherms are due to oxidation-reduction reactions leading to ignition in all cases.

The kinetics of thermal decomposition of salts **4c-4n** were evaluated using fourteen mechanism based kinetic models as given in Table 4.18. The set of reaction models [41-44] were used to analyse the isothermal TG data (in the range 200-240 °C for **4c-4f** (Fig. 4.63), 290-330 °C for **4g-4j** (Fig. 4.66) and 230-270 °C for **4k-4n** (Fig. 4.69), to calculate the E_a values for thermal decomposition which were done in the range of decomposition/vaporization using indigenously fabricated TG apparatus. The activation energy values are reported in Table 4.19-4.21. In the model fitting method, the kinetics is analysed by choosing a “best fit” model based on the value of the correlation coefficient r close to 1. Among various values of r calculated from different models, the highest value of r for salts **4c**, **4e**, **4g-4j**, **4k**, **4m** corresponds to model 14, for **4d** and **4f** corresponds to model 4, for **4l** corresponds to model 11 and for salts **4n** corresponds to model 1. An average value 55.5, 64.3, 67.0, 55.0, 78.7, 42.3, 37.2, 39.0, 20.4, 48.3, 109.8 and 48.6 kJ mol⁻¹ have been obtained as activation energy for isothermal decomposition of **4c-4n** salts. The isoconversional method is known to permit estimation of activation energy independent of the model used. Realistic kinetics parameters can only be extracted in a way that is independent of the reaction model. In our case, we have adopted the isoconversional method reported by Vyazovkin [45, 46]. This approach indicates that the decomposition of these salts is not simple as indicated by model fitting method. According to Fig. 4.64, 4.67, 4.70, for a particular salt each activation energy has a separate value at different α . Although these salts are stable at room temperature but ignite when subjected to sudden high temperature. Further to evaluate the sensitivity of these salts, their ignition delay measurement were carried out in temperature ranges 340-380 °C for salts **4c-4f** and 380-420 °C for **4g-4n** (Table 4.22-4.23). For salts **4c-4n**, E_a^* was determined from the slope of a plot of $\ln(D_i)$ vs. $1/T$ as shown in Fig. 4.65, 4.68, 4.71. The energy of activation for ignition is 28.6, 29.3, 46.4 and 37.7 kJ mol⁻¹ for salts **4c-4f**, respectively. From the ignition delay measurements, it is clear that the salt **4e** is highly thermal stable than **4c**, **4d** and **4f** as it

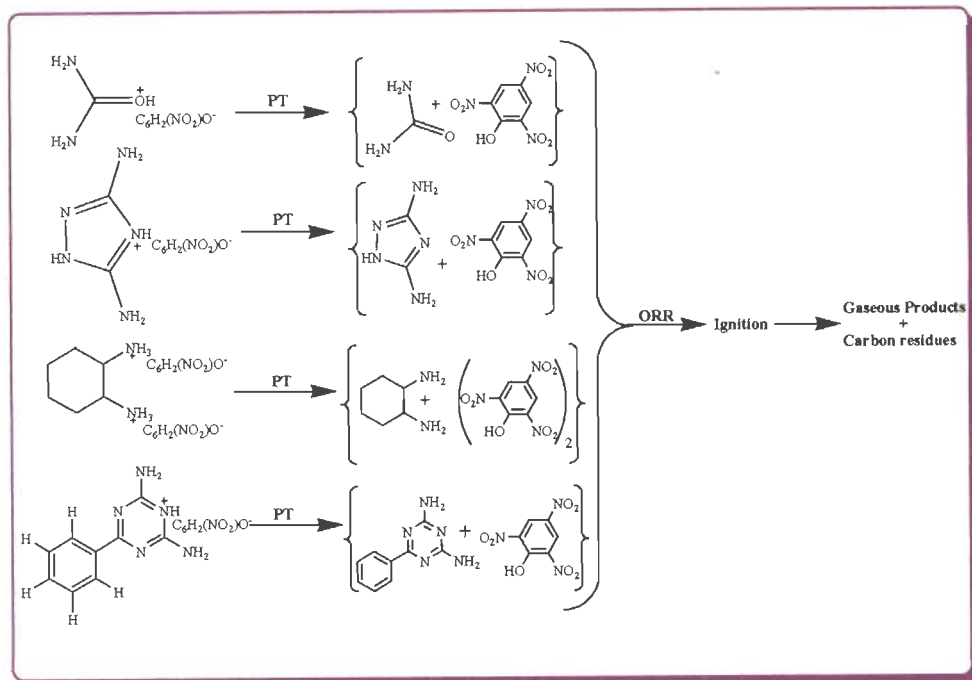
has the highest activation energy of ignition delay. The energy of activation for ignition is 79.6, 89.2, 99.9 and 108.3 kJ mol⁻¹ for salts **4g-4j**, respectively, and the energy of ignition delay for **4j** is highest as compared to **4g-4i** salts, may be due to stabilization of molecule by highest number of non-covalent interactions and highest hydrogen bond interaction energy. The energy of activation for ignition is 92.8, 69.4, 47.3 and 43.4 kJ mol⁻¹ for salts **4k-4n**, respectively and salt **4n** is less stable as compared to **4k-4m**. The activation energy (calculated by isothermal TG) and ignition delay measurement has different values which may be due to the different temperature ranges. The oxygen balance values reported in Table 4.22-4.23, suggest that these salts belong to low explosers. The thermal decomposition process of energetic materials often involves a concert of bond breaking and bond forming steps under condensed or gas phase reaction. The weakening of a particular bond seems to enhance the tendency to have a predominant, identified path to decomposition. The overall process of decomposition takes place at higher temperature by transfer of proton (N-H bond cleavage) from secondary organic nitrogen-rich heterocyclic moieties to picrates, and form the corresponding O...H bond in the condensed phase prior to ignition to form finally gaseous products leaving a black carbon residues [47] (Scheme 4.4-4.6).



Scheme 4.4: Proton transfer mechanism leading to ignition in salts **4c-4f**



Scheme 4.5: Proton transfer mechanism leading to ignition in salts **4g-4j**



Scheme 4.6: Proton transfer mechanism leading to ignition in salts **4k-4n**

PT = Proton Transfer, ORR = Oxidation-Reduction Reaction

CONCLUSION

Hydrogen bonding is important for generation of robust and supramolecular heterosynthons to give entirely different three dimensional packing views. Accordingly, we have successfully synthesized supramolecular networks containing common picric acid and heterocyclic organic moieties.

In salt **4c-4f**, the host molecules self assembled due to various types of non-covalent interactions and form different shaped cavity. On the other hand the solvent molecules as water, methanol and acetonitrile behave as the guest molecule and occupied the cavity in salt **4c**, **4e-4f**. The variation of substituent groups on pyrazole ring plays an important role in controlling the structure of the co-crystals.

In case of salts **4g-4j**, the non-covalent interactions increase on increasing the number of nitrogen atoms in secondary organic moieties. The presence of a maximum number of non-covalent interactions in salt **4j** may be responsible for the creation of a pseudocavity for trapping the 2,4,6-tris(2-pyridyl)-1,3,5-triazine as a guest molecule.

In salt **4k** and **4l**, one dimensional ribbon shaped chains while in **4m** and **4n**, two dimensional networks are formed by the hydrogen bonds between the picrate molecules. As the size (steric hindrance) of diamines increases, the drastic change was observed in the cavity size. The diversity of supramolecular structures in present chapter may be due to the difference in the structures of secondary organic moieties.

Theoretical studies suggested that structures are same in both solid and gaseous phase, and hydrogen bond interaction energy largely depends on the functional moieties, involved in the interaction. The ignition delay measurements suggest that the steric strain effects cause weakening of N-H bond, favouring proton transfer and the enhancement of the rate of decomposition in **4c-4f** and **4k-4n** salts.

Table 4.1: Crystal data and structure refinement for [2PA⁻.2PzH₂⁺.OH₂] (4c)

Empirical formula	C ₁₈ H ₁₆ N ₁₀ O ₁₅
Color	Yellow
Formula weight (g mol ⁻¹)	612.41
Crystal System	Triclinic
Space Group	P-1
a (Å)	7.679(2)
b (Å)	11.827(2)
c (Å)	13.529(3)
α (°)	98.54(10)
β (°)	101.78(10)
γ (°)	91.84(10)
V (Å ³)	1187.04(5)
Crystal size (mm)	0.27 x 0.19 x 0.13
Z	2
ρ _{calcd} (g m ⁻³)	1.713
μ	0.152
F (000)	628
θ range for data collection	1.56-30.93
limiting indices	-10 ≤ h ≤ 11 -17 ≤ k ≤ 19 -19 ≤ l ≤ 19
No. of measured reflections	7439
No. of observed reflections	6133
Data/ restraints/parameters	7439/0/412
R1 ^b (I > 2σ(I))	0.038
R1 (all data)	0.049
wR2 ^c (I > 2σ(I))	0.109
wR2(all data)	0.129

Table 4.2: Crystal data and structure refinement for [PA⁻.Pz^{Me2}H₂⁺] (4d)

Empirical formula	C ₁₁ H ₁₁ N ₅ O ₇
Color	Yellow
Formula weight (g mol ⁻¹)	325.25
Crystal System	Triclinic
Space Group	P-1
a (Å)	7.802(3)
b (Å)	8.245(3)
c (Å)	10.945(4)
α (°)	101.13(2)
β (°)	92.80(3)
γ (°)	90.56(2)
V (Å ³)	689.89(4)
Crystal size (mm)	0.27 x 0.21 x 0.17
Z	2
ρ _{calcd} (g m ⁻³)	1.566
μ	0.133
F (000)	336
θ range for data collection	2.52-31.85
limiting indices	-11 ≤ h ≤ 11 -11 ≤ k ≤ 12 -16 ≤ l ≤ 16
No. of measured reflections	4679
No. of observed reflections	3140
Data/ restraints/parameters	4679/0/214
R1 (I > 2σ(I))	0.049
R1 (all data)	0.072
wR2 (I > 2σ(I))	0.123
wR2 (all data)	0.150

Table 4.3: Crystal data and structure refinement for [PA⁻.Pz^{Ph,Me}H₂⁺.CH₃OH] (4e)

Empirical formula	C ₁₇ H ₁₇ N ₅ O ₈
Color	Yellow
Formula weight (g mol ⁻¹)	419.36
Crystal System	Monoclinic
Space Group	P 21/c
a (Å)	14.730(10)
b (Å)	7.089(5)
c (Å)	17.543(12)
α (°)	90.00
β (°)	93.95(3)
γ (°)	90.00
V (Å ³)	1827.7(2)
Crystal size (mm)	0.34 x 0.29 x 0.23
Z	4
ρ _{calcd} (g m ⁻³)	1827.7(2)
μ	1827.7(2)
F (000)	1827.7(2)
θ range for data collection	1.39-28.26
limiting indices	-19 ≤ h ≤ 19 -9 ≤ k ≤ 9 -18 ≤ l ≤ 23
No. of measured reflections	4457
No. of observed reflections	3194
Data/ restraints/parameters	4457/0/282
R1 (I > 2σ(I))	0.040
R1 (all data)	0.070
wR2 (I > 2σ(I))	0.116
wR2 (all data)	0.147

Table 4.4: Crystal data and structure refinement for [2PA⁻.2H₂dmpzH⁺.CH₃CN] (4f)

Empirical formula	C ₃₄ H ₃₇ N ₁₅ O ₁₄
Color	Yellow
Formula weight (g mol ⁻¹)	879.79
Crystal System	Monoclinic
Space Group	P 21/c
a (Å)	16.076(2)
b (Å)	21.176(3)
c (Å)	11.591(15)
α (°)	90.00
β (°)	94.07(7)
γ (°)	90.00
V (Å ³)	3935.9(9)
Crystal size (mm)	0.23 x 0.19 x 0.13
Z	4
ρ _{calcd} (g m ⁻³)	1.485
μ	0.118
F (000)	1832
θ range for data collection	1.27-28.40
limiting indices	-21 ≤ h ≤ 21 -27 ≤ k ≤ 28 -15 ≤ l ≤ 15
No. of measured reflections	9793
No. of observed reflections	7226
Data/ restraints/parameters	9793/0/601
R1 (I>2σ(I))	0.056
R1 (all data)	0.080
wR2 (I>2σ(I))	0.184
wR2 (all data)	0.202

Table 4.5: Crystal data and structure refinement for [PA⁻.phenH⁺.CH₃OH] (4g)

Empirical formula	C ₁₉ H ₁₅ N ₅ O ₈
Color	Yellow
Formula weight (g mol ⁻¹)	441.36
Crystal System	Triclinic
Space Group	P-1
a (Å)	9.874(3)
b (Å)	10.102(2)
c (Å)	10.903(3)
α (°)	67.23(13)
β (°)	71.29(13)
γ (°)	82.67(14)
V (Å ³)	949.8(4)
Crystal size (mm)	0.24 x 0.19 x 0.11
Z	2
ρ _{calcd} (g m ⁻³)	1.543
μ	0.123
F (000)	456
θ range for data collection	2.19-30.89
limiting indices	-14 ≤ h ≤ 14
	-14 ≤ k ≤ 13
	-15 ≤ l ≤ 12
No. of measured reflections	5856
No. of observed reflections	3119
Data/ restraints/parameters	5856/0/295
R1 (I>2σ(I))	0.049
R1 (all data)	0.105
wR2 (I>2σ(I))	0.130
wR2 (all data)	0.169

Table 4.6: Crystal data and structure refinement for [2PA⁻.terpyH₂⁺²] (4h)

Empirical formula	C ₂₇ H ₁₇ N ₉ O ₁₄
Color	Yellow
Formula weight (g mol ⁻¹)	691.50
Crystal System	Monoclinic
Space Group	P 21/c
a (Å)	16.835(12)
b (Å)	22.038(16)
c (Å)	7.628(5)
α (°)	90.00
β (°)	95.85(3)
γ (°)	90.00
V (Å ³)	2815.7(3)
Crystal size (mm)	0.31 x 0.26 x 0.22
Z	4
ρ _{calcd} (g m ⁻³)	1.631
μ	0.135
F (000)	1416
θ range for data collection	3.03-25.00
limiting indices	-20 ≤ h ≤ 20 -26 ≤ k ≤ 26 -9 ≤ l ≤ 8
No. of measured reflections	4950
No. of observed reflections	3533
Data/ restraints/parameters	4639/0/459
R1 (I > 2σ(I))	0.081
R1 (all data)	0.102
wR2 (I > 2σ(I))	0.216
wR2 (all data)	0.242

Table 4.7: Crystal data and structure refinement for [PA.hmta] (4i)

Empirical formula	C ₁₂ H ₁₅ N ₇ O ₇
Color	Yellow
Formula weight (g mol ⁻¹)	369.31
Crystal System	Monoclinic
Space Group	P2(1)/c
a (Å)	12.486(5)
b (Å)	6.579(2)
c (Å)	18.530(7)
α (°)	90.00
β (°)	107.04(2)
γ (°)	90.00
V (Å ³)	1455.44(9)
Crystal size (mm)	0.24 x 0.19 x 0.14
Z	4
ρ _{calcd} (g m ⁻³)	1.685
μ	0.141
F (000)	768
θ range for data collection	1.71-28.91
limiting indices	-16 ≤ h ≤ 16 -8 ≤ k ≤ 8 -25 ≤ l ≤ 23
No. of measured reflections	3778
No. of observed reflections	2973
Data/ restraints/parameters	3778/0/235
R1 (I > 2σ(I))	0.044
R1 (all data)	0.061
wR2 (I > 2σ(I))	0.146
wR2 (all data)	0.169

Table 4.8: Crystal data and structure refinement for [3PA⁻.tptzH₃⁺³] (4j)

Empirical formula	C ₃₆ H ₂₁ N ₁₅ O ₂₁
Color	Yellow
Formula weight (g mol ⁻¹)	999.68
Crystal System	Triclinic
Space Group	P-1
a (Å)	12.000(12)
b (Å)	12.449(12)
c (Å)	14.396(14)
α (°)	70.36(5)
β (°)	87.59(5)
γ (°)	73.85(5)
V (Å ³)	1942.7(3)
Crystal size (mm)	0.31 x 0.27 x 0.21
Z	2
ρ _{calcd} (g m ⁻³)	1.709
μ	0.145
F (000)	1020
θ range for data collection	1.50-28.57
limiting indices	-16 ≤ h ≤ 16 -16 ≤ k ≤ 16 -19 ≤ l ≤ 19
No. of measured reflections	9852
No. of observed reflections	7789
Data/ restraints/parameters	9852/0/661
R1 (I>2σ(I))	0.049
R1 (all data)	0.066
wR2 (I>2σ(I))	0.143
wR2 (all data)	0.171

Table 4.9: Crystal data and structure refinement for [PA⁻.Uronium] (4k)

Empirical formula	C ₇ H ₇ N ₅ O ₈
Color	Yellow
Formula weight (g mol ⁻¹)	289.18
Crystal System	Monoclinic
Space Group	P 21/c
a (Å)	3.886(11)
b (Å)	25.824(8)
c (Å)	11.167(3)
α (°)	90.00
β (°)	93.71(11)
γ (°)	90.00
V (Å ³)	1118.4(6)
Crystal size (mm)	0.32X0.26X0.21
Z	4
ρ _{calcd} (g m ⁻³)	1.717
μ	0.158
F (000)	592
θ range for data collection	1.58-28.29
limiting indices	-5 ≤ h ≤ 4 -34 ≤ k ≤ 34 -13 ≤ l ≤ 14
No. of measured reflections	2754
No. of observed reflections	1934
Data/ restraints/parameters	2754/0/182
R1 (I>2σ(I))	0.046
R1 (all data)	0.073
wR2 (I>2σ(I))	0.146
wR2 (all data)	0.181

Table 4.10: Crystal data and structure refinement for [PA⁻.3,5-diamino-1,2,4-triazolium] (4I)

Empirical formula	C ₈ H ₈ N ₈ O ₇
Color	Yellow
Formula weight (g mol ⁻¹)	328.22
Crystal System	Monoclinic
Space Group	C 2/c
a (Å)	22.834(14)
b (Å)	4.808(3)
c (Å)	22.557(14)
α (°)	90.00
β (°)	94.17
γ (°)	90.00
V (Å ³)	2470(3)
Crystal size (mm)	0.24X0.21X0.17
Z	8
ρ _{calcd} (g m ⁻³)	1.765
μ	0.156
F (000)	1344
θ range for data collection	1.79-29.56
limiting indices	-30 ≤ h ≤ 30 -6 ≤ k ≤ 6 -29 ≤ l ≤ 30
No. of measured reflections	3353
No. of observed reflections	2137
Data/ restraints/parameters	3353/0/224
R1 (I>2σ(I))	0.044
R1 (all data)	0.076
wR2 (I>2σ(I))	0.125
wR2 (all data)	0.154

Table 4.11: Crystal data and structure refinement for [PA⁻.1/2cyclohexane-1,2-diamin-ium] (4m)

Empirical formula	C ₁₈ H ₂₀ N ₈ O ₁₄
Color	Yellow
Formula weight (g mol ⁻¹)	572.42
Crystal System	Monoclinic
Space Group	C 2/c
a (Å)	22.105(8)
b (Å)	8.165(3)
c (Å)	14.524(5)
α (°)	90.00
β (°)	117.74(16)
γ (°)	90.00
V (Å ³)	2319.8(14)
Crystal size (mm)	0.31X0.27X0.21
Z	4
ρ _{calcd} (g m ⁻³)	1.639
μ	0.143
F (000)	1184
θ range for data collection	2.87-28.43
limiting indices	-29 ≤ h ≤ 29 -10 ≤ k ≤ 10 -19 ≤ l ≤ 19
No. of measured reflections	2749
No. of observed reflections	1700
Data/ restraints/parameters	2749/0/182
R1 (I>2σ(I))	0.086
R1 (all data)	0.132
wR2 (I>2σ(I))	0.273
wR2 (all data)	0.296

Table 4.12: Crystal data and structure refinement for [PA⁻.6-phenyl-2,4-diamino-1,3,5-triazinium] (4n)

Empirical formula	C ₁₅ H ₁₂ N ₈ O ₇
Color	Yellow
Formula weight (g mol ⁻¹)	416.33
Crystal System	Triclinic
Space Group	P -1
a (Å)	7.604(16)
b (Å)	7.940(19)
c (Å)	14.596(4)
α (°)	88.56(9)
β (°)	81.72(9)
γ (°)	77.43(9)
V (Å ³)	851.3(3)
Crystal size (mm)	0.29X0.19X0.13
Z	2
ρ _{calcd} (g m ⁻³)	1.624
μ	0.133
F (000)	428
θ range for data collection	1.41-27.21
limiting indices	-9 ≤ h ≤ 9 -10 ≤ k ≤ 10 -18 ≤ l ≤ 18
No. of measured reflections	3678
No. of observed reflections	1609
Data/ restraints/parameters	3678/0/275
R1 (I>2σ(I))	0.090
R1 (all data)	0.150
wR2 (I>2σ(I))	0.168
wR2 (all data)	0.288

Table 4.13: Non-covalent interactions for 4c-4n (Å and °)

S. N	D-H...A	d(D-H)	d(H-A)	d(D-A)	<(DHA)>
1.	[2PA⁻.2PzH₂⁺.OH₂] (4c)				
	O15-H16A...O1	0.847(22)	2.037(23)	2.804(2)	150.23(228)
	O15-H16A...O7	0.847(22)	2.317(24)	2.904(2)	126.77(201)
	O15-H15A...O8	0.831(25)	1.969(24)	2.721(2)	150.29(215)
	O15-H15A...O14	0.831(25)	2.259(22)	2.837(2)	126.94(198)
	N7-H7A...O1	0.877(22)	1.852(23)	2.693(2)	160.07(210)
	N8-H8A...O15	0.920(24)	1.783(24)	2.679(2)	163.91(219)
	N9-H9B...O15	0.869(19)	1.921(19)	2.724(2)	152.96(197)
	N10-H10A...O8	0.851(22)	1.930(21)	2.764(2)	166.39(220)
2.	[PA⁻.Pz^{Me2}H₂⁺] (4d)				
	N4-H4A...O1	0.954(21)	1.678(21)	2.596(4)	166.44(218)
	N4-H4A...O7	0.954(21)	2.298(24)	2.834(4)	114.87(162)
	N5-H5...O7	0.860(2)	2.362(4)	2.837(5)	115.19(9)
	C2-H2...O6	0.930(1)	2.603(2)	3.418(2)	146.62(8)
	C7-H7A...O1	0.960(2)	2.606(3)	3.374(5)	137.17(12)
	C9-H9...O4	0.930(2)	2.639(4)	3.516(6)	157.53(9)
	C11-H11B...O5	0.959(2)	2.478(4)	3.420(5)	167.26(12)
3.	[PA⁻.Pz^{Ph,Me}H₂⁺.CH₃OH] (4e)				
	N1-H1...O1	0.912(23)	1.782(23)	2.647(4)	157.43(206)
	N1-H1...O2	0.912(23)	2.315(21)	2.888(4)	120.65(176)
	N2-H2A...O8	1.014(22)	1.664(22)	2.660(3)	166.12(197)
	O8-H8A...O1	0.820(1)	2.151(3)	2.846(4)	142.64(9)
	O8-H8A...O6	0.820(1)	2.225(3)	2.900(3)	139.92(10)
	C1-H1C...O2	0.960(2)	2.355(2)	3.170(3)	142.32(13)
	C6-H6...O7	0.931(2)	3.149(2)	3.600(4)	111.83(12)
	C6-H6...O8	0.929(2)	2.859(2)	3.728(4)	156.29(12)
	C7-H7...O7	0.930(2)	2.592(3)	3.323(4)	135.81(13)
	C17-H17B...O5	0.960(3)	2.687(3)	3.577(5)	154.55(14)
	C17-H17C...O6	0.960(2)	3.020(2)	3.730(3)	131.81(14)
	C17-H17C...O7	0.960(2)	2.636(2)	3.593(3)	174.87(14)
4.	[2PA⁻.2H₂dmpzH⁺.CH₃CN] (4f)				
	N13-H13A...O14	0.947(23)	2.792(25)	2.989(9)	143.64(22)
	N14-H1AA...O8	0.901(25)	1.800(25)	2.679(8)	164.75(227)
	N14-H1AA...O14	0.901(25)	2.284(25)	2.776(11)	114.67(34)
	C2-H2...N15	0.930(2)	2.433(9)	3.193(11)	138.85(16)

	C19-H9B...O11	0.960(2)	2.575(2)	3.471(3)	155.35(14)
	C21-H21C...N15	0.960(3)	2.413(3)	3.240(4)	144.19(19)
	C22-H22A...O11	0.960(2)	2.605(5)	3.491(5)	153.47(14)
	C30-H30A...O2	0.960(3)	2.685(7)	3.349(11)	126.77(14)
	C30-H30C...O5	0.960(4)	2.761(9)	3.592(13)	145.26(15)
	C32-H32A...O8	0.960(4)	2.914(2)	3.649(6)	134.26(14)
	C33-H33B...O14	0.959(4)	2.600(3)	3.331(6)	133.18(22)
5.	[PA⁻.phenH⁺.CH₃OH] (4g)				
	O8-H8...O1	0.820	2.002(3)	2.2.767	155.1
	O8-H8...O4	0.820	2.419(19)	2.993	127.8
	N1-H1B...O8	0.896	1.831 (29)	2.682	157.7
	C7-H7A...O1	0.930	2.338(18)	3.218	157.7
	C7-H7A...O2	0.930	2.404(9)	3.114	133.0
	C9-H9...O3	0.930	3.016(19)	3.757	137.7
	C11-H11...O3	0.930	2.628(9)	3.457	148.8
	C12-H12...O6	0.930	2.840(21)	3.741	163.5
	C14-H14...O7	0.930	2.41(2)	3.300	160.3
	C15-H15...O8	0.930	2.839(5)	3.340	115.0
	C16-H16...O8	0.929	2.807(4)	3.338	117.4
	C19-H19C...O3	0.930	2.746(7)	3.620	151.5
6.	[2PA⁻.terpyH₂⁺²] (4h)				
	N1-H1A...O8	0.964	2.031(110)	2.718	126.6
	N3-H3A...O8	0.997	1.727(49)	2.694	162.4
	C4-H4...O12	0.929	2.697(3)	3.595	162.7
	C7-H7...O11	0.931	2.714(3)	3.450	136.6
	C7-H7...O12	0.931	2.619(3)	3.524	164.3
	C8-H8...O5	0.930	2.949(8)	3.618	130.1
	C9-H9...O1	0.930	2.287(5)	3.178	160.2
	C12-H12...O1	0.930	2.380(4)	3.305	172.9
	C13-H13...O2	0.930	2.489(8)	3.098	123.2
	C13-H13...O11	0.930	2.600(3)	3.361	139.3
	C14-H14...O5	0.929	2.121(7)	3.707	143.2
	C15-H15...O4	0.930	2.328(7)	3.147	146.7
7.	[PA.hmta] (4i)				
	O1-H1...O3	0.820	3.228(2)	3.697	119.0
	O1-H1...N6	0.820	2.119(1)	2.663	123.7
	C7-H7A...O4	0.970	2.607(2)	3.206	120.1
	C7-H7A...O6	0.970	3.255(4)	3.612	103.8
	C7-H7B...O6	0.970	3.042(4)	3.612	118.9
	C8-H8A...O3	0.970	2.972(2)	3.773	140.6
	C8-H8A...O4	0.970	3.159(2)	3.925	137.0
	C9-H9B...O7	0.970	2.627(1)	3.450	142.8
	C10-H10A...O4	0.969	2.707(1)	3.326	122.1

	C10-H10A...O5	0.969	3.017(2)	3.511	113.0
	C10-H10A...O6	0.969	2.599(1)	3.525	159.7
	C11-H11A...O7	0.970	2.676(2)	3.177	112.5
	C7-H7A...N7	0.970	2.800(2)	3.662	148.4
	C8-H8A...N5	0.970	2.858(1)	3.394	115.7
	C9-H9B...N2	0.970	2.924(2)	3.856	161.3
	C10-H10A...N3	0.969	2.977(2)	3.670	129.4
	C10-H10B...N7	0.971	2.801(3)	3.662	148.2
	C12-H12B...N7	0.969	2.908(3)	3.379	111.0
8.	[3PA⁻.tptzH₃³⁺] (4j)				
	N10-H10...O17	0.831	2.637(24)	3.084	115.1
	N12-H12A...O8	0.867	1.931(26)	2.791	170.3
	N15-H15...O20	1.102	2.243(29)	3.262	152.7
	N15-H15...O21	1.102	2.777(29)	3.590	130.3
	C19-H19...O14	0.931	2.484(5)	3.327	150.6
	C19-H19...O17	0.931	2.795(8)	3.197	107.2
	C20-H20...O17	0.930	2.633(5)	3.175	117.8
	C21-H21...O18	0.930	2.661(2)	3.540	157.9
	C22-H22...O20	0.930	2.839(8)	3.608	140.7
	C28-H28...O15	0.930	2.649(6)	3.238	121.8
	C28-H28...O16	0.930	2.534(6)	3.454	169.5
	C29-H29...O15	0.930	2.601(6)	3.217	124.1
	C33-H33...O8	0.929	1.955(4)	2.872	168.4
9.	[PA⁻.Uronium] (4k)				
	O11-H11...O1	0.821	1.740(2)	2.547	167.0
	O11-H11...O7	0.821	2.340(9)	2.762	112.6
	N6-H6A...O1	0.861	2.135(6)	2.817	135.7
	N6-H6A...O2	0.861	2.651(4)	3.453	155.4
	N6-H6B...O6	0.860	2.701(2)	3.384	137.2
	N6-H6B...O7	0.860	2.373(10)	3.218	167.5
	N7-H7A...O2	0.860	2.246(8)	3.076	161.9
	N7-H7A...O3	0.860	2.968(2)	3.753	152.7
	N7-H7B...O4	0.860	2.625(5)	3.106	116.5
	N7-H7B...O6	0.860	2.224(3)	3.024	154.5
	C3-H3...O3	0.930	2.587(7)	3.478	160.6
	C5-H5...O5	0.930	2.999(15)	3.884	159.4
10.	[PA⁻.3,5-diamino-1,2,4-triazolium] (4l)				
	N1-H1...O1	0.877	1.932(27)	2.674	141.4
	N2-H2...O4	0.894	2.357(29)	3.229	165.0
	N4-H4A...O5	0.867	2.689(35)	3.037	105.4
	N4-H4B...O5	0.867	2.688(49)	3.034	105.5
	N5-H5A...O3	0.861	2.203(26)	3.034	161.0
	N5-H5B...O1	0.860	2.234(28)	2.914	136.0

	N4-H4B...N3	0.867	2.115(31)	2.967	167.5
	C7-H7...O6	0.929	2.699(6)	3.042	102.7
11.	[PA⁻.1/2cyclohexane-1,2-diaminium] (4m)				
	N4-H4A...O1	0.889	2.092(18)	2.755	141.6
	N4-H4A...O7	0.889	2.385(6)	2.928	119.5
	N4-H4B...O7	0.890	2.293(16)	3.126	155.9
	N4-H4C...O1	0.890	1.928(8)	2.755	153.9
	N4-H4C...O2	0.890	2.428(10)	2.940	116.9
	C2-H2B...O6	0.969	2.431(22)	3.347	157.3
12.	[PA⁻.6-phenyl-2,4-diamino-1,3,5-triazinium] (4n)				
	N6-H6...O1	0.810	1.920(37)	2.685	157.3
	N6-H6...O7	0.810	2.567(63)	3.159	131.0
	N7-H7A...O2	0.859	2.389(15)	3.144	146.9
	N7-H7A...O3	0.850	2.377(9)	3.172	154.0
	N7-H7B...O1	0.860	1.964(8)	2.710	144.4
	N7-H7B...O2	0.860	2.227(12)	2.902	135.2
	N8-H8B...O7	0.860	2.113(11)	2.925	157.0
	N8-H8A...N5	0.861	2.248(13)	3.062	157.8
	C12-H12...O4	0.930	2.593(8)	3.223	125.5
	C13-H13...O4	0.930	2.728(11)	3.297	120.3
	C14-H14...O5	0.930	2.537(11)	3.376	150.2
	C15-H15...O3	0.930	3.012(16)	3.906	161.8

Table 4.14: Hydrogen bond interaction energy (Kcal/mol)

S. N	Salts	Hydrogen bond interaction energy (Kcal/mol)
1.	[2PA ⁻ .2PzH ₂ ⁺ .OH ₂] (4c)	13.39
2.	[PA ⁻ .Pz ^{Me2} H ₂ ⁺] (4d)	14.51
3.	[PA ⁻ .Pz ^{Ph,Me} H ₂ ⁺ .CH ₃ OH] (4e)	26.56
4.	[2PA ⁻ .2H ₂ dmpzH ⁺ .CH ₃ CN] (4f)	21.96
5.	[PA ⁻ .phenH ⁺ .CH ₃ OH] (4g)	9.46
6.	[2PA ⁻ .terpyH ₂ ⁺²] (4h)	12.50
7.	[PA ⁻ .hmta] (4i)	18.72
8.	[3PA ⁻ .tptzH ₃ ³⁺] (4j)	21.49
9.	[PA ⁻ .Uronium] (4k)	19.83
10.	[PA ⁻ .3,5-diamino-1,2,4-triazolium] (4l)	17.32
11.	[PA ⁻ .1/2cyclohexane-1,2-diaminium] (4m)	15.33
12.	[PA ⁻ .6-phenyl-2,4-diamino-1,3,5-triazinium] (4n)	10.26

Table 4.15: Comparison of energy in Solid phase and Gasous phase

S. N	Salts	Energy of optimized str. (gaseous phase)	CIF-Energy of optimized str. (solid phase)
1.	[2PA ⁻ .2PzH ₂ ⁺ .OH ₂] (4c)	1147.0008	1146.9993
2.	[PA ⁻ .Pz ^{Me2} H ₂ ⁺] (4d)	1225.6003	1225.6543
3.	[PA ⁻ .Pz ^{Ph,Me} H ₂ ⁺ .CH ₃ OH] (4e)	1417.1913	1417.2243
4.	[2PA ⁻ .2H ₂ dmpzH ⁺ .CH ₃ CN] (4f)	1529.2960	1529.3021
5.	[PA ⁻ .phenH ⁺ .CH ₃ OH] (4g)	1491.9409	1492.5091
6.	[2PA ⁻ .terpyH ₂ ⁺²] (4h)	2583.0971	2584.4358
7.	[PA. hmta] (4i)	1375.1767	1375.4929
8.	3PA ⁻ .tptzH ₃ ³⁺] (4j)	3782.6183	3782.5788
9.	[PA ⁻ .Uronium] (4k)	1146.1599	1146.1047
10.	[PA ⁻ .3,5-diamino-1,2,4-triazolium] (4l)	1272.8796	1273.2988
11.	[PA ⁻ .1/2cyclohexane-1,2-diaminium] (4m)	2189.0005	2188.3719
12.	[PA ⁻ .6-phenyl-2,4-diamino-1,3,5-triazinium] (4n)	1543.1021	1543.0546

Table 4.16: Comparison of bond lengths (Å) and bond angles (°) in solid and gaseous phase for salts 4c-4n

S. N	Parameters	X-ray	B3LYP/6-31G(d,p)
1.	[2PA ⁻ .2PzH ₂ ⁺ .OH ₂] (4c)		
	Bond Lengths		
	N1-O2	1.228(2)	1.228
	O3-N1	1.231(2)	1.230
	O4-N2	1.233(2)	1.232
	O5-N2	1.228(2)	1.227
	O6-N3	1.230(2)	1.229
	O7-N3	1.228(2)	1.228
	N2-C4	1.449(2)	1.449
	C4-C3	1.386(2)	1.386
	C3-H3A	0.930(1)	0.929
	N3-C2	1.458(2)	1.458
	C3-C2	1.377(2)	1.376
	O1-C1	1.258(2)	1.257
	C2-C1	1.453(2)	1.453
	N1-C6	1.456(2)	1.455
	C1-C6	1.499(2)	1.449
	C4-C5	1.386(2)	1.386

C6-C5	1.378(2)	1.377
C5-H5A	0.929(1)	0.929
N9-N10	1.340(2)	1.341
N9-C16	1.335(2)	1.334
C16-H16	0.930(1)	0.930
C16-C17	1.386(2)	1.385
C17-H17	0.930(1)	0.930
N10-C18	1.336(2)	1.335
C17-C18	1.386(2)	1.385
C18-H18	0.930(1)	0.930
N9-H9B	0.869(19)	0.868
N10-H10A	0.851(22)	0.850
Bond Angles		
O2—N1—O3	122.88(11)	122
O2—N1—C6	118.62(10)	118.59
O3—N1—C6	118.41(10)	118.48
O5—N2—O4	124.15(11)	124.17
O5—N2—C4	118.04(11)	117.96
O4—N2—C4	117.81(10)	117.85
O7—N3—O6	123.26(12)	123.27
O7—N3—C2	118.9(1)	118.89
O6—N3—C2	117.82(10)	117.80
C5—C4—C3	121.64(11)	121.65
C5—C4—N2	118.94(11)	118.89
C3—C4—N2	119.38(10)	119.40
C2—C3—C4	118.57(11)	118.54
C2—C3—H3A	120.69(12)	120.73
C4—C3—H3A	120.74(12)	120.71
C3—C2—C1	124.60(11)	124.61
C3—C2—N3	115.83(10)	115.80
C1—C2—N3	119.57(10)	119.57
O1—C1—C6	125.11(11)	125.12
O1—C1—C2	123.04(11)	123.02
C6—C1—C2	111.74(10)	111.74
C5—C6—C1	124.14(10)	124.14
C5—C6—N1	115.42(10)	115.39
C1—C6—N1	120.42(10)	120.44
C6—C5—C4	119.02(11)	119.00
C6—C5—H5A	120.49(12)	120.49
C4—C5—H5A	120.48(12)	120.50
C17—C16—H16	125.94(13)	125.98
C18—C17—C16	105.63(11)	105.61
C18—C17—H17	127.22(12)	127.20
C16—C17—H17	127.15(13)	127.17
N10—C18—C17	108.35(11)	108.39
N10—C18—H18	125.79(12)	125.79

	C17—C18—H18	125.86(12)	125.81
	N10—N9—H9B	117.83(138)	117.80
	N9—N10—H10A	118.75(150)	118.75
2.	[PA⁻.Pz^{Me2}H₂⁺] (4d)		
	Bond Lengths		
	O1—C6	1.251(2)	1.318
	O2—N1	1.220(2)	1.251
	O3—N1	1.216(2)	1.220
	O4—N2	1.226(2)	1.227
	O5—N2	1.225(2)	1.232
	O6—N3	1.226(2)	1.228
	O7—N3	1.224(3)	1.224
	N1—C1	1.458(2)	1.454
	N2—C3	1.448(3)	1.466
	N3—C5	1.450(2)	1.473
	N4—C8	1.330(2)	1.335
	N4—N5	1.340(2)	1.356
	N4—H4A	0.954(21)	1.061
	N5—C10	1.337(3)	1.358
	N5—H5	0.860(2)	1.009
	C1—C2	1.364(3)	1.391
	C1—C6	1.447(2)	1.423
	C2—C3	1.389(2)	1.384
	C2—H2	0.930(1)	1.081
	C3—C4	1.377(2)	1.400
	C4—C5	1.379(3)	1.381
	C4—H4	0.930(2)	1.093
	C5—C6	1.442(2)	1.415
	C7—C8	1.480(3)	1.498
	C7—H7A	0.960(2)	1.091
	C7—H7B	0.960(2)	1.096
	C7—H7C	0.960(2)	1.095
	C8—C9	1.390(3)	1.417
	C9—C10	1.377(3)	1.383
	C9—H9	0.930(2)	1.080
	C10—C11	1.488(3)	1.495
	C11—H11A	0.960(2)	1.096
	C11—H11B	0.959(2)	1.096
	C11—H11C	0.960(3)	1.091
	Bond Angles		
	O3—N1—O2	123.70(13)	124.58
	O3—N1—C1	118.36(12)	119.02
	O2—N1—C1	117.93(12)	117.79
	O5—N2—O4	123.42(15)	124.58
	O5—N2—C3	118.36(12)	117.67
	O4—N2—C3	118.22(13)	117.74

	O7—N3—O6	122.52(13)	126.25
	O7—N3—C5	118.98(12)	117.32
	O6—N3—C5	118.48(12)	116.39
	C8—N4—N5	108.71(12)	104.85
	C8—N4—H4A	127.47(132)	126.74
	N5—N4—H4A	123.80(149)	122.79
	C10—N5—N4	109.89(12)	113.26
	C10—N5—H5	125.06(14)	128.52
	N4—N5—H5	125.04(13)	118.24
	C2—C1—C6	125.70(12)	122.01
	C2—C1—N1	117.22(11)	117.71
	C6—C1—N1	117.06(11)	120.26
	C1—C2—C3	117.70(12)	118.83
	C1—C2—H2	121.12(13)	120.12
	C3—C2—H2	121.18(13)	121.03
	C4—C3—C2	121.56(12)	121.98
	C4—C3—N2	119.01(12)	119.86
	C2—C3—N2	119.42(11)	118.14
	C3—C4—C5	119.85(12)	117.97
	C3—C4—H4	120.11(13)	122.31
	C5—C4—H4	120.04(13)	119.63
	C4—C5—C6	123.24(12)	123.19
	C4—C5—N3	115.99(11)	117.56
	C6—C5—N3	120.74(11)	119.24
	O1—C6—C5	127.02(12)	120.03
	O1—C6—C1	120.97(12)	123.97
	C5—C6—C1	111.91(11)	115.96
	C8—C7—H7A	109.46(15)	110.72
	C8—C7—H7B	109.47(15)	111.31
	C8—C7—H7C	109.47(16)	110.94
	N4—C8—C9	107.62(12)	110.60
	N4—C8—C7	120.77(13)	121.25
	C9—C8—C7	131.59(14)	128.14
	C10—C9—C8	106.82(13)	105.84
	C10—C9—H9	126.60(15)	126.62
	C8—C9—H9	126.57(14)	127.52
	N5—C10—C9	106.95(13)	105.48
	N5—C10—C11	121.49(14)	122.75
	C9—C10—C11	131.51(14)	131.76
	C10—C11—H11A	109.46(15)	111.75
	C10—C11—H11B	109.46(16)	110.03
	C10—C11—H11C	109.44	111.80
3.	PA⁻.Pz^{Ph,Me}H₂⁺.CH₃OH] (4e)		
	Bond Lengths		
	N1- N2	1.350(3)	1.370
	N1- C2	1.330(2)	1.357

N1- H1	0.912(23)	1.011
N2- C4	1.347(3)	1.360
N2 - H2A	1.014(22)	1.011
C3- H3	0.930(2)	1.078
C3 -C2	1.389(2)	1.386
C3- C4	1.387(3)	1.408
C6 -H6	0.931(2)	1.087
C6- C5	1.392(2)	1.410
C6 -C7	1.386(3)	1.389
C5- C10	1.400(3)	1.408
C5- C4	1.467(3)	1.447
C2 -C1	1.488(3)	1.491
C10- H10	0.930(2)	1.085
C10- C9	1.381(3)	1.389
C8- H8	0.930(2)	1.084
C8- C7	1.382(3)	1.399
C8- C9	1.383(3)	1.398
C7- H7	0.930(2)	1.085
C9- H9	0.930(2)	1.088
C1- H1A	0.960(2)	1.095
C1- H1B	0.959(2)	1.090
C1- H1C	0.960(2)	1.093
C15- H15	0.930(2)	1.081
C15- C16	1.377(2)	1.368
C15- C14	1.380(3)	1.407
C12-C13	1.369(2)	1.368
C12-C11	1.450(3)	1.485
C12-N5	1.453(3)	1.461
C13-H13	0.930(2)	1.081
C13-C14	1.385(3)	1.407
C16-C11	1.452(3)	1.485
C16-N3	1.452(3)	1.460
C11-O1	1.249(2)	1.225
C14-N4	1.446(2)	1.410
N3-O3	1.235(2)	1.241
N3-O2	1.232(2)	1.227
N5-O7	1.232(2)	1.241
N5-O6	1.229(2)	1.227
N4-O5	1.230(2)	1.251
N4-O4	1.236(2)	1.253
Bond Angles		
C2—N1—N2	109.57(14)	108.68
C2—N1—H1	132.79(136)	126.97
N2—N1—H1	117.64(142)	119.58
C4—N2—N1	108.79(14)	109.28
C4—N2—H2A	133.09(119)	125.46

N1—N2—H2A	117.54(119)	119.37
C16—C15—C14	119.65(16)	120.05
C16—C15—H15	120.17(17)	119.79
C14—C15—H15	120.18(16)	120.14
C13—C12—C11	125.07(15)	124.24
C13—C12—N5	115.74(14)	116.01
C11—C12—N5	119.19(14)	119.74
C12—C13—C14	118.78(15)	120.06
C12—C13—H13	120.65(16)	119.80
C14—C13—H13	120.57(17)	120.13
C15—C16—N3	115.59(15)	116.02
C15—C16—C11	123.93(16)	124.25
N3—C16—C11	120.46(14)	119.72
O1—C11—C12	122.88(15)	124.47
O1—C11—C16	125.80(16)	124.44
C12—C11—C16	111.32(14)	111.08
C15—C14—C13	121.05(15)	120.21
C15—C14—N4	119.77(14)	119.89
C13—C14—N4	119.16(14)	119.88
C4—C3—C2	106.87(15)	107.86
C4—C3—H3	126.53(17)	126.04
C2—C3—H3	126.60(18)	126.07
C7—C6—C5	120.37(16)	119.79
C7—C6—H6	119.82(17)	119.56
C5—C6—H6	119.81(17)	120.58
C6—C5—C10	118.99(16)	119.62
C6—C5—C4	121.84(15)	121.12
C10—C5—C4	119.16(16)	119.24
N1—C2—C3	107.53(15)	107.48
N1—C2—C1	121.92(15)	121.70
C3—C2—C1	130.51(16)	130.77
C9—C10—C5	120.05(16)	120.30
C9—C10—H10	119.94(17)	119.54
C5—C10—H10	120.01(17)	120.11
C7—C8—C9	119.73(17)	120.57
C7—C8—H8	120.15(19)	121.32
C8—C7—C6	120.27(17)	120.06
C8—C7—H7	119.82(18)	120.21
C6—C7—H7	119.90(18)	119.71
N2—C4—C3	107.24(14)	106.30
N2—C4—C5	122.46(15)	122.66
C3—C4—C5	130.26(15)	131.02
C10—C9—C8	120.59(17)	119.62
C10—C9—H9	119.71(19)	121.09
C8—C9—H9	119.71(18)	119.27
C2—C1—H1A	109.51(17)	110.74

	C2—C1—H1B	109.48(17)	109.85
	C2—C1—H1C	109.49(17)	111.47
	O2—N3—O3	122.08(14)	123.98
	O2—N3—C16	119.38(14)	118.50
	O3—N3—C16	118.53(14)	117.48
	O6—N5—O7	122.76(14)	124.00
	O6—N5—C12	119.11(14)	118.49
	O7—N5—C12	118.07(14)	117.48
	O5—N4—O4	123.41(15)	121.93
	O5—N4—C14	118.31(14)	119.18
	O4—N4—C14	118.27(13)	118.87
4.	2PA·2H₂dmpzH⁺·CH₃CN] (4f)		
	Bond Lengths		
	C4—O1	1.266(3)	1.222
	C4—C5	1.430(3)	1.486
	C4—C3	1.434(3)	1.485
	C1—C2	1.391(4)	1.403
	C1—C6	1.372(4)	1.415
	C1—N2	1.447(4)	1.406
	C5—C6	1.383(4)	1.363
	C5—N1	1.454(3)	1.466
	C3—C2	1.356(4)	1.370
	C3—N3	1.464(4)	1.453
	C2—H2	0.930(2)	1.079
	C6—H6	0.930(3)	1.082
	O2—N1	1.227(4)	1.225
	O3—N1	1.227(3)	1.235
	O4—N2	1.224(4)	1.230
	O5—N2	1.222(4)	1.281
	O6—N3	1.208(3)	1.222
	O7—N3	1.210(4)	1.253
	C16—C21	1.480(3)	1.489
	C16—N10	1.341(5)	1.340
	N9—N10	1.348(3)	1.352
	N9—H9AA	0.875(32)	1.010
	N10—H10A	0.882(34)	1.059
	N8—N7	1.353(3)	1.354
	N7—H7AA	0.898(25)	1.008
	C18—N9	1.331(3)	1.349
	C21—H21A	0.959(3)	1.092
	C21—H21B	0.960(3)	1.091
	C21—H21C	0.960(3)	1.095
	C18—C22	1.494(5)	1.491
	C22—H22A	0.960(2)	1.091
	C22—H22B	0.960(2)	1.095
	C22—H22C	0.960(4)	1.094

C17—C14	1.467(4)	1.467
C14—C15	1.383(3)	1.430
C13—C14	1.412(5)	1.395
C13—C19	1.476(3)	1.495
C19—H19A	0.960(4)	1.095
C19—H19B	0.960(2)	1.090
C19—H19C	0.961(4)	1.095
C15—N7	1.353(5)	1.328
C15—C20	1.486(3)	1.498
C20—H20A	0.960(3)	1.091
C20—H20B	0.959(2)	1.095
C20—H20C	0.959(3)	1.096
C13—N8	1.337(3)	1.354
Bond Angles		
O1—C4—C5	127.56(19)	124.55
O1—C4—C3	120.00(19)	124.45
C5—C4—C3	112.41(19)	110.98
C6—C1—C2	121.34(21)	119.87
C6—C1—N2	119.52(21)	120.28
C2—C1—N2	119.13(21)	119.83
C6—C5—C4	122.62(20)	123.88
C6—C5—N1	116.40(19)	115.92
C4—C5—N1	120.97(19)	120.18
C2—C3—C4	126.20(21)	124.71
C2—C3—N3	118.76(21)	116.30
C4—C3—N3	115.04(19)	118.98
C3—C2—C1	117.30(22)	119.78
C3—C2—H2	121.30(23)	120.10
C1—C2—H2	121.39(23)	120.10
C1—C6—C5	120.11(21)	120.66
C1—C6—H6	119.92(23)	120.79
C5—C6—H6	119.98(22)	118.50
O6—N3—O7	124.34(22)	124.94
O6—N3—C3	118.03(20)	117.77
O7—N3—C3	117.63(21)	117.25
O2—N1—O3	122.34(19)	123.46
O2—N1—C5	119.14(19)	119.54
O3—N1—C5	118.51(19)	116.98
O5—N2—O4	123.77(24)	120.52
O5—N2—C1	118.17(22)	120.50
O4—N2—C1	118.06(22)	118.97
C18—C17—C16	105.66(18)	105.95
C18—C17—C14	127.96(19)	127.22
C16—C17—C14	126.36(18)	126.81
N8—C13—C14	110.92(17)	111.02
N8—C13—C19	122.62(19)	120.35

C14—C13—C19	126.46(19)	128.61
N9—C18—C17	108.50(18)	108.01
N9—C18—C22	121.63(18)	122.13
C17—C18—C22	129.8(2)	129.83
C15—C14—C13	105.25(18)	105.24
C15—C14—C17	127.59(18)	127.39
C13—C14—C17	127.16(18)	127.35
N10—C16—C17	107.91(17)	107.15
N10—C16—C21	121.77(20)	122.39
C17—C16—C21	130.32(20)	130.45
N7—C15—C14	106.16(17)	104.96
N7—C15—C20	122.91(19)	122.48
C14—C15—C20	130.93(20)	132.54
C18—N9—N10	109.11(17)	108.79
C18—N9—H9AA	128.88(203)	133.44
N10—N9—H9AA	122.00(226)	117.03
C16—N10—N9	108.80(18)	110.07
C16—N10—H10A	121.69(212)	130.41
N9—N10—H10A	129.5(22)	119.51
C13—N8—N7	104.79(17)	104.55
C15—N7—N8	112.87(17)	114.21
C15—N7—H7AA	126.69(155)	125.96
N8—N7—H7AA	120.27(160)	118.81
5. [PA⁻.phenH⁺.CH₃OH] (4g)		
Bond Lengths		
O1—C1	1.242(9)	1.243
O2—N4	1.219(7)	1.236
O3—N4	1.221(6)	1.233
O4—N3	1.218(10)	1.245
O5—N3	1.218(4)	1.235
O6—N5	1.218(5)	1.235
O7—N5	1.234(11)	1.235
N1—C7	1.325(4)	1.337
N1—C18	1.361(11)	1.366
N1—H1B	0.896(28)	1.044
N2—C16	1.320(5)	1.321
N2—C17	1.355(9)	1.413
N3—C6	1.449(7)	1.444
N4—C2	1.452(11)	1.457
N5—C4	1.450(11)	1.450
C1—C6	1.451(11)	1.466
C1—C2	1.454(5)	1.466
C2—C3	1.373(10)	1.375
C3—C4	1.376(11)	1.402
C3—H3A	0.930(4)	1.082
C4—C5	1.380(6)	1.391

C5—C6	1.37(1)	1.385
C5—H5A	0.930(7)	1.081
C7—C8	1.383(10)	1.399
C7—H7A	0.930(8)	1.088
C8—C9	1.370(11)	1.380
C8—H8A	0.931(3)	1.082
C9—C10	1.399(5)	1.414
C9—H9	0.930(7)	1.086
C10—C18	1.402(10)	1.414
C10—C11	1.437(12)	1.434
C11—C12	1.347(5)	1.362
C11—H11	0.930(7)	1.085
C12—C13	1.426(10)	1.433
C12—H12	0.930(8)	1.086
C13—C14	1.405(5)	1.414
C13—C17	1.408(12)	1.420
C14—C15	1.358(10)	1.379
C14—H14	0.930(8)	1.086
C15—C16	1.403(11)	1.413
C15—H15	0.930(4)	1.084
C17—C18	1.433(5)	1.440
Bond Angles		
C7—N1—C18	122.63(17)	123.170
C7—N1—H1B	116.78(141)	117.90
C18—N1—H1B	120.56(155)	118.89
C16—N2—C17	116.82(16)	118.14
O5—N3—O4	122.5(2)	122.04
O5—N3—C6	118.40(18)	118.82
O4—N3—C6	119.02(17)	119.11
O2—N4—O3	122.1(2)	123.76
O2—N4—C2	119.22(19)	118.06
O3—N4—C2	118.64(18)	118.12
O6—N5—O7	124.00(23)	124.22
O6—N5—C4	118.57(19)	117.80
O7—N5—C4	117.42(21)	117.96
O1—C1—C6	124.01(17)	124.09
O1—C1—C2	124.47(16)	123.65
C6—C1—C2	111.52(15)	112.22
C3—C2—N4	116.45(17)	117.11
C3—C2—C1	124.13(16)	123.77
N4—C2—C1	119.33(16)	119.10
C2—C3—C4	119.25(19)	119.41
C2—C3—H3A	120.35(18)	120.43
C4—C3—H3A	120.4(2)	120.13
C3—C4—C5	121.48(18)	121.00
C3—C4—N5	119.68(19)	119.46

	C5—C4—N5	118.80(18)	119.48
	C6—C5—C4	119.09(18)	119.72
	C6—C5—H5A	120.45(20)	120.10
	C4—C5—H5A	120.46(19)	120.16
	C5—C6—N3	116.27(17)	116.99
	C5—C6—C1	124.45(17)	123.23
	N3—C6—C1	119.26(16)	119.77
	N1—C7—C8	120.13(18)	119.76
	C7—C8—H8A	120.26(20)	115.14
	C8—C9—C10	120.48(19)	120.56
	C8—C9—H9	119.82(21)	120.44
	C10—C9—H9	119.7(2)	118.98
	C9—C10—C18	118.04(17)	117.98
	C9—C10—C11	123.49(18)	123.05
	C18—C10—C11	118.46(17)	118.96
	C12—C11—C10	120.61(19)	120.93
	C12—C11—H11	119.7(2)	120.74
	C10—C11—H11	119.68(20)	118.32
	C11—C12—C13	121.62(19)	121.03
	C11—C12—H12	119.16(20)	120.35
	C13—C12—H12	119.22(21)	118.60
	C14—C13—C17	116.56(17)	116.62
	C14—C13—C12	123.60(18)	123.49
	C17—C13—C12	119.82(18)	119.87
	C15—C14—C13	119.53(19)	119.39
	C15—C14—H14	120.22(21)	121.03
	C13—C14—H14	120.25(20)	119.56
	C14—C15—C16	119.44(20)	119.02
	C14—C15—H15	120.3(2)	121.13
	C16—C15—H15	120.26(20)	119.83
	N2—C16—C15	123.52(19)	119.02
	N2—C16—H16	118.23(20)	119.83
	C15—C16—H16	118.25(21)	121.13
	N2—C17—C13	124.12(17)	123.71
	N2—C17—C18	117.80(16)	117.83
	C13—C17—C18	118.05(16)	118.45
	N1—C18—C10	119.16(17)	119.05
	N1—C18—C17	119.39(16)	120.26
	C10—C18—C17	121.44(16)	120.68
	N1—C7—H7A	119.92(20)	115.14
	C8—C7—H7A	119.95(21)	125.05
	C9—C8—C7	119.5(2)	119.41
	C9—C8—H8A	120.24(20)	121.76
6.	[2PA⁻.terpyH₂⁺²] (4h)		
	Bond Lengths		
	O1—C21	1.225(6)	1.240

O2—N4	1.149(10)	1.140
O3—N4	1.186(9)	1.230
O4—N5	1.170(9)	1.233
O5—N5	1.179(8)	1.242
O6—N6	1.223(8)	1.237
O7—N6	1.231(7)	1.238
O8—C22	1.271(5)	1.272
O9—N7	1.225(5)	1.236
O10—N7	1.221(5)	1.227
O11—N8	1.223(5)	1.237
O12—N8	1.217(5)	1.232
O13—N9	1.213(5)	1.231
O13—N9	1.213(5)	1.232
N1—C1	1.343(5)	1.339
N1—C5	1.355(5)	1.359
N1—H1A	0.964(102)	1.038
N2—C6	1.336(5)	1.333
N2—C10	1.341(5)	1.334
N3—C15	1.328(5)	1.344
N3—C11	1.357(5)	1.356
N3—H3A	0.997(49)	1.058
N4—C16	1.446(8)	1.464
N5—C20	1.466(7)	1.461
N6—C18	1.447(5)	1.459
N7—C23	1.467(5)	1.458
N8—C27	1.475(5)	1.449
N9—C25	1.462(5)	1.444
C1—C2	1.373(5)	1.382
C1—H1	0.930(4)	1.081
C2—C3	1.390(6)	1.389
C2—H2	0.931(4)	1.081
C3—C4	1.388(5)	1.398
C3—H3	0.930(4)	1.081
C4—C5	1.385(5)	1.383
C4—H4	0.929(4)	1.081
C5—C6	1.481(5)	1.478
C6—C7	1.388(5)	1.404
C7—C8	1.395(5)	1.391
C7—H7	0.931(4)	1.083
C8—C9	1.395(6)	1.394
C8—H8	0.930(4)	1.084
C9—C10	1.392(5)	1.399
C9—H9	0.930(4)	1.083
C10—C11	1.487(5)	1.479
C11—C12	1.372(5)	1.394
C12—C13	1.400(6)	1.393

C12—H12	0.930(4)	1.082
C13—C14	1.377(6)	1.395
C13—H13	0.930(4)	1.085
C14—C15	1.384(5)	1.387
C14—H14	0.929(4)	1.083
C15—H15	0.930(4)	1.085
C16—C17	1.343(6)	1.394
C16—C21	1.463(6)	1.452
C17—C18	1.389(6)	1.386
C17—H17	0.930(4)	1.008
C18—C19	1.389(6)	1.394
C19—C20	1.370(7)	1.378
C19—H19	0.930(4)	1.082
C20—C21	1.444(6)	1.451
C22—C27	1.429(5)	1.469
C22—C23	1.435(5)	1.469
C23—C24	1.380(5)	1.385
C24—C25	1.371(6)	1.392
C24—H24	0.930(4)	1.081
C25—C26	1.388(5)	1.403
C26—C27	1.358(5)	1.371
C26—H26	0.930(4)	1.082
Bond Angles		
C1—N1—C5	123.32(32)	124.65
C1—N1—H1A	140.07(594)	118.31
C5—N1—H1A	95.07(644)	96.99
C6—N2—C10	118.55(31)	119.56
C15—N3—C11	122.74(34)	123.41
C15—N3—H3A	112.68(264)	115.81
C11—N3—H3A	124.57(290)	120.76
O2—N4—O3	110.55(74)	124.94
O2—N4—C16	122.99(62)	123.80
O3—N4—C16	121.18(57)	120.39
O4—N5—O5	117.80(69)	117.66
O4—N5—C20	119.31(50)	117.59
O5—N5—C20	122.88(54)	118.53
O6—N6—O7	124.03(60)	122.92
O6—N6—C18	116.85(39)	117.39
O7—N6—C18	119.11(37)	117.66
O10—N7—O9	124.21(36)	122.61
O10—N7—C23	117.50(31)	118.39
O9—N7—C23	118.29(32)	118.95
O12—N8—O11	124.59(38)	124.61
O12—N8—C27	117.61(34)	117.73
O11—N8—C27	117.79(31)	117.83
O13—N9—O14	123.80(33)	122.39

O13—N9—C25	118.77(31)	118.76
O14—N9—C25	117.42(30)	119.43
N1—C1—C2	120.23(33)	120.56
N1—C1—H1	119.80(36)	117.88
C2—C1—H1	119.97(40)	123.44
C1—C2—C3	118.45(38)	118.66
C1—C2—H2	120.76(36)	119.23
C3—C2—H2	120.78(36)	122.04
C4—C3—C2	120.14(34)	119.94
C4—C3—H3	119.94(35)	119.03
C2—C3—H3	119.92(41)	119.03
C5—C4—C3	120.03(33)	119.47
C5—C4—H4	119.95(39)	121.07
C3—C4—H4	120.02(36)	119.03
N1—C5—C4	117.83(34)	118.82
N1—C5—C6	115.54(31)	116.45
C4—C5—C6	126.62(32)	124.61
N2—C6—C7	122.87(35)	122.03
N2—C6—C5	114.80(31)	114.83
C7—C6—C5	122.33(32)	123.12
C6—C7—C8	118.42(33)	118.23
C6—C7—H7	120.80(39)	121.16
C8—C7—H7	120.78(36)	120.59
C7—C8—C9	119.18(34)	119.73
C7—C8—H8	120.43(35)	120.11
C9—C8—H8	120.38(41)	120.14
C10—C9—C8	118.08(36)	117.79
C10—C9—H9	120.99(35)	121.74
C8—C9—H9	120.93(36)	120.45
N2—C10—C9	122.89(32)	122.63
N2—C10—C11	114.80(31)	114.08
C9—C10—C11	122.30(34)	123.28
N3—C11—C12	119.03(33)	118.13
N3—C11—C10	116.50(33)	116.69
C12—C11—C10	124.46(34)	125.13
C11—C12—C13	119.34(35)	119.83
C11—C12—H12	120.30(36)	119.71
C13—C12—H12	120.36(41)	120.41
C14—C13—C12	119.83(40)	120.02
C14—C13—H13	120.12(38)	120.29
C12—C13—H13	120.05(40)	119.67
C13—C14—C15	118.90(34)	118.56
C13—C14—H14	120.55(43)	121.69
C15—C14—H14	120.55(39)	119.74
N3—C15—C14	120.13(35)	120.01
N3—C15—H15	119.90(39)	115.03

C14—C15—H15	119.97(36)	124.94
C17—C16—N4	115.52(43)	115.62
C17—C16—C21	125.82(41)	122.87
N4—C16—C21	118.66(43)	121.49
C16—C17—C18	119.15(37)	120.06
C16—C17—H17	120.31(38)	119.70
C18—C17—H17	120.54(42)	120.23
C17—C18—C19	120.2(4)	120.92
C17—C18—N6	118.19(36)	119.62
C19—C18—N6	121.59(37)	119.44
C20—C19—C18	119.81(43)	118.89
C20—C19—H19	120.14(47)	120.71
C18—C19—H19	120.05(44)	120.38
C19—C20—C21	124.39(43)	124.39
C19—C20—N5	116.47(45)	115.89
C21—C20—N5	119.14(39)	119.70
O1—C21—C20	127.17(44)	121.06
O1—C21—C16	122.23(42)	126.19
C20—C21—C16	110.59(38)	112.69
O8—C22—C27	124.21(35)	125.68
O8—C22—C23	124.18(33)	122.71
C27—C22—C23	111.60(31)	111.57
C24—C23—C22	124.39(33)	124.63
C24—C23—N7	116.48(33)	116.78
C22—C23—N7	119.12(31)	118.56
C25—C24—C23	118.46(35)	119.09
C25—C24—H24	120.77(36)	119.89
C23—C24—H24	120.77(36)	120.98
C24—C25—C26	121.62(34)	120.68
C24—C25—N9	118.98(33)	119.49
C26—C25—N9	119.31(31)	119.78
C27—C26—C25	118.14(32)	120.24
C27—C26—H26	120.93(38)	119.86
C25—C26—H26	120.93(36)	119.87
C26—C27—C22	125.43(35)	123.18
C26—C27—N8	117.77(31)	116.23
C22—C27—N8	116.68(31)	120.57
7. [PA.hmta] (4i)		
Bond Lengths		
O1—C1	1.245(2)	1.317
O1—H1	0.820(1)	0.994
O2—N1	1.207(2)	1.226
O3—N1	1.223(2)	1.229
O4—N3	1.236(2)	1.227
O5—N3	1.227(2)	1.227
O6—N2	1.227(2)	1.220

O7—N2	1.232(2)	1.252
N1—C6	1.470(2)	1.474
N2—C2	1.446(2)	1.455
N3—C4	1.441(2)	1.472
N4—C11	1.445(2)	1.480
N4—C7	1.473(2)	1.486
N4—C8	1.477(2)	1.481
N5—C9	1.441(2)	1.475
N5—C8	1.471(2)	1.473
N5—C12	1.476(2)	1.477
N6—C11	1.515(2)	1.474
N6—C10	1.517(2)	1.476
N6—C9	1.520(2)	1.479
N7—C10	1.447(2)	1.476
N7—C7	1.468(2)	1.474
N7—C12	1.474(2)	1.474
C1—C2	1.458(2)	1.424
C1—C6	1.459(2)	1.416
C2—C3	1.372(3)	1.392
C3—C4	1.378(2)	1.384
C3—H3	0.930(1)	1.081
C4—C5	1.391(2)	1.398
C5—C6	1.366(3)	1.383
C5—H5	0.930(2)	1.094
C7—H7A	0.970(1)	1.094
C7—H7B	0.970(2)	1.093
C8—H8A	0.970(2)	1.095
C8—H8B	0.970(2)	1.094
C9—H9A	0.970(2)	1.095
C9—H9B	0.970(2)	1.095
C10—H10A	0.969(2)	1.095
C10—H10B	0.971(1)	1.095
C11—H11A	0.970(1)	1.093
C11—H11B	0.971(2)	1.093
C12—H12A	0.970(2)	1.095
C12—H12B	0.969(2)	1.095
Bond Angles		
C1—O1—H1	109.43(15)	106.56
O2—N1—O3	122.33(17)	126.08
O2—N1—C6	119.93(13)	117.70
O3—N1—C6	117.73(14)	116.16
O6—N2—O7	121.19(14)	123.13
O6—N2—C2	118.89(13)	119.08
O7—N2—C2	119.92(15)	117.72
O5—N3—O4	122.89(14)	125.43
O5—N3—C4	119.13(13)	117.69

O4—N3—C4	117.97(15)	116.86
C11—N4—C7	109.16(12)	107.49
C11—N4—C8	108.70(12)	107.79
C7—N4—C8	108.25(11)	107.79
C9—N5—C8	109.17(13)	107.93
C9—N5—C12	109.13(12)	108.04
C8—N5—C12	108.22(12)	107.83
C11—N6—C10	108.54(11)	107.90
C11—N6—C9	108.66(11)	107.66
C10—N6—C9	108.42(11)	107.71
C10—N7—C7	108.99(13)	107.95
C10—N7—C12	108.71(12)	107.86
C7—N7—C12	108.66(12)	108.09
O1—C1—C2	125.79(16)	123.78
O1—C1—C6	122.54(16)	120.35
C2—C1—C6	111.66(14)	115.82
C3—C2—N2	115.57(15)	117.63
C3—C2—C1	124.07(14)	122.13
N2—C2—C1	120.36(13)	120.22
C2—C3—C4	119.27(16)	118.84
C2—C3—H3	120.38(14)	120.27
C4—C3—H3	120.35(14)	120.88
C3—C4—C5	121.48(13)	118.84
C3—C4—N3	119.49(15)	118.55
C5—C4—N3	119.00(13)	119.62
C6—C5—C4	119.11(13)	118.25
C6—C5—H5	120.44(17)	119.24
C4—C5—H5	120.46(14)	122.49
C5—C6—C1	124.22(16)	123.06
C5—C6—N1	115.75(13)	116.68
C1—C6—N1	120.03(13)	120.24
N7—C7—N4	112.04(12)	112.41
N7—C7—H7A	109.18(12)	108.77
N4—C7—H7A	109.25(13)	108.54
N7—C7—H7B	109.20(15)	109.51
N4—C7—H7B	109.19(14)	109.02
H7A—C7—H7B	107.89(13)	108.49
N5—C8—N4	112.09(11)	112.59
N5—C8—H8A	109.20(15)	108.90
N5—C8—H8B	109.20(13)	109.33
N4—C8—H8A	109.20(12)	108.73
N4—C8—H8B	109.18(13)	108.50
H8A—C8—H8B	107.87(15)	108.69
N5—C9—N6	109.76(11)	112.67
N5—C9—H9A	109.72(14)	109.12
N6—C9—H9A	109.72(13)	108.83

	N5—C9—H9B	109.73(15)	109.09
	N6—C9—H9B	109.75(12)	108.72
	H9A—C9—H9B	108.14(15)	108.30
	N7—C10—N6	110.03(12)	112.74
	N7—C10—H10A	109.66(15)	108.86
	N6—C10—H10A	109.66(13)	108.89
	N7—C10—H10B	109.65(13)	108.93
	N6—C10—H10B	109.65(13)	108.95
	H10A—C10—H10	108.16(13)	108.35
	N4—C11—N6	109.95(14)	112.82
	N4—C11—H11A	109.64(13)	109.01
	N6—C11—H11A	109.69(12)	108.54
	N4—C11—H11B	109.64(14)	108.63
	N6—C11—H11B	109.70(13)	109.26
	H11A—C11—H11B	108.20(15)	108.46
	N7—C12—N5	111.87(12)	112.58
	N7—C12—H12A	109.21(13)	109.08
	N5—C12—H12A	109.29(14)	108.88
	N7—C12—H12B	109.26(12)	108.99
	N5—C12—H12B	109.24(14)	108.85
	H12A—C12—H12B	107.89(17)	108.35
8.	[3PA⁻.tptzH₃³⁺] (4j)		
	Bond Lengths		
	O1—C1	1.239(4)	1.239
	O2—N1	1.232(5)	1.228
	O3—N1	1.230(4)	1.236
	O4—N2	1.232(4)	1.233
	O5—N2	1.233(4)	1.231
	O6—N3	1.237(3)	1.229
	O7—N3	1.229(3)	1.232
	O8—C8	1.257(4)	1.231
	O9—N4	1.229(3)	1.242
	O10—N4	1.232(3)	1.230
	O11—N5	1.233(4)	1.235
	O12—N5	1.223(4)	1.235
	O13—N6	1.231(5)	1.229
	O14—N6	1.230(5)	1.217
	O15—C15	1.231(4)	1.257
	O16—N7	1.243(5)	1.229
	O17—N7	1.231(3)	1.230
	O18—N8	1.235(3)	1.222
	O19—N8	1.236(3)	1.232
	O20—N9	1.230(4)	1.231
	O21—N9	1.218(5)	1.228
	N1—C6	1.448(5)	1.451
	N2—C4	1.436(5)	1.436

N3—C2	1.452(4)	1.448
N4—C7	1.457(5)	1.442
N5—C11	1.452(5)	1.441
N6—C9	1.460(4)	1.456
N7—C16	1.442(3)	1.460
N8—C18	1.442(5)	1.451
N9—C14	1.456(4)	1.456
N10—C19	1.339(4)	1.338
N10—C23	1.350(4)	1.351
N10—H10A	0.831(31)	0.830
N11—C24	1.333(3)	1.332
N11—C26	1.335(4)	1.335
N12—C31	1.337(4)	1.336
N12—C27	1.359(4)	1.359
N12—H12A	0.867(26)	0.867
N13—C25	1.330(4)	1.330
N13—C26	1.337(4)	1.336
N14—C25	1.332(4)	1.331
N14—C24	1.334(4)	1.334
C33—C34	1.340(4)	1.338
C33—C32	1.356(4)	1.356
C33—H33	0.929(2)	0.929
C1—C2	1.459(5)	1.459
C1—C6	1.460(4)	1.459
C2—C3	1.367(5)	1.381
C3—C4	1.390(4)	1.367
C3—H3	0.929(3)	0.929
C4—C5	1.385(5)	1.367
C5—C6	1.382(5)	1.367
C5—H5	0.930(3)	0.929
C7—C12	1.380(4)	1.368
C7—C8	1.451(4)	1.471
C12—C11	1.374(5)	1.395
C12—H12	0.930(3)	0.930
C11—C10	1.394(4)	1.380
C10—C9	1.376(4)	1.376
C10—H10	0.930(3)	0.930
C9—C8	1.454(5)	1.465
C15—C16	1.466(4)	1.453
C15—C14	1.472(4)	1.451
C14—C13	1.369(5)	1.381
C13—C18	1.396(4)	1.373
C13—H13	0.931(2)	0.930
C18—C17	1.381(4)	1.394
C17—C16	1.376(5)	1.375
C17—H17	0.930(3)	0.929

C19—C20	1.383(4)	1.382
C19—H19	0.931(3)	0.930
C20—C21	1.387(5)	1.386
C20—H20	0.930(3)	0.931
C21—C22	1.390(5)	1.390
C21—H21	0.930(3)	0.930
C22—C23	1.377(4)	1.376
C22—H22	0.930(3)	0.930
C23—C24	1.480(4)	1.480
C25—C32	1.474(4)	1.473
C26—C27	1.480(4)	1.479
C27—C28	1.378(4)	1.377
C28—C29	1.398(4)	1.397
C28—H28	0.930(3)	0.930
C29—C30	1.385(4)	1.384
C29—H29	0.930(3)	0.931
C30—C31	1.383(4)	1.383
C30—H30	0.930(3)	0.930
C31—H31	0.930(3)	0.930
C32—N15	1.381(4)	1.381
N15—C36	1.390(5)	1.390
N15—H15	1.102(28)	1.101
C36—C35	1.384(5)	1.384
C36—H36	0.930(3)	0.929
C35—C34	1.372(4)	1.371
C35—H35	0.930(3)	0.929
C34—H34	0.930(3)	0.930
Bond Angles		
O3—N1—O2	123.00(19)	122.39
O3—N1—C6	118.39(18)	118.25
O2—N1—C6	118.61(18)	119.33
O4—N2—O5	123.21(20)	122.72
O4—N2—C4	118.13(18)	118.41
O5—N2—C4	118.66(18)	118.85
O7—N3—O6	123.88(18)	121.78
O7—N3—C2	118.68(17)	118.78
O6—N3—C2	117.41(17)	119.40
O9—N4—O10	122.02(19)	123.17
O9—N4—C7	119.63(18)	118.82
O10—N4—C7	118.34(18)	117.99
O12—N5—O11	123.46(22)	123.44
O12—N5—C11	118.70(19)	118.68
O11—N5—C11	117.84(20)	117.86
O14—N6—O13	123.17(17)	122.03
O14—N6—C9	118.81(17)	119.63
O13—N6—C9	118.02(18)	118.32

O17—N7—O16	121.77(18)	123.86
O17—N7—C16	118.81(15)	117.41
O16—N7—C16	119.39(15)	118.69
O18—N8—O19	122.74(16)	123.18
O18—N8—C18	118.84(17)	118.15
O19—N8—C18	118.41(16)	118.66
O21—N9—O20	122.36(18)	122.96
O21—N9—C14	119.35(18)	118.42
O20—N9—C14	118.27(17)	118.60
C19—N10—C23	122.62(17)	122.55
C19—N10—H10A	119.60(175)	119.63
C23—N10—H10A	117.76(178)	117.78
C24—N11—C26	113.30(17)	113.33
C31—N12—C27	122.10(18)	122.11
C31—N12—H12A	115.54(177)	115.51
C27—N12—H12A	122.35(171)	122.36
C25—N13—C26	114.59(15)	114.55
C25—N14—C24	113.66(17)	113.66
C34—C33—C32	121.01(18)	121.01
C34—C33—H33	119.48(17)	119.52
C32—C33—H33	119.51(18)	119.46
O1—C1—C2	122.68(18)	124.99
O1—C1—C6	126.47(19)	124.36
C2—C1—C6	110.84(17)	110.59
C3—C2—N3	116.01(17)	114.88
C3—C2—C1	125.77(18)	124.67
N3—C2—C1	118.20(17)	120.19
C2—C3—C4	118.44(19)	119.72
C2—C3—H3	120.78(20)	120.17
C4—C3—H3	120.78(21)	120.10
C5—C4—C3	121.18(20)	121.17
C5—C4—N2	119.93(19)	118.86
C3—C4—N2	118.87(18)	116.04
C6—C5—C4	119.75(19)	118.44
C6—C5—H5	120.12(20)	120.78
C4—C5—H5	120.13(21)	120.76
C5—C6—N1	115.90(18)	116.04
C5—C6—C1	123.89(19)	125.72
N1—C6—C1	120.20(18)	118.20
C12—C7—C8	123.76(19)	124.77
C12—C7—N4	115.77(19)	116.10
C8—C7—N4	120.47(18)	119.12
C11—C12—C7	119.62(20)	119.31
C11—C12—H12	120.20(22)	120.33
C7—C12—H12	120.19(21)	120.35
C12—C11—C10	121.42(21)	121.02

C12—C11—N5	118.59(19)	120.48
C10—C11—N5	119.98(20)	119.58
C9—C10—C11	118.71(20)	118.46
C9—C10—H10	120.63(21)	120.13
C11—C10—H10	120.66(22)	120.28
C10—C9—C8	124.34(19)	124.67
C10—C9—N6	115.84(18)	114.88
C8—C9—N6	119.75(18)	120.44
O8—C8—C7	124.21(19)	124.36
O8—C8—C9	123.71(18)	124.99
C7—C8—C9	112.07(18)	110.59
O15—C15—C16	124.96(19)	124.19
O15—C15—C14	124.40(17)	123.71
C16—C15—C14	110.60(16)	112.08
C13—C14—N9	116.09(18)	115.82
C13—C14—C15	124.81(17)	124.34
N9—C14—C15	119.10(16)	119.74
C14—C13—C18	119.26(19)	118.69
C14—C13—H13	120.36(18)	120.64
C18—C13—H13	120.38(18)	120.66
C17—C18—C13	121.06(17)	121.46
C17—C18—N8	118.46(16)	118.54
C13—C18—N8	120.44(18)	119.98
C16—C17—C18	119.57(17)	119.59
C16—C17—H17	120.18(20)	120.14
C18—C17—H17	120.25(19)	120.26
C17—C16—N7	114.87(16)	114.85
C17—C16—C15	124.66(18)	123.73
N7—C16—C15	120.47(16)	120.48
N10—C19—C20	119.51(19)	119.53
N10—C19—H19	120.23(19)	120.19
C20—C19—H19	120.26(19)	120.27
C19—C20—C21	119.24(19)	119.28
C19—C20—H20	120.39(21)	120.40
C21—C20—H20	120.37(21)	120.31
C20—C21—C22	119.88(20)	119.84
C20—C21—H21	120.06(20)	120.08
C22—C21—H21	120.06(22)	120.07
C23—C22—C21	119.07(20)	119.04
C23—C22—H22	120.46(19)	120.50
C21—C22—H22	120.47(20)	120.45
N10—C23—C22	119.67(16)	119.72
N10—C23—C24	117.82(17)	117.77
C22—C23—C24	122.50(18)	122.48
N11—C24—N14	126.86(17)	126.83
N11—C24—C23	118.78(17)	118.81

	N14—C24—C23	114.34(17)	114.32
	N13—C25—N14	125.67(18)	125.67
	N13—C25—C32	118.12(16)	118.13
	N14—C25—C32	116.17(17)	116.16
	N11—C26—N13	125.72(18)	125.69
	N11—C26—C27	118.30(17)	118.29
	N13—C26—C27	115.85(16)	115.89
	N12—C27—C28	119.96(17)	119.95
	N12—C27—C26	116.10(17)	116.07
	C28—C27—C26	123.69(16)	123.71
	C27—C28—C29	118.80(17)	118.80
	C27—C28—H28	120.61(19)	120.60
	C29—C28—H28	120.59(19)	120.59
	C30—C29—C28	119.71(19)	119.74
	C30—C29—H29	120.14(20)	120.09
	C28—C29—H29	120.14(19)	120.60
	C31—C30—C29	119.50(19)	119.45
	C31—C30—H30	120.25(19)	120.27
	C29—C30—H30	120.26(21)	120.16
	N12—C31—C30	119.86(18)	119.87
	N12—C31—H31	120.11(20)	120.17
	C30—C31—H31	120.03(20)	119.94
	C33—C32—N15	120.49(19)	120.45
	C33—C32—C25	117.54(17)	117.55
	N15—C32—C25	121.97(17)	121.98
	C32—N15—C36	118.49(19)	118.52
	C32—N15—H15	121.72(132)	121.73
	C36—N15—H15	119.73(130)	119.67
	C35—C36—N15	120.06(21)	120.00
	C35—C36—H36	119.94(23)	119.93
	N15—C36—H36	120.0(2)	119.10
	C34—C35—C36	119.10(21)	119.10
	C34—C35—H35	120.45(21)	120.48
	C36—C35—H35	120.45(22)	120.40
	C33—C34—C35	120.84(19)	120.87
	C33—C34—H34	119.55(21)	119.53
	C35—C34—H34	119.60(22)	119.59
9.	[PA.Uronium] (4k)		
	Bond Lengths		
	O1—C1	1.246(2)	1.256
	C5—C6	1.374(3)	1.383
	C5—C4	1.376(3)	1.392
	C5—H5	0.930(4)	1.081
	C4—C3	1.387(6)	1.392
	C4—N2	1.453(2)	1.456
	C6—C1	1.442(6)	1.457

C6—N3	1.451(4)	1.457
C3—C2	1.366(3)	1.382
C3—H3	0.930(2)	1.081
C1—C2	1.450(3)	1.457
C2—N1	1.459(6)	1.459
N3—O7	1.208(2)	1.239
N3—O6	1.218(6)	1.231
N2—O4	1.221(4)	1.233
N2—O5	1.227(6)	1.233
N1—O3	1.205(4)	1.231
N1—O2	1.209(3)	1.239
O11—C8	1.297(5)	1.335
O11—H11	0.821(1)	0.967
N6—C8	1.305(3)	1.315
N6—H6A	0.861(2)	1.034
N6—H6B	0.860(3)	1.008
C8—N7	1.304(3)	1.321
N7—H7A	0.860(3)	1.041
N7—H7B	0.860(3)	1.007
Bond Angles		
C6—C5—C4	119.72(17)	119.66
C6—C5—H5	120.16(17)	120.09
C4—C5—H5	120.13(17)	120.24
C5—C4—C3	121.08(17)	121.05
C5—C4—N2	119.63(16)	119.46
C3—C4—N2	119.28(16)	121.05
C5—C6—C1	123.68(17)	123.20
C5—C6—N3	116.37(16)	116.09
C1—C6—N3	119.95(15)	120.69
C2—C3—C4	118.84(17)	119.61
C2—C3—H3	120.55(18)	120.12
C4—C3—H3	120.61(19)	120.25
O1—C1—C6	125.63(17)	123.67
O1—C1—C2	122.32(17)	123.12
C6—C1—C2	112.04(16)	113.13
C3—C2—C1	124.37(17)	123.27
C3—C2—N1	116.33(17)	116.11
C1—C2—N1	119.28(16)	120.61
O7—N3—O6	121.10(18)	122.79
O7—N3—C6	121.21(16)	119.29
O6—N3—C6	117.68(16)	117.89
O4—N2—O5	123.73(19)	124.63
O4—N2—C4	118.47(16)	117.67
O5—N2—C4	117.80(16)	117.68
O3—N1—O2	122.13(20)	122.78
O3—N1—C2	118.88(17)	117.76

	O2—N1—C2	118.95(18)	119.43
	C8—O11—H11	109.49(16)	111.64
	C8—N6—H6A	119.96(19)	119.84
	C8—N6—H6B	120.01(19)	119.07
	H6A—N6—H6B	120.03(21)	121.08
	O11—C8—N7	115.74(18)	115.55
	O11—C8—N6	121.42(18)	121.97
	N7—C8—N6	122.84(19)	122.46
	C8—N7—H7A	120.08(20)	120.20
	C8—N7—H7B	120.04(20)	121.50
	H7A—N7—H7B	119.87(25)	118.91
10.	[PA⁻.3,5-diamino-1,2,4-triazolium] (4I)		
	Bond Lengths		
	O1—C3	1.252(3)	1.252
	O2—N6	1.224(7)	1.249
	O3—N6	1.236(4)	1.229
	O4—N7	1.231(4)	1.233
	O5—N7	1.225(16)	1.232
	O6—N8	1.223(11)	1.231
	O7—N8	1.226(3)	1.235
	N1—C1	1.345(22)	1.343
	N1—C2	1.378(5)	1.385
	N1—H1	0.877(25)	1.054
	N2—C1	1.325(6)	1.347
	N2—N3	1.397(13)	1.397
	N2—H2	0.894(25)	1.006
	N3—C2	1.308(9)	1.317
	N4—C2	1.341(20)	1.347
	N4—H4A	0.867(25)	1.018
	N4—H4B	0.867(27)	1.007
	N5—C1	1.318(4)	1.347
	N5—H5A	0.861(14)	1.007
	N5—H5B	0.860(3)	1.019
	N6—C4	1.448(21)	1.444
	N7—C6	1.445(3)	1.456
	N8—C8	1.460(7)	1.463
	C3—C8	1.443(23)	1.457
	C3—C4	1.454(8)	1.461
	C4—C5	1.375(3)	1.388
	C5—C6	1.379(21)	1.387
	C5—H5	0.929(4)	1.081
	C6—C7	1.391(7)	1.398
	C7—C8	1.359(3)	1.377
	C7—H7	0.929(14)	1.082
	Bond Angles		
	C1—N1—C2	107.21(15)	107.14

	C1—N1—H1	124.65(164)	129.69
	C2—N1—H1	128.11(160)	122.95
	C1—N2—N3	111.88(14)	112.49
	C1—N2—H2	126.15(137)	128.26
	N3—N2—H2	121.68(144)	119.19
	C2—N3—N2	103.32(15)	102.55
	C2—N4—H4A	119.38(159)	118.46
	C2—N4—H4B	121.31(170)	117.45
	H4A—N4—H4B	117.05(240)	118.41
	C1—N5—H5A	120.00(17)	118.64
	C1—N5—H5B	120.05(16)	118.04
	H5A—N5—H5B	119.95(19)	117.23
	O2—N6—O3	122.38(16)	122.41
	O2—N6—C4	120.05(16)	119.36
	O3—N6—C4	117.56(14)	118.19
	O5—N7—O4	122.64(16)	124.67
	O5—N7—C6	118.60(16)	117.61
	O4—N7—C6	118.77(16)	117.71
	O6—N8—O7	123.21(15)	123.48
	O6—N8—C8	117.99(14)	117.41
	O7—N8—C8	118.80(14)	119.07
	N5—C1—N2	129.32(15)	128.52
	N5—C1—N1	124.50(16)	125.48
	N2—C1—N1	106.17(15)	105.93
	N3—C2—N4	126.01(18)	127.38
	N3—C2—N1	111.42(16)	111.87
	N4—C2—N1	122.55(17)	120.72
	O1—C3—C8	123.48(17)	122.33
	O1—C3—C4	124.96(16)	124.62
	C8—C3—C4	111.45(14)	112.93
	C5—C4—N6	117.06(16)	116.18
	C5—C4—C3	123.44(16)	123.12
	N6—C4—C3	119.45(14)	120.69
	C4—C5—C6	120.02(17)	119.61
	C4—C5—H5	120.03(18)	120.18
	C6—C5—H5	119.95(18)	120.19
	C5—C6—C7	120.67(17)	121.09
	C5—C6—N7	120.45(17)	119.42
	C7—C6—N7	118.83(16)	119.46
	C8—C7—C6	118.69(16)	119.60
	C8—C7—H7	120.64(19)	120.19
	C6—C7—H7	120.66(17)	120.20
	C7—C8—C3	125.55(17)	123.48
	C7—C8—N8	116.42(15)	116.47
	C3—C8—N8	117.92(14)	120.03
11.	[PA·1/2cyclohexane-1,2-diaminium] (4m)		

Bond Lengths			
O1—C4	1.256(6)		1.265
O2—N1	1.179(6)		1240
O3—N1	1.217(16)		1.228
O4—N2	1.214(16)		1.231
O5—N2	1.235(7)		1.231
O6—N3	1.232(5)		1.228
O7—N3	1.219(9)		1.241
N1—C5	1.450(5)		1.458
N2—C7	1.442(7)		1.459
N3—C9	1.446(18)		1.457
N4—C3	1.488(7)		1.505
N4—H4A	0.889(8)		1.049
N4—H4B	0.890(4)		1.044
N4—H4C	0.890(3)		1.020
C1—C1 [†]	1.429(14)		1.536
C1—C2	1.466(8)		1.537
C1—H1A	0.969(9)		1.097
C1—H1B	0.971(12)		1.094
C2—C3	1.479(8)		1.532
C2—H2A	0.969(7)		1.097
C2—H2B	0.969(13)		1.096
C3—C3i	1.438(15)		1.540
C3—H3	0.980(9)		1.093
C4—C5	1.449(19)		1.453
C4—C9	1.451(7)		1.452
C5—C6	1.371(7)		1.385
C6—C7	1.376(7)		1.390
C6—H6	0.930(12)		1.082
C7—C8	1.393(18)		1.391
C8—C9	1.360(7)		1.383
C8—H8	0.930(5)		1.082
Bond Angles			
O2—N1—O3	120.23(40)		123.25
O2—N1—C5	121.63(37)		118.56
O3—N1—C5	118.10(29)		118.14
O4—N2—O5	122.38(38)		124.93
O4—N2—C7	119.39(37)		117.51
O5—N2—C7	118.23(37)		117.54
O7—N3—O6	122.37(36)		123.01
O7—N3—C9	119.90(29)		118.77
O6—N3—C9	117.71(30)		118.79
C3—N4—H4A	109.43(37)		112.78
C3—N4—H4B	109.50(31)		111.19
H4A—N4—H4B	109.52(28)		110.62
C3—N4—H4C	109.45(33)		106.68

H4A—N4—H4C	109.47(35)	106.95	
H4B—N4—H4C	109.46(32)	108.44	
C1 ¹ —C1—C2	116.84(45)	111.87	
C1 ¹ —C1—H1A	108.11(51)	110.24	
C2—C1—H1A	108.16(50)	109.57	
C1 ¹ —C1—H1B	107.98(56)	109.48	
C2—C1—H1B	108.08(64)	108.93	
H1A—C1—H1B	107.31(93)	106.56	
C1—C2—C3	113.55(42)	110.23	
C1—C2—H2A	108.8(6)	110.78	
C3—C2—H2A	108.85(55)	110.06	
C1—C2—H2B	108.86(39)	109.40	
C3—C2—H2B	108.90(39)	109.25	
H2A—C2—H2B	107.73(50)	107.04	
C3i—C3—C2	115.9(4)	114.56	
C3i—C3—N4	116.53(39)	115.70	
C2—C3—N4	112.41(35)	112.03	
C3i—C3—H3	103.26(55)	108.95	
C2—C3—H3	103.14(51)	109.61	
N4—C3—H3	103.17(47)	104.84	
O1—C4—C5	125.53(30)	123.27	
O1—C4—C9	122.50(33)	123.62	
C5—C4—C9	111.92(26)	113.01	
C6—C5—C4	123.52(32)	123.44	
C6—C5—N1	116.04(33)	116.03	
C4—C5—N1	120.44(24)	120.51	
C5—C6—C7	119.85(36)	119.48	
C5—C6—H6	120.12(39)	120.20	
C7—C6—H6	120.03(37)	120.30	
C6—C7—C8	121.25(35)	120.98	
C6—C7—N2	120.21(36)	119.48	
C8—C7—N2	118.53(37)	119.52	
C9—C8—C7	118.50(39)	119.62	
C9—C8—H8	120.73(41)	120.06	
C7—C8—H8	120.77(37)	120.30	
C8—C9—N3	115.41(36)	115.92	
C8—C9—C4	124.96(36)	123.25	
N3—C9—C4	119.62(30)	120.81	
12.	[PA⁻.6-phenyl-2,4-diamino-1,3,5-triazinium] (4n)		
	Bond Lengths		
	O1—C1	1.258(7)	1.252
	O2—N1	1.240(8)	1.235
	O3—N1	1.222(9)	1.231
	O4—N2	1.206(7)	1.232
	O5—N2	1.241(8)	1.232
	O6—N3	1.235(8)	1.229

O7—N3	1.241(8)	1.248
N1—C2	1.453(9)	1.463
N2—C4	1.449(8)	1.457
N3—C6	1.444(7)	1.444
N4—C7	1.318(8)	1.341
N4—C8	1.327(8)	1.335
N5—C9	1.332(9)	1.332
N5—C7	1.349(9)	1.346
N6—C9	1.348(8)	1.367
N6—C8	1.360(9)	1.374
N6—H6	0.810(61)	1.044
N7—C8	1.308(9)	1.326
N7—H7A	0.859(6)	1.008
N7—H7B	0.860(6)	1.026
N8—C9	1.315(9)	1.333
N8—H8A	0.861(5)	1.007
N8—H8B	0.860(6)	1.019
C1—C2	1.444(9)	1.458
C1—C6	1.445(9)	1.461
C2—C3	1.371(8)	1.379
C3—C4	1.393(9)	1.396
C3—H3A	0.930(6)	1.082
C4—C5	1.375(8)	1.388
C5—C6	1.377(8)	1.387
C5—H5A	0.931(6)	1.082
C7—C10	1.494(9)	1.477
C10—C11	1.395(9)	1.404
C10—C15	1.401(9)	1.404
C11—C12	1.383(8)	1.391
C11—H11	0.930(7)	1.083
C12—C13	1.395(10)	1.397
C12—H12	0.930(6)	1.085
C13—C14	1.378(10)	1.397
C13—H13	0.930(6)	1.086
C14—C15	1.401(8)	1.391
C14—H14	0.930(7)	1.085
C15—H15	0.930(6)	1.083
Bond Angles		
O3—N1—O2	122.62(43)	123.21
O3—N1—C2	118.38(39)	117.41
O2—N1—C2	118.99(40)	119.35
O4—N2—O5	123.95(46)	124.73
O4—N2—C4	118.93(43)	117.61
O5—N2—C4	117.12(40)	117.64
O6—N3—O7	122.42(43)	122.55
O6—N3—C6	118.20(38)	119.17

O7—N3—C6	119.38(40)	118.26
C7—N4—C8	116.14(42)	116.05
C9—N5—C7	115.13(42)	116.54
C9—N6—C8	119.08(40)	118.56
C9—N6—H6	129.56(402)	128.50
C8—N6—H6	111.05(409)	117.91
C8—N7—H7A	120.09(49)	117.08
C8—N7—H7B	119.95(49)	121.87
H7A—N7—H7B	119.96(52)	120.97
C9—N8—H8A	119.99(43)	116.67
C9—N8—H8B	120.02(47)	122.22
H8A—N8—H8B	119.99(48)	121.08
O1—C1—C2	122.97(41)	123.13
O1—C1—C6	125.04(40)	123.93
C2—C1—C6	111.77(40)	112.93
C3—C2—C1	125.32(43)	123.28
C3—C2—N1	115.86(40)	116.13
C1—C2—N1	118.58(40)	120.57
C2—C3—C4	118.33(42)	119.80
C2—C3—H3A	120.84(48)	120.04
C4—C3—H3A	120.84(51)	120.14
C5—C4—C3	120.77(44)	121.07
C5—C4—N2	120.80(42)	119.45
C3—C4—N2	118.36(40)	119.47
C4—C5—C6	120.24(43)	119.47
C4—C5—H5A	119.89(46)	120.28
C6—C5—H5A	119.87(45)	120.23
C5—C6—N3	117.32(41)	116.24
C5—C6—C1	123.51(41)	123.38
N3—C6—C1	119.1(4)	120.35
N4—C7—N5	126.59(48)	125.45
N4—C7—C10	115.71(43)	117.34
N5—C7—C10	117.68(41)	117.20
N7—C8—N4	119.65(44)	120.51
N7—C8—N6	119.03(43)	118.26
N4—C8—N6	121.31(43)	121.21
N8—C9—N5	119.97(44)	119.70
N8—C9—N6	118.36(42)	118.72
N5—C9—N6	121.66(43)	121.56
C11—C10—C15	119.20(45)	119.46
C11—C10—C7	122.01(42)	120.31
C15—C10—C7	118.62(41)	120.22
C12—C11—C10	121.42(44)	120.14
C12—C11—H11	119.30(46)	120.89
C10—C11—H11	119.28(52)	118.95
C11—C12—C13	118.79(43)	120.09

C11—C12—H12	120.57(48)	119.81
C13—C12—H12	120.64(53)	120.08
C14—C13—C12	120.98(51)	120.03
C14—C13—H13	119.51(48)	119.97
C12—C13—H13	119.50(46)	119.98
C13—C14—C15	120.12(45)	120.10
C13—C14—H14	119.9(6)	120.08
C15—C14—H14	119.97(46)	119.81
C14—C15—C10	119.47(43)	120.14
C14—C15—H15	120.20(48)	120.92
C10—C15—H15	120.33(52)	118.93

Table 4.17: TG-DTG-DTA phenomenological data of 4c-4n under air atmosphere

S. N	Stage	TG		DTA		DTG
		T range / °C	Observed mass loss (%)	Peak temp. / °C	nature	Peak temp. / °C
1.	[2PA⁻.2PzH₂⁺.OH₂] (4c)					
	I	71-205	23.4	159	endo	135
	II	205-279	72.8	280	exo	268
2.	[PA⁻.Pz^{Me2}H₂⁺] (4d)					
	I	92-200	28.2	102	endo	190
	II	200-324	68.5	278	exo	271
3.	[PA⁻.Pz^{Ph,Me}H₂⁺.CH₃OH] (4e)					
	I	101-225	7.1	162	endo	161
	II	225-295	52.8	281	exo	275
	III	505-666	35.9	589	exo	592
4.	[2PA⁻.2H₂dmpzH⁺.CH₃CN] (4f)					
	I	99-151	4.6	154	endo	147
	II	240-289	49.7	293	exo	282
	III	289-689	45.1	686	exo	678
5.	[PA⁻.phenH⁺.CH₃OH] (4g)					
	I	100-200	7.0	206	endo	215

	II	250-337	49.1	319	exo	320
	III	337-600	41.8	537	exo	549
6.	[2PA⁻.terpyH₂⁺²] (4h)					
	I	200-314	62.1	301	exo	299
	II	420-620	34.2	531	exo	536
7.	[PA.hmta] (4i)					
	I	178-342	60.3	270	exo	267
	II	512-711	36.4	585	exo	555
8.	[3PA⁻.tptzH₃³⁺] (4j)					
	I	175-306	94.5	301	exo	295
9.	[PA⁻.Uronium] (4k)					
	I	136-264	76.2	188°C	exo	205
	II	264-412	20.4	312°C	exo	324
10.	[PA⁻.3,5-diamino-1,2,4-triazolium] (4l)					
	I	225-330	68.1	264°C	exo	262
	II	455-689	30.3	677°C	exo	666
11.	[PA⁻.1/2cyclohexane-1,2-diaminium] (4m)					
	I	200-327	76.4	301°C	exo	299
	II	470-620	19.2	531°C	exo	536
12.	[PA⁻.6-phenyl-2,4-diamino-1,3,5-triazinium] (4n)					
	I	221-322	51.4	299°C	exo	300
	II	524-634	43.6	588°C	exo	617

Table 4.18: Set of reaction models applied to describe thermal decomposition of solids

Model no.	Reaction model	$f(\alpha)$	$g(\alpha)$
1.	Power law	$4 \alpha^{3/4}$	$\alpha^{1/4}$
2.	Power law	$3 \alpha^{2/3}$	$\alpha^{1/3}$
3.	Power law	$2 \alpha^{1/2}$	$\alpha^{1/2}$
4.	Power law	$2/3 \alpha^{-1/2}$	$\alpha^{3/2}$
5.	One-dimensional diffusion	$1/2 \alpha^{-1}$	α^2
6.	Mampel (first order)	$1 - \alpha$	$-\ln(1 - \alpha)$
7.	Avrami-Erofeev	$4(1 - \alpha)[- \ln(1 - \alpha)]^{3/4}$	$[- \ln(1 - \alpha)]^{1/4}$
8.	Avrami-Erofeev	$3(1 - \alpha)[- \ln(1 - \alpha)]^{2/3}$	$[- \ln(1 - \alpha)]^{1/3}$
9.	Avrami-Erofeev	$2(1 - \alpha)[- \ln(1 - \alpha)]^{1/2}$	$[- \ln(1 - \alpha)]^{1/2}$
10.	Contracting sphere	$3(1 - \alpha)^{2/3}$	$1 - (1 - \alpha)^{1/3}$
11.	Three-dimensional diffusion	$2(1 - \alpha)^{2/3} [1 - (1 - \alpha)^{1/3}]^{-1}$	$[1 - (1 - \alpha)^{1/3}]^2$
12.	Contracting cylinder	$2(1 - \alpha)^{1/2}$	$1 - (1 - \alpha)^{1/2}$
13.	Prout-Tomkins	$\alpha (1 - \alpha)$	$\ln(\alpha / 1 - \alpha)$
14.	Ginstling-Brounshtein	$3/2[(1 - \alpha)^{-1/3} - 1]^{-1}$	$[1 - (2\alpha / 3)] - (1 - \alpha)^{2/3}$

Table 4.19: Arrhenius parameters for isothermal decomposition of 4c-4f

Salts	(4c)		(4d)		(4e)		(4f)	
	E_a	r	E_a	r	E_a	r	E_a	r
1	61.5	0.971	66.0	0.998	62.8	0.964	60.5	0.948
2	61.3	0.972	65.8	0.998	62.9	0.965	60.2	0.949
3	60.9	0.972	65.4	0.998	63.3	0.966	59.4	0.950
4	58.5	0.975	64.3	0.999	65.0	0.972	55.0	0.953
5	57.4	0.976	64.1	0.999	65.8	0.975	53.1	0.953
6	56.2	0.976	64.6	0.999	66.3	0.976	53.9	0.951
7	58.6	0.975	64.6	0.998	64.7	0.971	57.4	0.951
8	59.1	0.974	65.4	0.998	64.4	0.970	58.1	0.949
9	58.3	0.975	65.1	0.999	64.9	0.972	57.1	0.950
10	57.5	0.936	64.6	0.999	65.6	0.974	55.0	0.952
11	54.5	0.975	64.7	0.957	67.9	0.956	50.4	0.888
12	58.0	0.976	64.6	0.999	65.2	0.973	55.6	0.952
13	59.0	0.973	65.9	0.998	64.3	0.969	59.0	0.948
14	55.5	0.977	64.3	0.998	67.0	0.978	51.2	0.951

^a Enumeration of the model is as given in Table 4.18.

E_a = kJ/mol

Table 4.20: Arrhenius parameters for isothermal decomposition of 4g-4j

Salts	(4g)		(4h)		(4i)		(4j)	
	E_a	r	E_a	r	E_a	r	E_a	r
1	81.7	0.997	45.6	0.896	35.4	0.899	38.2	0.980
2	81.6	0.997	45.6	0.897	35.5	0.900	38.1	0.980
3	81.4	0.997	45.4	0.900	35.7	0.900	38.2	0.980
4	80.0	0.997	44.1	0.914	36.7	0.907	38.1	0.983
5	79.3	0.997	43.2	0.919	37.0	0.911	38.2	0.984
6	79.9	0.997	43.5	0.915	36.6	0.908	39.0	0.985
7	80.7	0.997	45.3	0.912	36.0	0.902	38.4	0.983
8	81.1	0.997	44.9	0.903	35.8	0.902	38.5	0.983
9	80.8	0.997	44.6	0.906	36.0	0.903	38.6	0.984
10	80.1	0.997	44.0	0.912	37.3	0.907	38.6	0.985
11	78.6	0.998	41.8	0.905	36.5	0.902	39.7	0.951
12	80.3	0.997	44.2	0.911	36.4	0.906	38.4	0.984
13	81.4	0.997	45.1	0.922	35.5	0.901	38.7	0.983
14	78.7	0.997	42.3	0.923	37.2	0.915	39.0	0.985

Table 4.21: Arrhenius parameters for isothermal decomposition of 4k-4n

Salts	(4k)		(4l)		(4m)		(4n)	
	E_a	r	E_a	r	E_a	r	E_a	r
1	18.4	0.964	51.0	0.701	120.5	0.976	48.6	0.985
2	18.6	0.964	50.9	0.706	120.1	0.976	48.4	0.985
3	18.8	0.964	50.8	0.718	119.1	0.977	48.2	0.984
4	19.7	0.966	49.7	0.777	113.5	0.979	47.3	0.983
5	20.0	0.967	49.1	0.799	110.7	0.980	47.4	0.983
6	20.2	0.967	49.3	0.818	115.0	0.978	47.7	0.983
7	19.6	0.965	50.4	0.771	116.7	0.979	47.6	0.984
8	19.3	0.965	50.4	0.760	119.2	0.977	48.2	0.984
9	19.6	0.966	50.1	0.776	118.2	0.977	48.0	0.984
10	19.9	0.966	49.6	0.795	115.4	0.978	47.6	0.983
11	20.7	0.962	48.3	0.837	110.0	0.915	48.0	0.912
12	19.8	0.966	49.8	0.784	115.6	0.978	47.6	0.983
13	19.3	0.965	50.5	0.759	120.7	0.976	48.6	0.984
14	20.4	0.968	48.5	0.831	109.8	0.980	47.6	0.982

Table 4.22: Ignition delay activation energy for thermal ignition (E^*) and correlation coefficient (r) for salts 4c-4f

S. N	D_i /s at temperature/ °C					$E^*/kJmol^{-1}$ (KJ/mol)	r	OB
	340 ± 1	350 ± 1	360 ± 1	370 ± 1	380 ± 1			
1.	[2PA ⁻ .2PzH ₂ ⁺ .H ₂ O] (4c)							
	109	99	93	82	78	28.58	0.993	-57.6
2.	[PA ⁻ .Pz ^{Me₂} H ₂ ⁺] (4d)							
	97	85	79	74	67	29.30	0.993	-66.17
3.	[PA ⁻ .Pz ^{Ph,Me} H ₂ ⁺ .CH ₃ OH] (4e)							
	107	89	79	68	61	46.45	0.997	-79.78
4.	[2PA ⁻ .2H ₂ dmpzH ⁺ .CH ₃ CN] (4f)							
	112	93	80	77	70	37.75	0.974	-71.5

Table 4.23: Ignition delay activation energy for thermal ignition (E^*) and correlation coefficient (r) for salts 4g-4n

S. N	D_i /s at temperature/ °C					$E^*/kJmol^{-1}$ (KJ/mol)	r	OB
	380 ± 1	390 ± 1	400 ± 1	410 ± 1	420 ± 1			
5.	[PA ⁻ .phenH ⁺ .CH ₃ OH] (4g)							
	163	125	92	80	71	79.6	0.984	-86.17
6.	[2PA ⁻ .terpyH ₂ ⁺²] (4h)							
	118	82	69	53	45	89.2	0.992	-79.85
7.	[PA.hmta] (4i)							
	225	175	128	100	79	99.9	0.999	-59.75
8.	[3PA ⁻ .tptzH ₃ ³⁺] (4j)							
	138	90	67	55	42	108.3	0.992	-72.58
9.	[PA ⁻ .Uronium] (4k)							
	65	48	36	30	24	92.8	0.996	-46.2
10.	[PA ⁻ .3,5-diamino-1,2,4-triazolium] (4l)							
	108	78	65	58	50	69.4	0.980	-38.7
11.	[PA ⁻ .1/2cyclohexane-1,2-diaminium] (4m)							
	78	66	59	54	46	47.3	0.994	-63.3
12.	[PA ⁻ .6-phenyl-2,4-diamino-1,3,5-triazinium] (4n)							
	103	92	81	73	65	43.4	0.999	-66.6

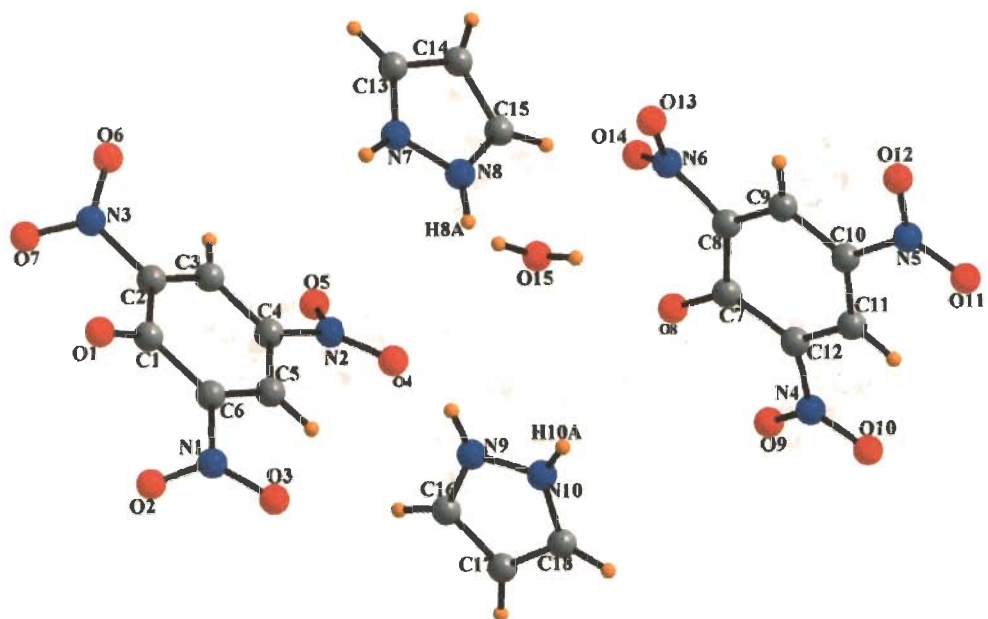


Fig. 4.8: Crystal structure of $[2\text{PA}\cdot 2\text{PzH}_2^+\cdot \text{OH}_2]$ (**4c**). Color code: C, grey; H, orange; O, red; N, blue

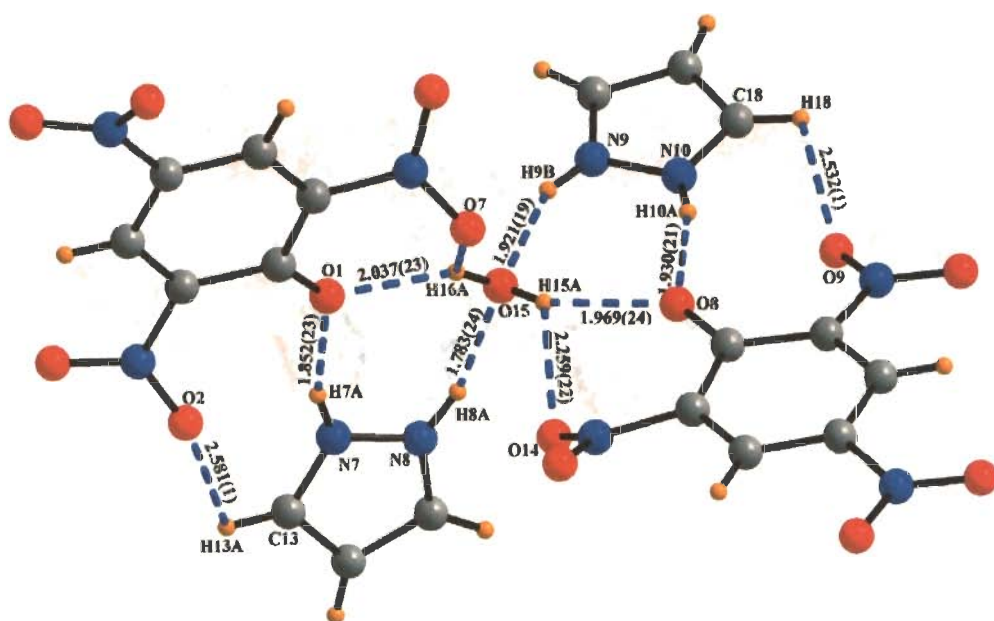


Fig. 4.9: Various N-H \cdots O and O-H \cdots O non-covalent interactions in **4c**. Color code: C, grey; H, orange; O, red; N, blue

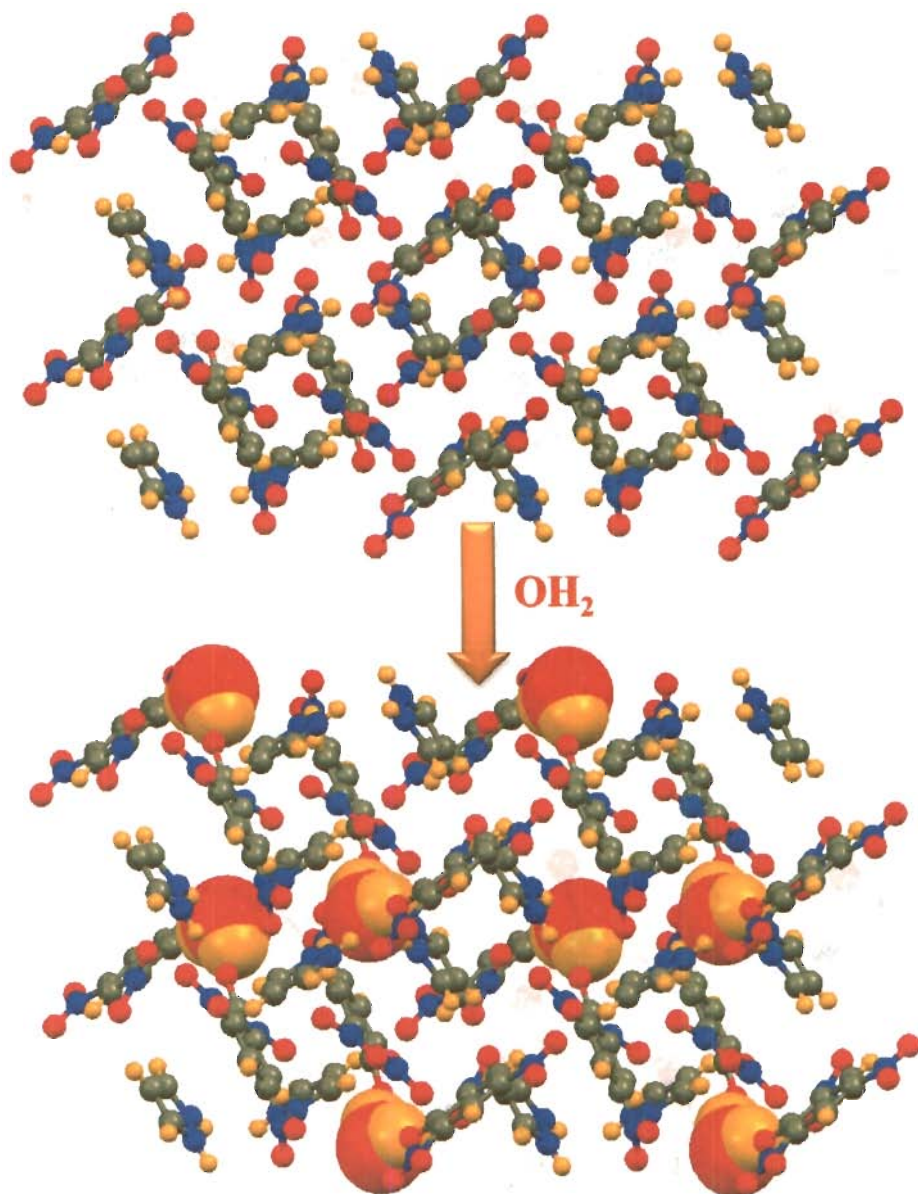


Fig. 4.10: Host-guest supramolecular motif via N-H \cdots O, C-H \cdots O, O-H \cdots O non-covalent interactions in **4c**. Color code: C, grey; H, orange; O, red; N, blue; H $_2$ O, guest

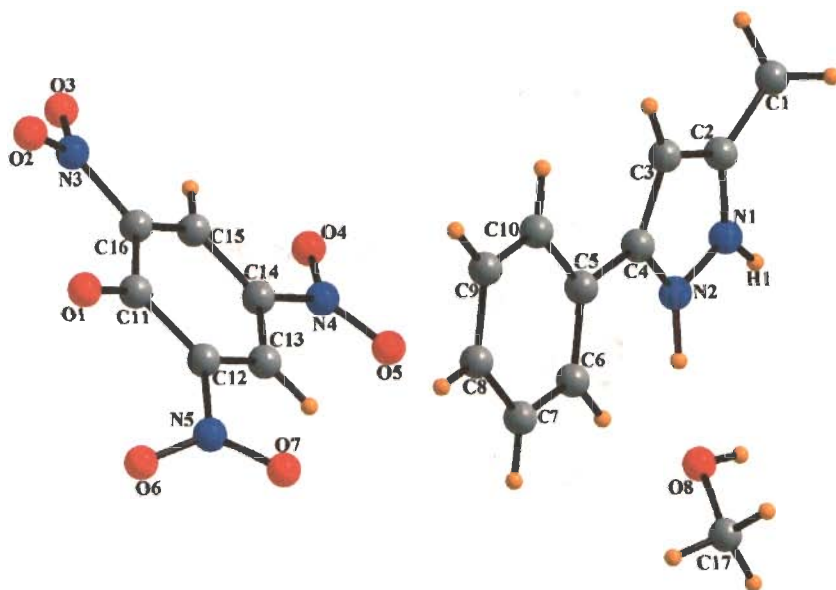


Fig. 4.13: Crystal structure of $[\text{PA}^-\cdot\text{Pz}^{\text{Ph,Me}}\text{H}_2^+\cdot\text{CH}_3\text{OH}]$ (**4e**). Color code: C, grey; H, orange; O, red; N, blue

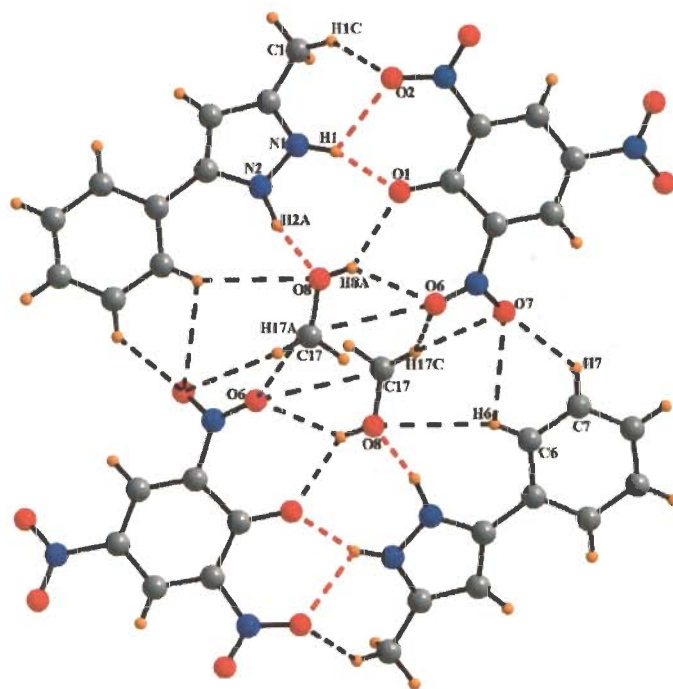


Fig. 4.14: Various N-H...O and C-H...O non-covalent interactions in **4e**. Color code: C, grey; H, orange; O, red; N, blue

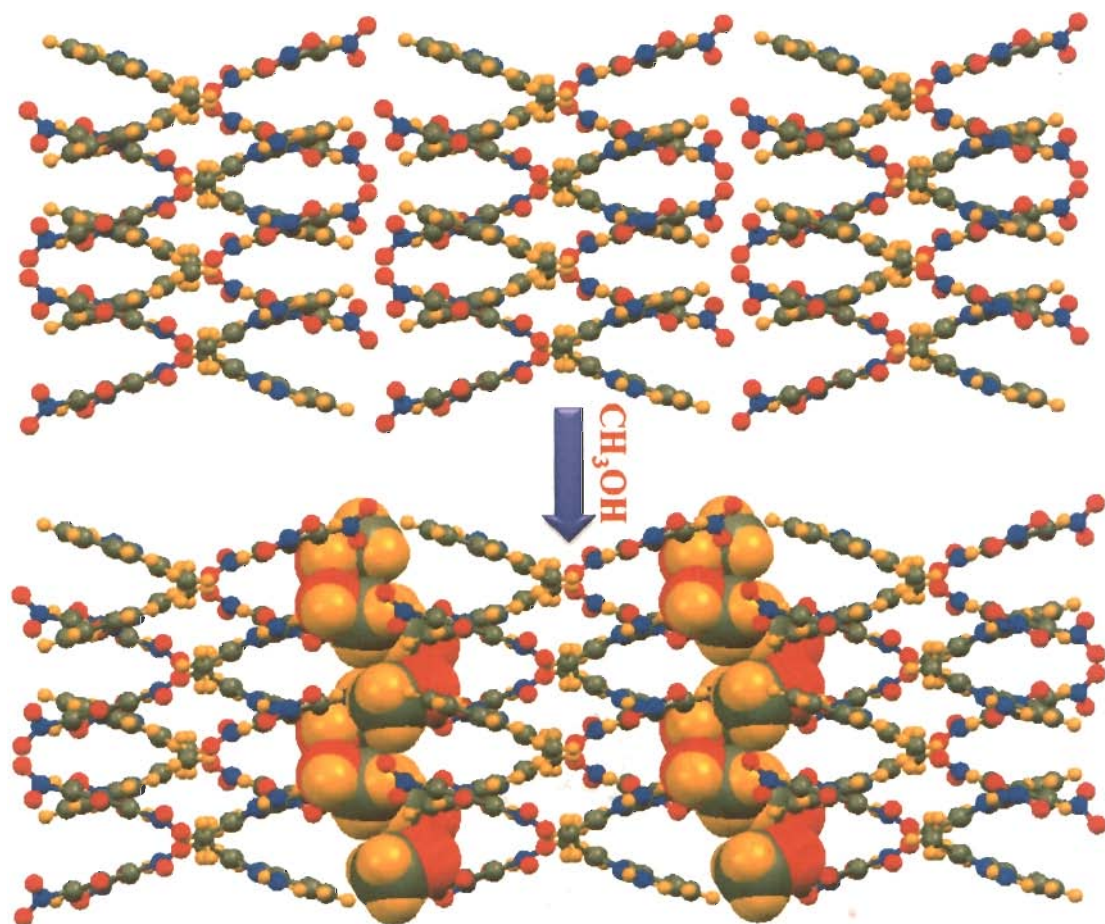


Fig. 4.15: Host-guest supramolecular motif via N-H \cdots O, C-H \cdots O non-covalent interactions in **4e**. Color code: C, grey; H, orange; O, red; N, blue; CH₃OH, guest

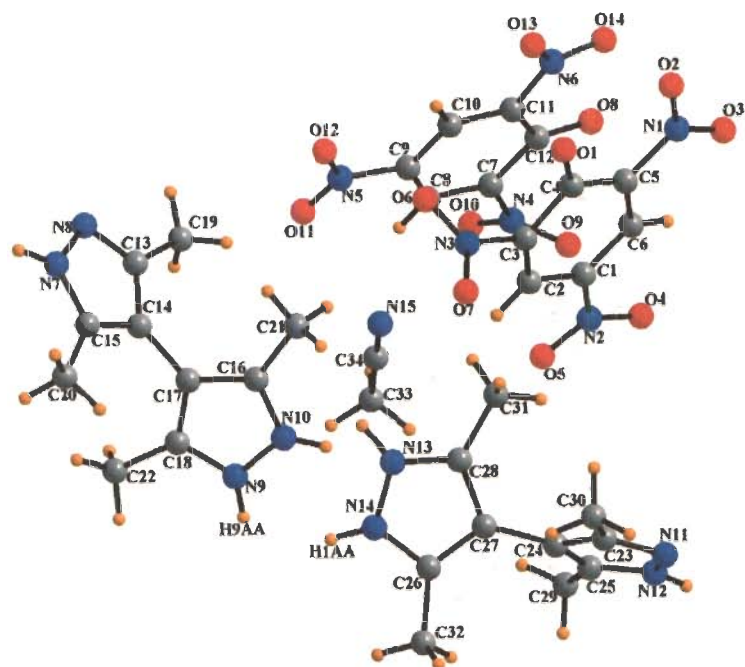


Fig. 4.16: Crystal structure of $[2\text{PA}^-.2\text{H}_2\text{dmPzH}^+.\text{CH}_3\text{CN}]$ (**4f**). Color code: C, grey; H, orange; O, red; N, blue

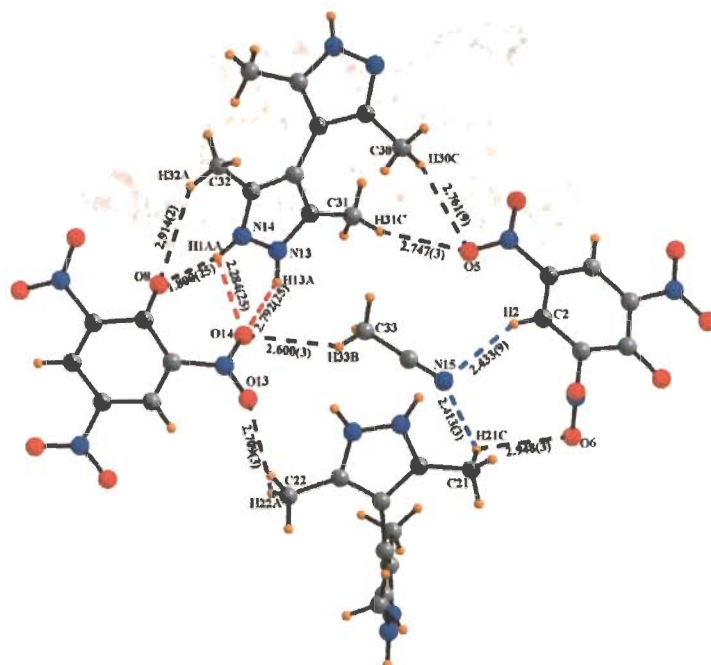


Fig. 4.17: Various N-H...O, C-H...O and C-H...N non-covalent interactions in **4f**. Color code: C, grey; H, orange; O, red; N, blue

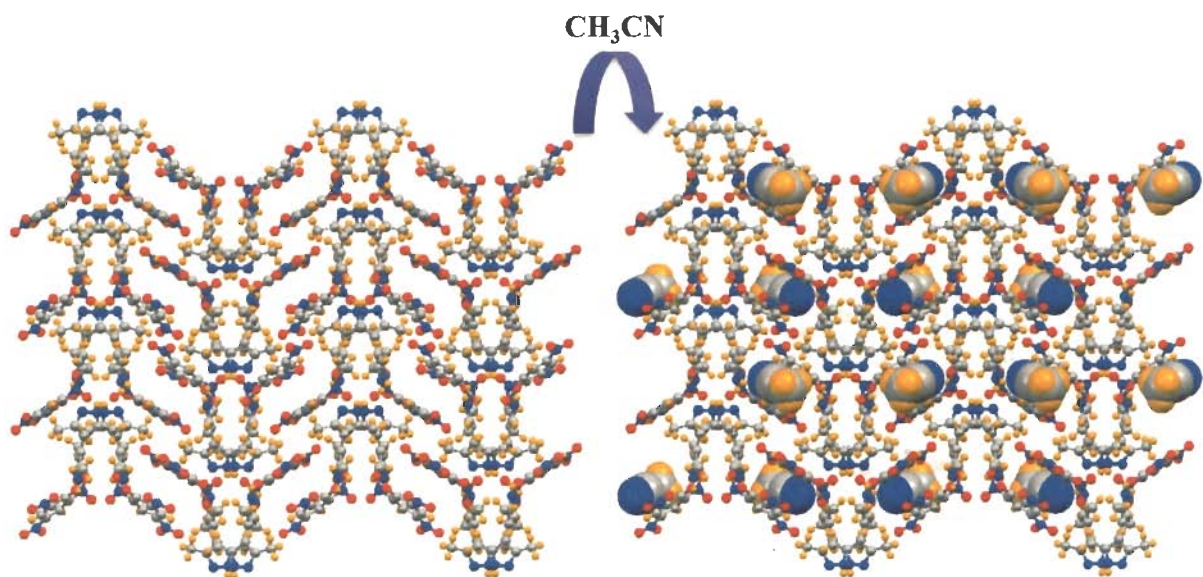


Fig. 4.18: Host-guest supramolecular motif via N-H \cdots O, C-H \cdots O, C-H \cdots N non-covalent interactions in **4f**. Color code: C, grey; H, orange; O, red; N, blue; CH₃CN, guest

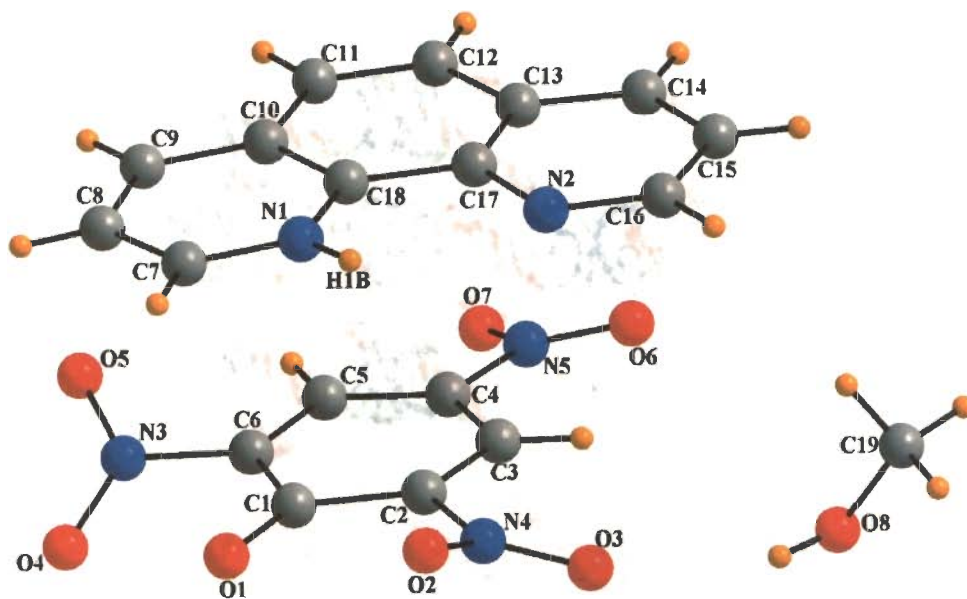


Fig. 4.19: Crystal structure of [PA \cdot phenH⁺·CH₃OH] (**4g**). Color code: C, grey; H, orange; O, red; N, blue

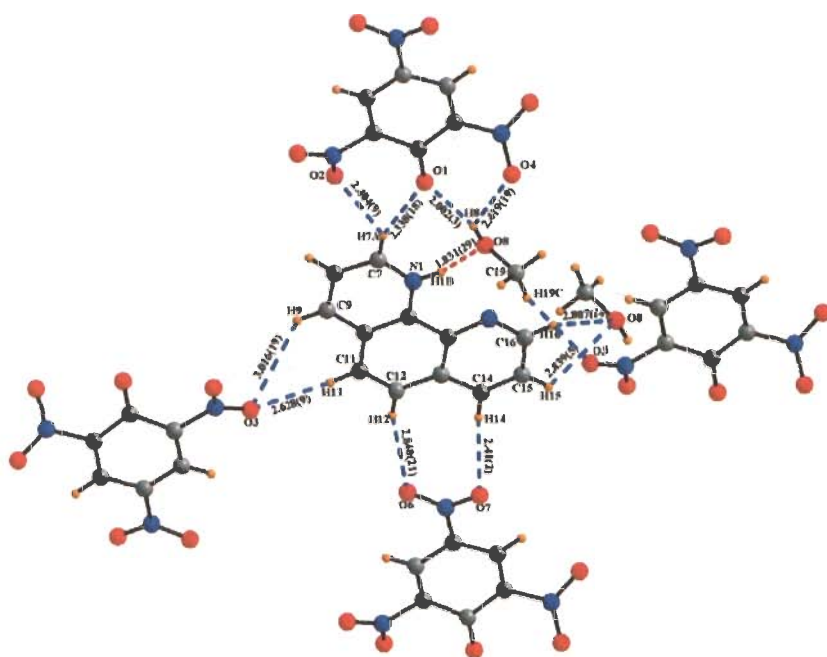


Fig. 4.20: Various non-covalent interactions in **4g**. Color code: C, grey; H, orange; O, red; N, blue

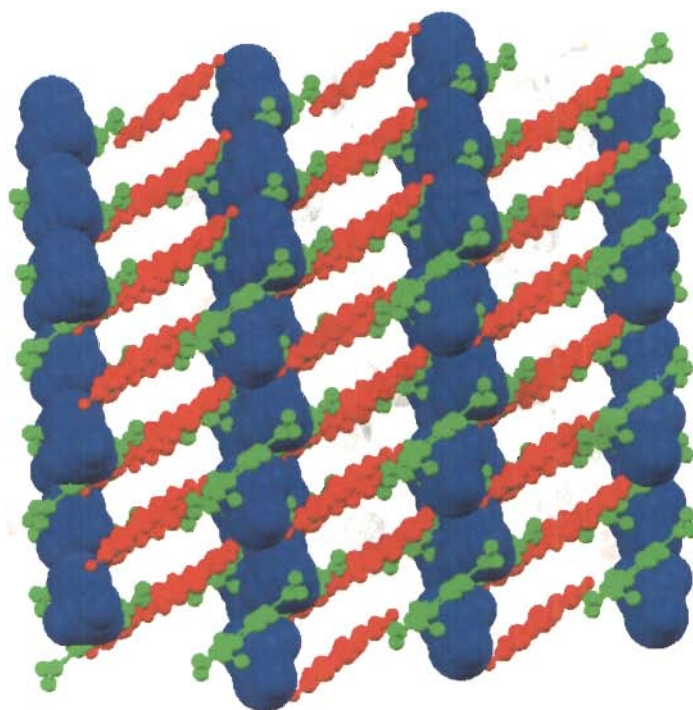


Fig. 4.21: Three dimensional ladders like molecular arrangement in **4g**. Color code: PA⁻, green; phen, red; CH₃OH, blue

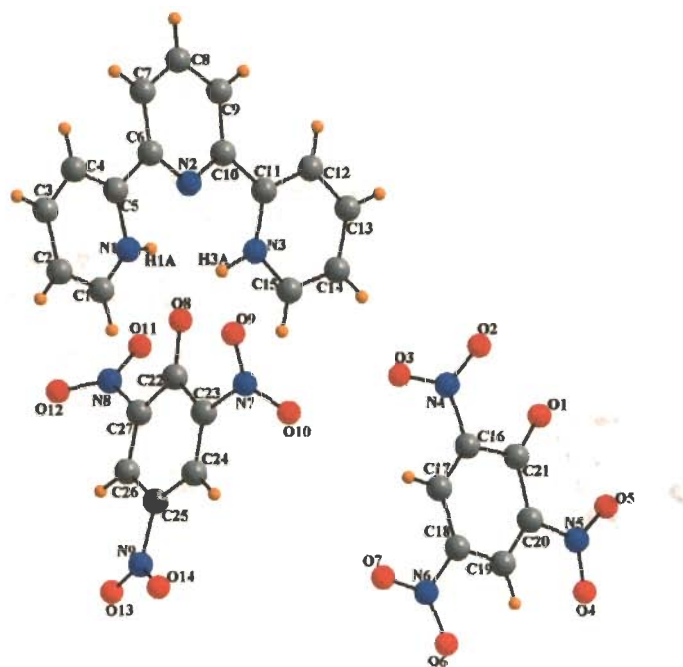


Fig. 4.22: Crystal structure of $[2\text{PA}^{\ominus}.\text{terpyH}_2^{2+}]$ (**4h**). Color code: C, grey; H, orange; O, red; N, blue

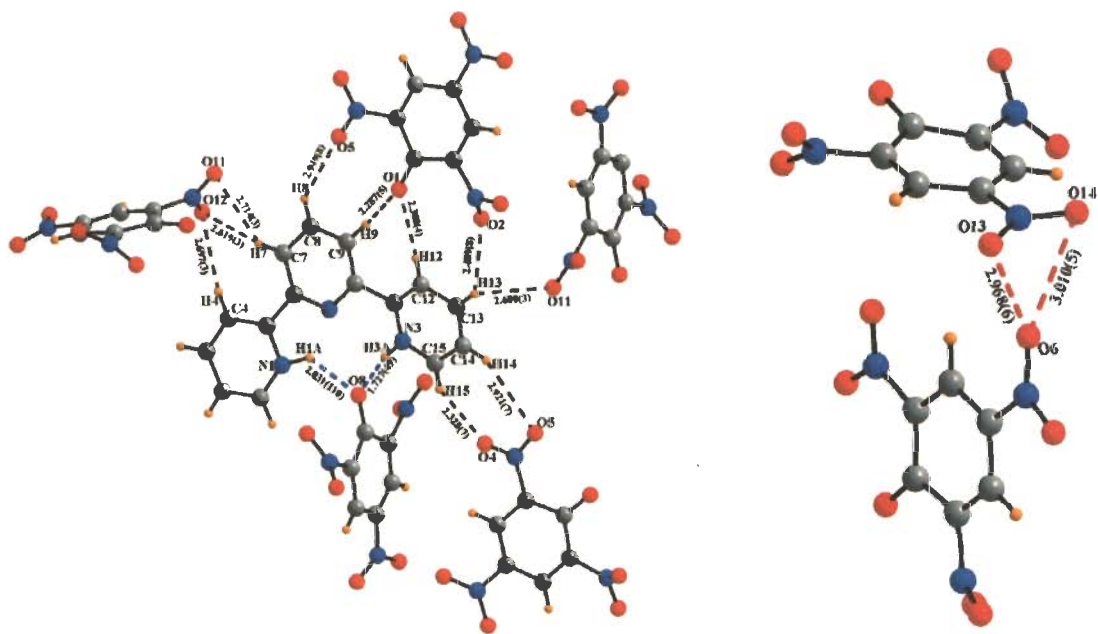


Fig. 4.23: Various non-covalent interactions in **4h**. Color code: C, grey; H, orange; O, red; N, blue

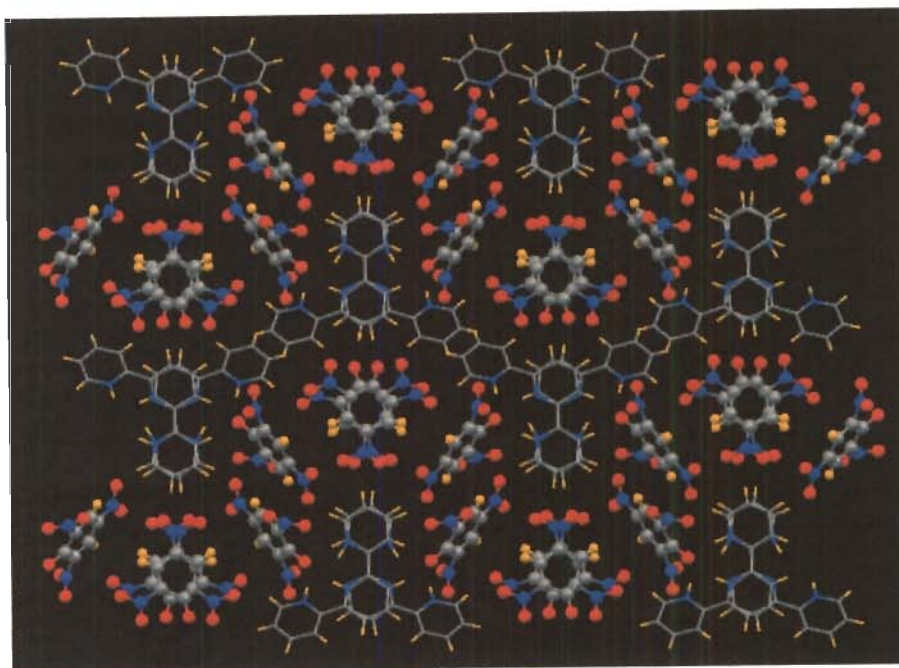


Fig. 4.24: Three dimensional mat like supramolecular motif along the 'c' axis in **4h**. Color code: C, grey; H, orange; O, red; N, blue

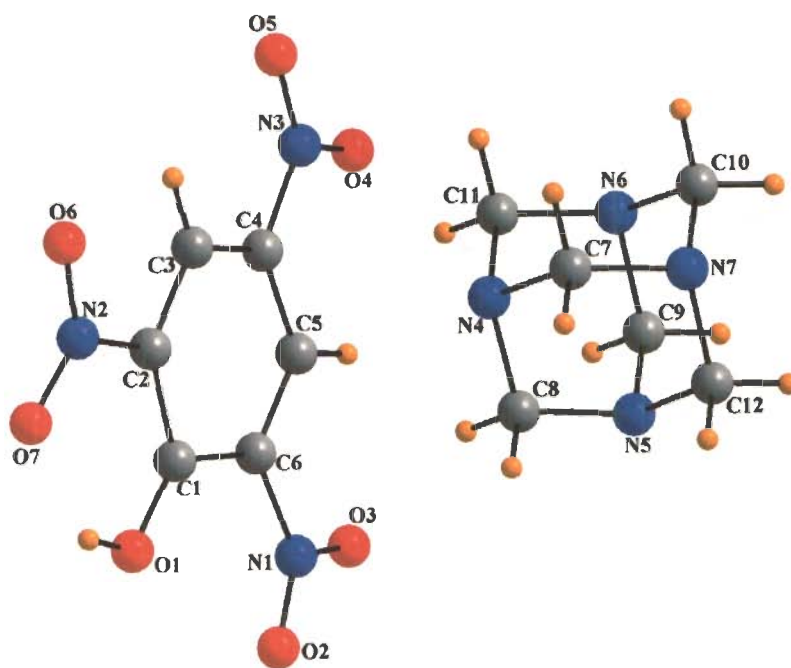


Fig. 4.25: Crystal structure of [PA.hmta] (**4i**). Color code: C, grey; H, orange; O, red; N, blue

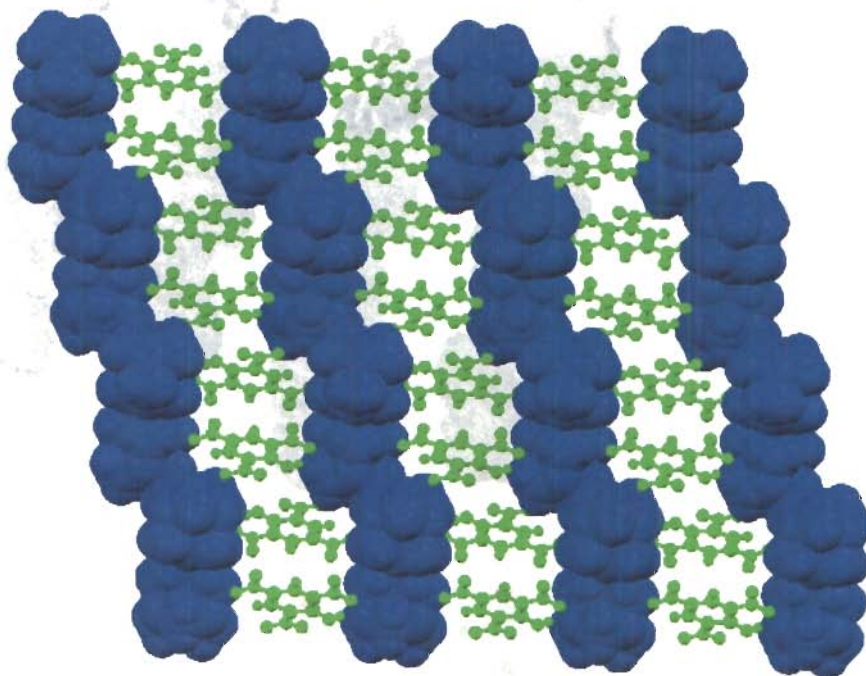


Fig. 4.27: Three dimensional packing in **4i** as alternate channels of picric acid and hmta along the 'b' axis. Color code: PA, green; hmta, blue

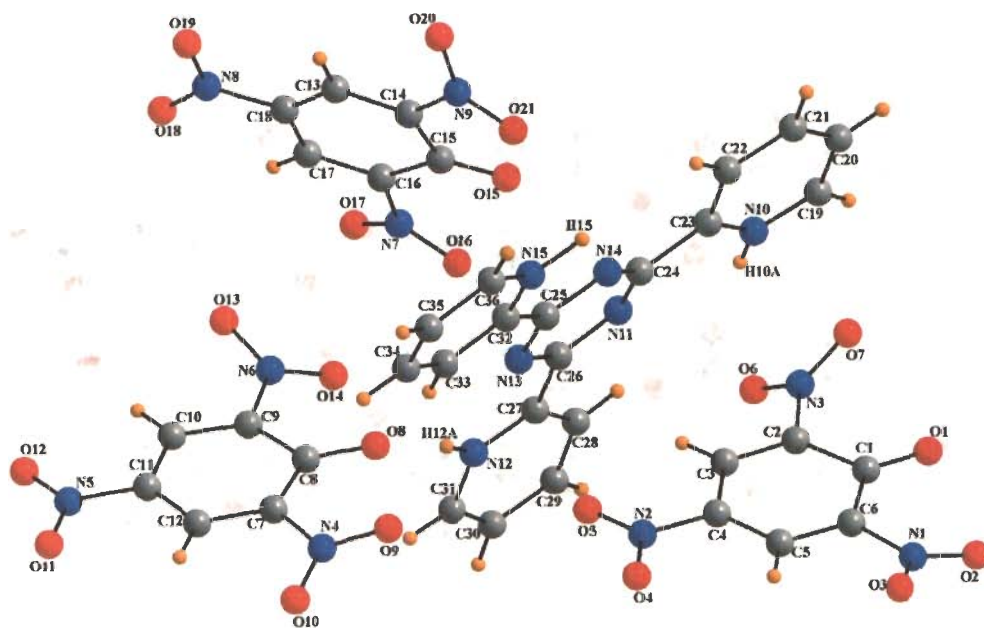


Fig. 4.28: Crystal structure of $[3\text{PA}\cdot\text{tptzH}_3^{+3}]$ (**4j**). Color code: C, grey; H, orange; O, red; N, blue

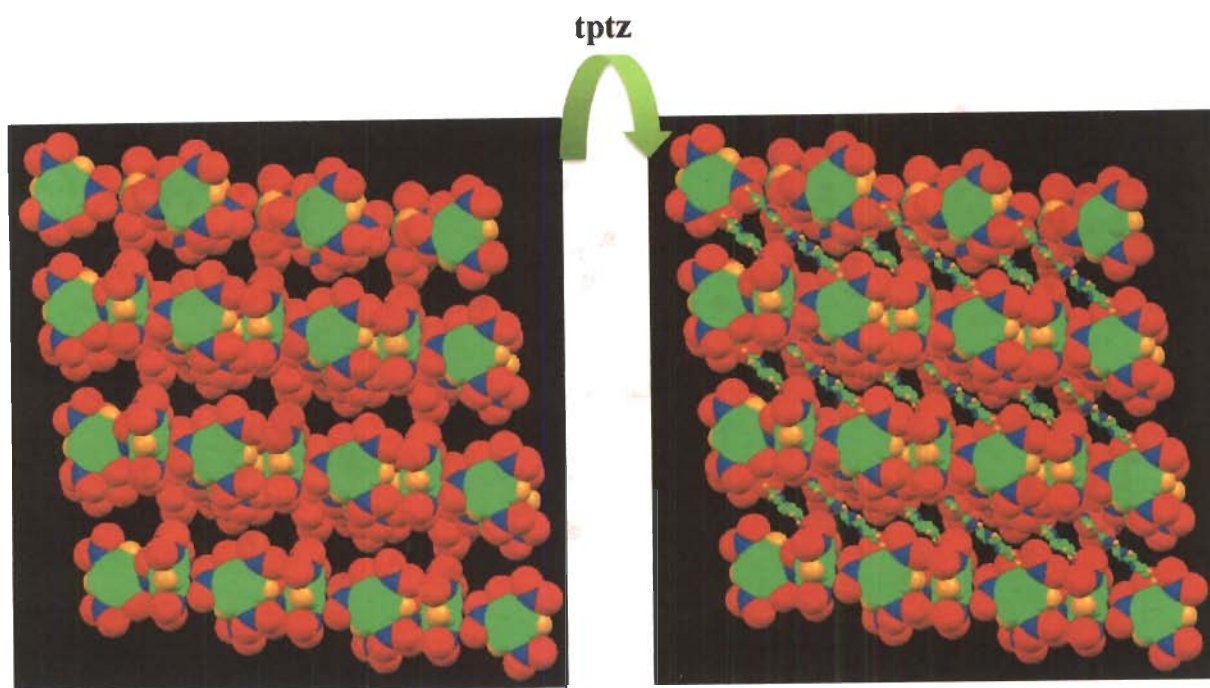


Fig. 4.31: Three dimensional perspective view of cationic-anionic host-guest structure along 'c' axis in **4j**. Color code: C, green; H, orange; O, red; N, blue

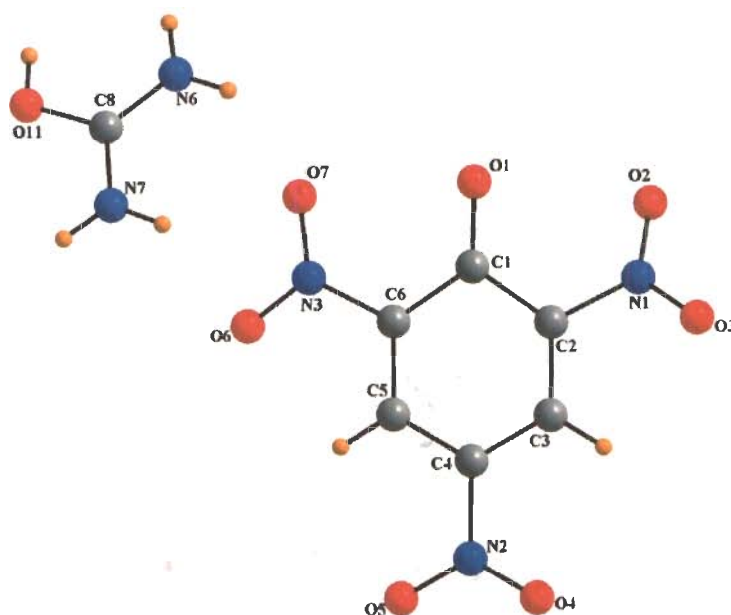
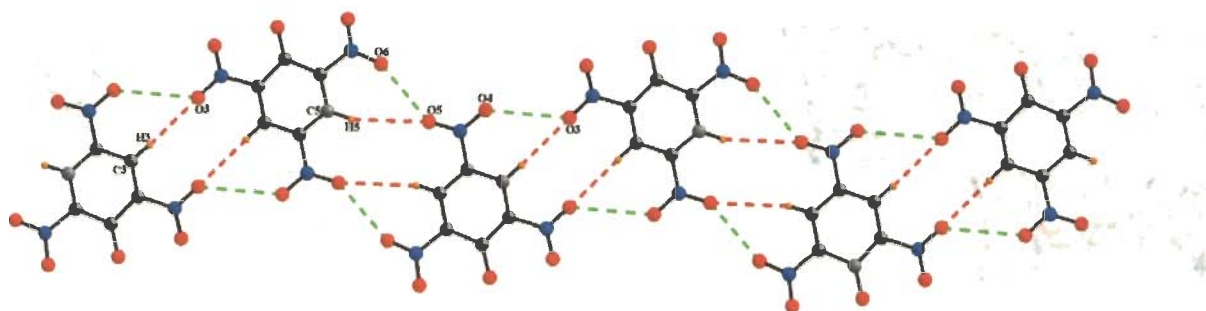
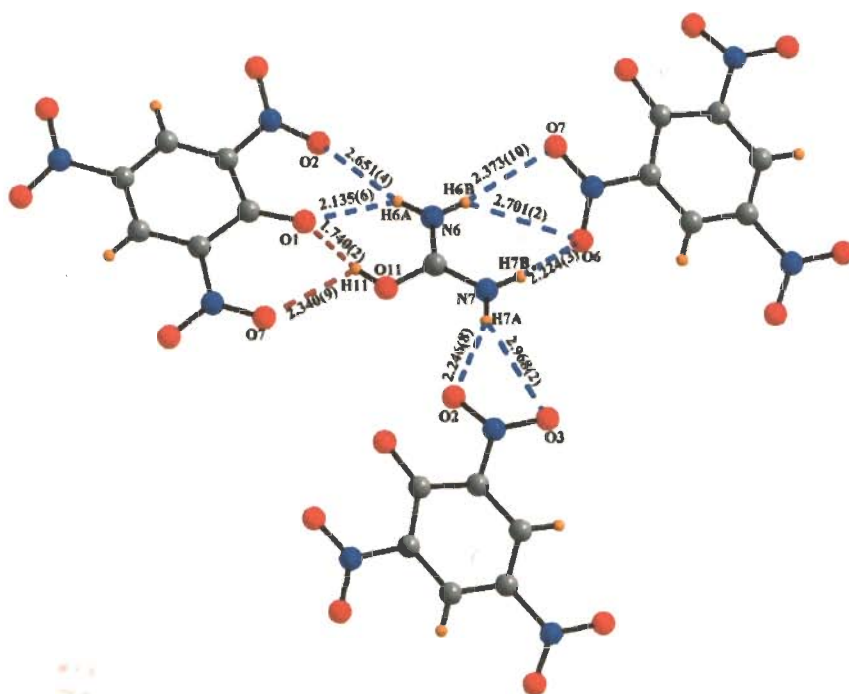


Fig. 4.32: Crystal structure of [PA⁻.Uronium] (**4k**). Color code: C, grey; H, orange; O, red; N, blue



(a)



(b)

Fig. 4.33: (a) One dimensional spiral molecular arrangement among picrates (b) Various N-H...O and O-H...O non-covalent interactions in **4k**. Color code: C, grey; H, orange; O, red; N, blue

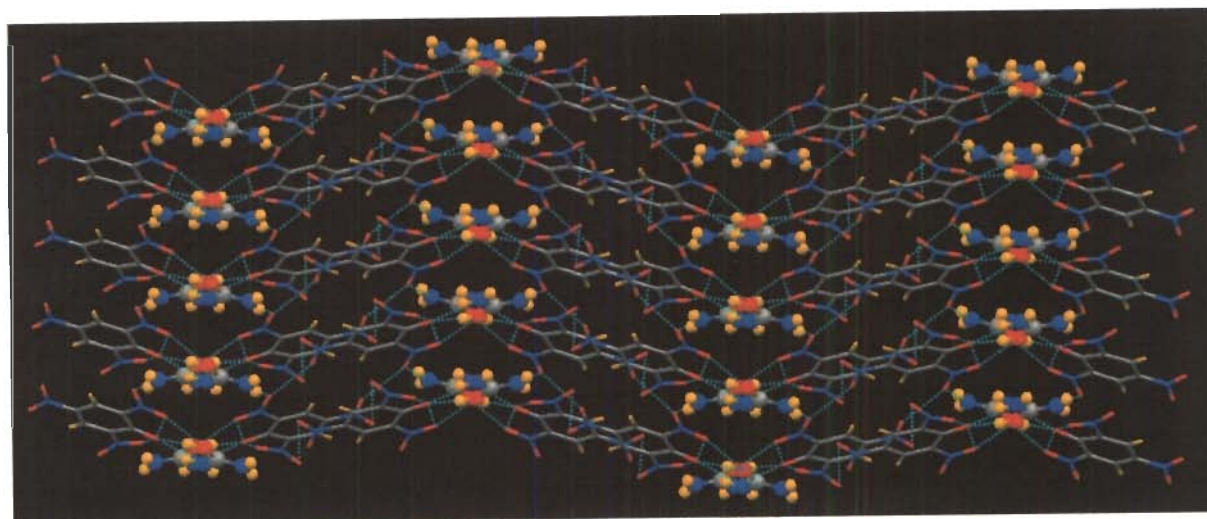


Fig. 4.34: Three dimensional zig-zag molecular arrangement along the 'c' axis in **4k**. Color code: C, grey; H, orange; O, red; N, blue

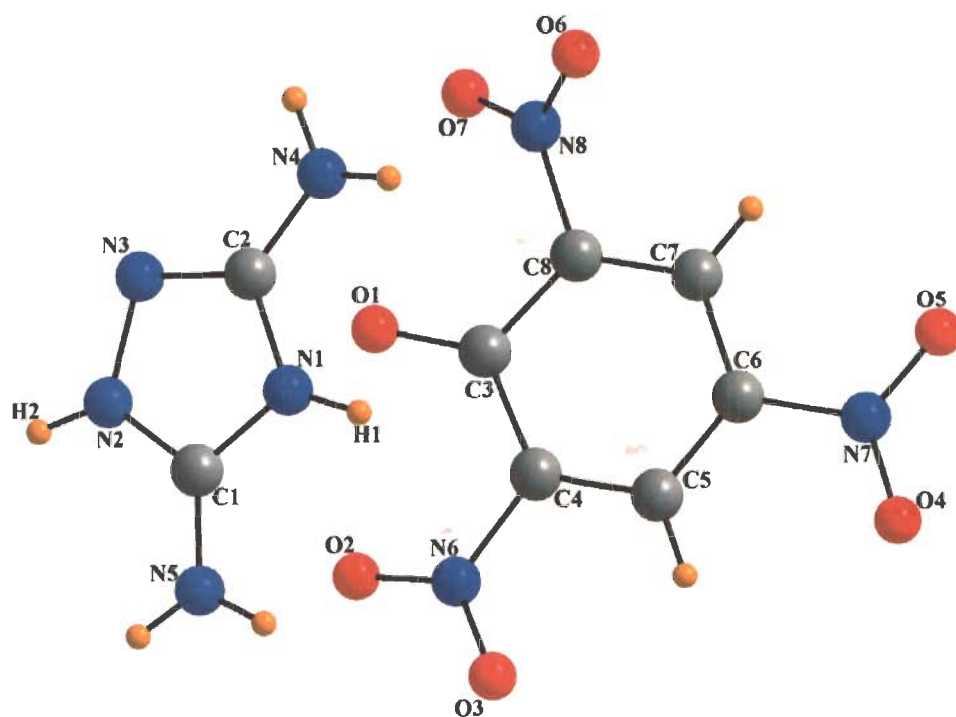
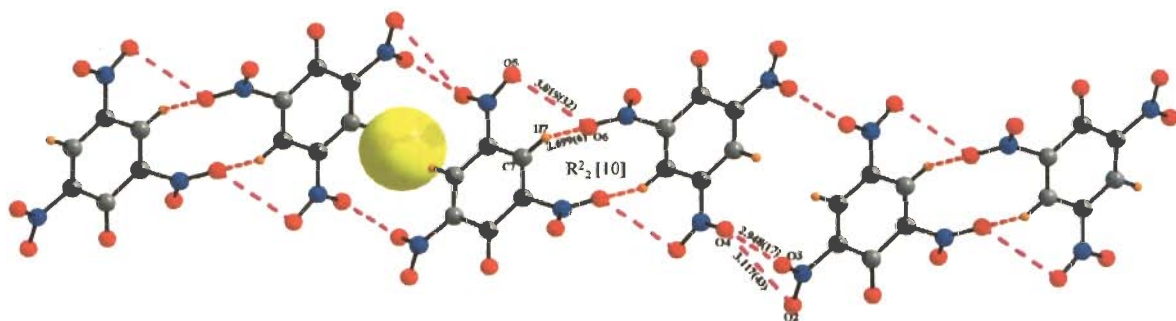
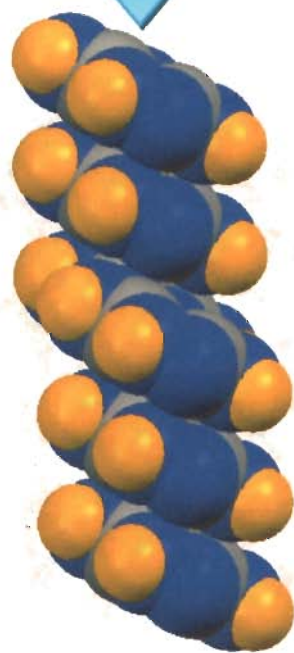
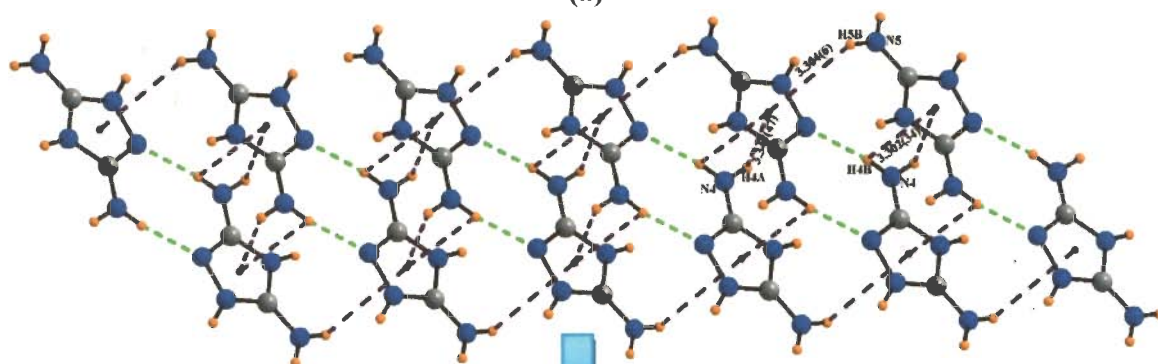


Fig. 4.35: Crystal structure of [PA⁻.3,5-diamino-1,2,4-triazolium] (**4l**). Color code: C, grey; H, orange; O, red; N, blue



(a)



(b)

Fig. 4.36: (a) One dimensional ribbon shaped packing along 'ac' plane among picrates (b) Two dimensional layered along 'c' axis among 3,5-diamino-1,2,4-triazolium in **4I**. Color code: C, grey; H, orange; O, red; N, blue

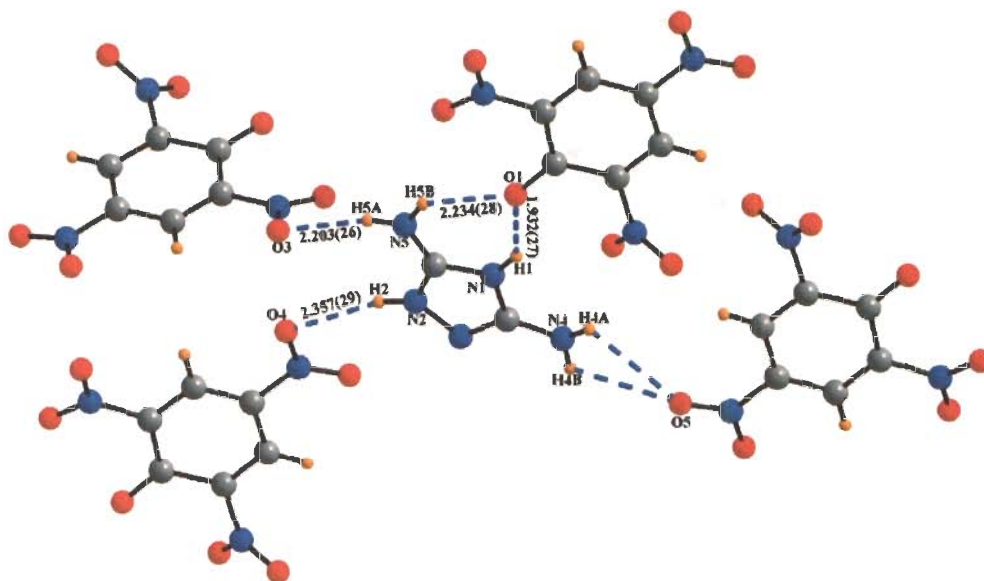


Fig. 4.37: Various N-H...O non-covalent interactions in **4I**. Color code: C, grey; H, orange; O, red; N, blue

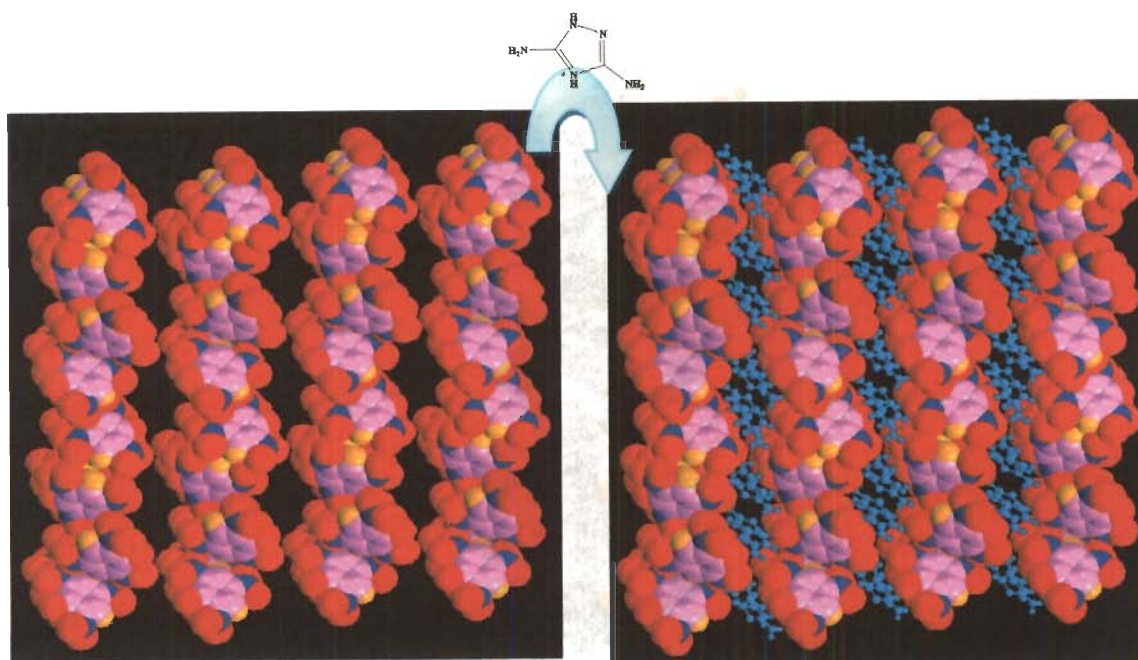


Fig. 4.38: Three dimensional packing as alternate channels of picrates and 3,5-diamino-1,2,4-triazolium along the 'c' axis in **4I**. Color code: C, pink; H, orange; O, red; N, blue; cation, blue

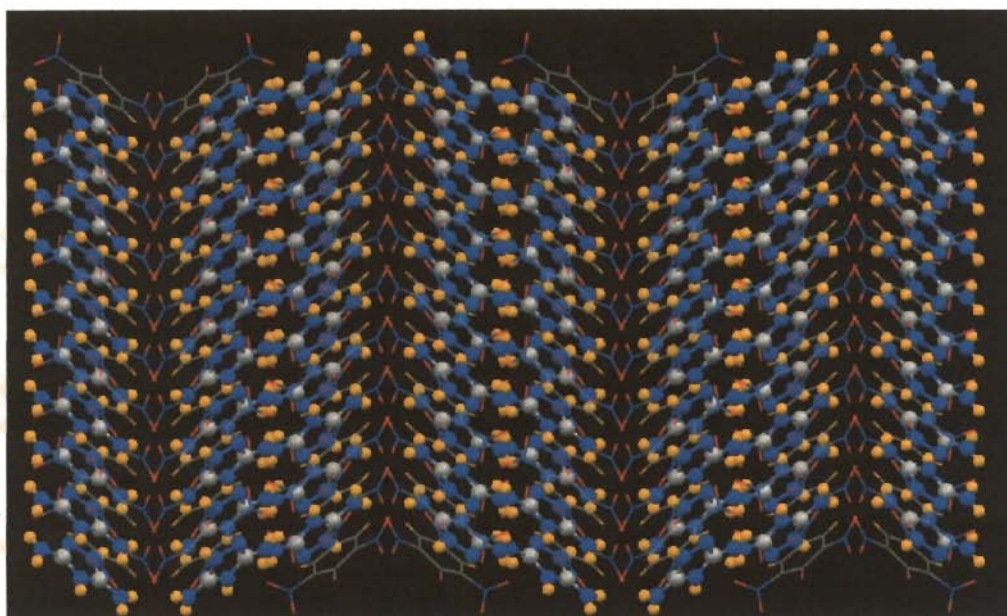


Fig. 4.39: Mat-like supramolecular architecture along the 'a' axis in **4l**. Color code: C, grey; H, orange; O, red; N, blue

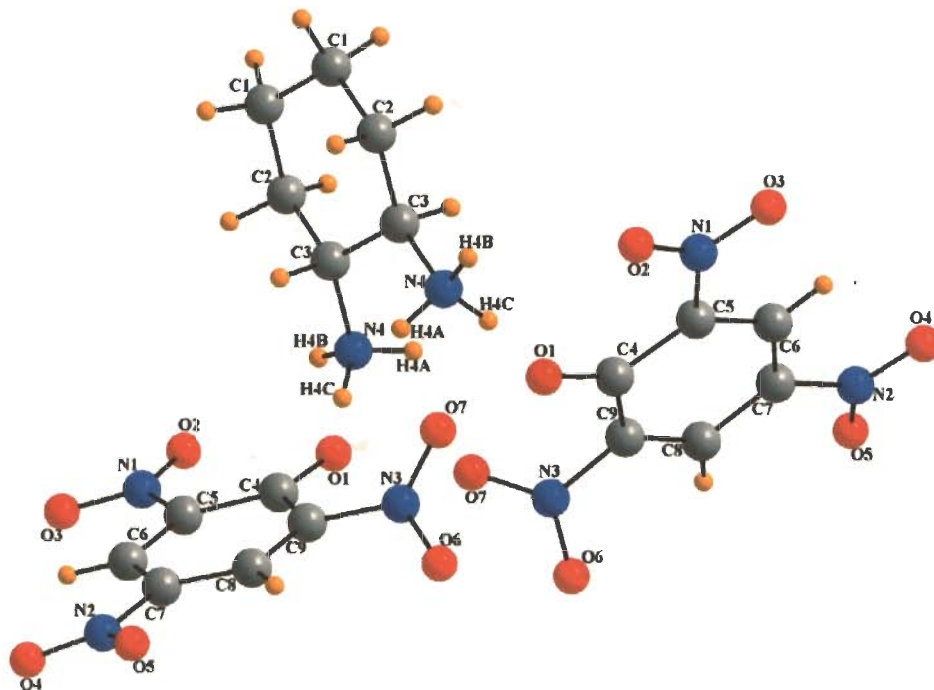


Fig. 4.40: Crystal structure of [PA·1/2cyclohexane-1,2-diaminium] (**4m**). Color code: C, grey; H, orange; O, red; N, blue

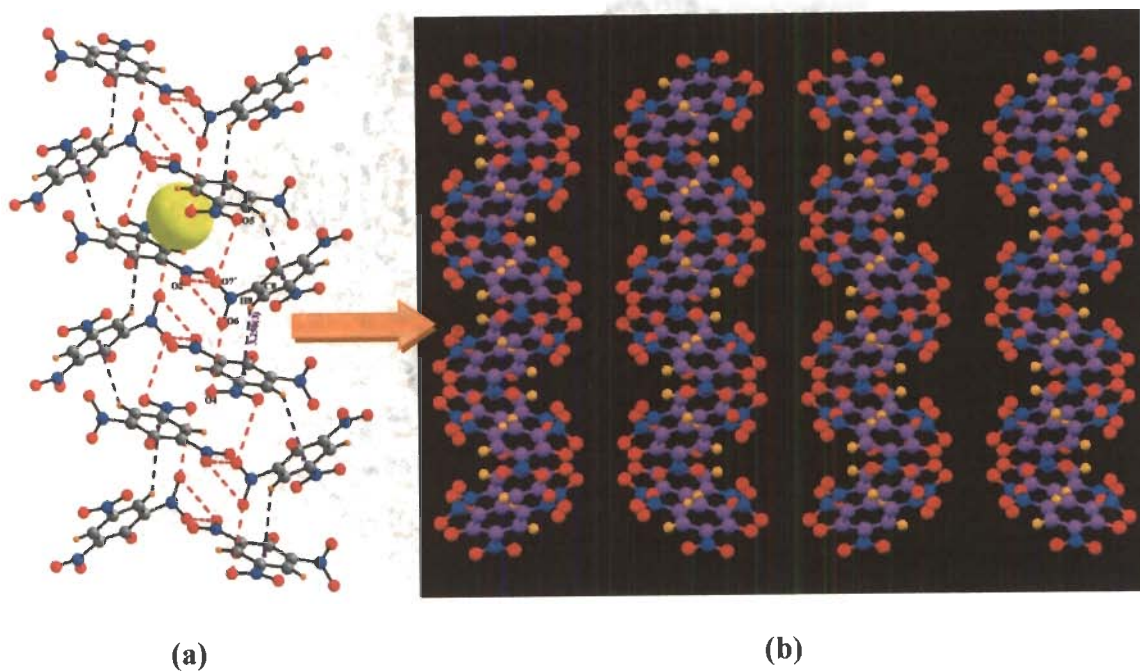


Fig. 4.41: (a) Formation of cavity via non-covalent interactions (b) Three dimensional spiral packing among picrate anions in **4m**. Color code: C, grey/purple; H, orange; O, red; N, blue

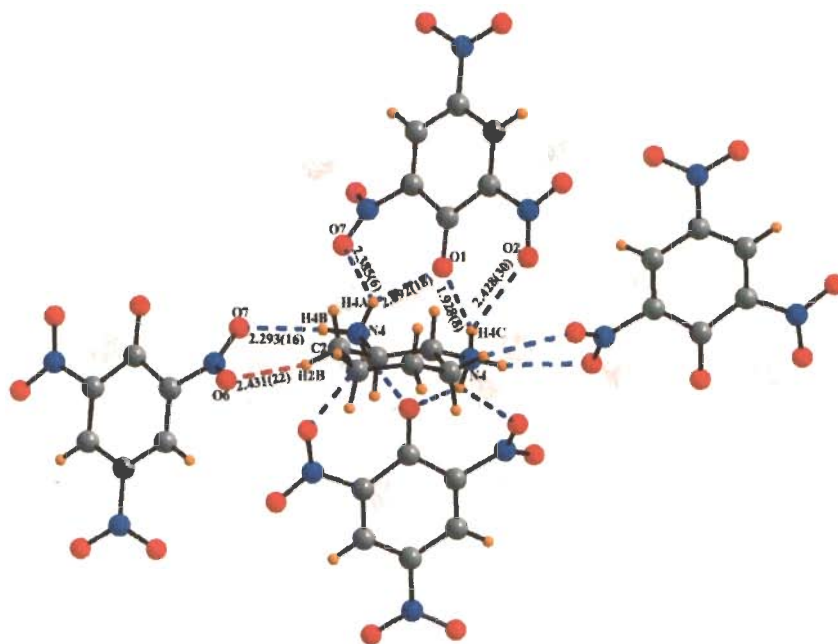


Fig. 4.42: Various C-H...O and N-H...O non-covalent interactions in **4m**. Color code: C, grey; H, orange; O, red; N, blue

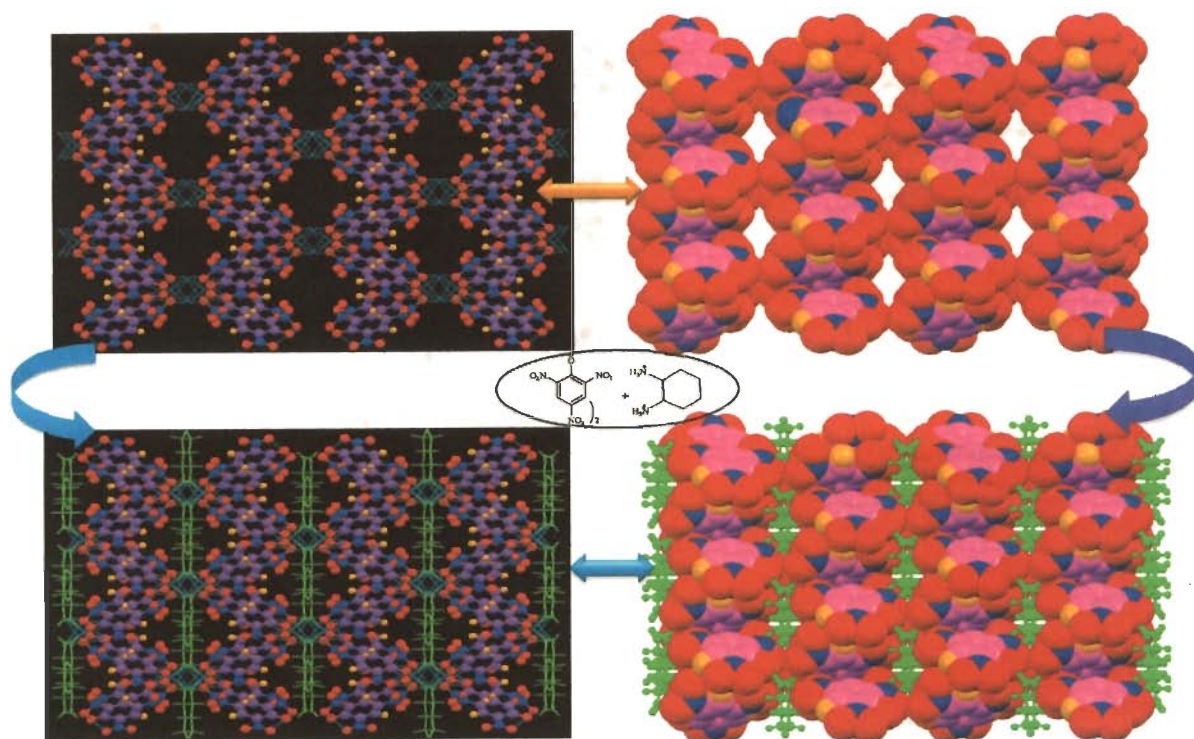


Fig. 4.43: Perspective view of the supramolecular motif in **4m**. Color code: C, pink/purple; H, orange; O, red; N, blue; 1/2cyclohexane-1,2-diaminium, green

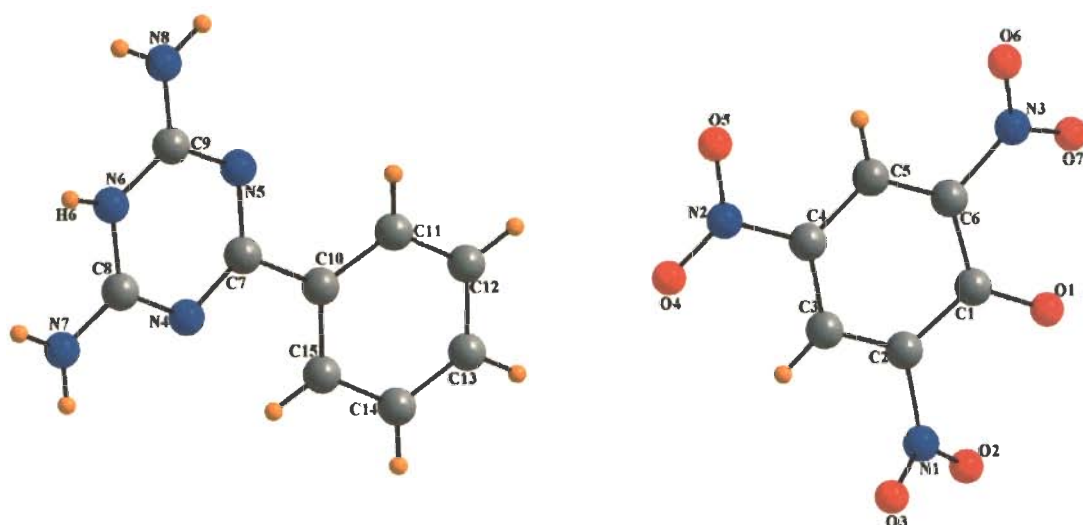


Fig. 4.44: Crystal structure of [PA·6-phenyl-2,4-diamino-1,3,5-triazinium] (**4n**). Color code: C, grey; H, orange; O, red; N, blue

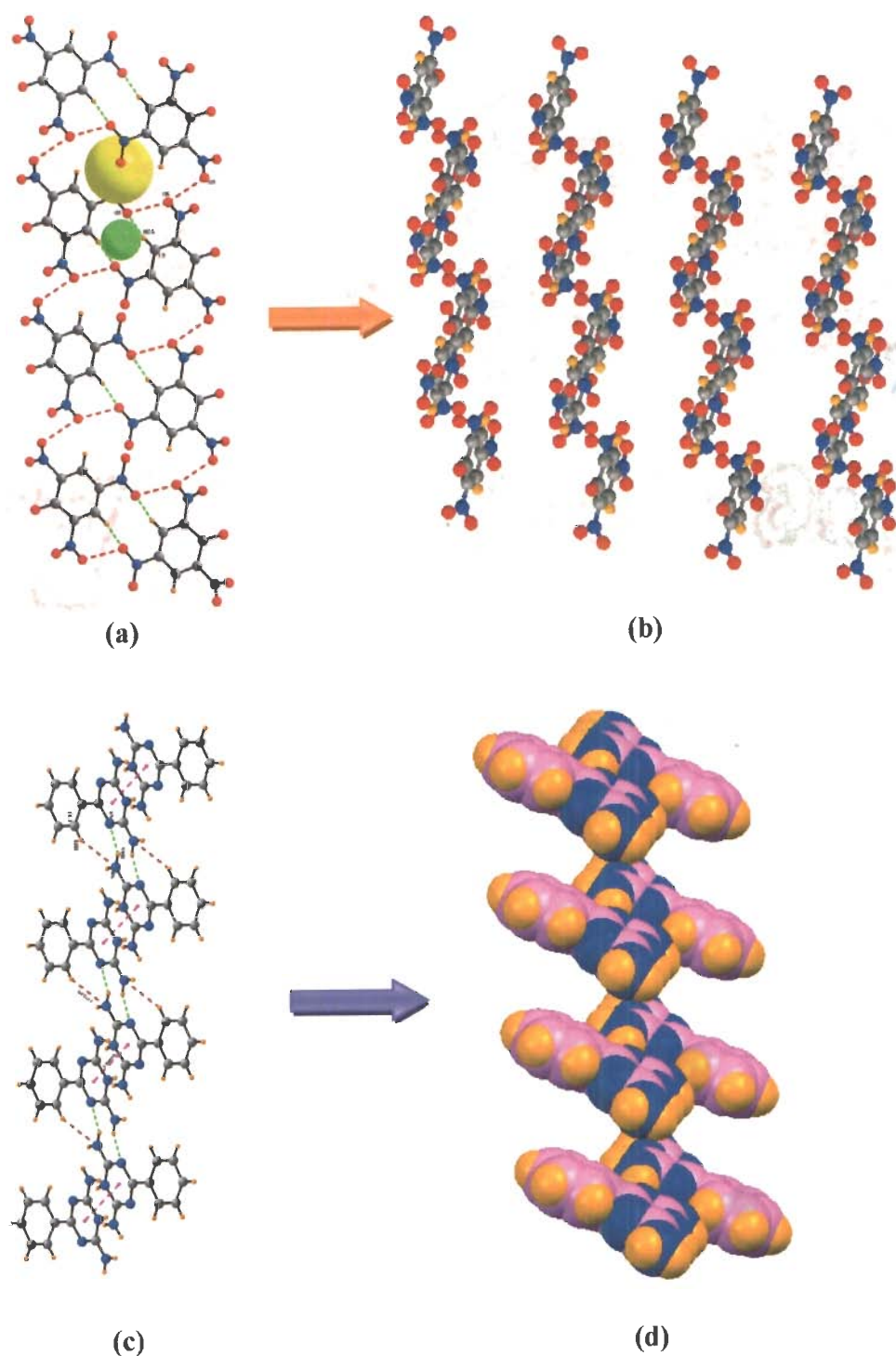


Fig. 4.45: (a) Formation of cavity via intermolecular interactions (b) Three dimensional zig-zag molecular arrangement among picrates (c) Spiral molecular arrangement and (d) Stacking among 6-phenyl-2,4-diamino-1,3,5-triazinium via various non-covalent interactions in **4n**. Color code: C, grey/pink; H, orange; O, red; N, blue.

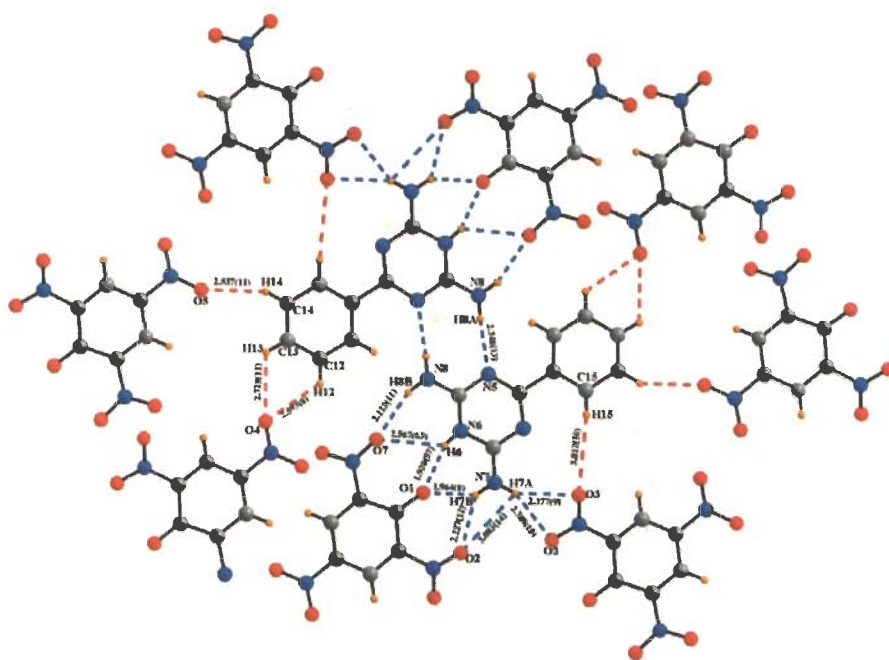


Fig. 4.46: Various C-H...O and N-H...O non-covalent interactions in **4n**. Color code: C, grey; H, orange; O, red; N, blue

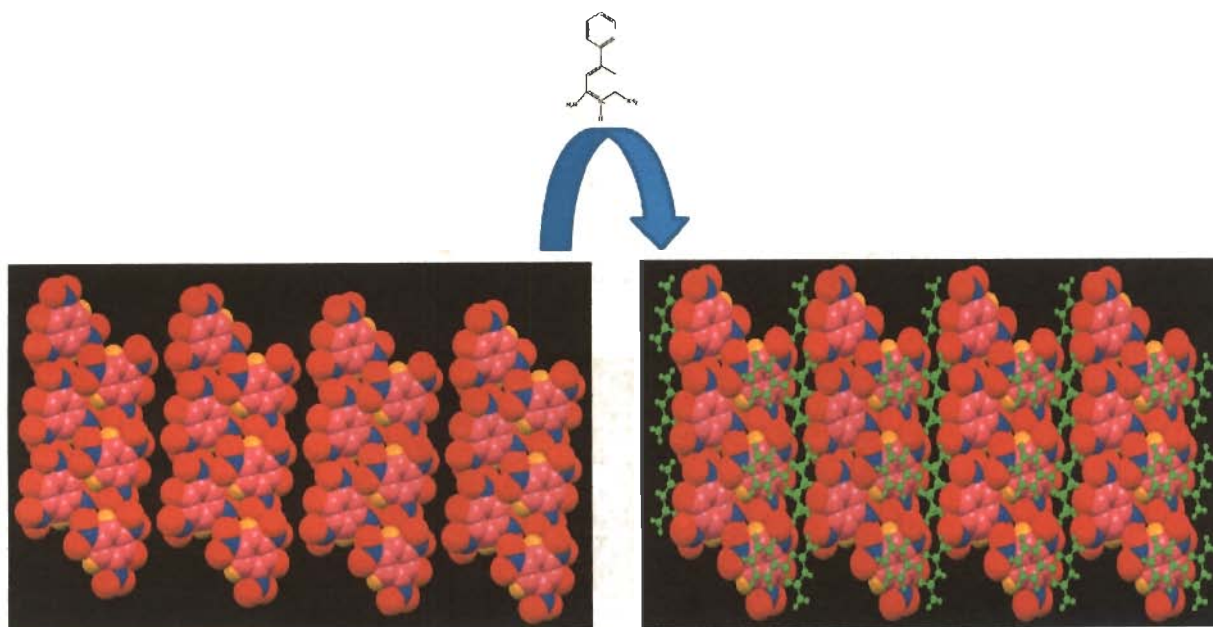
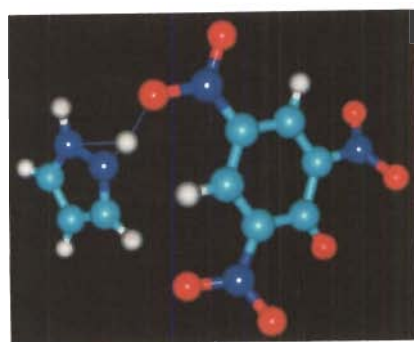
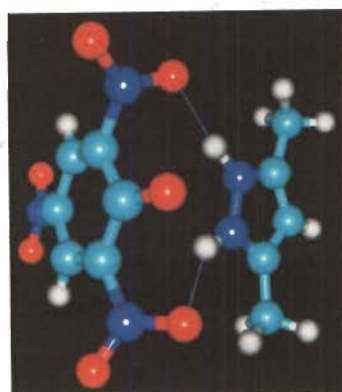


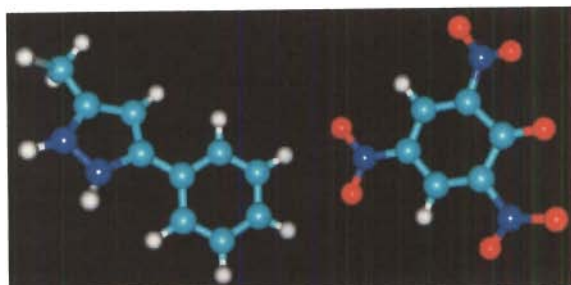
Fig. 4.47: Three dimensional packing as alternate channels of picrates and 6-phenyl-2,4-diamino-1,3,5 triazinium in **4n**. Color code: C, pink; H, orange; O, red; N, blue; 6-phenyl-2,4-diamino-1,3,5 triazine, green



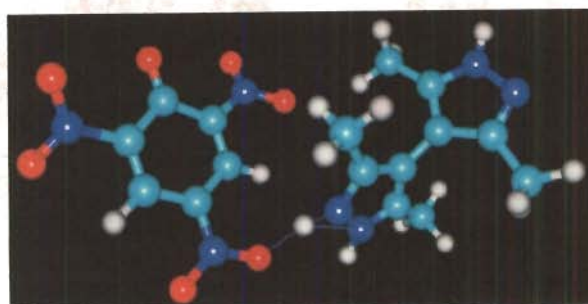
(a)



(b)

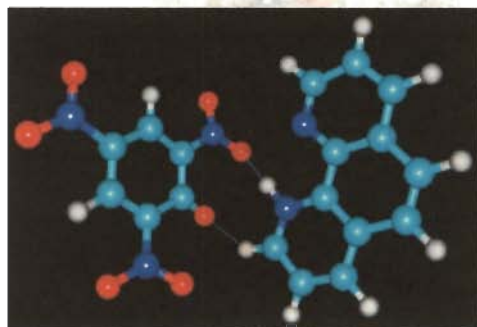


(c)

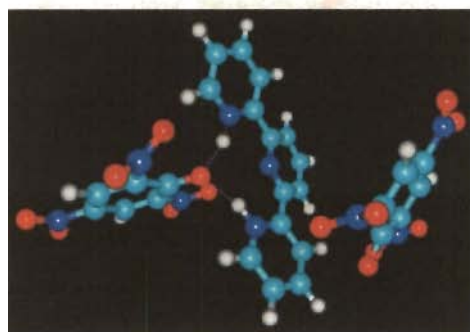


(d)

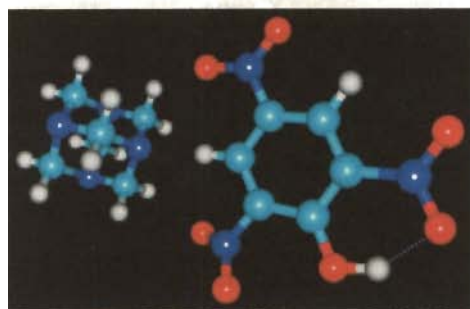
Fig. 4.48: Optimized geometry of salts (a) 4c (b) 4d (c) 4e (d) 4f. Color code: C, cyan; H, white; O, red; N, blue



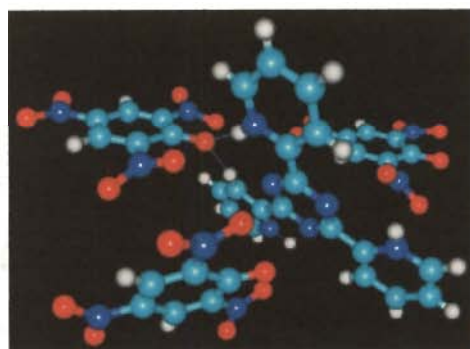
(a)



(b)

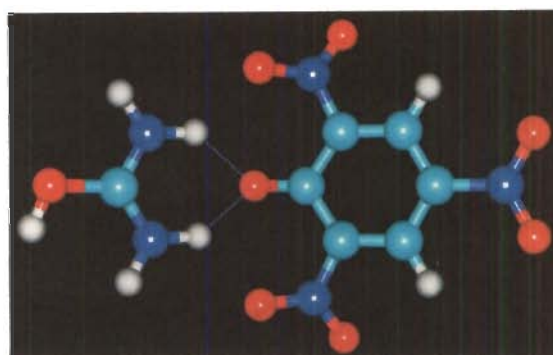


(c)

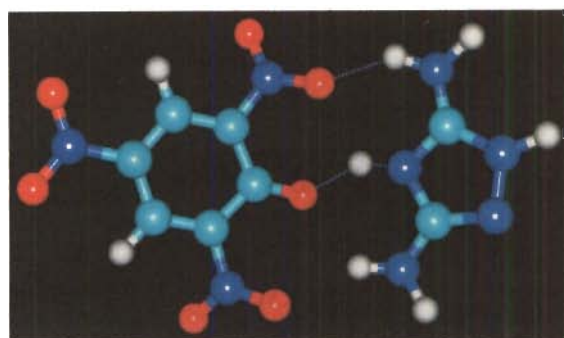


(d)

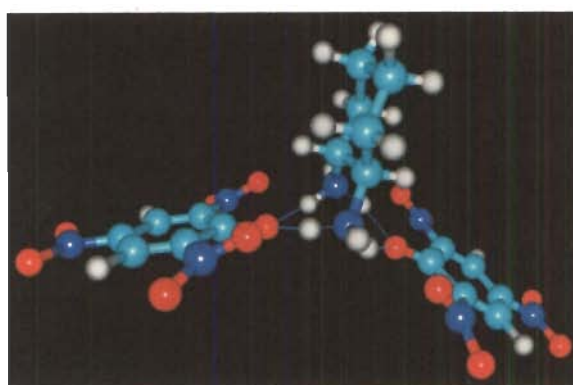
Fig. 4.49: Optimized geometry of salts (a) 4g (b) 4h (c) 4i (d) 4j. Color code: C, cyan; H, white; O, red; N, blue



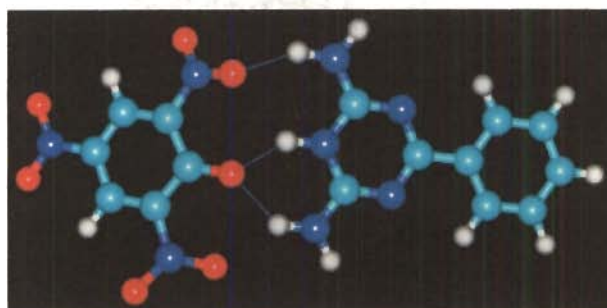
(a)



(b)



(c)



(d)

Fig. 4.50: Optimized geometry of salts (a) 4k (b) 4l (c) 4m (d) 4n. Color code: C, cyan; H, white; O, red; N, blue

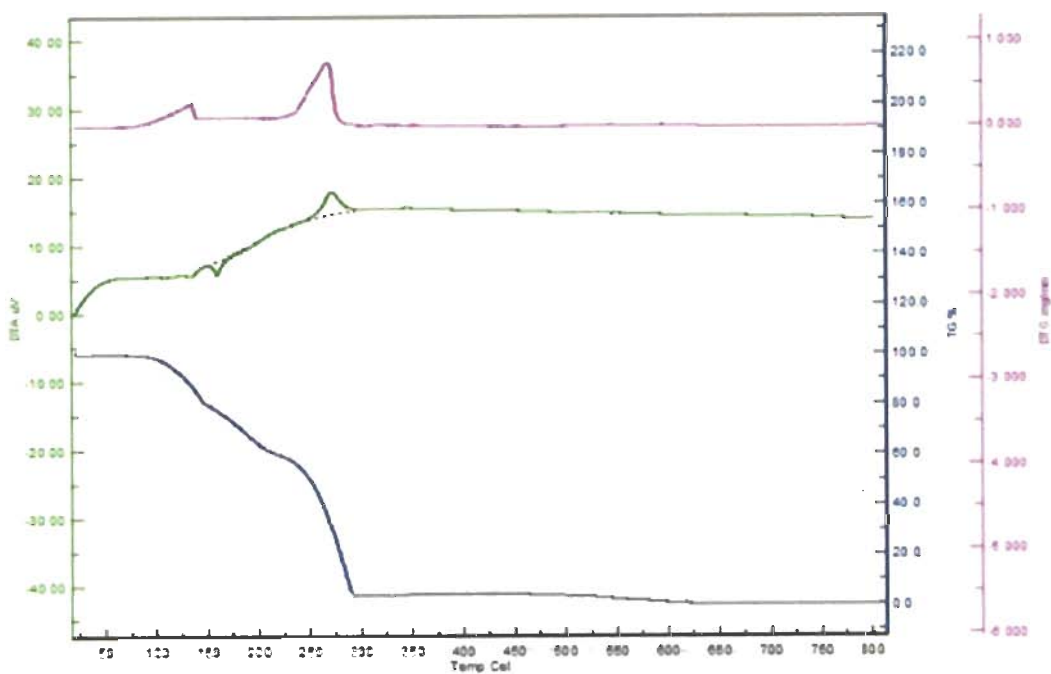


Fig. 4.51: Non-isothermal TG-DTA in air at standard atmospheric condition of $[2PA^- \cdot 2PzH_2^+ \cdot OH_2]$ (**4c**)

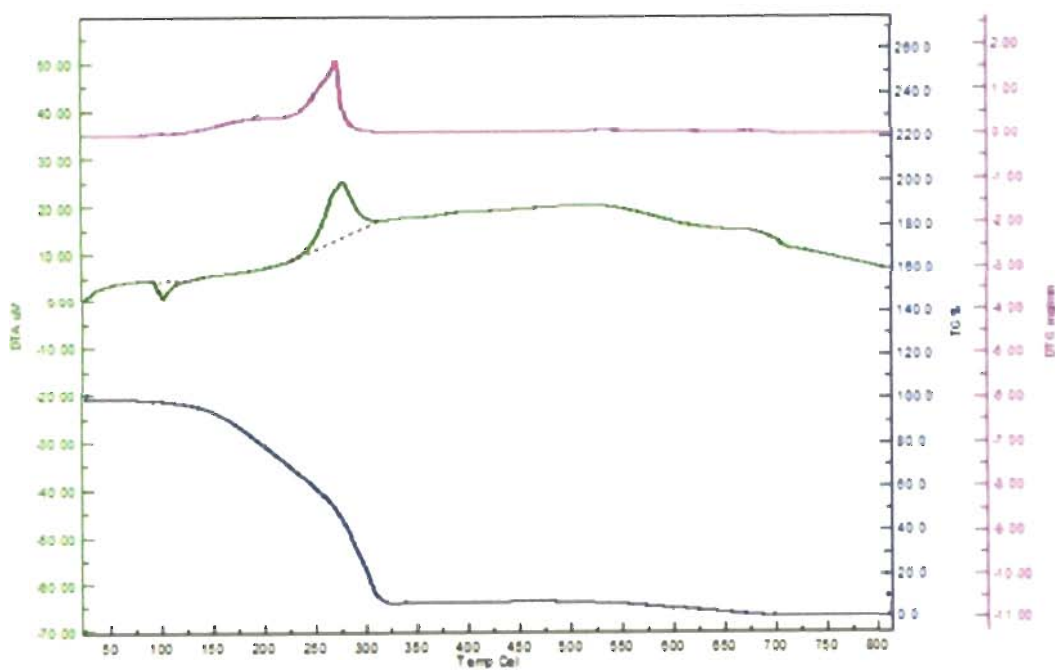


Fig. 4.52: Non-isothermal TG-DTA in air at standard atmospheric condition of $[PA^- \cdot Pz^{Me_2}H_2^+]$ (**4d**)

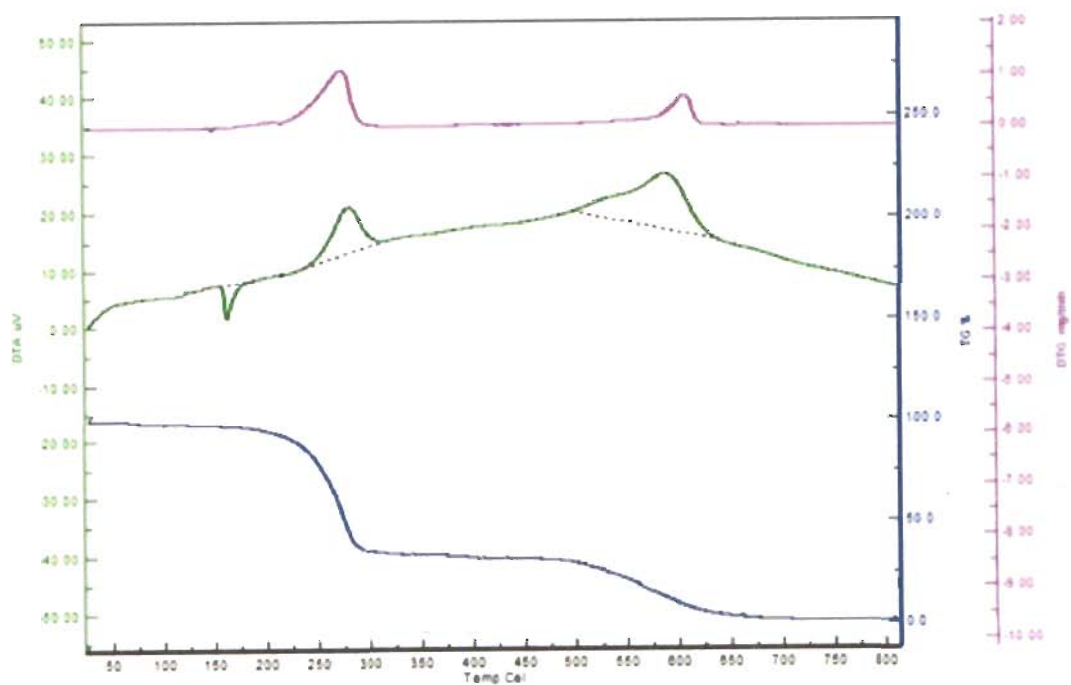


Fig. 4.53: Non-isothermal TG-DTA in air at standard atmospheric condition of $[PA^- \cdot Pz^{Ph,Me} H_2^+ \cdot CH_3OH]$ (**4e**)

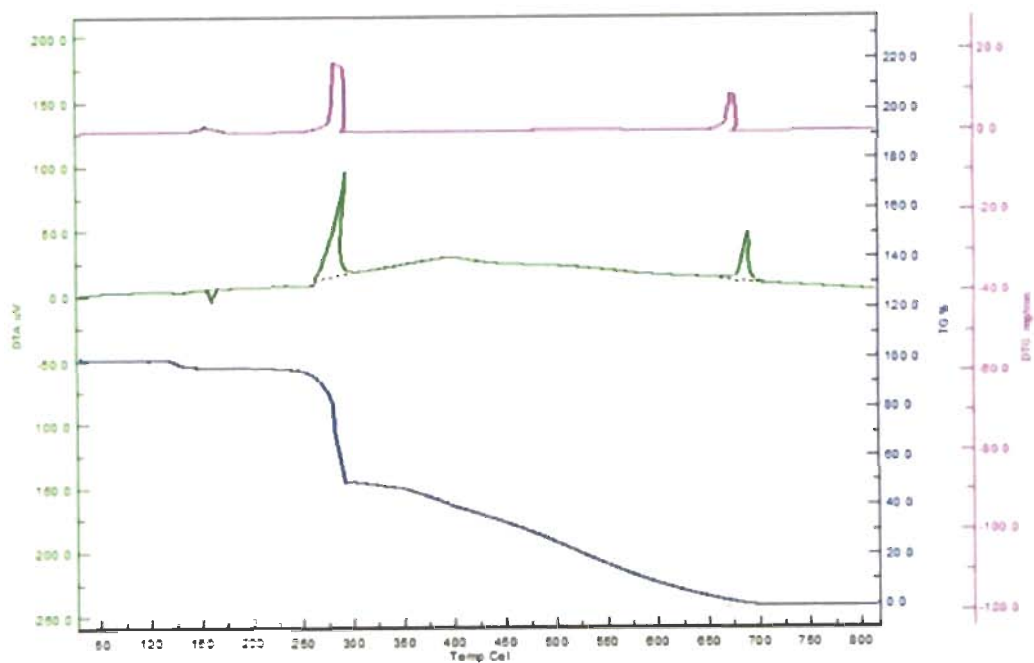


Fig. 4.54: Non-isothermal TG-DTA in air at standard atmospheric condition of $[2PA^- \cdot 2H_2dmPzH^+ \cdot CH_3CN]$ (**4f**)

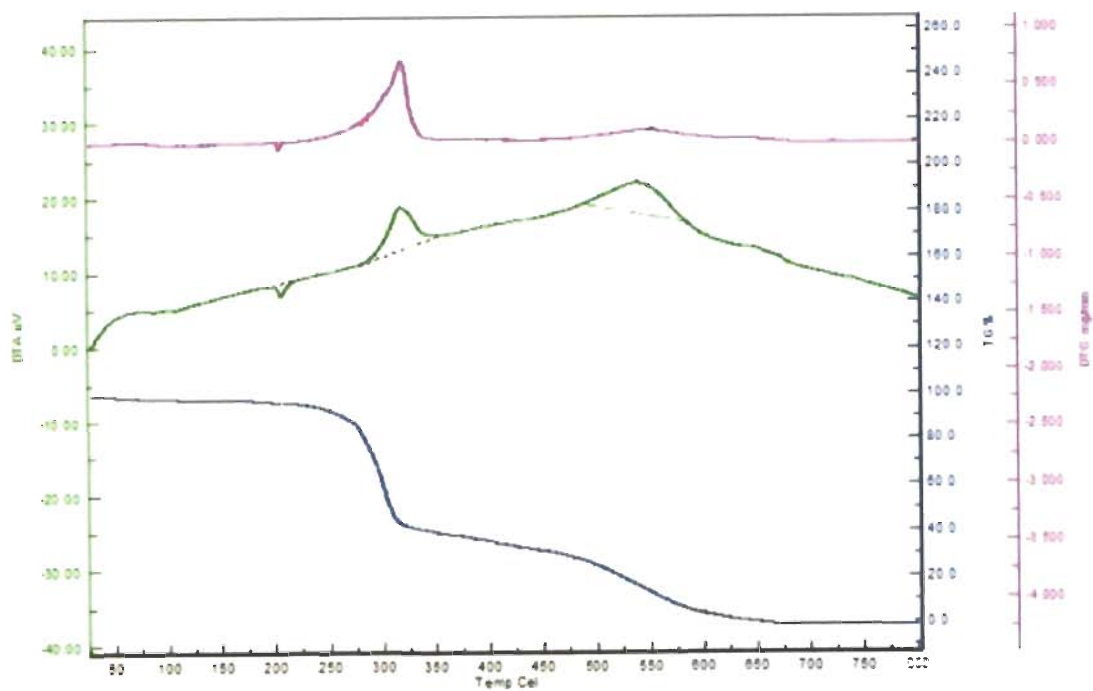


Fig. 4.55: Non-isothermal TG-DTA in air at standard atmospheric condition of [PA⁻.phenH⁺.CH₃OH] (4g)

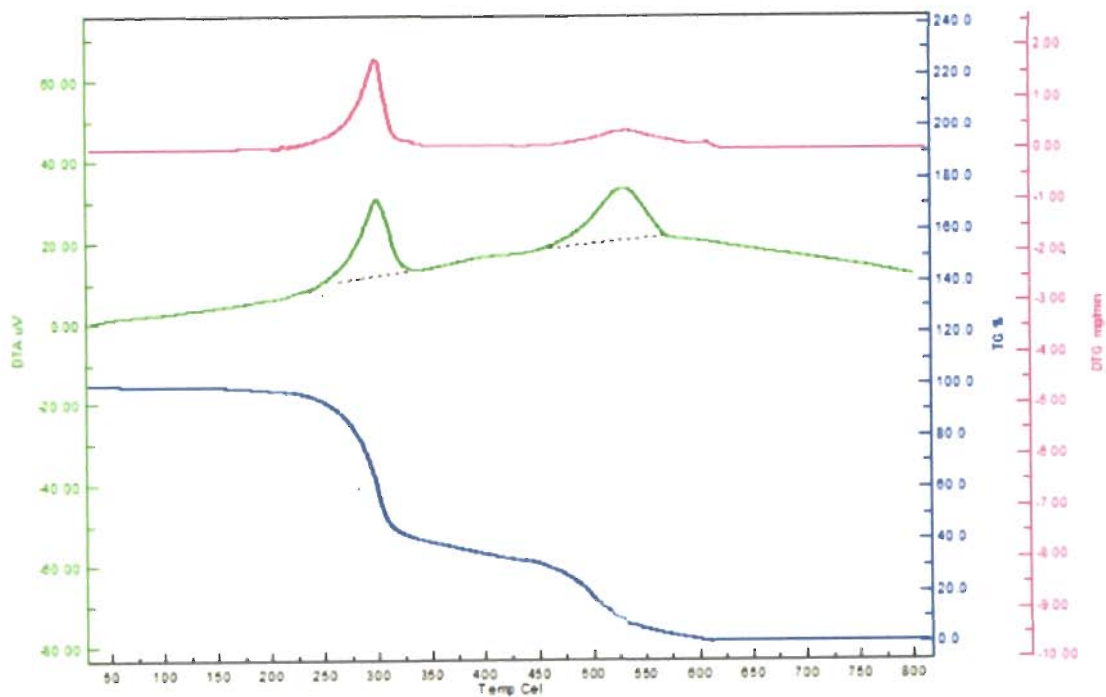


Fig. 4.56: Non-isothermal TG-DTA in air at standard atmospheric condition of [2PA⁻.terpyH₂⁺²] (4h)

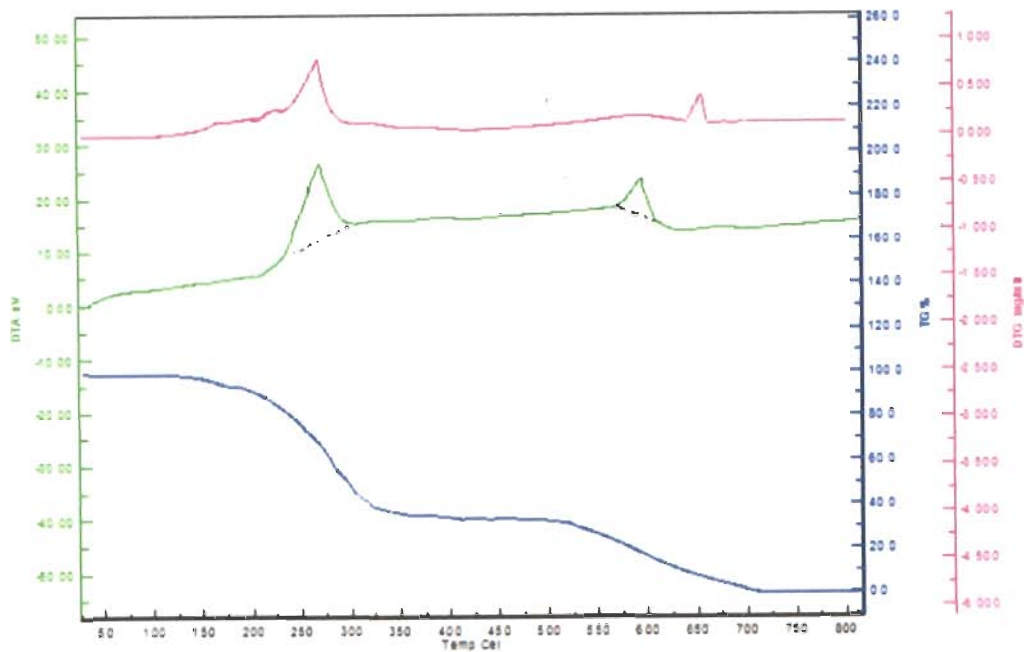


Fig. 4.57: Non-isothermal TG-DTA in air at standard atmospheric condition of [PA. hmta] (4i)

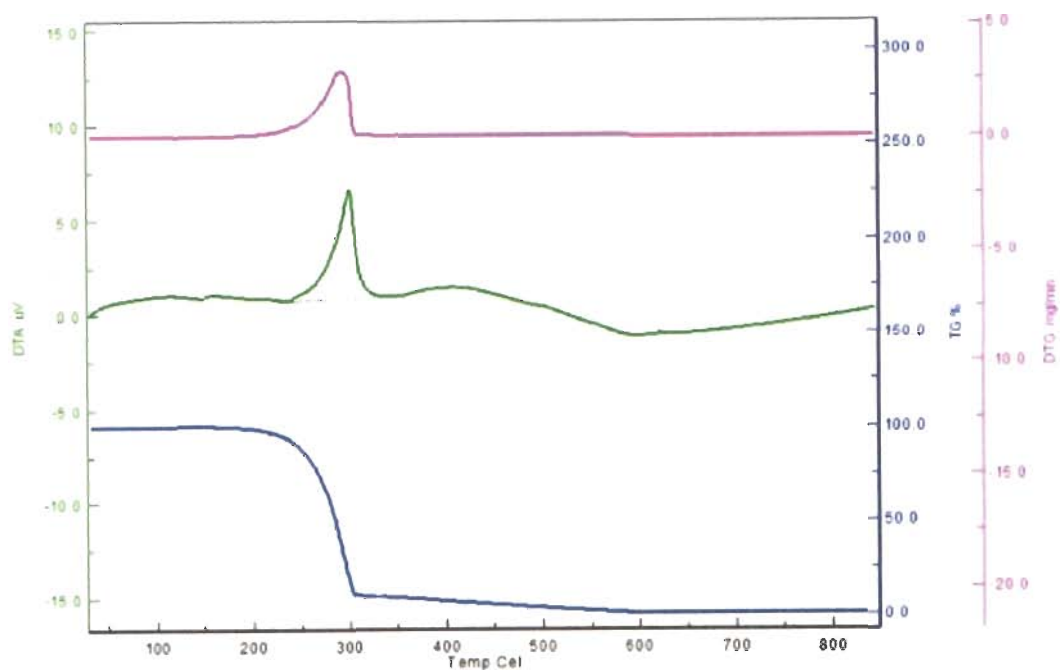


Fig. 4.58: Non-isothermal TG-DTA in air at standard atmospheric condition of [3PA. tptzH₃⁺3] (4j)

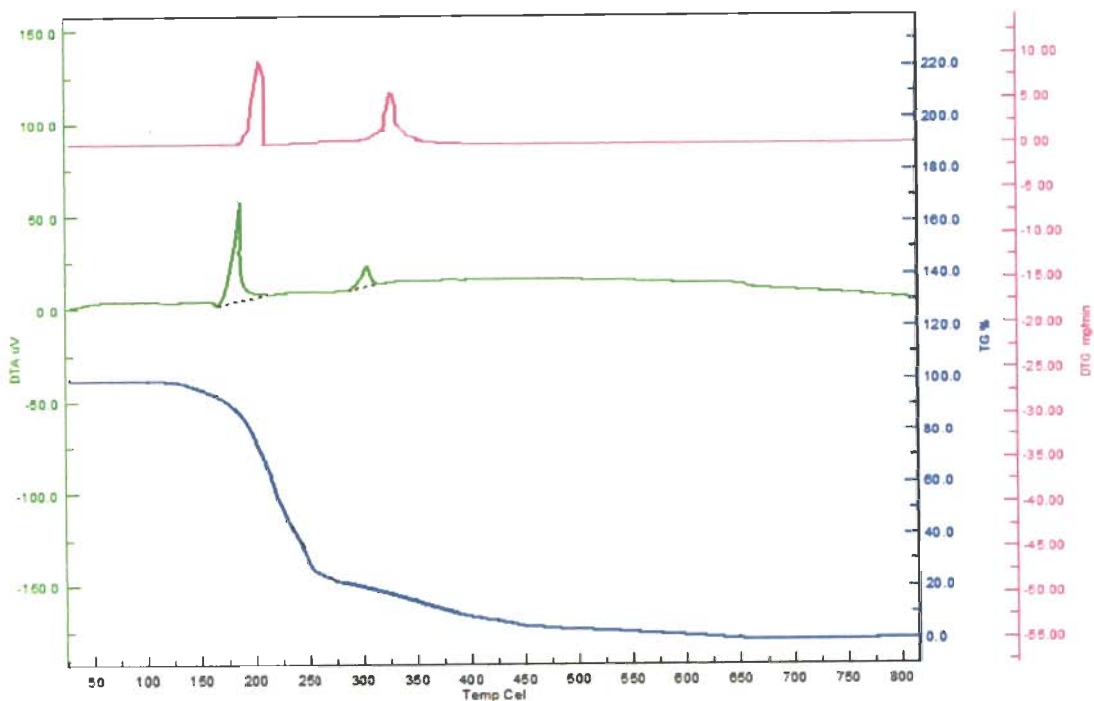


Fig. 4.59: Non-isothermal TG-DTA in air at standard atmospheric condition of [PA³.Uronium] (4k)

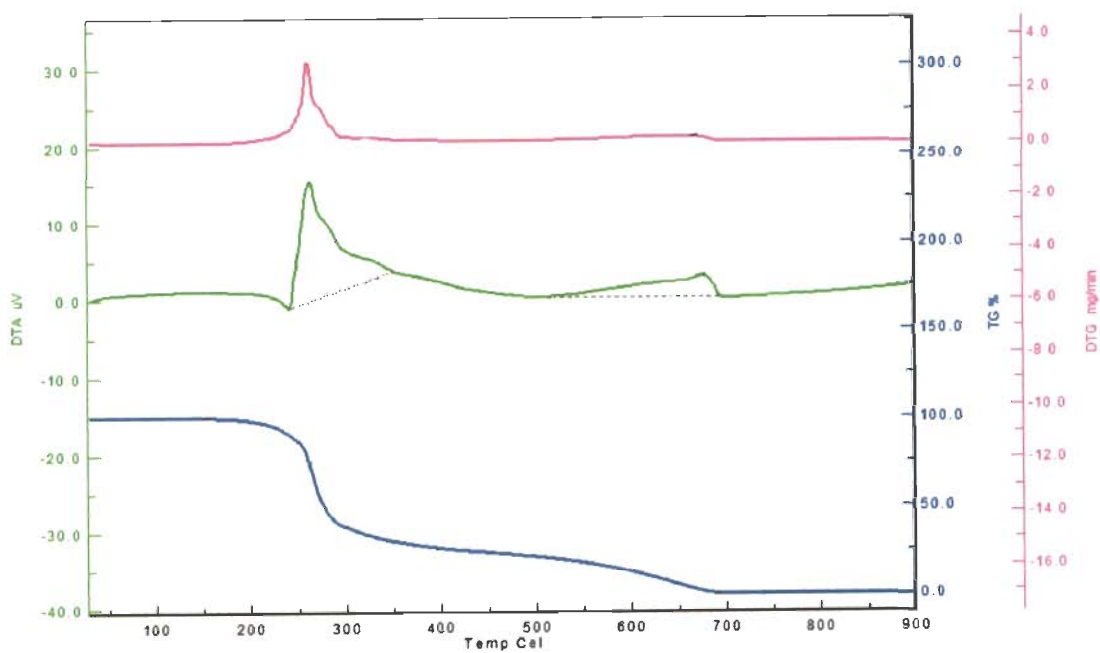


Fig. 4.60: Non-isothermal TG-DTA in air at standard atmospheric condition of [PA³,5-diamino-1,2,4-triazolium] (4l)

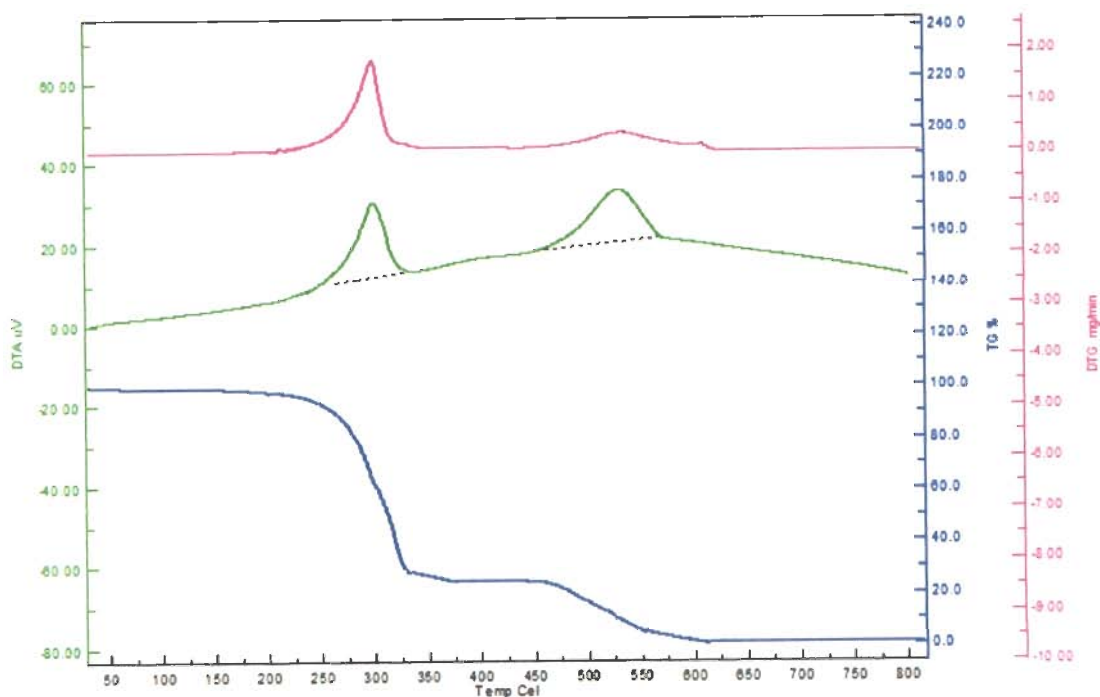


Fig. 4.61: Non-isothermal TG-DTA in air at standard atmospheric condition of [PA⁻.1/2cyclohexane-1,2-diaminium] (**4m**)

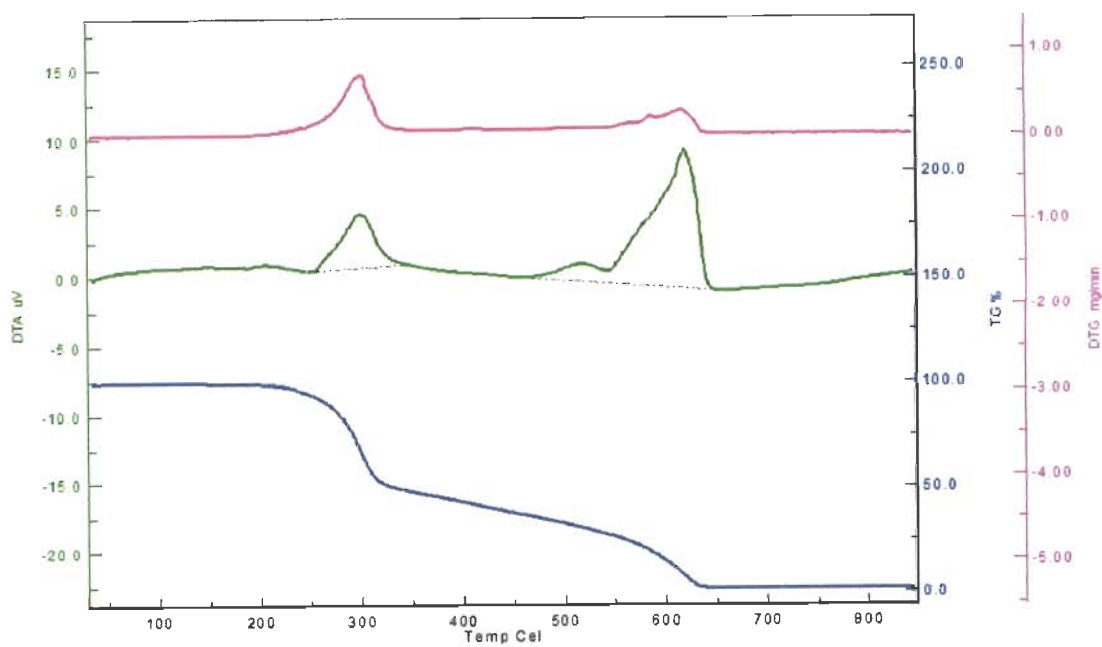
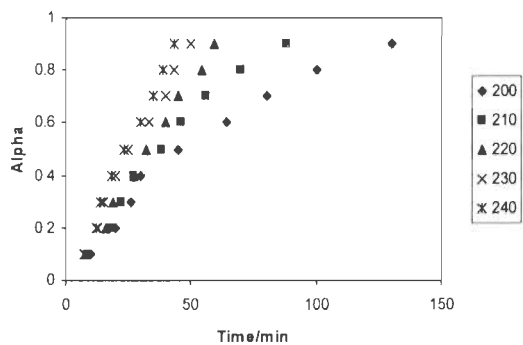
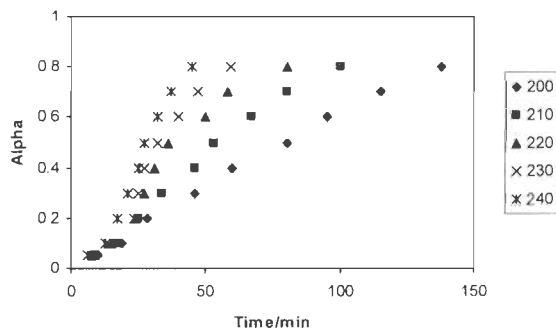


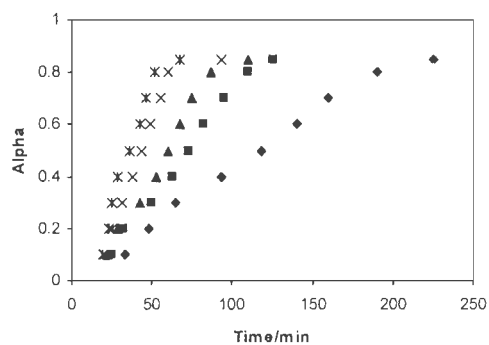
Fig. 4.62: Non-isothermal TG-DTA in air at standard atmospheric condition of [PA⁻.6-phenyl-2,4-diamino-1,3,5-triazinium] (**4n**)



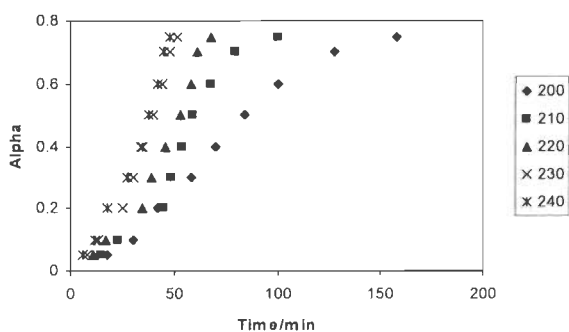
(a)



(b)



(c)



(d)

Fig. 4.63: Isothermal TG in static air atmosphere for salts 4c-4f (a) 4c (b) 4d (c) 4e (d) 4f

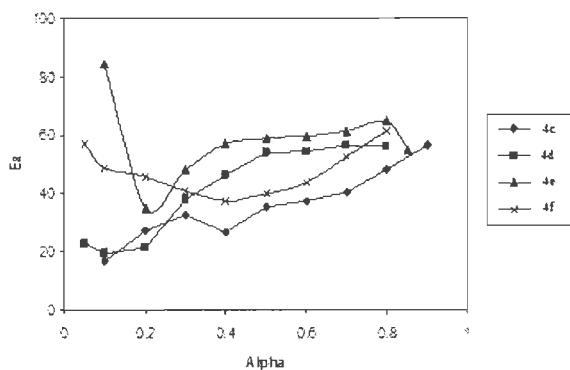


Fig. 4.64: Dependence of activation energy (E_a) on the extent of conversion (α) for 4c-4f

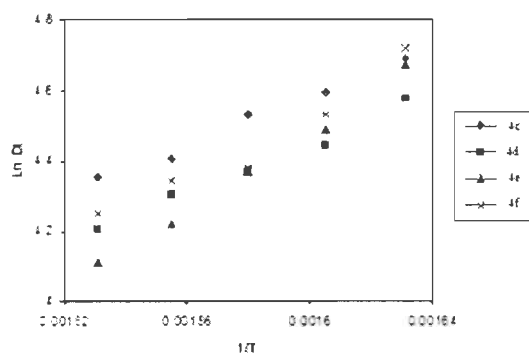
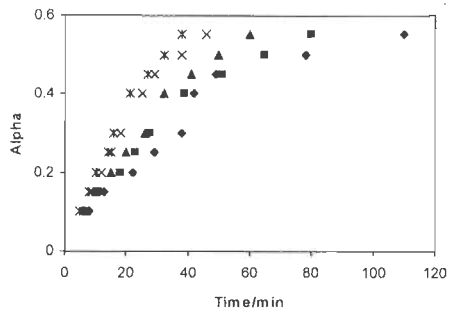
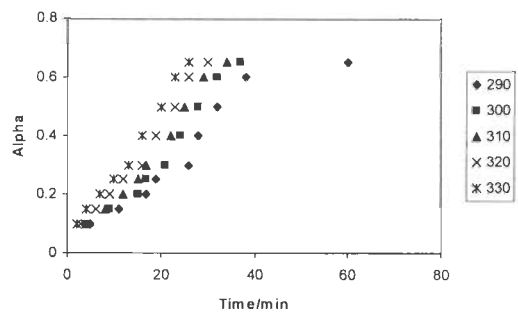


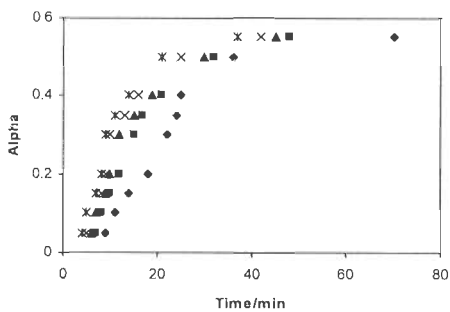
Fig. 4.65: Graph of $\ln D_i$ vs $1/T$ for 4c-4f



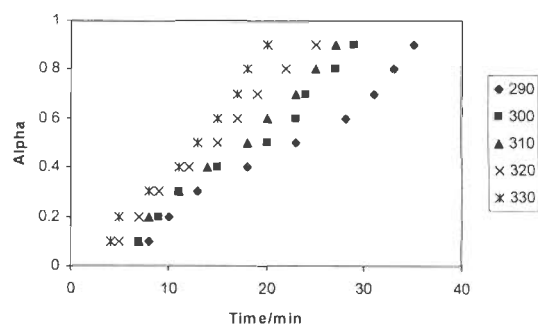
(a)



(b)



(c)



(d)

Fig. 4.66: Isothermal TG in static air atmosphere for salts 4g-4j (a) 4g (b) 4h (c) 4i (d) 4j

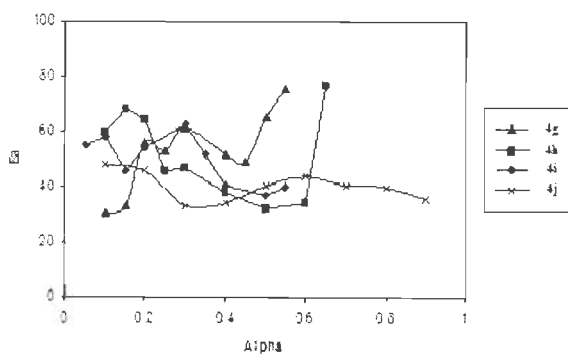


Fig. 4.67: Dependence of activation energy (E_a) on the extent of conversion (α) for 4g-4j

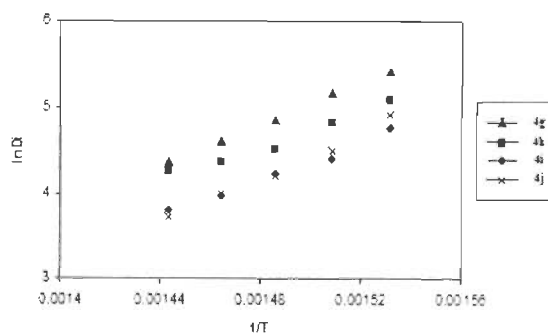
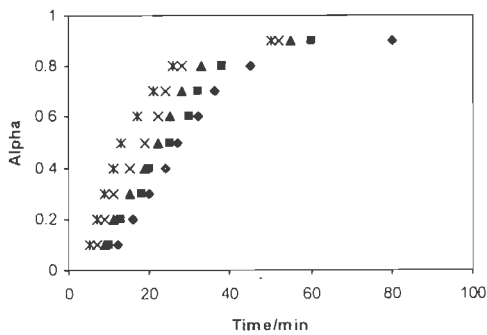
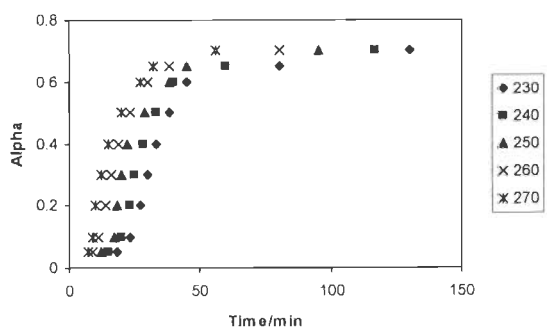


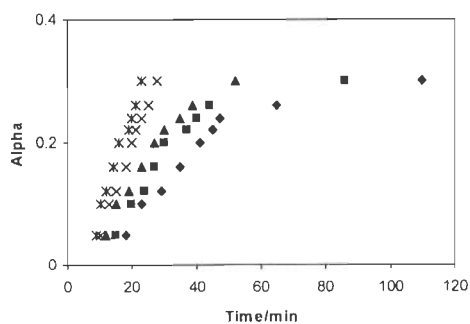
Fig. 4.68: Graph of $\ln D_i$ vs $1/T$ for 4g-4j



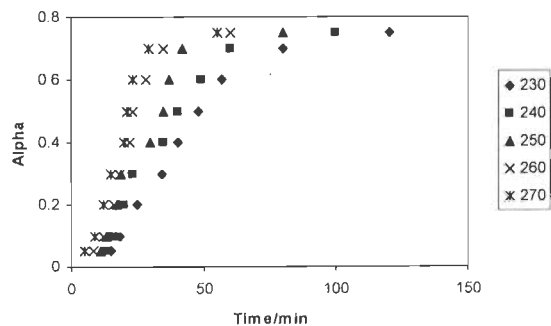
(a)



(b)



(c)



(d)

Fig. 4.69: Isothermal TG in static air atmosphere for salts 4k-4n (a) 4k (b) 4l (c) 4m (d) 4n

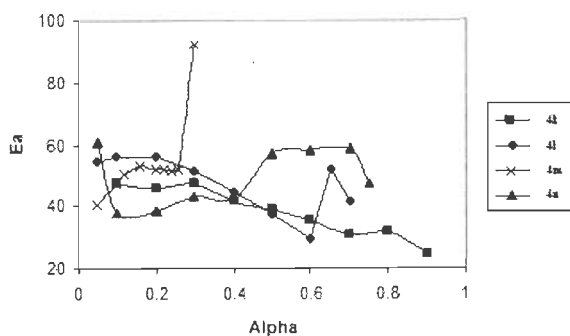


Fig. 4.70: Dependence of activation energy (E_a) on the extent of conversion (α) for 4k-4n

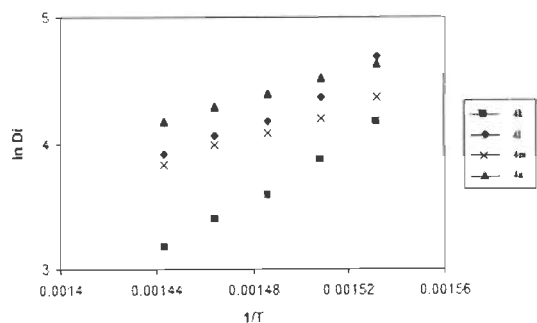


Fig. 4.71: Graph of $\ln D_i$ vs $1/T$ for 4k-4n

REFERENCES

1. Brill, T. B., Zhang, T. L. and Tappan, B. C., "Thermal decomposition of energetic materials 74. volatile metal isocyanates from flash pyrolysis metal-NTO and metal-picrate salts and an application hypothesis", *Combust. Flame.*, **121**, 662 (2000).
2. (a) Harrowfield, J. M., Lu, W., Skelton, B. W. and White, A. H., "Structural systematics of rare earth complexes. I. structural characterization of lanthanoid (III) picrate hydrates: Monoclinic ($P2_1/C$) (Quasi-)dodecahydrates of the related La→Pr and Nd→Tb families", *Aus. J. Chem.*, **47**, 321 (1994). (b) Harrowfield, J. M., Lu, W., Skelton, B. W. and White, A. H., "Structural systematics of rare earth complexes. II. structural characterization of lanthanoid (III) picrate hydrates: The triclinic $P1$, 11.5 hydrates of the later rare earths and yttrium", *Aus. J. Chem.*, **47**, 339 (1994). (c) Harrowfield, J. M., Lu, W., Skelton, B. W. and White, A. H., "Structural systematics of rare earth complexes. III. structural characterization of lanthanoid (III) picrate hydrates: Gadolinium picrate dodecahydrate—an X-ray-induced phase modification?—and some general aspects of the structural chemistry of lanthanoid picrates", *Aus. J. Chem.*, **47**, 349 (1994). (d) Harrowfield, J. M., Skelton, B. W. and White, A. H., "Structural systematics of rare earth complexes. IV. structural characterization of lanthanoid (III) picrate hydrates: The quasi-undecahydrate of samarium (III) picrate", *Aus. J. Chem.*, **47**, 359 (1994).
3. Chen, C. S., Chao, H. E., Wang, S. J. and Wu, S. C., "Spectrophotometric studies on the solvent extraction of lithium picrate with dibenzo-14-crown-4 and its analogs", *Inorg. Chim. Acta*, **145**, 85 (1988).
4. Melo, W. C., Zain, M., Matos, J. R., Isolani, P. C., Zinner, K. and Zinner, L. B., "Studies of neodymium, europium and terbium picrate complexes with benzyl-t-butyl sulphoxide", *J. Alloys Comp.*, **225**, 344 (1995).
5. Urbanski, T.; "Chemistry and technology of explosives", Pergamon Press, Oxford, (1984) Vol. 4, Ch. 7.
6. Pagoria, P. F., Lee, G. S., Mitchell, A. R. and Schmidt, R. D., "A review of energetic materials synthesis", *Thermochim. Acta*, **384**, 187 (2002).
7. Sikder, A. K. and Sikder, N. J., "A review of advanced high performance, insensitive and thermally stable energetic materials emerging for military and space applications", *J. Hazard. Mater.*, **112**, 1 (2004).

8. Agarwal, J. P., "Recent trends in high-energy materials", *Prog. Energy Combust. Sci.*, **24**, 1 (1998).
9. Christe, K. O., Wilson, W. W., Sheehy, J. A. and Boatz, J. A., "N₅: A novel homoleptic polynitrogen ion as a high energy density material", *Angew. Chem. Int. Ed.*, **38**, 2004 (1999).
10. Chavez, D. E., Hiskey, M. A. and Gilardi, R. D., "3,3'-azobis (6-amino-1,2,4,5-tetrazine): A novel high nitrogen energetic material", *Angew. Chem. Int. Ed.*, **39**, 1791 (2000).
11. Hammer, A., Klapotke, T. M., Noth, H., Warchhold, M. and Holl, G., "Synthesis, structure, molecular orbital and valence bond calculations for tetrazole azide, CHN₇", *Propellants, Explos. Pyrotech.*, **28**, 165 (2003).
12. Neutz, J., Grosshardt, O., Schaufele, S., Schuppler, H. and Schweikert, W., "Synthesis, characterization and thermal behaviour of guanidinium-5-aminotetrazolate (GA) - A new nitrogen-rich compound", *Pyrotech.*, **28**, 181 (2003).
13. Jin, C. M., Ye, C., Piekarski, C., Twamley, B. and Shreeve, J. M., "Mono and bridged azolium picrates as energetic salts", *Eur. J. Inorg. Chem.*, **10**, 3760 (2005).
14. Llamas-Saiz, A. L., Foces-Foces, C., Echevarría, A. and Elguero, J., "The relative basicities of tris(pyrazol-1-yl)-1,3,5-triazine (TPT), water and the picrate anion in the solid state", *Acta Cryst.*, **C51**, 1401 (1995).
15. Infantes, L., Foces-Foces, C., Claramunt, R. M., López, C. and Elguero, J., "Aminopyrazoles and their conjugated acids. An X-ray study of 3,5-dimethyl-4-aminopyrazole and the picrate of 3(5)-aminopyrazole", *J. Heterocycl. Chem.*, **36**, 595 (1999).
16. Zaderenko, P., Gil, M. S., López, P., Ballesteros, P., Fonseca, I. and Albert, A., "Diethyl 2-benzimidazol-1-ylsuccinate-picric acid (1/1) - An inclusion molecular complex", *Acta Cryst.*, **B53**, 961 (1997).
17. Hammerl, A. and Klapotke, T. M., "Tetrazolypentazoles: Nitrogen-rich compounds", *Inorg. Chem.*, **41**, 906 (2002).
18. Dobrowolska, W. S., Bator, G., Sobczyk, L., Grech, E., Scheibe, J. N., Pawlukoja, A. and Wuttke, J., "The (2:1) complex of picric acid with tetramethylpyrazine: The structure, IR spectra and tunnel splitting of methyl groups", *J. Mol. Struct.*, **975**, 298 (2010).
19. Jin, S., Zhang, W., Wang, D., Gao, V., Zhou, J. Z., Chen, R. and Xu, X., "Crystal and molecular structure of the 1:2 adduct formed between N,N'-butylenebis(imidazole) and carboxylic acid derivatives", *J. Chem. Crystallogr.*, **40**, 87 (2009).

20. Chandramohan, A., Bharathikannan, R., Kandhaswamy, M. A. and Chandrasekaran, J., "Synthesis, crystal growth, spectral, thermal and optical properties of acenaphthene picrate", *Cryst. Res. Technol.*, **43**, 93 (2008).
21. Narayana, B., Sarojini, B. K., Kamath, K. P., Yathirajan, H. S. and Bolte, M., "2-Aminopyrimidinium picrate", *Acta Cryst.*, **E64**, o117 (2008).
22. Smith, G., Wermuth, U. D. and Healy, P. C., "A second crystal polymorph of anilinium picrate", *Acta Cryst.*, **E60**, o1800 (2004).
23. MacDonald, J. C., Yigit, M. V. and Mychajlonka, K., "Two concomitant polymorphs of a supramolecular model of the asp...his...ser catalytic triad", *Cryst. Growth Des.*, **5**, 2248 (2005).
24. Garcia, M. S. and Toscano, R. A., "Crystal and molecular structure of 4-(3-indolyl)butyric acid-picric acid 2/2 π complex", *J. Crystallogr. Spectrosc. Res.*, **17**, 207 (1987).
25. Yamaguchi, S. I., Goto, M., Takayanagi, H. and Ogura, H., "The crystal structure of phenanthrene:picric acid molecular complex", *Bull Chem. Soc. Jpn.*, **61**, 1026 (1988).
26. Darwich, C., Klapotke, T. M. and Sabate, C. M., "Structural and preliminary explosive property characterization of new 3,4,5-triamino-1,2,4-triazolium salts", *Propellants, Explos. Pyrotech.*, **33**, 333 (2008).
27. Yathirajan, H. S., Narayana, B., Swamy, M. T., Sarojini, B. K. and Bolte, M., "Phthalazin-1(2H)-one-picric acid (1/1)", *Acta Cryst.*, **E64**, o119 (2008).
28. Muthamizchelvan, C., Saminathan, K., Fraanje, J., Peschar, R. and Sivakumar, K., "Crystal structure of 2-chloroanilinium picrate", *Anal. Sci.*, **21**, x61 (2005).
29. Singh, R. P., Verma, R. D., Meshri, D. T. and Shreeve, J. M., "Energetic nitrogen-rich salts and ionic liquids", *Angew. Chem. Int. Ed.*, **45**, 3584 (2006).
30. Klapotke, T. M., Karaghiosoff, K., Mayer, P., Poenger, A. and Welch, J. M., "Synthesis and characterization of 1,4-dimethyl-5-aminotetrazolium 5-nitrotetrazolate", *Propellants, Explos. Pyrotech.*, **31**, 188 (2006).
31. Xue, H., Gao, Y., Twamley, B. and Shreeve, J. M., "New energetic salts based on nitrogen-containing heterocycles", *Chem. Mater.*, **17**, 191 (2005).
32. Xue, H., Arritt, S. W., Twamley, B. and Shreeve, J. M., "Energetic salts from N-aminoazoles", *Inorg. Chem.*, **43**, 7972 (2004).
33. Huynh, M. V., Hiskey, M. A., Hartline, E. L., Montoya, D. P. and Gilardi, R., "Polyazido high-nitrogen compounds: Hydrazo and azo-1,3,5-triazine", *Angew. Chem. Int. Ed.*, **43**, 4924 (2004).

34. Chavez, D. E., Hiskey, M. A. and Naud, D. L., "Tetrazine explosives", *Propellants, Explos. Pyrotech.*, **29**, 209 (2004).
35. Puerta, D. T. and Cohen, S. M., "[$(\text{Tp}^{\text{Me,Ph}})_2\text{Zn}_2(\text{H}_3\text{O}_2)]\text{ClO}_4$: A new H_3O_2 species relevant to zinc proteinases", *Inorg. Chim. Acta*, **337**, 459 (2002).
36. Mosby, W. L., "The reaction of some 1:4-dicarbonyl system with hydrazine", *J. Chem. Soc.*, xxx, 3997 (1957).
37. Ghazaryan, V. V., Fleck, M. and Petrosyan, A. M., "Glycine glycinium picrate-reinvestigation of the structure and vibrational spectra", *Spectrochim. Acta*, **A78**, 128 (2011).
38. Ikeda, C., Nagahara, N., Motegi, E., Yoshioka, N. and Inoue, H., "Self-assembly of monopyrazolporphyrins by hydrogen bonding in solution", *Chem. Commun.*, **43**, 1759 (1999).
39. Silverstein, R. M., Bassler, G. C. and Morrill, T. C., "Spectrometric identification of organic compounds", 5th Ed., John Wiley, New York (1991).
40. Brown, M. E., Dollimore, D. and Galway, A. K., "Reaction in the solid state, in: *Comprehensive chemical kinetics*", Elsevier, Amsterdam, The Netherlands, **22**, 1 (1960).
41. Hameed, A. S. H., Ravi, G., Dhanasekaran, R. and Ramasamy, P., "Studies on organic indole-3-aldehyde single crystals", *J. Cryst. Growth*, **212**, 227 (2000).
42. Satava, V., "Mechanism and kinetics from non-isothermal TG traces", *Thermochim. Acta*, **2**, 423 (1971).
43. Sharp, J. H., Brindley, G. W. and Achar, B. N. N., "Numerical data for some commonly used solid state reaction equations", *J. Am. Ceram. Soc.*, **49**, 379 (1966).
44. Masuda, Y., Iwata, K., Ito, R. and Ito, Y., "Kinetics of the thermal dehydration of magnesium oxalate dihydrate in a flowing atmosphere of dry nitrogen", *J. Phys. Chem.*, **91**, 6543 (1987).
45. Vyazovkin, S., "Computational aspects of kinetic analysis. Part C. The ICTAC kinetics project-the light at the end of the tunnel?", *Thermochim. Acta*, **355**, 155 (2000).
46. Vyazovkin, S. and Wight, C. A., "Kinetics in solids", *Annu. Rev. Phys. Chem.*, **48**, 125 (1997).
47. Kapoor, I. P. S., Kapoor, M., Singh, G., Singh, U. P. and Goel, N., "Preparation, characterization and thermolysis of nitrate and perchlorate salts of 2,4,6-trimethylaniline", *J. Hazard. Mater.*, **173**, 173 (2010).

MATERIALS

All manipulations were carried out under air atmosphere. Ethanol, acetonitrile, chloroform and methanol were carefully purified and distilled under nitrogen prior to use by the literature method [1]. Pyrazole (PzH), 3,5-dimethylpyrazole (Pz^{Me2}H), 2,6-dinitrophenol (2,6-DNP), 1,10-phenanthroline (phen), 2,2';6',2''-terpyridine (terpy), 2,4,6-tris(2-pyridyl)-1,3,5-triazine (tptz), 1H-1,2,4-triazole-3,5-diamine (guanazole), cyclohexane-1,2-diamine, 6-phenyl-1,3,5-triazine-2,4-diamine (benzoguanamine), GdCl₃.6H₂O, EuCl₃.6H₂O, TbCl₃.6H₂O of the highest grade were purchased from Sigma-Aldrich, Chemical company, USA. 2,2'-bipyridine (bipy), hexamethylenetetramine (hmta), urea, Gd(NO₃)₃.6H₂O and benzoic acid were commercially available from s.d.fine-chem Limited, Mumbai. The sodium salt of benzoic acid was prepared by reacting with the appropriate amount of sodium hydroxide in water. Potassium thiocyanate was purchased from Loba Chemie, Mumbai.

INSTRUMENTATION

Crystalline complexes and salts were carefully dried under vacuum for several hours prior to elemental analysis on CHNS analyzer Elementar Vario EL III. IR spectra were obtained on a Thermo Nicolet Nexus FT-IR spectrometer in KBr. Absorption spectra were recorded on Perkin Elmer UV-visible Spectrophotometer, (Lambda 35) equipped with thermostated bath (Julabo). The emission spectra were measured on Perkin-Elmer LS-55 model spectrophotometer.

X-RAY CRYSTALLOGRAPHIC STUDY

The X-ray data collection were performed on a Bruker Kappa Apex four circle-CCD diffractometer using graphite monochromated MoK α radiation ($\lambda = 0.71070 \text{ \AA}$). In the reduction of data, Lorentz and polarization corrections, empirical absorption corrections were applied [2]. Crystal structures were solved by Direct and Patterson methods. Structure solution, refinement and data output were carried out with the SHELXTL program [3, 4]. Non-hydrogen atoms were refined anisotropically. Hydrogen atoms were placed in geometrically calculated positions using a riding model. Images and hydrogen bonding interactions were created in the crystal lattice with DIAMOND and MERCURY softwares [5, 6].

COMPUTATIONAL STUDY

Geometry optimization of different species involved both for salts and co-crystals were done by using Density Functional Method (B3LYP) with 6-31G(d,p) basis set as implemented

in the Gaussian 03 suite of program [7]. The input for the simulation was the Z matrix generalized by Gauss view [8, 9] that was also used for visualizing the optimized structures of molecules. ChemCraft, Version 1.5 software was used for comparing the optimized structure with the crystallographic one.

THERMAL ANALYSIS

Non-isothermal and Isothermal TG

Non-isothermal TG of complexes and salts were recorded in the temperature range 10–800 °C at a heating rate of 10 °C min⁻¹ in static air using Perkin-Elmer's (pyris Diamond) thermogravimetry analyzer. The accuracy of the furnace was ±1°C, while the isothermal TG studies (Wt. 0.03 g, 100-200 mesh) of complexes and salts were also performed at appropriate temperature in static air using indigenously fabricated TG apparatus [10] fitted with temperature cum controller.

Ignition Delay Measurements

The ignition delay (D_i) data were recorded using tube furnace technique [11] (mass 0.02 g, 100-200 mesh) in appropriate temperature range (±1°C). Each run was repeated five times. The D_i data were found to fit in the following equation [12-14]

$$D_i = A e^{E_a^*/RT}$$

where E_a^* is the activation energy for thermal ignition, A is the pre-exponential factor and T is the absolute temperature. E_a^* was determined from the slope of a plot of $\ln(D_i)$ vs. $1/T$.

Percent Oxygen Balance

The percent oxygen balance (OB) for metal complexes and salts were calculated by following equation, suggested by Martin and Yallop [15].

For metal complexes-

$$OB = -1600(2x + y/2 + M - Z)/ \text{molecular weight}$$

where x, y and z are the respective number of C, H, O atoms and M is the number of metal atom.

For salts-

$$OB = [(z - 2x - y/2) 100]/ n$$

where x, y and z are the respective number of C, H, O atoms and n is the total number of atoms in the molecule.

CHAPTER-5

Experimental

Kinetics Analysis of Isothermal TG Data

Kinetic analysis of solid state decomposition is usually based on a single step kinetic eq. [16]

$$d\alpha / dt = k (T) f (\alpha) \quad \dots\dots\dots (1)$$

where t is the time, T is the temperature, α is the extent of conversion ($0 < \alpha < 1$), k (T) is the rate constant and f (α) is the reaction model [17], which describes the dependence of the reaction rate on the extent of reactions. The value of α is experimentally derived from the global mass loss in TG experiments. The reaction model may take various forms; the temperature dependence of k (T) can be satisfactorily described by the Arrhenius eq., whose substitution into eq. (1) yields

$$d\alpha / dt = A \exp (-E/RT).f (\alpha) \quad \dots\dots\dots (2)$$

where, A is pre exponential factor, E is activation energy and R is the gas constant.

Model Fitting Method

Rearrangement and integration of equation (1) for isothermal conditions gives

$$g_j (\alpha) = k_j (T) t \quad \dots\dots\dots (3)$$

where $g (\alpha) = \int_0^\alpha [f (\alpha)]^{-1} d\alpha$ is the integrated form of the reaction model. The subscript j has been introduced to emphasize that substituting a particular reaction model in eq. (3) results in evaluating the corresponding rate constant, which is determined from the slope of a plot of $g_j (\alpha)$ verses t. For each reaction model selected, the rate constants are evaluated at several temperatures T_i and Arrhenius parameters are determined using the Arrhenius eq. (4) in its logarithmic form

$$\ln k_j (T_i) = \ln A_j - E_j / RT_i \quad \dots\dots\dots (4)$$

Arrhenius parameters were evaluated for isothermal experimental data by the model fitting method.

Model Free Isoconversional Method

This method allows the activation energy to be evaluated without making any assumptions about the reaction model. Additionally, the method evaluates the effective activation energy as a function of the extent of conversion which allows one to explore multistep kinetics. The basic assumption of the isoconversional method [17] is that the reaction model as defined in eq. (1) is not dependent on temperature or heating rate. Under isothermal conditions, on combining eq. (3) & (4) we get-

$$-\ln t_{\alpha,i} = \ln [A_{\alpha}/g(\alpha)] - E_{\alpha}/RT_i \quad \dots\dots\dots(5)$$

where E_{α} is evaluated from the slope of the plot of $-\ln t_{\alpha,i}$ against T_i^{-1} . Thus, E_{α} at various α_i for complexes and salts have been evaluated.

SYNTHESES OF COMPLEXES AND SALTS

Chapter-2

(i) Synthesis of [Eu(phen)₂Cl₃CH₃OH] (2a)

To the methanolic solution of EuCl₃.6H₂O (0.18 g, 0.5 mmol), 0.19 g, 1.0 mmol of 1,10-phenanthroline in 10.0 ml methanol was added drop wise and the reaction mixture was stirred for 8 hrs. The solution was filtered on celite and the solvent was evaporated under vacuum. The resultant solid in 69.2% (0.45 g, 0.69 mmol) yield was recrystallized from methanol at 4 °C. Anal. Calcd. (%) for C₂₅H₁₉Cl₃N₄OEu (649.76): C, 46.09; H, 3.07; N, 8.60. Found: C, 46.01; H, 2.95; N, 8.43. IR (KBr, cm⁻¹): 1626, 1581, 851, 722.

(ii) Synthesis of [Eu(2,6-DNP)₃phenCH₃OH] (2b)

To the methanolic solution of **2a**, added the methanolic solution of 2,6-DNP (0.04 g, 0.25 mmol) having pH 6-7 with continuous stirring. The reaction mixture was further stirred for 8 hrs at room temperature. The precipitate was filtered and washed with 95% methanol. The suitable crystals in yellow color were obtained from slow evaporation of solvent with in 1 week. Yield: 67.3% (0.61 g, 0.67 mmol). Anal. Calcd. (%) for C₃₁H₂₁N₈O₁₆Eu (913.53): C, 40.81; H, 2.21; N, 12.28. Found: C, 40.61; H, 2.19; N, 12.17. IR (KBr, cm⁻¹): 1609, 1577, 1567, 1533, 1360, 1344.

(iii) Synthesis of [Eu(2,6-DNP)₃phen(OH)].Hphen (2c)

The complex **2c** was prepared and crystallized in 72.8% (0.79 g, 0.72 mmol) yield by the method as described for **2b** except the pH of 2,6-DNP solution was 4-5 during reaction. Anal. Calcd. (%) for C₄₂H₂₇N₁₀O₁₆Eu (1079.71): C, 46.72; H, 2.52; N, 12.97. Found: C, 46.51; H, 2.38; N, 12.84. IR (KBr, cm⁻¹): 1612, 1586, 1569, 1540, 1357, 1333.

(iv) Synthesis of [Eu(2,6-DNP)₃bipyOH₂] (2d)

Complex **2d** was prepared and crystallized in 68.3% (0.59 g, 0.68 mmol) yield by the method as outlined for **2b** using 2,2'-bipyridine (0.03 g, 0.25 mmol) instead of 1,10-phenanthroline. Anal. Calcd. (%) for C₂₈H₁₇N₈O₁₆Eu (873.47): C, 38.50; H, 1.96; N, 12.82. Found: C, 38.39; H, 1.84; N, 12.67. IR (KBr, cm⁻¹): 1609, 1582, 1567, 1536, 1358, 1342.

(v) Synthesis of [Eu(2,6-DNP)₃bipy(OH)].Hbipy (2e)

Complex **2e** was prepared and crystallized in 72.3% (0.75 g, 0.72 mmol) yield by the method as outlined for **2b** using 2,2'-bipyridine (0.03 g, 0.25 mmol) at pH 4-5. Anal. Calcd. (%) for C₃₈H₂₇N₁₀O₁₆Eu (1031.67): C, 44.24; H, 2.63; N, 13.57. Found: C, 44.19; H, 2.53; N, 13.32. IR (KBr, cm⁻¹): 1610, 1581, 1565, 1538, 1355, 1347.

(vi) Synthesis of [Gd(phen)₂(NO₃)₃] (2f)

Solutions of Gd(NO₃)₃.6H₂O (0.21 g, 0.5 mmol) in methanol (10.0 ml) and 1,10-phenanthroline (0.19 g, 1.0 mmol) in methanol (10.0 ml) were mixed slowly. The resulting solution was stirred for 8 hrs and filtered on celite. The filtrate was dried under vacuum to afford a powder solid in 73.0% (0.51 g, 0.73 mmol) yield. The compound was recrystallized from methanol at room temperature. The suitable colorless crystals were obtained from slow evaporation of solvent within 5 days. Anal. Calcd. (%) for C₂₄H₁₆N₇O₉Gd (703.69): C, 40.96; H, 2.29; N, 13.93. Found: C, 40.79; H, 2.13; N, 13.81. IR (KBr, cm⁻¹): 1627, 1583, 1561, 1553, 1361, 1347, 847, 719.

(vii) Synthesis of [Gd(2,6-DNP)₃phenCH₃OH] (2g)

Complex **2g** was prepared and crystallized in 69.4% (0.63 g, 0.69 mmol) yield by the method as outlined for **2b** using GdCl₃.6H₂O (0.02 g, 0.5 mmol) instead of EuCl₃.6H₂O. Anal. Calcd. (%) for C₃₁H₂₁N₈O₁₆Gd (918.81): C, 40.52; H, 2.30; N, 12.19. Found: C, 40.23; H, 2.19; N, 12.11. IR (KBr, cm⁻¹): 3445, 1623, 1595, 1553, 1421, 1335, 1262, 1098, 1021, 845, 726, 675.

(viii) Synthesis of [Gd(2,6-DNP)₃phen(OH)]₂.(Hphen)₂ (2h)

The complex **2h** was prepared and crystallized in 66.8% (0.72 g, 0.66 mmol) yield by the method as described for **2c**. Anal. Calcd. (%) for C₈₄H₅₄N₂₀O₃₂Gd₂ (2169.95): C, 46.49; H, 2.51; N, 12.91. Found: C, 46.33; H, 2.44; N, 12.73. IR (KBr, cm⁻¹): 3365, 1614, 1548, 1521, 1464, 1429, 1338, 1249, 1012, 910, 850.

(ix) Synthesis of [Gd(2,6-DNP)₃bipyOH₂] (2i)

Complex **2i** was prepared and crystallized in 69.8% (0.61 g, 0.69 mmol) yield by the method as outlined for **2d**. Anal. Calcd. (%) for C₂₈H₁₉N₈O₁₆Gd (880.74): C, 38.18; H, 2.17; N, 12.72. Found: C, 38.11; H, 2.09; N, 12.53. IR (KBr, cm⁻¹): 3417, 1618, 1524, 1433, 1331, 1266, 1012, 869, 739.

(x) Synthesis of [Gd(2,6-DNP)₃bipy(OH)].Hbipy (2j)

Complex **2j** was prepared and crystallized in 71.6% (0.74 g, 0.71 mmol) yield by the method as outlined for **2e**. Anal. Calcd. (%) for C₃₈H₂₇N₁₀O₁₆Gd (1036.95): C, 44.01; H, 2.62; N, 13.50. Found: C, 43.89; H, 2.56; N, 13.39. IR (KBr, cm⁻¹): 3402, 1615, 1525, 1435, 1338, 1257, 1021, 906, 874.

Chapter-3

(i) Synthesis of [Gd(tptz)Cl₂(OH₂)₄].Cl.4H₂O (3a)

Solutions of GdCl₃.6H₂O (0.37 g, 1.0 mmol) in methanol (10.0 ml) and 2,4,6-tris(2-pyridyl)-1,3,5-triazine (0.31 g, 1.0 mmol) in methanol (10.0 ml) were mixed and the resulting solution was stirred overnight. The solution was filtered on celite and the filtrate was dried under vacuum to afford a powder solid in 82.01% (0.57 g, 0.82 mmol) yield. The compound was dissolved in water-methanol mixture and the suitable colorless crystals were obtained from slow evaporation of solvent at room temperature (about one week). Anal. Calcd. (%) for C₁₈H₁₂N₆O₈Cl₃Gd (703.94): C, 30.71; H, 1.72; N, 11.94. Found: C, 30.59; H, 1.63; N, 11.71. IR (KBr, cm⁻¹): 3433, 1551, 1522, 1379, 1252, 768, 670.

(ii) Synthesis of [Gd(tptz)(SCN)₃(CH₃OH)₂OH₂].CH₃OH (3b)

A mixture of potassium thiocyanate (0.15 g, 1.5 mmol) and 2,4,6-tris(2-pyridyl)-1,3,5-triazine (0.15 g, 0.5 mmol) in 15.0 ml methanol was added to the methanolic solution of GdCl₃.6H₂O (0.19 g, 0.5 mmol). The reaction mixture was stirred at room temperature for 8 hrs and the solution was filtered. The filtrate was dried under vacuum to afford a powder solid in 79.8% (0.60 g, 0.79 mmol) yield. The compound was recrystallized from methanol at 4 °C. Anal. Calcd. (%) for C₂₄H₂₂N₉O₄S₃Gd (753.97): C, 38.23; H, 2.94; N, 16.71. Found: C, 38.11; H, 2.87; N, 16.65. IR (KBr, cm⁻¹): 3443, 2067, 1630, 1545, 1519, 1381, 1256, 756, 627.

(iii) Synthesis of [Gd(tptz)(OBz)₂(μ-OBz)OH₂]₂.H₂O (3c)

A mixture of sodium benzoate (0.21 g, 1.5 mmol) and 2,4,6-tris(2-pyridyl)-1,3,5-triazine (0.15 g, 0.5 mmol) in 15.0 ml methanol was added to the methanolic solution of GdCl₃.6H₂O (0.19 g, 0.5 mmol) and the mixture was stirred at room temperature for 4 hrs. The solution was filtered on celite and the filtrate was dried under vacuum to afford a powder solid in 74.2% (1.3 g, 0.74 mmol) yield. Anal. Calcd. (%) for C₇₈H₅₄N₁₂O₁₆Gd₂ (1729.83): C, 54.15; H, 3.15; N, 9.72. Found: C, 54.01; H, 3.08; N, 9.59. IR (KBr, cm⁻¹): 3425, 1612, 1599, 1537, 1421, 1017, 718, 676.

(iv) Synthesis of $[\text{Gd}(\text{phen})\text{Cl}_2(\text{OH}_2)_4]\cdot\text{Cl}\cdot\text{CH}_3\text{OH}$ (**3d**)

To the methanolic solution of $\text{GdCl}_3\cdot 6\text{H}_2\text{O}$ (0.37 g, 1.0 mmol), 1,10-phenanthroline (0.19 g, 1.0 mmol) solution in methanol (10.0 ml) was added drop wise and the resulting solution was stirred for 8 hrs. The reaction mixture was filtered on celite and the solvent was evaporated under vacuum. The resultant solid in 81.02% (0.44 g, 0.81 mmol) yield was recrystallized from water-methanol mixture at room temperature. Anal. Calcd. (%) for $\text{C}_{13}\text{H}_{19}\text{N}_2\text{O}_5\text{Cl}_3\text{Gd}$ (546.86): C, 28.55; H, 3.56; N, 5.12;. Found: C, 28.43; H, 3.49; N, 5.06. IR (KBr, cm^{-1}): 3456, 1624, 1591, 1465, 1372, 847, 763, 670.

(v) Synthesis of $[\text{Gd}(\text{phen})_2(\text{SCN})_3\text{CH}_3\text{OH}]\cdot\text{phen}$ (**3e**)

A mixture of potassium thiocyanate (0.14 g, 1.5 mmol) and 1,10-phenanthroline (0.10 g, 0.5 mmol) in 15.0 ml methanol was added to methanolic solution of $\text{GdCl}_3\cdot 6\text{H}_2\text{O}$ (0.19 g, 0.5 mmol). The suspension was stirred at room temperature for 8 hrs and the solution was filtered. The filtrate was dried under vacuum to afford a powder solid in 69.8% (0.63 g, 0.70 mmol) yield. Anal. Calcd. (%) for $\text{C}_{40}\text{H}_{28}\text{N}_9\text{OS}_3\text{Gd}$ (904.13): C, 53.13; H, 3.12; N, 13.94. Found: C, 52.98; H, 3.07; N, 13.85. IR (KBr, cm^{-1}): 3346, 1596, 1568, 1467, 1377, 848, 769.

(vi) Synthesis of $[\text{OH}_2(\text{phen})(2\text{-pyca})_2\text{Gd}_1(\mu\text{-ox})\text{Gd}_2(2\text{-pyca})_2(\text{phen})\text{OH}_2]\cdot 6\text{H}_2\text{O}$ (**3f**)

A mixture of $\text{GdCl}_3\cdot 6\text{H}_2\text{O}$ (0.37 g, 1.0 mmol), 2-pyrazine carboxylic acid (0.24 g, 2.0 mmol), 1,10-phenanthroline (0.19 g, 1.0 mmol), water (10.0 ml) and methanol (5.0 ml) in a 25 ml Teflon-lined autoclave under autogenous pressure was heated at 170°C for 7 days. Colorless crystals of **3f** were obtained by cooling the reaction mixture at room temperature. Yield: 79.6% (1.10 g, 0.79 mmol). Anal. Calcd. (%) for $\text{C}_{46}\text{H}_{28}\text{N}_{12}\text{O}_{20}\text{Gd}_2$ (1383.31): C, 39.94; H, 2.04; N, 12.15. Found: C, 39.83; H, 1.95; N, 12.09. IR (KBr, cm^{-1}): 3380, 1639, 1459, 1392, 845, 735.

(vii) Synthesis of $[\text{Eu}(\text{tptz})\text{Cl}_3(\text{CH}_3\text{OH})_2]\cdot\text{CH}_3\text{OH}$ (**3g**)

Complex **3g** was prepared in 79.1% (0.44 g, 0.79 mmol) yield by the method as outlined for **3a** using $\text{EuCl}_3\cdot 6\text{H}_2\text{O}$ (0.18 g, 0.5 mmol) instead of $\text{GdCl}_3\cdot 6\text{H}_2\text{O}$. Anal. Calcd. (%) for $\text{C}_{21}\text{H}_{24}\text{N}_6\text{O}_3\text{Cl}_3\text{Eu}$ (558.65): C, **45.15**; H, 4.33; N, 15.03. Found: C, 25.63; H, 4.27; N, 14.91. IR (KBr, cm^{-1}): 3431, 1553, 1519, 1376, 1249, 763, 667.

(viii) Synthesis of $[\text{Eu}(\text{tptz})(\text{SCN})_3(\text{CH}_3\text{OH})_2\text{OH}_2]\cdot\text{CH}_3\text{OH}$ (**3h**)

Complex **3h** was prepared and crystallized in 77.4% (0.58 g, 0.77 mmol) yield by the method as outlined for **3b** using $\text{EuCl}_3\cdot 6\text{H}_2\text{O}$ (0.18 g, 0.5 mmol) instead of $\text{GdCl}_3\cdot 6\text{H}_2\text{O}$. Anal.

Calcd. (%) for $C_{24}H_{23}N_9O_4S_3Eu$ (749.69): C, 38.45; H, 3.08; N, 16.81. Found: C, 38.29; H, 2.99; N, 16.69. IR (KBr, cm^{-1}): 3449, 2066, 1630, 1543, 1378, 1260, 1156, 1013, 763, 675.

(ix) Synthesis of $[OH_2(OBz)_2(tptz)Eu_1(\mu-OBz)_2Eu_2(tptz)(OBz)_2OH_2].CH_3OH.7H_2O$ (3i)

Complex **3i** was prepared and crystallized in 68.7% (1.26 g, 0.68 mmol) yield by the method as outlined for **3c** using $EuCl_3.6H_2O$ (0.18 g, 0.5 mmol) instead of $GdCl_3.6H_2O$. Anal. Calcd. (%) for $C_{79}H_{58}N_{12}O_{22}Eu_2$ (1831.32): C, 51.81; H, 3.19; N, 9.18. Found: C, 51.69; H, 3.11; N, 9.09. IR (KBr, cm^{-1}): 3445, 1614, 1599, 1541, 1421, 1021, 766, 718.

(x) Synthesis of $[Eu(phen)_2(SCN)_3CH_3OH].phen$ (3j)

Complex **3j** was prepared in 72.9% (0.65 g, 0.73 mmol) yield by the method as outlined for **3e** using $EuCl_3.6H_2O$ (0.18 g, 0.5 mmol). Anal. Calcd. (%) for $C_{40}H_{27}N_9OS_3Eu$ (897.89): C, 53.51; H, 3.14; N, 14.04. Found: C, 53.33; H, 3.10; N, 13.93. IR (KBr, cm^{-1}): 3344, 1596, 1569, 1464, 1375, 846, 769.

(xi) Synthesis of $[OH_2(phen)(2-pyca)_2Eu_1(\mu-ox)Eu_2(2-pyca)_2(phen)OH_2].6H_2O$ (3k)

Complex **3k** was prepared in 77.3% (1.07 g, 0.77 mmol) yield by the method as outlined for **3f** using $EuCl_3.6H_2O$ (0.36 g, 1.0 mmol). Anal. Calcd. (%) for $C_{46}H_{44}N_{12}O_{20}Eu_2$ (1388.78): C, 39.78; H, 3.19; N, 12.10. Found: C, 39.67; H, 3.11; N, 11.97. IR (KBr, cm^{-1}): 3382, 1638, 1454, 1393, 847, 733.

(xii) Synthesis of $[Tb(tptz)Cl_3(CH_3OH)_2].CH_3OH$ (3l)

Complex **3l** was prepared in 81.02% (0.46 g, 0.81 mmol) yield by the method as outlined for **3a** using $TbCl_3.6H_2O$ (0.19 g, 0.5 mmol) instead of $GdCl_3.6H_2O$. Anal. Calcd. (%) for $C_{21}H_{24}N_6O_3Cl_3Tb$ (565.62): C, 44.53; H, 4.27; N, 14.85. Found: C, 25.34; H, 4.19; N, 14.71. IR (KBr, cm^{-1}): 3437, 1556, 1519, 1371, 1256, 765, 675.

(xiii) Synthesis of $[Tb(tptz)(SCN)_3(CH_3OH)_2OH_2].CH_3OH$ (3m)

Complex **3m** was prepared and crystallized in 74.9% (0.57 g, 0.75 mmol) yield by the method as outlined for **3b** using $TbCl_3.6H_2O$ (0.19 g, 0.5 mmol). Anal. Calcd. (%) for $C_{24}H_{23}N_9O_4S_3Tb$ (756.65): C, 38.09; H, 3.06; N, 16.66. Found: C, 37.91; H, 2.97; N, 16.52. IR (KBr, cm^{-1}): 3420, 2059, 1621, 1541, 1377, 1086, 763, 675.

(xiv) Synthesis of $\{[Tb_1(tptz)(OBz)_2(\mu-OBz)]_2.[Tb_2(tptz)(OBz)_3CH_3OH]\}.CH_3OH.2H_2O$ (3n)

A mixture of sodium benzoate (0.21 g, 1.5 mmol) and 2,4,6-tris(2-pyridyl)-1,3,5-triazine (0.15 g, 0.5 mmol) in a water-methanol mixture (v/v %, 1:4, 10 ml) was added to the methanolic solution of $TbCl_3.6H_2O$ (0.19 g, 0.5 mmol). The suspension was stirred at room

temperature for 6 hrs and filtered on celite. The filtrate was dried under vacuum to afford a powder solid in 72.9% (1.92 g, 0.72 mmol) yield. Anal. Calcd. (%) for $C_{119}H_{89}N_{18}O_{22}Tb_3$ (2599.95): C, 54.99; H, 3.41; N, 9.70. Found: C, 54.67; H, 3.34; N, 9.57. IR (KBr, cm^{-1}): 3441, 1612, 1599, 1532, 1421, 1255, 1008, 854, 768, 722.

(xv) Synthesis of $[Tb(phen)_2Cl_3OH_2].CH_3OH$ (**3o**)

The methanolic solutions (10 ml) of $TbCl_3.6H_2O$ (0.19 g, 0.5 mmol) and 1,10-phenanthroline (0.09 g, 0.5 mmol) was stirred overnight and filtered on celite. The filtrate was dried under vacuum to afford a powder solid in 78.0% (0.53 g, 0.78 mmol) yield. The compound was recrystallized from methanol at 4 °C. Anal. Calcd. (%) for $C_{25}H_{22}N_4O_2Cl_3Tb$ (675.75): C, 44.43; H, 3.28; N, 8.29. Found: C, 44.31; H, 3.13; N, 8.15. IR (KBr, cm^{-1}): 3356, 1625, 1590, 1382, 640.

(xvi) Synthesis of $[Tb(phen)_2(SCN)_3CH_3OH].phen$ (**3p**)

Complex **3p** was prepared in 73.4% (0.66 g, 0.73 mmol) yield by the method as outlined for **3e** using $TbCl_3.6H_2O$ (0.19 g, 0.5 mmol). Anal. Calcd. (%) for $C_{40}H_{28}N_9OS_3Tb$ (905.81): C, 53.03; H, 3.11; N, 13.99. Found: C, 52.89; H, 3.03; N, 13.83. IR (KBr, cm^{-1}): 3343, 1594, 1566, 1459, 1373, 843, 764.

(xvii) Synthesis of $[OH_2(phen)(2-pyca)_2Tb_1(\mu-ox)Tb_2(2-pyca)_2(phen)OH_2].6H_2O$ (**3q**)

Complex **3q** was prepared in 67.8% (0.95 g, 0.68 mmol) yield by the method as outlined for **3f** using $TbCl_3.6H_2O$ (0.37 g, 1.0 mmol). Anal. Calcd. (%) for $C_{46}H_{44}N_{12}O_{20}Tb_2$ (1402.72): C, 39.38; H, 3.16; N, 11.98. Found: C, 39.21; H, 3.09; N, 11.87. IR (KBr, cm^{-1}): 3378, 1637, 1461, 1389, 843, 729.

Chapter-4

3-phenyl-5-methylpyrazole [$Pz^{Ph,Me}H$] [Ref. 35 of chapter 4] (**4a**), 4-(3,5-dimethyl-4H-pyrazole-4-yl)-3,5-dimethyl-1H-pyrazole [H_2mdpz] [Ref. 36 of chapter 4] (**4b**) were synthesized by the literature method.

(i) Synthesis of $[2PA^-.2PzH_2^+.OH_2]$ (**4c**)

Picric acid (0.22 g, 1.0 mmol) and pyrazole (0.06 g, 1.0 mmol) were mixed in a water-methanol mixture (v/v %, 1:4, 10 ml). The resulting solution was stirred for 6 hrs and filtered through celite. The filtrate was evaporated to dryness under vacuum and the yellow solid obtained was redissolved in methanol. The yellow crystals of salt **4c** in 69.0% (0.42 g, 0.69 mmol) yield, suitable for X-ray data collection were obtained by slow evaporation of solvent at room temperature. Anal. Calcd. (%) for $C_{18}H_{16}N_{10}O_{15}$ (612.41): C, 76.49; H, 2.37; N, 23.56.

Found: C, 76.35; H, 2.31; N, 23.47. IR (KBr, cm^{-1}): 3218, 3141, 2996, 1843, 1611, 1567, 1539, 1494, 1360, 1321, 1278, 1162, 1134, 1077, 909, 769, 711, 608, 543.

(ii) Synthesis of $[\text{PA}^-\text{Pz}^{\text{Me}_2}\text{H}_2^+]$ (4d)

Salt **4d** was prepared by same procedure as outlined above for **4c** using 3,5-dimethyl pyrazole (0.09 g, 1.0 mmol) in methanol (10 ml) with 63.2% (0.20 g, 0.63 mmol) yield. Anal. Calcd. (%) for $\text{C}_{11}\text{H}_{11}\text{N}_5\text{O}_7$ (325.25): C, 40.62; H, 3.40; N, 21.53. Found: C, 40.43; H, 3.29; N, 21.39. IR (KBr, cm^{-1}): 3191, 3126, 1586, 1469, 1336, 1298, 1154, 1032, 1008, 835, 737.

(iii) Synthesis of $[\text{PA}^-\text{Pz}^{\text{Ph,Me}}\text{H}_2^+\cdot\text{CH}_3\text{OH}]$ (4e)

Salt **4e** was prepared by same procedure as outlined above for **4c** using 3-phenyl-5-methyl pyrazole (0.16 g, 1.0 mmol) in methanol (10 ml) with 71.8% (0.30 g, 0.72 mmol) yield. Anal. Calcd. (%) for $\text{C}_{17}\text{H}_{17}\text{N}_5\text{O}_8$ (419.36): C, 48.69; H, 4.08; N, 16.70. Found: C, 48.49; H, 3.97; N, 16.53. IR (KBr, cm^{-1}): 3308, 3102, 1860, 1627, 1533, 1431, 1341, 1260, 1151, 1082, 834, 780, 702, 534.

(iv) Synthesis of $[2\text{PA}^-\cdot 2\text{H}_2\text{mdpzh}^+\cdot\text{CH}_3\text{CN}]$ (4f)

Salt **4f** was prepared by same procedure as outlined above for **4c** using 4-(3,5-dimethyl-4H-pyrazole-4-yl)-3,5-dimethyl-1H-pyrazole (0.19 g, 1.0 mmol) in an acetonitrile-methanol mixture (v/v %, 1:4, 10 ml) with 68.9% (0.61 g, 0.68 mmol) yield. Anal. Calcd. (%) for $\text{C}_{34}\text{H}_{37}\text{N}_{15}\text{O}_{14}$ (879.79): C, 46.41; H, 4.23; N, 23.88. Found: C, 46.37; H, 4.19; N, 23.73. IR (KBr, cm^{-1}): 3347, 1830, 1626, 1581, 1536, 1426, 1313, 1165, 1072, 907, 812, 710, 616.

(v) Synthesis of $[\text{PA}^-\text{phenH}^+\cdot\text{CH}_3\text{OH}]$ (4g)

Salt **4g** was prepared by same procedure as outlined above for **4c** using 1,10-phenanthroline (0.19 g, 1.0 mmol) in an acetonitrile-methanol mixture (v/v %, 1:4, 10 ml) with 62.5% (0.27 g, 0.62 mmol) yield. Anal. Calcd. (%) for $\text{C}_{19}\text{H}_{15}\text{N}_5\text{O}_8$ (441.36): C, 51.71; H, 3.42; N, 15.86; Found: C, 51.59; H, 3.33; N, 15.63. IR (KBr, cm^{-1}): 3357, 3056, 1514, 1364, 1312, 1263, 1159, 1076, 1016, 909, 847, 785, 744, 715, 619.

(vi) Synthesis of $[2\text{PA}^-\cdot\text{terpyH}_2^{2+}]$ (4h)

Salt **4h** was prepared by same procedure as outlined above for **4c** using 2,2';6',2''-terpyridine (0.23 g, 1.0 mmol) with 72.8% (0.50 g, 0.72 mmol) yield. Anal. Calcd. (%) for $\text{C}_{27}\text{H}_{17}\text{N}_9\text{O}_{14}$ (691.50): C, 46.90; H, 2.47; N, 18.23. Found: C, 46.78; H, 2.32; N, 18.09. IR (KBr, cm^{-1}): 3429, 3098, 1860, 1635, 1527, 1435, 1337, 1269, 1160, 1080, 915, 834, 780, 704.

(vii) Synthesis of [PA.hmta] (4i)

Salt **4i** was prepared by same procedure as outlined above for **4g** using hexamethylenetetramine (0.14 g, 1.0 mmol) with 73.7% (0.27 g, 0.73 mmol) yield. Anal. Calcd. (%) for $C_{12}H_{15}N_7O_7$ (369.31): C, 39.03; H, 4.09; N, 26.55. Found: C, 38.89; H, 3.93; N, 26.42. IR (KBr, cm^{-1}): 3438, 2917, 2552, 1629, 1562, 1483, 1433, 1404, 1361, 1287, 1257, 1156, 1014, 978, 820, 791, 708.

(viii) Synthesis of [3PA⁻.tptzH₃³⁺] (4j)

Salt **4j** was prepared by same procedure as outlined above for **4g** using 2,4,6-tris(2-pyridyl)-1,3,5-triazine (0.31 g, 1.0 mmol) with 68.9% (0.68 g, 0.68 mmol) yield. Anal. Calcd. (%) for $C_{36}H_{21}N_{15}O_{21}$ (999.68): C, 43.25; H, 2.11; N, 21.01. Found: C, 43.08; H, 2.09; N, 20.87. IR (KBr, cm^{-1}): 3426, 3104, 1860, 1633, 1609, 1531, 1434, 1342, 1272, 1155, 1087, 918, 830, 778, 732, 705, 660.

(ix) Synthesis of [PA⁻.Uronium] (4k)

Salt **4k** was prepared by same procedure as outlined above for **4g** using urea (0.06 g, 1.0 mmol) with 71.5% (0.21 g, 0.71 mmol) yield. Anal. Calcd. (%) for $C_7H_7N_5O_8$ (289.18): C, 29.07; H, 2.43; N, 24.22; Found: C, 28.93; H, 2.34; N, 24.17. IR (KBr, cm^{-1}): 3412, 3103, 2882, 1856, 1709, 1635, 1534, 1432, 1345, 1148, 1082, 926, 826, 774, 729, 530.

(x) Synthesis of [PA⁻.3, 5-diamino-1,2,4-triazolium] (4l)

Picric acid (0.22 g, 1.0 mmol) and 1H-1,2,4-triazole-3,5-diamine (0.09 g, 1.0 mmol) were mixed in a water-methanol mixture (v/v %, 1:4, 10 ml). The resulting solution was refluxed for 2 hrs and filtered through celite. The filtrate was evaporated to dryness under vacuum and the yellow solid obtained was redissolved in methanol. The yellow diamond shaped crystals of salt **4l** in 77.8% (0.25 g, 0.77 mmol) yield were obtained by slow evaporation of solvent at room temperature. Anal. Calcd. (%) for $C_8H_8N_8O_7$ (328.22): C, 29.37; H, 2.15; N, 34.25. Found: C, 29.23; H, 2.05; N, 34.11. IR (KBr, cm^{-1}): 3460, 3418, 3354, 3168, 1839, 1689, 1627, 1548, 1430, 1329, 1272, 1163, 1076, 999, 912, 788, 711, 656.

(xi) Synthesis of [1PA⁻.1/2cyclohexane-1,2-diaminium] (4m)

Salt **4m** was prepared by same procedure as outlined above for **4l** with cyclohexane 1,2-diamine (0.11 g, 0.5 mmol) with 69.7% (0.39 g, 0.69 mmol) yield. Anal. Calcd. (%) for $C_{18}H_{20}N_8O_{14}$ (572.42): C, 37.77; H, 3.52; N, 19.57; Found: C, 37.53; H, 3.41; N, 19.47. IR (KBr, cm^{-1}): 3429, 2926, 1633, 1547, 1489, 1428, 1342, 1265, 1084, 910, 780, 702, 628.

(xii) Synthesis of [PA⁻.6-phenyl-2,4 diamino-1,3,5-triazinium] (4n)

Salt **4n** was prepared by same procedure as outlined above for **4l** with 6-phenyl-1,3,5-triazine-2,4-diamine (0.18 g, 1.0 mmol) with 67.0% (0.27 g, 0.67 mmol) yield. Anal. Calcd. (%) for C₁₅H₁₂N₈O₇ (416.33): C, 43.28; H, 2.90; N, 26.91. Found: C, 43.19; H, 2.83; N, 26.49. IR (KBr, cm⁻¹): 3378, 3105, 2874, 1856, 1673, 1535, 1429, 1336, 1154, 1082, 976, 855, 778, 704, 534.

REFERENCES

1. Perrin, D. D., Armarego, W. L. and Perrin, D. R., "Purification of laboratory chemicals", 2nd ed., Pergamon, New York (1980).
2. Sheldrick, G. M., "Phase annealing in SHELX-90: Direct methods for larger structures", *Acta Cryst.*, **A46**, 467 (1990).
3. Sheldrick, G. M., "SHELXTL-NT 2000 version 6.12, reference manual", University of Göttingen, Göttingen, Germany.
4. Sheldrick, G. M., SADABS, University of Göttingen, Germany (1996).
5. Klaus, B., "Diamond: Visual crystal structure information system (Version 2.1d)", Bonn, Germany (2000).
6. Mercury, Cambridge Crystallographic Data Centre, 12 Union Road, Cambridge CB2 1EZ, United Kingdom. Available from: Website: <http://www.ccdc.cam.ac.uk/>.
7. Gaussian 03, Rev. C.02, Gaussian, Inc., Wallingford CT (2004).
8. Hariharan, P. C. and Pople, J. A., "The influence of polarization functions on molecular orbital hybridization energies", *Theo. Chem. Acta*, **28**, 213 (1972).
9. Frisch, A., Nielsen, A. B. and Holder, A. J., "Gauss view users manual, Gaussian Inc", Wallingford, CT (2003).
10. Singh, G. and Singh, R. R., "Indigenously fabricated apparatus for thermogravimetric analysis", *Res. Ind.*, **23**, 92 (1978).
11. Singh, G., Vasudeva, S. K. and Kapoor, I. P. S., "Thermolysis of AP-PS-additive mixture II", *Indian J. Tech.*, **29**, 589 (1991).
12. Zinn, J. and Rogers, R. N., "Thermal initiation of explosives", *J. Phys. Chem.*, **66**, 2646 (1962).
13. Semenov, N., "Chemical kinetics, chain reactions", Clarendon Press Oxford, Chap.18 (1935).
14. Freeman, E. S. and Gorden, S., "The application of the absolute rate theory of the nitrate-magnesium, sodium nitrate- magnesium", *J. Phys. Chem.*, **60**, 867 (1956).
15. Martin, A. R. and Yallop, H. J., "Some aspects of detonation of part I: Detonation velocity and chemical constitution", *Trans Faraday Soc.*, **54**, 257 (1958).
16. Brown, M. E., Dollimore, D. and Galway, A. K., "Reaction in the solid state, in: *Comprehensive chemical kinetics*", 22, Elsevier, Amsterdam, The Netherlands, 1 (1960).

17. Singh, G., Felix, P. S. and Pandey, D. K., "Studies on energetic compounds part 37: Kinetics of thermal decomposition of perchlorate complexes of some transition metals with ethylenediamine", *Thermochim. Acta*, **411**, 61 (2004).